SANDIA REPORT SAND84—0618 • TTC—0431

Printed March 1984

Gravel Gertie Confinement Verification Program – Final Report (U)

R. E. Luna, R. P. Sandoval, J. M. Taylor, N. R. Grandjean,
L. L. Keller, G. J. Newton

Prepared by
Sandia National Laboratories
Albuquerque, New Mexico 87185 and Livermore, California 94550
for the United States Department of Energy
under Contract DE-AC04-76DP00789

When printing a copy of any digitized SAND Report, you are required to update the markings to current standards.

SF2900QA(8-81)

SAND84-0618
TTC-0431

Printed March 1984

GRAVEL GERTIE CONFINEMENT VERIFICATION PROGRAM -- Final Report

Prepared by:
R. E. Luna
R. P. Sandoval
J. M. Taylor
N. R. Grandjean
L. L. Keller

Sandia National Laboratories
Division 6321
Albuquerque, NM 87185
for the United States Department of Energy
Under Contract DE-AC04-76DP00789

G. J. Newton
Lovelace Inhalation Toxicology Research Institute
Albuquerque, New Mexico 87185
Under Contract DE-AC04-76EV01013

ABSTRACT

An evaluation of the aerosol confinement capability of a Gravel Gertie assembly structure was conducted in 1982 by Sandia National Laboratories. This program included scale-model tests, confinement-chamber tests, and a single full-scale test. Explosive aerosol generators were designed and tested to confirm aerosol production quantities in both subscale and full-scale confined tests. A computer model was developed to provide a means of relating results of this test to earlier tests and future design changes. Measurements of tracer aerosols were made inside and outside the subscale and full-scale structure in order to evaluate the release of respirable aerosol. Results of the full-scale test indicate that a maximum of 4×10^{-3} of the respirable-size tracer aerosols produced from detonation of high explosives inside the structures was released through the gravel roof to the environment.

ACKNOWLEDGEMENTS

The authors would like to express their appreciation to all participating persons, organizations and institutions for their technical support and assistance in this study. In particular, a special note of appreciation is expressed to the following people.

Sandia National Laboratories

B. Holt, 7123	L. B. Neeley, 7124	B. G. Edwards, 7131
V. E. Kerr, 7131	A. Church, 7132	R. W. Durkee, 7132
H. E. Roberts, 7132	P. W. Cooper, 7132	A. Trujillo, 7135
W. L. Stevens, 7230	J. E. CDeBaca, 7522	R. J. Beyatte, 7522
E. L. Pedro (EG&G), 7522	F. H. Mathews, 7533	R. E. Bohannon, 7533
M. G. Perdue, 7533	J. P. Weber, 7533	S. A. Ingham, 7556
J. S. Llamas, 7556	L. W. Paulson, 7556	B. D. Zak, 6324
J. Sebastian, 6323	A. L. Jensen, 6324	B. T. Kenna, 6324
H. W. Church, 6324	E. Shirley, 6320	K. R. Dunbar, 5152
G. T. Gay, 6324	E. Sanchez, 3311	C. E. Gray, 3311
D. R. Parker, 3311	A. D. Romig, 1832	K. S. Varga, 1822
G. Grady, 1530	T. Bergstresser, 1530	

Lovelace Inhalation Toxicology Reserach Institute

R. McClellan	B. B. Boecker	S. C. Yeh
J. Evans	E. B. Barr	B. Wong

Los Alamos National Laboratories

W. R. Hansen	A. Stoker	E. Gladney
	D. Rose	

Holmes & Narver
P. Brebrick

New Mexico Word Processing Center

National Weather Service
B. Armstrong

EG&G, Mercury
R. Starbird and crew

Reynolds Electrical & Engineering Co.

B. Pritchett	M. Barr	W. Baker

Southwest Research Institute
W. E. Baker

Amman and Whitney
S. Weissman

Mason and Hanger, Silas Mason Co.
J. Burling

TABLE OF CONTENTS

	Page
Abstract	ii
Acknowledgements	iii
List of Figures	v
List of Tables	vii
List of Appendices	viii
Executive Summary	1
Main Report	4
Introduction	4
Historical Background	4
1982 Test Series	8
Scale Test Summary	8
Confinement Test Summary	10
Full-Scale Test Summary	12
Interpretation of Full-Scale Test Data	55
Comparison with Early Tests	56
Conclusions	57
References	58
Appendices	A-1

LIST OF FIGURES

		Page
2-1	Plan and Elevation View of Structure for 1956-1957 Test	6
2-2	Gravel Height Versus Time (1957 Test)	7
2-3	Subscale Test Facility (Plan View and Elevation View)	9
2-4	Confinement Chamber Test Facility	11
2-5	Particle Size Distribution from Confinement Test 8	13
2-6	Gravel Gertie Site Location at NTS	14
2-7	Plan View of Gravel Gertie Test Structure	15
2-8	Elevation View of Gravel Gertie Structure	16
2-9	Construction Details of Gravel Bed	17
2-10	Location of Sampler Arrays and Meteorological Equipment Near the Gravel Gertie Structure	20
2-11	GGASP Sampler Cross Section	21
2-12	Gravel Gertie Donut Sampling Array (GGDSA)	22
2-13	Gravel Gertie External Sampling Array (GGESA)	23
2-14	Gravel Gertie Balloon Sampling Array (GGBSA)	24
2-15	Gravel Gertie Pole Sampling Array (GGPSA)	25
2-16	Location of GGCTA Sampler Trays	27
2-17	Tunnel Sampling System	28
2-18	Design of HEAG Installation	30
2-19	Size Distribution of Sb_2O_3 Powder	31
2-20	Round Room Configuration at Test Time	32
2-21	Gravel Bed Behavior and Round Room Pressure	36
2-22	Gravel Bed Detail--T = 0 sec	37
2-23	Gravel Bed Detail--T = 0.5 sec	38
2-24	Gravel Bed Detail--T = 1.3 sec	39
2-25	Gravel Bed Detail--T = 2.0 sec	40

LIST OF FIGURES (CONT)

		Page
2-26	Gravel Bed Detail--T = 2.2 sec	41
2-27	Gravel Bed Detail--T = 2.8 sec	42
2-28	Gravel Bed Detail--T = 8.0 sec	43
2-29	Gravel Bed Profiles During Dome Rise	45
2-30	Gravel Bed Profile During Dome Collapse	46
2-31	Typical Round Room Pressure Signature	48
2-32	Typical Staging Area Pressure Signature	49
2-33	GGCTA Data Above Background	50
2-34	Size Distribution for GGBSA Impactors With Significant Collections	51
2-35	Cloud Outlines Versus Time (SE Station)	52
2-36	Cloud Outlines Versus Time (NE Station)	53

LIST OF TABLES

		Page
2-1	Review of 1956-1957 Full-Scale Gravel Gertie Tests	5
2-2	Aerosol Sampling System Descriptions	19
2-3	Brief Event Chronology	35
2-4	Meteorological Data Near Shot Time	54

LIST OF APPENDICES

		Page
A.	Subscale Test Details	A-1
B.	Scaled Source Term Autoclave Tests	B-1
C.	Full-Scale Test Construction Details	C-1
D.	Aerosol Sampling System Details and Data	D-1
E.	Full-Scale Test Pressure and Temperature Records	E-1
F.	Fragmentation Experiments Conducted During Full-Scale Test	F-1
G.	Full-Scale Test Blast Valve Experiment	G-1
H.	Full-Scale Test Meteorological Monitoring System Details and Data	H-1
I.	Photographic System	I-1
J.	Calculation of Internal Aerosol Release Mass for Full-Scale Test	J-1
K.	Analysis of Respirable Aerosol Release Fraction for Full-Scale Test	K-1
L.	Analysis of Cloud Growth, Release, and Particle Trajectories	L-1
M.	Analytical Prediction of Results Using Diffusion Modelling	M-1
N.	Analysis of Control Samples, Background Soil, and Background Air Samples	N-1
O.	Dynamic Analysis	O-1

EXECUTIVE SUMMARY

Introduction

The Gravel Gertie Confinement Verification Program (GGCVP) was initiated in early 1982 to provide information on the ability of Gravel Gertie structures to contain the respirable-sized plutonium aerosols that would be produced in an accident involving detonation of a nuclear weapon's high explosive. Earlier tests of the Gravel Gertie design during the mid-1950s were primarily concerned with the degree to which the structure minimized ground deposit of plutonium aerosols. However, those tests did not address the exposure to respirable material of persons nearby and at site boundaries which is the principal measure, under current radiation protection standards, of hazards to man.

The full GGCVP contained three major components:

1. Scaled Tests--To explore in a quick and inexpensive manner the possible impact of structural design features which could not be duplicated in the full-scale test and which were not included in earlier tests,

2. Confinement Vessel Tests--To verify the high explosive/uranium aerosol generator (HEAG) design in terms of the amounts of respirable aerosol produced, and

3. Full-Scale Test--To verify in full scale the capture efficiency of a Gravel Gertie structure for aerosolized materials produced.

Subscale Test Program

The subscale test series confirmed the predicted scaling law behavior for overall gravel bed movement and proved the viability of the GGASP aerosol monitoring equipment. In addition, the variability introduced by either an off-center detonation or the inclusion of a dropped ceiling were found to be insignificant.

Confinement Test Program

A series of subscale explosive tests were performed in a spherical steel confinement chamber to verify the hydrocode predictions of aerosol quantity produced by the HEAG as well as to determine a particle size distribution for the aerosols produced. The high explosive aerosol generator used for these experiments was scaled from the device designed for the full-scale test. The results of these tests suggested a respirable fraction of between 6% and 7%. When possible secondary aerosolization mechanisms such as liquid droplet breakup were considered, these values were consistent with hydrocode predictions of 2-3 percent vaporization.

Full-Scale Test Program

The site chosen for the full-scale Gravel Gertie test was that used for the Gravel Gertie concept tests in the mid-1950s. The structure was fully excavated and, after inspection by structural consultants, was found to be suitable for additional testing. The staging area used in the 50s test series did not simulate actual geometry and volume of current designs. As a result, a new staging area was designed and constructed using appropriate lengths of 10-ft-diameter steel culvert.

Since the principal goal of the full-scale test was to determine the capture efficiency of the gravel roof of the structure, aerosol measurement systems were designed to characterize the aerosol inside the structure before gravel bed collapse as well as any aerosol escaping from the structure.

Within the structures were a set of six blast-hardened and fragment-shielded samplers. Four were in the round room and two in the staging area to sample respirable aerosols prior to gravel bed collapse. Outside the structure were a number of air sampler systems designed to obtain data to characterize the aerosol emissions by quantity, size distribution and location. These included filters, impactors, electrostatic precipitators, and fallout trays.

Pressure measurements were made at four locations in the round room, and various points in the staging area. In addition, a series of pressure measurements were made inside and outside the structure by Southwest Research Institute.

Uranium was selected to be the primary tracer because of its physical similarity to plutonium. The uranium aerosol was generated by four high explosive aerosol generators (HEAG), each composed of a hollow high explosive shell surrounding a hollow uranium shell. Powdered antimony oxide (Sb_2O_3) was used as a secondary tracer.

The test was documented by still photographs, video tapes, and motion pictures spanning construction, test, and recovery phases of the event.

At approximately 0840 Pacific Standard Time on November 20, 1982, the high explosive aerosol generators were detonated. Initial indications were that all operational systems functioned and all data to be recorded was being received. During and after the test, winds remained steady from the east at 0.5-1.0 m/sec.

Onsite personnel were released into the test area at T + 20 min to recover samplers and dissassemble sampling arrays. At T + 4 days, the tunnel door was reopened to allow access for sampling and preliminary equipment recovery operations. At T + 14 days, soil and gravel fall-back were removed from the round room to allow access to the round room samplers.

Extrapolation of the aerosol concentration in the mass of gas captured by inside samplers to the total mass of gas in the structure provided an estimate of the total uranium aerosol mass inside the Gravel Gertie structure. The total quantity of uranium aerosol inside the structure was measured to be 195 g $\pm$ 40 g with 90 to 98 percent in the respirable size regime.

Estimating the mass of respirable aerosol external to the structure was done in two largely independent ways. One involved fitting air sampler data with a diffusion model. The second involved using air sampler results together with photographic evidence of cloud volumes sampled to form a concentration-volume product which yielded aerosol mass. Both processes indicated a released aerosol mass of 0.6 to 1.0 grams.

The fallout tray data indicated a few locations where significant deposits were received within 125 meters of the test structure; the remaining values were generally indistinguishable from background.

The test result of principal interest is the respirable aerosol release fraction. This quantity was obtained by dividing the estimates of uranium aerosols external to the structure by the measured quantity inside before roof collapse. This yields a total aerosol release fraction of $4 \times 10^{-3} \pm 1.5 \times 10^{-3}$ with a respirable component of $3 \times 10^{-3} \pm 1.1 \times 10^{-3}$.

The results obtained in this test were not fully consistent with the results of the 50s test. In that test none of the fallout trays received deposits above that received by the same trays uncovered for a comparable time before the test. In addition, qualitative review of test films also indicates that gravel bed behavior was somewhat different in the two tests. In searching for possible reasons for these discrepancies, several differences between the tests were noted. The three most important relate to the quantity of aerosol produced, the construction of the gravel bed, and the volume and configuration of the staging areas. Since the specification for Gravel Gerties at Pantex includes about 20% more gravel and greater gravel bed depth in the areas above the round room periphery than used on this test, the use of 4×10^{-3} as a release fraction for assessing gravel bed confinement capability is clearly conservative.

A dynamic model was formulated to relate system response to construction variations, scale, and HE quantities. This model was formulated to match the results of this test and compared satisfactorily with earlier tests and the scaled tests performed in this program. The model indicated that a Gravel Gertie constructed according to Pantex specification should show slightly greater confinement capability than this test unit.

The Gravel Gertie Confinement Verification Program has provided a significant increase in the understanding of the behavor of Gravel Gertie structures under high explosive detonation conditions. Taken together, the program components provide confidence in the Department of Energy's use of the Gravel Gertie to mitigate consequences of high explosive detonation during weapon assembly operations.

2.0 Main Report

Introduction

The Gravel Gertie Confinement Verification Program (GGCVP) was initiated in early 1982 to provide information on the ability of Gravel Gertie structures to contain respirable plutonium aerosols that would be produced in an accidental detonation of the explosive component of a nuclear weapon. Tests of the Gravel Gertie design during the mid-1950s were primarily concerned with the capability of the structure to minimize ground deposit of plutonium aerosols. However, those tests did not address exposure to respirable material of persons nearby and at site boundaries.

The full GGCVP contained three major components: scaled tests, confinement vessel tests, and a full-scale test. In addition, there were two other separately funded components of the GGCVP: a demonstration of the operation of two prototype blast check valves proposed for use in a LANL test device assembly building, and an experiment to obtain data on shock and pressure levels both inside and outside the structure.

Historical Background

Since the initial Gravel Gertie design concept was suggested in the mid-1950s there have been three test series of significance. The first of these was a full-scale test series conducted in the United States in 1956-1957; the second was a scale model test series conducted in the United Kingdom in 1962, and the third is the test series reported in this document.

1956-1957 US Test Series

A set of four tests was conducted to evaluate the Gravel Gertie as a potential containment structure [Co57, Co58]. Significant aspects of each of these tests are given in Table 2-1, and plan and elevation views of the structure used in these tests are shown on Figure 2-1. The principal aerosol measurement instrumentation in the three tests at NTS was a large grid of fallout trays, consisting of metal sheets covered with a sticky alkyd resin material. This system was designed to detect particles large enough to fall out of the cloud and adhere to the surface. While this is a reasonable approach for detection of relatively large (>100 μm) particles, it is not a good technique for detection of small (<10 μm) particles which are of concern from the current radiological safety point-of-view. Hence, the utility of these earlier tests in the context of comparison to dosimetric limits is open to question. The Amarillo test was also of limited use since (1) the comparability of lanthanum to actual weapon materials is questionable; (2) no particle size discrimination was carried out; and (3) the gamma-ray "shine" from nonreleased material was difficult to distinguish from the radiation emitted by released material.

Despite the "hindsight" problems identified with the 1956-1957 test series, the data which was collected can be used to benchmark the current test to the earlier tests. Three types of measurements were made during Test 4: meteorological, gravel behavior, and aerosol. Figure 2-2 shows the gravel height as a function of time. No uranium levels above background were

TABLE 2-1

Review of 1956-1957 Full-Scale
Gravel Gertie Tests

Test No.	Location	Tracer	HE Quantity (lb)	Door Position
1	Amarillo	La-140	120	Closed
2	NTS	None	250	Open
3	NTS	U	550	Open
4	NTS	U	550	Closed

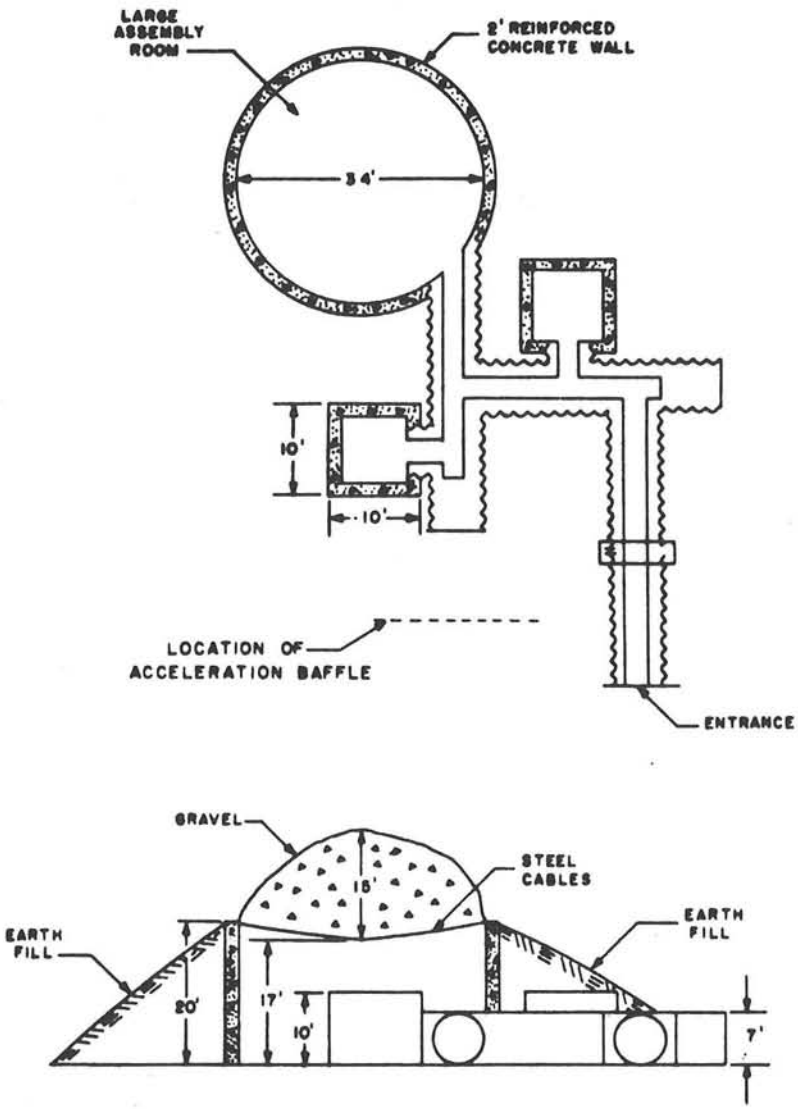

Figure 2-1. Plan and Elevation View of Structure for 1956-1957 Test

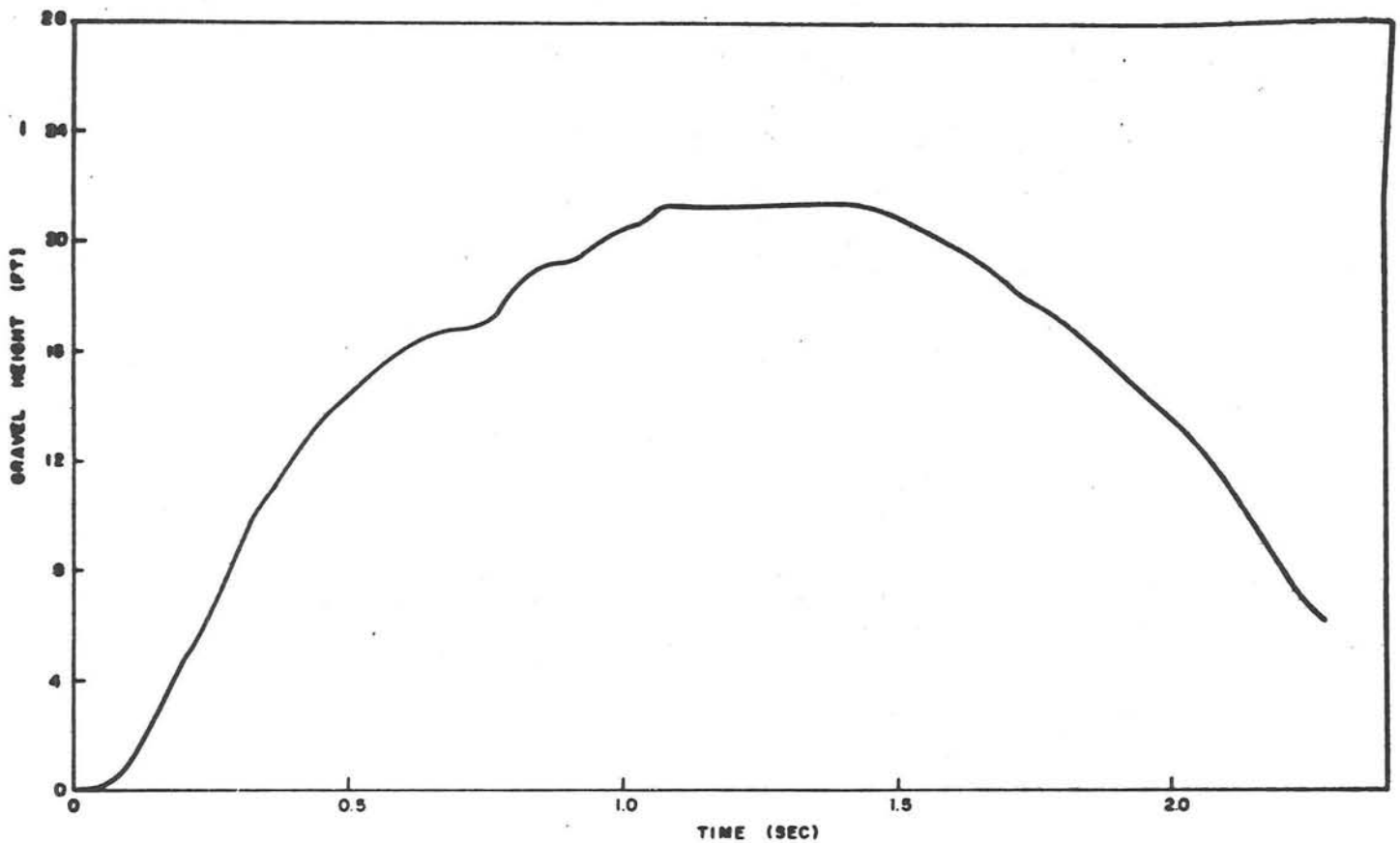

Figure 2-2. Gravel Height Versus Time (1957 Test)

detected in any of the 920 fallout trays. In fact, background levels exceeded the measured levels in several trays, presumably due to their location along heavily traveled dirt roads. The application of the 1982 test data to the 1956-1957 experiment will be discussed later in the report.

1962 UK Test Series

The test series conducted by the UK consisted of three distinct sets of experiments conducted on 0.118-scale model units, all designed to elicit Gravel Gertie structural response data [Ja63, Wo63a, Wo63b].

Four principal conclusions were drawn from the 15 test shots:

1. Pressure variations were due to a superposition of shock pressures and a gradual rise to a quasi-static pressure of 32 psi;

2. Incident shock strength decreased with distance from the round room;

3. Blast attenuating cavities were much more effective if filled with foam, plastic, or steel wool rather than gravel; and

4. Structural blast loading was static rather than impulsive, except in the round room itself, where impulsive loadings were significant.

The objective of the second series of tests was to evaluate various schemes for roof mounding. The results of these 13 tests suggested that little or no venting occurred when 0.84 m (scaled from 7.09 m) of cover was provided. In fact, it appeared that a thickness of slightly more than 5.8 m would be adequate. A cover of 4.6 m was shown to be insufficient. When a smooth shear plane was introduced between the gravel bed and the side mounding, slightly more roof elevation was achieved.

The third test set evaluated the reinforced concrete sidewall response. Seven experiments were conducted using a scaled round room with no associated staging area volume. The model was constructed aboveground and bermed, and a scaled gravel roof was installed. Two conclusions were drawn: that the proposed sidewall construction was adequate and that the mounding would probably contain any contamination.

1982 Test Series

Scale Test Summary

The scaled test program, fully described in Appendix A, consisted of five experiments. Each of these tests was run on a 0.176 scale facility shown in Figure 2-3. The scale test series had four principal objectives: (1) To evaluate the viability of replica scaling; (2) To evaluate the effect of placing the explosive charge off-center in the round room; (3) To evaluate the

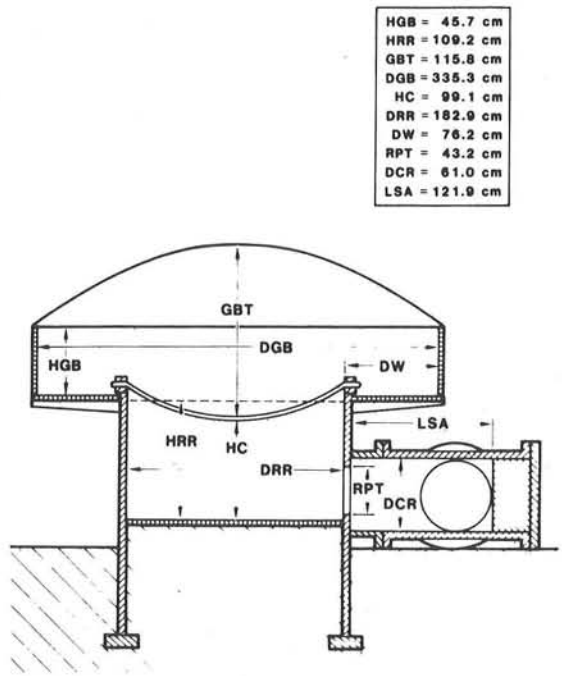

SUBSCALE TEST FACILITY - ELEVATION VIEW

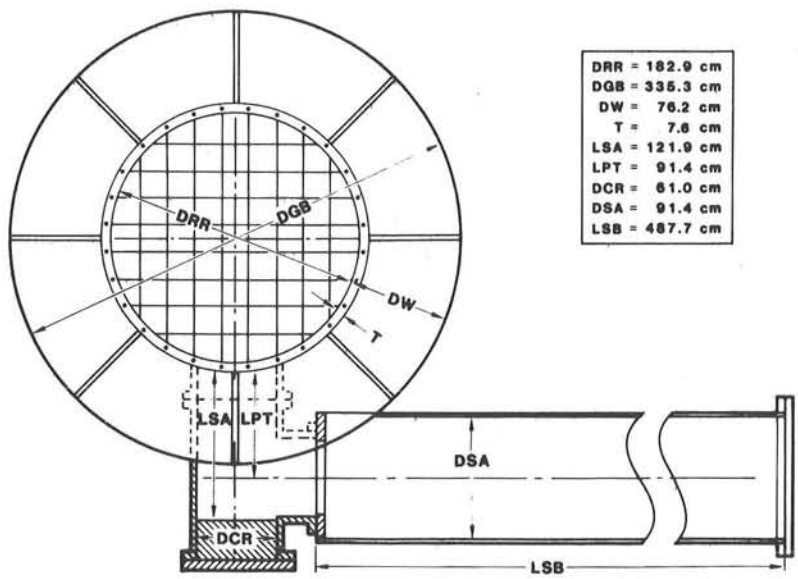

SUBSCALE TEST FACILITY - PLAN VIEW

Figure 2-3. Subscale Test Facility

effect of the dropped ceiling on gravel bed behavior; and (4) To verify the performance of the aerosol sampling systems.

The first two tests were designed to check out the test facility and instrumentation and to obtain correct scaling factors for the roof and the explosive charge. The third test examined the effects of an off-center charge by moving the charge from the center of the round room to a point 15 cm from the wall. The fourth test served as a subscale proof test of the aerosol sampling systems intended for use in the full-scale test. The fifth, and final, subscale test served to evaluate the impact of the dropped ceiling on overall gravel bed dynamics.

The following conclusions were drawn from the subscale test series:

(1) The dynamic behavior of the gravel bed (height of rise, velocity, etc.) can be scaled satisfactorily and basically follows a $W^{1/3}$ rule, where W is the mass of the gravel bed;

(2) Material strengths, in particular cable failures and membrane thicknesses, are more complex and do not follow simple scaling laws;

(3) At early times the gravel bed appears to act as a solid body and transmits significant shear force to the walls confining the gravel bed;

(4) The presence of a dropped ceiling has no discernable effect on overall gravel bed behavior;

(5) Overall gravel bed behavior was not changed by moving the charge away from the center of the chamber, suggesting that the system is responding to quasi-static pressure forces rather than to impulsive shock loading;

(6) A respirable uranium aerosol release fraction of $5.1 \times 10^{-3} \pm 4.0 \times 10^{-3}$ was determined for the subscale Gravel Gertie structure. This is within the experimental error of the full-scale NTS release estimate.

Confinement Test Summary

A series of source term generation experiments, fully described in Appendix B, were carried out in an explosive containment chamber. These tests were designed to validate the hydrocode predictions of aerosol quantity from the proposed full-scale high explosive aerosol generator (HEAG).

The confinement chamber test series consisted of eight experiments using one of three explosive configurations: a solid sphere of high explosive, a uranium shell surrounded by high explosive representing a 1/8-scale replica of the full-scale HEAG, and a uranium shell surrounded by high explosive representing a 1/3-scale replica HEAG. All eight experiments were conducted in the six-foot diameter steel pressure vessel shown in Figure 2-4.

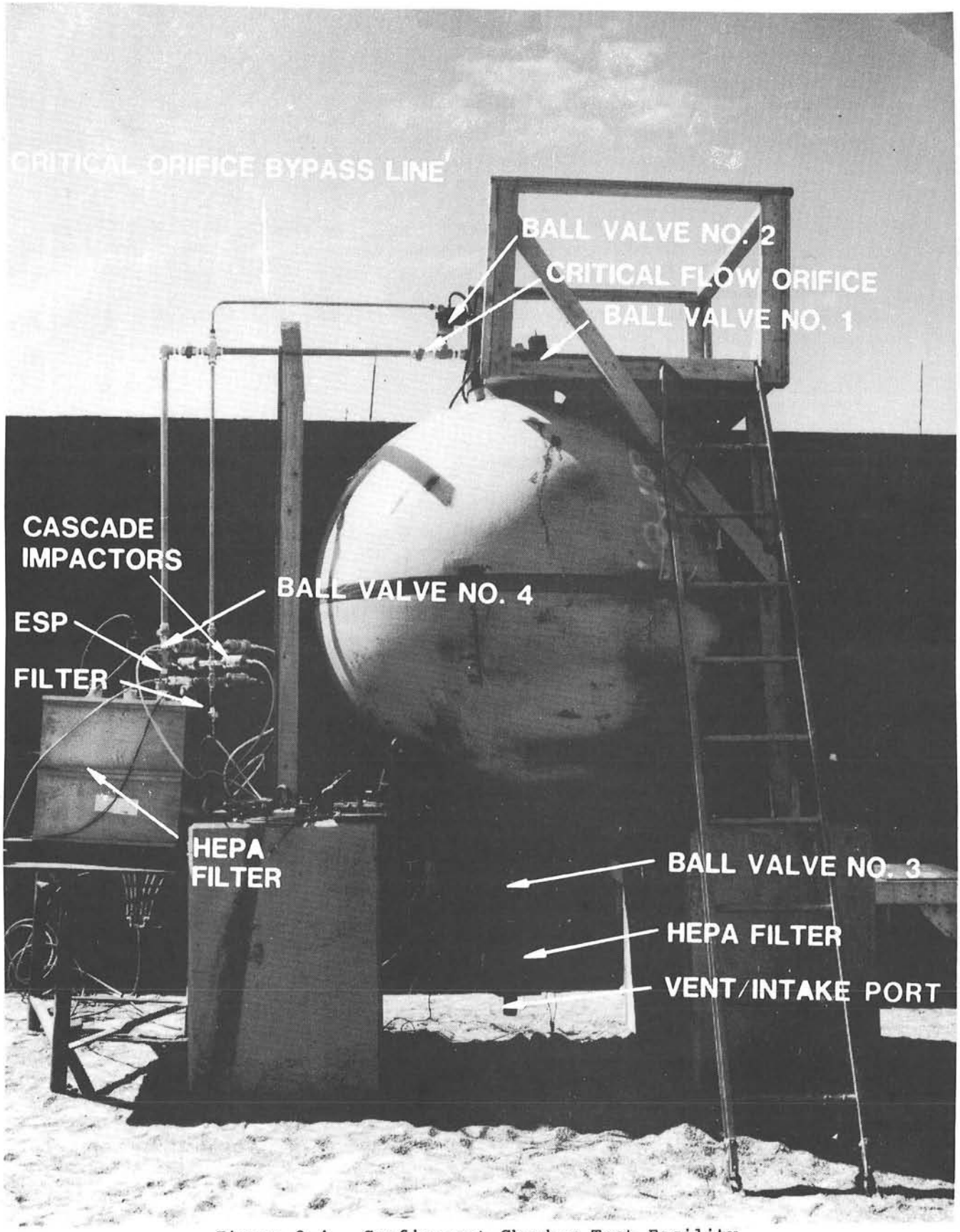

Figure 2-4. Confinement Chamber Test Facility

The aerosols generated by the detonation of aerosol generators were collected through a plumbing system attached to the top closure plate of the confinement chamber. This system included valves and orifices to allow the relatively fragile aerosol measurement equipment to monitor the relatively high pressure, high temperature gases in the chamber after detonation.

Four of the eight tests were used to check out the firing and sampling systems. The remaining four tests were used to obtain aerosol quantity and size distribution measurements. The tests done at 1/8 scale (1000 grams of HE and 44 grams of U) produced approximately 6 $\pm$ 1% of the uranium as a respirable aerosol (<10 μm AD). This compares quite favorably with the hydrocode prediction of 2.3% when secondary aerosolization mechanisms such as droplet breakup are included. Test 8 at 1/3 scale confirmed this result by yielding 7% $\pm$ 1% uranium in the respirable size range. The particle size distribution measured during Test 8 is shown in Figure 2-5.

Full-Scale Test Summary

Site Construction

The site chosen for the full-scale Gravel Gertie test was the same one used in the mid-1950s (see Figure 2-6). Since the assembly cell or round room was originally built for multiple tests it was felt that, to save time and money, it might be used again. The structure was fully excavated and, after inspection by structural consultants, was deemed to be suitable for additional testing. After considering options for simulating the effects of a staging area as it exists in the Pantex configuration, it was decided that the important features of the staging area for the purpose of this experiment were volume and round room entrance cross-section. The staging area was simulated using appropriate lengths of 3-m diameter steel culvert. The actual construction configuration is shown in Figures 2-7, 2-8, and 2-9 and discussed in detail in Appendix C. The enclosed volume was sealed by the compacted overburden and a leak-tight blast door so that all exhaust was forced to pass through the gravel roof of the round room.

Figure 2-9 shows the gravel bed specifications per reference HN82 (item 2). As a result of oversight during construction, the actual gravel bed profile was constructed as shown by the dashed line on Figure 2-9. As a result of this deviation from design, the actual gravel depth at a radius of 5.2 m was approximately one meter shallower than called for on HN82. The effects of this deviation on the experimental results are discussed in later sections of this report.

Aerosol Measurement Systems

Since the principal goal of the full-scale test was to determine the capture efficiency of the gravel roof of the structure, aerosol measurement systems were designed to characterize both the aerosol inside the structure before collapse of the gravel bed and the aerosol escaping from the area. These systems, outlined in Table 2-2, shown on Figure 2-10, and fully described in Appendix D, are briefly described as follows:

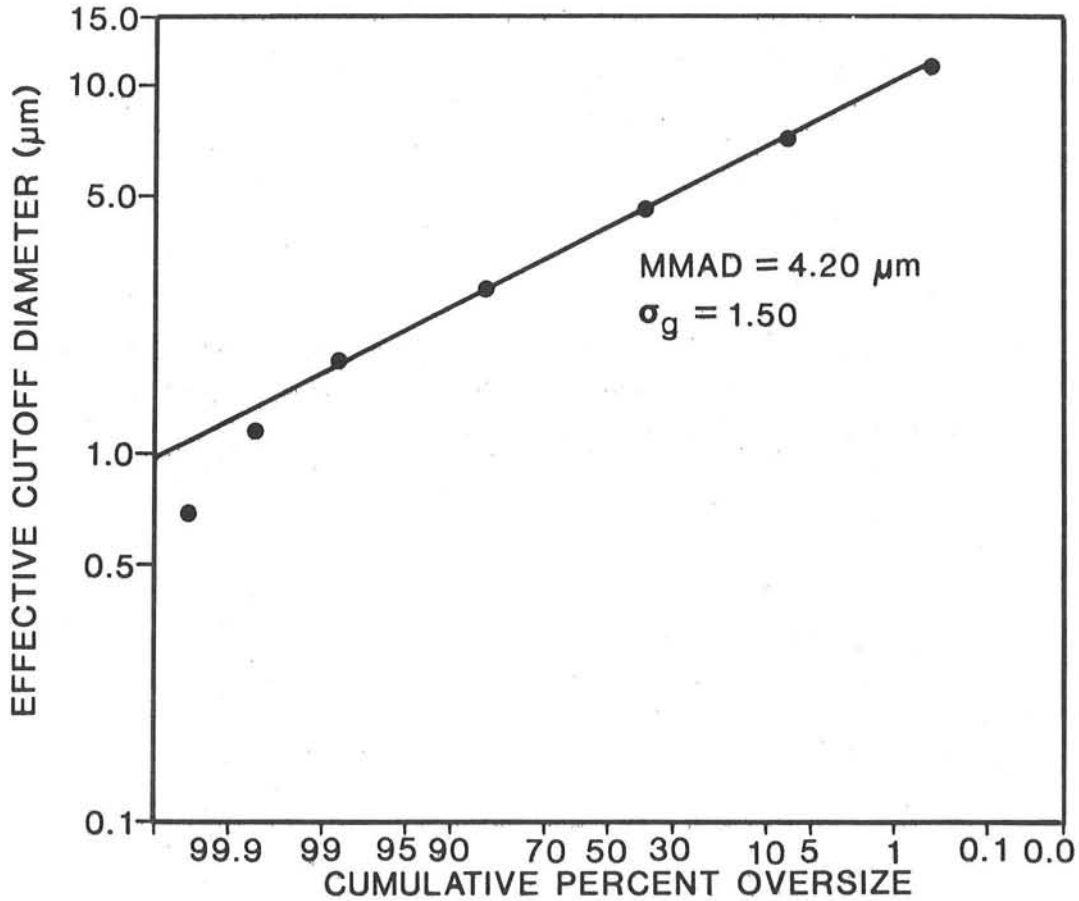

Figure 2-5. Particle Size Distribution From Confinement Test 8

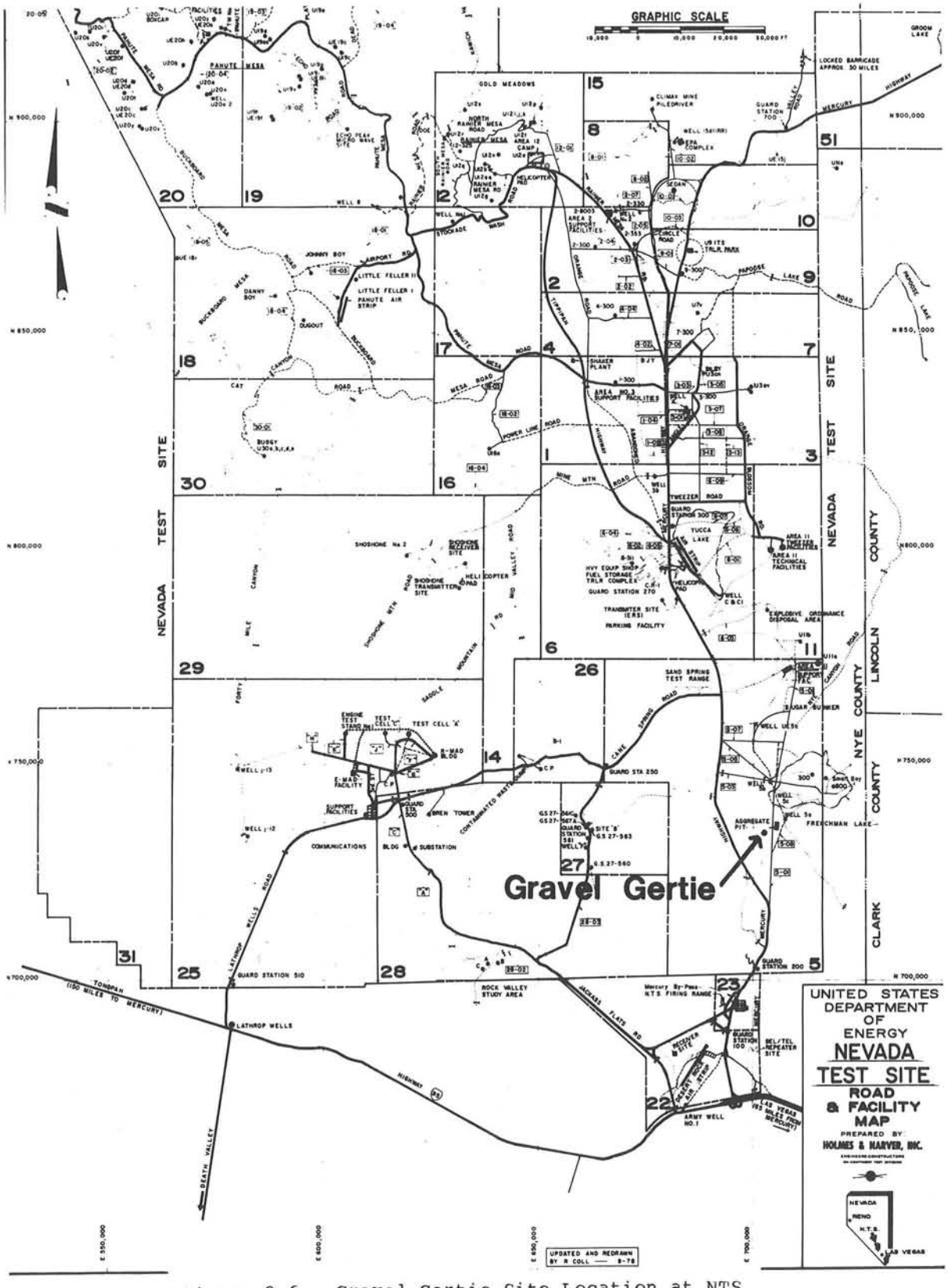

Figure 2-6. Gravel Gertie Site Location at NTS

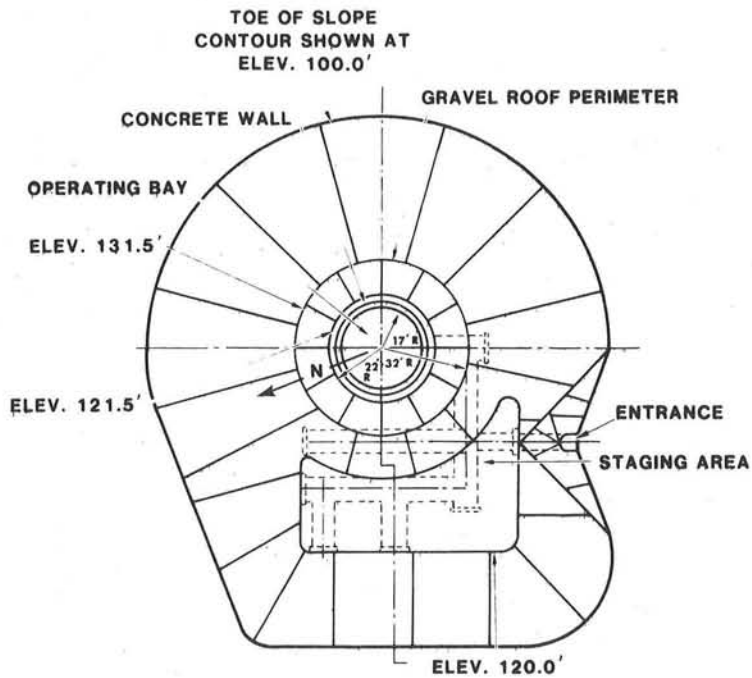

Figure 2-7. Plan View of Gravel Gertie Test Structure

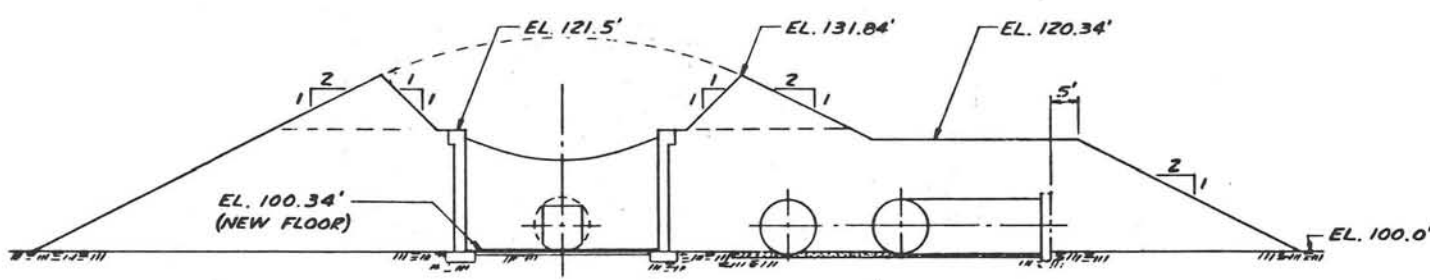

Figure 2-8. Elevation View of Gravel Gertie Structure

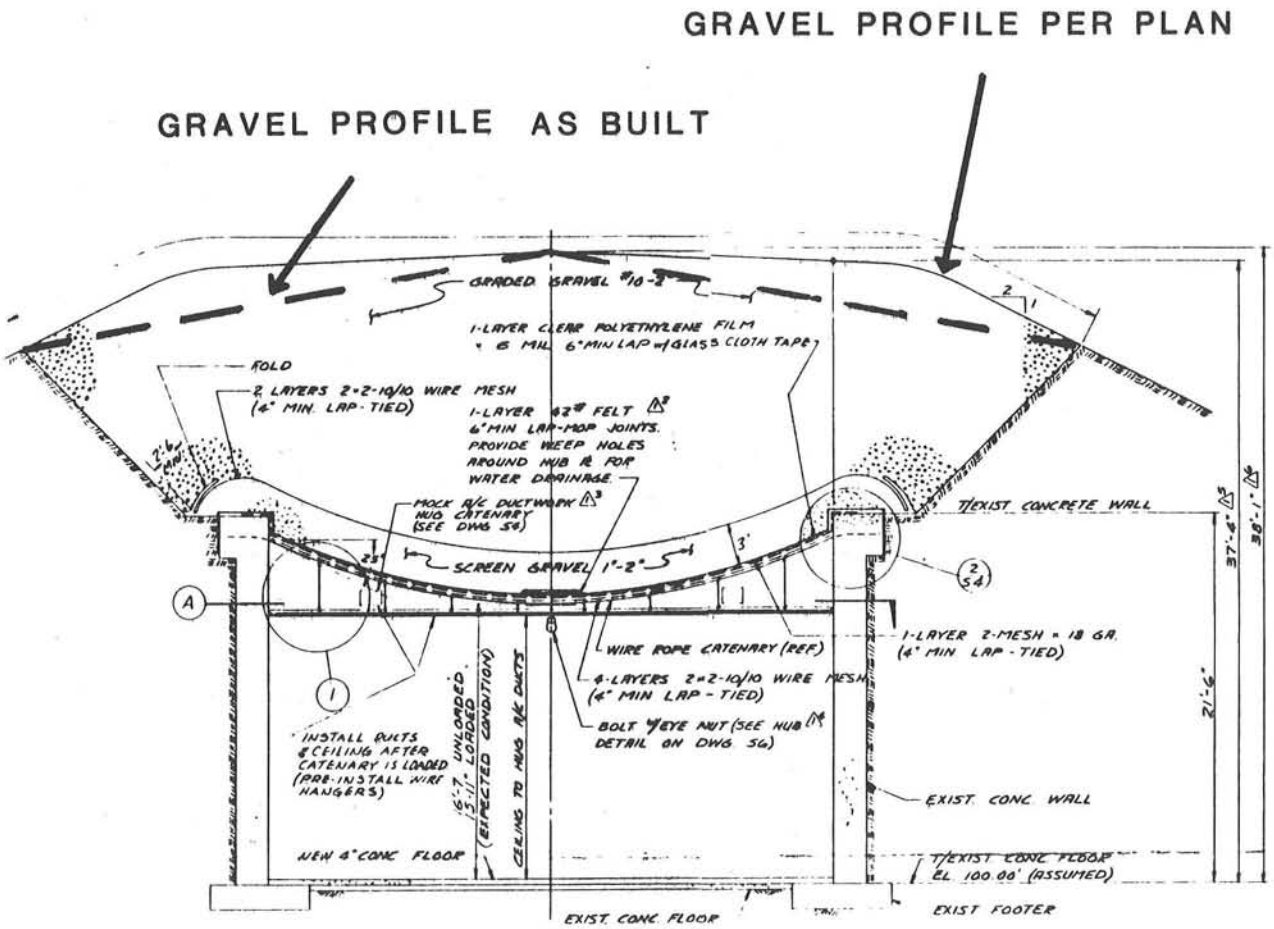

Figure 2-9. Construction Details of Gravel Bed

1. GGASP--A set of six samplers, hardened and shielded to withstand blast, fragments, and gravel bed collapse, were located within the test structure. Each sampler consisted of an evacuated chamber connected to filter and cascade impactor aerosol measurement instruments. By opening a remotely-activated solenoid valve, the evacuated chamber was filled with aerosol-laden air in the time period between detonation and roof collapse, and then was closed off. A pump drew the sample through the instruments and recirculated it to the chamber for approximately 7-1/2 minutes. Deposition samples from within the chamber were retrieved for electron microscopy. Internal (to the sampler) temperature and pressure, and external pressure were measured at each station. Sampler locations are shown in Figure 2-10. Construction details of the GGASP Samplers are shown in Figure 2-11.

2. GGDSA--A set of filter samplers were located external to the structure on the overburden, near the edge of the gravel-overburden interface. Eight 2-m stakes were located 10.4 m from the center of the round room on 45° spacing, starting from north. Fourteen battery-operated personnel aerosol monitors were attached at heights of 1 m and 2 m on the stakes (two of the stakes had only one instrument). Instruments were manually turned on before the test and turned off afterwards. See Figure 2-12 for locations.

3. GGESA--An array of filters, impactors, electrostatic precipitators, and deposition samplers was suspended from a cable over the center of the round room at a height of 19 m. Samplers were mounted on a fixed horizontal beam and on a boom that was deployed to a vertical orientation after the rise and fall of the gravel bed. The deployed boom and the beam formed a cross over the center of the round room to allow sampling from 4 to 22 m above the preshot height of the gravel and $\pm$ 6 m crosswind at the 19 m height. Instruments in the array were turned on and off manually. See Figure 2-13.

4. GGBSA--A set of 48 filter samplers was supported by four helium balloons and formed a sampler curtain to intercept and sample released aerosols before they were transported by winds beyond the near vicinity of the test structure. The balloons were positioned at shot time to be 45.7 m downwind of the center of the test structure between azimuths 240° and 300°. Eight strings of samplers at six heights (2.4, 10.7, 16.8, 22.9, 29.0, and 45.7 m) were used in forming the sampler curtain. See Figure 2-14.

5. GGPSA--Four poles were set at 0°, 90°, 180°, and 270° azimuths and at distances ranging from 15.2 to 45.7 m from the center of the round room. Each pole had three measurement levels at 10.4, 15.2, and 22.9 m where filter samples, fallout trays and electrostatic precipitator samplers were located. See Figure 2-15.

TABLE 2-2

AEROSOL SAMPLING SYSTEM DESCRIPTIONS

System	Number of Units	Type of Sampler(s)	Location(s)
GGASP Aerosol Sampling Package	6	Sampling Chamber, Total Filter; Mercer Impactor	4 in round room 2 in staging area
GGESA External Sampling Array	13 stations 4 vert, 9 hor	13 Total Filters 13 LMJ* Impactors 13 Deposition Collectors 13 Planchets	Suspended at a height of 18.8 m over center of round room
GGDSA "Donut" Sampling Array	8	14 Filter Samplers	On 1.8 m stakes 45° apart on overburden 10.4 m from center
GGBSA/RSA Balloon Sampling Array	1	48 Filters 8 Mercer Impactors	At 45 m radius, west of ground zero 8 vertical strings with 6 heights per string
GGCTA Collector Tray Array	120	Grease coated biscuit pans; planchets	In square grid on 61 m spacing to 914 m in all directions
GGPSA Pole Sampling Array	4	2 LMJ Impactors 3 Deposition Samplers 3 Planchets 1 Electrostatic Precipitator 2 Filters	West and east poles on 30 m radius, North pole on 15 m radius, South pole on 45 m radius
GGTSA Tunnel Sampling Array	2	1 Filter 1 LMJ Impactor	Southwest at 22 m and 26 m radius

*LMJ-Lovelace Multijet Impactor

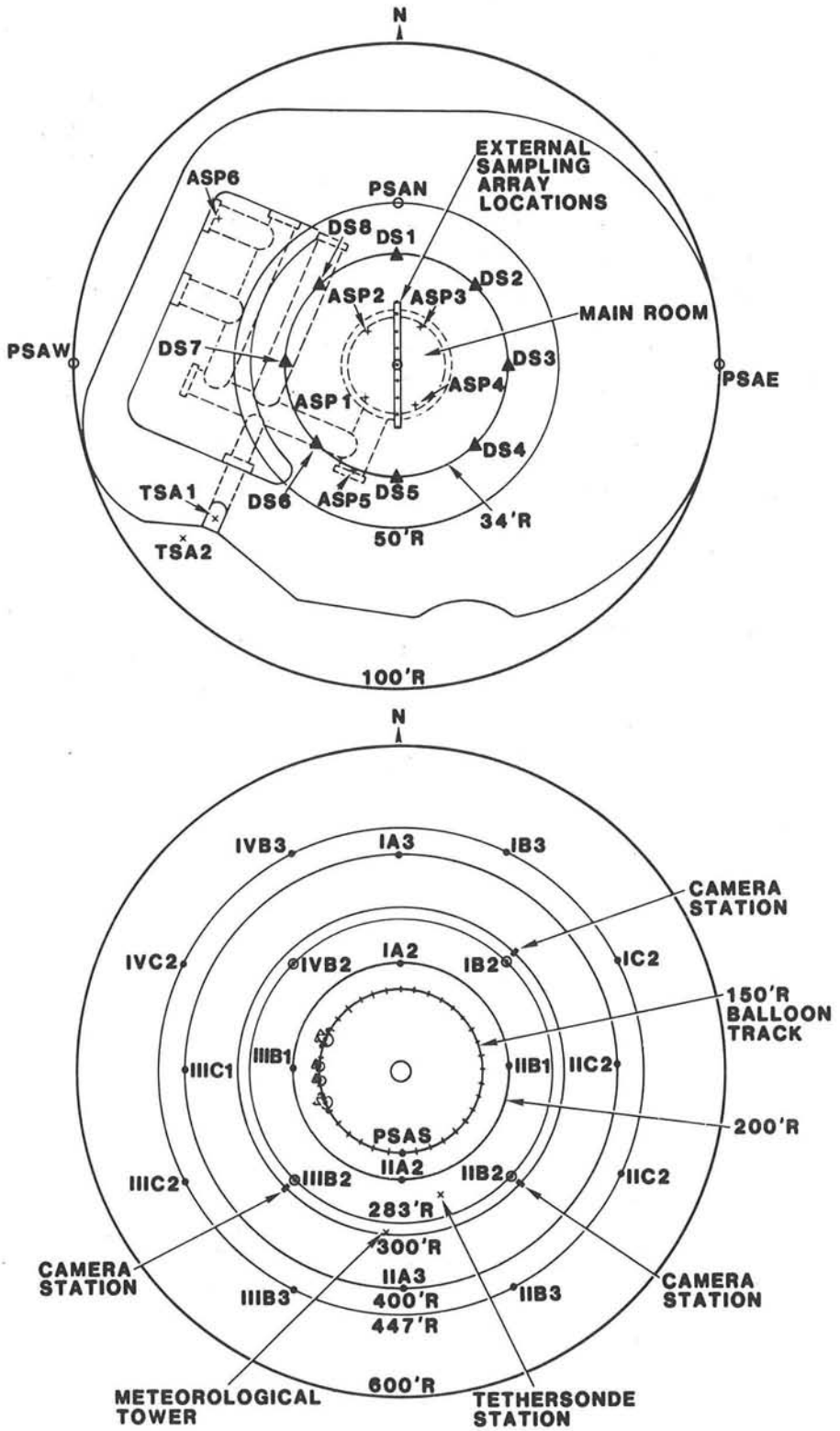

Figure 2-10. Location of Sampler Arrays and Meteorological Equipment Near the Gravel Gertie Structure

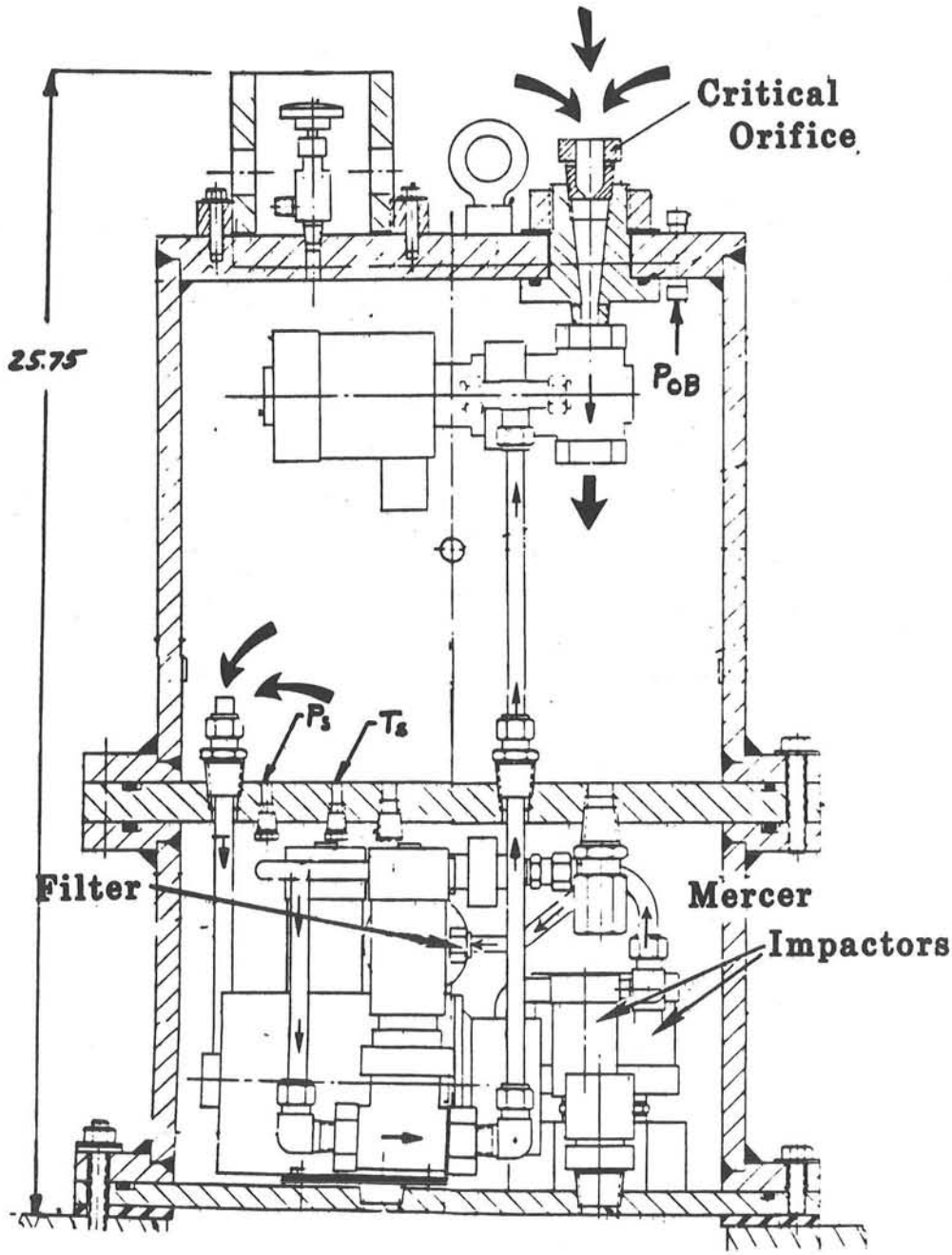

Figure 2-11. GGASP Sampler Cross Section

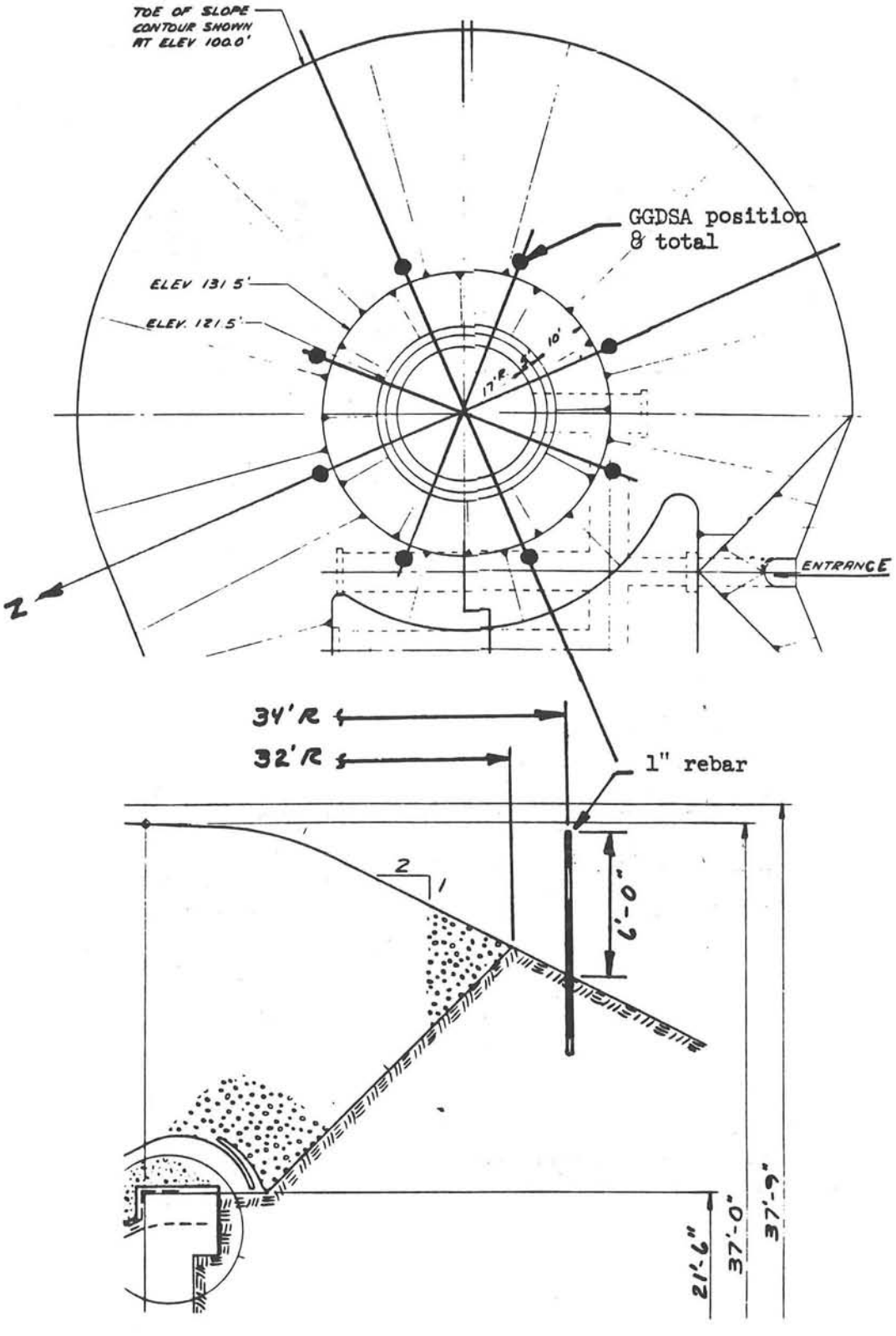

Figure 2-12. Gravel Gertie Donut Sampling Array (GGDSA)

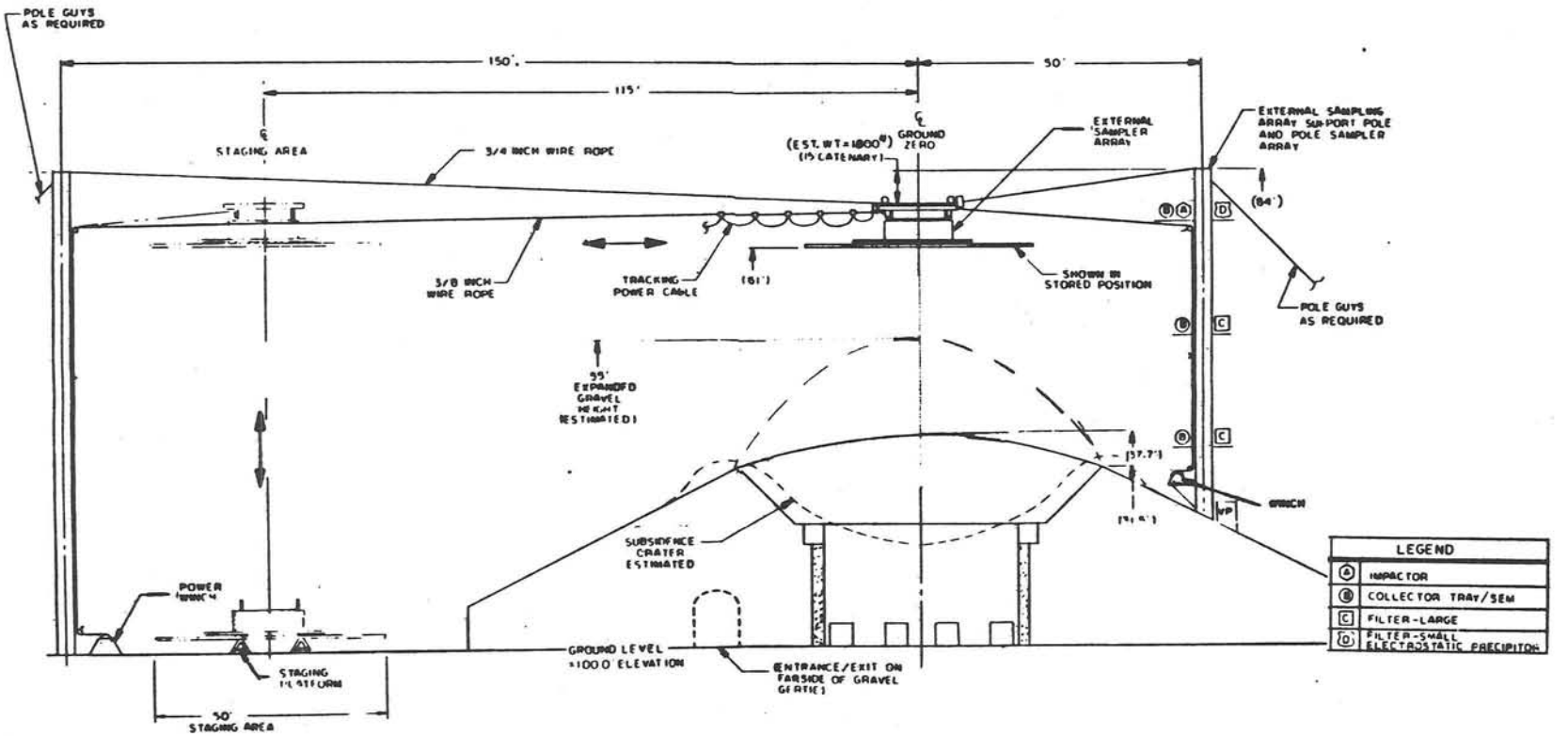

Figure 2-13. Gravel Gertie External Sampling Array (GGESA)

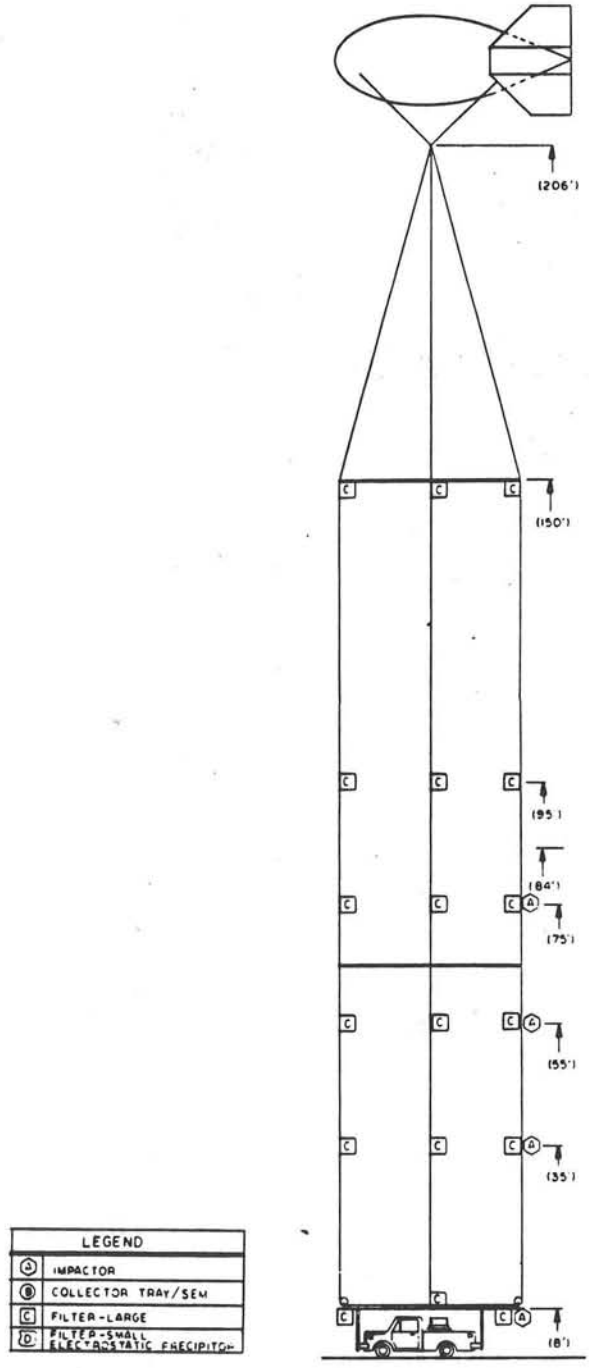

Figure 2-14. Gravel Gertie Balloon Sampling Array (GGBSA) (one of three units shown)

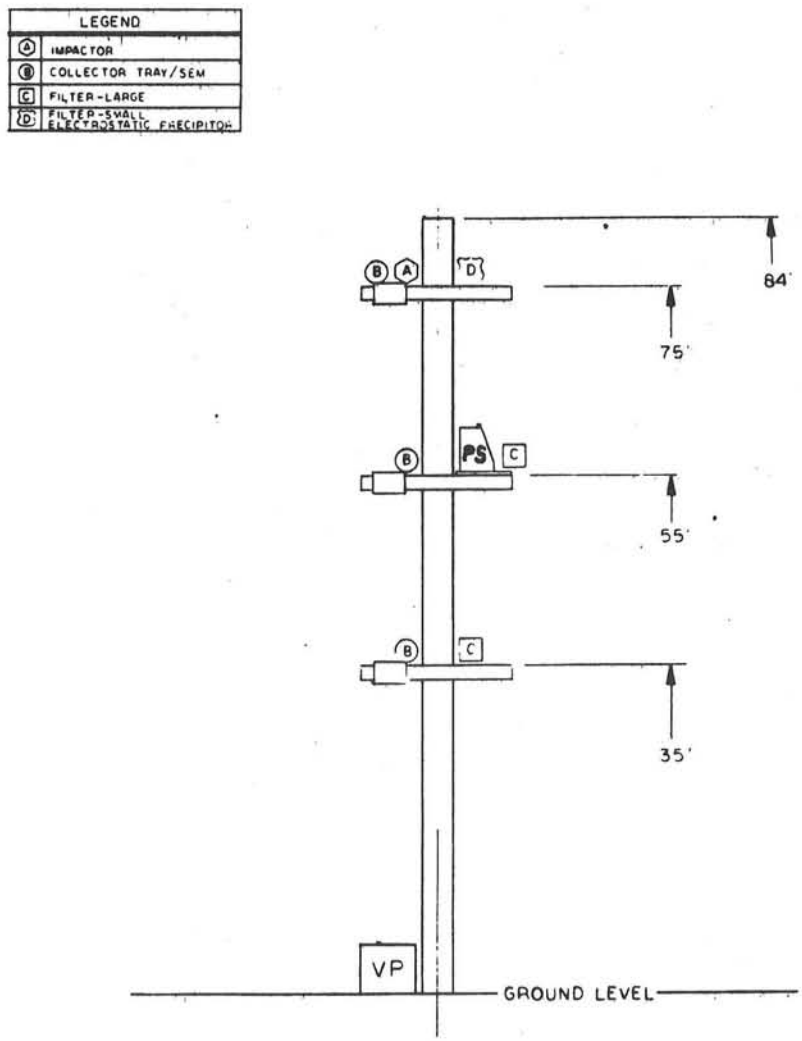

Figure 2-15. Gravel Gertie Pole Sampling Array (GGPSA)

6. GGCTA--To link data from this test to that obtained in the 1950s tests, fallout trays were located at distances up to 914 m from the site using approximately 120 selected locations within the original 1957-test deposition sampler array. Each sampler consisted of a 16.5 cm x 26 cm biscuit tray coated with a thin adhesive film designed to capture and retain particles. Forty trays contained planchets for particle examination by electron microscopy. Trays were deployed the day before the test and most were retrieved within two hours post-test. Some were retrieved just before the test to provide background uranium deposition data. Figure 2-16 shows the arrangement of samplers.

7. GGTSA--To document any leakage around the sealed exit door, two samplers were located outside the structure in the tunnel leading to the blast door and two were located about 3 m outside the tunnel exit. A filter and cascade impactor were used at each station. The tunnel samplers were hung at a height of 1.7 m and the external samplers were 1 m off the ground. See Figure 2-17.

8. GGRSA--A battery of eight impactors was located on strings No. 3 and 6 of the balloon curtain in an attempt to obtain a size distribution of the material which was collected on the balloon array.

Pressure and Temperature Measurements

Pressure measurements using Kulite pressure gages were made at each GGASP location, at the sealed exit door, and at the check valve experiment. Two pressure measurements were made at each GGASP, one located inside the sampling chamber and one located outside so as to be exposed to pressure within the GG structure. Temperatures inside the sampling chambers were also recorded at each GGASP location.

In addition to the pressure measurements made at GGASP locations, Southwest Research Institute (SWRI) made several pressure measurements both inside and outside the Gravel Gertie structure as a part of a separately-funded DOE contract to evaluate structural response [SW82]. These measurements were made using piezoelectric and piezoresistive gauges to observe both short-term shock pressures and longer-term quasi-static pressures.

Complete pressure-time histories for both the SNLA and SWRI measurements are provided in Appendix E.

Meteorological Measurements

Meteorological measurement support was provided by the National Weather Service at DOE/NVO and by SNL meteorologists. Three months prior to the scheduled test date, a 30 m meteorological tower was erected 100 m south of the center of the round room. Wind speed and direction sensors were placed at heights of 9 m and 23 m on the tower. Temperature sensors were located at 3 and 28 m. Data from these instruments were telemetered to a central recording station. Baseline data for the three months prior to the full-scale test were used to estimate test-time meteorological parameters. A few days prior to the scheduled test date, a second set of speed and direction sensors was placed on

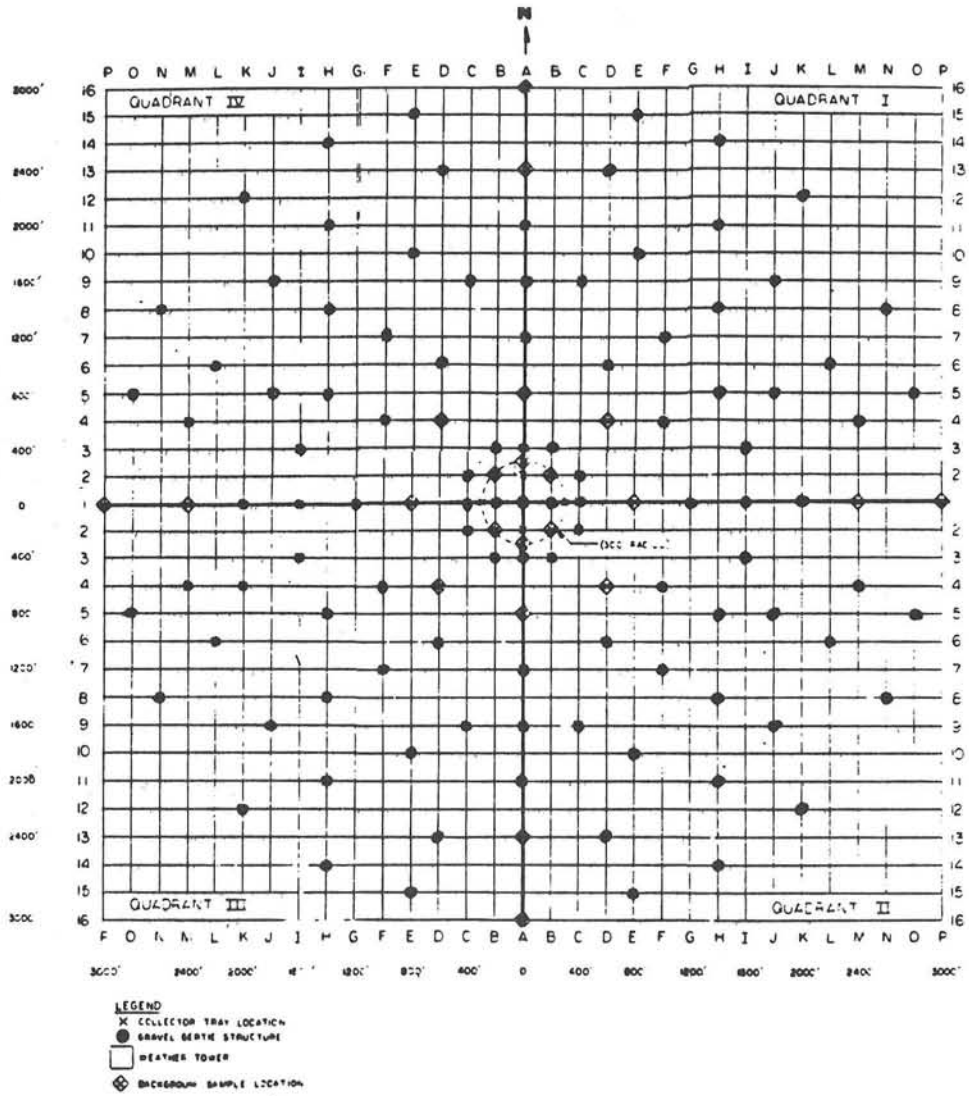

Figure 2-16. Location of GGCTA Sampler Trays

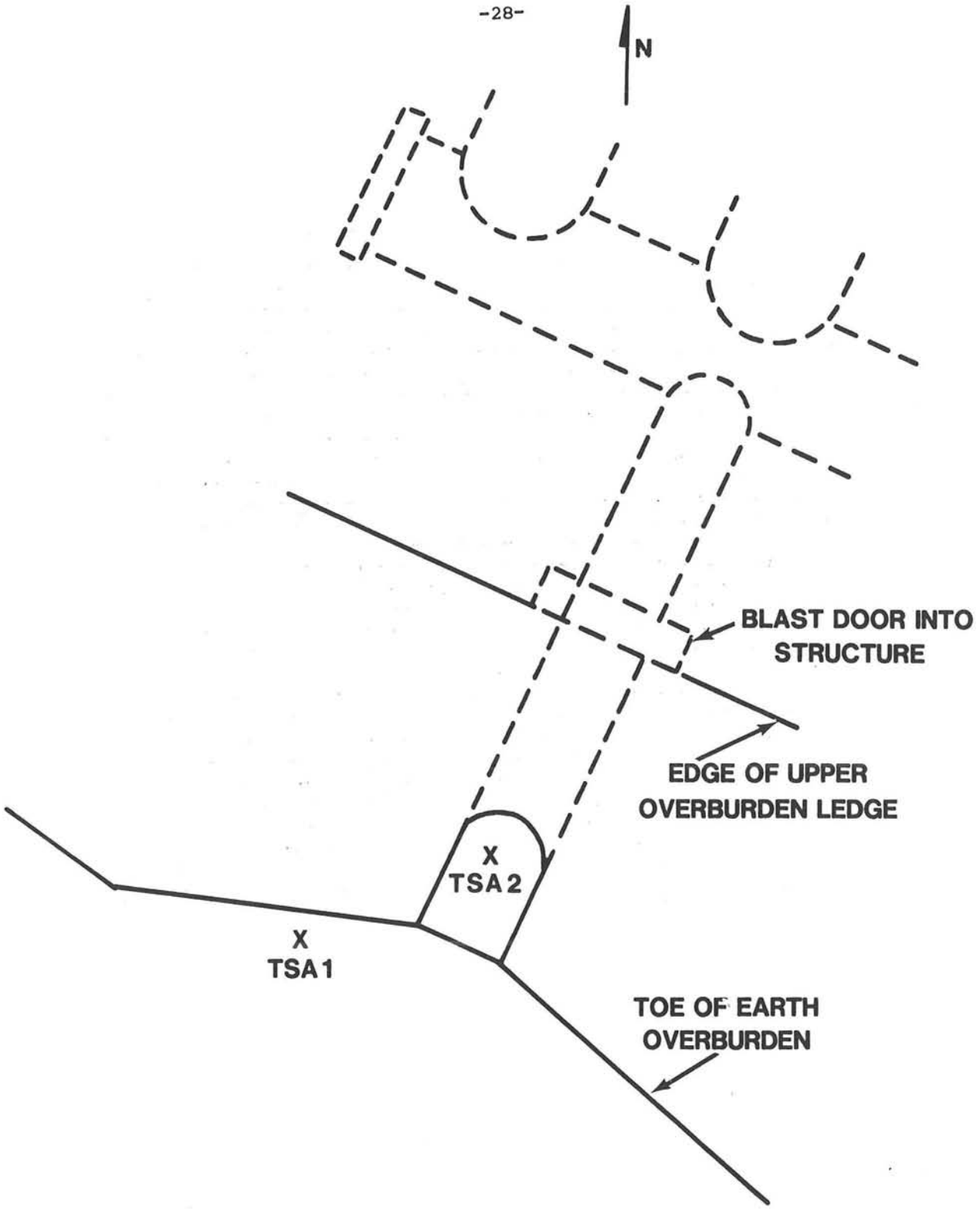

Figure 2-17. Tunnel Sampling System

the tower to allow meteorological conditions to be monitored during the test. Pilot balloons (PIBALs) were released at the site and tracked between 4.5 and 1.5 hours preshot to obtain upper level wind speed and direction information. In addition, a tethersonde system was deployed near the control trailer to allow detailed measurements of wind speed and direction versus height in the first 1000 m above the site. See Figure 2-10 for the location of the tethersonde.

Tracer Generation

Two tracers were used in the full-scale Gravel Gertie test. Uranium was selected to be the primary tracer because of its physical similarity to plutonium and because the uranium aerosol could be generated in a manner analogous to that expected in an actual accident. Antimony oxide (Sb_2O_3) powder of a known size distribution was used as a secondary tracer.

The uranium aerosol was generated by four High Explosive Aerosol Generators (HEAG), each composed of a hollow HE shell surrounding a hollow 2 kg uranium shell. Four such aerosol generators were suspended from the ceiling in nylon harnesses, as shown in Figures 2-18 and 2-19. Detonation of each HEAG was accomplished by one detonator/booster assembly located on the surface nearest the floor. Hydrocode calculation of energy deposition in the uranium suggested that from 2 to 3 percent of the uranium would be vaporized. Confinement vessel tests of a geometrically scaled generator indicated that 6 to 7 percent of the uranium would be converted to respirable-sized aerosols. When the effects of extractive sampling line geometry and pressure vessel wall were considered, these values were consistent with hydrocode predictions of 2 to 3 percent.

The antimony tracer was contained in four packets made of ashless filter paper, each containing 250 g of Sb_2O_3 powder. Figure 2-19 shows the size distribution of this material. The packets were suspended on wires 3 m above the floor. It was expected that the shock and high temperatures produced by the HE detonation would destroy the filter paper and release the tracer. The geometric arrangement is shown in Figure 2-20.

Documentary Photography

The test was documented by still photographs, TV tapes, and motion pictures spanning construction, test, and recovery phases of the event.

1. Motion picture coverage was obtained from three viewpoints with cameras operating at three framing rates. One camera at each station was set to operate at 400 frames per second and was closely focused on the structure itself to permit documentation of the gravel rise and fall-back phenomena. A second camera, operating at 24 frames per second, covered a wider view of the test setup to document cloud growth and transport. The third camera used a wide-angle lens and operated at 10 frames per second to document cloud dynamics on a larger time and space scale. Camera stations were located at a radius of 91.4 m from round room center on azimuths of 45°, 135°, and 225°.

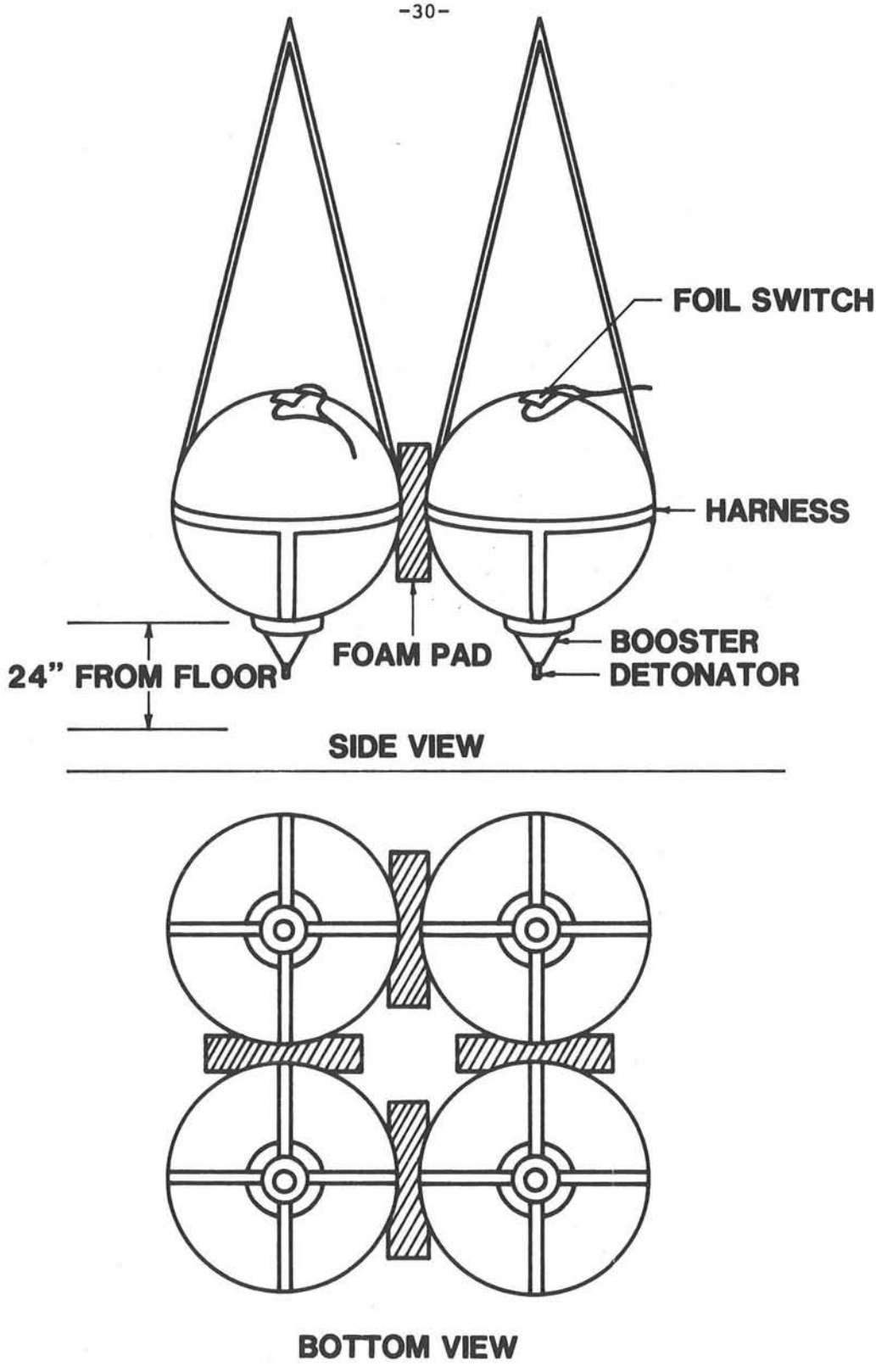

Figure 2-18. Design of HEAG Installation

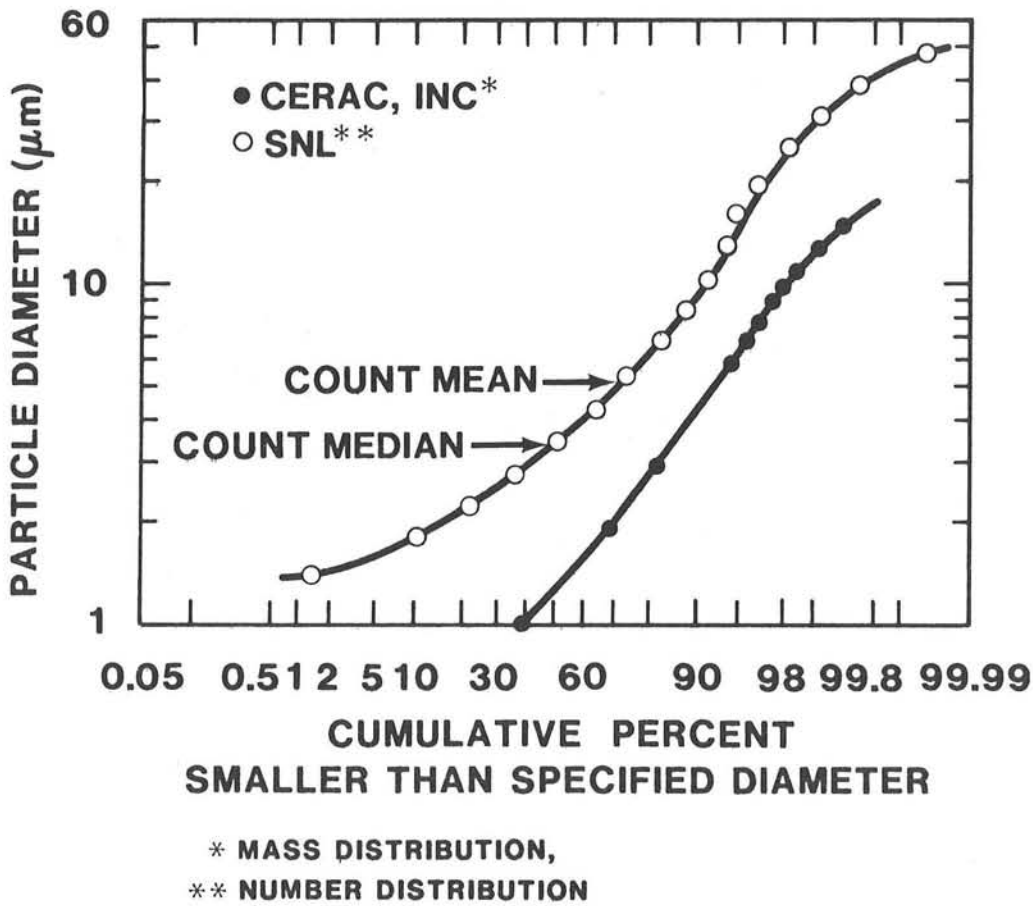

Figure 2-19. Size Distribution of Sb_2O_3 Powder

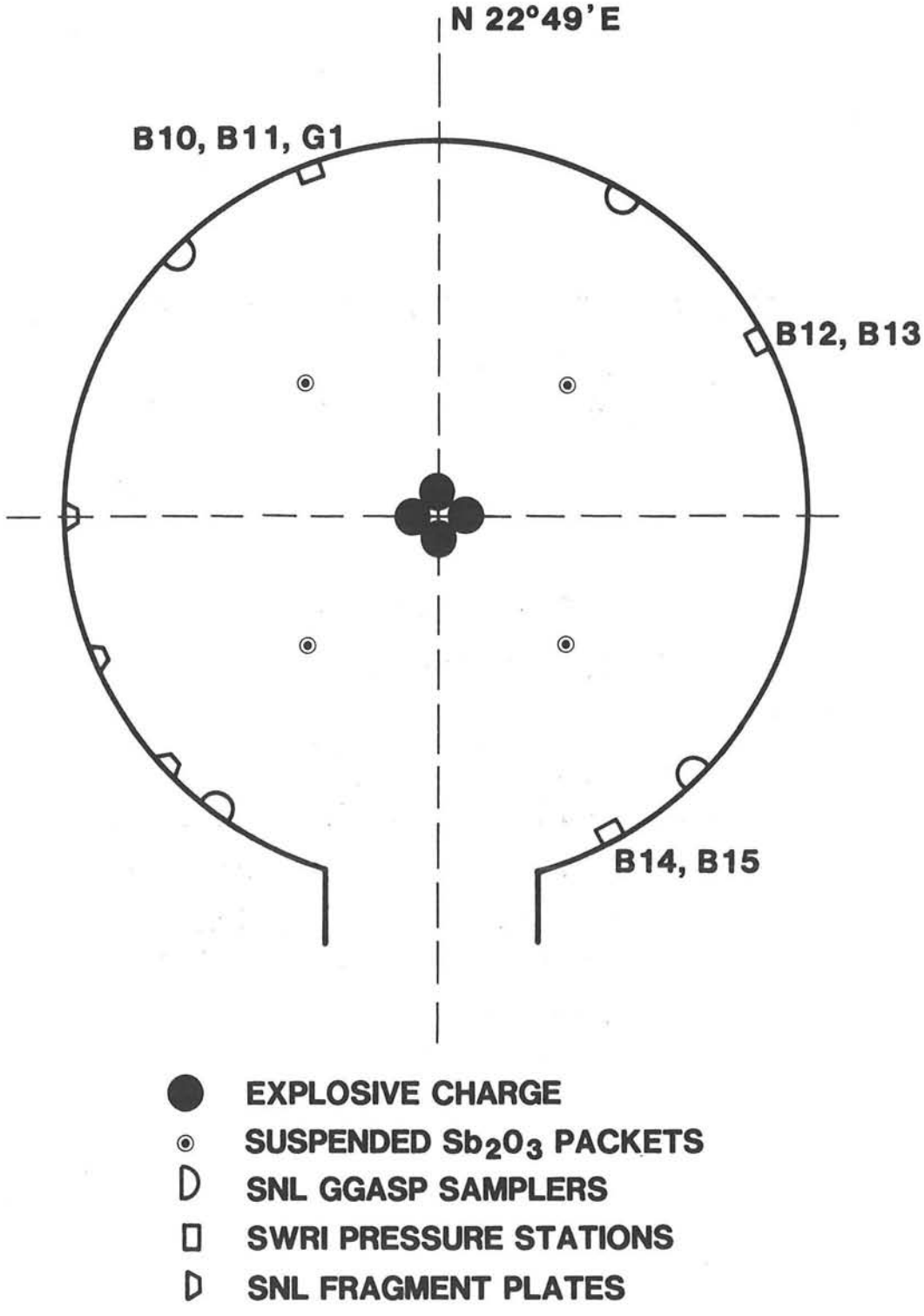

Figure 2-20. Round Room Configuration at Test Time

2. TV coverage was largely documentary in nature and was accomplished from two locations. One station was at about 125 m radius on an azimuth of 200°. The second was the viewing station on road 05-01, approximately 1300 m away on an azimuth of 170°.

3. A sequence of still photographs of the test were taken from a vantage point approximately 450 m away on an azimuth of about 110°.

Full-Scale Test Execution

On Friday, November 19, 1982, test preparations had been completed and meteorological indications were favorable for a possible test on Saturday morning, November 20. The earliest possible shot time was at 0700 (1/2-hour after sunrise) in order to have sufficient light for photography, but meteorological records indicated that favorable winds were more likely two to three hours after sunrise. Site operations began at 0400 with the collection and replacement of the background GGCTA deposition samplers and the final checkout of data links and equipment operation. Aerosol samplers were turned on between 0500 and 0600. Personnel not required for onsite operations were sent to the observation point at 0630. Meteorological instruments indicated light and variable winds.

At 0700 the tethersonde was brought to a height of 20 m (between tower instrument levels) for continuous speed/direction monitoring at a height just above the top of the Gravel Gertie. A cloud deck was limiting light for photography, but clouds were clearing rapidly. After positioning the balloon array three times to accommodate large shifts in wind directions, an east wind started and became steady at a speed of about 0.5-0.7 m/sec. The balloon array was moved to the west side of the structure and its operators went to their shelter. At 0840:31 Pacific Standard Time on November 20, 1982, the High Explosive Aerosol Generators were detonated. Initial indications were that all operational systems functioned and all data to be recorded was being received. During and after the test, winds remained steady from the east at 0.5-1.0 m/sec. After about 20 minutes, health physics monitors came in to survey the area. Finding little or no surface contamination above background, onsite personnel were released from their shelter at T + 40 minutes for test recovery. Samplers were turned off; the process of retrieving samples was begun; and documentary photography commenced. Observers were restricted from the site until about T + 2 hours to streamline the recovery and documentation phases.

On T + 4 days, the tunnel door was reopened under the supervision of health physics personnel, who sampled for aerosolized uranium and toxic gases. Entry was made by personnel in full face masks and anticontamination clothing to survey damage and to take deposit samples from walls and floor. Reentry was made after a week of ventilation to recover the GGASP samplers, pressure transducers, and check valve experiments in the staging area.

During the second week in December, a ramp was built on the overburden and a crane with clamshell bucket was brought in to remove the soil and gravel fall-back from the round room. The four GGASP samplers, impact plates, and pressure transducers were retrieved. All operations were documented with photographs.

Post-Shot: Staging Area:

Reentry to the staging area revealed relatively little damage to the basic corrugated steel culvert structure and no evidence of leakage paths to the environment. In a few places there were cracks (no larger than 0.5 mm) in the rolled joints of the culvert section. In one location farthest from the round room entrance, a tensile failure was found in the butt weld joint in one strip from which the culvert was rolled. This provided an escape path about 2.5 cm wide and 61 cm long. Although no specific measurements were made outside the overburden at this point, this opening was so remote from the entrance and was covered by at least 4 meters of consolidated fill that it is unlikely there was any leakage.

The staging area was covered with a thick and fairly uniform film of dust which was sampled with a vacuum cleaner-filter arrangement. These samples were not been analyzed because they were intended as a backup to the GGASP samples.

Post-Shot: Round Room

Excavation of the round room using a clamshell and crane was not conducive to observation of subtle features of either the gravel fall-back or cable locations. However, it was observed that the cables along the south rim of the round room were generally intact (i.e., were hanging along the wall while those in the north quadrant were generally severed right at the wall). The load spreader seemed to fall toward the southeast area of the round room. Mesh from the roof lay against the wall in the southeast quadrant and formed a bridge between the wall and floor which protected the GGASP (GGASP 4) in that location from being completely covered with gravel. This appearance might suggest that failure of cables at the north wall occurred first, but how the failure occurred and what impact it might have had on structure dynamics is not known.

Test Results

Dynamic Behavior

The first few seconds following the detonation of the HE charges revealed several significant aspects of the response of Gravel Gertie to large internal pressure transients. In order to evaluate this behavior, four specific aspects will be discussed. Initially, a time line graph which allows correlation of gravel bed movement with internal pressures will be presented. Secondly, a brief chronology of significant events in the first 10 seconds will be provided together with frames taken from the SE and SW high-speed cameras showing various gravel bed features. Thirdly, behavior of certain ballistic particles will be described; and fourthly a model which has been developed to analyze the dynamic response of a Gravel Gertie will be presented.

The chronology in Table 2-3 shows some of the highlights. Gravel bed behavior and round room pressure are shown in Figure 2-21.

Figures 2-22 through 2-28 are photographs extracted from the high-speed films taken from the SW and SE camera locations.

Table 2-3

Brief Event Chronology

TIME (Approximate)	Event
0	HE detonated.
0 +	Peak shock pressure of 270 psig in round room.
70 msec	First discernable movement of gravel bed.
125 msec	Peak shock pressure of 88 psig at end of staging area.
580 msec	Layering and petal-like structure begin to appear in rising gravel dome.
990 msec	First appearance of light colored base surge precursors.
700 msec	Net pressure reduced to 0 psig in round room.
1300 msec	Peak dome rise.
1800 msec	Side petals enveloped in base surge; dome still apparent in center. First indication of jets to east and southeast.
2000 msec	Jet to NNW visible from SW camera above base surge.
2300 msec	Dome drops below base surge.
2700 msec	ESA boom fully deployed. First visible ballistic particles on SW slope.
3300 msec	First particles visible moving to SE; dark jet from center first appears.
3800 msec	Light roiling begins towards SE in front of dark jet.
5650 msec	Base surge envelopes tunnel entrance.

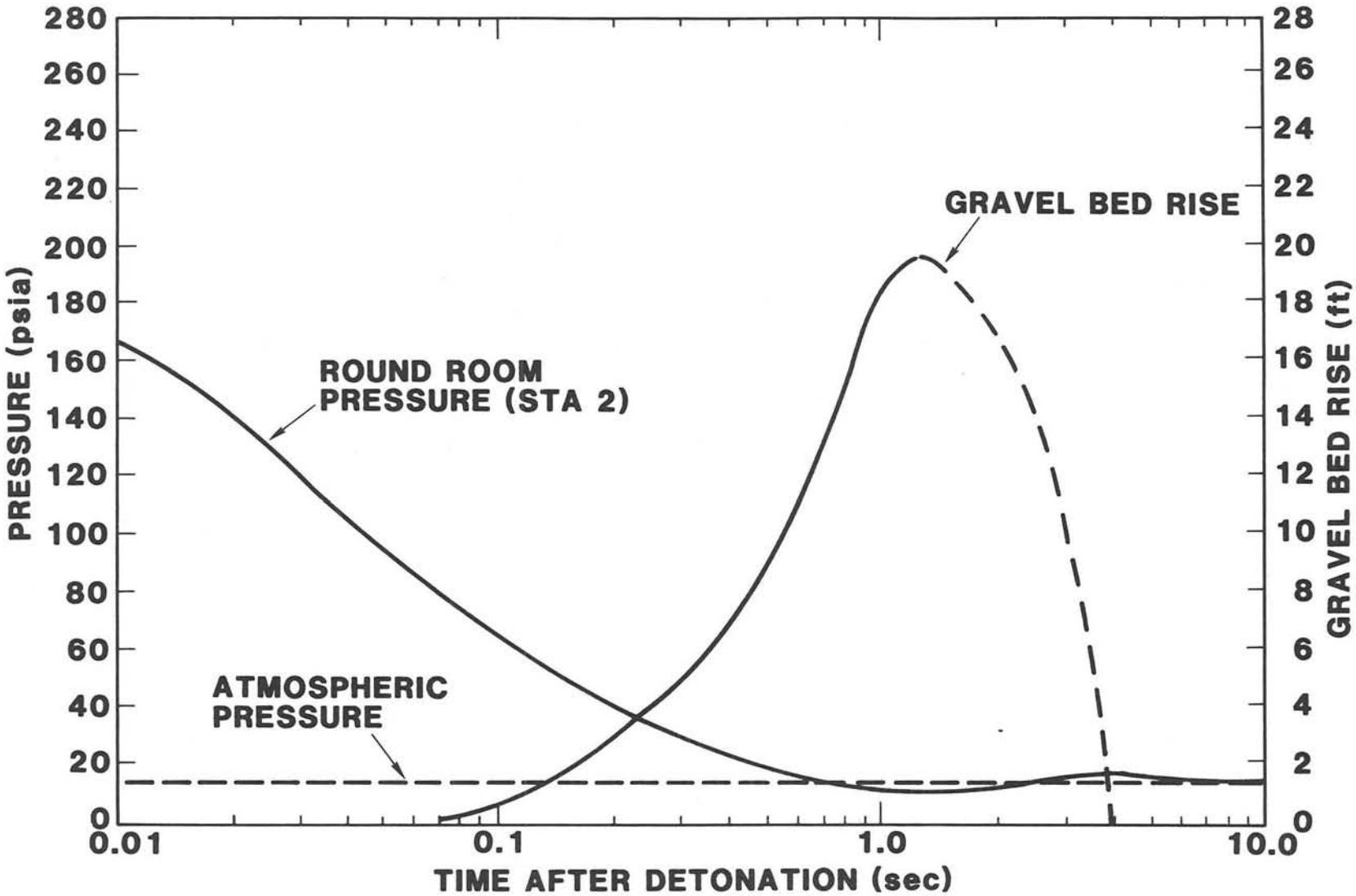

Figure 2-21. Gravel Bed Behavior and Round Room Pressure

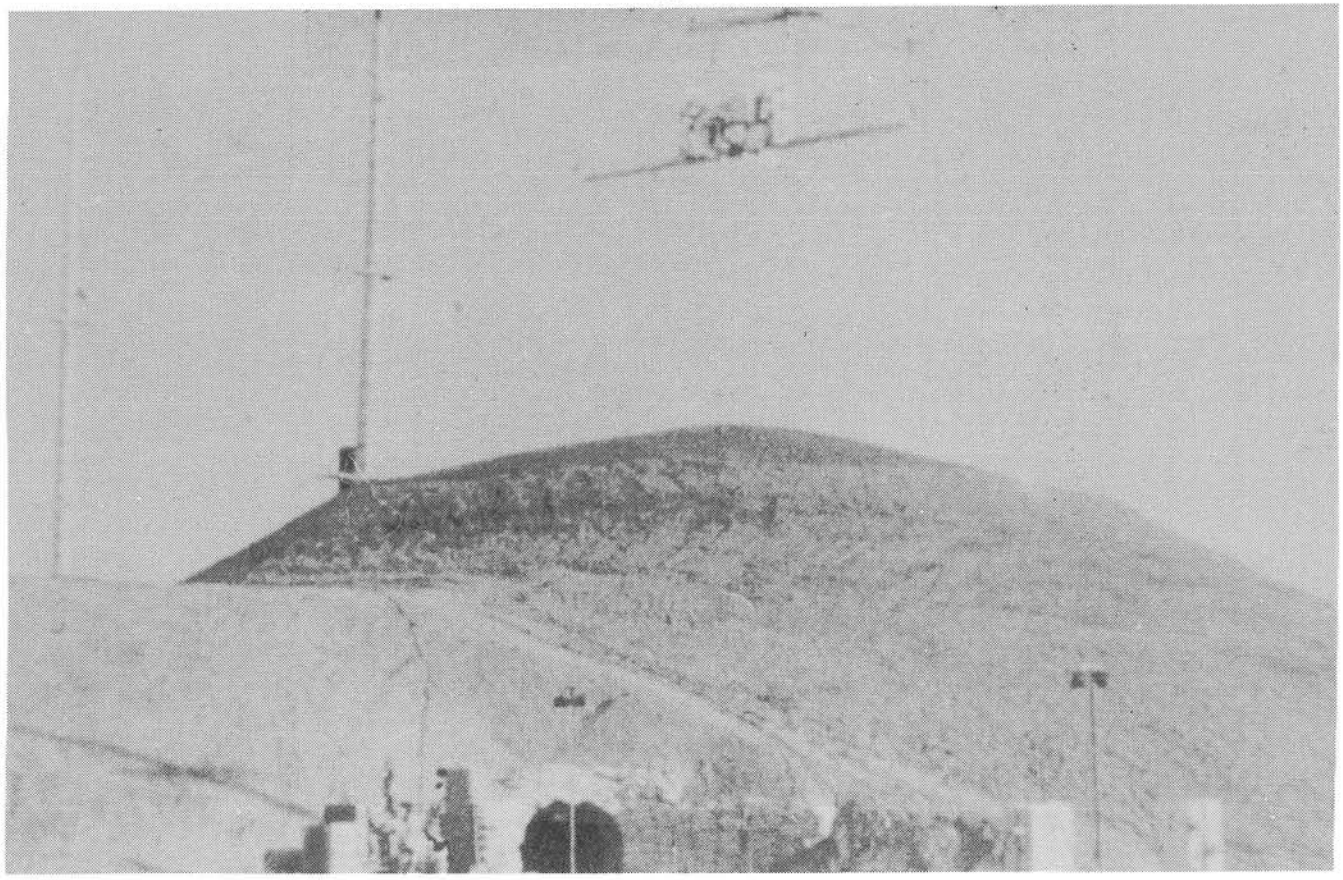

SW view

preshot

SE view

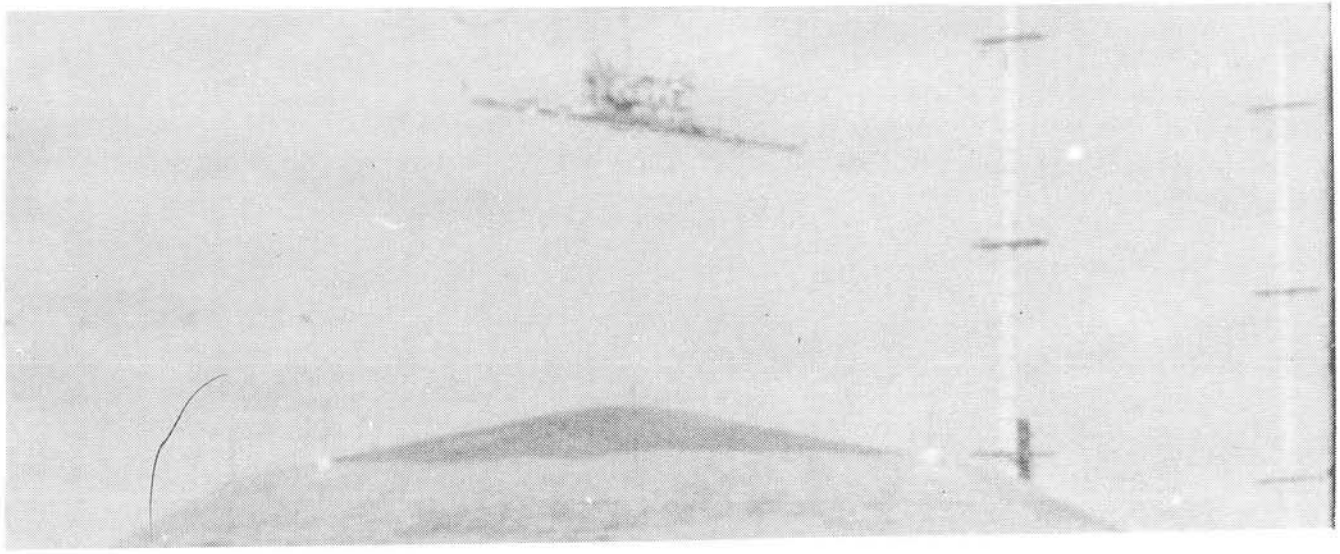

Figure 2-22. Gravel Bed Detail--T = 0 Sec

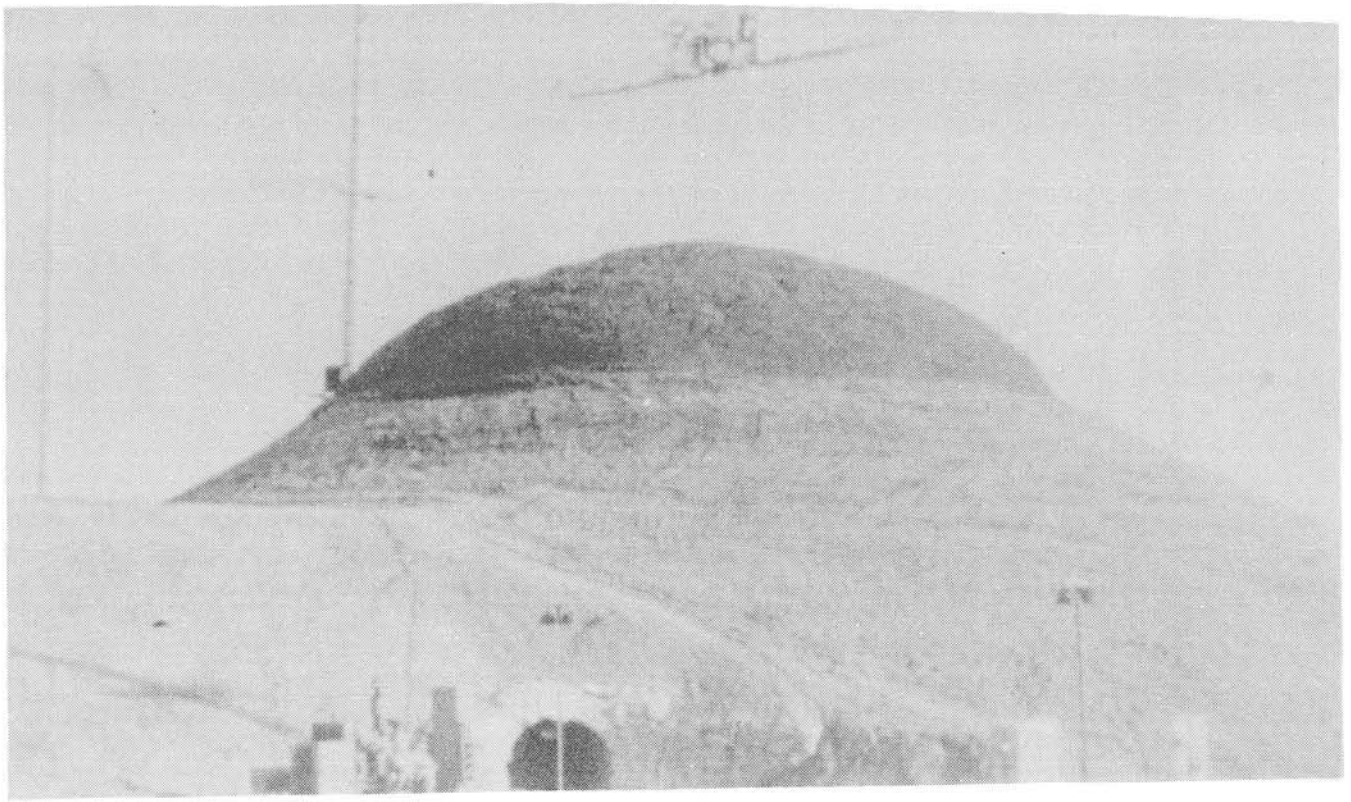

SW view

0.5 seconds

SE view

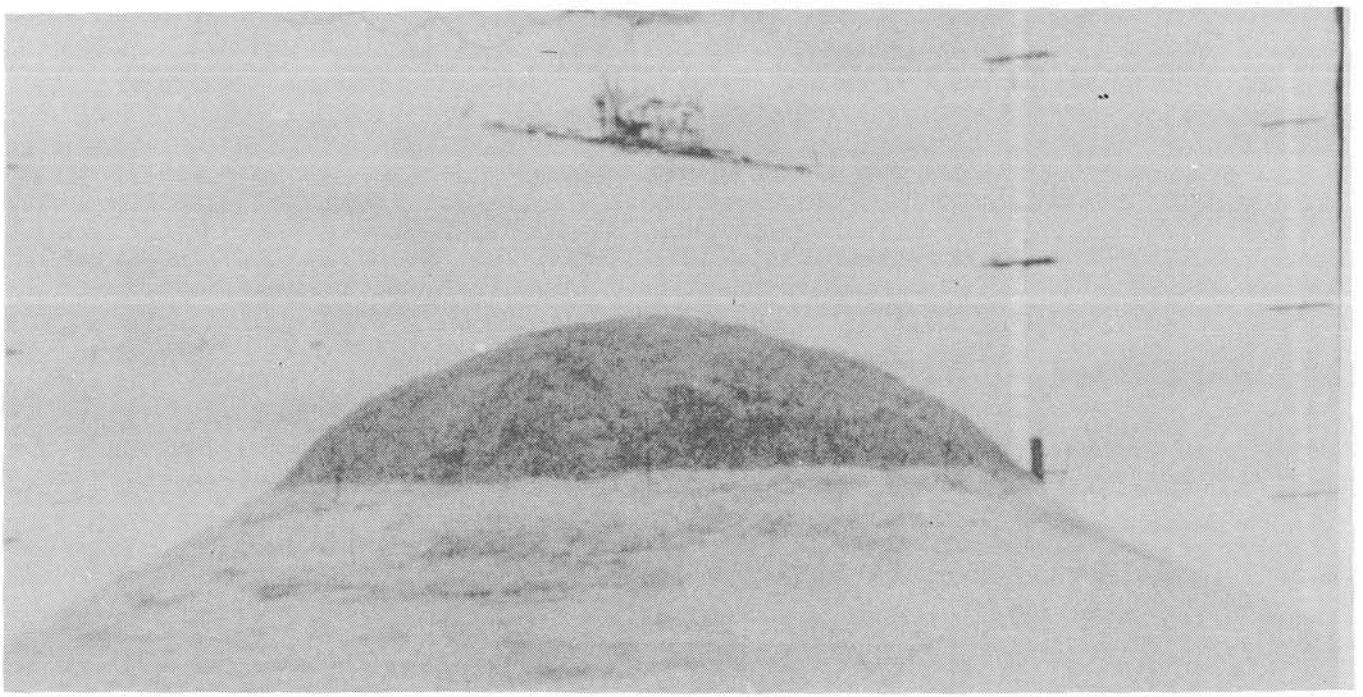

Figure 2-23. Gravel Bed Detail--T = 0.5 Sec

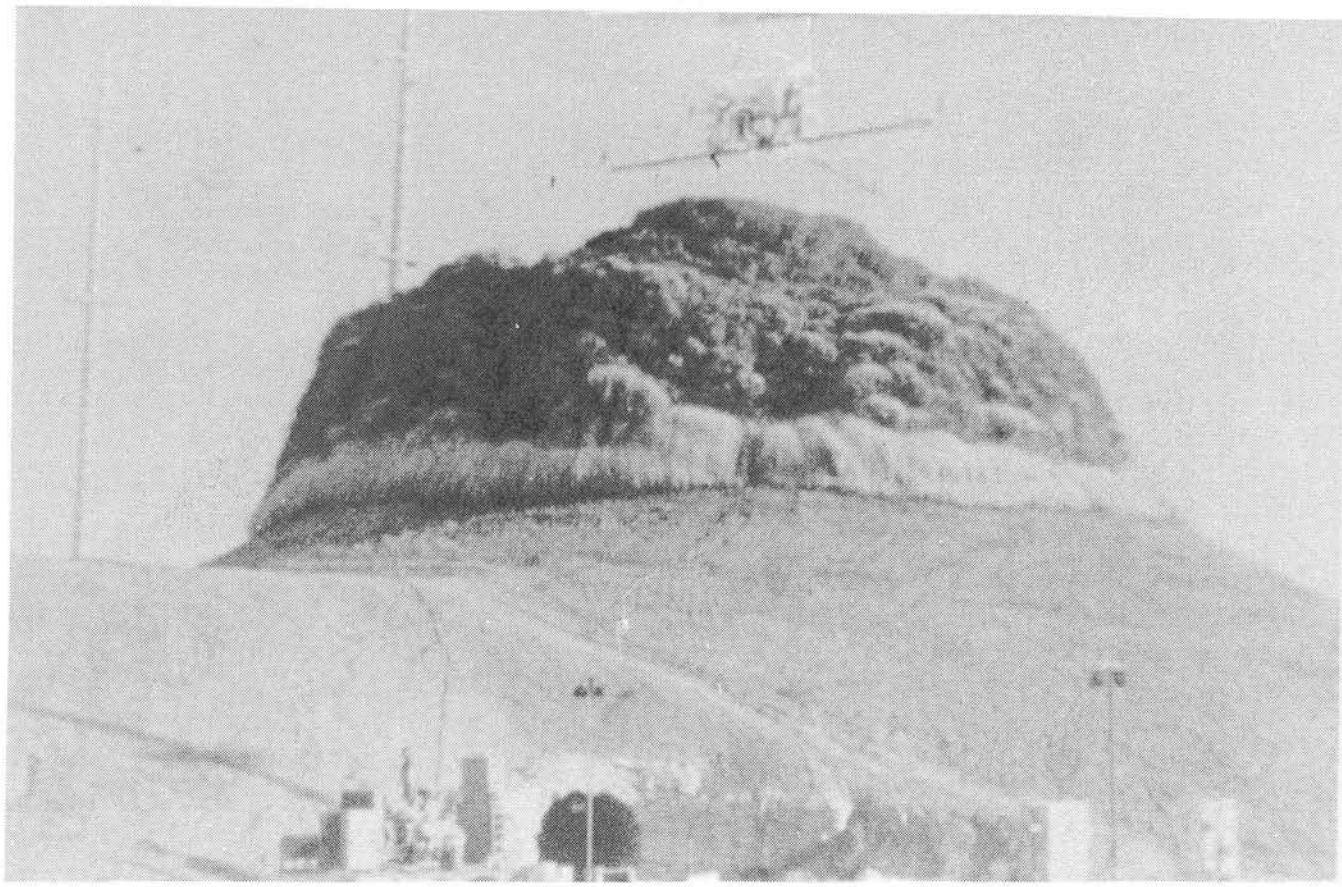

1.3 seconds

SW view

SE view

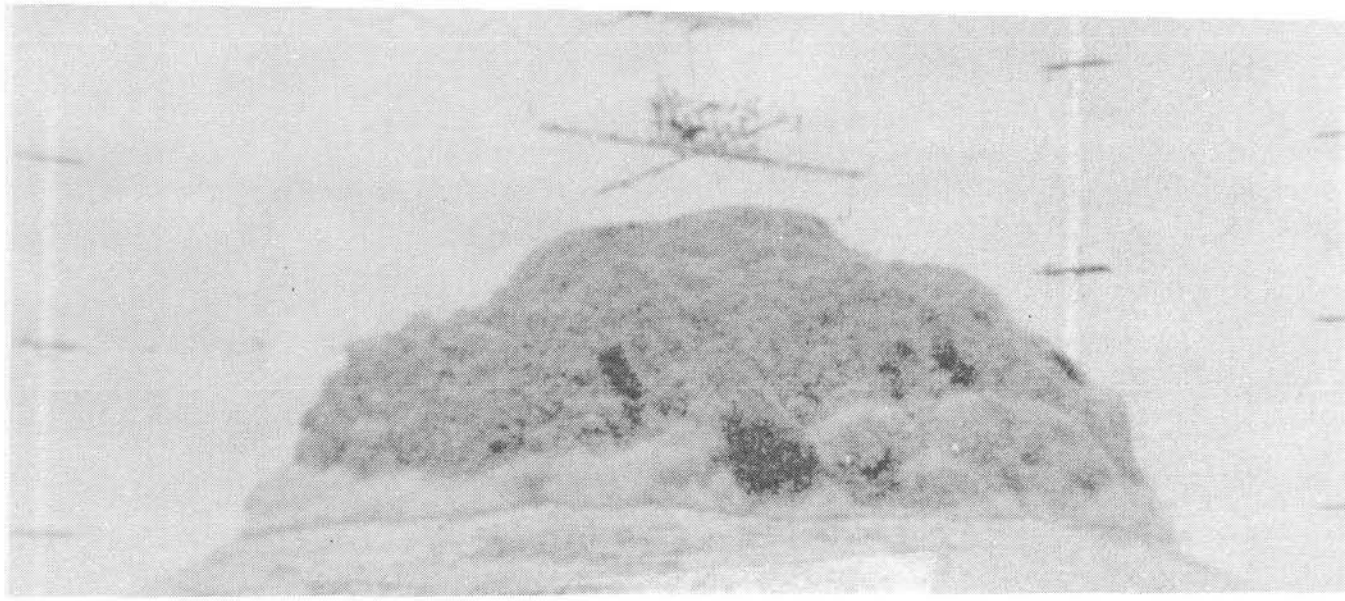

Figure 2-24. Gravel Bed Detail--T = 1.3 Sec

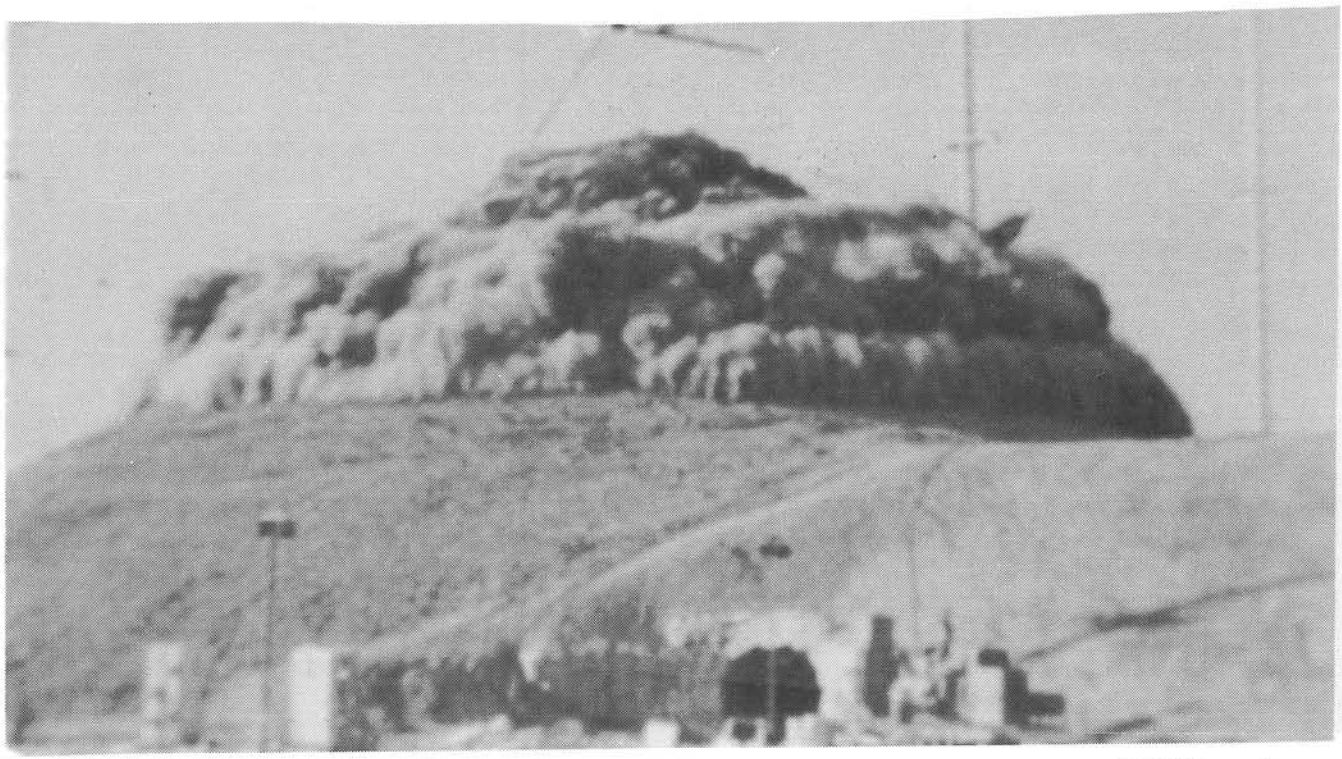

SW view

2.0 seconds

SE view

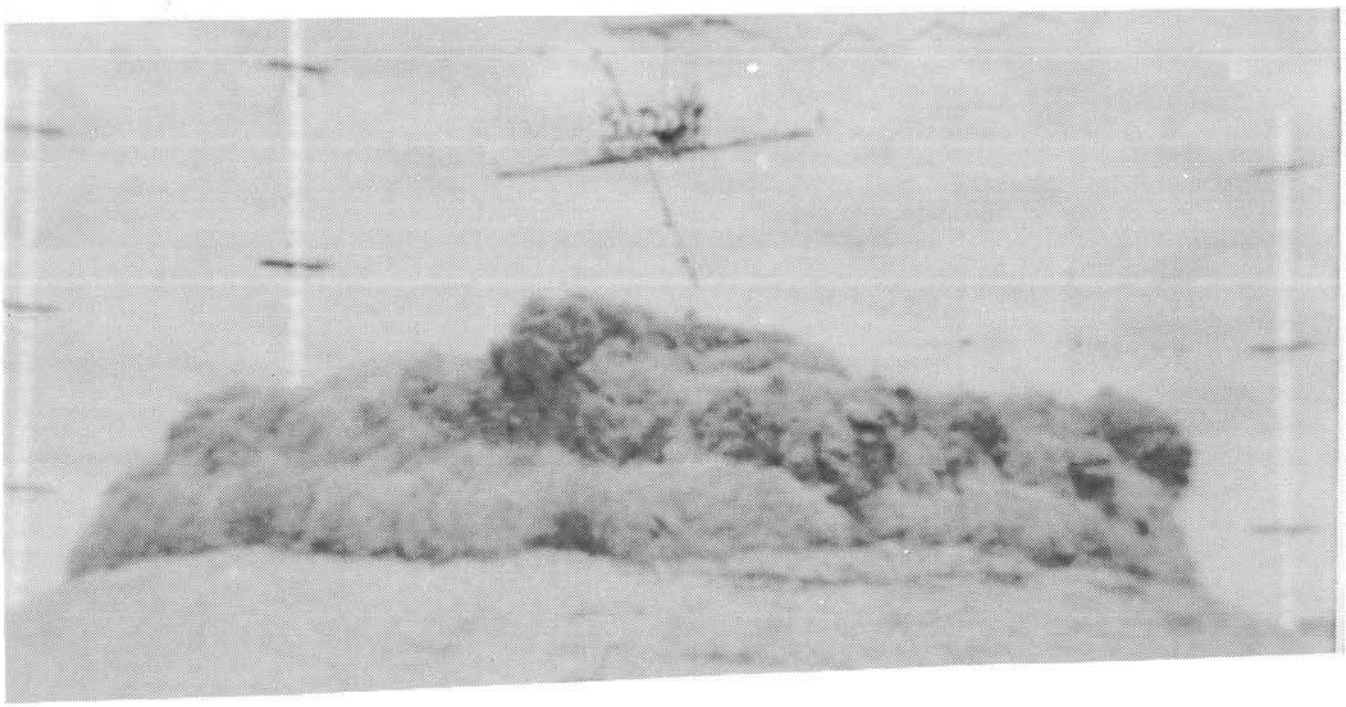

Figure 2-25. Gravel Bed Detail--T = 2.0 Sec

SW view

2.2 seconds

SE view

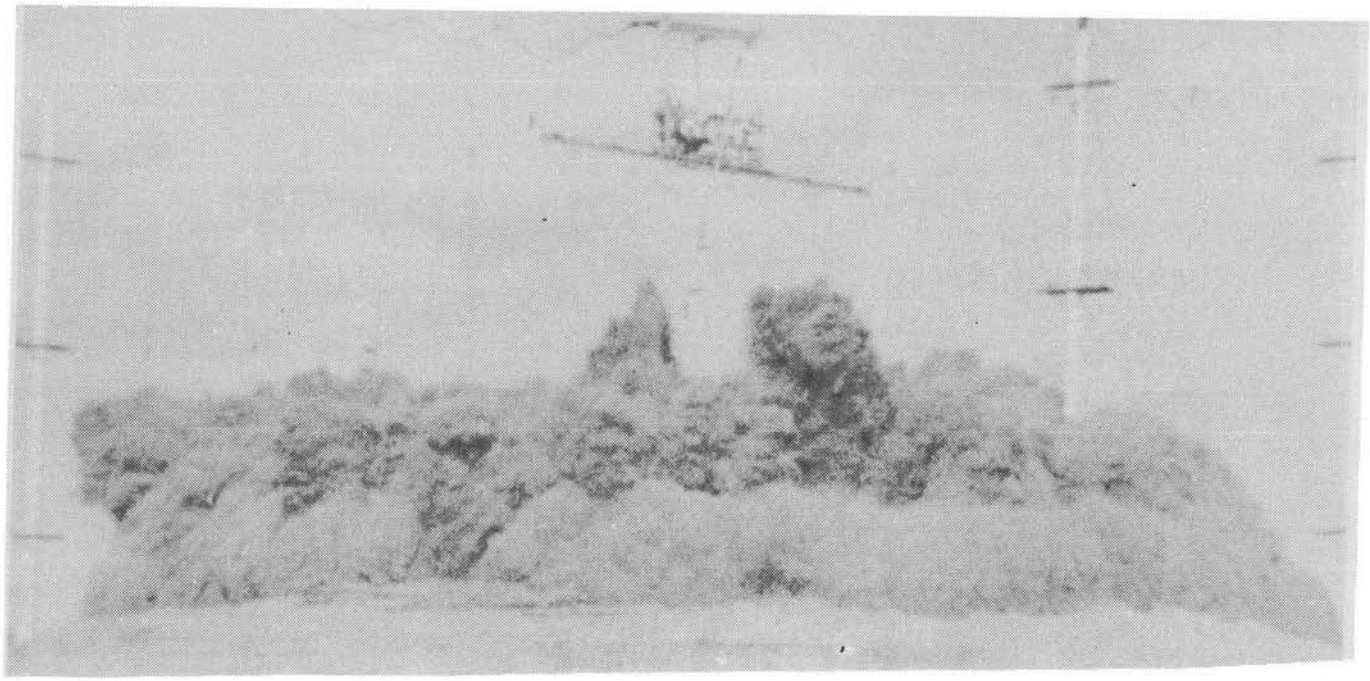

Figure 2-26. Gravel Bed Detail--T = 2.2 Sec

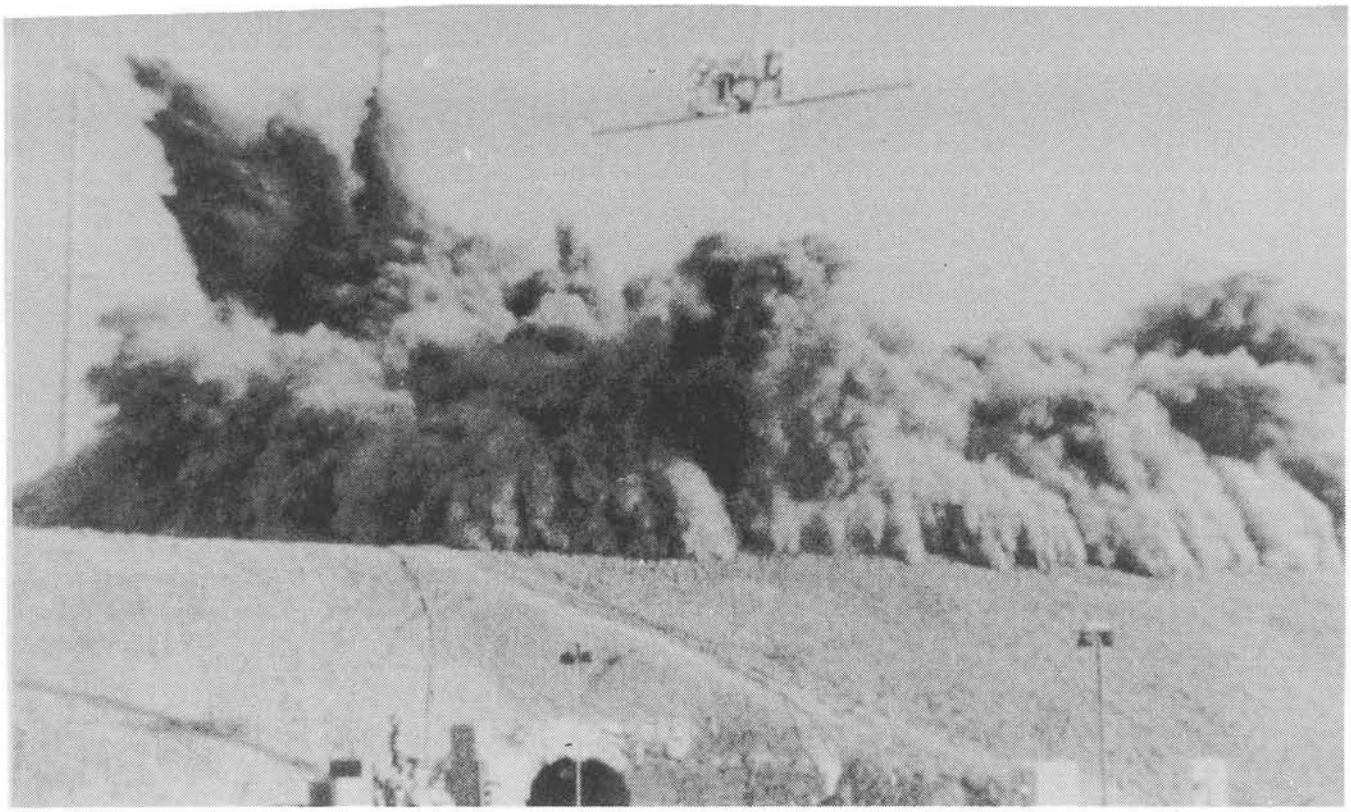

SW view

2.8 seconds

SE view

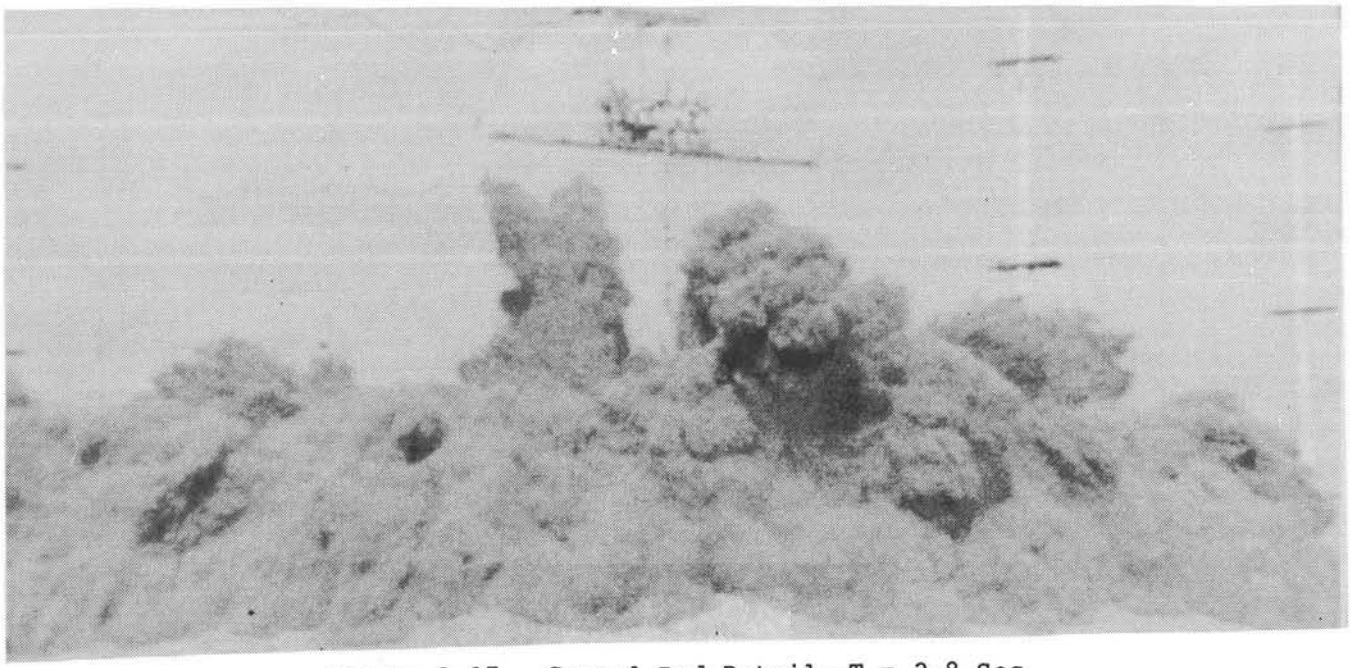

Figure 2-27. Gravel Bed Detail--T = 2.8 Sec

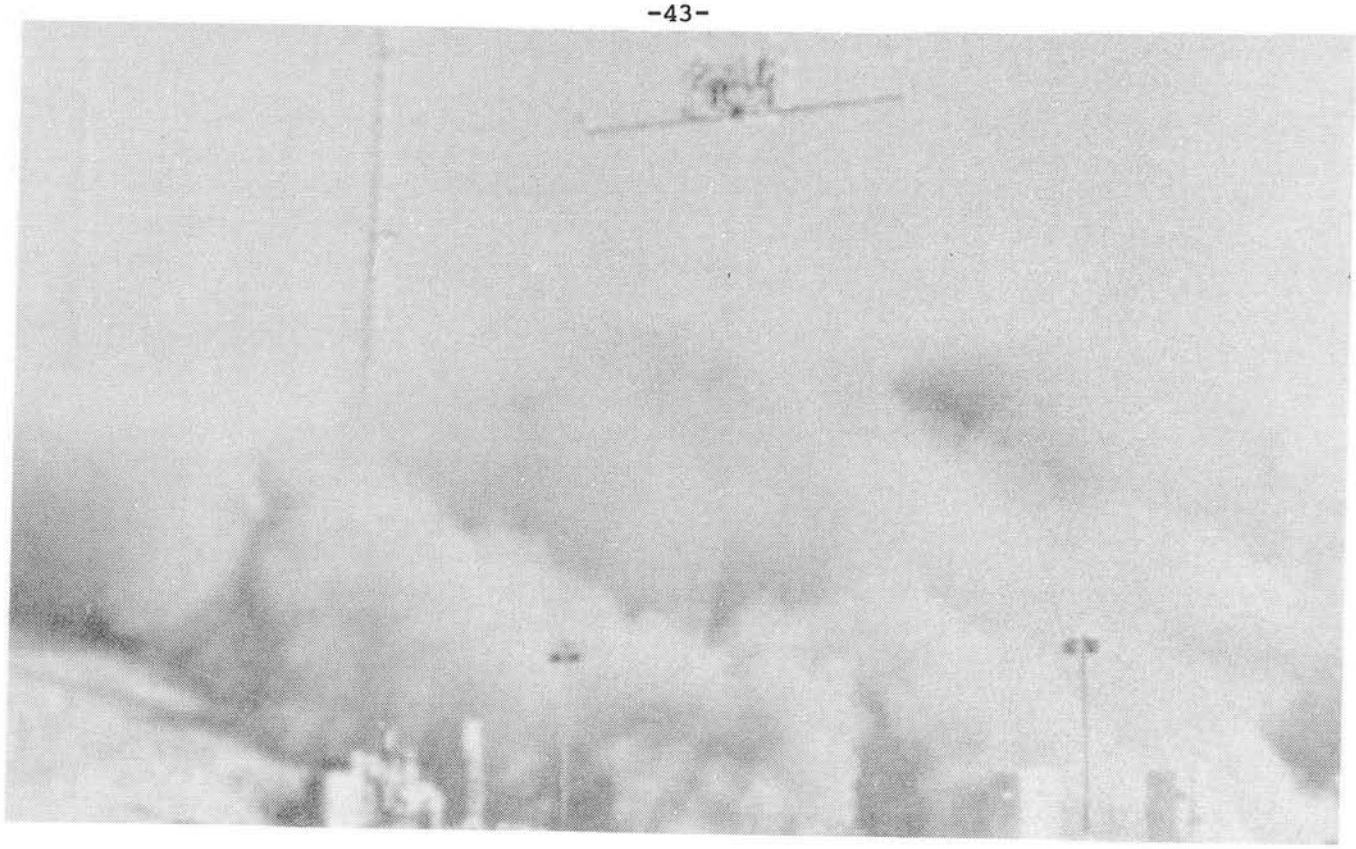

SW view

8.0 seconds

SE view

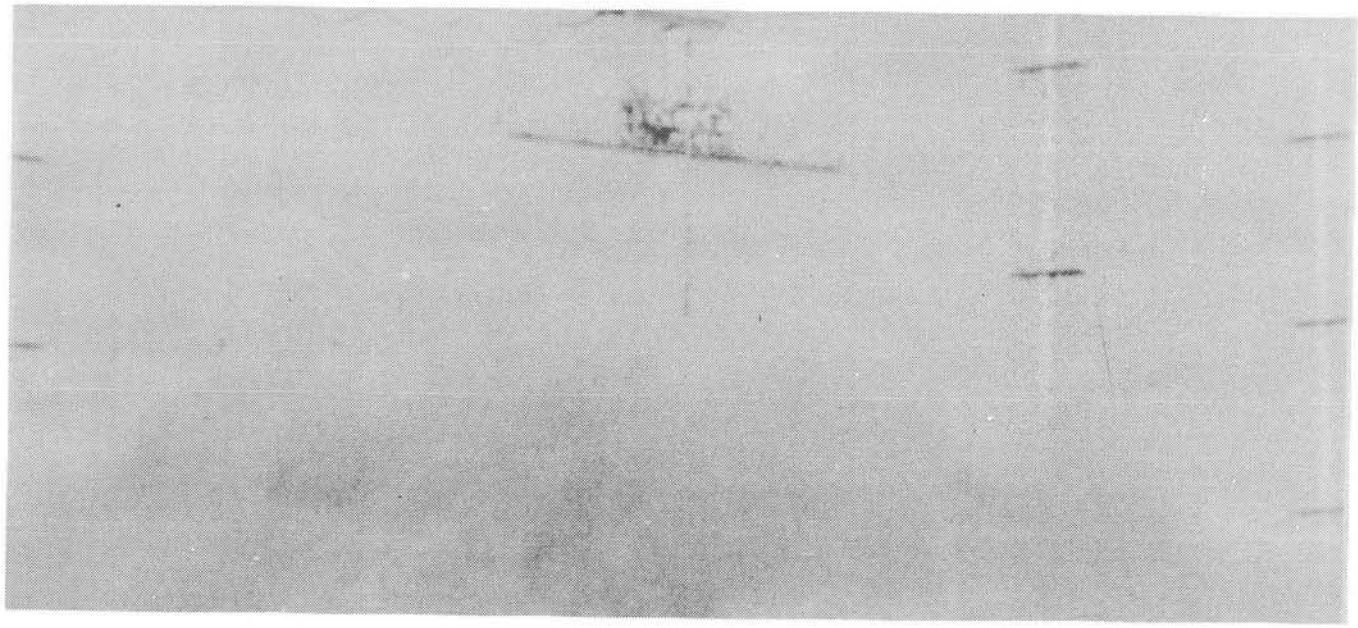

Figure 2-28. Gravel Bed Detail--T = 8.0 Sec

In the early phases of the gravel dome rise (up to approximately 0.6 seconds), the dome approximates a spherical section with slight expansion at the edges and marked growth in the center. As it nears its peak height (~ 1.3 second) a distinctive center section, or "plug," appears with the outer "shell" exhibiting more horizontal movement and beginning to "petal." The plug appears to correspond to the section of gravel immediately above the cylindical round room structure. At 2.0 seconds, the dome is collapsing and a base surge is forming. The "shell" begins to collapse onto the upper portion of the overburden. The "plug" is still distinguishable from the SW although it has become somewhat obscured by roiling dust when viewed from the SE. At 2.2 seconds, the first of several dark jets appear. These first two are moving to the NNW and ENE and are fully developed with essentially ballistic trajectories by 2.8 seconds. As collapse continues, more jets appear and the base surge grows until by 8.0 seconds, the entire structure is obscured in a light-colored dust cloud.

The relative symmetery of dome behavior through the first half second can be seen in Figure 2-29. From 0.6 to 1.3 seconds, the emergence of the "plug and shell" configuration becomes apparent. The relatively disorganized collapse profiles shown in Figure 2-30 suggest that failures in the gravel bed structure and its cable supports were inhomogeneous and probably reflect complex material interactions.

High-speed films show a set of light-colored, "twinkling" objects falling in ballistic trajecteries down the southern faces of the structures between times 2.5 and 5.0 seconds. Trajectory analysis suggests that these particles are large rocks from the lower layers in the Gravel Gertie structure. They appear to be launched by initial roof expansion and the subsequent rebound from the elastic cables as the roof collapes. A more detailed description of this phenomenon is provided in Appendix L.

A dynamic model, fully described in Appendix O, has been developed to predict the response of a Gravel Gertie structure under various internal pressure loading environments.

Aerosols Inside Test Structure

Extrapolation of the aerosol concentration in the mass of gas captured by each GGASP to the total mass of gas in the structure provided an estimate of the total aerosol produced in the structure. This value, multiplied by the fraction respirable, provided an estimate of the respirable aerosol mass in the structure.

Estimation of the mass of gas sampled by each GGASP was obtained from calculations using the pressures inside and outside the GGASP sample chamber during the time when the inlet valve was open. Details of this calculation are provided in Appendix J.

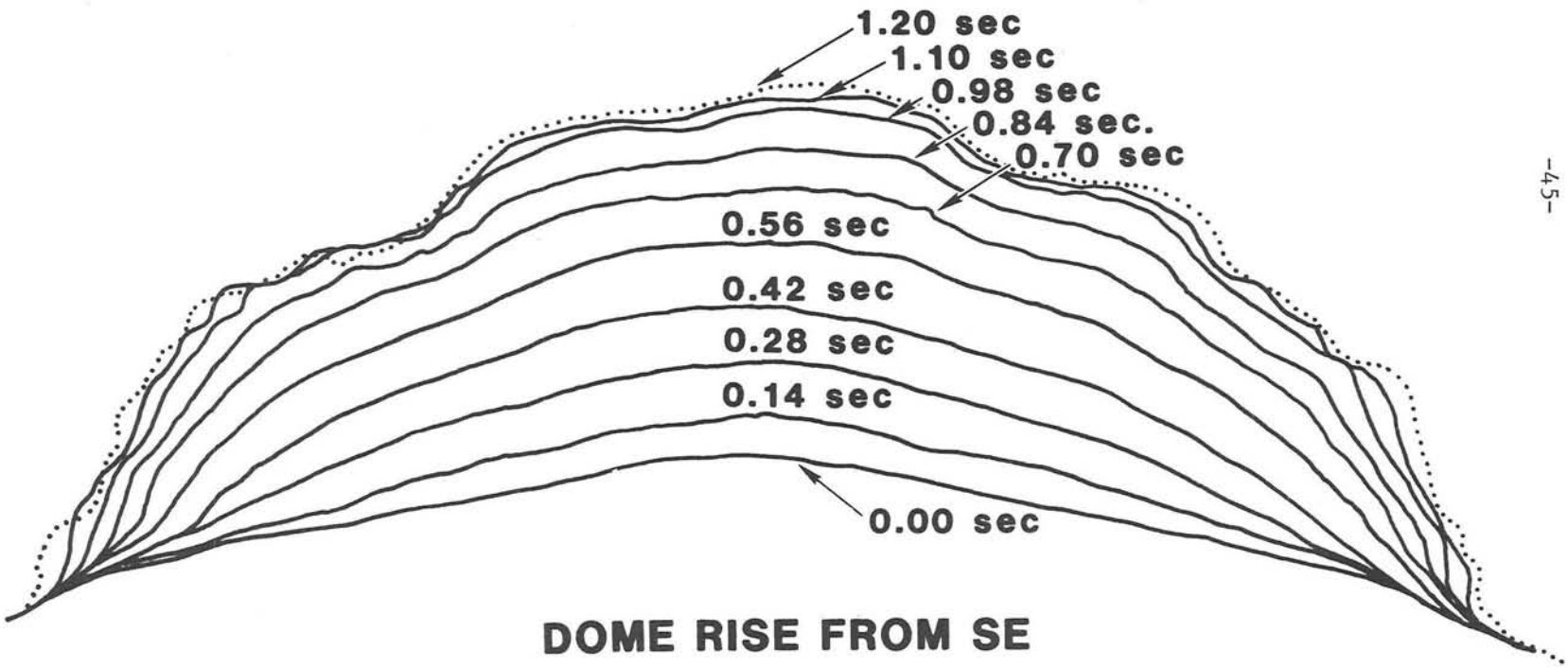

Figure 2-29. Gravel Bed Profiles During Dome Rise

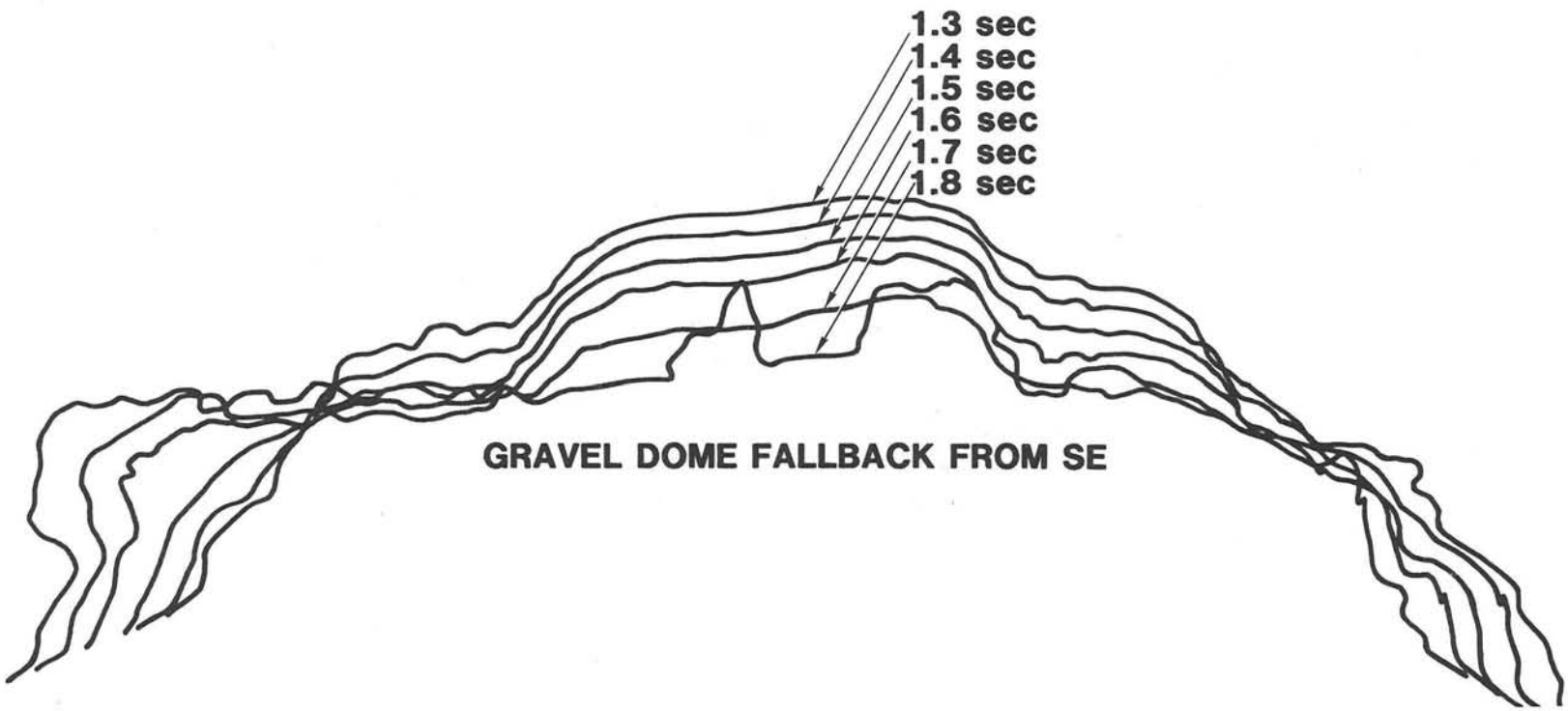

Figure 2-30. Gravel Bed Profile During Dome Collapse

GGASP Pressure/Temperature Data. The pressures and temperatures measured at the GGASP stations are provided in Appendix E. While records varied somewhat by location in the test structure, depending on distance from the HE mass, pressure signatures were similar in nature. Figure 2-31 shows a typical pressure and temperature record for a GGASP within the round room. Figure 2-32 is the record from the GGASP at the far end of the staging area.

In each case, the pressure difference and pressure ratio across the orifice were calculated to ensure that the inlet flow was "critical" and to obtain the mass flow rate of gas into the GGASP.

GGASP Aerosol Data. Results of uranium analysis of the GGASP samples are presented in Appendix D. Results indicate successful collection of aerosols for all samplers. This permitted assessment of the total quantity of material drawn into the sampling chamber and the size distribution of the aerosol sampled.

Aerosols Escaping From Test Structure

Data obtained from the various close-in external aerosol sampler arrays are provided in Appendix D. Data which remained after subtracting estimates of background and removing data for which the mean value was of the same order as the assay uncertainty, consisted of data from the samplers at tunnel exits, the lowest tier of GGBSA, a few samplers at upper levels on the GGBSA, five samplers on the DSA array, and two samplers from the GGESA array.

Aerosols Deposited in GGCTA Deposition Samples. All GGCTA samplers were assayed for uranium. Resulting assay values are shown in Appendix D. The values shown in Figure 2-33 are statistically significant values remaining after adjusting for background deposits. Deposits to the west beyond 121.9 meters are small compared with the close-in deposits and may be artifacts of background and assay and not from the test.

Aerosol Size Distributions. Data from cascade impactors were examined to determine the average size distribution of any escaping aerosols. The data from all cascade impactors, as well as the analysis which leads to respirable fraction estimates, are contained in Appendix D. The size distribution measured in the GGBSA is shown on Figure 2-34.

Cloud Volume Measurements. Frames from the 10 frame per second camera were projected on a paper surface and outlines of the cloud were traced at various times after detonation. Also traced on the sheets were specific fixed objects in the field of view. These fiducial objects allowed removal of the dimensional distortion introduced by the wide-angle lens. The results of the cloud outline studies are shown in Figures 2-35 and 2-36.

Meteorological Measurements. Meteorological information obtained as a result of the test is provided in Appendix H. Readouts of the wind speed, direction, and temperature which are most relevant to interpretation of the test results are shown in Table 2-4.

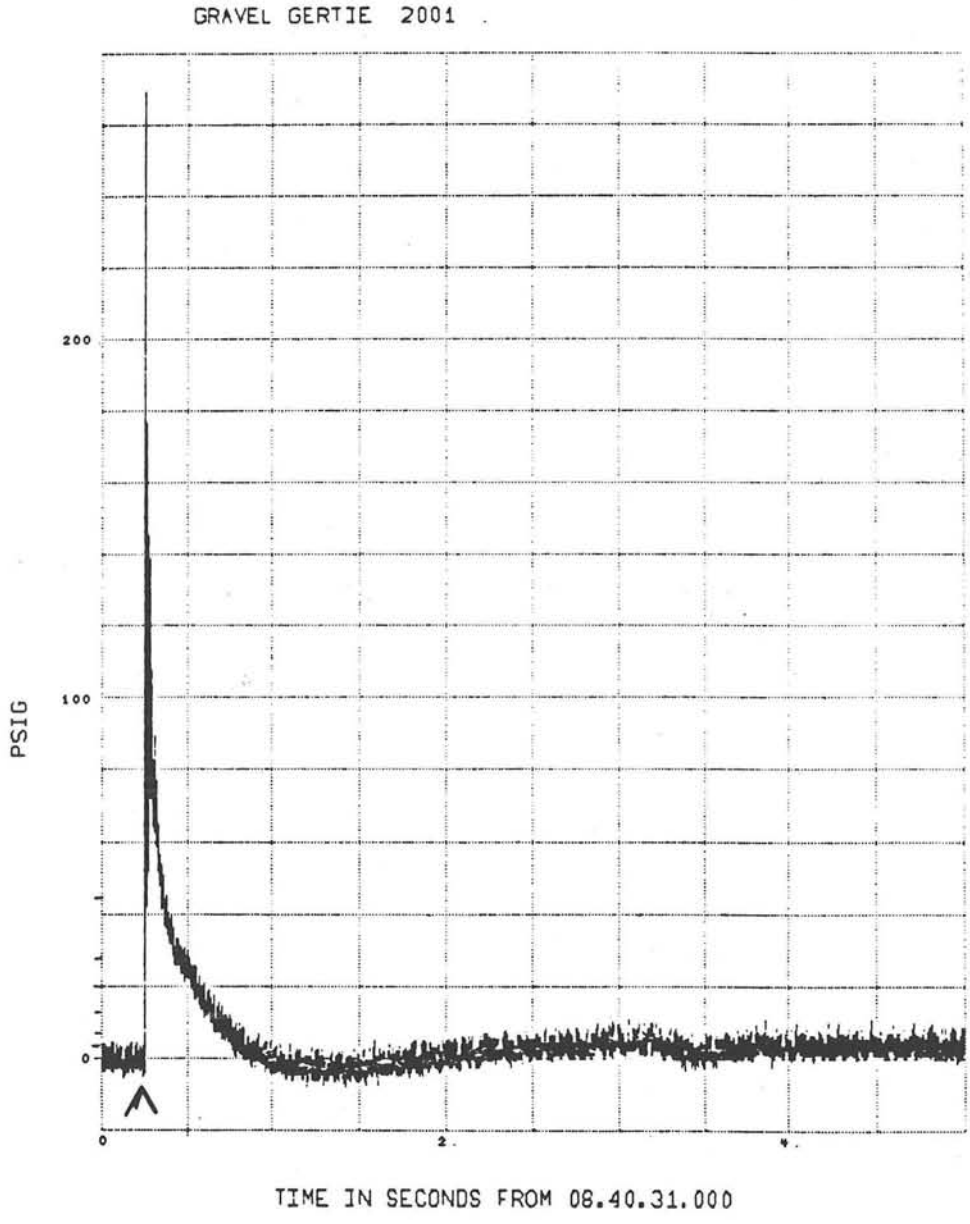

Figure 2-31. Typical Round Room Pressure Signature

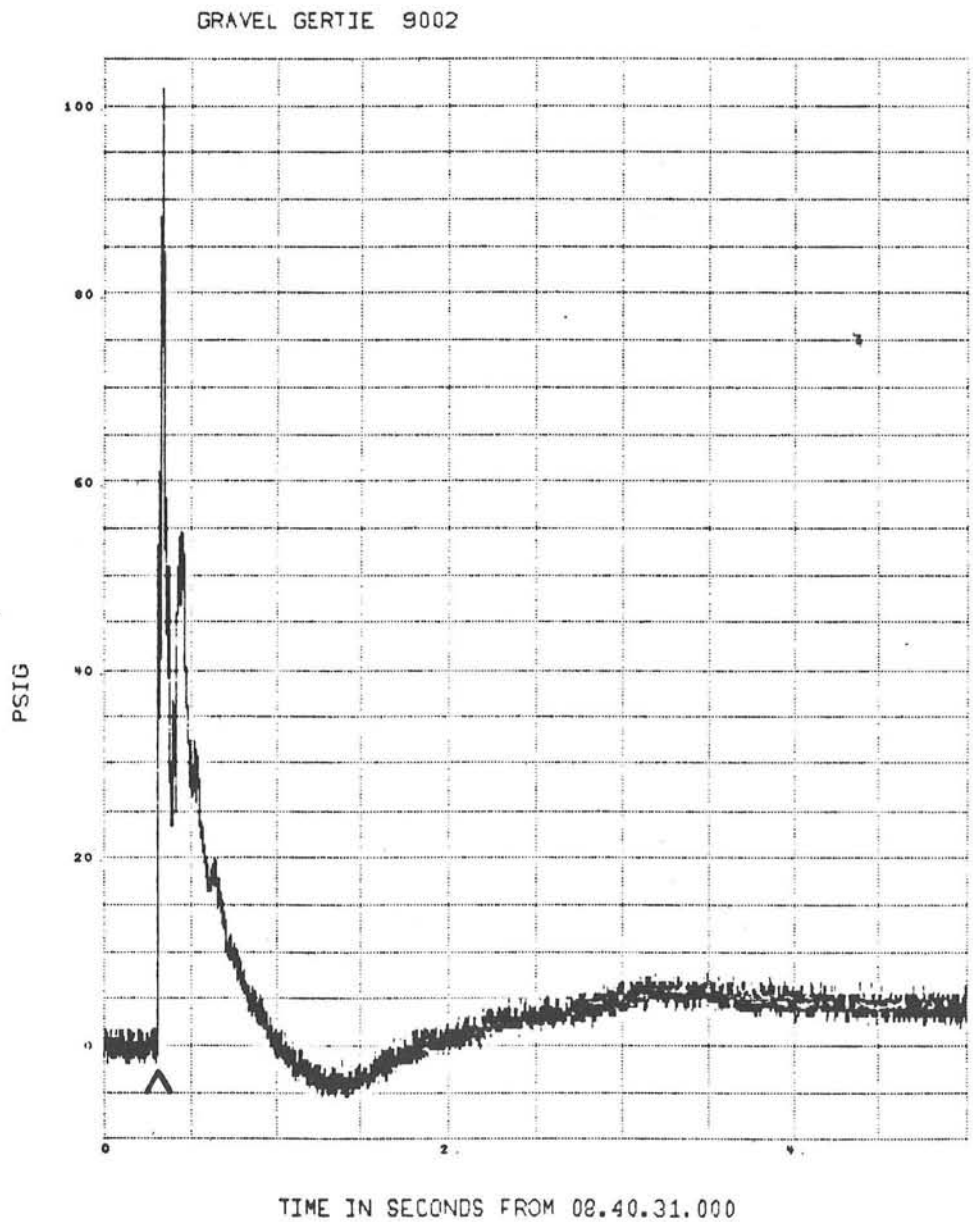

Figure 2-32. Typical Staging Area Pressure Signature

GRAVEL GERTIE CTA ARRAY DATA
VALUES IN MICROGRAMS/M**2
BACKGROUND REMOVED

	P	O	N	M	L	K	J	I	H	G	F	E	D	C	B	A	B	DISTANCE METRES
7	-	-	-	-	-	-	-	-	-	-	-	-	-	-	-	-	-	365.76
6	-	-	-	-	-	-	-	-	-	-	-	-	-	-	-	-	-	304.80
5	-	-	-	-	-	-	-	-	3.01	-	-	-	-	-	-	-	-	243.84
4	-	-	-	-	-	-	-	-	-	-	-	-	0.61	-	-	-	-	182.88
3	-	-	-	-	-	-	-	3.01	-	-	-	-	-	-	2.85	52.84	-	121.92
2	-	-	-	-	-	-	-	-	-	-	-	-	-	9.20	297.10	312.26	-	60.96
1	-	-	-	0.77	-	0.68	-	1.67	-	2.59	-	2.88	-	210.74	386.66	GZ	-	-
2	-	-	-	-	-	-	-	-	-	-	-	-	-	1.31	9.20	-	0.73	60.96
3	-	-	-	-	-	-	-	-	-	-	-	-	-	-	-	0.73	-	121.92
4	-	-	-	-	-	-	-	-	-	-	-	-	-	-	-	-	-	182.88
5	-	-	-	-	-	-	-	-	-	-	-	-	-	-	-	-	-	243.84
6	-	-	-	-	-	-	-	-	-	-	-	-	-	-	-	-	-	304.80
7	-	-	-	-	-	-	-	-	-	-	-	-	-	-	-	-	-	365.76
DIST	914.40	853.44	792.48	731.52	670.56	609.60	548.64	487.68	426.72	365.76	304.80	243.84	182.88	121.92	60.96	-	60.96	-
(M)	-	-	-	-	-	-	-	-	-	-	-	-	-	-	-	-	-	-

Statistically Significant GGCTA Uranium Deposition* above Background**

*Values greater than 0.49 $\mu g/m^2$ after subtraction of background
**Background estimated at 0.30 $\mu g/m^2$

Figure 2-33. GGCTA Data Above Background

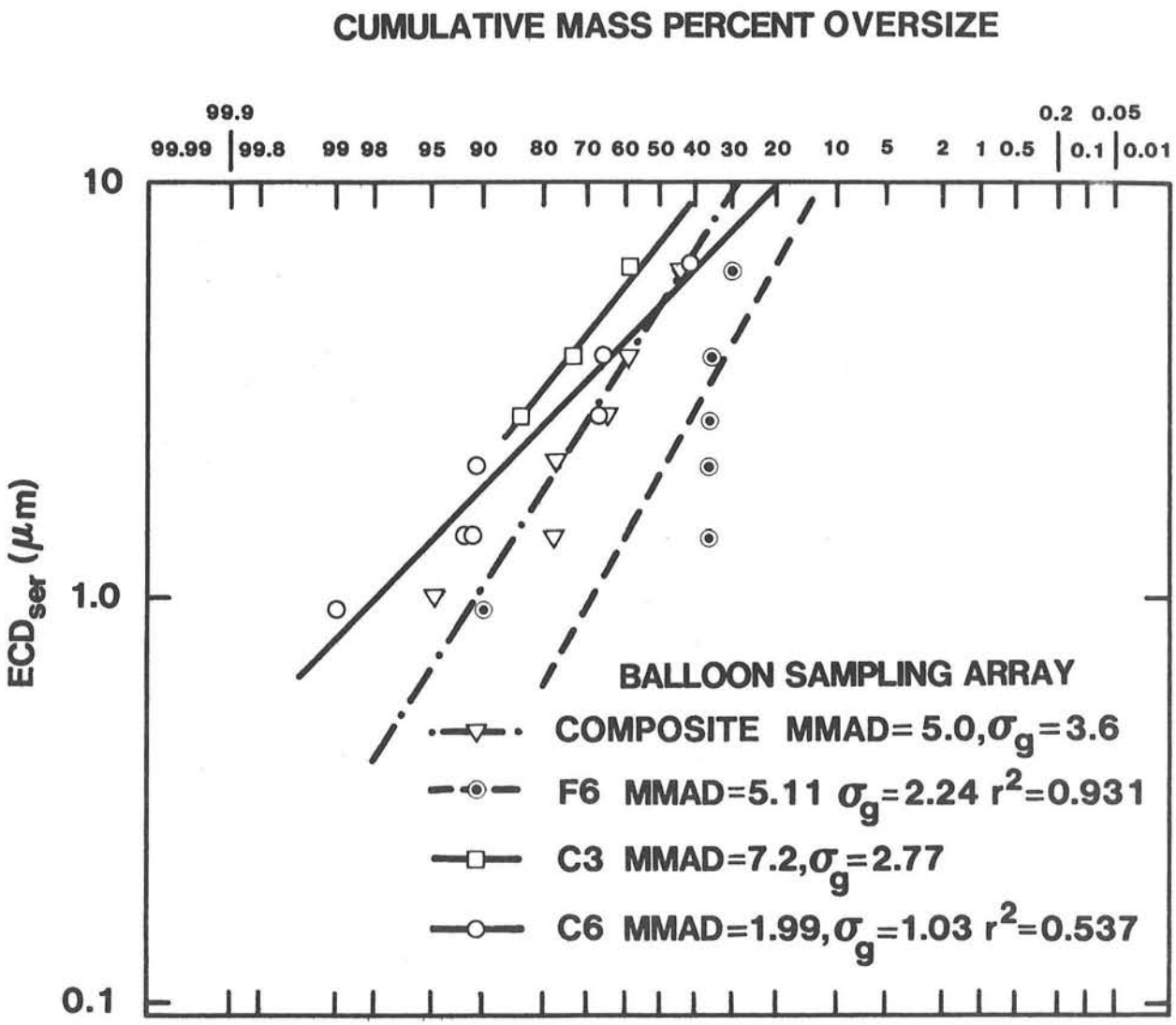

Figure 2-34. Size Distribution for GGBSA Impactors With Significant Collections

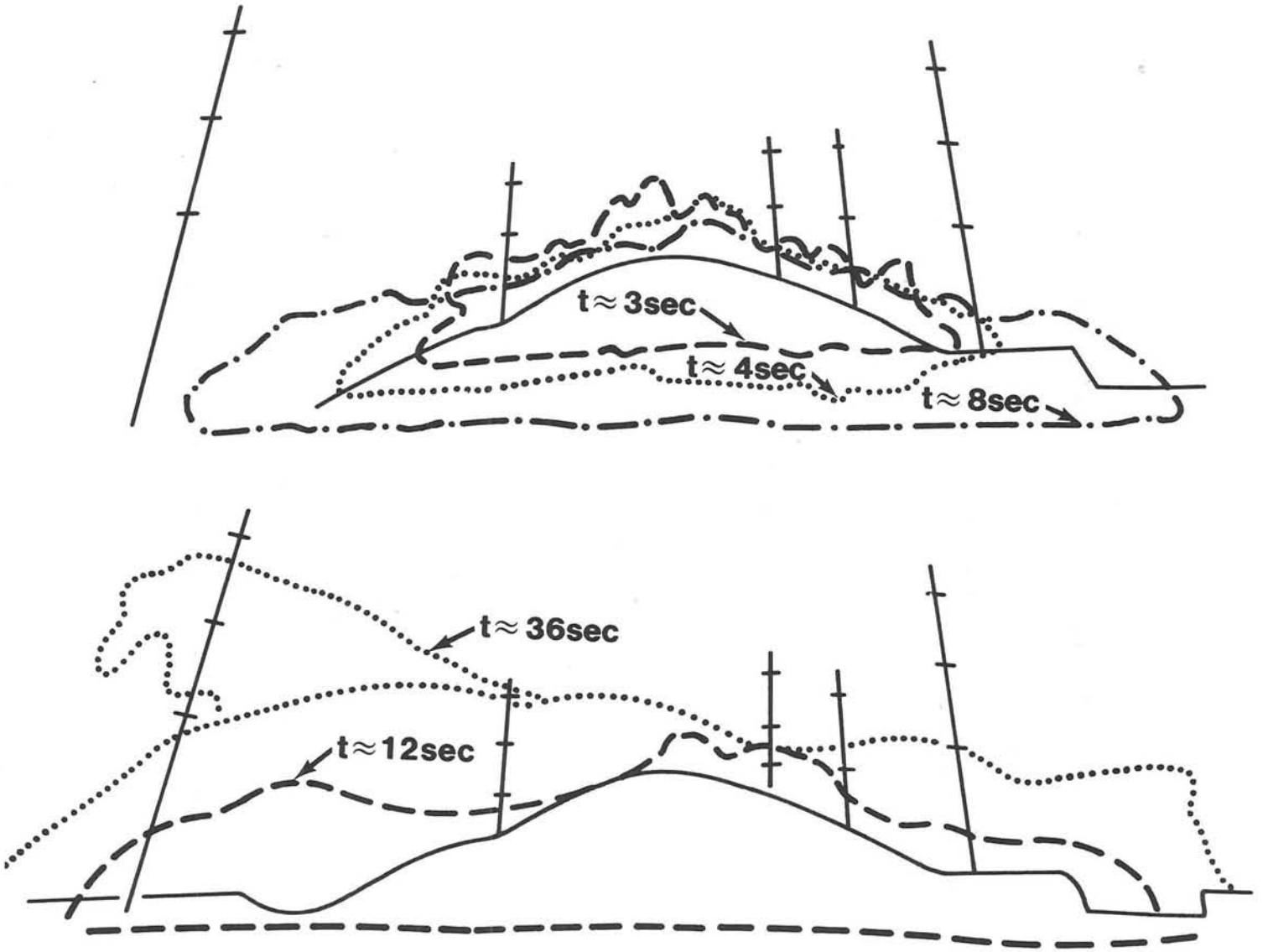

Figure 2-35. Cloud Outlines Versus Time (SE Station)

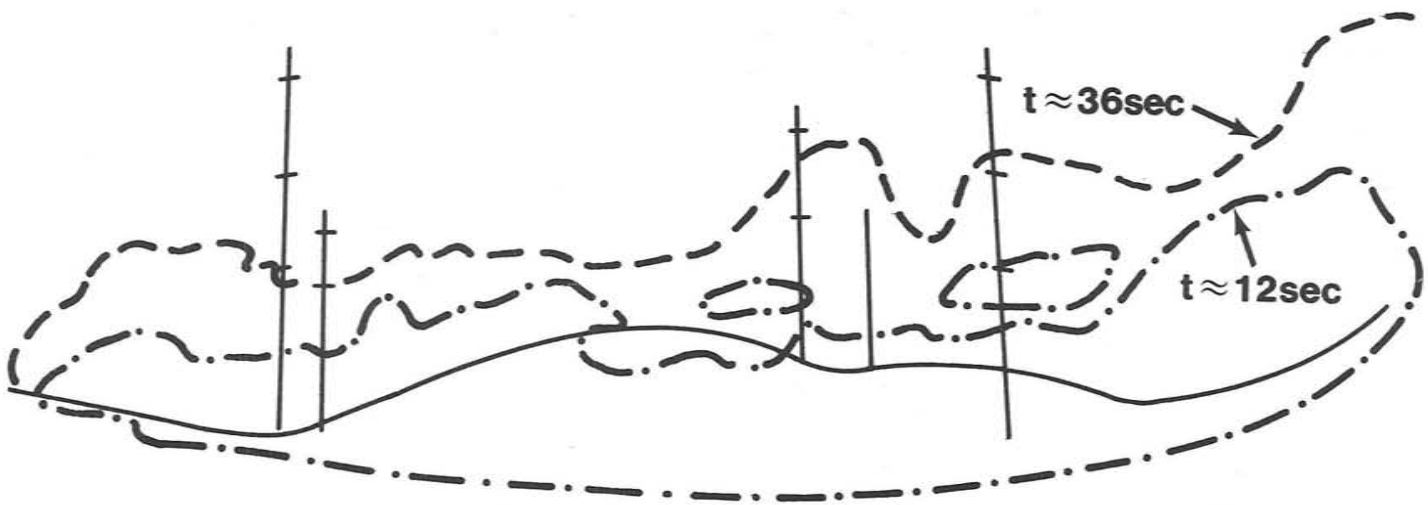

Figure 2-36. Cloud Outlines Versus Time (NE Station)

TABLE 2-4

METEOROLOGICAL DATA NEAR SHOT TIME

Time	Height (m)	Wind Speed (m/s)	Wind Direction*	Temperature (°C)	Relative Humidity
0835	9	1.0	110	--	--
	18	0.6	140	5.3	66
	23	1.0	085	--	--
0840	9	1.0	075	--	--
(Shot Time)	18	0.4	082	5.6	63
	23	2.0	085	--	--
0845	9	1.0	090	--	--
	18	0.4	071	6.5	61
	23	2.5	095	--	--

*degrees east of true north

Interpretation of Full-Scale Test Data

The total mass of tracer aerosol within the round room cannot be determined solely from the GGASP data because the GGASP collection efficiency decreases rapidly with particle size above 12 to 15 micrometers. In addition, because of expected blast and fragment environments, the inlets of the samplers were protected by a blast shield that prevented direct exposure of the GGASP to the incident aerosol. Because respirable particles are easily carried with gas flow and because of the extraordinary turbulence and gas movement in the structure, it has been assumed that the aerosol particles which are of primary concern were well mixed with the gas and that sampling was representative. If this assumption was invalid the aerosolized mass would have been somewhat larger. Data from cascade impactors within the GGASP units suggested that 90 to 98 percent of the aerosol collected by the GGASPs was in the respirable size range. The total mass of GGASP-collectable uranium aerosol in the structure is estimated to be 195 g $\pm$ 40 g. This value is the measured quantity from which release fraction may be calculated by comparison to samples of similar sized particles outside of the Gravel Gertie.

Establishing the mass of respirable aerosol external to the structure was approached in two largely-independent ways. One involved using air sampler results together with cloud volumes sampled to form a concentration-volume product yielding aerosol mass. This process, which is shown in detail in Appendix L, indicates a value of 0.60 to 0.98 grams.

Multiplying by respirable fraction estimates from impactor data yields an estimated respirable released mass. Dividing this by the respirable mass inside the structure gives the efficiency. Thus, the indicated release fraction (using a central estimate) is:

$$\text{release fraction} = \frac{\text{Aerosol mass outside}}{\text{Aerosol mass inside}}$$

$$\text{release fraction} = \frac{0.8\ \text{g} \pm 0.2}{195\ \text{g} \pm 40} = 4 \times 10^{-3} \pm 1.5 \times 10^{-3}$$

Data from impactors on the GGBSA indicated a respirable fraction of 0.7 $\pm$ 0.1. Data from GGASP samplers indicated 0.95 $\pm$ 0.05 respirable fraction. Applying these factors to the release fraction yields the following estimate of respirable release fraction (f_{rr}):

$$f_{rr} = 3.0 \times 10^{-3} \pm 1.1 \times 10^{-3}$$

The second method used in estimating the external aerosol mass is based on the use of atmospheric transport and diffusion codes. In this technique, several possible source configurations are postulated, each with a source of 1 g of material. Comparing predicted time-integrated concentration values at each sampler location with the corresponding measurements permitted selection of source masses which best fit the observed data. In this technique, source cloud configurations, meteorology, and particle size distributions were all specified to approximate those observed in the experiment. When a reasonable

fit was achieved, the respirable aerosol masses in each source were summed to form an estimate of the total released mass equal to 0.9 grams. This technique is detailed in Appendix M.

The estimate matched respirable predictions against actual filter measurements. Since the actual measurements include particles as large as 15 to 20 micrometers, this estimate must be reduced by the fraction of external aerosol less than 10 micrometers. Data from the BSA samplers indicated that 0.70 of the total released aerosol was respirable. Using this fact and the respirable fraction of 0.95 indicated by the GGASP samplers, the release fraction should be reduced by the ratio 0.70/0.95. The results for the uranium aerosol mass release fractions are:

$$\text{release fraction} = \frac{0.9\ \text{g} \pm .4}{195\ \text{g} \pm 40} = 4.6 \times 10^{-3} \pm 2.3 \times 10^{-3}$$

$$\text{respirable release fraction} = f_{rr} = 3 \times 10^{-3} \pm 3 \times 10^{-3}$$

The indicated release fraction by these two methods is fairly consistent.

An analysis of the Sb_2O_3 secondary tracer deposits on Balloon Sampling Array filters and cascade impactors was also performed. This analysis (Appendix L) indicated that 106 $\pm$ 64 mg of respirable Sb was released from the GG round room to the surrounding area. This quantity corresponds to a respirable release fraction of $1.1 \times 10^{-4} \pm 6.4 \times 10^{-5}$ of the initial Sb_2O_3 tracer mass (1 kg) in the round room. The respirable release fraction for the uranium tracer is 27 times larger than the release fraction for the Sb_2O_3 tracer. In retrospect because the Sb_2O_3 powder responded differently to the high temperatures and shock environment in the round room, Sb_2O_3 was not considered to be an acceptable secondary tracer.

Comparison With Earlier Tests

The results obtained in this test are not fully consistent with the results of Experiment 3 of the mid-1950s test series, which was conducted in the same round room. In that test, the fallout trays received no deposits above that received by the same trays uncovered for a comparable time before the test. However, in this test, deposits of uranium were observed in locations downwind of the structure. Qualitative review of test films also indicates that gravel bed behavior was somewhat different in the two tests. In searching for possible reasons for this lack of consistency several differences were noted. The three most important relate to the configuration of the test device(s), the construction of the gravel bed, and the volume and configuration of the staging areas. Among other less obvious differences were HE composition, number of charges, casing of the units, proximity to floor, and cable geometry.

Calculations of energy deposition for a HEAG of the same charge-to-mass ratio as the aerosol generator used in the 1950s test device suggest that a significantly larger quantity of respirable aerosol would have been produced in the 1957 test series.

A somewhat more important result of the dynamic model development was the importance of staging area volume in the predicated gravel rise. Calculations indicate that for a fixed amount of HE and round room gravel geometery, the gravel rise increases as staging area volume increases. This apparently results from the ability of the staging area to act as a pressure reservoir to lengthen the duration of the positive pressure phase. This increases the impulse on the gravel bed and produces greater displacements. While the expected effect of greater internal volume is to reduce the early pressure (to reduce impulse if the duration in unaffected), the reservoir effect is dominant. This result suggests that changes in Gravel Gertie design, especially those that affect enclosed volumes, be considered very carefully for effects on the dynamic behavior of the structure.

Inclusion of a staging area of comparable volume to those Gravel Gerties in use at Pantex produced an additional very significant difference between this test and the earlier test series. The extra volume (620 m^3 compared with 140 m^3) and door area (6 m^2 compared with 3.6 m^2) meant that initial gas pressures in the round room in this test should have been lower, but that the duration of positive pressure might be longer than that of the mid-1950 test series. It seemed plausible that flow channels might develop in the roof near the area above the entrance to the staging area since that is the last reservoir of pressurized gases to be vented. Although this proposed mechanism for a release path is conjectural, there is adequate reason to believe that the fluid dynamic situation was very different in these two tests. Thus, there is no lack of possible reasons for differences between this result and that obtained in earlier tests. However, with the exception of the construction deviation, this test was much like current Pantex Gravel Gertie geometries/volumes.

Conclusions

The Gravel Gertie Confinement Verification Program has provided a significant increase in the understanding of the behavior of Gravel Gertie structures under high explosive detonation conditions. The confinement vessel tests provided a needed design value for the aerosol measuring system. The full-scale test, scaled tests, and dynamic model each provided a major component of that understanding and indicated that the basic design of the structure is sound. The scaled tests indicated that HE placement in the structure and details of ceiling construction had little impact on gravel bed behavior and that aerosol leaks were most likely to occur at the gravel periphery. The dynamic model has indicated how dynamic behavior and aerosol collection efficiency are related to system design parameters, especially staging area volume. The full-scale test provided a direct measurement of a specific value for respirable release fraction, i.e., 3×10^{-3}, as well as other information on pressure, gravel motions, residual aerosols, and external aerosol deposits. Taken together the program components provide confidence in DOE's use of the Gravel Gertie to mitigate consequences of HE detonation during weapon assembly operations.

References

An61 Annberg, B. T.; "Review of Critical Flowmeters for GS Flow Measurements"; ASME 61-WA-181.

BA82 "Explosion Hazards and Evaluation; Baker et al.; Elsevier Press; 1982.

Co57 "Fallout Measurements From a Test of a Gravel Gertie (U)"; M. Cowan; SNLA, Ref Sym 7223(376); 1/15/57; SRD.

Co58 "April '57 Test of Gravel Gertie (U)"; M. Cowan; SCTM196-58(51); 5/58; CRD.

Gl80 Gladney, et al. "Nuclear Techniques for the Chemical Analysis of Environmental Materials"; Los Alamos Scientific Laboratory Report LA-8192-MS; January 1980

HN82 Holmes and Narver, Inc.; Gravel Gertie Test Structure Drawing; 1982.

JS-005-030-S1	Floor Plan
JS-005-030-S2	Grading & Backfill
JS-005-030-S3	Operating Bay Covering & Ceiling
JS-005-030-S4	Misc. Details
JS-005-030-S5	Catenary Cables, Lacing & Procedure
JS-005-030-S6	Catenary Cables, Hub & Ring Assy. & Lacing
JS-005-030-S7	Blast Bulkheads
JS-005-030-S8	Operating Bay Slab & Blast Shields
JS-005-030-S9	External Sampler Cable Tram
JS-005-030-S10	External Sampler Cable Tram Details
JS-005-030-S11	Corrugated Conduit, Shoring & Joints
JS-005-030-S12	Corrugated Conduit, Pre& Post-Shot Dim.
JS-005-030-S13	Tram Poles Stiffening Detail
JS-005-030-E1	Aerosol Sampling Conduit System
JS-005-030-E2	Aerosol Junction Box Details
JS-005-030-C1	Collector Tray Array

Ja63 "Model Experiments to Obtain the Pressure-Time Relationship at Various Points in the Gravel Gertie Structure (U)"; D. J. James, R. D. Rowe; AWRE Report No. E8/63; SRD.

Jt76 J. Throck Watson; Introduction to Mass Spectrometry: Biomedical, Environmental, and Forensic Applications; 1976

Lu69 "DIFOUT: A Model for Computation of Aerosol Transport and Diffusion in the Atmosphere;" R. E. Luna, H. W. Church, Sandia National Laboratories, Albuquerque, NM, January 1969, SC-RR-66-555.

MI74 "Filtration of Airborne Particles by Gravel Filters"; Miyamato, A. and Pohn, H. L.; Journal of Air Pollution Control Assoc.; Vol 24, No. 11, November 1974; pp 1051-1054.

Ne79 T. R. Neal, "Charge Rating System for a Confinement Vessel," Los Alamos Scientific Laboratory, University of California (January 15, 1979).

Nw82 G. J. Newton, et al, "High-Temperature--High-Pressure Cascade Impactor Design, Performance, and Data Analysis Methods," J. of Colloid and Interface Science, 87, No. 1, May 1982.

Pr53 Price, Ferretli, Schwartz; Analytical Chemistry, Vol 25, pp 322-323; 1953

PX1 Pantex Assembly Cell 8 Drawing List
D12-44-8A3 Floor Plan
D12-44-8A5 Architectural Sections and Elevations
D12-44-8A9 Safety Door
D12-44-8A12 Wall Framing Plan
D12-44-8A17 Catenary and Ceiling Details
D12-44-8A18 Catenary Layout
D12-44-8A20 Sections and Details

PX2 Original Pantex Drawings for NTS Gravel Gertie Test Structure

NTS-A-3 Test Structure at NTS - Plan

NTS-A-4 Test Structure at NTS - Sections

NTS-S-1 Test Structure at NTS - Wall Section

NTS-S-2 Test Structure at NTS - Catenary Cable Layout and Details

NTS-S-3 Test Structure at NTS - Storage By Layout Plan and Sections

NTS-S-4 Test Structure at NTS - Entrance Door

NTS-S-5 Test Structure at NTS - Backfill Plan

NTS-S-6 Test Structure at NTS - Tunnel Baffles

SL82 Sandia National Laboratory; Gravel Gertie Aerosol Measurement System Drawings; 1982.

14213 T87419	Sampler, Main Room (GGASP)
14213 LD-T88392	Drawing Tree--Gravel Gertie
14213 T88392	Aerosol Sampling Systems
14213 T88393	External Sampler Array--Horizontal & Vertical
14213 T88394	Weldment--Equipment Rack, External Array
14213 T88395	Vertical Mast Ext. Array

14213 T88396	Horizontal Beam Ext. Array
14213 T88397	Strong Back, External Array
14213 T88398	Weldment, Clevis, Sheave Mounting
14213 T88399	Bushing, CRES, Vertical Pivot
14213 T88401	Collector Tray Array
14213 T88402	Platform, Staging Area (GGESA)
14213 T88403	Pole Sampler Array
14213 T88994	Balloon Sampler Array
14213 T91745	Gravel Gertie Schematic

Sw82 "Blast Measurements for the Full-Scale Gravel Gertie Test at Nevada Test Site;" E. D. Esparza, W. T. Baker; Southwest Research Institute, San Antonio, TX; Dec. 1982; SWRI-7394.

Sw82b "Effects of Combustibles on Internal Blast Loads in the Damaged Weapons Facility--Final Report for Phase IV;" J. C. Hokanson, E. D. Esparza, R. Sandoval, W. E. Baker; Southwest Research Institute; September, 1982.

Th79 S. L. Thompson, CSQII--An Eulerian Finite Difference Program for Two-Dimensional Material Response--Part F, Materials Section, SAND77-1330 (Albuquerque: Sandia National Laboratories, 1979).

Wo63a "Grevel Gertie: Investigation Into the Effectiveness of Roof Mounding in the Case of an Incident (U)"; A. J. Wood; AWRE Report No. E9/63; SRD.

Wo63b "Gravel Gertie: Investigation Into the Effectiveness of the Side Walls (U)"; A. J. Wood; AWRE Report No. E10/63; SRD.

Appendix A
Subscale Test Details

Introduction

A set of five subscale tests was performed at Sandia's Coyote Test Field (CTF) near Bldg. 9927 on a 0.176-scaled version of the Gravel Gertie structure. Cell 8 at Pantex was used as a model for specifying the roof construction, operating bay dimensions, and staging area volume (Reference PX1).

Objectives

The objectives of the subscale test series were to:

a. Evaluate the effect of Cell 8 dropped ceiling on roof behavior;

b. Evaluate the effect of off-center HE charge on roof behavior;

c. Evaluate the aerosol capture efficiency of the gravel roof; and

d. Verify the performance of the primary aerosol sampling systems for use on the full-scale test.

Test Facility

A resuable test facility was constructed of steel pipe and weldments to produce a 0.176-scale replica of Cell 8. The basic structure is illustrated in Figures A-1, A-2, and A-3. The staging area beyond the right angle turn is representative of Cell 8 volume, but not its geometric configuration. The definition of the roof and high explosive charge varied with each test as different objectives were evaluated.

Test Description

Five subscale tests were performed in achieving the test objectives. The test variables included the HE charge size, HE charge position, and the roof construction. In all tests, the impervious outer weather covering used on Cell 8 was omitted. The tests are reviewed individually as to their objective(s), configuration, and results.

SGG 1 Roof Development. The first subscale test was performed to check out the test facility and to evaluate the concept of replica scaling as applied to Gravel Gertie. A spherical HE charge of 0.58 pounds of PBX 9501 was used. The test configuration is illustrated in Figure A-4.

The test results were as follows:

a. Because of premature firing, high-speed camera coverage was lost; only video tape was obtained.

HGB =	45.7 cm
HRR =	109.2 cm
GBT =	115.8 cm
DGB =	335.3 cm
HC =	99.1 cm
DRR =	182.9 cm
DW =	76.2 cm
RPT =	43.2 cm
DCR =	61.0 cm
LSA =	121.9 cm

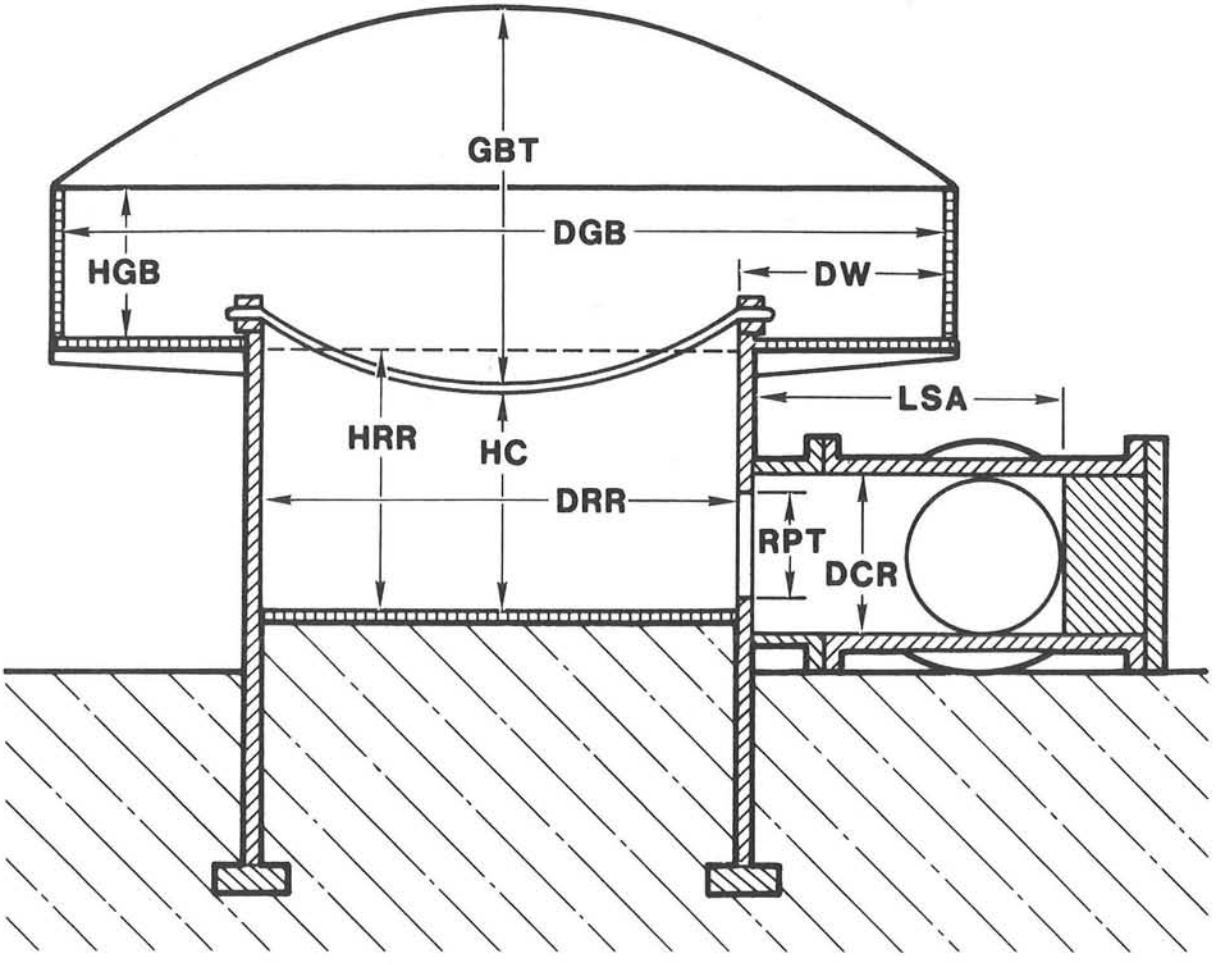

Figure A-1. Subscale Test Facility - Elevation View

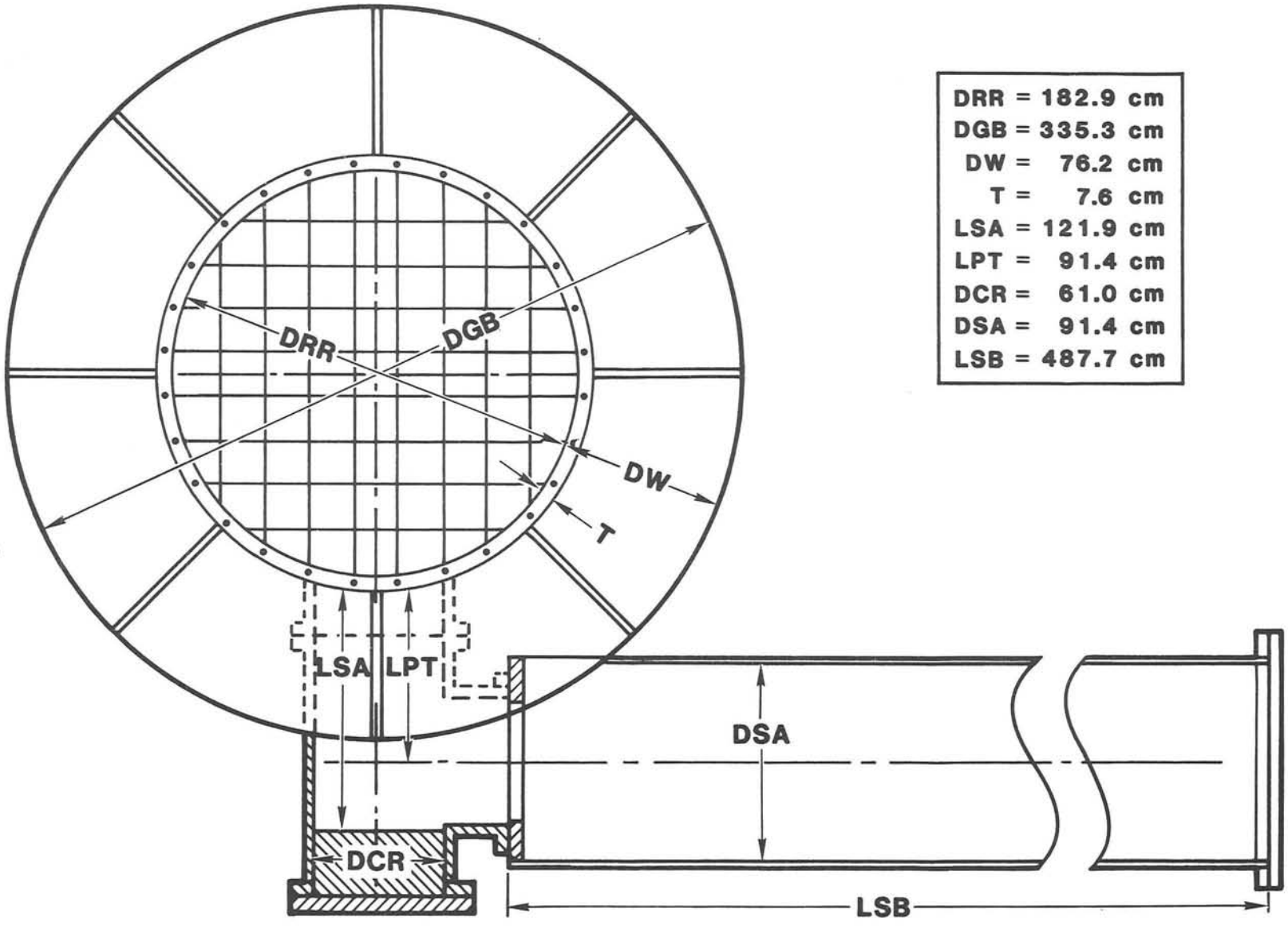

Figure A-2. Subscale Test Facility - Plan View

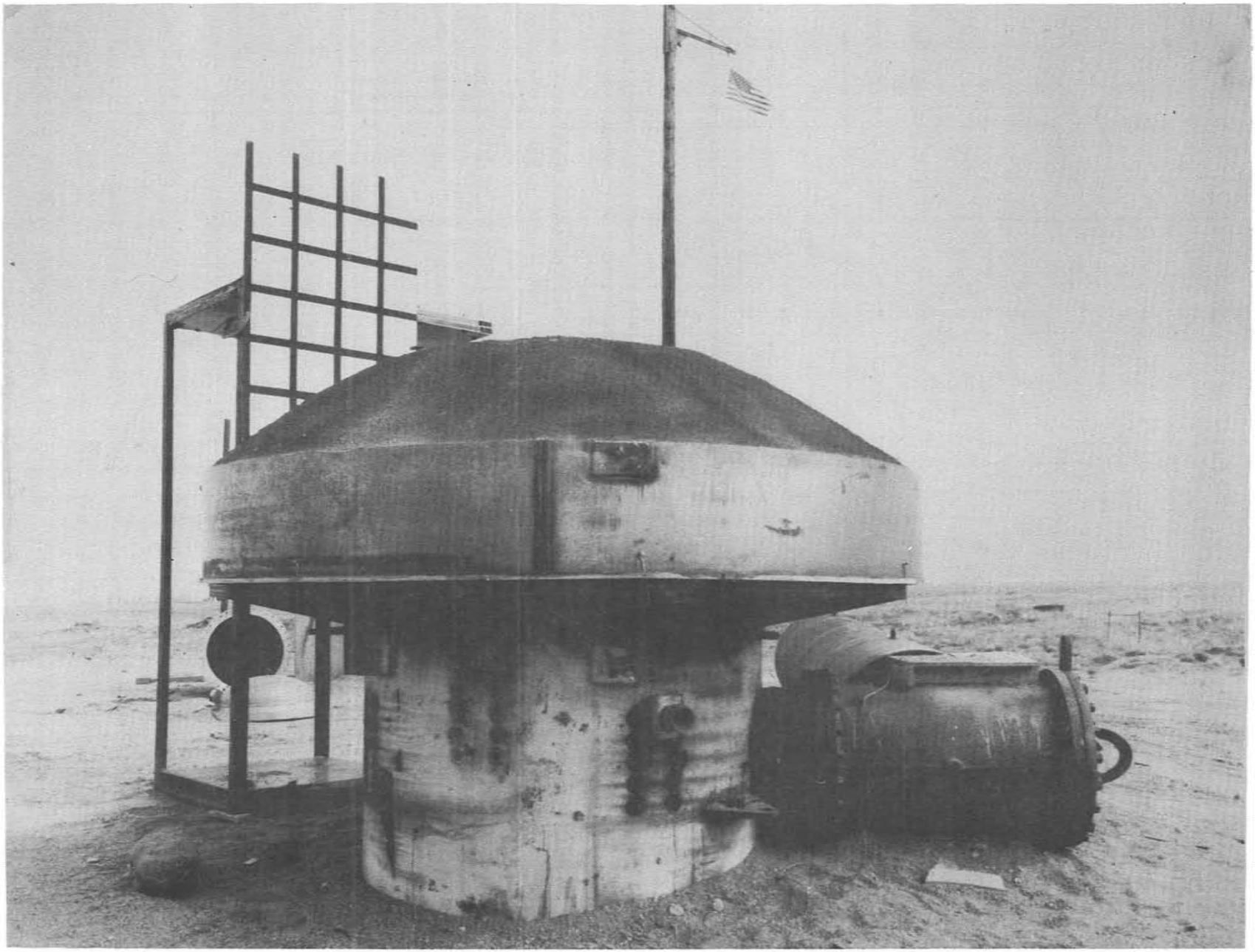

Figure A-3. Subscale Test Facility

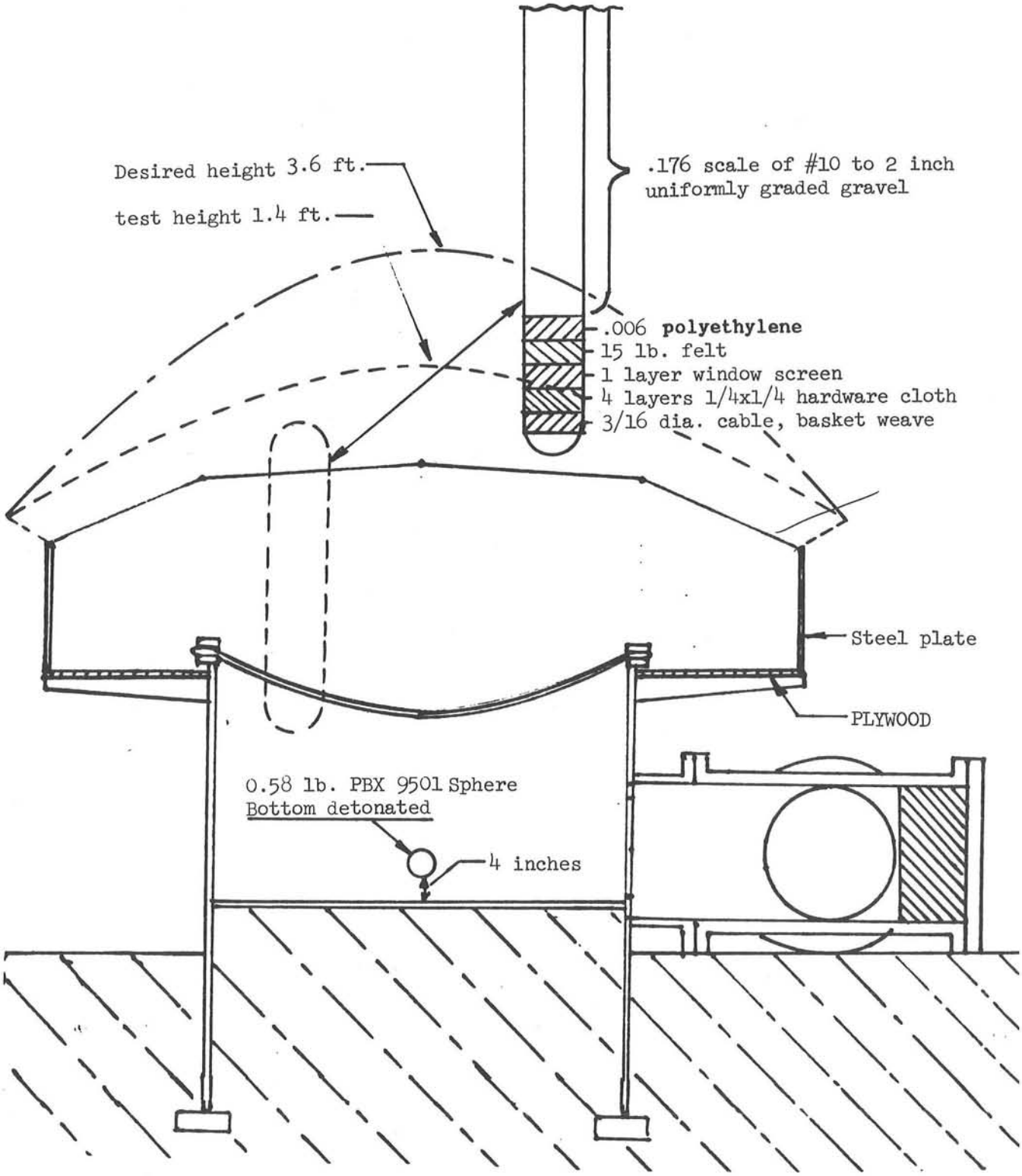

Figure A-4. SGG-1 Test Configuration and Performance

b. The gravel roof moved upward as a uniform "bubble" with no significant jetting--similar to the full-scale Gravel Gertie tests in the 1950s.

c. A crater was formed as a result of gravel spillover at the edge of the test fixture. The response to the explosion was in a camoufler mode in which there is no significant venting and no true ejecta as would occur for cratering mode.

d. The design goal for the displacement of the gravel top was 1.1 m (3.6 feet). The actual movement was 0.43 m (1.4 feet). At the time of the test, it was assumed that this shortfall was a result of an incorrect assumption in scaling the HE mass. However, subsequent testing showed the problem to be primarily in the loss of gas pressure at the steel cylinder/plywood interface. Because the plywood floor and outer rim were not rigidly connected to the cylinder, shear forces transmitted through the gravel were able to lift the plywood/rim assembly and allow a direct flow path for HE gases from the cell to the surroundings below the plywood.

e. The polyethylene and felt vapor barriers were not scaled properly. They were included essentially in full-scale configurations and were too strong. As a result, they were not severely damaged during the test. This problem in design was corrected in test SGG-3.

f. The cables supporting the roof did not break during the test as observed in the 1956 full-scale test series.

g. Because of fragment damage to the pressure transducer, no pressure data was obtained for this test.

SGG-2: Roof Development-Configuration. The second subscale test was designed to incorporate changes indicated by SGG-1, and achieve the desired (i.e., scaled) Gravel Gertie roof behavior. The test charge was increased to 0.522 kg (1.151 pounds) of PBX-9501. The test configuration is illustrated in Figure A-5.

The test results were as follows:

a. The gravel roof moved upward as a uniform "bubble" with no significant jetting.

b. An apparent crater was formed as a result of gravel spillover at the edge of the test fixture. The response to the explosion was in the camouflet mode.

c. The design goal for the upward movement of the gravel was 0.92 m (3.0 feet), the actual movement was 0.96 m (3.15 feet).

d. The cables supporting the roof did not break during the test.

e. High-speed films showed venting beneath the plywood floor which was not seen in the earlier test. This led to correction of the design for subsequent tests.

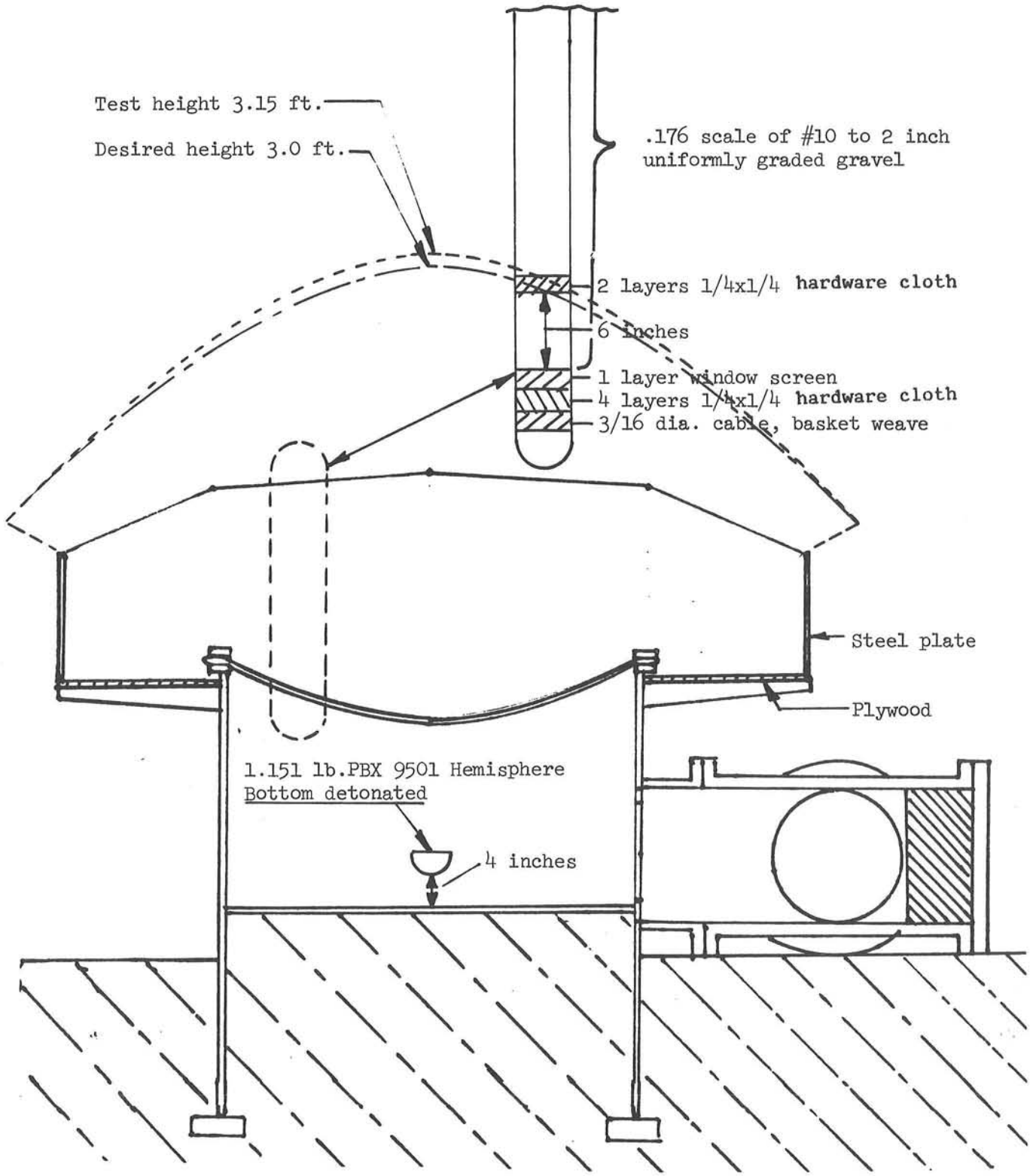

Figure A-5. SGG-2 Test Configuration and Performance

f. Figure A-6 is a plot of gauge pressure measured in the structure for test no. 2.

SGG-3: Off-Center Charge. The third subscale test was designed to evaluate the effect of an off-center HE charge on roof behavior. The configuration was the same as SGG-2 except (a) the charge was placed 0.15 m (6 inches) from the operating bay wall (scaled from minimum HE-to-wall separation permitted at Pantex), and (b) a scaled representation of the vapor barriers was included. The test configuration is illustrated in Figure A-7.

The test results were as follow:

a. The gravel roof moved upward as a uniform "bubble" with no significant jetting.

b. The shape of the "bubble" was essentially the same as for a centrally located HE charge.

c. The cables supporting the roof broke in the area above the charge. This may have resulted from the shape of the charge (a hemisphere) and/or proximity of the wall.

d. Figure A-8 is a plot of guage pressure inside the structure as a function of time for test SGG-3.

SGG-4: Gravel Roof Filter Efficiency Without Dropped Ceiling. The fourth subscale test was designed to verify the performance of primary aerosol sampling systems to be used on the full-scale test at NTS. The sealed interface between the steel cylinder and the skirt required that the HE charge be reduced to the original 0.26 kg (0.58 pounds) (SGG-1). Since no aerosol generator test devices with this quantity of HE existed in the inventory, 1.074 g of UO_2 powder was placed in the simulated operating bay together with 5 g of the secondary aerosol (Sb_2O_3 powder) planned for use at NTS. The UO_2 powder was not sized prior to testing. The Sb_2O_3 powder was sized before testing and Figure 2-19 shows the size distribution.

Two aerosol sampler trains were connected to a port (position RR of Figure A-9) in the side of the scaled assembly cell. One was the actual configuration of the in situ sampler (GGASP) to be used in the full-scale event. The second was a "straight-through" pipe and valve arrangement connected to a filter and impactor similar to that used in the GGASP. The objective of the test was to sample the tracer aerosols with similar instrumentation to evaluate the effect of losses in the more complex GGASP plumbing.

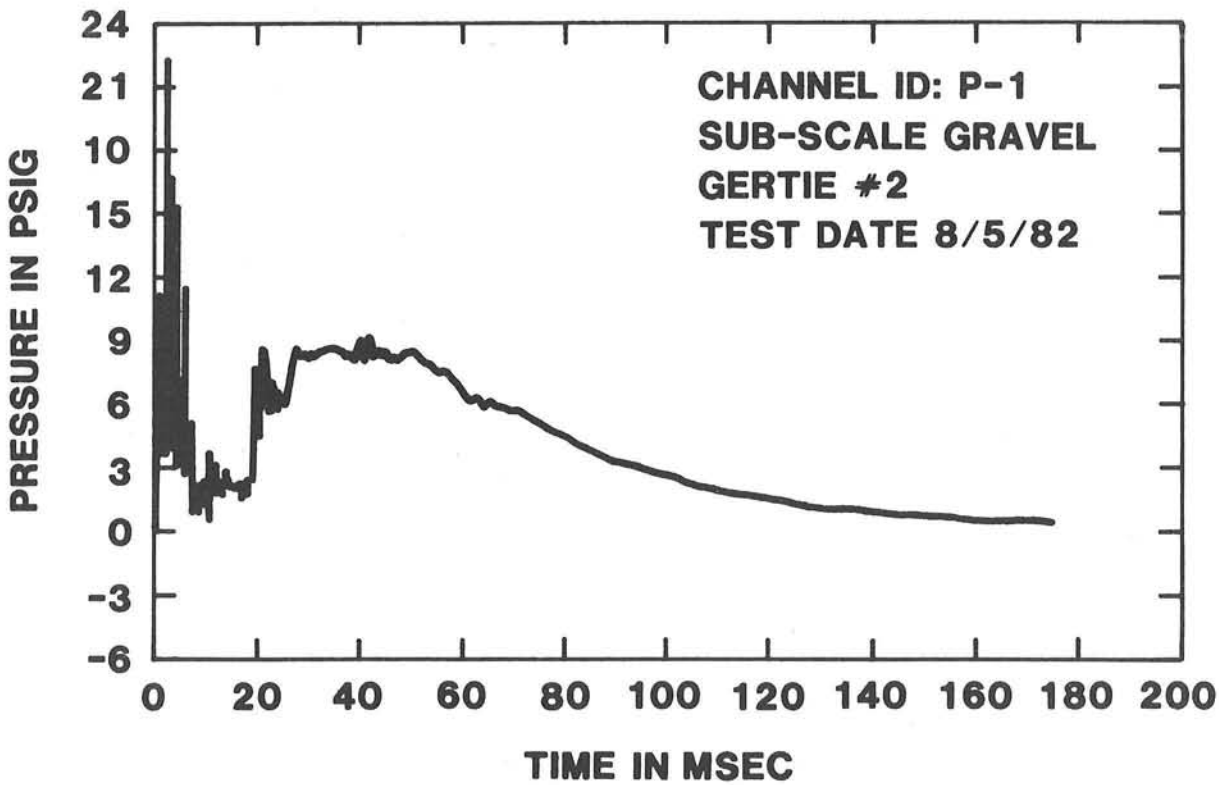

Figure A-6. Pressure Signature for Subscale Test No. 2

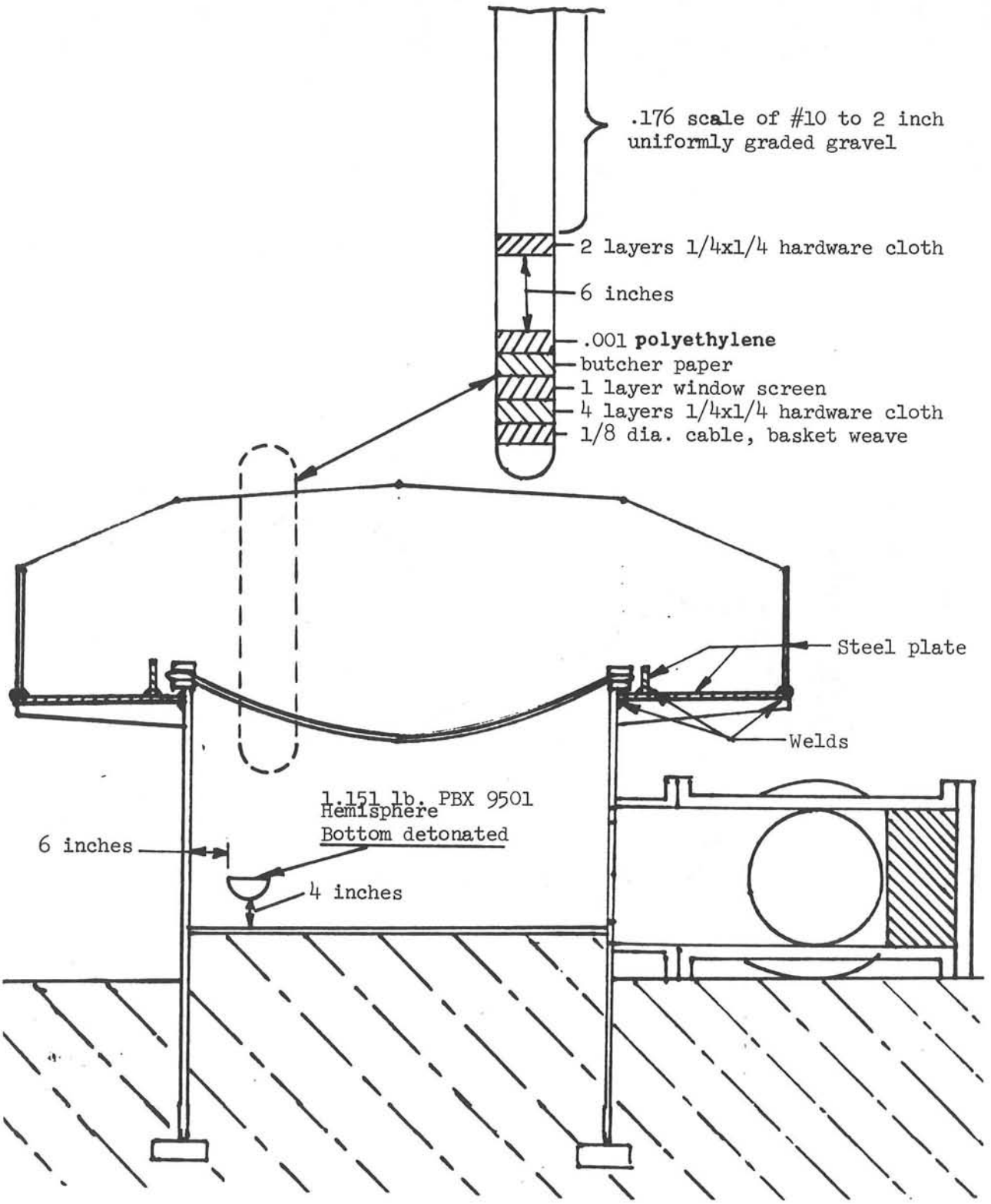

Figure A-7. SGG-3 Test Configuration

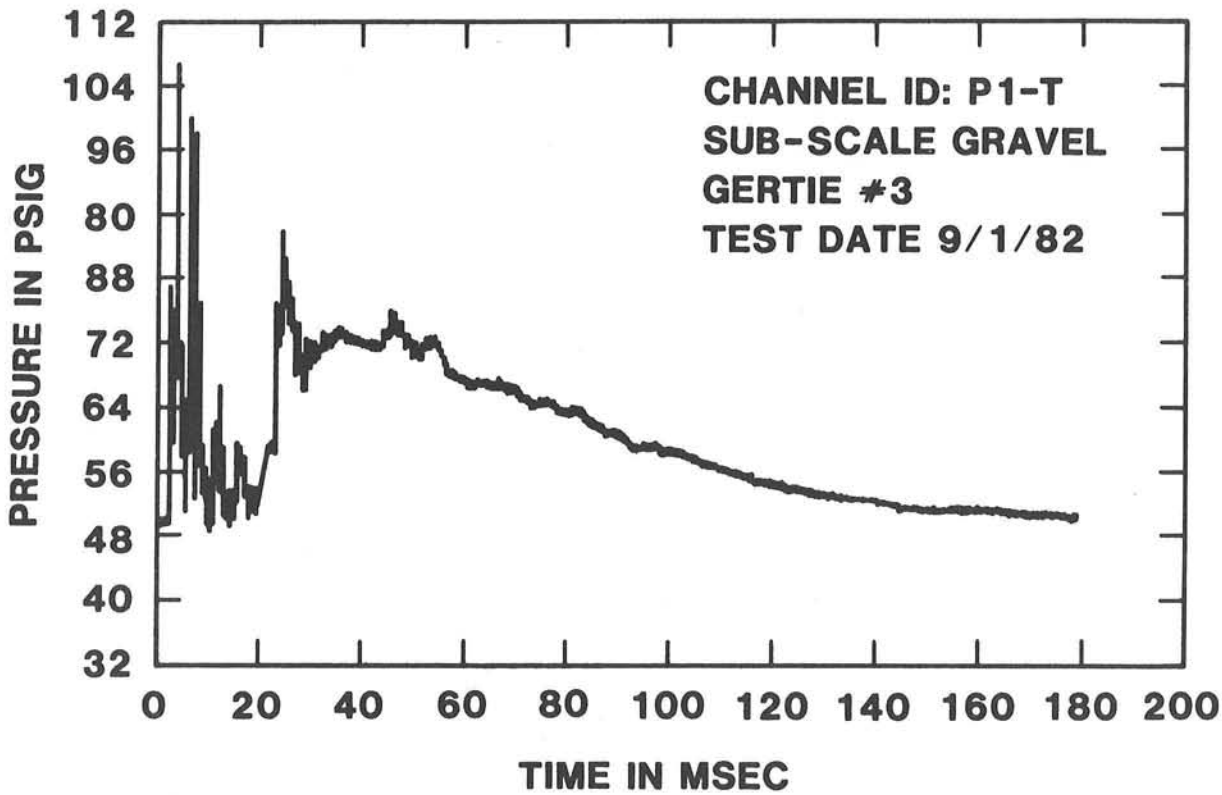

Figure A-8. Pressure Signature for Subscale Test No. 3

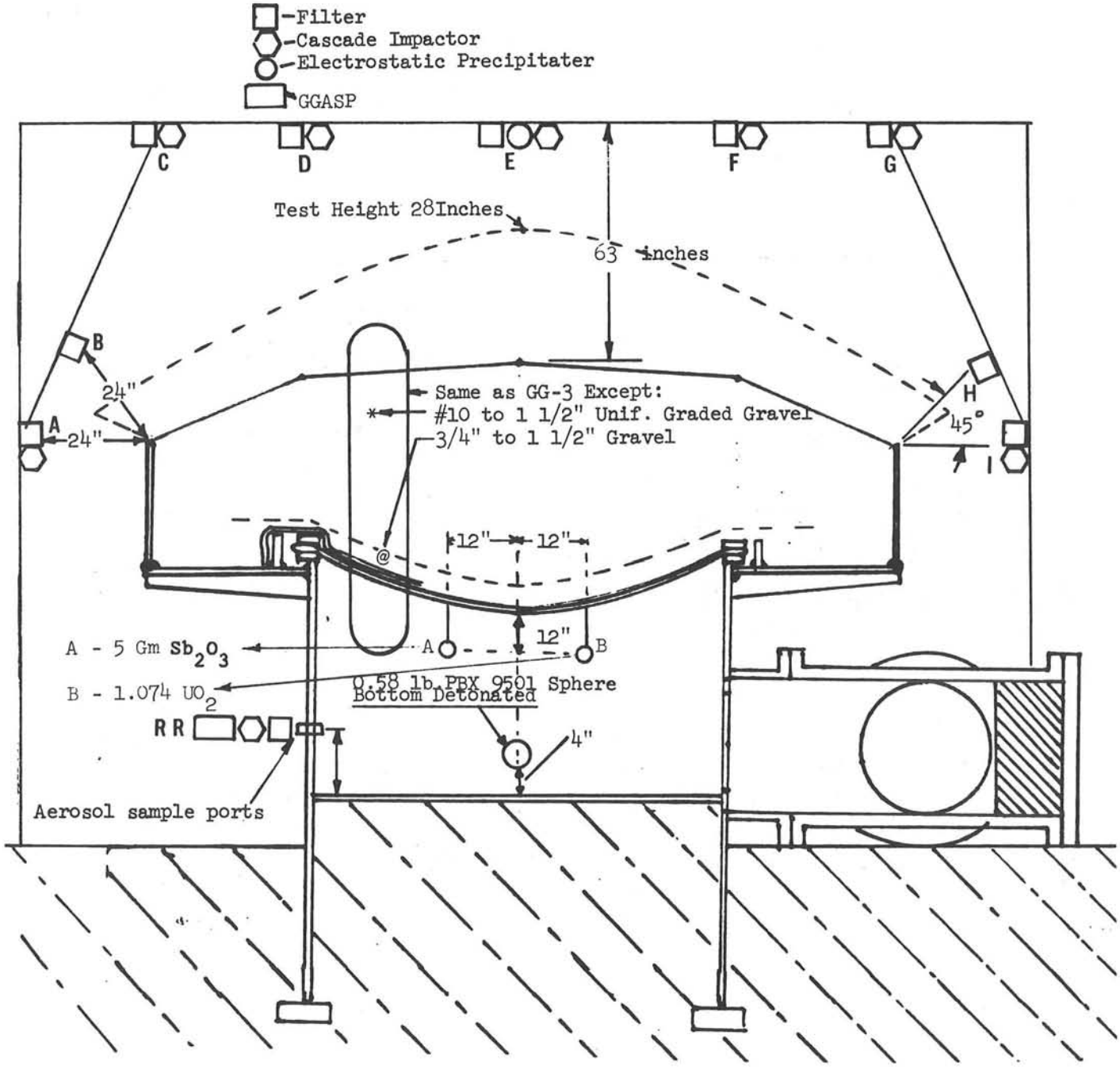

Figure A-9. SGG-4 Test Configuration

Aerosol samplers were also arranged over and around the test cell on a vertical plane passing through the center of the cell. This was an attempt to document the escape of the aerosols included in the test cell. The test configuration is illustrated in Figure A-9.

The SGG-4 test results are as follows:

a. The gravel roof moved upward as a uniform "bubble" with no significant jetting. The height achieved was 0.71 m (28 inches) above the as-built elevation.

b. An apparent crater was formed as a result of gravel spillover at the edge of the test fixture. The response to the explosion was in the camouflet mode.

c. The cables supporting the roof were not broken during the test.

d. Aerosol Sampling Results

Table A-1 summarizes the impactor and filter sampler data for test SGG-4. The GGASP samples indicated a uranium mass concentration inside the round room of 8.01 μg/ℓ for the 30 second period after detonation. A mass median aerodynamic diameter (MMAD) of 3.1 μm at 30 seconds after detonation was measured by the GGASP impactors. This is in good agreement with samples obtained from the filter and LMJ cascade impactor which sampled round room air at a sampling port adjacent to the GGASP port. These samples indicated a uranium mass concentration of 9.84 μg/ℓ during the initial 30 seconds after detonation and a MMAD of 3.6 μm. The average uranium concentration in the round room during the initial 30 seconds after detonation was therefore 8.93 μg/ℓ. A plot of the uranium particle size distribution in the round room for a LMJ impactor and one of the GGASP impactors is shown in Figures A-10 and A-11.

TABLE A-1
ROUND ROOM AEROSOL SAMPLER DATA FROM TEST SGG-4

SAMPLE ID NO.	LOCATION	TYPE	FLOW RATE (ℓ/min)	URANIUM MASS (ng)	CUM%	ECD (μm)	MMAD (μm)	T (min.)	URANIUM CONCENTRATION (μg/ℓ)	AVERAGE URANIUM CONCENTRATION (μg/ℓ)	TOTAL URANIUM AEROSOL (g)	TEST URANIUM MASS (g)	% AEROSOLIZATION IN STRUCTURE
G11001	RR	47F	4.8	1.39×10^4	-	-	-	0.5	5.79	8.93	5.07×10^{-2}	1.025	
G10041	RR	LMJC	16.5	2.30×10^4	19.1	12.20	3.6	0.5	13.9				4.95
G10042	RR	LMJC	16.5	1.54×10^4	32.5	7.55							
G10043	RR	LMJC	16.5	1.75×10^4	47.7	4.87							
G10044	RR	LMJC	16.5	1.40×10^4	59.9	2.97							
G10045	RR	LMJC	16.5	1.12×10^4	69.7	1.89							
G10046	RR	LMJC	16.5	1.05×10^4	78.8	1.18							
G10047	RR	LMJC	16.5	1.15×10^4	88.8	0.71							
G10048	RR	LMJC	16.5	1.33×10^4	-	-							
			TOTAL	1.15×10^5									
G1GASP47F	RR	47F	10.8	4.68×10^4	-	-	-	0.5	8.67				
G1GASP25F	RR	25F	10.8	4.53×10^4	-	-	-	0.5	8.39				
G1 MO5-1	RR	Mercer	1.4	4.03×10^1	1.9	7.07	1.4	0.5	6.97				
G1 MO5-2	RR	Mercer	1.4	1.91×10^2	5.8	4.67							
G1 MO5-3	RR	Mercer	1.4	2.58×10^2	11.0	3.17							
G1 MO5-4	RR	Mercer	1.4	3.50×10^2	18.2	2.14							
G1 MO5-5	RR	Mercer	1.4	3.34×10^2	25.1	1.61							
G1 MO5-6	RR	Mercer	1.4	2.21×20^3	70.4	1.08							
G1 MO5-7	RR	Mercer	1.4	3.54×10^2	77.7	0.72							
G1 MO5-8	RR	Mercer	1.4	1.09×10^3	-	-							
			TOTAL	4.88×10^3									
G1 M14-1	RR	Mercer	1.4	1.15×10^2	0.1	7.07	4.8	0.5	5.01				
G1 M14-2	RR	Mercer	1.4	2.28×10^2	0.3	4.67							
G1 M14-3	RR	Mercer	1.4	1.97×10^2	0.5	3.17							
G1 M14-4	RR	Mercer	1.4	2.46×10^2	0.7	2.14							
G1 M14-5	RR	Mercer	1.4	1.02×10^5	86.3	1.61							
G1 M14-6	RR	Mercer	1.4	8.22×10^3	93.2	1.08							
G1 M14-7	RR	Mercer	1.4	4.29×10^3	96.8	0.72							
G1 M14-8	RR	Mercer	1.4	3.80×10^3	-	-							
			TOTAL	1.19×10^5									

RR: Round Room Sampling Port (see Figure A-9)
LMJ: Lovelace Multijet Impactor
Mercer: Mercer Impactor

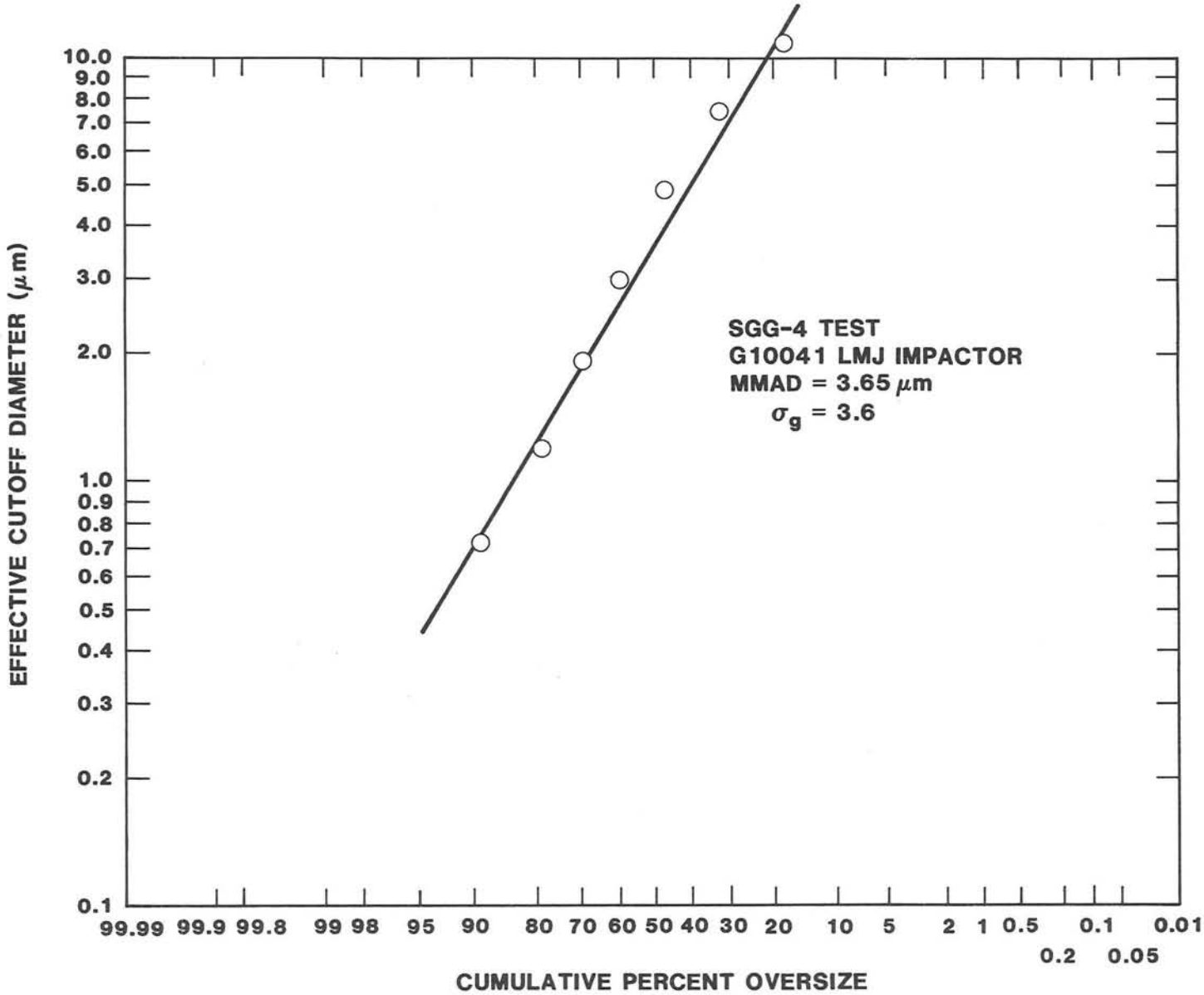

Figure A-10. LMJ Impactor Particle Size Distribution in Round Room for Subscale Test No. 4

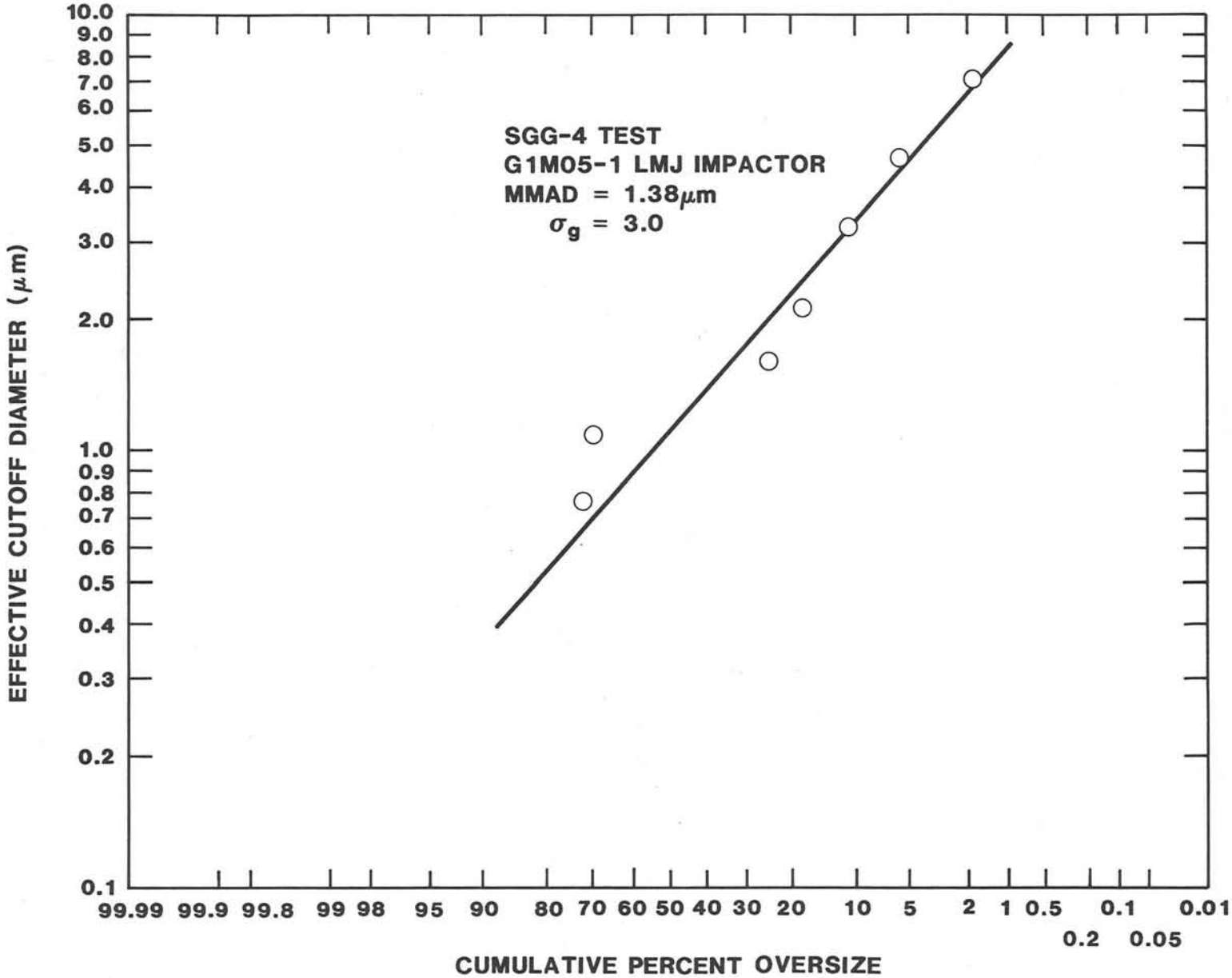

Figure A-11. GGASP Impactor Particle Size Distribution in Round Room for Subscale Test No. 4

A round room free volume of 2.97 m^3 and a staging room volume of 3.11 m^3 was used to calculate the total volume of gas available for sampling by the GGASP and impactor/filter assembly. Ninety-three percent of of the combustion products, round room air, and staging room air were assumed to be available for sampling. This is the same assumption made for the full-scale test gas volume calculation in Appendix J. A total volume of gas in the subscale structure was estimated to be 5.68×10^3 ℓ. A total respirable uranium particle mass of 5.07×10^{-2} g was produced in the structure, assuming a spatially uniform uranium mass concentration of 8.93 μg/ℓ. Based upon an initial UO_2 powder mass of 1.025 g, five percent of the initial UO_2 mass was aerosolized to a respirable size (aerodynamic diameter $\leq$10 μm).

e. Figure A-12 is a plot of guage pressure inside the structure as a function of time.

f. Results of SEM-EDS Analysis

Carbon planchet samples from the GGASP used in Subscale Gravel Gertie Test No. 4 were analyzed by SEM-EDS. Particles examined ranged in size from $\leq$ 0.1 μm to 2 μm. All particles analyzed contained a mixture of U, Fe, Cu, Zn, Si, Al, and Ba. The particles were physical mixtures of uranium, metal components and "dirt." It was not possible to resolve any structural details of the uranium constituents contained within the particles. Figure A-13 shows an area of this sample. All of the particles in this field of view which were analyzed contained uranium. Figure A-14 shows a typical x-ray spectra measured from one of the particles examined. Characteristic lines of U, Cu, Fe, Zn, Al, and Ba were observed.

Table A-2 summarizes the data for samplers located on the vertical overhang outside the round room (see Figure A-9). Impactors located at positions A and G indicated an average uranium concentration in the released plume of 4.8×10^{-2} μg/ℓ. The uranium concentration at position A was 5.8×10^{-2} μg/ℓ or about two times higher than at position G (2.6×10^{-2} μg/ℓ). This fact is explainable from photometric observations which show a denser cloud at position A than at positions G and H. The median aerodynamic diameter (MMAD) of uranium particles in the released cloud was about 4.2 μm averaged over the cloud volume. Figures A-15 and A-16 show log-probability plots of uranium particle-size distributions measured by impactors at A and G positions. A measurement of the released cloud spatial profile was made photometrically. An estimate of the stabilized cloud volume during the time of sampling (one-minute post-detonation) was made from the cloud profile. A cloud volume as large as 9.62×10^3 and as small as 1.1×10^3 ℓ was determined. Assuming an average uranium mass concentration for the cloud of 4.8×10^{-2} μg/ℓ, an upper bound of 4.6×10^{-4} g and a lower bound of 5.3×10^{-5} g of respirable-size uranium particles in the cloud was determined. Based upon the measured respirable-size uranium mass produced in the Gravel Gertie structure (4.97×10^{-2} g), a release fraction (respirable uranium) of no larger than 9.1×10^{-3} and no smaller than 1.1×10^{-3} was calculated. This estimate is in agreement with the respirable release fraction estimate (4×10^{-3}) of the full-scale Gravel Gertie test at NTS.

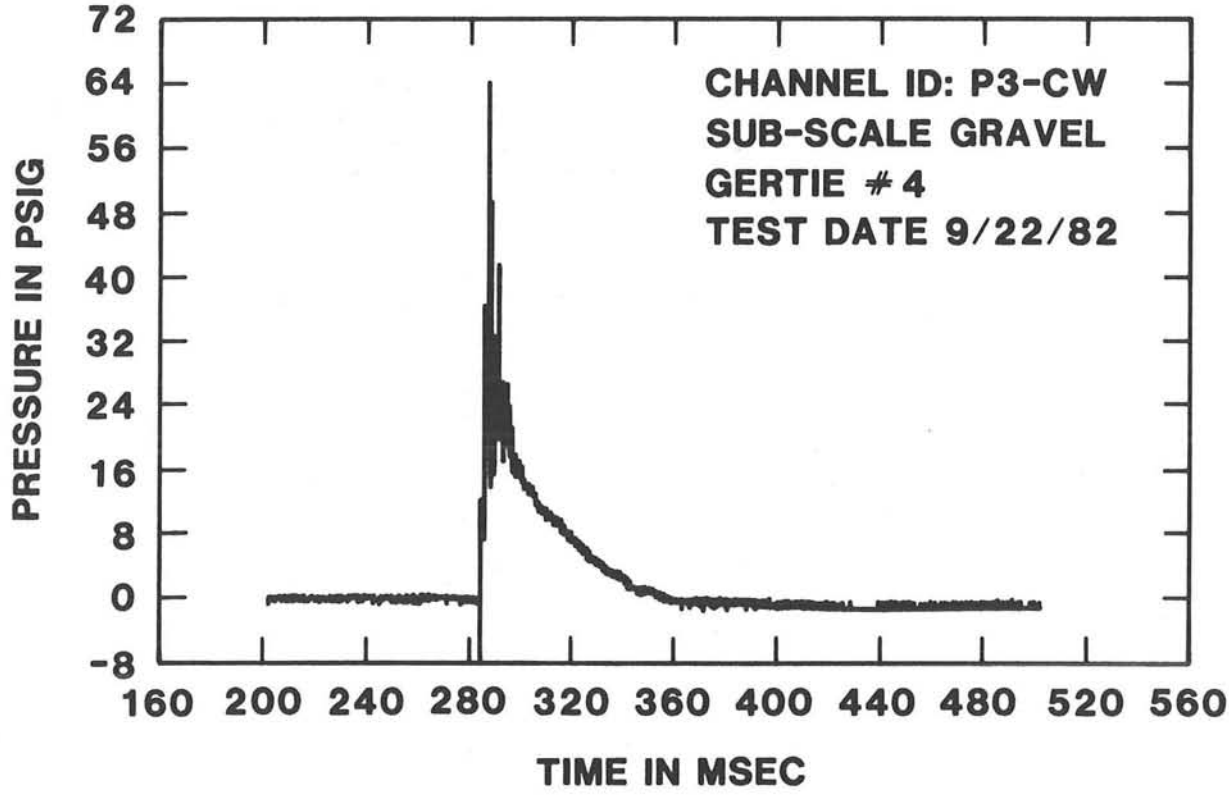

Figure A-12. Pressure Signature for Subscale Test No. 4

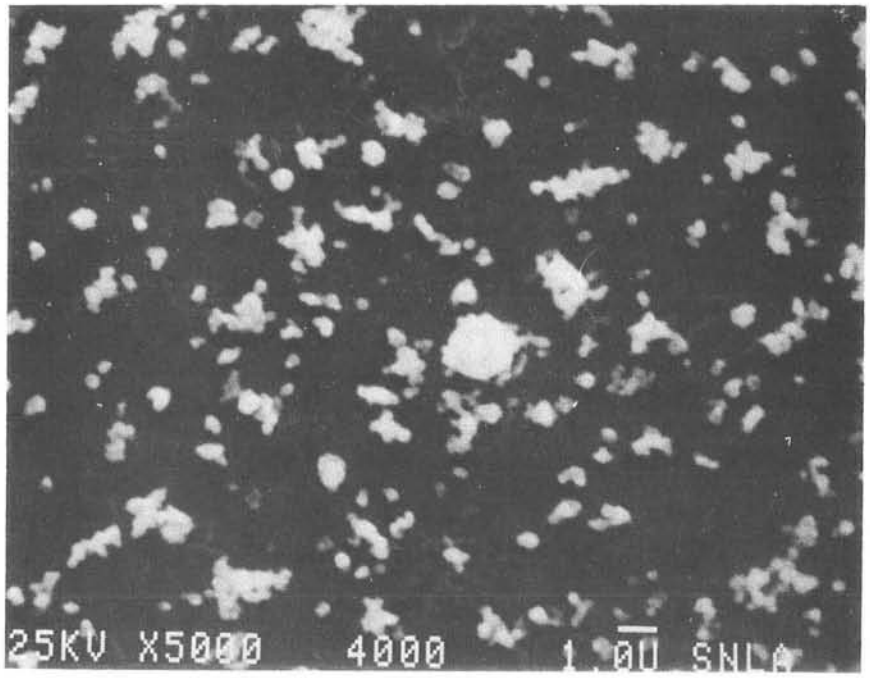

Figure A-13. Planchet From SGG-4 GGASP Chamber. A large number of particles rich in U, Fe, Cu, Zn, Si, Aℓ, and Ba. Size ranges from <0.1 μm to 2 μm.

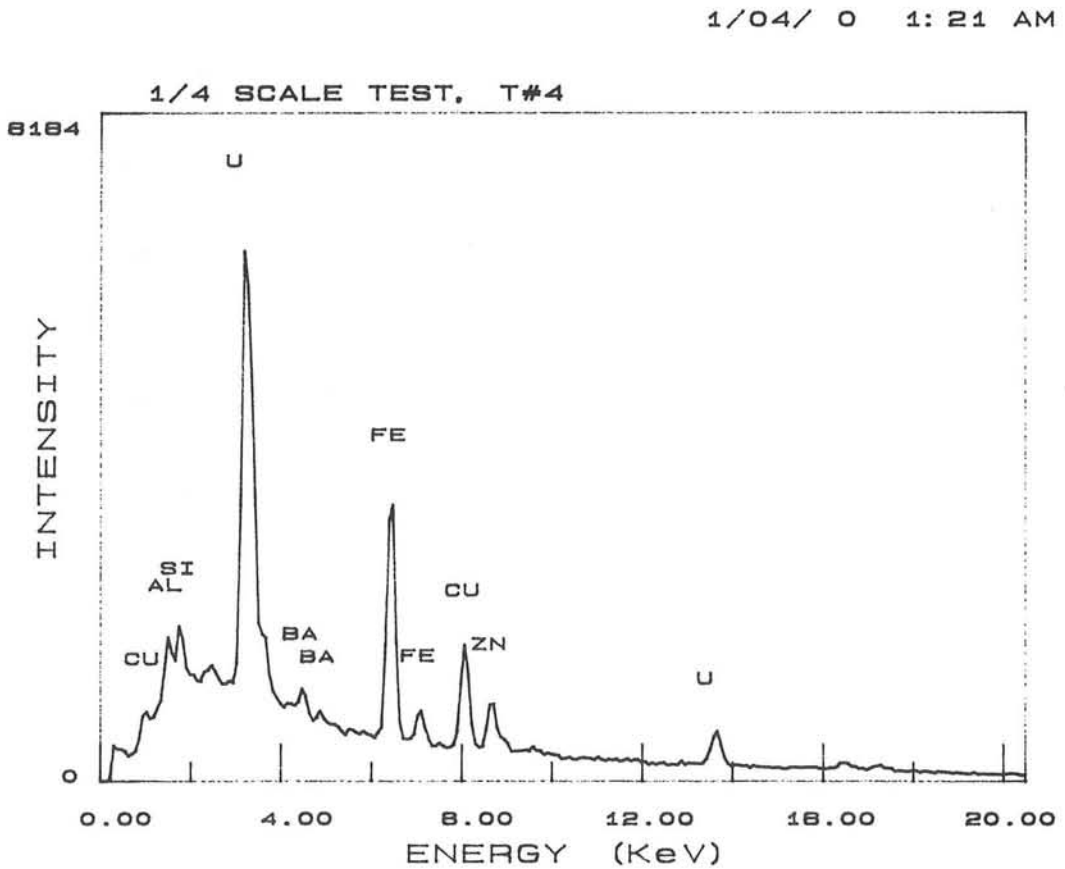

Figure A-14. X-ray Spectra from a Typical Particle Taken from SGG-4 GGASP Sample. Characteristic lines for U, Cu, Fe, Zn, Si, Aℓ, and Ba are clearly shown.

TABLE A-2
EXTERNAL AEROSOL SAMPLER DATA FROM TEST SGG-4

SAMPLE ID NO.	LOCATION	TYPE	FLOW RATE (ℓ/min)	URANIUM MASS (ng)	CUM%	ECD (μm)	MMAD (μm)	T (min.)	URANIUM CONCENTRATION ($\mu g/\ell$)	AVERAGE URANIUM CONCENTRATION ($\mu g/\ell$)	AVERAGE CLOUD VOLUME (ℓ)	URANIUM AEROSOL IN CLOUD (g)
G11010	A	47F	4.8	1.06×10^{2}	-	-	-	1	2.2×10^{-2}	4.8×10^{-2}	9.62×10^{3}(M)	4.6×10^{-4}(M)
G10051	A	LMJP	19.0	5.30×10^{2}	29.3	11.68	6.2	1	9.5×10^{-2}		1.1×10^{3}(N)	5.3×10^{-5}(N)
G10052	A	LMJP	19.0	2.45×10^{2}	42.8	7.27						
G10053	A	LMJP	19.0	8.79×10^{1}	47.7	4.68						
G10054	A	LMJP	19.0	5.04×10^{1}	50.5	2.86						
G10055	A	LMJP	19.0	6.66×10^{2}	87.3	1.82						
G10056	A	LMJP	19.0	1.19×10^{2}	93.8	1.14						
G10057	A	LMJP	19.0	6.29×10^{1}	97.4	0.70						
G10058	A	LMJP	19.0	3.84×10^{1}	-	-						
			TOTAL	1.81×10^{3}								
G10091	G	LMJN	18.9	0*	0	11.40	2.0	1	2.6×10^{-2}			
G10092	G	LMJN	18.9	3.24×10^{1}*	6.6	7.09						
G10093	G	LMJN	18.9	3.09×10^{1}*	12.9	4.57						
G10094	G	LMJN	18.9	6.39×10^{1}*	25.9	2.79						
G10095	G	LMJN	18.9	2.03×10^{2}*	67.4	1.77						
G10096	G	LMJN	18.9	5.79×10^{1}*	79.2	1.11						
G10097	G	LMJN	18.9	6.09×20^{1}*	91.6	0.68						
G10098	G	LMJN	18.9	4.14×20^{2}*	-	-						
			TOTAL	4.90×10^{2}								

A: See Figure A-8
G: See Figure A-8
LMJ: Lovelace Multijet Cascade impactor
47F: 47mm Cellulose Nitrate Filter
25F: 25mm Cellulose Nitrate Filter
*: These values are below the limit of detectability (71ng)
M: Maximum
N: Minimum

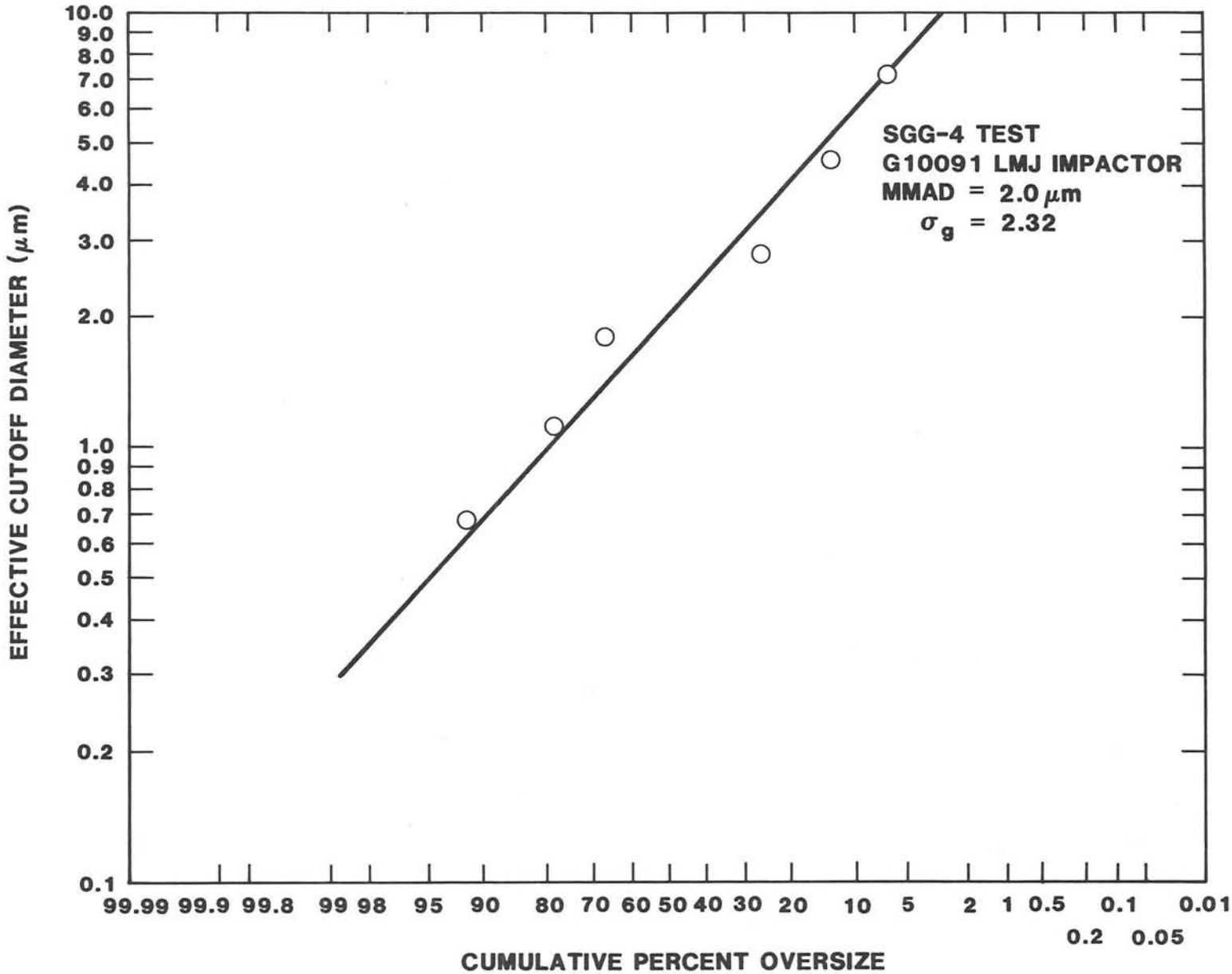

Figure A-15. Uranium Particle Size Distribution at Position G on Subscale Test No. 4

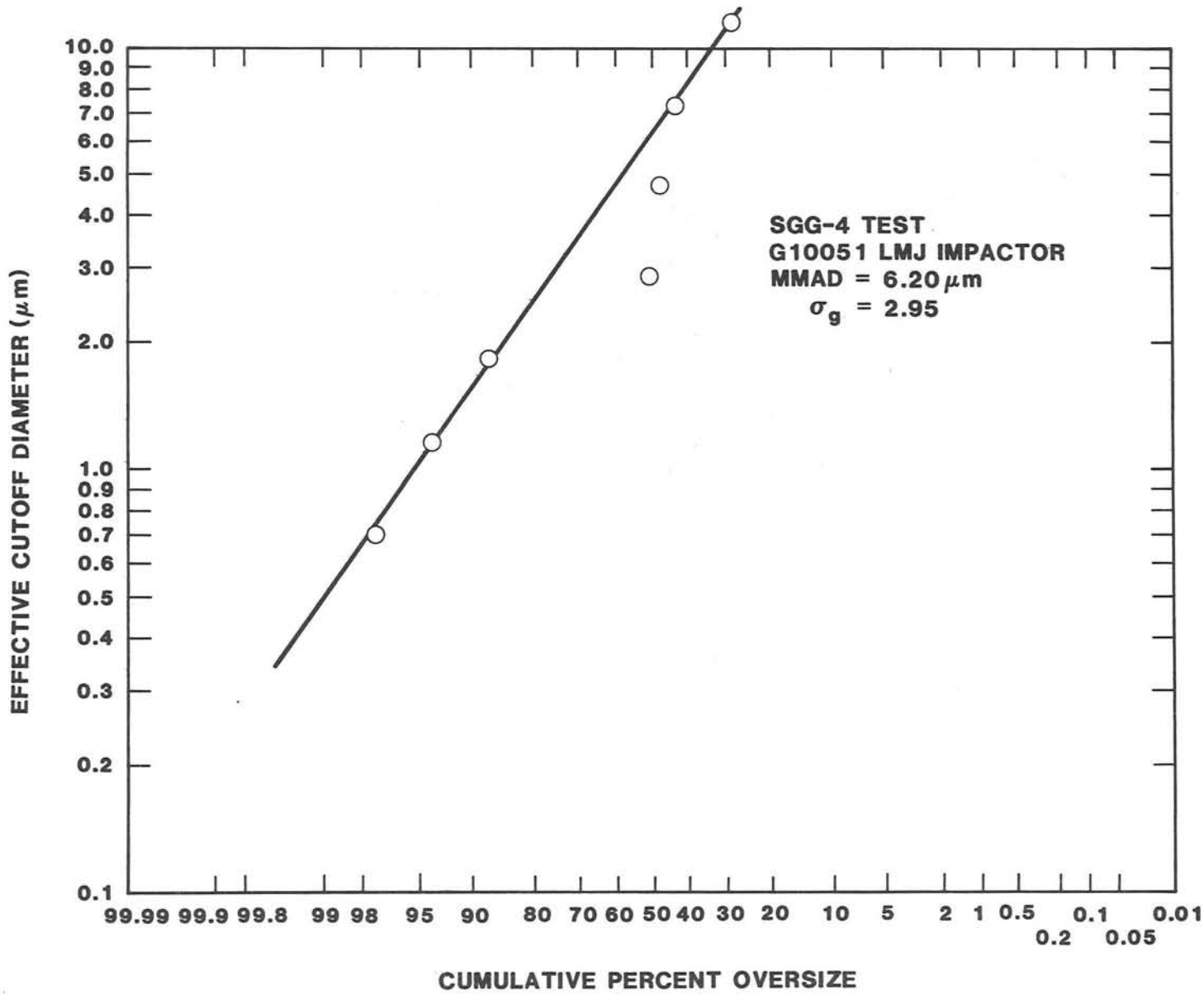

Figure A-16. Uranium Particle Size Distribution at Position A on Subscale Test No. 4

SGG-5: Gravel Roof Filter Efficiency With Dropped Ceiling. The fifth subscale test was designed to simulate the as-built Gravel Gertie configuration at NTS, and, in particular, to evaluate the effect on roof behavior of the dropped ceiling used in Cell 8 and other cells at Pantex. The test configuration was essentially the same as SGG-4, the principal differences being the addition of (a) a scaled gypsum board ceiling, (b) cable cutters to assure collapse of the ceiling following the HE explosion, and (c) "salting" of the gravel under the painted layer to visualize the cloud of escaping gas. The test configuration is illustrated in Figure A-17.

The test results are as follows:

a. The gravel roof moved upward as a uniform "bubble" with no significant jetting.

b. Gravel spilled over the edge of the test fixture as in previous tests, but there was complete collapse of the ceiling as a result of successful operations of the cable cutters.

c. The hardware cloth and window screen bridged in some areas on the floor of the cell, leaving air pockets in the collapsed roof.

d. The vapor barriers (polyethelene and butcher paper as a surrogate for roofing felt) and the dropped ceiling (gypsum board) fragmented sufficiently to give the aerosols free access to the gravel roof.

Aerosol Sampling Results

Tables A-3 and A-4 summarize the aerosol results for test SSG-5. Cascade impactor and filter samples indicated an average uranium aerosol mass concentration of 14.5 μg/ℓ inside the round room during the initial 51 seconds after detonation. A median aerodynamic diameter of ~1.8 μm was indicated by the same samples for this time period. A plot of the uranium particle size distribution inside the structure is shown in Figure A-18. A round room free volume of 2.97 m^3 and a staging room volume of 3.11 m^3 was used to calculate the total volume of gas available for sampling in the structure. Ninety-three percent of the round room and staging room volume were assumed to be available for sampling by the GGASP samplers. The total volume of gas available for sampling in the structure was estimated to be 5.68 m^3. Assuming a spatially uniform mass concentration of 14.5 μg/ℓ, a total respirable uranium aerosol mass in the structure was estimated to be 8.2×10^{-2} g. Based upon an initial UO_2 powder mass of 1.025 g, eight percent of the initial UO_2 mass was aerosolized to a respirable size.

Table A-4 summarizes the analytical results of samples taken external to the subscale structure. Impactors and filters indicated an average uranium aerosol concentration in the released cloud of 4.75×10^{-2} μg/ℓ. The median aerodynamic uranium particle diameter ranged from 1.2 ℓm (location C) to 4.0 μm (location E).

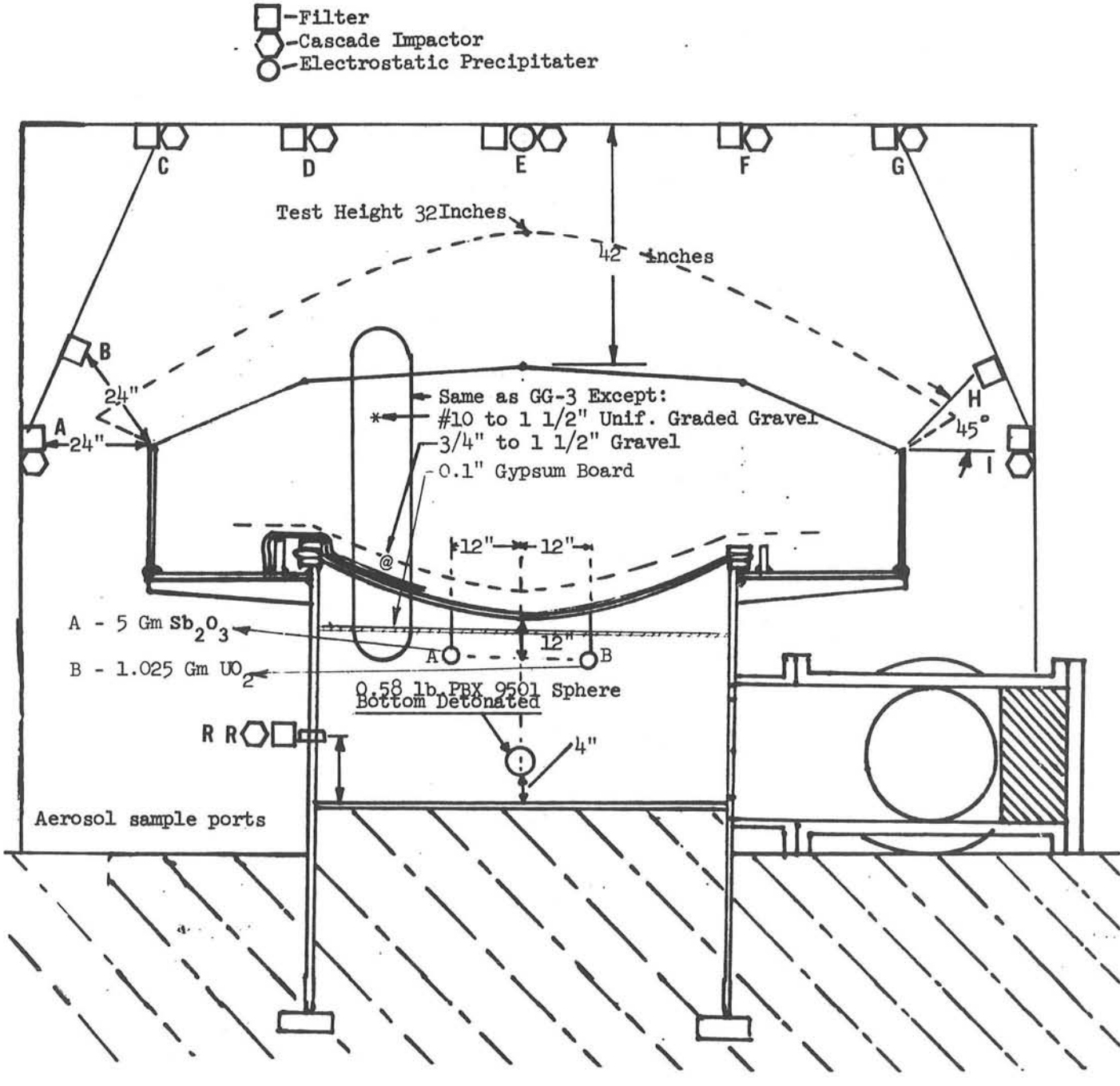

Figure A-17. SGG-5 Test Configuration

TABLE A-3
ROUND ROOM AEROSOL SAMPLER DATA FROM TEST SGG-5

SAMPLE ID NO.	LOCATION	TYPE	FLOW RATE (ℓ/min)	URANIUM MASS (ng)	Σ%	ECD (μm)	MMAD (μm)	T (min.)	URANIUM CONCENTRATION (μg/ℓ)	AVERAGE URANIUM CONCENTRATION (μg/ℓ)	URANIUM AEROSOL IN STRUCTURE (g)	TEST URANIUM MASS IN STRUCTURE (g)	% AEROSOLIZATION IN STRUCTURE
G20051	RR	LMJH	18.9	6.95×10^{3}	1.3	11.40	1.4	0.85	3.3×10^{1}	14.5	8.2×10^{-2}	1.025	8.0
G20052	RR	LMJH	18.9	1.98×10^{4}	5.0	7.05							
G20053	RR	LMJH	18.9	2.81×10^{4}	10.3	4.55							
G20054	RR	LMJH	18.9	4.62×10^{4}	19.0	2.77							
G20055	RR	LMJH	18.9	5.96×10^{4}	30.2	1.76							
G20056	RR	LMJH	18.9	1.38×10^{5}	56.1	1.10							
G20057	RR	LMJH	18.9	1.32×10^{5}	80.9	0.66							
G20058	RR	LMJH	18.9	1.02×10^{5}	-	-							
			TOTAL	5.32×10^{5}									
G20071	RR	LMJH	11.5	6.12×10^{3}	6.7	14.61	2.1	0.85	9.3				
G20072	RR	LMJH	11.5	1.00×10^{4}	17.7	9.09							
G20073	RR	LMJH	11.5	8.50×10^{3}	27.1	5.86							
G20074	RR	LMJH	11.5	1.21×10^{4}	40.4	3.57							
G20075	RR	LMJH	11.5	9.44×10^{3}	50.8	2.27							
G20076	RR	LMJH	11.5	7.10×10^{3}	58.6	1.42							
G20077	RR	LMJH	11.5	7.71×10^{3}	67.1	0.87							
G20078	RR	LMJH	11.5	2.99×10^{4}	-	-							
			TOTAL	9.09×10^{4}									
G21004	RR	47F	4.8	4.74×10^{3}	-	-		0.85	1.16				

RR: Round Room Sampling Port (see Figure A-17)
LMJ: Lovelace Multijet Impactor
47F: 47 mm Diameter Cellulose Nitrate Filter

TABLE A-4
EXTERNAL AEROSOL SAMPLER DATA FROM TEST SGG-5

SAMPLE ID NO.	LOCATION	TYPE	FLOW RATE (ℓ/min)	URANIUM MASS (ng)	%	ECD (μm)	MMAD (μm)	URANIUM MASS CONCENTRATION (μg/ℓ)	AVERAGE URANIUM CONCENTRATION (μg/ℓ)	AVERAGE CLOUD VOLUME (ℓ)	URANIUM AEROSOL IN CLOUD (g)
G20091	A	LMJN	18	8.46×10^{2}	13.7	11.68	*	*	4.75×10^{-2}	3.0×10^{3}	1.42×10^{-4}
G20092	A	LMJN	18	4.12×10^{3}	80.2	7.27					
G20093	A	LMJN	18	5.30×10^{2}	88.8	4.68					
G20094	A	LMJN	18	1.43×10^{2}	91.1	2.86					
G20095	A	LMJN	18	1.31×10^{2}	93.2	1.82					
G20096	A	LMJN	18	1.06×10^{2}	94.9	1.14					
G20097	A	LMJN	18	1.94×10^{2}	98.1	0.70					
G20098	A	LMJN	18	1.22×10^{2}	-	-					
		TOTAL		6.19×10^{2}							
G20021	C	LMJF	18	1.49×10^{2}	0.33	11.68	1.2	2.47×10^{-1}			
G20022	C	LMJF	18	1.76×10^{2}	0.73	7.23					
G20023	C	LMJF	18	1.16×10^{2}	0.99	4.66					
G20024	C	LMJF	18	2.51×10^{3}	6.63	2.84					
G20025	C	LMJF	18	5.57×10^{3}	19.1	1.81					
G20026	C	LMJF	18	2.07×10^{4}	65.7	1.13					
G20027	C	LMJF	18	9.89×10^{3}	87.9	0.68					
G20028	C	LMJF	18	5.34×10^{3}	-	-					
		TOTAL		4.44×10^{4}							
G20041	E	LMJP	18	2.62×10^{2}	24.5	11.68	4.0	6.11×10^{-3}			
G20042	E	LMJP	18	9.09×10^{1}	33.0	7.27					
G20043	E	LMJP	18	2.08×10^{1}	52.4	4.68					
G20044	E	LMJP	18	5.94×10^{1}	58.0	2.86					
G20045	E	LMJP	18	1.69×10^{2}	73.7	1.82					
G20046	E	LMJP	18	8.34×10^{1}	81.6	1.14					
G20047	E	LMJP	18	7.44×10^{1}	88.5	0.70					
G20048	E	LMJP	18	1.22×10^{2}	-	-					
		TOTAL		1.07×10^{3}							
G21001	C	47F	4.9	1.34×10^{2}		-	-	2.7×10^{-3}			
G21002	E	47F	4.9	4.25×10^{2}		-	-	8.7×10^{-3}			
G21005	B	47F	4.8	4.25×10^{2}		-	-	8.7×10^{-3}			
G21007	A	47F	4.9	2.45×10^{3}		-	-	5.0×10^{-2}			
G21008	A	47F	4.9	4.55×10^{2}		-	-	9.5×10^{-3}			
G21010											

A,B,C,E,H,I: Location of samplers on external array (see Figure A-17)
LMJ: Lovelace Multijet Impactor
47F: 47mm diameter filter
25F: 25 mm diameter filter
*: Values not determinable because of leaking impactor

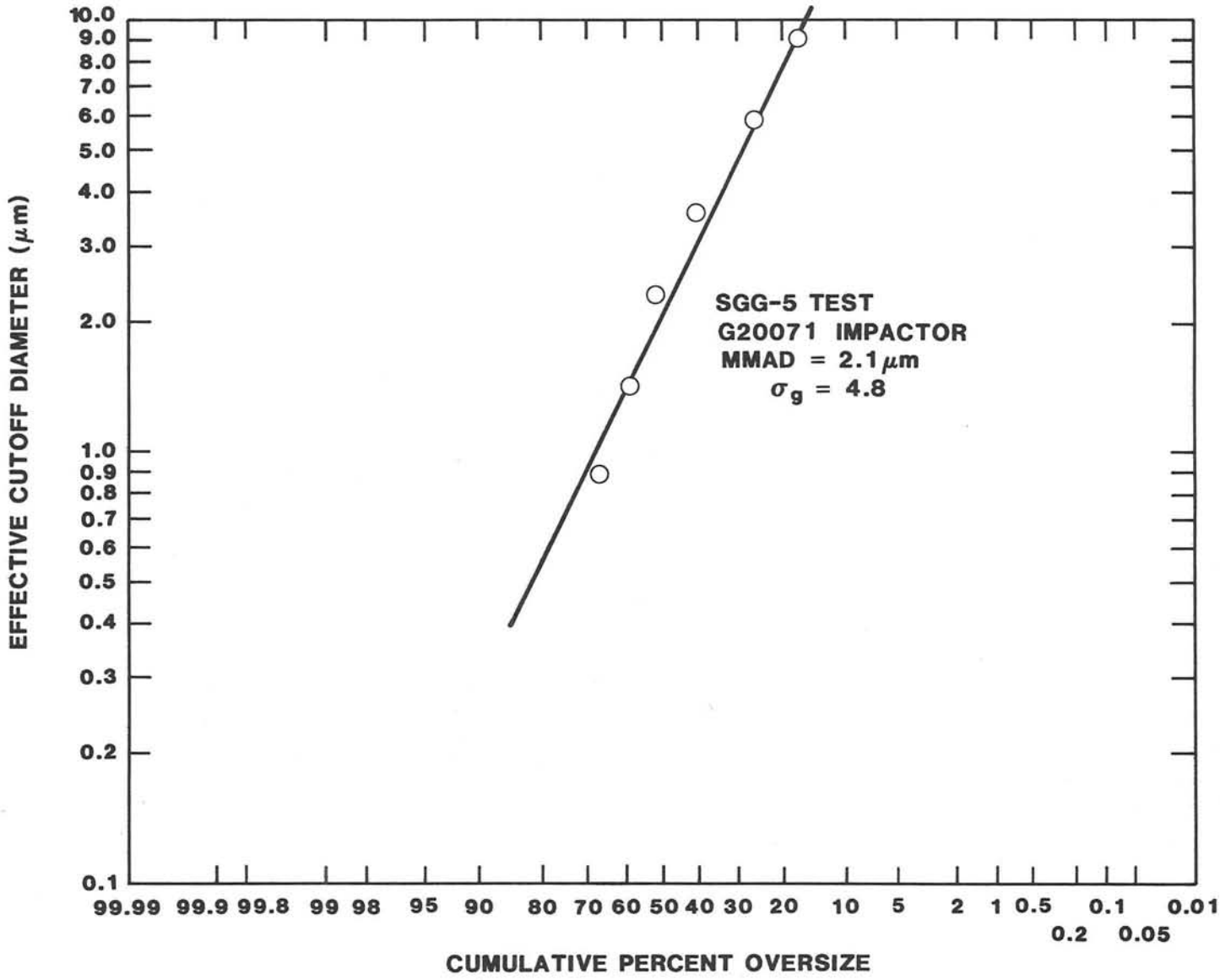

Figure A-18. Uranium Particle Size Distribution in Round Room for Subscale Test 5

Figure A-19 shows a log-probability plot of uranium particle size for location E of the sampler array. An estimate of the stabilized cloud volume during the 10-minute sampling period after detonation was made from the photometric film. A cloud volume of 3.0 m^3 was estimated. Assuming a uniform uranium respirable mass concentration of 4.75×10^{-2} μg/ℓ, a total respirable uranium mass in the cloud was estimated to be 1.42×10^{-4} g.

Based upon a calculated uranium aerosol mass inside the Gravel Gertie structure of 8.2×10^{-2} g, a respirable uranium release fraction of 1.7×10^{-3} was estimated. This is within the release fraction estimate (4×10^{-3}) of the full-scale Gravel Gertie test at NTS.

From these data, it is concluded that the dropped ceiling and vapor barriers had no significant effect on the filtration efficiency of the gravel roof.

e. The technique to increase the aerosol cloud density (for photographic purposes) by adding carbon black to the gravel surface was not satisfactory. The indications are that the carbon black should be placed in fragile, waterproof containers which will rupture during the roof expansion.

f. Figure A-20 is a plot of guage pressure inside the structure as a function of time.

Results and Conclusions

The results of the subscale test series as noted above verified that replica scaling of the Gravel Gertie roof structure is feasible and basically follows a $W^{1/3}$ law where W is the roof mass. Scaling HE and strength of materials is more complex. Behavior of the gravel roof was satisfactorily modeled. The objectives of the test were accomplished and the following conclusions can be made:

a. The presence of the dropped ceiling had no significant effect on roof behavior;

b. Roof behavior was not sensitive to the location of the HE at the time of explosion; and

c. Aerosol sampling equipment was found to operate satisfactorily. Aerosol samples were found to adequately measure the quantity of aerosols produced.

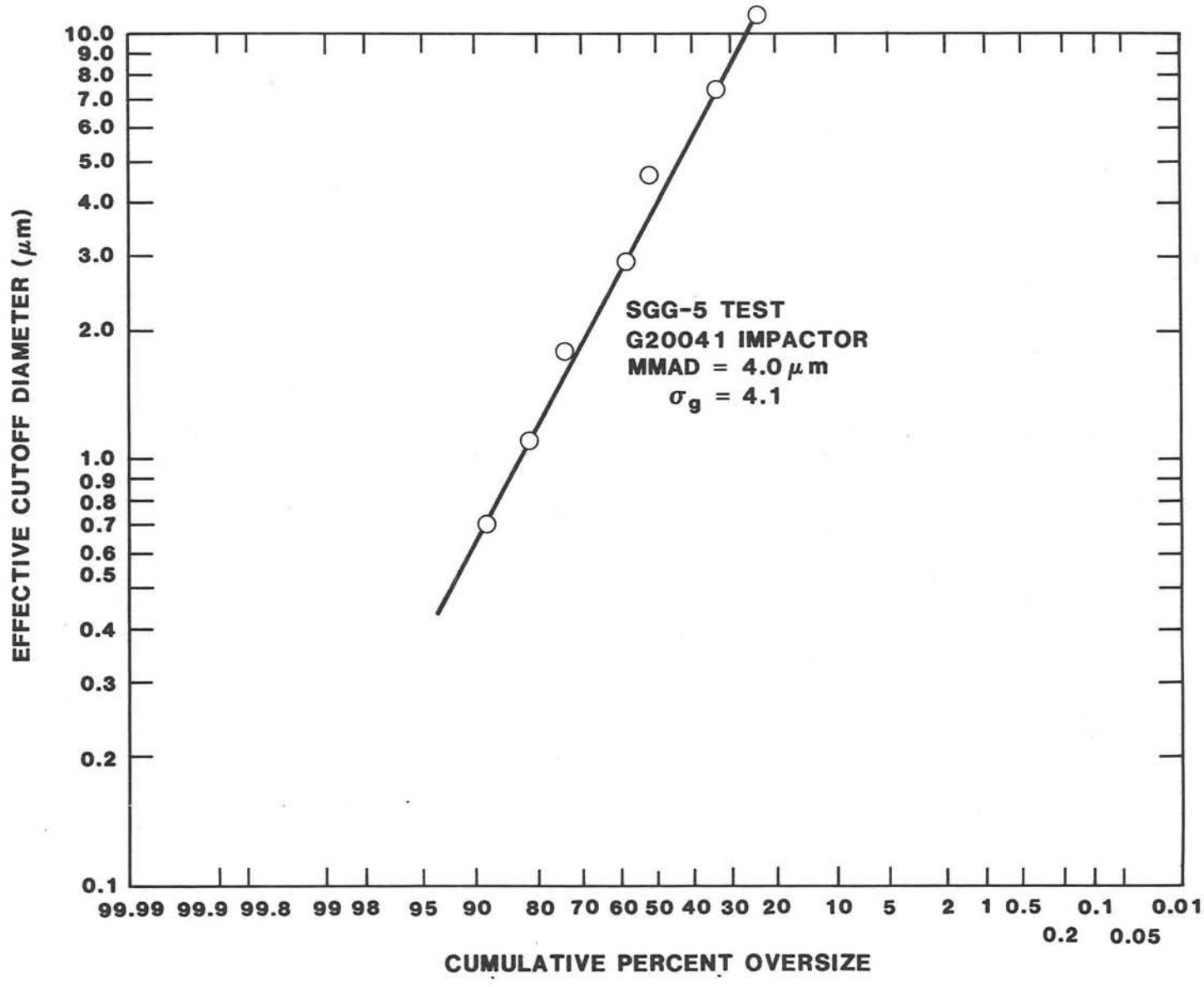

Figure A-19. Uranium Particle Size Distribution at Position E for Subscale Test 5

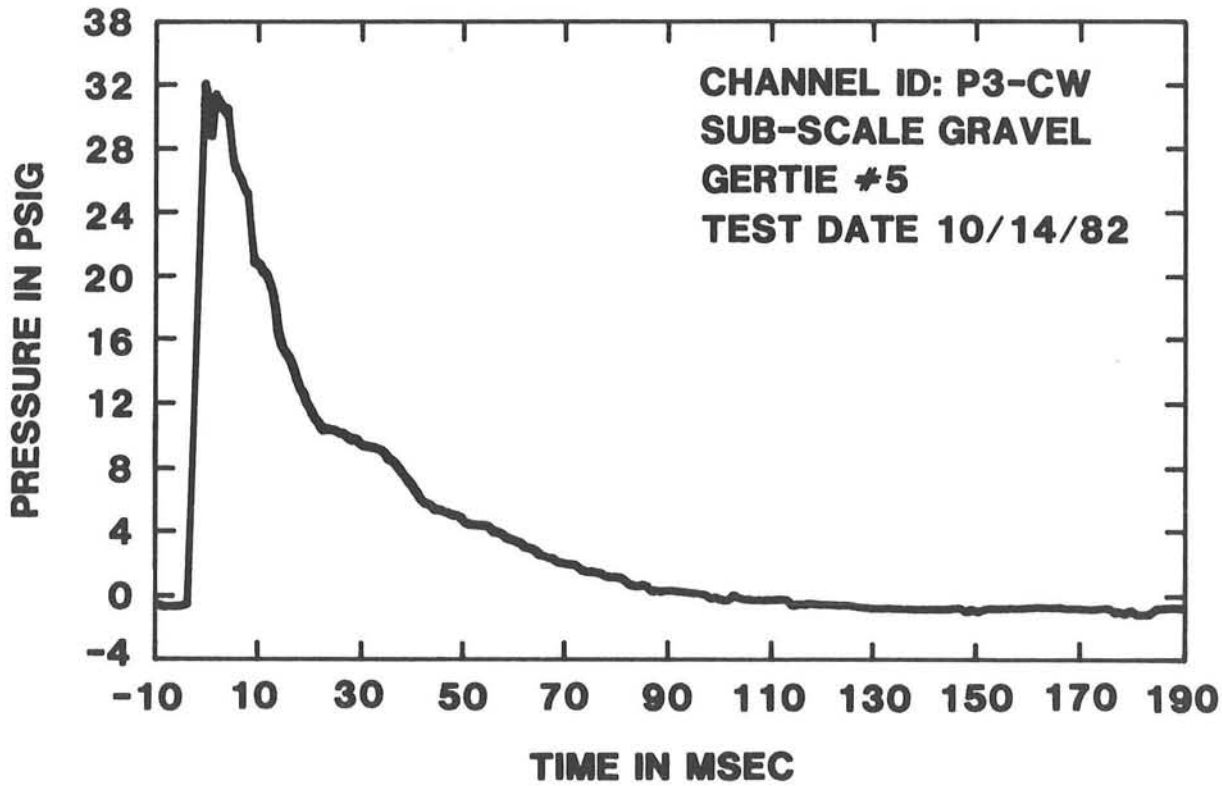

Figure A-20. Pressure Signature for Subscale Test No. 5

Appendix B
Scaled Source Term Autoclave Tests

I. Introduction

A series of eight subscale High Explosive Aerosol Generator (HEAG) tests were conducted in a 1.83-meter-diameter pressure sphere to evaluate the following:

1. The mass fraction of uranium produced as respirable airborne particles from detonation of scaled HEAG devices having selected charge-to-mass ratios (CTM);

2. The particulate size fraction of material less than 10 μm aerodynamic diameter produced;

3. The morphological characteristics of the surrogate aerosols produced;

4. The applicable scaling law predicting fraction of mass produced as a respirable (less than 10 μm aerodynamic diameter) aerosol for selected CTMs.

The experimental data were used to validate design estimates of the fraction of aersolized uranium calculated using a two-dimensional Eulerian Wave code CSQ II [Th79]. The code simulated the detonation of HEAG configurations ranging from CTMs of about 5 to 24 to establish that the design goal of 2.3% or more aerosol production could be achieved with uranium at a CTM of 24. The estimate of 2.3% was based on the quantity of uranium initially vaporized by detonation of the HE under the assumption that the majority of particles smaller than 10 μm aerodynamic diameter consist of vaporized materials.

II. Experimental Configuration

A 1.83-m-diameter spherical pressure vessel was selected to contain the high explosive (HE) gases and test material fragments produced from detonation of the scaled HE test devices. The pressure vessel was made of 2.54-cm-thick ASTM-A-537 Class 2 steel and had two diametrically opposed closure cutouts, one 20 cm and the other 41 cm in diameter. The spherical pressure vessel is shown in Figure B-1. The limiting charge for this vessel, defined to be the largest charge that, when detonated at the center of the vessel, does not cause the chamber to undergo plastic deformation, is a 15-lb sphere of PBX-9501 [Ne79].

The 41-cm-diameter bulkhead closure plate was fitted with a high-pressure ball valve (2.54 cm orifice) and HEPA filter for controlling air flow in and out of the vessel. The 20 cm diameter bulkhead closure plate was fitted to a high pressure critical flow orifice, three high pressure ball valves, a high pressure HEPA filter, and an aerosol sampling tree via 2.5-cm-diameter

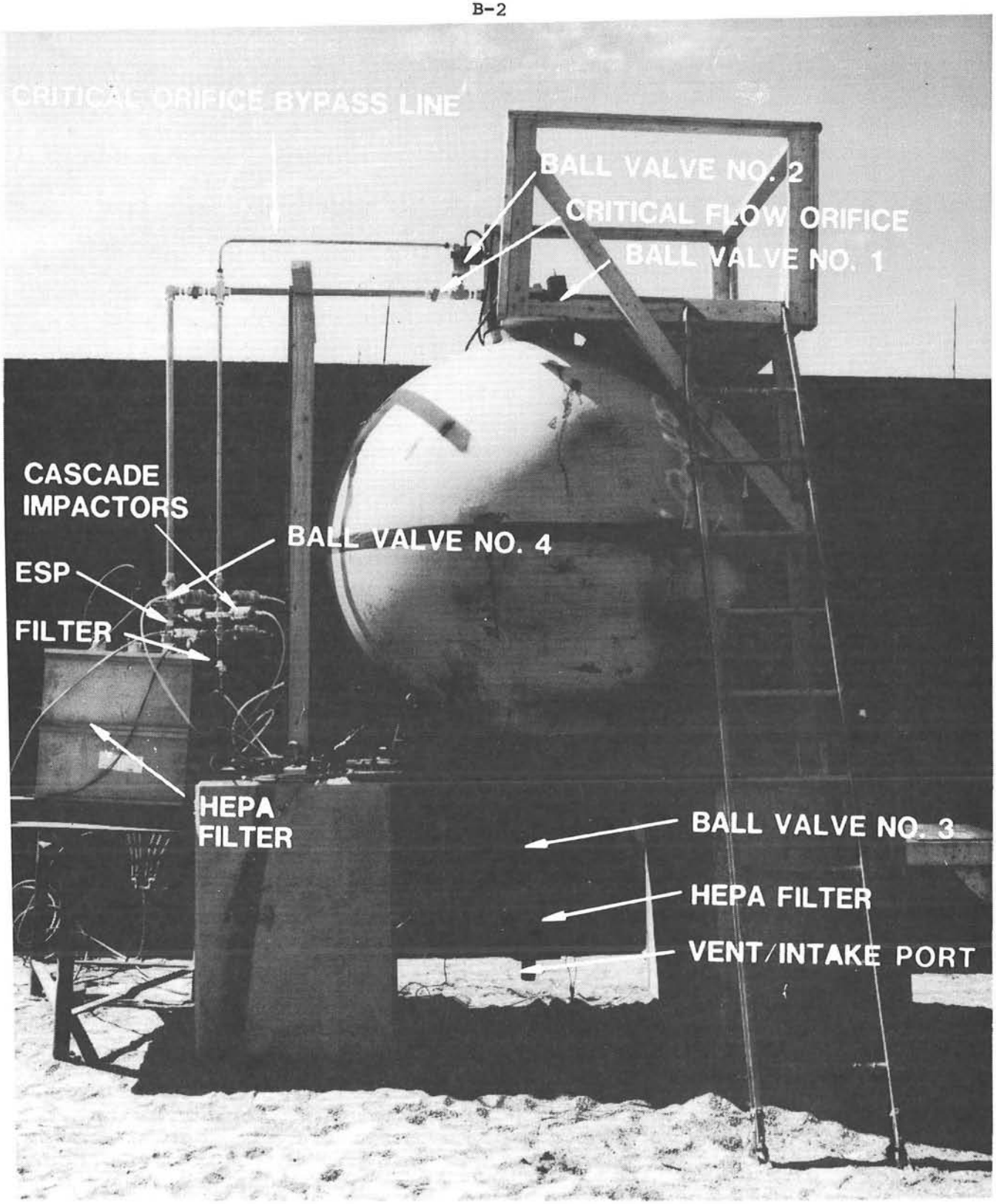

Figure B-1. Spherical Pressure Vessel

stainless steel pipe. The aerosol sampling tree consisted of 5 Lovelace Multijet cascade impactors [NW82], one electrostatic precipitator sampler, and one 47 mm filter. A schematic of the containment vessel, aerosol instruments, and plumbing is shown in Figure B-2.

For test procedure shakedown, Tests 1, 2, and 7 included high explosive only charges. The PBX-9501 HE sphere used in Tests 1, 2, and 7 is shown in Figure B-3. Charges of 1.045 kg of PBX-9501 and 43.5 g of depleted uranium metal were used in Tests 3, 4, and 5; and charges of 3.632 kg of PBX-9501 and 151 g of depleted uranium metal were used in Tests 6 and 8. A schematic of these test charges is shown in Figure B-4. The test charges were hung from the top 20 cm diameter bulkhead by nylon nets in all tests, with the exception of Test numbers 7 and 8, in which a fine copper wire (0.81 mm dia) was used to support the test charges. Figure B-5 shows a photograph of the nylon net and test charge used in Test number 3. The test charges were detonated using a single tetryl pellet and an RP-83 detonator on the top surface of the sphere. The charges were positioned at the center of the pressure vessel.

Aerosols and gases produced by the detonated test charges were extracted via 2.5 cm diameter stainless steel pipe connected to the top 20 cm diameter bulkhead closure plate. A 300 psi remotely-operated pneumatic ball valve, which remained closed during detonation, was opened 10 seconds after detonation to allow the high pressure (from 220 to 260 psig) high temperature ($\sim$600°C) gases and aerosols to flow through a critical flow orifice into an aerosol sampling tree of cascade impactors, an electrostatic precipitator sampler, and filters. A cubic, 61-cm fiberglass paper HEPA filter was connected in parallel to the critical flow orifice (shown in Figure B-2) to vent the overflow of hot, high-pressure gases from the pressure vessel to the atmosphere. The purpose of the critical flow orifice was to meter the gas flow rate and to provide an accurate measure of the gas flow rate into the aerosol samplers. The critical orifice was designed to operate at gas pressures of 300 psig and temperatures of 400°C. When the hot gas pressures dropped below 3 psig, the pneumatic ball valve at position 4 (see Figure B-2) was closed and ball valves No. 2 and No. 3 were opened remotely to allow extraction of the aerosol and gases through the sampling tree using vacuum pumps. The smaller HEPA filter at position 3 allowed outside air to replace the gases extracted from the pressure vessel.

Table B-1 shows the test number, test date, purpose of each test, the type and number of aerosol samplers used, and the types of analyses performed for each test.

Up to six cascade impactors were operated sequentially in time from t = 10 seconds to 15 minutes postdetonation to provide a time history of the uranium particle size distribution. Up to seven 47 mm cellulose acetate paper filters were operated sequentially in time from t = 10 seconds to t = 15 minutes to provide a history of the total and uranium mass concentration. One electrostatic precipitator was operated from t = 17 seconds to t = 1.5 minutes to provide information on the morphology and real size of the airborne particles produced from the HE test device. The Gravel Gertie Aerosol Sampling Package

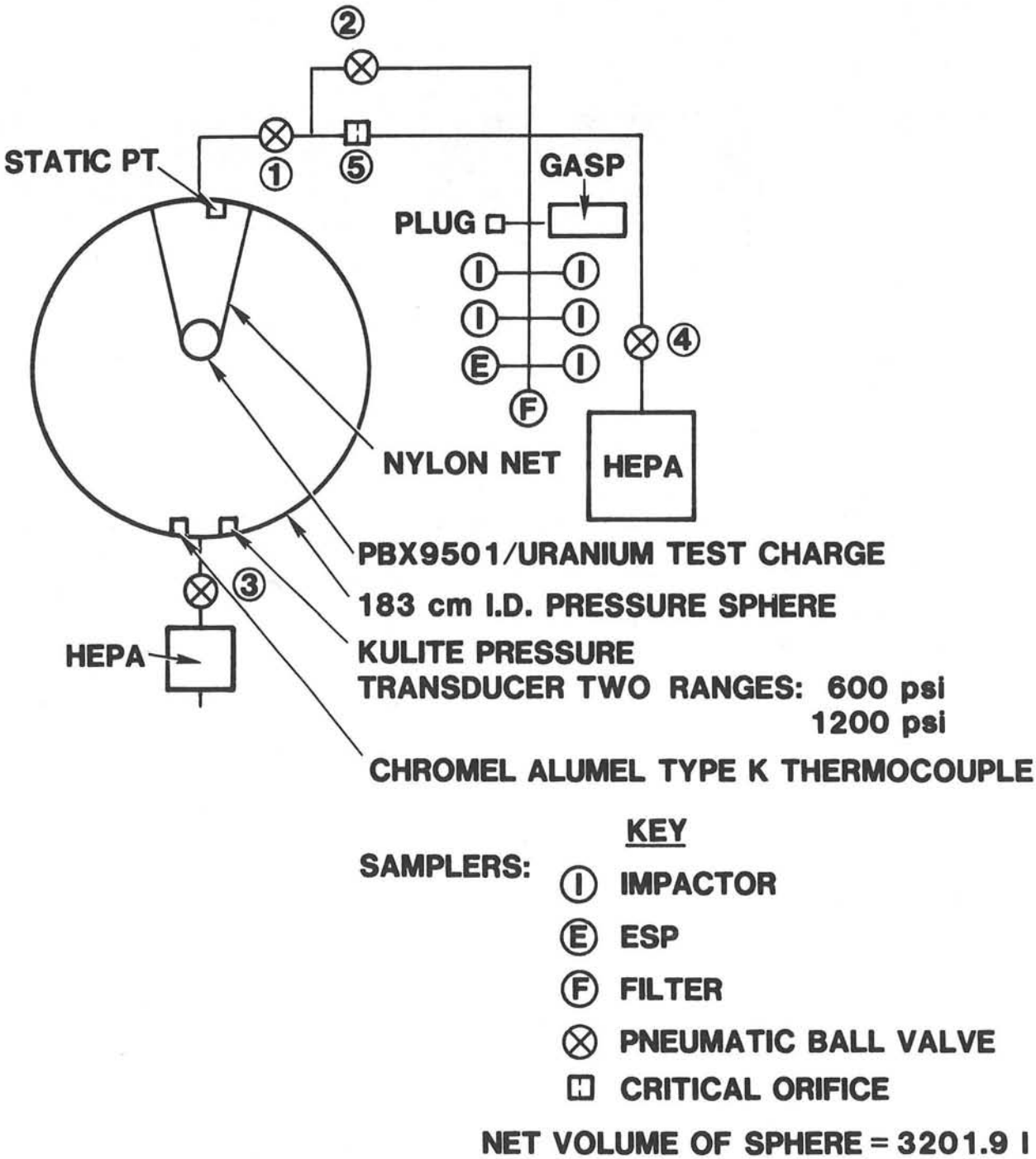

Figure B-2. Confinement Chamber Plumbing Schematic

PBX9501 HE CHARGE

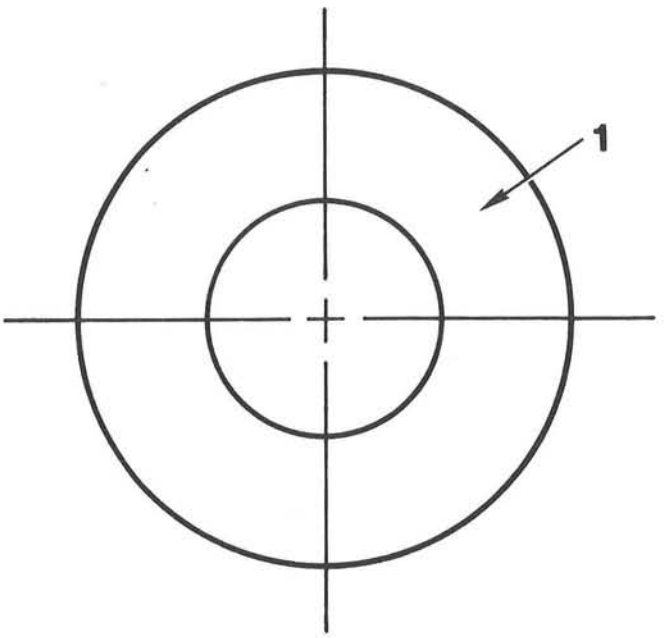

GG TEST CHARGE ASSY[b]				
TEST CHARGE[a] ASSY. NO.	ITEM 1 SK. NO. GG-1		O. D. cm	HE WT. kg
	QTY	IT. NO.		
GG-4-1	2	2	10.3	1.045
GG-4-3	2	3	15.6	3.624

a. MTL: PBX9501

b. SKTCH NO GG-4

Figure B-3. PBX-9501 HE Charge Shell

PBX9501 HE CHARGE/URANIUM SHELL

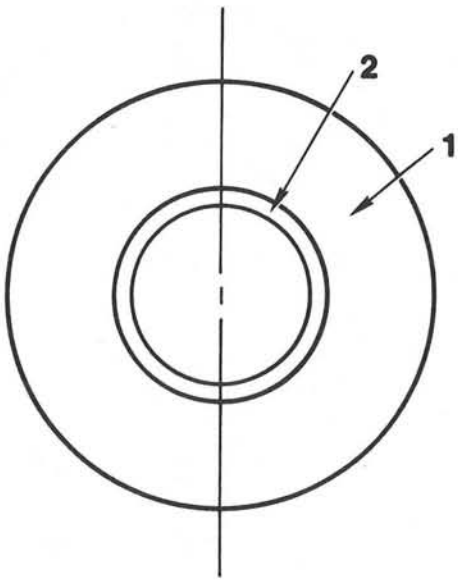

GG TEST CHARGE ASSY [b]									
TEST CHARGE [a] ASSY. NO.	ITEM 1		ITEM 2		O. D. cm	WEIGHT, kg			CTM
	SK. NO. GG-1		SK. NO. GG-2			HE	U	TOTAL	
	QTY	IT. NO.	QTY	IT. NO.					
GG-3-2	2	2	1	2	10.3	1.045	0.043	1.088	24
GG-3-3	2	3	1	3	15.6	3.624	0.151	3.775	24

a. MTL: PBX9501/DEP URANIUM

b. SKCH NO. GG-3

Figure B-4. PBX 9501 HEAG Charge/Uranium Shell

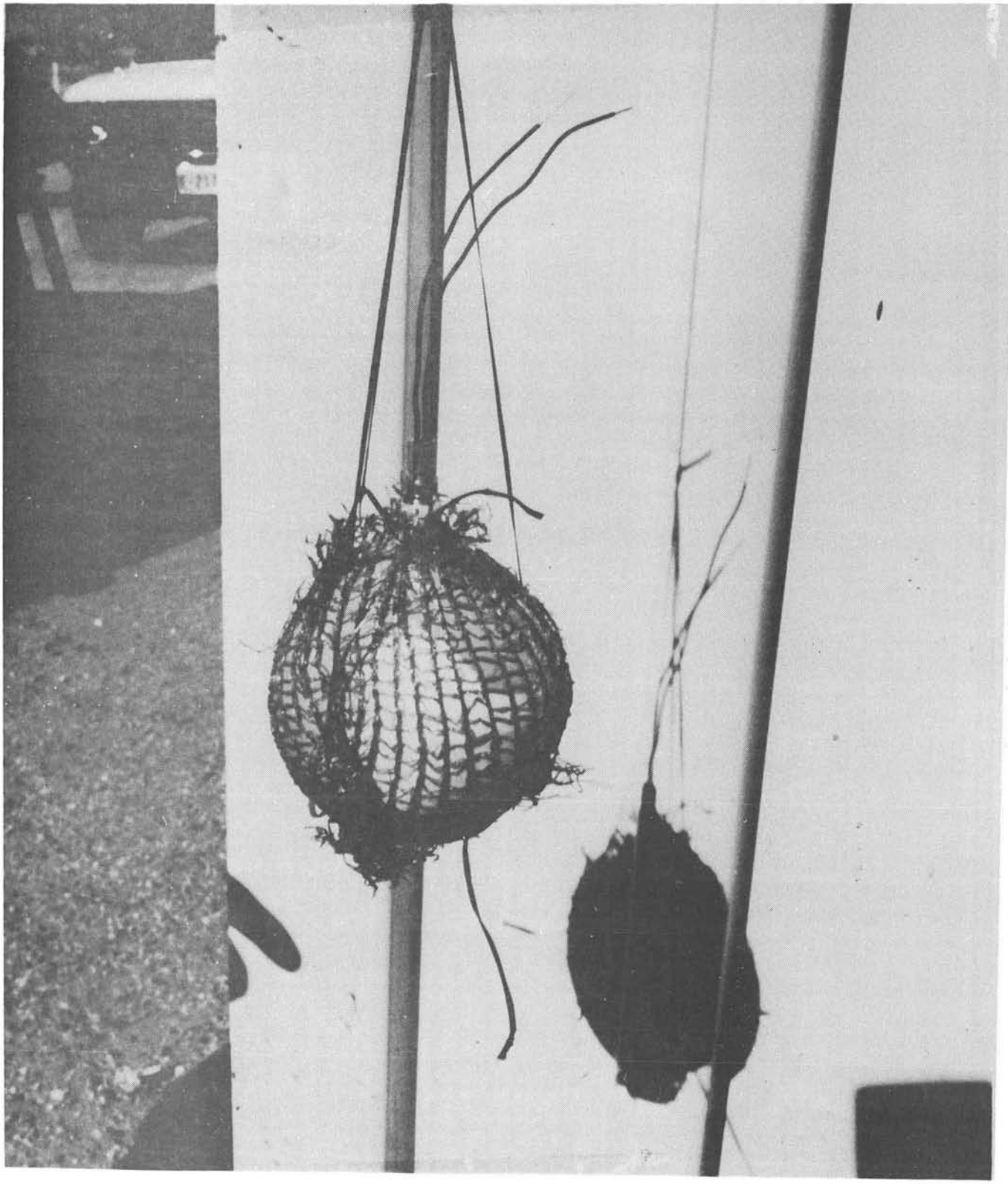

Figure B-5. Test Charge for Containment Chamber Tests No. 1, 2, 3, 4, 5, and 6 in Nylon Net

TABLE B-1

Aerosol Sampling Instrumentation and Analyses

Test No.	Test Date	Test Purpose	Aerosol Samplers Used	Analysis Performed
1	8/20/82	Test configuration checkout	LMJ Imp[c] (5) Filters[d] (2) ESP[e] (1)	none none none
2	8/24/82	Repeat Test No. 1	LMJ Imp (5) Filters (1) ESP (1)	Grav[a] (5) Grav[a] (1) SEM[b] (1)
3	8/27/82	Determine aerosol fraction and size fraction	LMJ Imp (6) Filters (3) ESP (1)	Grav (2)/Flo[f] (0) Grav (3)/Flo (3) SEM (1)
4	9/03/82	Confirm results of test No. 3 and checkout GGASP sampler	LMJ Imp (6) Filters (2) ESP (1) GGASP IMP[g] (2)	Grav (1)/Flo (1) Grav (0)/Flo (0) SEM (0) Flo (1)
5	9/30/82	Repeat Test No. 4	LMJ Imp (5) Filters (7) ESP (1) GGASP Filter[h] (2)	Grav (5)/Flo (1) Grav (7)/Flo (4) SEM (1) Grav (2)/Flo (2)
6	10/11/82	Determine fraction aerosolized and size fraction	LMJ Imp (3) Filters (3) ESP (1)	Grav (3)/Flo (2) Grav (3)/Flo (3) SEM (1)
7	12/17/82	System checkout	LMJ Imp (4) Filters (5) ESP (1)	Grav (4) Grav (4) SEM (0)
8	12/22/82	Determine fraction aerosolized and size fraction	LMJ Imp (5) Filters (7) ESP (1)	Grav (5)/Flo (5) Grav (7)/Flo (7) SEM (1)

a = Gravimetric Analysis
b = Scanning Electron Microscopic Analysis
c = Lovelace Multijet Cascade Impactor
d = 47 mm Cellulose Acetate Filter
e = Electrostatic-Precipitator
f = Uranium Fluorometric Analysis
g = Gravel Gertie Aerosol Sampling Package Mercer Impactor
h = Gravel Gertie Aerosol Sampling Package 25 and 47 mm Filters

(GGASP) was used in Tests 4 and 5 to provide particle size and aerosol concentration data for evaluation and comparison with aerosol parameter data provided by the external sampling tree.

Gravimetric analysis and scanning electron microscopy (SEM) were performed on those samples collected in tests in which only HE was used (Tests 2 and 7). Gravimetric, uranium fluorometric, and SEM analyses were performed on samples collected from tests utilizing uranium metal in the test charge (Tests 3, 4, 5, 6, and 8). The critical flow orifice and stainless steel plumbing were carefully washed with a 1 molar solution of HNO_3 between tests in which uranium tracers were used.

Two Kulite piezoelectric pressure transducers (Model XTM-1-190) were mounted on the inner surface of the upper 20 cm and the lower 41 cm diameter bulkhead cover plates to provide internal shock and pressure data. One Type K Chromel/Alumel 5 mil wire thermocouple was placed on the inner surface of the 41 cm diameter bottom cover plate to measure internal temperatures.

III. Test Results and Discussion

Table B-2 summarizes the test results for each test performed in the source term evaluation series. Valve problems were encountered in Test 1 in which 1045 g of PBX-9501 was used to check out the experimental configurations. Test 2 was a repeat of Test 1 and provided useful information concerning the background aerosols and HE combustion products produced from detonation in a confined volume.

Table B-3 summarizes the uranium aerosol size, uranium mass concentration, and total mass concentration results obtained for each test. No uranium above detection limits was measured in background aerosols sampled in Test 2 (no uranium in test device).

In Test 3, 1045 g of PBX-9501 and 43.5 g of uranium metal (CTM = 24) were used in the test charge to determine explosively generated uranium aerosol mass fraction and uranium size fractions less than 10 μm (aerodynamic diameter). Approximately 6 percent (2 g) of the initial uranium mass in the test charge was measured as respirable aerosol during the period t = 9.6 seconds to t = 40 seconds. The median aerodynamic diameter of the uranium aerosol produced during this time period was 1.2 μm.

Test 4 was performed to confirm the results of Test 3 for the same HE charge to uranium mass configuration. However, problems with vent valve 3 were encountered and samples collected for this test were not analyzed.

TABLE B-2

Summary of Source Term Test Results

Test No.	Date	Charge/Mass Configuration	Test Results
1	8/20/82	1045 g PBX-9501	Valves 1 and 3 open during test: no data
2	8/24/82	1045 g PBX-9501	Successful system checkout
3	8/27/82	1045 g PBX-9501/43.5 g U CTM = 24	6 percent of uranium mass generated as respirable aerosol, MMAD* = 1.2 μm
4	9/03/82	1045 g PBX-9501/43.5 g U CTM = 24	Vent valve open during test; data obtained but no conclusion possible
5	9/30/82	1045 g PBX-9501/43.5 g U CTM = 24	6 percent of uranium mass generated as respirable aerosol MMAD* = 1.3 μm
6	10/11/82	3632 g PBX-9501/151.6 g U CTM = 24	A & F program sequencer failure, orifice plugged
7	12/17/82	3632 g PBX-9501	System checkout successful
8	12/22/82	3632 g PBX-9501/151.3 g U CTM = 24	7 percent of test charge uranium mass generated as respirable aerosol MMAD* = 4.2 μm

* Mass median aerodynamic diameter

Test 5 was performed to confirm the results of Test 3. The experimental configuration of Test 5 was similar to that of Test 3. The filter and cascade impactor data of Test 5 are summarized in Table B-3. Uranium aerosol mass concentration (mg/ℓ) was computed from Table B-3 (plotted in Figure B-6) as a function of time after detonation. From Figure B-6, it may be seen that at t ≈ 0 the uranium mass concentration was approximately 0.85 mg/ℓ. The net free volume of the test sphere was calculated to be 3202 ℓ. The total uranium suspended aerosol at t $\approx$ 0 was therefore calculated to be approximately 2.7 $\pm$ 0.5 g. This suspended uranium aerosol mass corresponds to 6.2 percent of the total initial uranium mass available in the test charge (43.5 g). Figure B-7 shows a plot of the particle size distribution determined from LMJ 41 for Test No. 5. The MMAD of the suspended uranium aerosol during t = 12 seconds to t = 42 seconds was 1.32 μm.

Test 6 was performed to quantify the total uranium respirable aerosol produced from a test charge containing 3632 g of PBX-9501 and 151.6 g of uranium metal (CTM = 24). The test charge mass of Test 6 was $\sim$3.5 times larger than that of Tests 3, 4, and 5. However, because of an arming and firing program sequencer failure, no information was obtained from Test 6.

As a result of the program sequencer failure of Test 6, it was decided to perform Test 7 with HE only in order to reconfirm program sequencer performance. No uranium was included. Uranium fluorometric analyses were performed on selected filter samples from Test 7. No uranium above the minimum detectable limit (10 ng) was detected. This again confirmed background was smaller than detectable limits.

Test 8 used a test charge consisting of 3632 g of PBX-9501 and 151.3 g of uranium metal (CTM = 24). The filter analyses data are shown in Table B-3. No uranium fluorometric analyses were performed on cascade impactor samples taken for this test. Figure B-8 shows a plot of uranium mass concentration as a function of time for the filter data of Test 8. Initial uranium aerosol concentration was approximately 3.5 $\pm$ 0.5 mg/ℓ at t $\leq$ 10 seconds. Assuming a uniformly distributed uranium aerosol, the initial total uranium mass was 11.2 $\pm$ 1.6 g. This corresponds to a respirable uranium aerosol fraction of 7 $\pm$ 1.0 percent of the initial uranium test mass. Figure B-9 is a plot of the uranium particle size distribution for Test No. 8. The MMAD of the airborne uranium aerosol during t = 12 seconds to t = 42 seconds was 4.2 μm.

Table B-4 summarizes the results of measurements with the GGASP for Tests 4 and 5. Each GGASP unit, fully described in Appendix D, consisted of two Mercer impactors and one 25 mm filter at the intake port of the pump and one 47 mm filter at the exhaust port of the pump. Since the critical orifices were not used in either of these tests, flow metering was determined by the critical flow meter at position 5 (see Figure B-2) and by the critical flow meters located behind each of the two Mercer impactors and the 25 mm filter. The total flow rate of the GGASP sampling package for both Tests 4 and 5 was estimated to be $\sim$10.8 l/min. Flow rates, collected uranium aerosol mass, and sampling periods (ΔT), are shown in Table B-4. While calculated uranium aerosol mass concentrations and size distributions for Test 4 are shown, no interpretations and conclusions were made because the vent valve was not closed during the explosive phase.

TABLE B-3

Summary of Cascade Impactor and Filter Data

Test No.	Sampler Type	Time On (Minutes)	Time Off (Minutes)	Uranium Mass (mg)	Total Mass Concentration (mg/ℓ)	Flow Rate (ℓ/Min)	MMAD (μm)	σ_g
2	Filter	0.3	14.5	0	1.47	4.8	--	--
2	LMJC	0.3	1.3	0	1.36	16.3	1.2	1.7
2	LMJD	1.3	2.3	0	0.79	16.6	1.1	1.4
2	LMJH	2.75	5.25	0	0.72	16.7	1.4	1.4
2	LMJF	7.0	9.0	0	0.86	16.4	1.6	1.3
2	LMJP	10.0	14.0	0	--	16.5	2.0	1.5
3	Filter	0	5.0	1.98	1.87	5	--	--
3	Filter	18.5	20.5	6.89	2.02	5	--	--
3	LMJH	0.16	0.67	6.96	1.86	18.5	1.2	1.5
3	LMJC	1.75	2.25	18.9	1.76	18.0	2.2	1.6
5	Filter	0.16	1.16	4.05	--	4.8	--	--
5	Filter	3.0	3.5	0.304	9.12	4	--	--
5	Filter	6.0	6.5	0.261	6.03	4	--	--
5	Filter	17.0	17.4	0.042	4.99	4	--	--
5	LMJ41	0.17	0.67	4.54	1.75	17.6	1.2	1.6
6	Filter	0.5	1.0	0.009	1.34	4.8	--	--
6	Filter	3.0	3.5	0.13	0.25	4.8	--	--
6	Filter	44.0	48.0	0.11	0.13	4.8	--	--
6	LMJ31	0.5	1.0	0.67	0.91	17.3	2.7	1.6
8	Filter	0.17	1.0	11.93	6.7	4.8	--	--
8	Filter	1.5	2.5	5.12	2.4	4.8	--	--
8	Filter	3.5	4.5	0.98	0.4	4.8	--	--
8	Filter	6.0	7.0	0.43	0.2	4.8	--	--
8	Filter	14.0	15.0	0.11	0.05	4.8	--	--
8	Filter	20.0	21.0	0.09	0.08	4.8	--	--
8	Filter	31.0	33.0	0.15	0.03	4.8	--	--

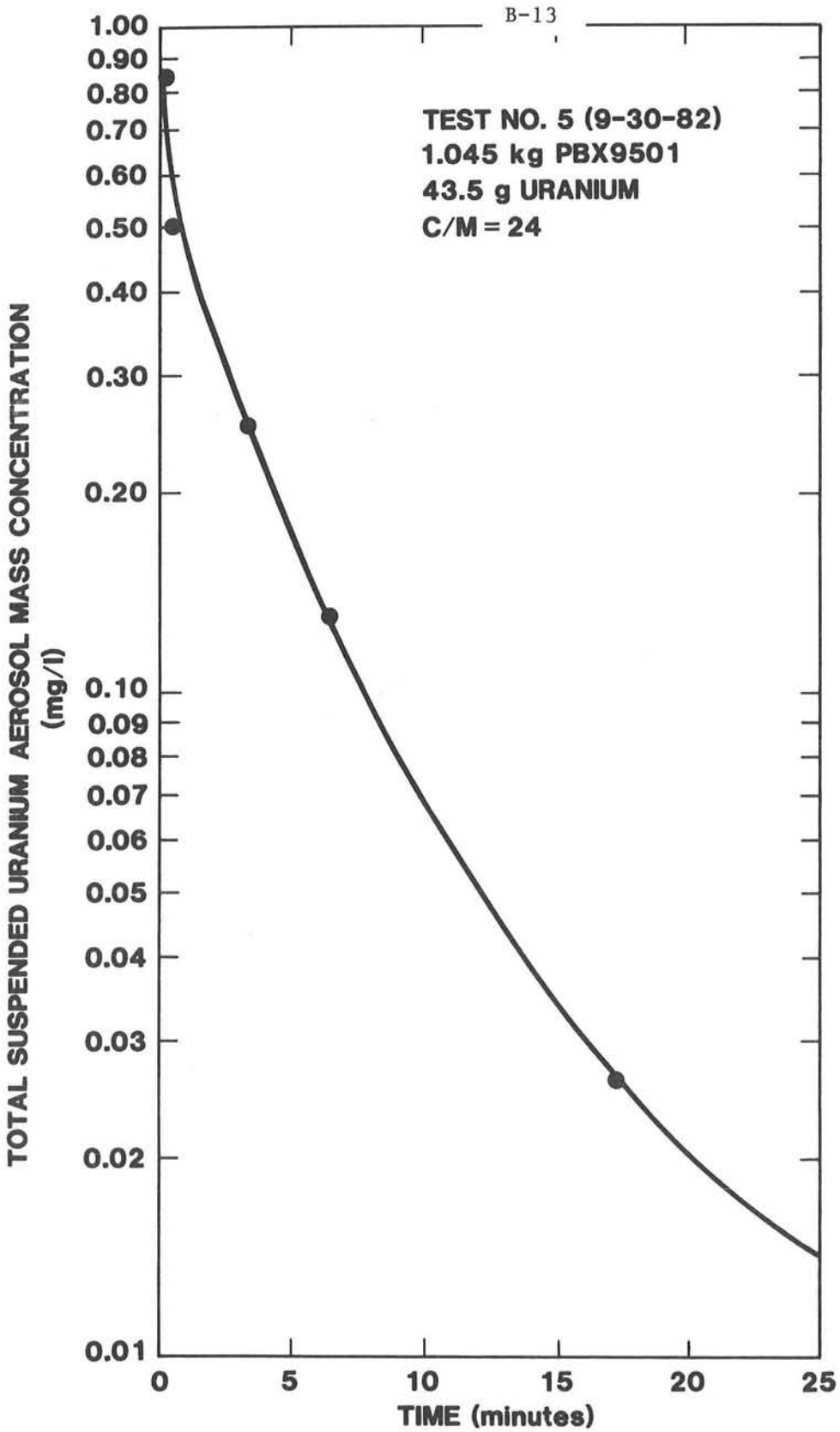

Figure B-6. Total Suspended Uranium Aerosol Mass Concentration-Confinement Test No. 5

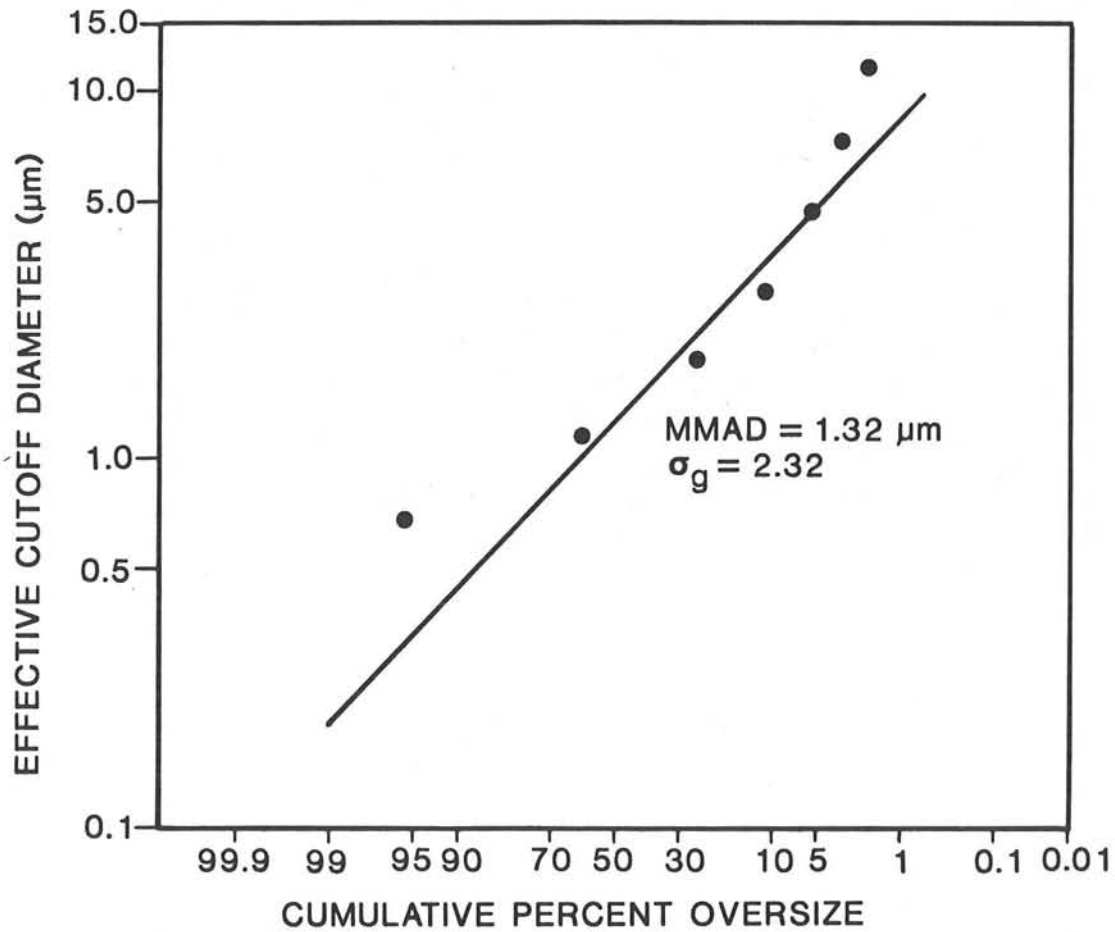

Figure B-7. Plot of Particle Size Distribution for STAT Test No. 5

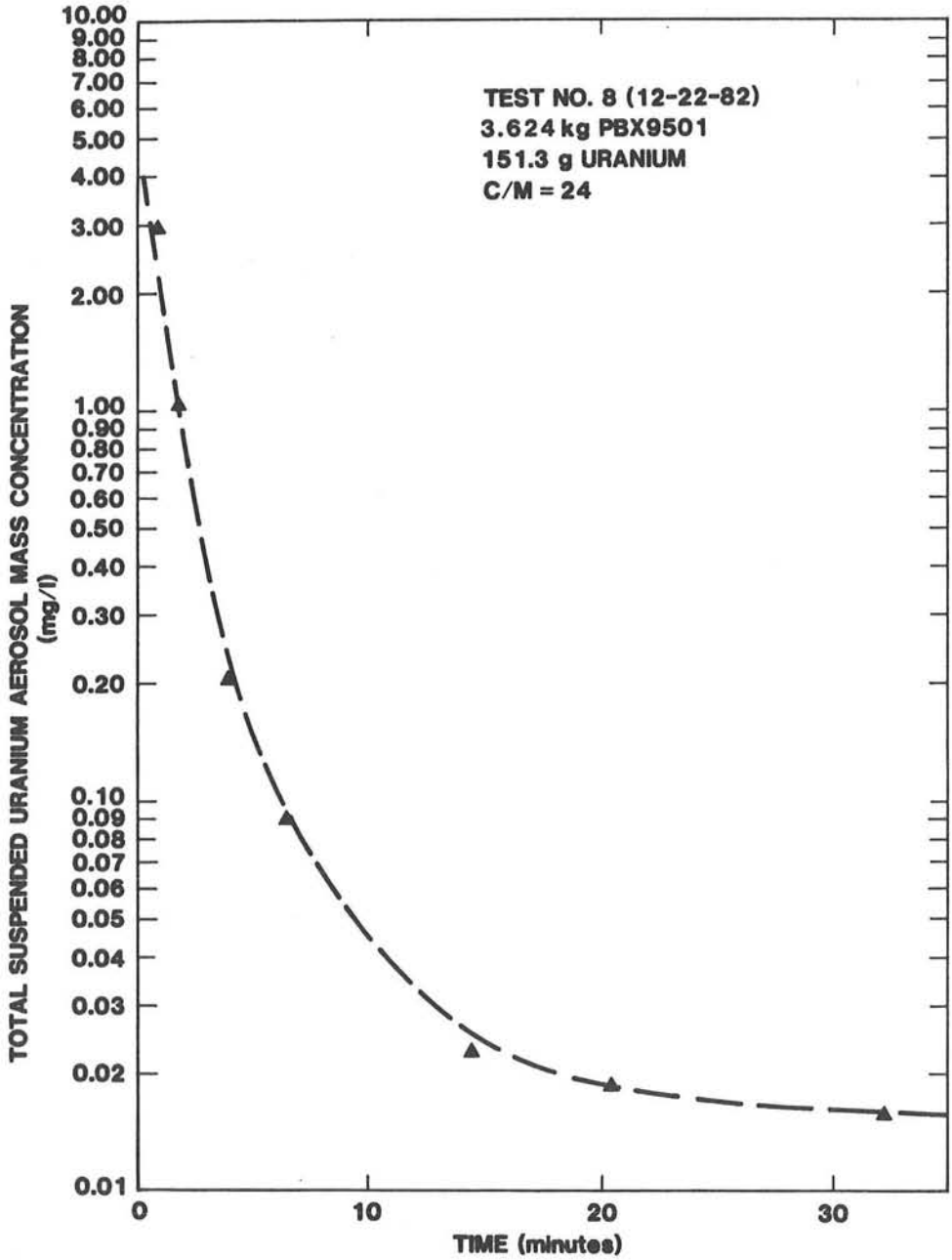

Figure B-8. Total Suspended Uranium Aerosol Mass Concentration-Confinement Test No. 8

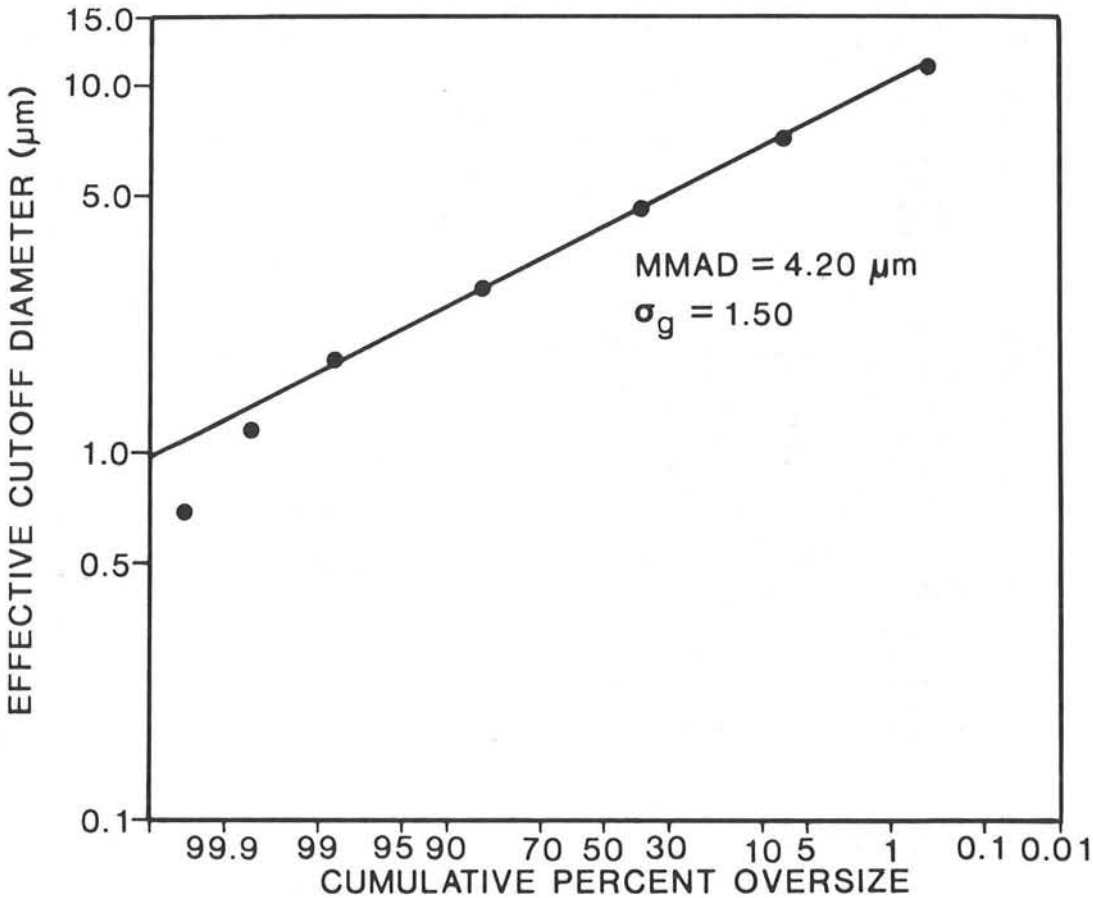

Figure B-9. Plot of Uranium Particle Size Distribution for STAT Test No. 8

TABLE B-4

Summary of GGASP Measurements

Test No.	Test Date	Sampler Type	Uranium Mass (mg)	Flow[a] Rate (ℓ/min)	Uranium Mass Concentration (μg/ℓ)	ΔT (Min)	MMAD (μm)	σ_g (μm)
4	09/03/82	Filter (25)[b]	--ruptured during test				--	
		Filter (47)[b]	0.39	10.8	120	1.0	--	--
		Mercer 1	0.156	1.4		1.0	0.9	1.7
		Mercer 2	0.158	1.4		1.0	1.1	1.3
		Wash	0.33	--		--	--	--
		Total 1	1.03					
5	09/30/82	Filter (47)[b]	0.16	10.8	60	1.0	--	--
		Filter (25)[b]	0.317	8.0		1.0	--	--
		Mercer 1	0.074	1.4		1.0	--	--
		Mercer 2	0.039	1.4		1.0	1.0	1.6
		Wash	0.15	--		--		
		Total	0.45	--		--		

a = best estimate
b = size of filter in mm

Calculations of uranium aerosol mass concentrations and median aerosol size for Test No. 5 are shown in Table B-4. Based upon the results of Test No. 5 and the previous confinement chamber tests it was not possible to come to a definitive conclusion concerning the ability of the GGASP to quantify the aerosol concentration generated from the explosive test device. For Test No. 5, the aerosol mass concentration measured by the GGASP package (120 $\mu g/\ell$) was comparable to the uranium mass concentration of 130 and 150 $\mu g/\ell$ as measured by two extractive filter samplers for that test. However, these tests did not duplicate the pressure, temperature and sampling geometry, (i.e., distance between samplers and aerosol generating device) of the full-scale Gravel Gertie test.

Table B-5 summarizes the pressure and temperature data obtained for each test. Table B-5 shows test number, test date, HE test charge configuration, maximum pressure in the vessel (averaged over the chamber volume), and maximum temperature of the chamber gases.

Figure B-10 shows a recording of the pressure history in the pressure vessel for Test 5. The peak dynamic pressure was ~140 psig. The average pressure (averaged over the volume of the vessel) was ~110 psig.

IV. Conclusions

The following statements summarize the conclusions of the confinement chamber tests:

- Two successful tests indicated an average uranium aerosol mass fraction yield of 6 $\pm$ 1 percent for a 1045 g PBX 9501/43.5 g uranium test charge (CTM = 24).

- A third test at a larger scale with a 3632 g PBX 9501/151.3 g uranium test charge (CTM = 24) indicated a uranium aerosol mass fraction yield of 7 $\pm$ 1 percent.

- At a constant explosive charge to uranium mass ratio of 24:1 and two different explosive charge masses, the mass fraction of respirable particles produced was between 6 and 7 percent.

- Within the experimental precision of these tests, no significant dependence of the fraction of respirable uranium aerosols on size of explosive charge masses was detected.

- MMAD increased by a factor of two as the mass of high explosives and uranium metal was increased by a factor of 3.5. This result is expected because the rate of agglomeration and therefore particle size increases for a fixed containment volume and increased aerosol concentration.

TABLE B-5

Pressure and Temperature Data

Test No.	Date	HE Charge/U Mass Configuration	Max Chamber Pressure (psig)	Max Temp (°C)
1	08/20/82	1045 g PBX-9501	none measured[d]	none measured
2	08/24/82	1045 g PBX-9501	229[a] 50[b]	415[c]
3	08/27/82	1045 g PBX-9501/43.5 g U	225[a] 75[b]	650[c]
4	09/03/82	1045 g PBX-9501/43.5 g U	190[a,d]	613[c]
5	09/30/82	1045 g PBX-9501/43.5 g U	110[a] 85[b]	401[c]
6	10/11/82	3632 g PBX-9501/151.6 g U	300[a,e]	358[c]
7	12/17/82	3632 g PBX-9501	220[a]	sensor damaged in test
8	12/22/82	3632 g PBX-9501/151.3 g U	260[a]	660

a = as measured by Kulite Pressure Transducer
b = as measured by Bourdon Tube
c = as measured by Chromel-Alumel Type K Thermocouple
d = vent valve open during test: compromised results
e = A&F misfire: compromised results

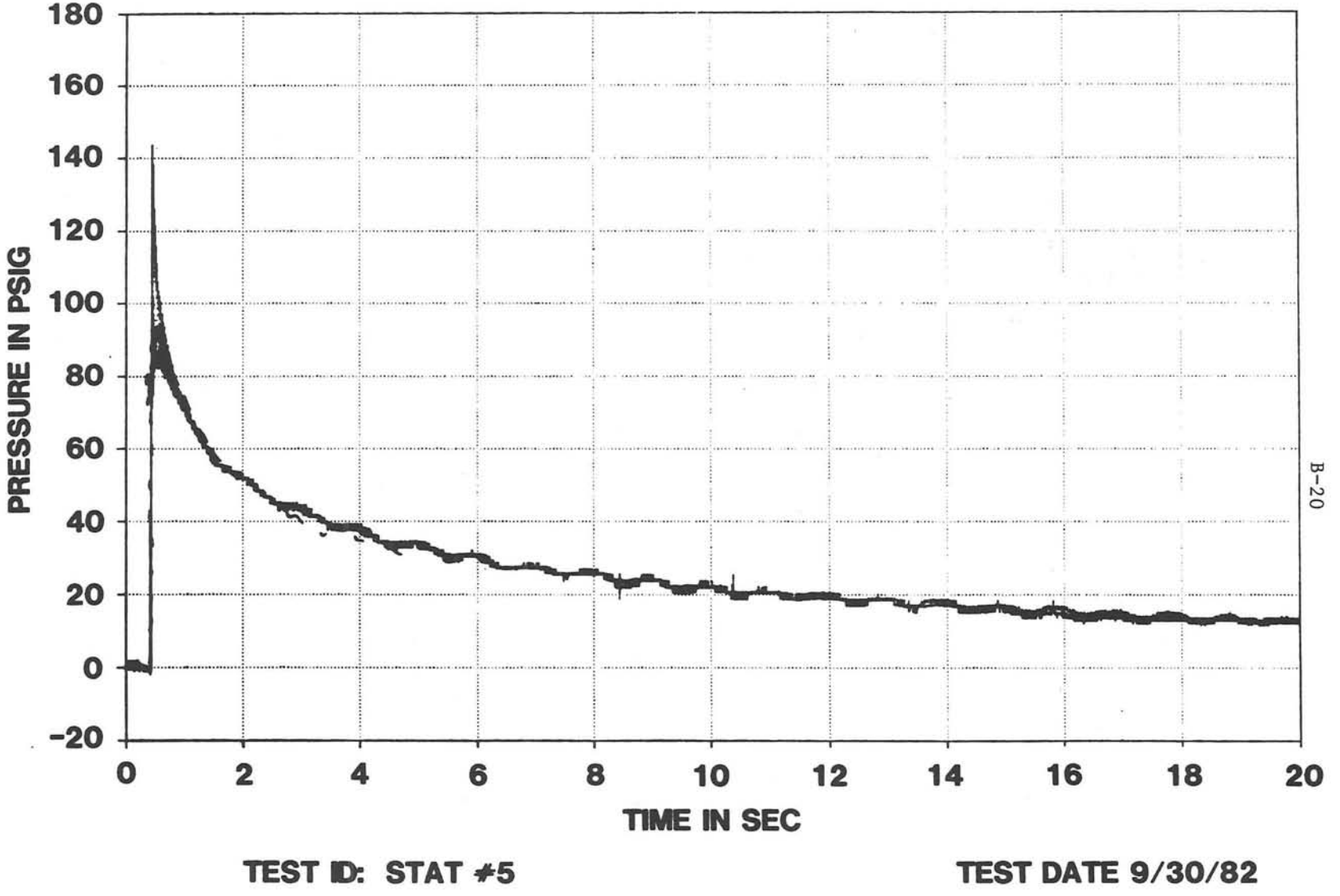

Figure B-10. Recording of Pressure in Pressure Sphere for STAT Test No. 5

Appendix C
Full-Scale Test Construction Details

The test facility for the full-scale test was constructed using a portion of the Gravel Gertie structure (assembly cell and blast door) used in the 1950s test series at NTS. The motivation to use this site was based primarily on DOE/ALO time scales for the Pantex Expansion Program. Other considerations included (1) a determination that the existing assembly cell (round room) was structurally adequate for use in an HE test; (2) a favorable preliminary cost estimate; (3) an existing Environmental Impact Statement; and (4) onsite organizations (Holmes & Narver, Inc. (H&N) and Reynolds Electrical & Engineering Co., Inc. (REECO)) who were familiar with general requirements for the design and construction of structures similar to the Gravel Gertie.

Test Organization

SNL

Dept. 7120 - Instrumentation, Data Recordings & Analysis
Dept. 7130 - Temporary Office Facilities and Electrical Power, A&F System, Test Device Handling and Placement, Documentary Still Photo, and Safe Operating Procedures
Dept. 7550 - Photometrics (event motion pictures)
Dept. 3310 - Radiological Procedures and Safety Guidelines
Dept. 3440 - Safety
Dept. 6320 - Project Management, Aerosol Sampling, Aerosol Data Analysis, and Meteorology
Holmes and Narver (H&N) - Test Facility Design
Amman & Whitney (A&W) - Consultants on Test Facility Design
Southwest Research Institute (SwRI) - Consultants on Test Facility Design and Blast Instrumentation
REECO - Test Facility Construction and Radiation Monitoring
WSNSO - Meteorology
WSI - Security and Access Control
ITRI - Aerosol Sampling System Design, Fielding and Analysis

Simulated Gravel Gertie Structure

A simulated Gravel Gertie was constructed using an existing assembly cell and entrance air lock and a newly constructed staging area, Figures C-1 and C-2. The cable roof design (radial spoke) was the same as in the 1950s tests rather than the currently-used grid array at Pantex due to the construction of the existing operating bay. However, the remainder of the roof and all overburden details were patterned after cell 8 at Pantex [PX1].

Gravel Backfill

Reference HN82 (item 2) specifies backfill details. However, the actual backfill procedure used did not follow the plan specifications. As shown on Figure C-3, the as-built configuration was a true cone with an angle

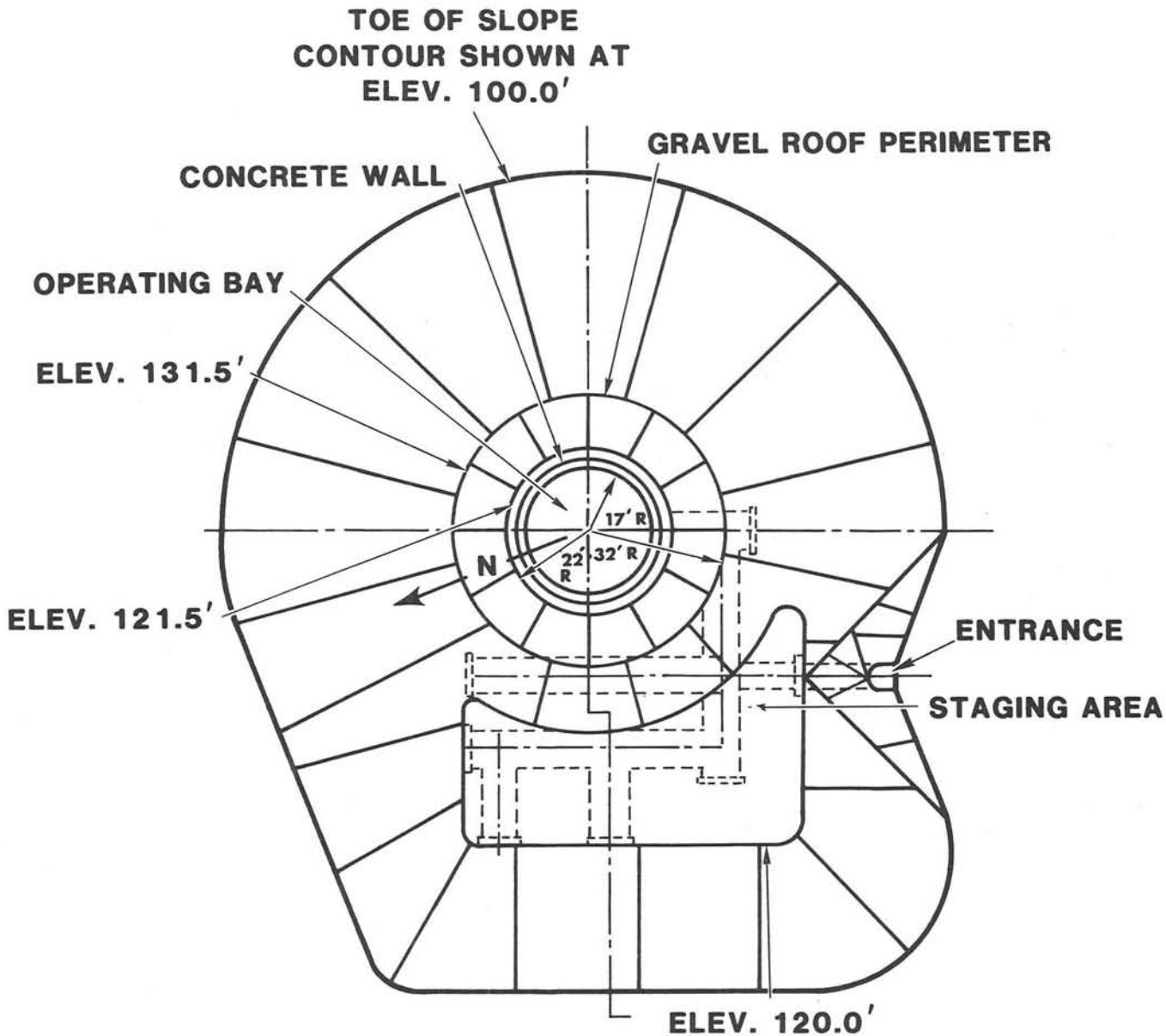

Figure C-1. Plan View of Gravel Gertie Structure

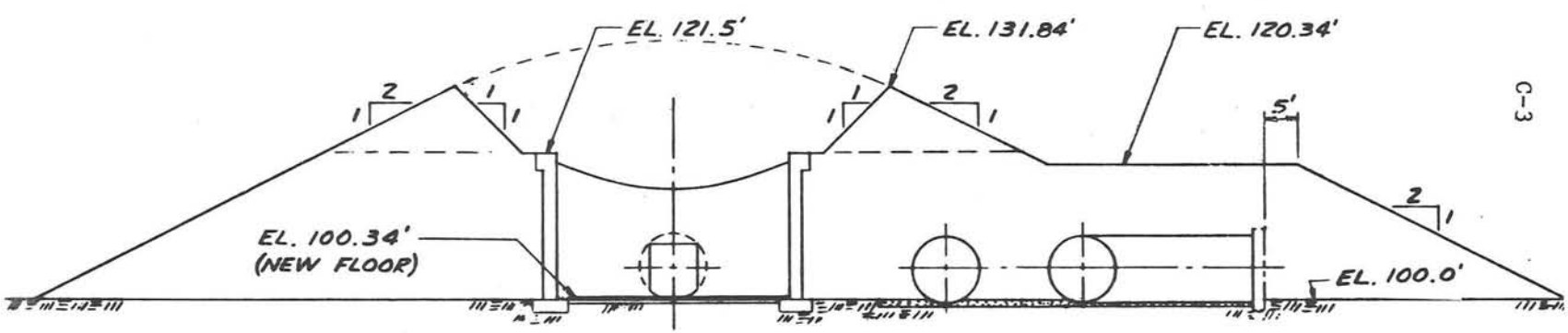

Figure C-2. Gravel Gertie Elevation View

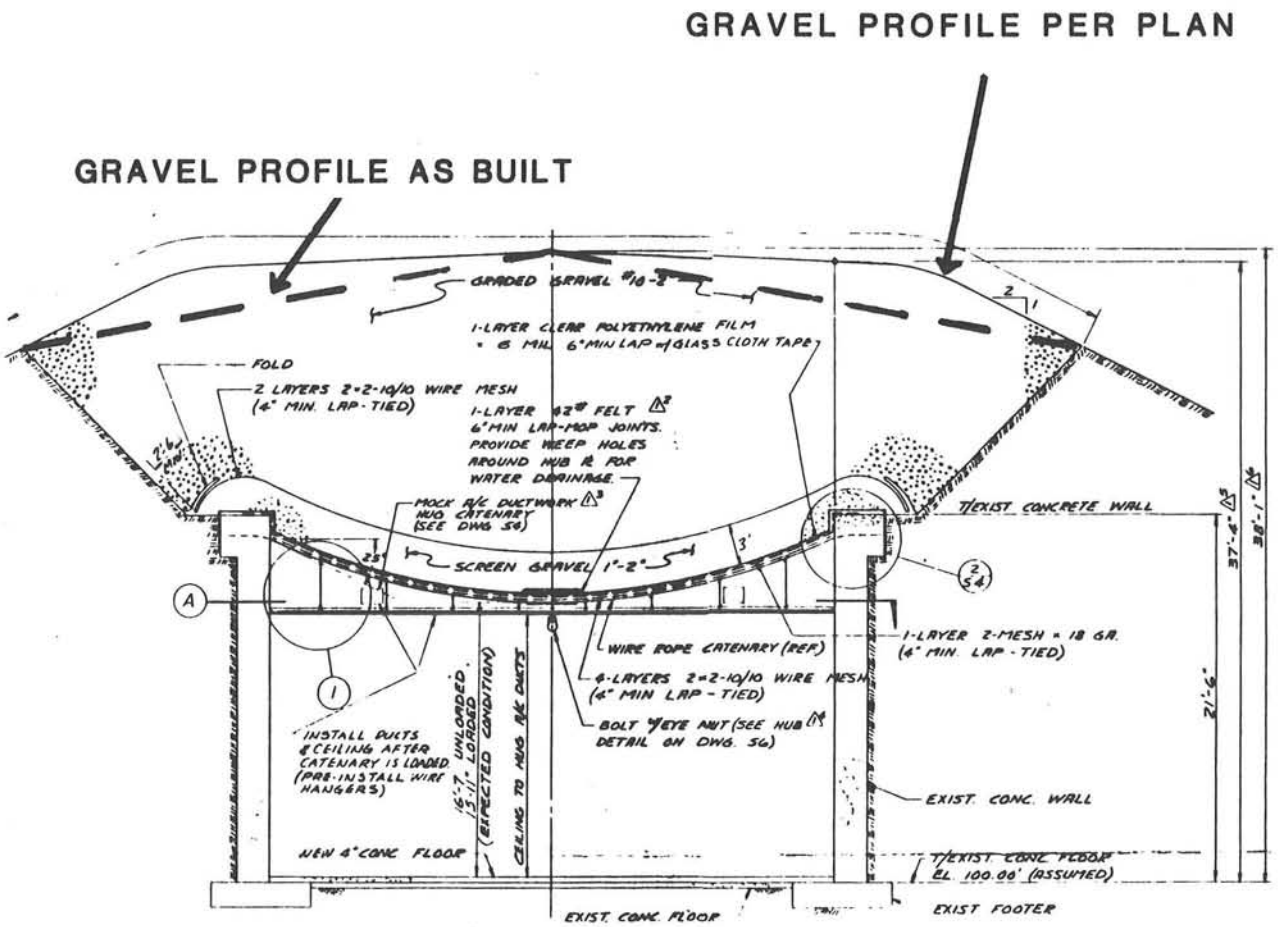

Figure C-3. Construction Details of Gravel Bed

approximately 12° with respect the horizontal instead of the specified 3° out to 5.5 m with an 2:1 slope beyond. This resulted in a overburden deficiency amounting to 1.1 m of gravel at the round room wall radius of 5.18 m. As discussed in the main body of the report, this deficit probably altered the filter efficiency of the roof.

The "Gulf Seal" cover was deleted from construction since it would not affect the filter efficiency of the gravel roof, as determined in the GG subscale tests (see Appendix A). A fluorescent orange paint was sprayed on the surface of the gravel roof to enhance photography. The simulated Gravel Gertie was documented in a set of drawings prepared by Holmes & Narver [HN82]. Acting as consultants for Dept. 6320, A&W and SwRI reviewed and approved the design. Figures C-4 through C-9 show the construction program from initial excavation of the 1956 structure through completion of the 1982 structure.

Assembly Cell--The assembly cell and the associated structures were originally constructed per Mason & Hanger drawings [PX2] to support the Gravel Gertie test series in the 1950s. In March 1982, the test structure was excavated, and the assembly cell was judged suitable for reuse, subject to some repair and modifying construction. Modifications were incorporated to accommodate instrumentation, false ceiling, air conditioning ducts, and a representative doorway.

Staging Area--The former staging area was removed and replaced with a new structure that was more representative of the round room entrance cross section and configuration, as well as total staging area volume of cell 8 at Pantex. The blast baffle/gravel pocket configuration used in cell 8 [PX1] was omitted to assure that all venting action occurred through the gravel roof. The personnel and equipment access doors were replaced with a single blast door salvaged from the 1950s structure.

High Explosive Aerosol Generator (HEAG)

Four HEAGs were used in the test. Each was detonated on the bottom surface using an SNLA arming and firing (A&F) system with a single EBW detonator and booster charge. The HE charges were located in the center of the operating bay with the bottom surface 61 cm (24 inches) above the floor. Each HEAG consisted of a 48-kilogram spherical charge of PBX-9501 with an internal depleted-uranium shell weighing 2 kilograms. The generator was uncased to minimize shrapnel damage to the instrumentation systems within the structure.

The HEAGs were suspend from the roof by a system consisting of nylon slings and a block and tackle attached to the cable hub, Figure C-10.

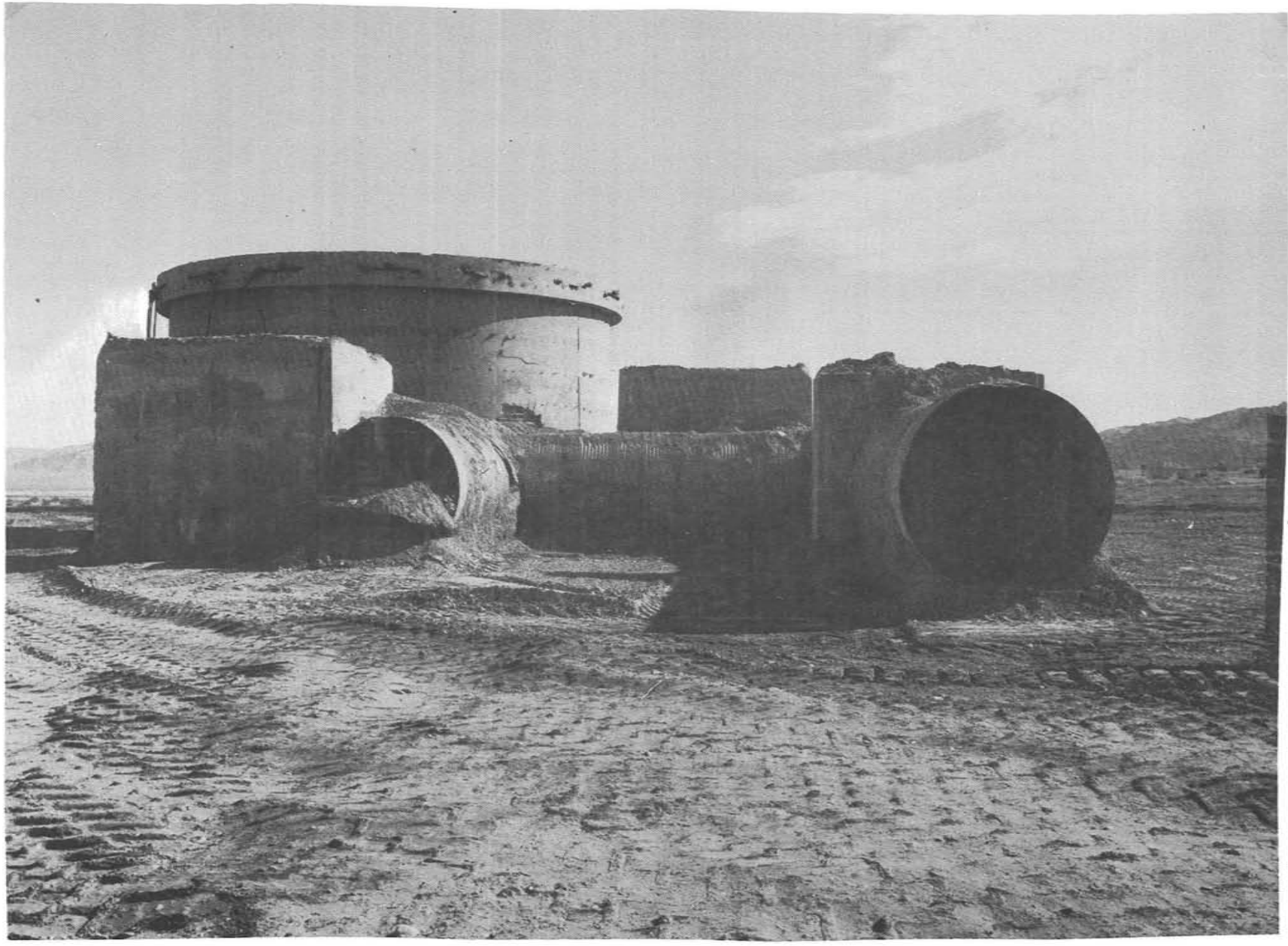

Figure C-4. Excavated 1956 Structure

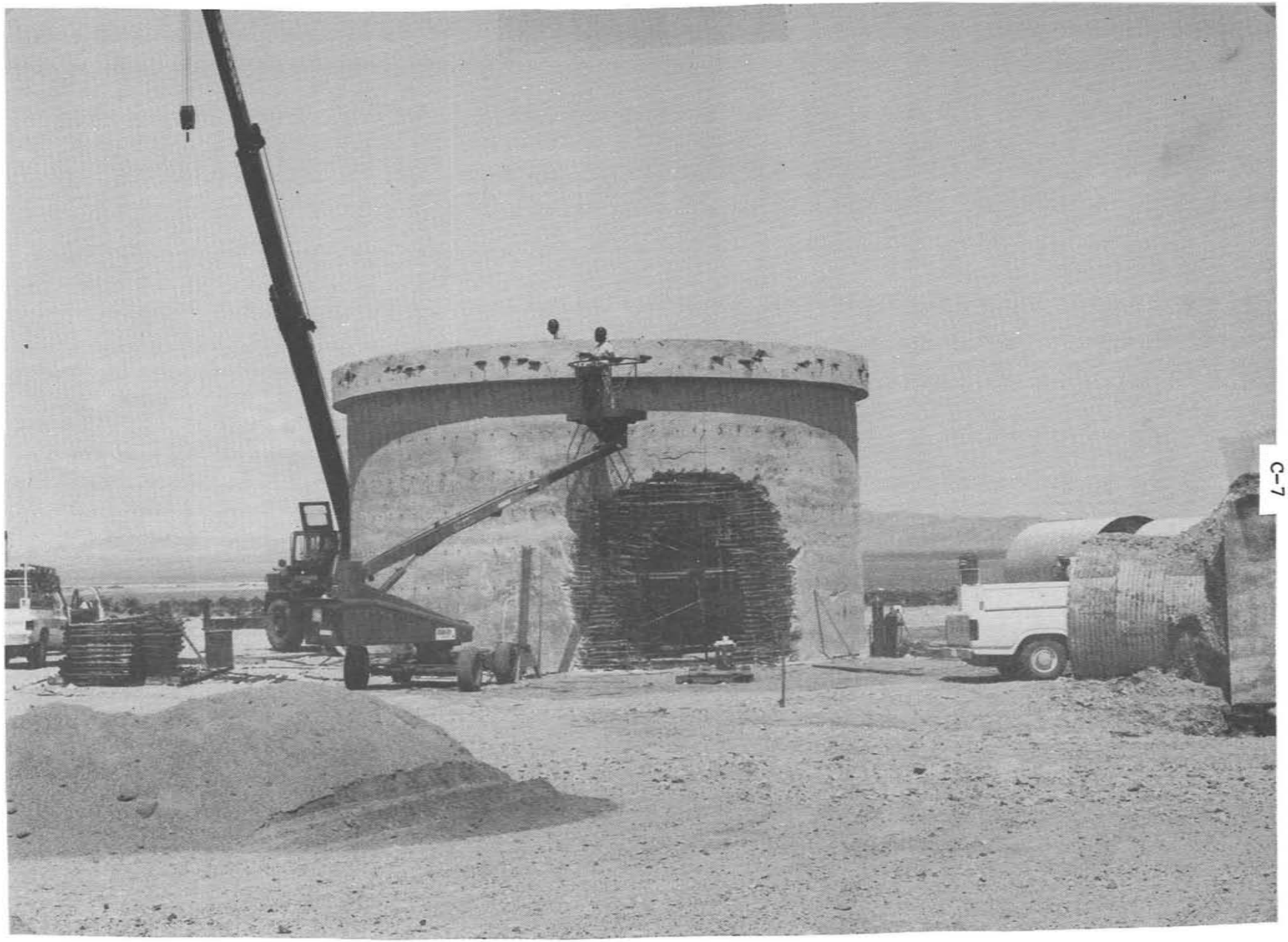

Figure C-5. Repair to Round Room Entrance

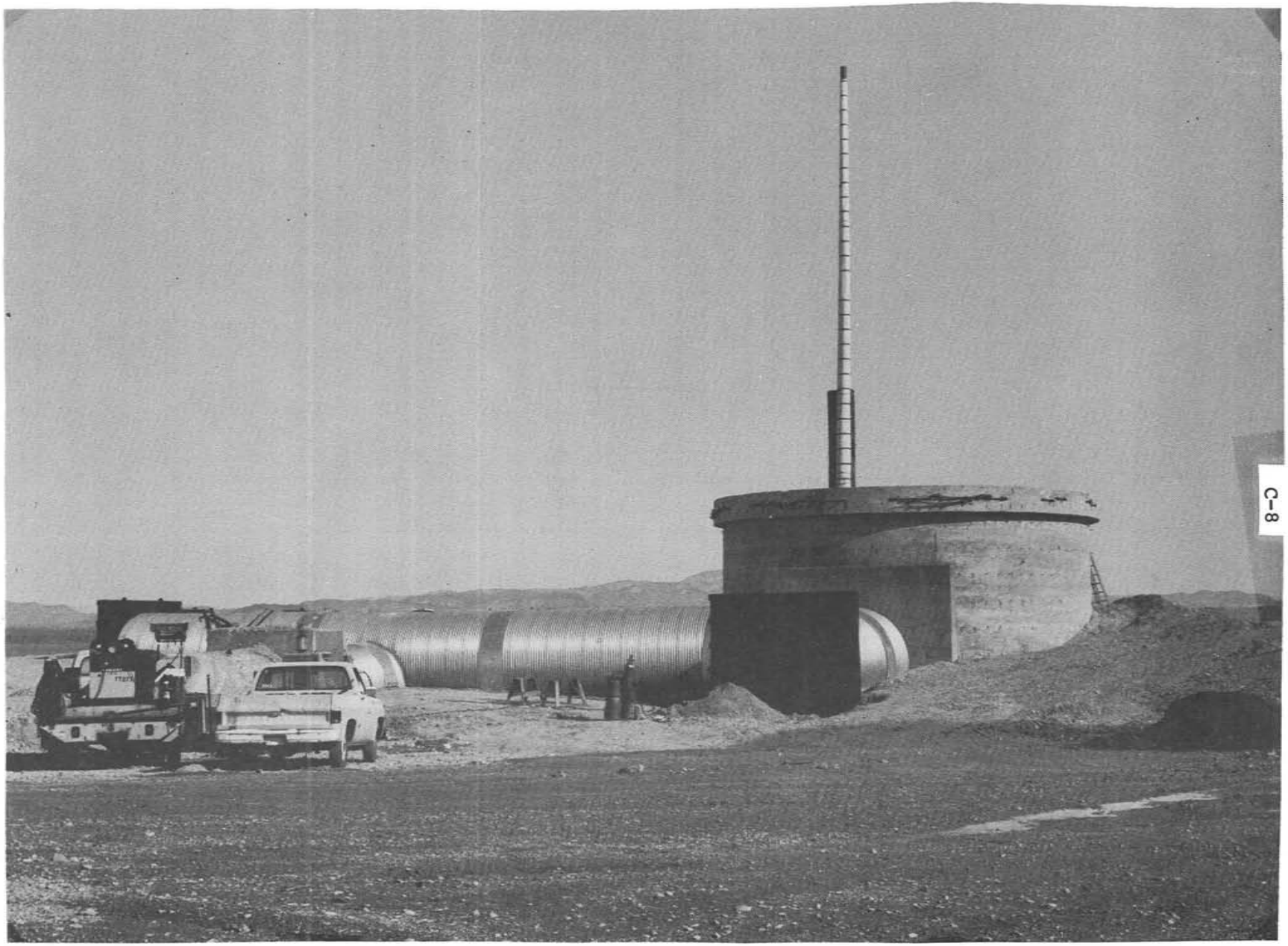

Figure C-6. Installation of Culvert Staging Area

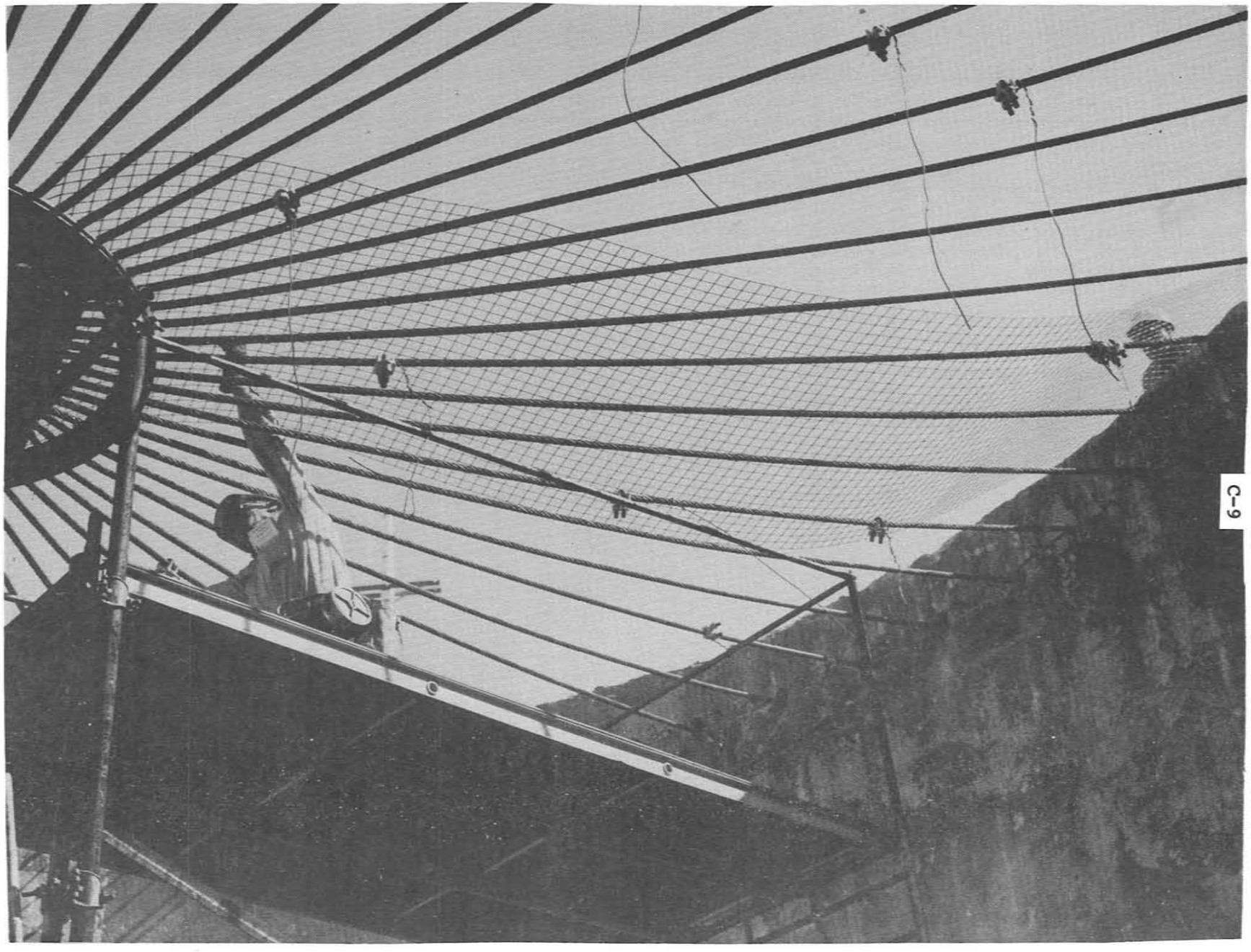

Figure C-7. Installation of Wire Roof Support

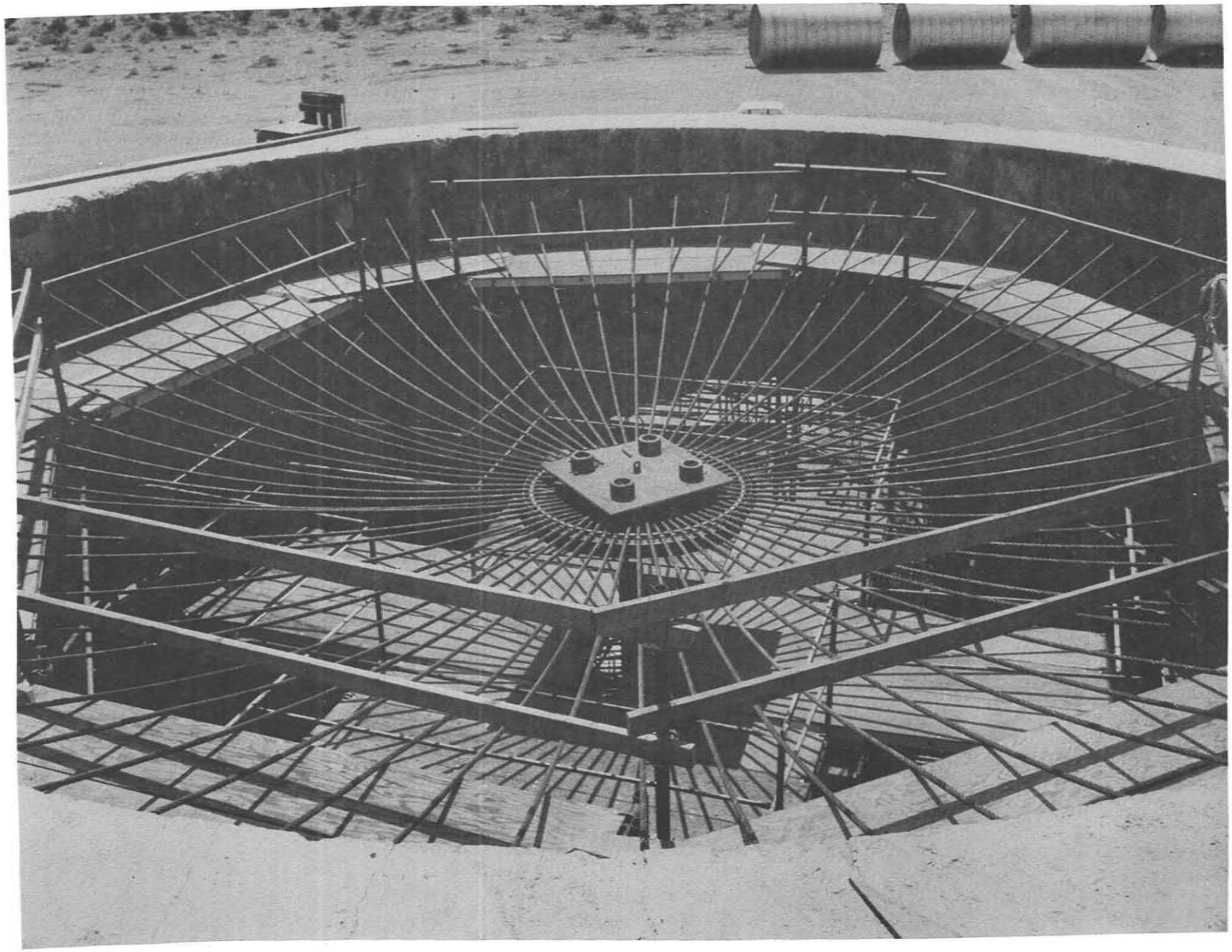

Figure C-8. Spider Ring and Main Cabling

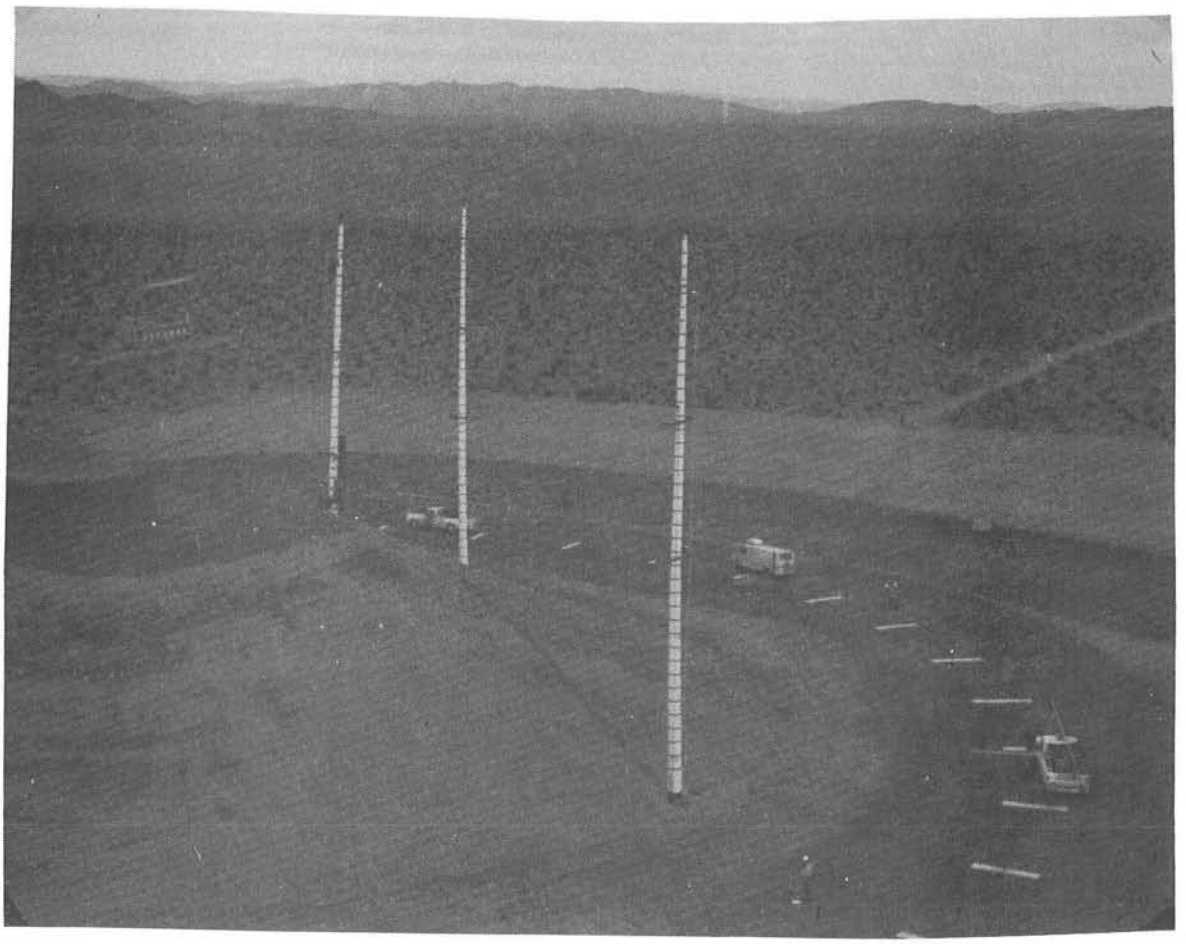

Figure C-9. Finished Structure

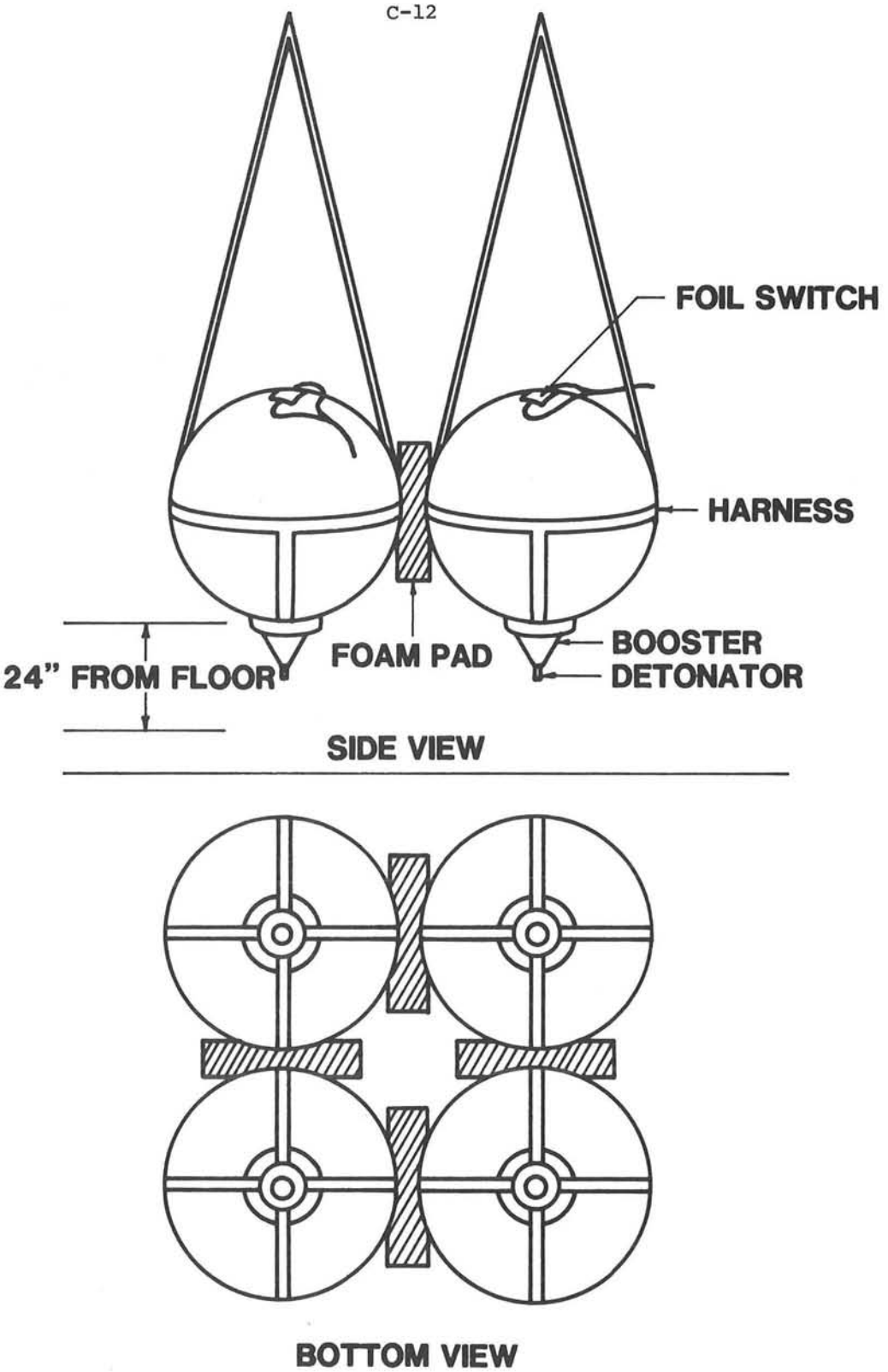

Figure C-10. Gravel Gertie--HEAG Arrangement

The four test devices were simultaneously detonated using SNLA A&F system, Figure C-11. Simultaneity of the detonation of the four test devices was determined by recording signals from foil switches bonded to the top surface of each device.

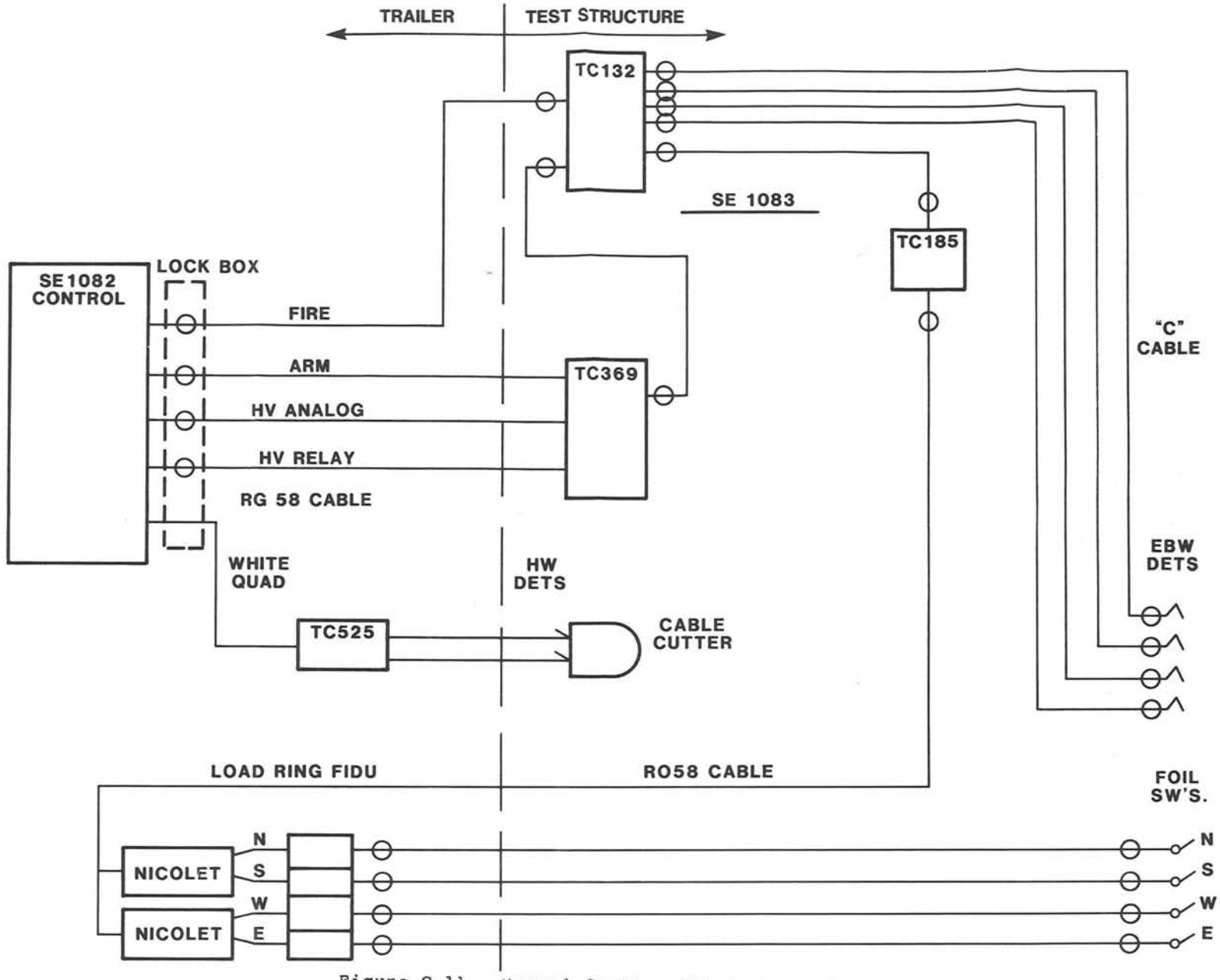

Figure C-11. Gravel Gertie--A&F System Schematic

Appendix D
Aerosol Sampling System Details and Data

This appendix summarizes the installation, performance and significant results from the various internal and external aerosol sampling systems installed in the full-scale Gravel Gertie experiment. In addition a general description of the procedures used to analyze and characterize aerosols is provided.

Aerosol Sampling Package (GGASP)

The GGASPs [SL82], Figures D-1 and D-2, were designed to be installed in the operating bay and the staging area for the collection of aerosols generatedby the test devices. They were designed to withstand the quasi-static over-pressure expected during the test, but were protected from fragments and the incident and reflected overpressures by shields provided by H&N/REECO [HN82]. A test sequencer in the instrumentation trailer operated a solenoid valve in each GGASP unit to capture a 20-liter sample of detonation-produced aerosols in an evacuated sample chamber. Subsequently, the same sequencer operated a pump in the GGASP to circulate the aerosol sampling through a filter assembly (FA) and two Mercer cascade impactors (CI) to remove the aerosols for analysis. Aerosols deposited in the aerosol chamber were sampled on SEM planchets, TEM grids, and were removed for quantitative analysis by an acid rinse.

"Doughnut" Sampling Array (DSA)

Consistent with the concept of sampling as close to the source as possible a sampler array was installed above the rim of the round room on the overburden. These samplers were intended to detect aerosol escaping from around the edge of the round room by mechanisms such as seepage or base surge entrainment that might result in aerosols of concern bypassing the other installed instrumentation.

Eight 2-cm-diameter bars extending 1.8 m above grade were installed in the earth backfill on a radius of approximately 10 meters from the center of the round room (see Figure D-3). Two Mesa Mine Safety Appliance 2G-2239-2 battery-powered total filter air samplers were attached to each of these stakes at heights of 0.9 and and 1.8 m. The samplers were installed prior to shot day with the sample ports plugged and the samplers de-energized. All samplers were turned on and checked for proper operation 1/2 hour preshot and de-energized approximately 45 minutes postshot. All samplers, with the exception of number 8L were recovered immediately. The lower sampler at Station 8 was never recovered and is assumed to be buried in crater rubble.

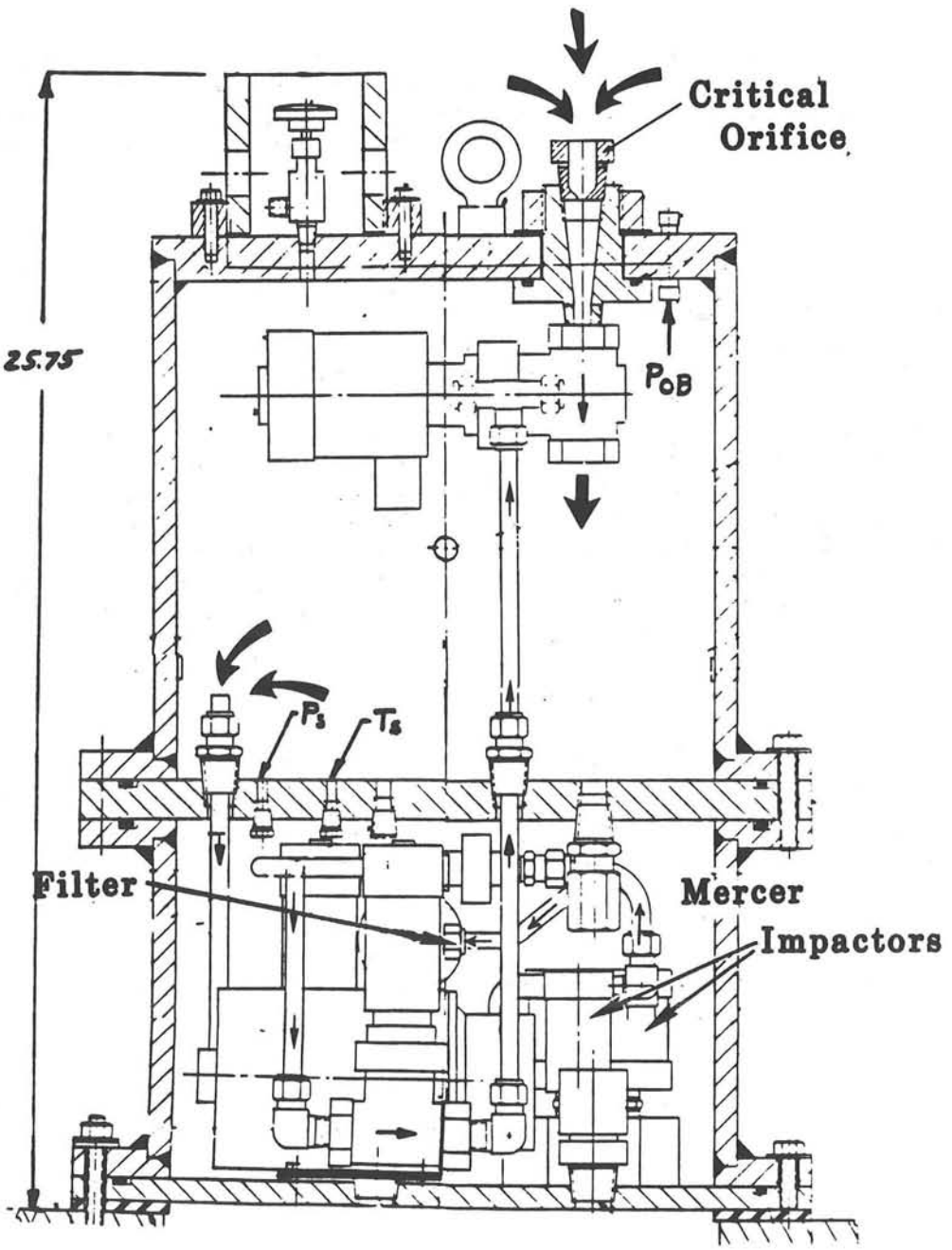

Figure D-1. GGASP Sampler Cross Section

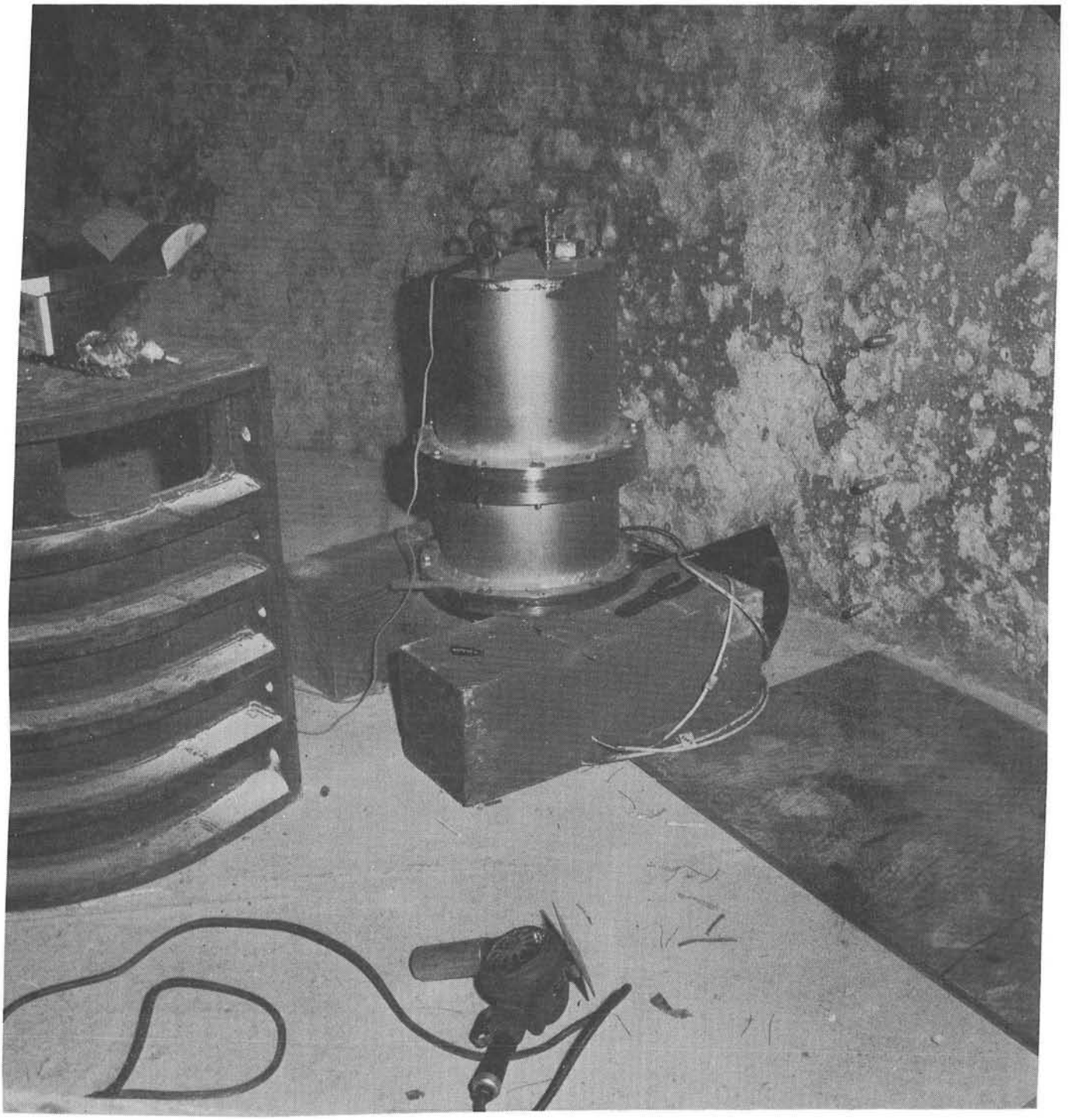

Figure D-2. GGASP Unit Ready for Installation

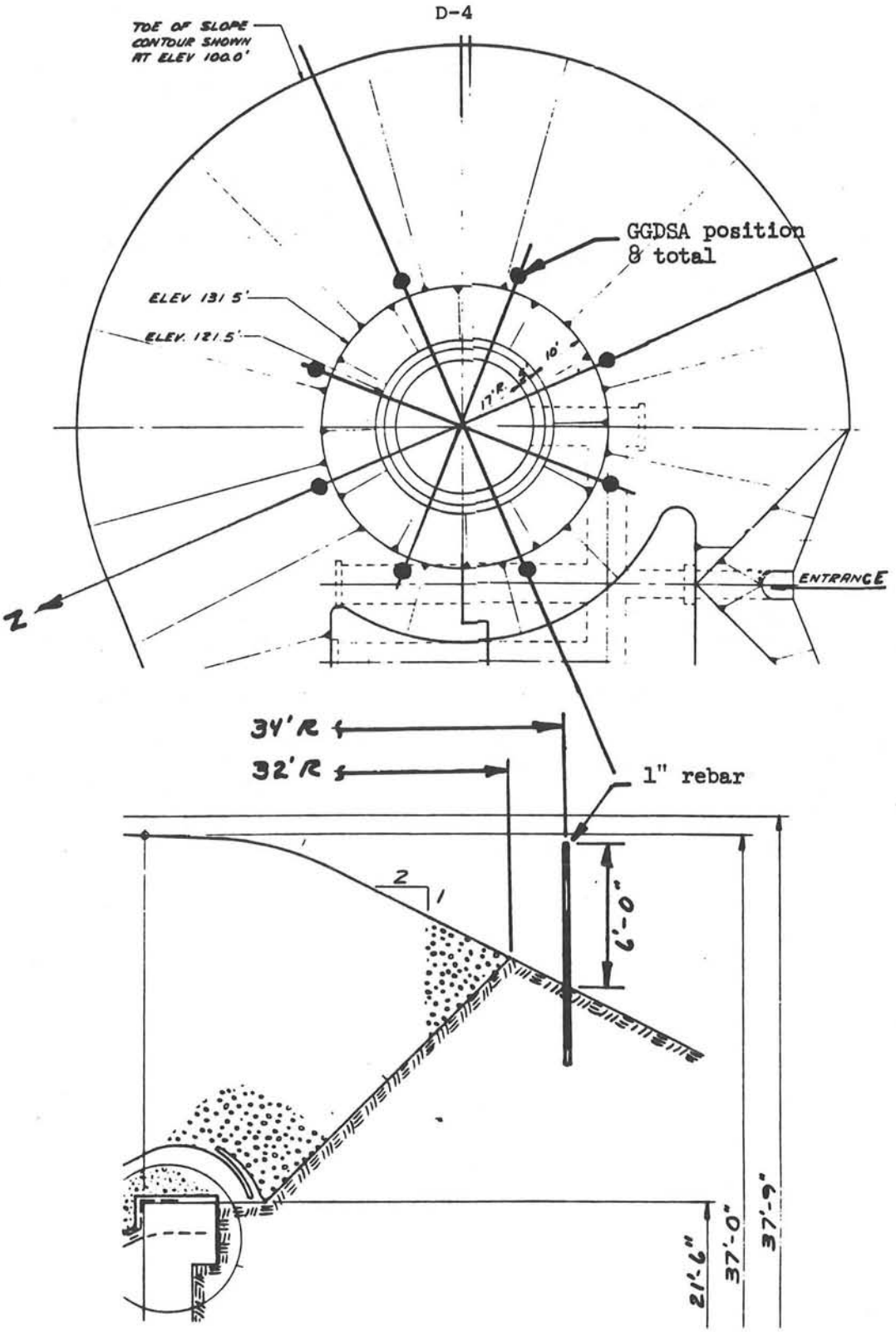

Figure D-3. Gravel Gertie Doughnut Sampling Array (GGDSA)

Results

Table D-1 summarizes the data and samples from the DSA which showed statistically significant uranium collections.

External Sampling Array (ESA)

The External Sampling Array (ESA) [SL82] was designed to obtain a sample of any tracer aerosol which might vent as the gravel roof expanded during the first few seconds postdetonation. The basic array, shown on Figure D-4, was suspended above the center of the round room, 7 m above the top of the undisturbed gravel mound.

Installation

The ESA was shipped to NTS in early November. Following a period of indoor assembly and testing, the unit was taken to the site and rigged between the north and south poles of the Pole Sampling Array. Power for pumps, electrostatic precipitators, etc, was fed to the ESA via a cable from the south support pole.

Operation

All ESA systems were energized and checked with the unit in the lowered position on 18 and 19 November. Samplers were unplugged and the unit was raised and placed in its test configuration on 19 November. During the test, the boom began to deploy at time t = 0.2 seconds and was fully deployed at time t $\cong$ 1.5 seconds. Figure D-5 shows the ESA in the fully deployed configuration.

The ESA was de-energized and was lowered for sample recovery within 2 hours postshot. Subsequently, the ESA was disassembled for shipment back to SNLA.

Tables D-2a and b show the data from the vertical and horizontal instruments of the ESA, respectively. Several ESA air samplers appeared to provide significant results: V1 at the lower end of the boom with about 310 μg-s/m^3, and V4 at the upper end of the boom with about 180 μg-s/m^3. On the horizontal beam, H1 with about 390 μg-s/m^3, H2 with about 1460 μg-s/m^3, H6 with about 480 μg-s/m^3, H8 with about 860 μg-s/m^3 and H9 with about 380 μg-s/m^3 were the only samplers with significant uranium collections. Because these data are the sum of several stages of an impactor with most stages only marginally above the detection limit, the significance of these data is also suspect. Also shown in the tables are filter data (FL) and collector tray data (CT).

TABLE D-1

Gravel Gertie Data DSA

(Bkgnd U @ 3.5 ppm in soil)

	FLOW RATE (LITERS/MIN)	URANIUM (NG)	URANIUM UNCERT (NG)	SIGNIFICANT URANIUM[c]	SOIL (MG)	BKGND U (NG)	NET U (μG-SEC/M**3)[d]
UPPER 1	1.9	32.9	10.0	y	0.4	1.4	1,015.6
LOWER 1	2.4	0.9	10.0	-	0.2	0.6	-
UPPER 2	1.9	21.9	10.0	y	1.0	3.6	565.8
LOWER 2	2.0	6.9	10.0	-	0.4	1.4	-
UPPER 3	1.9	21.9	10.0	y	0.3	1.1	641.4
LOWER 3 (ND)[a]	--	-	--	-	-	-	-
UPPER 4	1.8	123.9	10.0	y	0.4	1.3	4,014.4
LOWER 4	1.9	205.2	10.0	y	0.6	2.2	6,361.3
UPPER 5	1.6	72.0	10.0	y	0.4	1.3	2,596.6
LOWER 5	2.5	183.9	10.0	y	0.9	3.0	4,389.6
UPPER 6	0.9	144.9	10.0	y	0.2	0.8	9,646.9
LOWER 6	2.0	416.3	10.0	y	0.4	1.5	12,253.9
UPPER 7	2.2	29.4	10.0	y	0.3	0.9	767.5
LOWER 7 (ND)[a]	--	-	-	-	-	-	-
UPPER 8	1.7	3.9	10.0	-	0.6-	2.2	-
LOWER 8 (LIT)[b]	0.1	-	-	-	-	-	-

[a]ND-not deployed: unit disfunction prior to test time
[b]LIT-Lost in test, unit not recovered
[c]y indicates significant deposit of uranium
[d]time (in seconds) it takes cloud to traverse sampler.

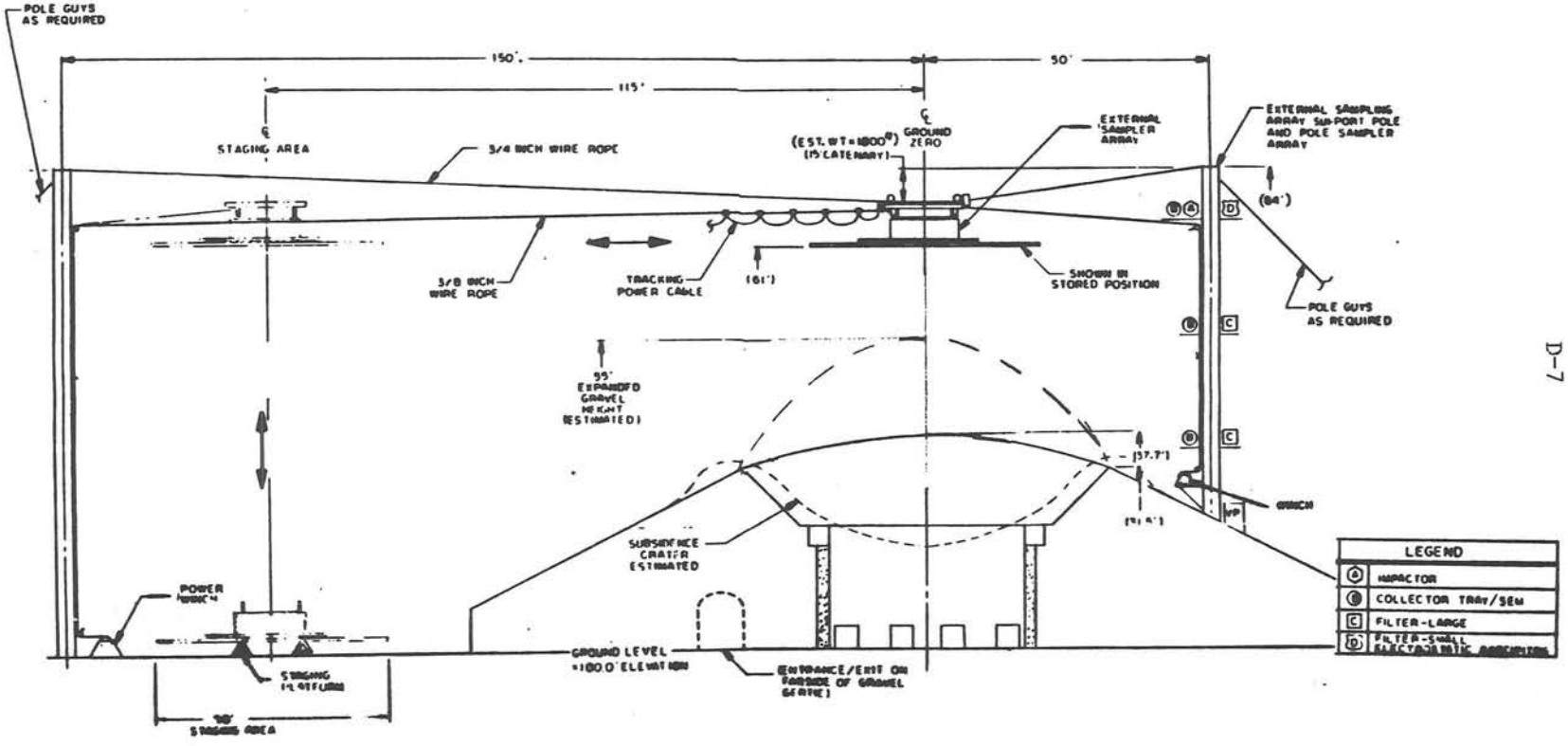

Figure D-4. Gravel Gertie External Sampling Array (GGESA)

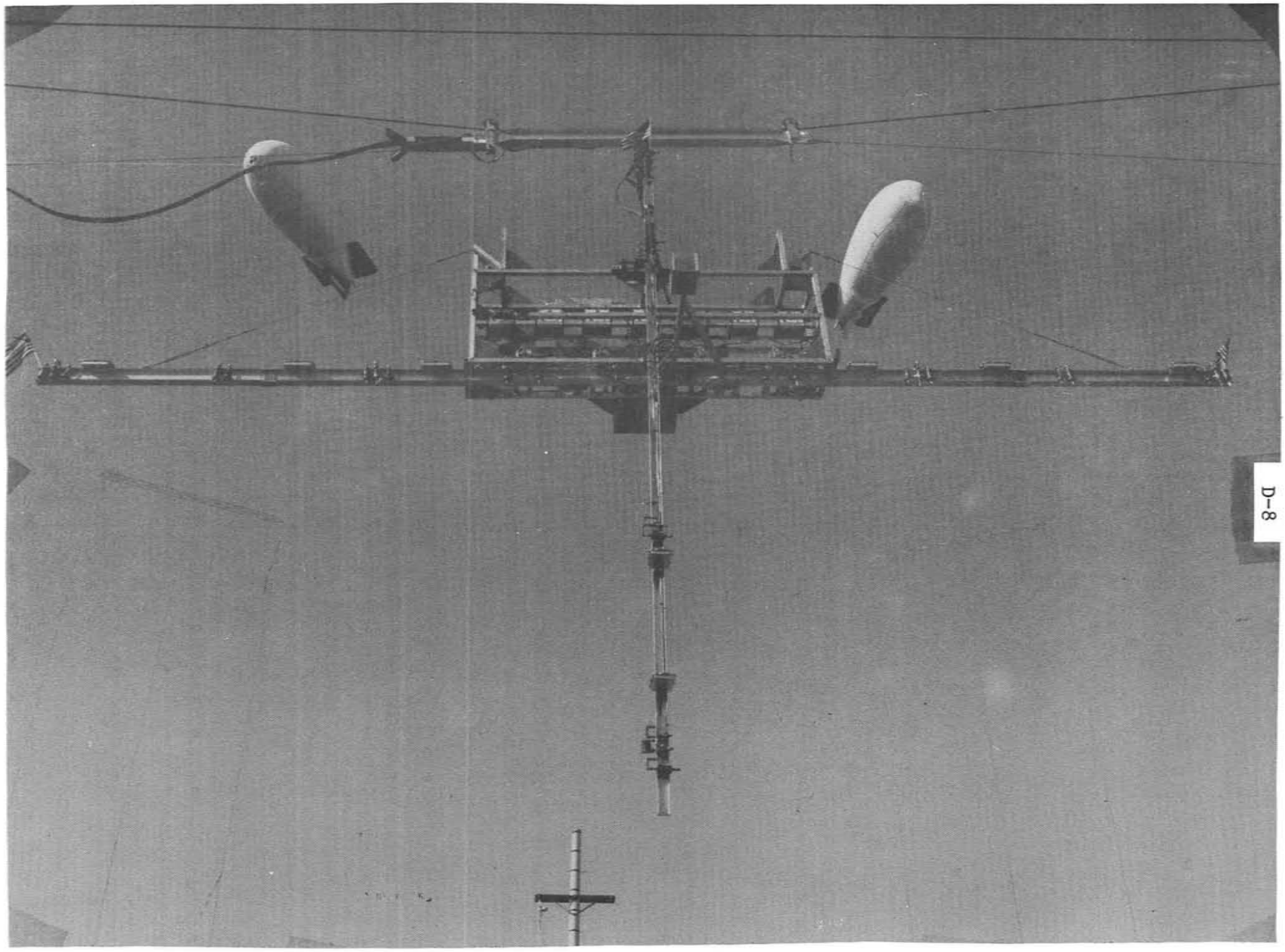

Figure D-5. ESA in Fully Deployed Configuration

TABLE D-2a

Gravel Gertie Data
ESA Vertical Boom Instruments

	FLOW RATE (LITERS/MIN)	MEAS. U (NG)	U UNCERT. (NG)	SIG.U NON-ZERO[a]	TOT. MASS (NG)	NET U (NG)	NET U (μG-S/M**3)	SIG U (μG-S/m**3)	U DEP (μG/M**2)
L1 V1	15.9	11.4	10.0	-	0.1	11.0	41.6	41.6	-
L2	15.9	11.4	10.0	-	-	11.4	43.0	43.0	-
L3	15.9	2.4	10.0	-	0.0	2.3	8.8	-	-
L4	15.9	-	-	-	-	-	-	-	-
L5	15.9	-	-	-	0.0	-	-	-	-
L6	15.9	15.9	10.0	1.0	-	15.9	60.0	60.0	-
L7	15.9	23.4	10.0	1.0	0.0	23.4	88.2	88.2	-
L8	15.9	20.2	10.0	1.0	0.4	18.9	71.3	71.3	-
TOT		84.7	60.0	-	0.6	82.9	312.9	312.9	-
L1 V2	15.9	5.4	10.0	-	0.2	4.5	17.1	-	-
L2	15.9	-	-	-	0.0	-	-	-	-
L3	15.9	2.4	10.0	-	0.1	2.1	7.8	-	-
L4	15.9	-	-	-	0.0	-	-	-	-
L5	15.0	-	-	-	-	-	-	-	-
L6	15.9	-	-	-	-	-	-	-	-
L7	15.9	-	-	-	0.0	-	-	-	-
L8	15.9	3.9	10.0	-	0.2	3.1	11.7	-	-
TOT		11.7	30.0	-	0.6	9.7	36.6	-	-
L1 V3	14.3	-	-	-	0.6	-	-	-	-
L2	14.3	-	-	-	0.2	-	-	-	-
L3	14.3	3.9	10.0	-	0.5	2.3	9.6	-	-
L4	14.3	-	-	-	0.3	-	-	-	-
L5	14.3	5.4	10.0	-	0.2	4.6	19.4	-	-
L6	14.3	2.4	10.0	-	0.3	1.5	6.4	-	-
L7	14.3	-	-	-	0.1	-	-	-	-
L8	14.3	-	-	-	0.4	-	-	-	-
TOT		11.7	30.0	-	2.5	8.4	35.4	-	-

[a]1.0 denotes significant quantity of uranium above background

TABLE D-2a (Cont.)

Gravel Gertie Data
ESA Vertical Boom Instruments

	FLOW RATE (LITERS/MIN)	MEAS. U (NG)	U UNCERT. (NG)	SIG.U NON-ZERO[a]	TOT. MASS (NG)	NET U (NG)	NET U (μG-S/M**3)	SIG U (μG-S/m**3)	U DEP (μG/M**2)
L1 V4	15.7	20.4	10.0	1.0	0.6	18.2	69.7	69.7	-
L2	15.7	3.9	10.0	-	0.4	2.7	10.2	-	-
L3	15.7	-	-	-	0.2	-	-	-	-
L4	15.7	9.9	10.0	-	0.1	9.4	36.1	-	-
L5	15.7	15.9	10.0	1.0	0.1	15.6	59.7	59.7	-
L6	15.7	-	-	-	0.1	-	-	-	-
L7	15.7	0.9	10.0	-	0.0	0.8	2.9	-	-
L8	15.7	0.9	10.0	-	0.3	-	-	-	-
TOT		51.9	60.0	-	1.8	46.7	178.6	-	-
V1 FL	8.6	-	-	-	0.5	-	-	-	-
V2 FL	8.4	-	-	-	0.4	-	-	-	-
V3 FL	8.4	-	-	-	0.4	-	-	-	-
V4 FL	8.4	-	-	-	0.5	-	-	-	-
V1 CT	-	-	10.0	-	-	-	-	-	-
V2 CT	-	-	10.0	-	-	-	-	-	-
V3 CT	-	1,284.4	10.0	1.0	-	1,284.4	-	-	26.5
V4 CT	-	47,944.1	10.0	1.0	-	47,944.1	-	-	987.5

[a]1.0 denotes significant quantity of uranium above background

TABLE D-2b
Gravel Gertie Data
ESA Horizontal Instruments

	FLOW RATE (LITERS/MIN)	MEAS. U (NG)	U UNCERT. (NG)	SIG.U NON-ZERO[a]	TOT. MASS (NG)	NET U (NG)	NET U (μG-S/M**3)	SIG U (μG-S/m**3)	U DEP (μG/M**2)
L1 H1	14.7	-	-	-	1.4	-	-	-	-
L2	14.7	-	-	-	0.3	-	-	-	-
L3	14.7	-	-	-	0.1	-	-	-	-
L4	14.7	27.9	10.0	1.0	0.1	27.7	113.2	113.2	-
L5	14.7	-	-	-	-	-	-	-	-
L6	14.7	15.9	10.0	1.0	0.0	15.9	64.8	64.8	-
L7	14.7	-	-	-	0.0	-	-	-	-
L8	14.7	60.9	10.0	1.0	0.6	59.0	240.7	240.7	-
TOT		104.7	30.0	1.0	2.4	96.2	392.6	392.6	-
L1 H2	17.3	296.1	10.0	1.0	1.0	292.6	1,014.8	1,014.8	-
L2	17.3	123.9	10.0	1.0	0.4	122.7	425.5	425.5	-
L3	17.3	5.4	10.0	-	0.8	2.7	9.5	-	-
L4	17.3	-	--	-	0.4	-	-	-	-
L5	17.3	-	--	-	0.4	-	-	-	-
L6	17.3	3.9	10.0	-	0.3	2.7	9.5	-	-
L7	17.3	-	-	-	0.2	-	-	-	-
L8	17.3	3.9	10.0	-	0.1	3.4	11.9	-	-
TOT		433.2	50.0	1.0	3.5	420.9	1,459.8	1,459.8	-
L1 H3	14.3	1.5	10.0	-	0.4	0.1	0.5	-	-
L2	14.3	4.5	10.0	-	0.5	2.8	11.8	-	-
L3	14.3	3.0	10.0	-	0.2	2.3	9.7	-	-
L4	14.4	1.5	10.0	-	0.2	0.9	3.9	-	-
L5	14.3	3.0	10.0	-	0.1	2.8	11.7	-	-
L6	14.3	1.5	10.0	-	0.1	1.3	5.4	-	-
L7	14.3	-	-	-	-	-	-	-	
L8	14.3	3.0	10.0	-	0.3	2.0	8.5	-	-
TOT		18.0	70.0	-	1.6	12.3	51.5	-	-

[a]1.0 denotes significant quantity of uranium above background

TABLE D-2b (Cont.)
Gravel Gertie Data
ESA Horizontal Instruments

	FLOW RATE (LITERS/MIN)	MEAS. U (NG)	U UNCERT. (NG)	SIG.U NON-ZERO[a]	TOT. MASS (NG)	NET U (NG)	NET U (μG-S/M**3)	SIG U (μG-S/m**3)	U DEP (μG/M**2)
L1 H4	15.0	0.9	10.0	-	0.6	-	-	-	-
L2	15.0	-	-	-	0.1	-	-	-	-
L3	15.0	-	-	-	0.2	-	-	-	-
L4	15.0	-	-	-	0.1	-	-	-	-
L5	15.0	8.4	10.0	-	0.2	7.8	31.1	-	-
L6	15.0	8.4	10.0	-		8.4	33.5	-	-
L7	15.0	-	-	-	0.2	-	-	-	-
L8	15.0	-	-	-	0.3	-	-	-	-
TOT		17.6	30.0	-	1.7	11.9	47.5	-	-
L1 H5	15.1	-	-	-	0.4	-	-	-	-
L2	15.1	-	-	-	-	-	-	-	-
L3	15.1	-	-	-	0.0	-	-	-	-
L4	15.1	-	-	-	-	-	-	-	-
L5	15.1	-	-	-	0.0	-	-	-	-
L6	15.1	-	-	-	-	-	-	-	-
L7	15.1	-	-	-	-	-	-	-	-
L8	15.1	-	-	-	0.3	-	-	-	-
TOT		-	-	-	0.8	-	-	-	-

[a]1.0 denotes significant quantity of uranium above background

TABLE D-2b (Cont.)
Gravel Gertie Data
ESA Horizontal Instruments

	FLOW RATE (LITERS/MIN)	MEAS. U (NG)	U UNCERT. (NG)	SIG.U NON-ZERO[a]	TOT. MASS (NG)	NET U (NG)	NET U (μG-S/M**3)	SIG U (μG-S/m**3)	U DEP (μG/M**2)
L1 N6	15.1	110.4	10.0	1.0	0.4	109.0	433.0	-	-
L2	15.1	-	-	-	0.3	-	-	-	-
L3	15.1	-	-	-	0.3	-	-	-	-
L4	15.1	-	-	-	0.1	-	-	-	-
L5	15.1	-	-	-	0.1	-	-	-	-
L6	15.1	6.9	10.0	-	0.0	6.8	26.9	-	-
L7	15.1	3.9	10.0	-	0.1	3.7	14.8	-	-
L8	15.1	5.4	10.0	-	0.6	3.4	13.5	-	-
TOT	15.1	126.6	40.0	1.0	1.8	120.3	477.9	-	-
L1 M7	15.2	1.5	10.0	-	0.6	-	-	-	-
L2	15.2	1.5	10.0	-	0.3	0.6	2.4	-	-
L3	15.2	3.0	10.0	-	0.1	2.7	10.5	-	-
L4	15.2	1.5	10.0	-	0.2	0.9	3.7	-	-
L5	15.2	1.5	10.0	-	0.2	0.9	3.4	-	-
L6	15.2	1.5	10.0	-	0.1	1.2	4.6	-	-
L7	15.2	-	-	-	-	-	-	-	-
L8	15.2	1.5	10.0	-	0.4	0.1	0.2	-	-
TOT	15.2	12.0	70.0	-	1.8	5.6	22.1	-	-
L1 H8	15.1	5.4	10.0	-	0.8	2.7	10.7	-	-
L2	15.1	5.4	10.0	-	0.2	4.9	19.4	-	-
L3	15.1	152.4	10.0	1.0	0.1	151.9	603.6	603.6	-
L4	15.1	-	-	-	-	-	-	-	-
L5	15.1	47.4	10.0	1.0	0.0	47.4	188.2	188.2	-
L6	15.1	-	-	-	0.0	-	-	-	-
L7	15.1	10.0	10.0	-	0.0	9.9	39.5	-	-
L8	15.1	-	-	-	0.3	-	-	-	-
TOT	15.1	220.6	50.0	1.0	1.4	215.7	857.1	857.1	-
L1 H9	15.1	-	-	-	0.1	-	-	-	-
L2	15.1	-	-	-	0.0	-	-	-	
L3	15.1	96.9	10.0	1.0	-	96.9	385.0	385.0	-

[a]1.0 denotes significant quantity of uranium above background

TABLE D-2b (Cont.)
Gravel Gertie Data
ESA Horizontal Instruments

	FLOW RATE (LITERS/MIN)	MEAS. U (NG)	U UNCERT. (NG)	SIG.U NON-ZERO[a]	TOT. MASS (NG)	NET U (NG)	NET U (μG-S/M**3)	SIG U (μG-S/m**3)	U DEP (μG/M**2)
L4	15.1	-	-	-	-	-	-	-	-
L5	15.1	-	-	-	0.0	-	-	-	-
L6	15.1	-	-	-	0.0	-	-	-	-
L7	15.1	-	-	-	0.1	-	-	-	-
L8	15.1	-	-	-	0.3	-	-	-	-
TOT	15.1	96.9	10.0	1.0	0.5	95.0	377.5	377.5	-
M1 FL	8.5	-	-	-	0.6	-	-	-	-
M2 FL	8.5	8.0	-	-	0.6	6.0	42.6	-	-
M3 FL	8.6	-	-	-	0.6	-	-	-	-
M4 FL	8.6	-	-	-	1.1	-	-	-	-
M5 FL	8.6	-	-	-	0.8	-	-	-	-
M6 FL	8.6	-	-	-	0.3	-	-	-	-
M7 FL	8.6	-	-	-	0.5	-	-	-	-
M8 FL	8.6	-	-	-	0.4	-	-	-	-
M9 FL	9.1	-	-	-	0.3	-	-	-	-
M1 CT	-	1,375.0	10.0	1.0	-	1,375.0	-	-	32.4
M2 CT	-	56.7	10.0	1.0	-	56.7	-	-	1.2
M3 CT	-	75.3	10.0	1.0	-	75.3	-	-	1.6
M4 CT	-	21.1	10.0	1.0	-	21.1	-	-	0.4
M5 CT	-	13.3	10.0	-	-	13.3	-	-	-
M6 CT	-	18.0	10.0	1.0	-	18.0	-	-	0.4
M7 CT	-	87.7	10.0	1.0	-	87.7	-	-	1.8
M8 CT	-	45.9	10.0	1.0	-	45.9	-	-	0.9
M9 CT	-	427.2	10.0	1.0	-	427.2	-	8.8	8.8

[a]1.0 denotes signiticant quantity of uranium above background

Balloon Sampling Array (BSA)

Introduction

In order to ensure maximum aerosol capture close to the Gravel Gertie without going to the expense of a 360° pole-mounted array, it was decided that a balloon suspension system, similar to that used on earlier explosive aerosol tests such as Operation Roller Coaster, would be useful.

System Description

Two 99 m^3 aerodynamically shaped balloons, each with a maximum lift capability of about 45 kg (depending upon altitude and air temperature), were each used to suspend three lines of the aerosol samplers. This is a similar approach to that used in the Roller Coaster experiments, but on a much smaller scale. The winches for controlling the large balloons were mounted in pickup trucks. The width of the balloon curtain was 47.8 meters. Two smaller balloons (7 m^3) were added to the system half way between the two larger balloons to increase the width of the array and each provided sufficient lifting capacity to suspend a fully instrumented sampler line.

The final configuration, shown in Figure D-6, consisted of eight cables, each supporting cascade impactors and/or filter samplers, suspended from a network of four balloons. Power supplies, pumps, flowmeters, etc, were located on each of the three vehicles.

Operation

The balloon sampling array (BSA) was initially fielded in mid-October and a ground crew was assembled and trained. During the final phases of site construction a "racetrack" for use of the balloon support vehicles was surveyed and marked at 10° increments around the perimeter of the Gravel Gertie at a radial distance of 45.75 m (150 ft) from the center of the round room.

On November 19, one day before the shot was scheduled, the filter and impactor samplers were unplugged and flow rates were measured. The results of these measurements are given in Table D-3.

The shot-time configuration of the BSA is shown on Figure D-7. Table D-4 shows the significant results above background for the BSA. All samplers at the lowest level (F) had significant collections and some of the higher levels, on strings 1 and 3, showed significant collections. Table D-5 and Figure D-8 shows data for impactors placed at selected locations on the BSA. While stages of some impactors showed some collection of uranium, quantities are generally not significant.

SAMPLE ARRAY VIEWED FROM GRAVEL GERTIE

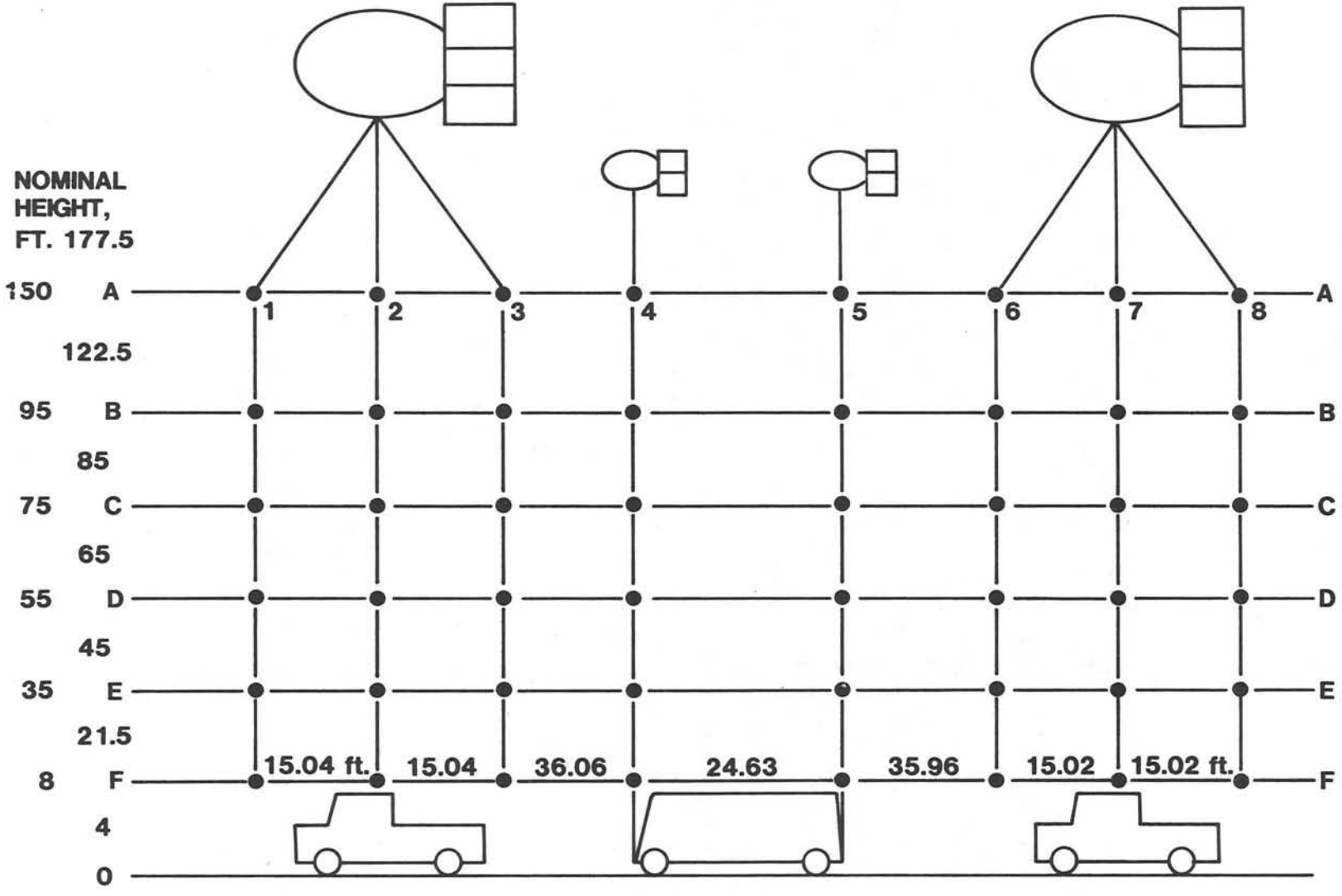

Figure D-6. GGBSA Viewed From the Gravel Gertie

TABLE D-3
BSA Flowrates

Sampler #				Flowrate (l/m)	Sampler #				Flowrate (l/m)
A6	181	022	R28	10	B1	102	12B	R05	10
A7	187	16C	R38	9	B2	108	41B	R11	10
A8	193	02C	R44	9	B3	114	07B	R17	10
B6	182	023	R27	10	C1	103	13B	R04	11
B7	188	21C	R37	10	C2	109	31B	R10	10
B8	194	09C	R43	9	C3	115	04B	R16	10
C6	183	027	R26	10	C3	65	09A	R22	0.6
C6	64	19A	R32	0.6	D1	104	14B	R03	11
C7	189	20C	R36	11	D2	110	30B	R09	10
C8	195	04C	R42	10	D3	116	08B	R15	10
D6	184	025	R25	11	D3	67	10A	R21	0.6
D6	66	18A	R31	0.635	E1	105	15B	R02	11
D7	190	19C	R35	10	E2	111	33B	R08	10
D8	196	06C	R41	10	E3	117	09B	R14	11
E6	185	024	R24	11	E3	61	11A	R20	0.625
E6	69	20A	R30	0.585	F1	106	10B	R01	11
E7	191	17C	R34	10	F2	112	38B	R07	11
E8	197	08C	R40	10	F3	118	06B	R13	10
F6	186	026	R23	11	F3	68	12A	R19	0.6
F6	63	17A	R29	0.6					
F7	192	18C	R33	11					
F8	198	07C	R39	10					
A4	119	10C	R50	9					
A5	125	002	R56	10					
B4	120	15C	R49	9					
B5	176	004	R55	9					
C4	121	12C	R48	10					
C5	177	009	R54	9					
D4	122	13C	R47	10					
D5	178	008	R53	10					
E4	123	11C	R46	10					
E5	179	007	R52	10					
F4	124	14C	R45	10					
F5	180	006	R51	10					
A1	101	11B	R06	10					
A2	107	29B	R12	9					
A3	113	02B	R18	9					

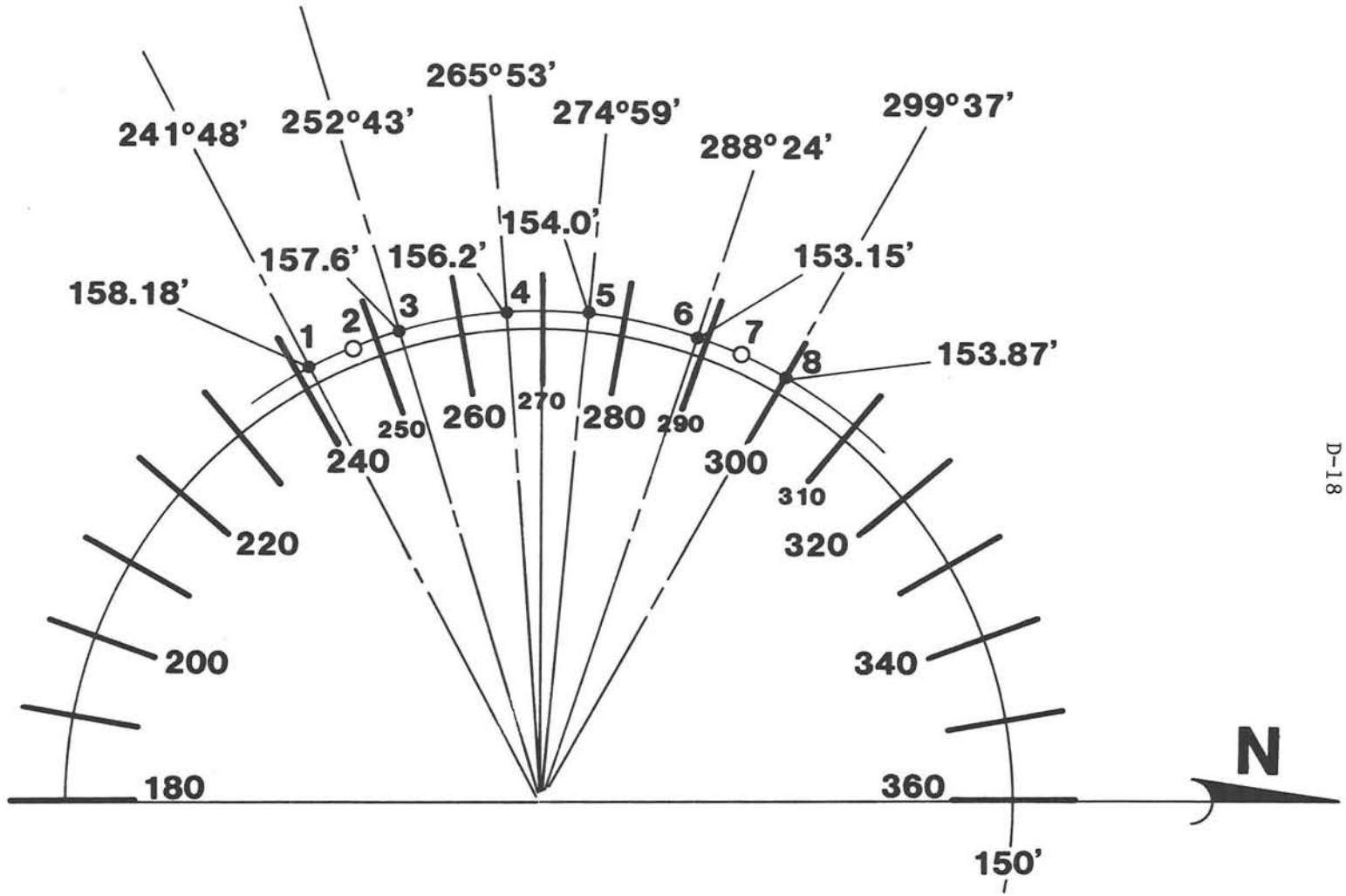

Figure D-7. Final Balloon Array During G.G. Test
Sampling Lines, Bottom Terminal Positions

TABLE D-4
GRAVEL GERTIE DATA BSA

	FLOW RATE (LITERS/MIN)	MEAS. U (IN NG)	U UNCERT.	SIG.U NON-ZERO	ANTIMONY (IN NG)	SCANDIUM (IN NG)	DEPLETED (U IN NG)	U/SC RATIO	SB/SC RATIO	U/SB RATIO	NET SB (μG-S/M**3)	NET U (μG-S/M**3)	
A1	10 0	10.0	8.0	-	4.0	1.1	33.7	30.6	4	8.4	22.7	-	A1
B1	10.0	-	-	-	-	1.0	(1.7)	(1.7)	-	-	(1.2)	-	B1
C1	11.0	16.0	9.0	-	34.0	5.1	48.1	9.4	7	1.4	179.9	-	C1
D1	11.0	25.0	9.0	1.0	5.0	0.8	87.4	105.4	6	17.5	26.4	477.0	D1
E1	11.0	66.0	5.0	1.0	27.0	4.2	227.4	54.1	6	8.4	142.7	1,240.2	E1
F1	11.0	118.0	12.0	1.0	75.0	5.2	410.5	78.9	14	5.5	403.4	2,239.2	F1
A2	9.0	-	-	-	-	-	-	-	-	-	-	-	A2
B2	10.0	9.0	8.0	-	-	1.2	29.9	24.9	-	-	(1.4)	-	B2
C2	10.0	9.0	8.0	-	-	1.2	10.9	5.8	-	-	(2.3)	-	C2
D2	10.0	10.0	8.0	-	10.0	2.1	5.9	4.6	2	2.6	53.3	-	D2
E2	10.0	50.0	9.0	1.0	11.0	2.5	172.9	61.8	4	15.7	62.6	1,037.5	E2
F2	11.0	143.0	13.0	1.0	.0		501.5	125.4	13	9.5	284.7	2,735.2	F2
A3	9.0	-	-	-	27.0	.5	.8	(1.7)	56	(0.0)	179.4	-	A3
B3	10.0	28.0	9.0	1.0	-	0.1	78.9	253.5	-	-	(0.5)	593.2	B3
C3	10.0	20.0	9.0	1.0	13.0	3.2	65.6	20.5	4	5.0	74.2	393.4	C3
D3	10.0	16.0	9.0	-	-	9.7	40.1	4.1	-	-	(11.6)	-	D3

TABLE D-4 (Continued)
GRAVEL GERTIE DATA BSA

	FLOW RATE (LITERS/MIN)	MEAS. U (IN NG)	U UNCERT.	SIG.U NON-ZERO	ANTIMONY (IN NG)	SCANDIUM (IN NG)	DEPLETED (U IN NG)	U/SC RATIO	SB/SC RATIO	U/SB RATIO	NET SB (µG-S/M**3)	NET U (µG-S/M**3)	
E3	11.0	34.0	9.0	1.0	37.0	7.6	107.7	14.2	5	2.9	193.5	187.7	E3
F3	10.0	40.0	9.0	1.0	21.0	5.2	133.2	25.6	4	6.3	119.8	799.3	F3
A4	9.0	-	-	-	-	-	-	-	-	-	-	-	A4
B4	9.0	1.0	8.0	-	2.0	0.9	2.0	2.3	2	1.0	12.2	-	B4
C4	10.0	8.0	8.0	-	2.0	0.3	27.9	90.0	6	14.0	11.6	-	C4
D4	10.0	-	-	-	6.0	1.7	(2.9)	(1.7)	4	(0.5)	34.0	-	D4
E4	10.0	4.0	8.0	-	14.0	-	14.2	-	-	1.0	84.0	-	E4
F4	10.0	53.0	9.0	1.0	2.0	1.3	186.2	143.2	2	93.1	10.4	1,117.0	F4
A5	10.0	-	-	-	-	-	-	-	0	-	-	-	A5
B5	9.0	-	-	-	-	0.4	(0.6)	(1.7)	-	-	(0.5)	-	B5
C5	9.0	9.0	8.0	-	-	0.1	31.8	264.9	-	-	(0.2)	-	C5
D5	10.0	12.0	8.0	-	22.0	3.8	36.1	9.5	6	1.6	127.4	-	D5
E5	10.0	4.0	8.0	-	-	-	14.2	-	-	-	-	-	E5
F5	10.0	26.0	9.0	1.0	4.0	1.8	89.3	49.6	2	22.3	21.8	535.9	F5
A6	10.0	-	-	-	2.0	0.5	(0.9)	(1.7)	4	(0.4)	11.4	-	A6
B6	10.0	-	-	-	-	-	-	-	-	-	-	-	B6
C6	10.0	-	-	-	5.0	-	-	-	-	-	-	-	C6
D6	11.0	-	-	-	-	-	-	-	-	-	-	-	D6

TABLE D-4 (Continued)

GRAVEL GERTIE DATA BSA

	FLOW RATE (LITERS/MIN)	MEAS. U (IN NG)	U UNCERT.	SIG.U NON-ZERO	ANTIMONY (IN NG)	SCANDIUM (IN NG)	DEPLETED (U IN NG)	U/SC RATIO	SB/SC RATIO	U/SB RATIO	NET SB (μG-S/M**3)	NET U (μG-S/M**3)	
E6	11.0	9.0	8.0	-	1.0	0.3	31.6	126.3	4	31.6	5.2	-	E6
F6	11.0	70.0	10.0	1.0	49.0	2.4	244.7	102.0	20	5.0	264.7	1,334.8	F6
A7	9.0	-	-	-	--	1.2	(2.1)	-	-	-	(1.6)	-	A7
B7	10.0	9.0	8.0	-	-	-	32.0	-	-	-	-	-	B7
C7	11.0	-	-	-	-	1.6	(2.8)	(1.7)	-	-	(1.7)	-	C7
D7	10.0	1.0	8.0	-	-	4.0	(3.4)	(0.8)	-	-	(4.8)	-	D7
E7	10.0	-	-	-	9.0	1.8	(3.1)	(1.7)	5	(0.3)	51.8	-	E7
F7	11.0	62.0	10.0	1.0	17.0	9.5	204.0	21.5	2	12.0	82.4	1,112.8	F7
A8	9.0	4.0	8.0	-	-	0.6	13.2	21.6	-	-	(0.8)	-	A8
B8	9.0	-	-	-	-	-	-	-	-	-	-	-	B8
C8	10.0	-	-	-	-	0.5	(0.9)	(1.7)	-	-	(0.6)	-	C8
D8	10.0	1.0	8.0	-	-	0.1	3.4	49.1	-	-	(0.1)	-	D8
E8	10.0	4.0	8.0	-	-	8.3	(0.1)	(0.0)	-	-	(0.1)	-	E8
F8	10.0	90.0	11.0	1.0	32.0	-	320.0	-	-	10.0	192.0	1,919.7	F8

TABLE D-5
GRAVEL GERTIE DATA
BSA IMPACTOR DATA

	FLOW RATE (LITERS/MIN)	MEAS. U (IN NG)	U UNCERT	SIG. U NON-ZERO	SIG U (μG-S/M**3)	SIG U (μG-S/M**3)		FLOW RATE (LITERS/MIN)	MEAS. U (IN NG)	U UNCERT.	SIG. U NON-ZERO	U IN (μG-S/M**3)	SIG U (μG-S/M**3)
61 1	0.6	-	-	-	-	-	66 1	0.6	-	-	-	-	-
61 2	0.6	2.5	10.0	-	238.1	-	66 2	0.6	0.9	10.0		87.9	-
61 3	0.6	-	-	-	-	-	66 3	0.6	0.9	10.0	-	-	-
61 4	0.6	-	-	-	-	-	66 4	0.6	-	-	-	-	-
61 5	0.6	-	-	-	-	-	66 5	0.6	-	-	-	-	-
61 6	0.6	-	-	-	-	-	66 6	0.6	0.9	10.0	-	-	-
61 7	0.6	-	-	-	-	-	66 7	0.6	--	-	-	-	-
61 8	0.6	4.0	10.0	-	386.9	-	66 8	0.6	-	-	-	-	-
61 TO	0.6	6.5	20.0	-	625.0	-	66 TO	0.6	1.9	20.0		175.7	-
63 1	0.6	35.4	10.0	1.0	3,540.0	3,540.0	67 1	0.6	-	-	-	-	-
63 2	0.6	17.4	10.0	1.0	1,740.0	1,740.0	67 2	0.6	0.9	10.0		93.0	-
63 3	0.6	0.9	10.0	-	90.0	-	67 3	0.6	-	-	-		-
63 4	0.6	18.9	10.00	1.0	1,890.0	1,890.0	67 4	0.6	-	-	-		-
63 5	0.6	0.9	10.0	-	90.0	-	67 5	0.6	-	-	-		-
63 6	0.6	5.4	10.0	-	540.0	-	67 6	0.6	-	-	-		-
63 7	0.6	-	-	-	-	-	67 7	0.6	-	-	-		-
63 8	0.6	-	-	-	-	-	67 8	0.6	-	-	-		-
63 TO	0.6	79.8	70.0	-	7,980.0	-	67 TO	0.6	0.9	10.0	-	93.0	-
64 1	0.6	21.9	10.0	1.0	2,190.0	2,190.0	68 1	0.6	-	-	-	-	-
64 2	0.6	3.9	10.0	-	390.0	-	68 2	0.6	0.9	10.0	-	93.0	-
64 3	0.6	-	-	-	-	-	68 3	0.6	-	-	-	-	-
64 4	0.6	-	-	-	-	-	68 4	0.6	-	-	-	-	-
64 5	0.6	-	-	-	-	-	68 5	0.6	-	-	-	-	-
64 6	0.6	38.4	10.0	1/0	3,840.0	3,840.0	68 6	0.6	-	-	-	-	-
64 7	0.6	8.4	10.0	-	840.0	-	68 7	0.6	-	-	-	-	-
64 8	0.6	-	-	-	-	-	68 8	0.6	-	-	-	-	-
64 TO	0.6	73.5	50.0	-	7,350.0	-	68 TO	0.6	0.9	10.0	-	93.0	-
65 1	0.6	65.4	10.0	1.0	6,540.0	6,540.0	69 1	0.6	-	-	-	-	-
65 2	0.6	14.4	10.0	-	1,440.0	-	69 2	0.6	-	-	-	-	-
65 3	0.6	12.9	10.0	-	1,290.0	-	69 3	0.6	-	-	-	-	-
65 4	0.6	17.4	10.0	1.0	1,740.0	1,740.0	69 4	0.6	-	-	-	-	-
65 5	0.6	-	-	-	-	-	69 5	0.6	-	-	-	-	-
65 6	0.6	-	-	-	-	-	69 6	0.6	0.9	10.0	-	95.4	-
65 7	0.6	-	-	-	-	-	69 7	0.6	-	-	-	-	-
65 8	0.6	-	-	-	-	-	69 8	0.6	0.9	10.0	-	95.4	-
65 TO	0.6	110.1	40.0	-	11,010.0	-	69 TOT	0.6	1.9	20.0	-	190.8	-

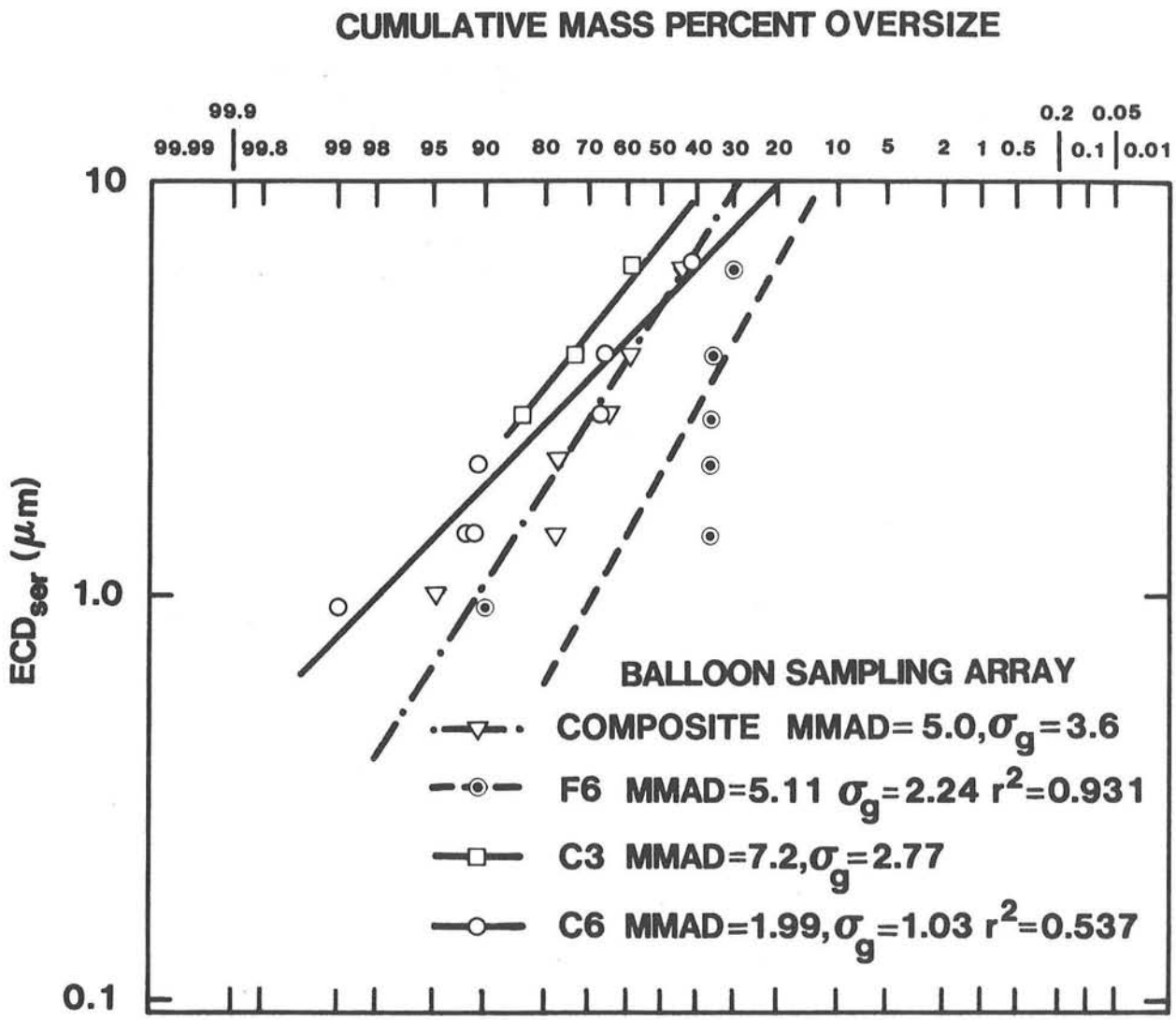

Figure D-8. Size Distributions for GGBSA Impactors with Significant Collections

Tunnel Sampling Array (TSA)

The only potential leakage path for hazardous aerosols from the round room other than through the gravel filter bed was through the sealed blast door which served as an access port during construction. In order to detect and quantify any leakage through this portal, a simple entryway aerosol sampling system was devised. Four aerosol samplers (two cascade impactors and two total filter samplers) were installed in the portal area outside the blast door as shown on Figure D-9. Two samplers inside the portal area were suspended from the overhead and hung at a height approximately 1.7 m feet above the ground. The two samplers outside the portal were affixed to an existing signpost and were approximately 1 meter above the ground.

The significant results from these samplers are shown on Table D-6. Significant collections were obtained in each sampler; but, because of the location of sampler 2 in the stagnant air region of the tunnel entrance, its collection is significantly larger than from samplers at location 1 outside.

Pole Sampling Array (PSA)

In order to make a close-in aerosol measurement which included components of base surge, levitated dust, and vented aerosol, a sampler array mounted on telephone poles was designed and installed.

Installation [SL82]

Four telephone poles were installed as shown on Figure D-10. Samplers were mounted and plumbed on each of the poles as shown on Figure D-11 and D-12.

Operation

All samplers were initially installed with sample ports covered. The ports were uncovered and flow rates were measured on November 19, 1982. All samplers were placed and energized in the test position at T - 120 minutes and were deenergized at T + 30 minutes.

Data obtained from the impactors (L1-L8), filters (FL) and deposition trays (CT) mounted on the poles surrounding the round room are shown in Table D-7. Significant collections were obtained on the North, West and South poles at the lowest intermediate levels. Only one significant collection was obtained on the East (upwind) pole.

Collector Tray Array

The only aerosol instrumentation used in the 1956 Gravel Gertie test program was an array of fallout trays positioned in a rectangular grid centered

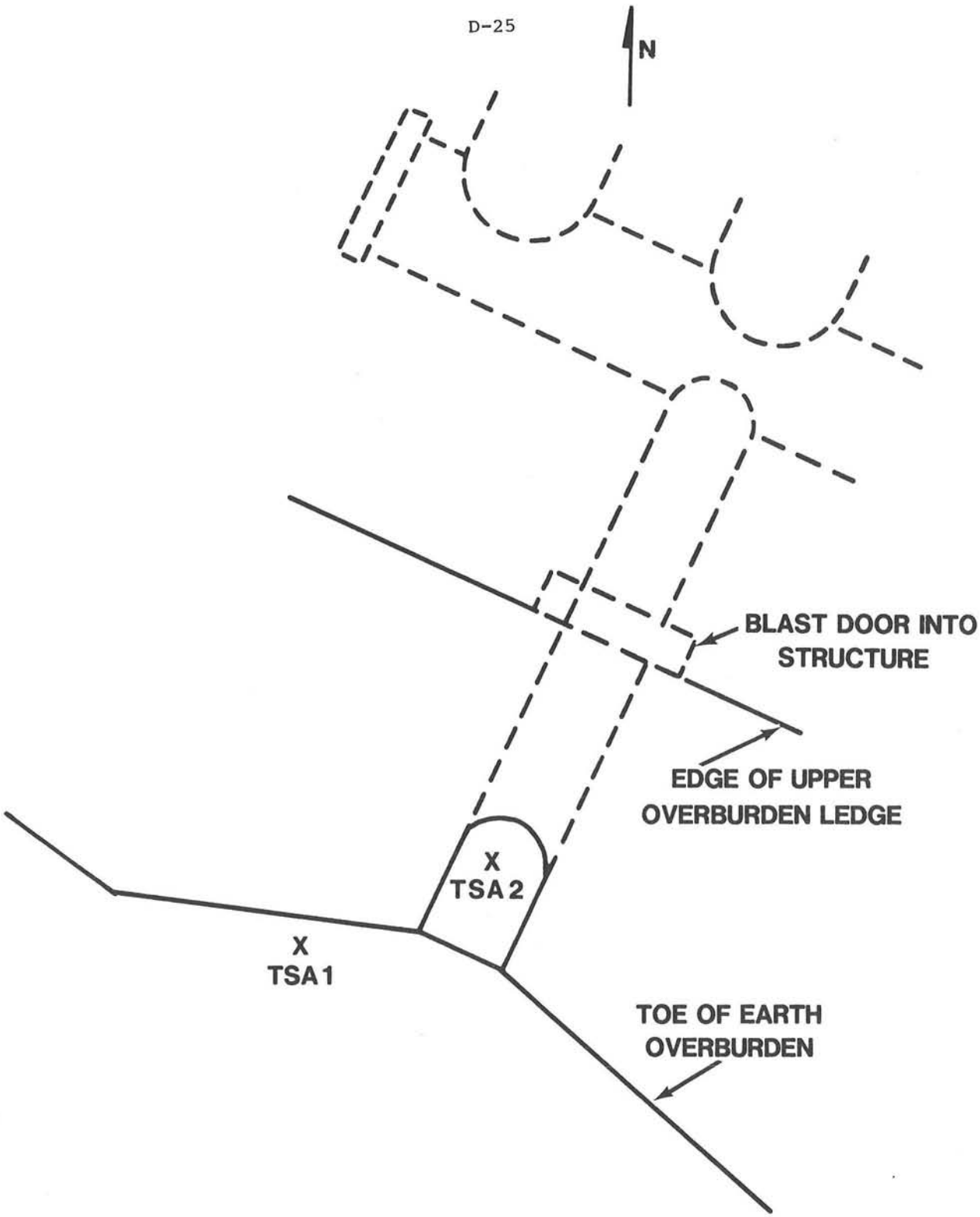

Figure D-9. Portal Sampling System

TABLE D-6

Gravel Gertie Data
Tunnel Sampler Array

	FLOW RATE (LITERS/MIN)	MEAS. U (IN NG)	U UNCERT.	SIG. U NON-ZERO	TOT. MASS (MG)	NET U (IN NG)	CONCEN. (μG-S/M**3)	SIG. CONCEN. (μG-S/M**3)
L1 1-18	15.1	1,829.1	10.0	1.0	4.9	1,812.0	7,219.2	7,219.2
L2	15.1	216.9	10.0	1.0	1.1	213.1	848.8	848.8
L3	15.1	272.4	10.0	1.0	0.5	270.5	1,077.9	1,077.9
L4	15.1	258.9	10.0	1.0	0.4	257.6	1,026.2	1,026.2
L5	15.1	233.4	10.0	1.0	0.3	232.5	926.3	926.3
L6	15.1	251.4	10.0	1.0	0.1	251.0	999.9	999.9
L7	15.1	164.4	10.0	1.0	0.0	164.3	654.6	654.6
L8	15.1	1,829.1	10.0	1.0	0.4	1,827.8	7,282.1	7,282.1
TOT	15.1	5,055.6	80.0	1.0	7.7	5,028.8	19,981.8	19,981.8
L1 2-21	15.3	27,500.0	10.0	1.0	9.7	27,466.1	107,992.3	107,992.3
L2	15.3	6,548.6	10.0	1.0	3.6	6,536.2	25,699.2	25,699.2
L3	15.3	5,992.4	10.0	1.0	3.2	5,981.4	23,517.9	23,517.9
L4	15.3	6,082.6	10.0	1.0	3.2	6,071.3	23,871.3	23,871.3
L5	15.3	5,526.5	10.0	1.0	2.6	5,517.5	21,694.0	21,694.0
L6	15.3	4,654.8	10.0	1.0	?	4,650.4	18,284.5	18,284.5
L7	15.3	6,593.7	10.0	1.0	0.5	6,591.8	25,918.0	25,918.0
L8	15.3	11,418.3	10.0	1.0	0.6	11,416.2	44,886.8	44,886.8
TOT	15.3	74,316.9	80.0	1.0	24.6	74,230.7	291,100.9	291,100.9
1 FL49	8.7	3,332.1	10.0	1.0	10.8	3,294.3	22,850.6	22,850.6
2 FL46	8.9	79,374.0	10.0	1.0	30.0	79,268.9	536,204.7	536,204.7

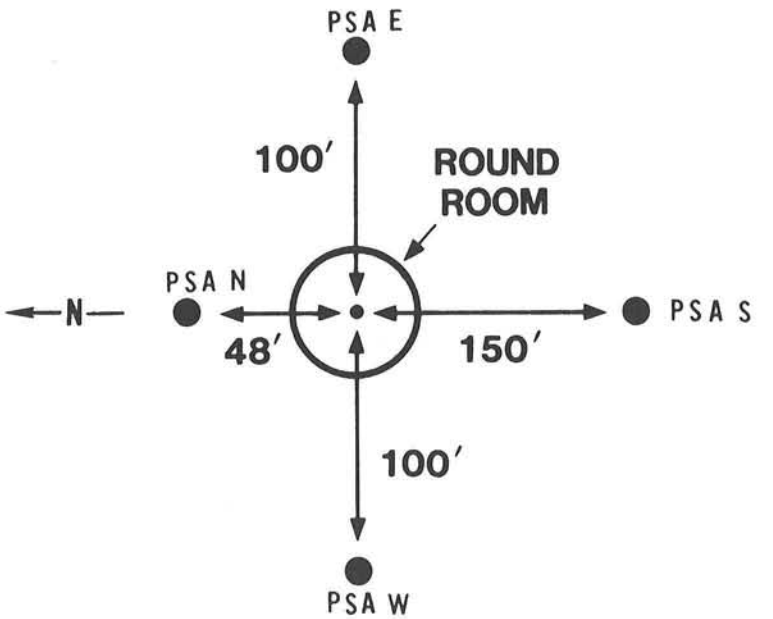

Figure D-10. Pole Sampling Array-Plan View

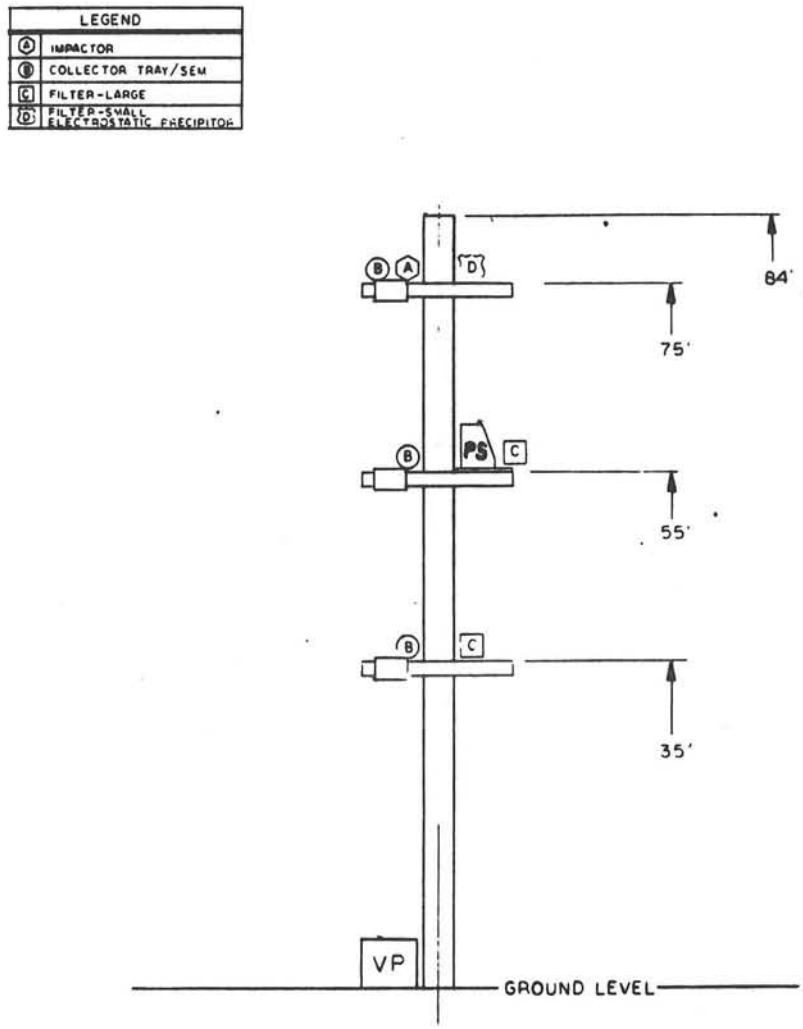

Figure D-11. Gravel Gertie Pole Sampling Array (GGPSA)

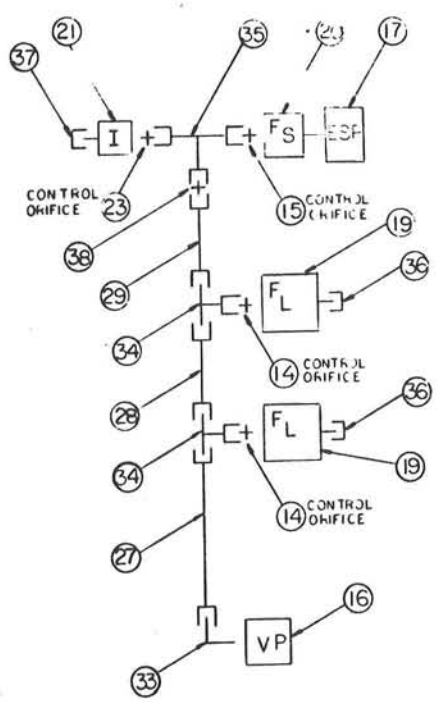

					40
					39
1	B 6004	UNION, 3/8 TUBE TO 3/8 TUBE	8		38
1	B-6-CP	CAP, 3/8 FNPT	8		37
2	B-4-CP	CAP 1/4 FNPT	8		36
1	B-4-T	TEE, 1/4 FNPT TO 3/8 TUBE	8		35
2	B-600-3 TTF	FEMALE BRANCH TEE, 1/4 FNPT TO 3/8 TUBE	8		34
1	B-600-2-6	MALE ELBOW, 3/8 MNPT TO 3/8 TUBE	8		33
					132
AR		ADHESIVE / HOLDER			31
					30
1		TUBE (55" TO 75")	W/F 25		29
1		TUBE (35" TO 55")	W/F 25		28
1		TUBE (PUMP TO 35")	W/F 25		27
					26
AR	ASTM-B75	TUBING, COPPER - OXYGEN FREE DRAWN TEMPER 075 OD 0.032 WALL STK NO 50,704			25
3		SEM-CARBON FLANGE			24
1		ORIFICE-CONTROL - IMPACTOR - MULTIJET			23
					22
1		IMPACTOR-MULTIJET, 20 LITER FLOW RATE	6		21
1		FILTER SMALL - 1/2 LITER FLOW RATE	6		20
2		FILTER LARGE - 15 LITER FLOW RATE	6		19
1		POWER SUPPLY - ELECTROSTATIC PRECIPITATOR	6		18
1		ELECTROSTATIC PRECIPITATOR - 1/2 LITER FLOW RATE	6		17
1	1022-V103-G272X	VACUUM PUMP	5		16
1		ORFICE-CONTROL-FILTER-SMALL			15
3		ORFICE-CONTROL-FILTER-LARGE			14

Figure D-12. Pole Sampling Array Plumbing Diagram

TABLE D-7

Gravel Gertie Data
PSA Instruments

	FLOW RATE (LITERS/MIN)	MEAS. U (IN NG)	U UNCERT.	SIG. U NON-ZERO	TOT. MASS (MG)	NET U (IN NG)	NET U (μG-S/M**3)	SIG U (μG-S/M**3)	U DEP (μG/M**2)
L1 N 2	15.5	1.4	10.0	-	0.0	11.4	44.1	-	-
L2	15.5	17.4	10.0	1.0	0.0	17.4	67.4	67.4	-
L3	15.5	21.9	10.0	1.0	-	21.9	85.0	85.0	-
L4	15.5	-	-	-	0.0	-	-	-	-
L5	15.5	3.9	10.0	-	-	3.9	15.1	-	-
L6	15.5	-	-	-	0.0	-	-	-	-
L7	15.5	29.4	10.0	1.0	0.0	29.3	113.8	113.8	-
L8	15.5	14.4	10.0	-	0.2	13.6	52.8	-	-
TOT	15.5	98.4	60.0	1.0	0.3	97.5	378.2	378.2	-
L1 N 3	15.3	8.4	10.0	-	-	8.4	32.9	-	-
L2	15.3	2.4	10.0	-	-	2.4	9.4	-	-
L3	15.3	2.4	10.0	-	0.0	2.4	9.3	-	-
L4	15.3	-	-	-	0.0	-	-	-	-
L5	15.3	8.4	10.0	-	0.2	7.9	30.9	-	-
L6	15.3	15.9	10.0	1.0	-	15.9	62.4	62.4	-
L7	15.3	15.9	10.0	1.0	-	15.9	62.4	62.4	-
L8	15.3	-	-	-	0.3	-	-	-	-
TOT	15.3	53.4	60.0	1.0	0.4	52.8	207.2	207.2	-
L1 E 2	15.4	-	-	-	0.1	-	-	-	-
L2	15.4	74.3	10.0	1.0	-	74.3	290.4	290.4	-
L3	15.4	-	-	-	-	-	-	-	-
L4	15.4	39.9	10.0	1.0	-	39.9	155.8	155.8	-
L5	15.4	0.9	10.0	-	0.0	0.8	3.2	-	-
L6	15.4	3.9	10.0	-	-	3.9	15.2	-	-
L7	15.4	3.9	10.0	-	-	3.9	15.2	-	-
L8	15.4	2.4	10.0	-	0.2	1.8	7.1	-	-
TOT	15.4	125.2	60.0	1.0	0.3	124.6	486.8	486.8	-
L1 E 3	15.6	5.4	10.0	-	0.9	2.3	8.7	-	-
L2	15.6	5.4	10.0	-	0.0	5.3	20.5	-	-
L3	15.6	-	-	-	-	-	-	-	-
L4	15.6	-	-	-	0.0	-	-	-	-
L5	15.6	-	-	-	0.1	-	-	-	-
L6	15.6	131.4	10.0	1.0	-	131.4	505.0	505.0	-
L7	15.6	-	-	-	0.0	-	-	-	-
L8	15.6	-	-	-	0.5	-	-	-	-
TOT	15.6	142.1	30.0	1.0	1.6	139.0	534.2	534.2	-

TABLE D-7 (continued)

	FLOW RATE (LITERS/MIN)	MEAS. U (IN NG)	U UNCERT.	SIG. U NON-ZERO	TOT. MASS (MG)	NET U (IN NG)	NET U (μG-S/M**3)	SIG U (μG-S/M**3)	U DEP (μG/M**2)
L1 S 2	15.3	5.4	10.0	-	0.1	5.1	20.1	-	-
L2	15.3	-	-	-	0.0	-	-	-	-
L3	15.3	8.4	10.0	-	-	8.4	32.9	-	-
L4	15.3	-	-	-	0.1	-	-	-	-
L5	15.3	-	-	-	0.0	-	-	-	-
L6	15.3	3.9	10.0	-	0.0	3.7	14.7	-	-
L7	15.3	-	-	-	-	-	-	-	-
L8	15.3	6.9	10.0	-	0.3	5.8	22.7	-	-
TOT	15.3	24.5	40.0	-	0.6	23.1	90.4	-	-
L1 S 3	14.6	5.4	10.0	-	0.3	4.3	17.7	-	-
L2	14.6	5.4	10.0	-	0.0	5.3	21.8	-	-
L3	14.6	-	-	-	-	-	-	-	-
L4	14.6	-	-	-	0.0	-	-	-	-
L5	14.6	-	-	-	-	-	-	-	-
L6	14.6	131.4	10.0	1.0	0.0	131.3	539.6	539.6	-
L7	14.6	-	-	-	-	-	-	-	-
L8	14.6	-	-	-	0.3	-	-	-	-
TOT	14.6	142.1	30.0	1.0	0.7	140.9	579.1	579.1	-
L1 W 2	15.0	17.4	10.0	1.0	0.0	17.3	69.3	69.3	-
L2	15.0	12.9	10.0	-	0.1	12.7	50.9	-	-
L3	15.0	15.9	10.0	1.0	0.1	15.7	62.8	62.8	-
L4	15.0	14.4	10.0	-	0.0	14.3	57.2	-	-
L5	15.0	14.4	10.0	-	-	14.4	57.6	-	-
L6	15.0	11.4	10.0	-	0.1	11.2	44.9	-	-
L7	15.0	14.4	10.0	-	0.1	14.1	56.5	-	-
L8	15.0	51.9	10.0	1.0	0.2	51.1	204.4	204.4	-
TOT	15.0	152.7	80.0	1.0	0.5	150.9	603.5	603.5	-
L1 W 3	15.8	-	-	-	0.1	-	-	-	-
L2	15.8	2.4	10.0	-	0.1	2.2	8.3	-	-
L3	15.8	20.4	10.0	1.0	-	20.4	77.4	77.4	-
L4	15.8	11.4	10.0	-	0.0	11.3	43.0	-	-
L5	15.8	5.4	10.0	-	-	5.4	20.5	-	-
L6	15.8	5.4	10.0	-	0.0	5.3	20.2	-	-
L7	15.8	-	-	-	0.0	-	-	-	-
L8	15.8	27.9	10.0	1.0	0.3	26.9	101.9	101.9	-
TOT	15.8	72.9	60.0	1.0	0.5	71.5	271.3	271.3	-

TABLE D-7 (continued)

	FLOW RATE (LITERS/MIN)	MEAS. U (IN NG)	U UNCERT.	SIG. U NON-ZERO	TOT. MASS (MG)	NET U (IN NG)	NET U (μG-S/M**3)	SIG U (μG-S/M**3)	U DEP (μG/M**2)
FL N1	8.5	195.9	10.0	1.0	2.3	187.9	1,321.8	1,321.8	-
FL N2	8.8	-	-	-	0.3	-	-	-	-
FL N3	-	-	-	-	-	-	-	-	-
FL E1	8.6	-	-	-	0.3	-	-	-	-
FL E2	8.8	-	-	-	0.3	-	-	-	-
FL E3	-	-	-	-	-	-	-	-	-
FL S1	8.3	104.4	10.0	1.0	0.8	101.7	735.2	735.2	-
FL S2	8.4	4.0	10.0	-	0.4	2.5	18.1	-	-
FL S3	-	-	-	-	-	-	-	-	-
FL W1	8.7	231.9	10.0	1.0	1.0	228.4	1,580.9	1,580.9	-
FL W2	8.1	7.0	10.0	-	0.3	5.9	43.0	-	-
FL W3	-	-	-	-	-	-	-	-	-
CT N1	-	455,145.0	10.0	1.0	80.0	454,865.0	-	-	9,369.0
CT N2	-	616.6	10.0	1.0	0.5	614.9	-	-	12.7
CT N3	-	81.5	10.0	1.0	-	81.5	-	-	1.7
CT E1	-	28.8	10.0	1.0	-	28.8	-	-	0.6
CT E2	-	39.7	10.0	1.0	-	39.7	-	-	0.8
CT E3	-	49.0	10.0	1.0	-	49.0	-	-	1.0
CT S1	-	461.3	10.0	1.0	-	461.3	-	-	9.5
CT S2	-	59.8	10.0	1.0	-	59.8	-	-	1.2
CT S3	-	59.8	10.0	1.0	-	59.8	-	-	1.2
CT W1	-	2,651.0	10.0	1.0	0.5	2,649.3	-	-	54.6
CT W2	-	185.4	10.0	1.0	-	185.4	-	-	3.8
CT W3	-	414.7	10.0	1.0	-	414.7	-	-	8.5

on the round room of the structure (see Figure D-13) [C58]. In order to benchmark the current test to the original one, a similar array (denoted Gravel Gertie Collector Tray Array or GGCTA) was installed for the 1982 full-scale test.

GGCTA Installation for 1982 Test [SL82]

The fallout tray array for the 1956 test was much more extensive than the array set out for this test. In the former case, sample stations were installed at approximately 980 grid points. The GGCTA for the 1982 test included only 124 stations set up as shown on Figure D-14. The grid points selected for this test were those from the earlier test which fell on or near the perimeter of circles centered, as before, on the middle of the round room.

There are five distinctive topographic zones in the 3.8×10^6 m^2 contained in the GGCTA grid. The first of these, lying to the west in Quadrants III and IV (see Figure D-14), consisted of relatively flat terrain with a gradual decrease in elevation of approximately 120 feet from the south to the north. The soil is generally quite rocky with some small patches of sand. The entire area is covered with greasewood bushes and other low desert flora. The bushes tend to grow 2 to 4 feet high and are spaced 10 to 30 feet apart.

The second terrain type occurs in the outer areas of Quadrants I and II. This consists of a series of deep arroyos running generally from southeast to northwest. These arroyos are between 15 and 20 feet deep and between 50 and 500 feet wide. As with Quadrants III and IV, this area contains low-desert shrubbery. Because of the presence of the arroyos, the soil in these areas is somewhat sandier than the soil in Quadrants III and IV.

The remaining three terrain types are all man-made but, because of their nature and location, has the potential for affecting the GGCTA test results. The first of these three types is located in Quadrants I and II, relatively close to the center. This terrain consists of a number of large gravel piles and pits which have been, or are being, used for gravel or fill dirt needs at NTS. The piles range in size from 10 to 20 feet high and from 40 to 200 feet long. The pits are between 20 and 50 feet deep and up to 300 feet across. In addition, there are a few large flat expanses between the Gravel Gertie and the gravel pit area used for access to the gravel by heavy equipment. Because of the radical nature of the surface roughness variations, no GGCTA samplers were installed in the gravel pit area.

The second man-made terrain feature is the road network in the immediate vicinity of the site. A paved road (5-01) runs from SSW to NNE passing approximately 400 feet to the east of the Gravel Gertie itself. A gravel road branches off Road 5-01 at approximately grid point II-C-16 and runs NNE to a large gravel pit area north of Quadrant I. In addition, 15 foot wide dirt roads were graded from the site outward along the N, S, and W radials.

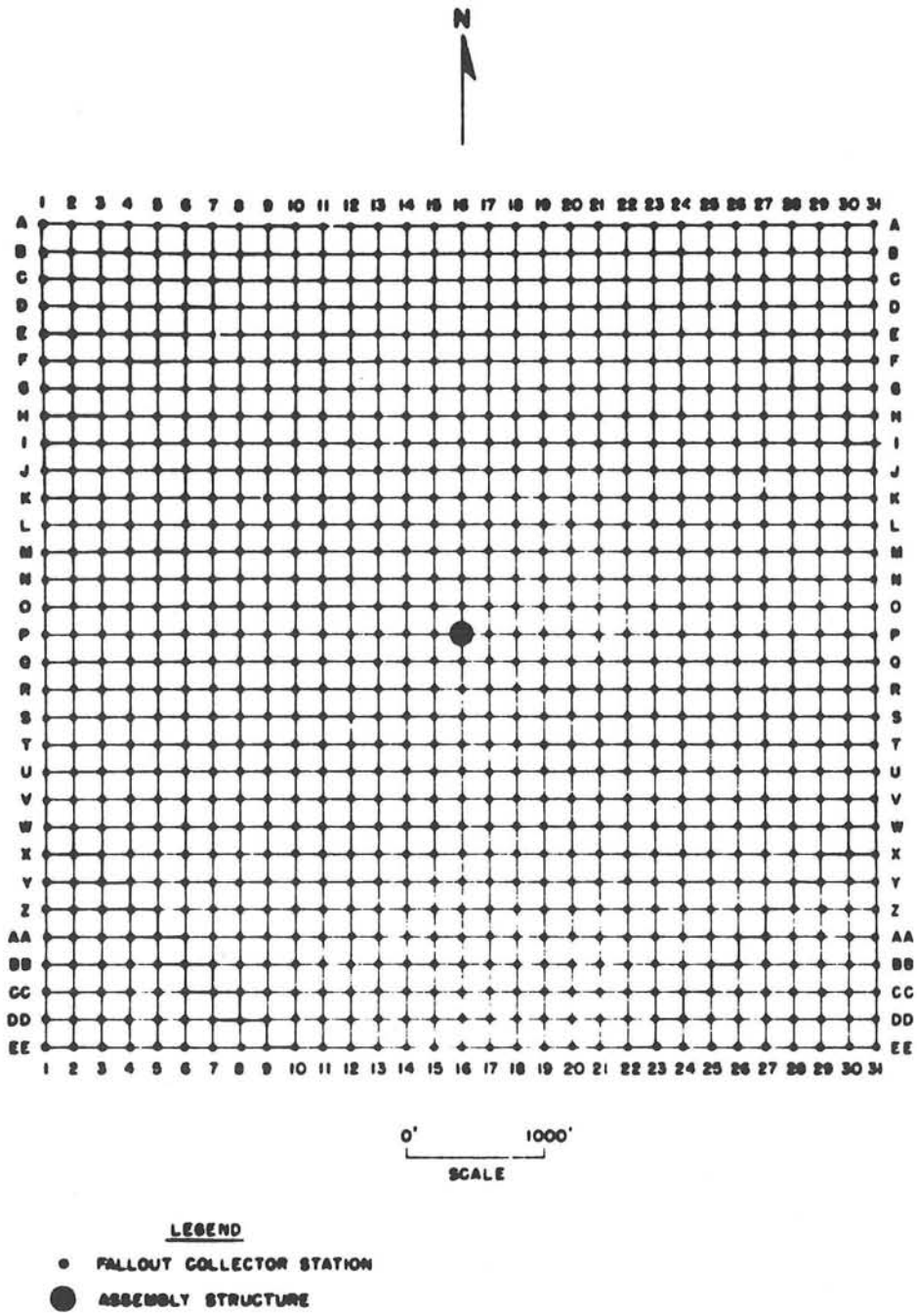

Figure D-13. 1956 Test Array

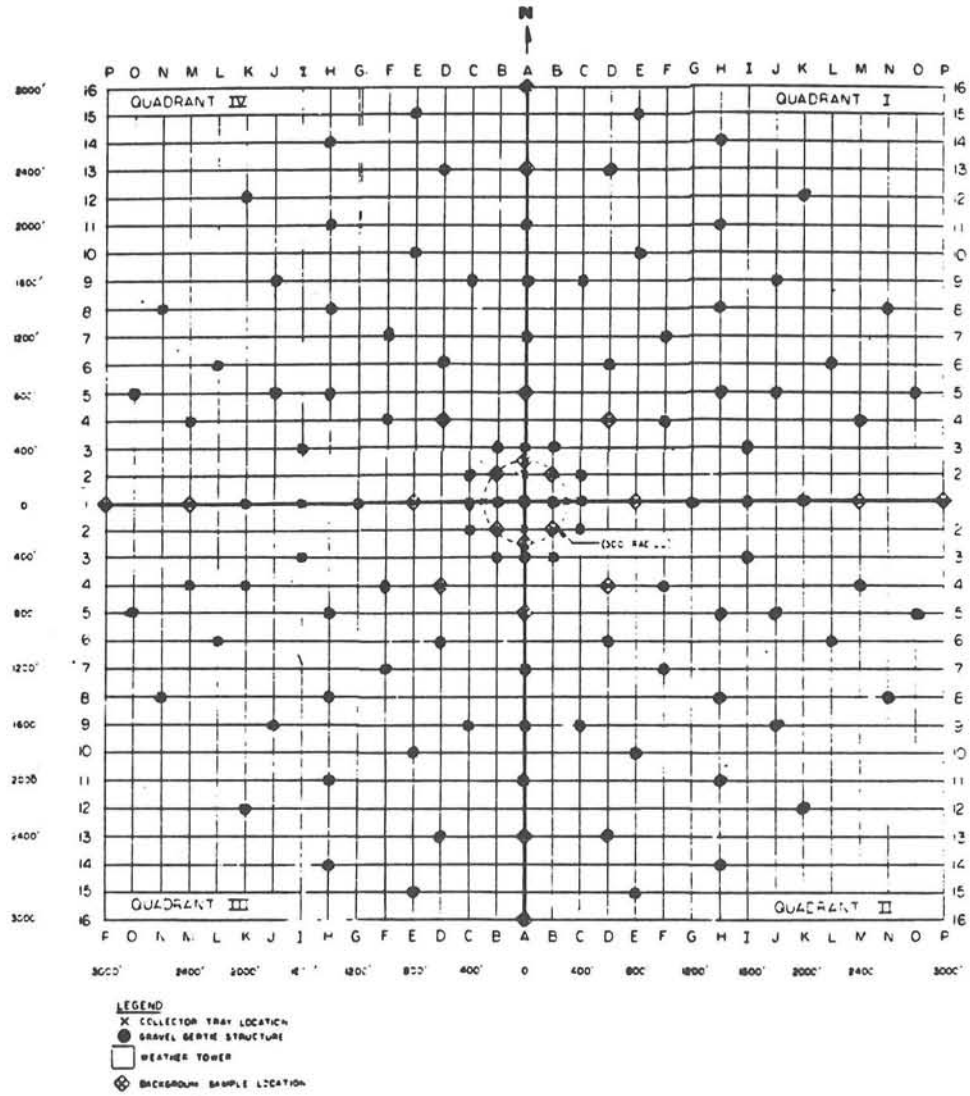

Figure D-14. Locations of GGCTA Sampler Trays

The third man-made terrain feature is the area of the site itself. An area approximately 800' x 800' was graded around the structure to permit required construction and test equipment access to the Gravel Gertie. This area was covered with a finer, dustier soil and was more prone to fugitive dust generation from vehicle and pedestrian traffic. Prior to shot time on November 20, this area was sprayed with water for dust control.

The concern, particularly with regard to the roads and site area, was that fugitive dirt would be resuspended due to vehicular traffic, pedestrian traffic, or high winds. This re-entrained material could deposit in opened trays, complicating the actual determination of shot-related deposition.

The trays themselves were installed on 1.27-cm-diameter rods as shown on Figure D-15. The trays were set at various heights, depending on the height of the top of the stake above grade. These heights varied from a minimum of about 50.8 cm to a maximum of 114 cm.

The trays were 27.3 cm x 17.8 cm x 3.8 cm (10-3/4" x 7" x 1-1/2") biscuit pans spray-coated with a mixture of Apiezon grease and toluene mixed 1:10. The coating was applied at SNL on October 12, 1982. The trays were immediately covered and boxed for shipment to NTS. They were installed on the stakes in the covered position on November 19, 1982 and November 20, 1982. The seven trays listed in Table D-8 were not installed because of their location in the gravel pit area or in the middle of one of the roads. Fortunately, the absence of these trays had little or no impact on the test results due to the easterly winds at shot time.

GGCTA Operation During 1982 Test

Table D-9 summarizes the pertinent times for each of the tray locations. The trays were initially placed in the test, or uncovered, position between 0930 and 1630 on November 19, 1982. The background sample trays were collected between 0400 and 0530 on shot day (November 20, 1982). The bulk of the trays were recovered and boxed for shipment between 0900 and 1300 on November 20, 1982. Trays in the immediate cleared area were recovered first (0900-0930) followed by those in Quadrants III and IV (0930-1130) and those in Quadrants I and II (1130-1345).

Data Analysis and Results

To arrive at a suitable background estimate three sets of data were examined: the actual background trays, deposit samples above line 5 in the upper half plane, and deposit samplers below line 5 in the lower half plane (Figure D-14). The latter two populations were selected as possible additional background samplers because the east wind at (and after) shot time could not have transported test uranium onto these samplers. Each population was subjected to averaging and determination of standard deviation. Results are as follows:

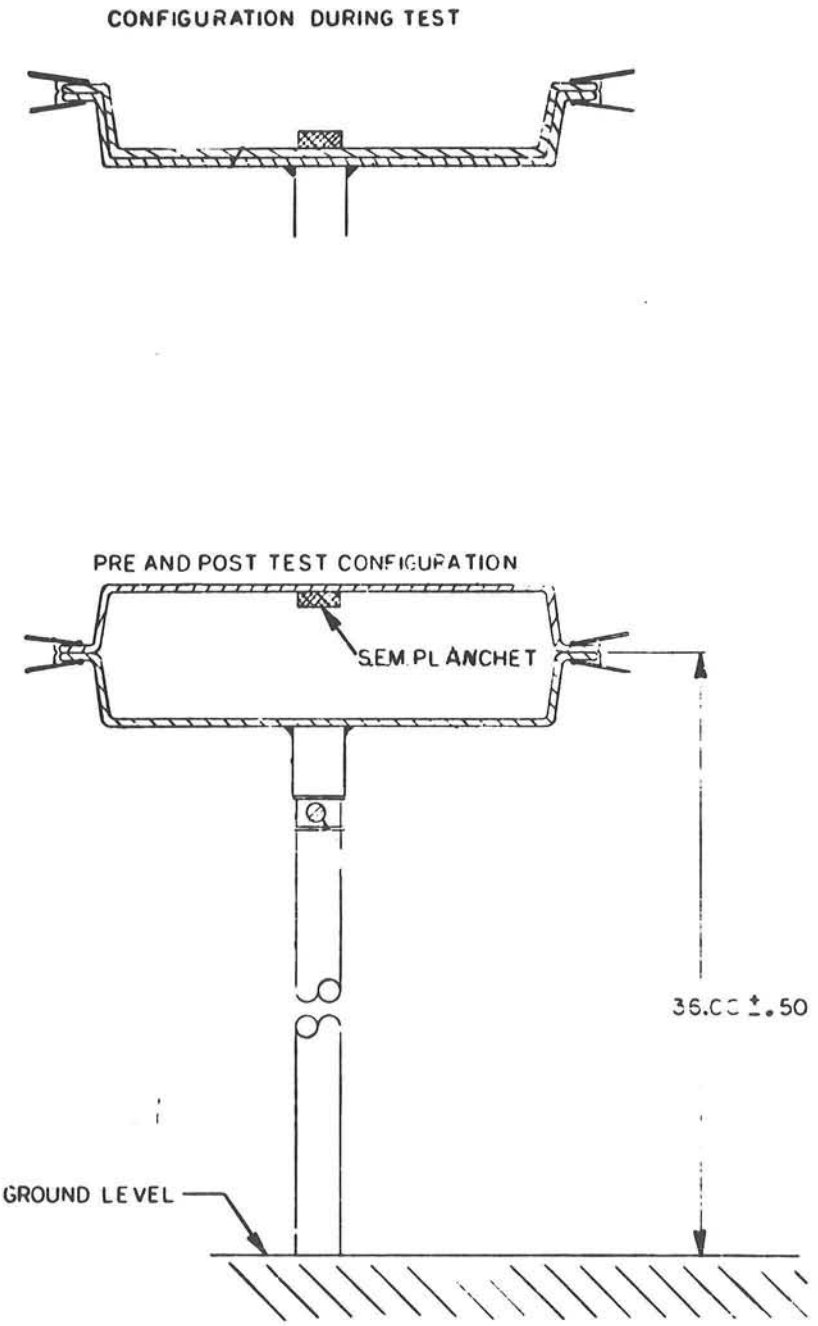

Figure D-15. GGCTA Installation

TABLE D-8

CTA Trays Not Installed

I-C-2

I-F-4

II-D-4

II-F-4

II-H-5

II-H-8

II-J-5

TABLE D-9
CTA DATA SUMMARY TABLE

*All Trays recovered on 11/20 between 0900 and 1330. Quadrants III & IV done 1st (09-11). Quadrants I & II done second. Trays in immediate cleared area around site done from 09-0930.

**May not have been used in test position

Tray Number	Test Position	Recovered	Tray Number	Test Position	Recovered
I-A2-000	11/19 1639	11/20 0900	II-A2-000	11/20 0513	11/20 0930
I-A3-000	11/19 1442	11/20 1200	II-A- 3-000	11/19 1141	11/20 0930
I-A- 5-BG1	11/19 1420	11/20 0422	II-A- 5-BG1	11/19 1137	11/20 0516
I-A- 5-000	11/20 0422	11/20 1200	II-A- 5-000	11/20 0516	11/20 1330
I-A- 7-000	11/19 1438	11/20 1200	II-A- 7-000	11/29 1132	11/20 1330
I-A- 9-000	11/19 1437	11/20 1200	II-A- 9-000	11/19 1130	11/20 1330
I-A-11-000	11/19 1435	11/20 1200	II-A-11-000	11/19 1121	11/20 1330
I-A-13-BG1	11/19 1253	11/20 0428	II-A-13-BG1	11/19 1119	11/20 0522
I-A-13-000	11/20 0428	11/20 1200	II-A-13-000	11/20 0422	11/20 1330
I-A-16-BG1	11/19 1253	11/20 0431	II-A-16-BG1	11/19 1115	11/20 0525
I-A-16-000	11/20 0431	11/20 1200	II-A-16-000	11/20 0424	11/20 1330
I-B- 2-BG1	11/19 1631	11/20 0419	II-B- 1-000	11/19 1209	11/20 0900
I-B- 2-000	11/20 0419	11/20 0900	II-B- 2-BG1	11/19 1620	11/20 0417
I-B- 3-000	11/19 1636	11/20 0900	II-B- 2-000	11/20 0417	11/20 0930
I-C- 2-000	Not Installed		II-B- 3-000	11/19 1621	11/20 0930
I-C- 9-000	11/19 1433	11/20 1200	II-C- 1-000	11/19 1641	11/20 1200
I-D- 4-BG1	11/19 1626	11/20 0413	II-C- 2-000	11/19 1503	11/20 1200
I-D- 4-000	11/20 0413	11/20 1200	II-C- 9-000	11/19 1355	11/20 1200
I-D- 6-000	11/19 1608	11/20 1200	II-D- 4-BG11		Not Installed
I-D-13-000	11/19 1259	11/20 1200	II-D- 4-0001		Not Installed
I-E-10-000	11/19 1431	11/20 1200	II-D- 6-000	11/19 1527	11/20 1200
I-E-15-000	11/19 1301	11/20 1200	II-D-13-000	11/20 0615	11/20 1200
I-F- 4-000	Not Installed		II-E- 1 BG1	11/19 1604	11/20 0411
I-F- 7-000**	11/19 1426	11/20 1200	II-E- 1-000	11/20 0411	11/20 1200
I-H-5-000	11/19 1422	11/20 1200	II-E-10-000	11/19 1353	11/20 1200
I-H- 8-000	11/19 1428	11/20 1200	II-E-15-000	11/19 1355	11/20 1200
I-H-11-000	11/19 1306	11/20 1200	II-F-4-000	Not Installed	

TABLE D-9 (Cont.)

Tray Number	Test Position	Recovered	Tray Number	Test Position	Recovered
I-H-14-000	11/19 1303	11/20 1200	II-F- 7-000	11/19 1537	11/20 1200
I-I- 3-000	11/19 1414	11/20 1200	II-G- 1-000	11/19 1539	11/20 1200
I-J- 5-000	11/19 1416	11/20 1200	II-H- 5-000	Not Installed	
I-J- 9-000	11/19 1311	11/20 1200	II-H- 8-000	Not Installed	
I-K-12-000	11/19 1308	11/20 1200	II-H-11-000	11/19 1351	11/20 1200
I-L- 6-000	11/19 1418	11/20 1200	II-H-14-000	11/19 1342	11/20 1200
I-M- 4-000	11/19 1319	11/20 1200	II-I- 1-000	11/19 1413	11/20 1200
I-N- 8-000	11/19 1314	11/20 1200	II-I- 3-000	11/19 1552	11/20 1200
I-0- 5-000	11/19 1317	11/20 1200	II-J- 5-000	Not Installed	
II-A- 2-BG1	11/19 1208	11/20 0513	II-J- 9-000	11/19 1401	11/20 1200
II-K- 1-000	11/19 1410	11/20 1200	III-L- 6-000	11/19 1006	11/20 1200
II-K-12-000	11/19 1337	11/20 1200	III-M- 1-BG1	11/19 1009	11/20 0453
II-L- 6-000	11/20 1406	11/20 1200	III-M- 1-000	11/20 0453	11/20 1200
II-M- 1-BG1	11/19 1325	11/20 0405	III-M- 4-000	11/19 1007	11/20 1200
II-M- 1-000	11/19 0405	11/20 1300	III-N- 8-000	11/19 1003	11/20 1200
II-M- 4-000	11/19 1328	11/20 1300	III-0- 5-000	11/19 1000	11/20 1200
II-N- 8-000	11/19 1333	11/20 1300	III-P- 1-BG1	11/19 0957	11/20 0456
II-0- 5-000	11/19 1330	11/19 1300	III-P- 1-000	11/20 0456	11/20 1000
II-P- 1-BG1	11/19 1323	11/20 0402	IV-B- 2-BG1	11/20 1218	11/20 0444
II-P- 1-000	11/20 0402	11/20 1300	IV-B- 2-000	11/20 0444	11/20 0920
III-B- 1-000	11/19 1225	11/20 0930	IV-B- 3-000	11/19 1229	11/20 1200
III-B- 2-000	11/20 0615	11/20 0930	IV-C- 2-000	11/20 1220	11/20 1200
III-B- 3-000	11/19 1630	11/21 0930	IV-C- 9-000	11/19 1240	11/20 1200
III-C- 1-000	11/19 1221	11/20 1200	IV-D- 4-BG1	11/19 1233	11/20 0441
III-C- 2-000	11/19 1222	11/20 1200	IV-D- 4-000	11/20 0441	11/20 1200
III-C- 9-000	11/19 1128	11/20 1200	IV-D- 6-000	11/19 1235	11/20 1200
III-D- 4-BG1	11/19 1653	11/20 0508	IV-D-13-000	11/19 1244	11/20 1200
III-D- 4-000	11/19 0508	11/20 1200	IV-E-10-000	11/19 1243	11/20 1200
III-D- 6-000	11/19 1135	11/20 1200	IV-E-15-000	11/19 1250	11/20 1200
III-D-13-000	11/19 1124	11/20 1200	IV-F- 4-000	11/19 1041	11/20 1200
III-E- 1-BG1	11/19 1648	11/20 0447	IV-F- 7-000	11/19 1033	11/20 1200
III-E- 1-000	11/20 0447	11/20 1200	IV-H- 5-000	11/19 1035	11/20 1200
III-E-10-000	11/19 1126	11/20 1200	IV-H- 8-000	11/19 1031	11/20 1200
III-E-15-000	11/19 1111	11/20 1200	IV-H-11-000	11/19 1028	11/20 1200

TABLE D-9 (Concluded)

Tray Number	Test Position	Recovered	Tray Number	Test Position	Recovered
III-F- 4-000	11/20 1649	11/20 1200	IV-H-14-000	11/17 1247	11/19 1200
III-F- 7-000	11/18 1057	11/20 1200	IV-I- 3-000	11/17 1344	11/20 1200
III-G- 1-000	11/20 1044	11/20 1200	IV-J- 5-000	11/17 1341	11/20 1200
III-H- 5-000	11/19 1055	11/20 1200	IV-J- 9-000	11/17 1228	11/20 1200
III-H- 8-000	11/19 1059	11/20 1200	IV-K-12-000	11/17 1234	11/20 1200
III-H-11-000	11/19 1103	11/20 1200	IV-L- 6-000	11/17 1351	11/20 1200
III-H-14-000	11/19 1109	11/20 1200	IV-M- 4-000	11/17 1352	11/20 1200
III-I- 1-000	11/19 1016	11/20 1200	IV-N- 8-000	11/17 1240	11/20 1200
III-I- 3-000	11/19 1050	11/19 1200	IV 0- 5-000	11/17 1356	11/20 1200
III-J- 9-000	11/19 1101	11/20 1200			
III-K- 1-000	11/19 1047	11/20 1200			
III-K- 4-000	11/19 1052	11/20 1200			
III-K-12-000	11/19 1106	11/20 1200			

A. Background Samplers
   Number: 18
   Average: 13.34 ngU
   Std. Dev.: 12.07 ngU

B. Upper Half Plane 5
   Number: 20
   Average: 15.71 ngU
   Std. Dev.: 9.72 ngU

C. Lower Half Plane 5
   Number: 18
   Average: 13.31 ngU
   Std. Dev.: 8.16 ngU

D. Combination of A and B
   Number: 38
   Average: 14.57 ngU

E. Combination of A, B, and C
   Number: 56
   Average: 14.7 ngU

It is clear from populations D and E that the A, B, and C distributions could be components of the same distribution. As a result, the background value for these deposit samples was chosen to be 14 ng. This value was subtracted from all deposit samples to account for background. All values were then screened to determine if they were larger than 24 ng (2 times the standard deviation of the background sampler distribution). Those above this level were converted to $\mu g/m^2$ and are shown in Figure D-16. This figure shows the significant deposition data from the Gravel Gertie Full-Scale experiment.

SAMPLE ANALYSIS: Procedure and Methods

Each sample was analyzed by at least one technique and, in those cases where specific information or confirmation was required, two or more techniques. Analysis for uranium was performed using uranium fluorometry, delayed neutron activation analysis (DNA) and scanning electron microscopy (SEM), including energy dispersive x-ray analysis (EDS). Samples were also analyzed for antimony (Sb) and Scandium (Sc) by instrumental thermal neutron activation analysis (ITNA). Total mass collected (including soil) was determined using gravimetric analysis. Atomic ratio of U-235 to U-238 was determined for selected samples using mass spectroscopic analysis (MSA). Table D-10 shows the type of analysis performed for each sampling system. Gravimetric analysis was performed on all samples with the exception of the Balloon Sampling Array (BSA) and the Collector Tray Array (CTA). Uranium fluorometry was performed on all samples of the Tunnel Sampling Array (TSA), Aerosol Sampling Package (GGASP), Doughnut Sampling Array (DSA) and Collector Tray Array (CTA). The

GRAVEL GERTIE CTA ARRAY DATA
VALUES IN MICROGRAMS/M**2
BACKGROUND REMOVED

	P	O	N	M	L	K	J	I	H	G	F	E	D	C	B	A	B	DISTANCE METRES
7	-	-	-	-	-	-	-	-	-	-	-	-	-	-	-	-	-	365.76
6	-	-	-	-	-	-	-	-	-	-	-	-	-	-	-	-	-	304.80
5	-	-	-	-	-	-	-	-	3.01	-	-	-	-	-	-	-	-	243.84
4	-	-	-	-	-	-	-	-	-	-	-	-	0.61	-	-	-	-	182.88
3	-	-	-	-	-	-	-	3.01	-	-	-	-	-	-	2.85	52.84	-	121.92
2	-	-	-	-	-	-	-	-	-	-	-	-	-	9.20	297.10	312.26	-	60.96
1	-	-	-	0.77	-	0.68	-	1.67	-	2.59	-	2.88	-	210.74	386.66	GZ	-	-
2	-	-	-	-	-	-	-	-	-	-	-	-	-	1.31	9.20	-	0.73	60.96
3	-	-	-	-	-	-	-	-	-	-	-	-	-	-	-	0.73	-	121.92
4	-	-	-	-	-	-	-	-	-	-	-	-	-	-	-	-	-	182.88
5	-	-	-	-	-	-	-	-	-	-	-	-	-	-	-	-	-	243.84
6	-	-	-	-	-	-	-	-	-	-	-	-	-	-	-	-	-	304.80
7	-	-	-	-	-	-	-	-	-	-	-	-	-	-	-	-	-	365.76
DIST	914.40	853.44	792.48	731.52	670.56	609.60	548.64	487.68	426.72	365.76	304.80	243.84	182.88	121.92	60.96	-	60.96	-
(M)	-	-	-	-	-	-	-	-	-	-	-	-	-	-	-	-	-	-

Figure D-16. Statistically Significant GGCTA Uranium Deposition* Above Background**

*Values greater than 0.49 $\mu g/m^2$ after subtraction of background
**Background estimated at 0.30 $\mu g/m^2$

TABLE D-10

Analytical Techniques Performed

Sampling System	Gravimetric	U Fluorometric	DNA	ITNA	SEM-EDS	MSA
GGASP	Y	Y	N	N	Y	N
ESA	Y	Y	M	M	Y	M
DSA	Y	Y	M	M	N	Y
BSA	N	M	Y	Y	N	Y
TSA	Y	Y	N	N	N	N
PSA	Y	Y	M	M	Y	M
CTA	N	Y	N	N	Y	N

DNA = Delayed Neutron Assay

ITNA = Instrumental Thermal Neutron Activation Analysis

SEM-EDS = Scanning Electron Microscopic and Energy Dispersive X-Ray Spectroscopy

MSA = Mass Spectroscopic Analysis

Y = Analysis performed on all samples

N = Analysis <u>not</u> performed

M = Analysis performed on selected samples

majority of samples from the External Sampling Array (ESA) and Pole Sampling Array (PSA) were analyzed using uranium fluorometry. Selected samples from the Balloon Sampling Array (BSA) were analyzed consecutively using DNA and uranium fluorometry to provide cross-check and confirmation of the two analytical techniques. DNA was performed on all samples of the BSA and selected samples of the ESA and PSA. DNA analysis of impactor samples from the GGASP, TSA, and CTA was not feasible because of substrate interference problems. All samples of the BSA and selected samples from the ESA, DSA, and PSA were analyzed for Sc and Sb using ITNA. ITNA analysis was not performed on samples of the GGASP, TSA, and CTA because of substrate interference problems. Selected samples from the GGASP, ESA, PSA, and CTA were analyzed for uranium and particle morophology using SEM-EDS. All samples from the DSA and BSA, and selected samples of the ESA and PSA were analyzed for atomic percent of U-235 using mass spectroscopy. The following is a brief description of each analytical technique.

Gravimetric Analysis

Gravimetric analysis was performed by weighing filters and cascade impactor substrates before and after sampling using a Cahn 26 Electrobalance with a mass resolution of 0.01 mg. All filter samples were dried in a desicator for 24 hours prior to weighing before and after sampling. Static charge on filters and substrates was neutralized by exposing each sample to a Po-210 source.

Uranium Fluorometry

After each sample was weighed, uranium fluorometric analysis was performed. Figure D-17 shows a flow chart of the analytical procedure. Samples are transferred to a glass beaker with water (soil sample) or toluene (filters or cascade impactor samples). The sample is then dried on a hot plate or in a drying oven and dry-ashed at 550°C for 24-48 hours. The sample is then wet-ashed with concentrated HNO_3 and 30% H_2O and evaporated dry on a hot plate. The dried powder is dissolved and diluted to known volume with 2 M HNO_3.

Uranium is then extracted from a 10 ml aliquot of the 2 M HNO_3 solution into 1 ml of tri-n-octyl phosphine oxide (TOPO). A 0.2-ml aliquot of TOPO is extracted from this solution and evaporated onto a pellet of 2% LiF in NaF and fused over a fusion burner. Finally, the uranium is measured by fluorometry using appropriate standards for calibration.

Instrumental resolution of uranium using this procedure is typically 10 nanograms. The procedure is described in greater detail in Reference PR53.

Delayed Neutron Activation Analysis

In this analytical technique, samples are irradiated with 0.1 kev thermal neutrons for approximately 60 seconds at the Los Alamos Omega West Reactor

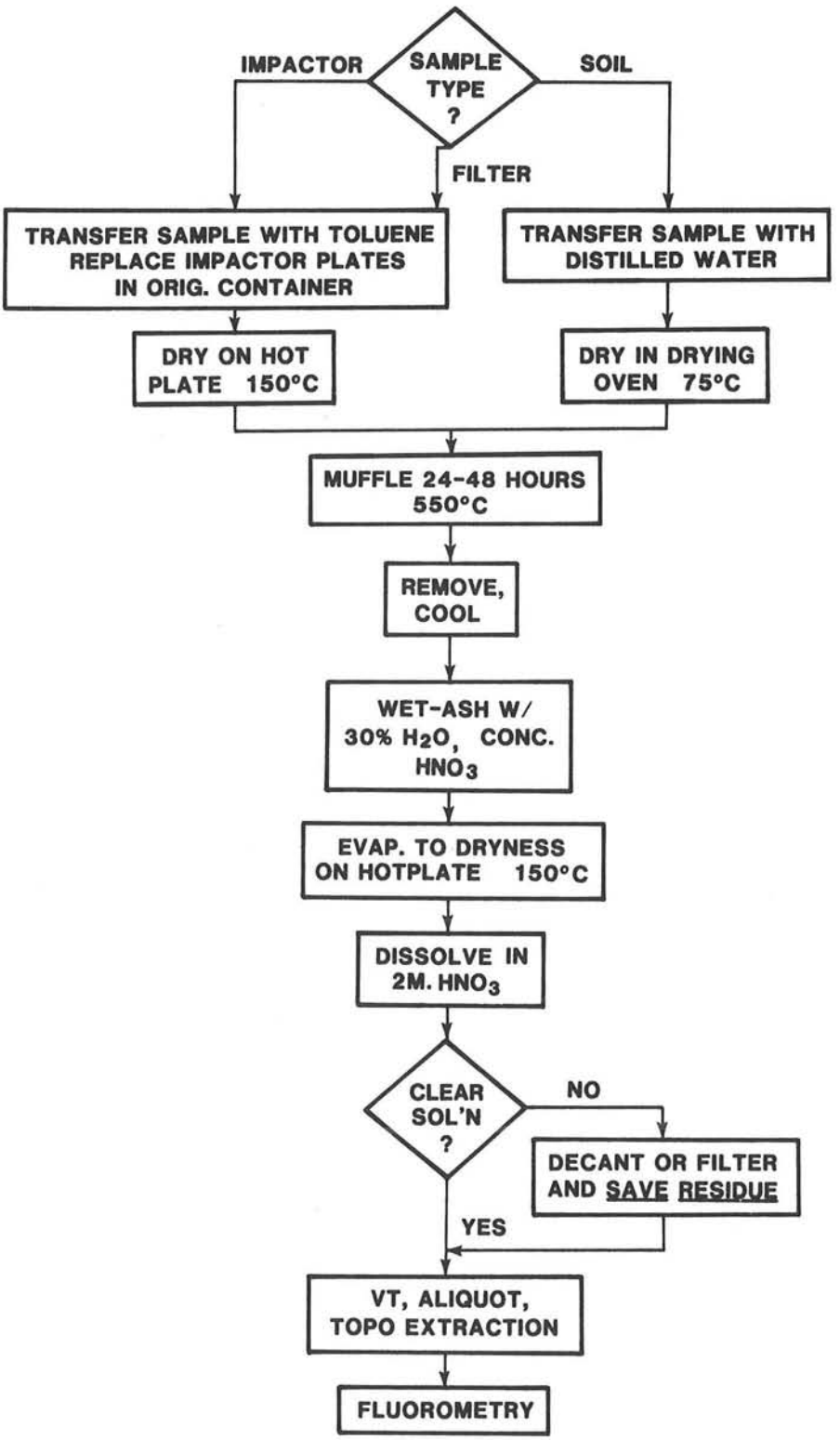

Figure D-17. Flow Chart of Uranium Fluorometric Procedure

(OWR). U-235 nuclei capture the thermal neutrons and fission into neutron-rich, highly unstable fission-products ranging in half-lives from 0.6 to 56 seconds. The fission-products decay by neutron emission and these neutrons can be distinguished from the prompt neutrons emitted during the fission process. A 60 second irradiation with a 20 second decay period preceeding a 60 second neutron count results in detection of 44% of all neutrons emitted. The delayed neutron flux is counted using a specially designed He-3 neutron detector. Standardization is accomplished by irradiating samples with a known U-235 content. NBS Standard Reference Material (SRM) 1648, "Urban Air Particulates" was used as the standard for this analysis. Excellent agreement between the Los Alamos analyses and NBS-certified values was achieved. Instrumental resolution for depleted uranium is typically 40 ng. The uranium DNA procedure is described in detail in Reference GL80.

Instrumental Thermal Neutron Activation-Analysis

Samples were irradiated with thermal neutrons in RT-4 of the OWR (Los Alamos Scientific Laboratory) for 1 hour at a neutron flux of 1×10^{13} neutrons/cm^2-sec with a decay period of approximately 10 days and a counting period of 8 to 16 hours per sample. The 1691 keV and 889 keV γ-transitions were used for quantitative analysis of Sb and Sc, respectively. The reactions for Sb and Sc are

$$^{123}Sb\ (n,\gamma)^{124}Sb \qquad (1)$$

$$^{45}Sc\ (n,\gamma)^{46}Sc \qquad (2)$$

Sc was selected as a tracer to quantify soil component on filter samples. Assuming that all Sc is soil derived, expected soil concentrations of U and Sb could be calculated for each filter. Quality assurance for Sb and Sc concentrations was provided by concurrent analysis of NBS Standard Reference Material (SRM) 1648: Urban Air Particulate. Excellent agreement was achieved for both elements. ITNA analysis is described further in Reference GL80.

Scanning Electron Microscopic-Energy Dispersive X-ray Analysis

The sample (usually a carbon disk 2.5 cm in diameter) is placed under a high energy electron probe which impinges a 10-500 Å diameter electron beam on the sample surface. The 20 keV electrons interact with the sample and generate several useful signals including secondary electrons and characteristic x-rays. The secondary electrons are those which carry the topographic information necessary to construct a visual image. The characteristic x-rays provide information on the electronic structure and therefore elemental identity of the sample. The SEM has a solid state x-ray detector (Si-drifted intrinsic Si-chip) which discriminates x-rays by energy, hence the descriptor "energy dispersive analysis." Routinely, this technique can detect elements only with atomic numbers greater than or equal to 11 (Na). For this program, the samples were analyzed on a JEOL JSM-35C. The detectability limit of

solvent element B in solvent element A is typically ≥ 0.5 wt%. The minimum detectable mass of an isolated particle is $\leq 10^{-18}$g which corresponds to a 100 Å diameter particle.

Mass Spectroscopic Analysis

Because DNA measures neutrons from only U-235 fission-products, the U-235/U-238 isotopic ratio must be known in order to translate the signal into total U present on the sample. It is important therefore that the atomic percent of U-235 in the sample be determined. Mass spectroscopic (MS) analysis of filter and soil samples was performed using the Los Alamos Scientific Laboratory PC-2 Mass Spectrometer (Group INC-7) to determine the isotopic ratio of U-235/U-238. MS analysis was performed on all samples of the DSA and selected samples of the BSA, PSA, and ESA. A detailed description of this technique is described in Reference JT76.

Results of SEM-EDS Analysis of Full-Scale Test Samples

This section summarizes the results of SEM-EDS analysis of the full-scale test samples. Table D-11 summarizes the analytical results of the full-scale test. Uranium was detected on three of the six GGASP station samples analyzed (Stations 1, 3, 4). No uranium was detected on samples taken from GGASP Stations 2, 5 and 6. No uranium was detected on samples taken external to the confinement structure. This includes samples taken from the PSA, ESA, and CTA systems. All of the samples analyzed contained elements (Si, Ca, Al, Fe) indicative of "dirt" or pulverized rock from the containment structure or surrounding desert floor. GGASP samples from Stations 5 and 6 contained significant quantities of Pb, Cu, and Zn which could have come from electrical wire and metal components used in the test. On several samples of the CTA (IIA2000, IIB2 BG2, IIE1 BG2, BG1, and III D4 BG1) organic residue was detected which came from the toluene used to coat the collector trays. The uranium particle size ranged from 1 μm to 10 μm and the dirt particle size ranged from <1 μm to 100 μm. Most of the uranium particles appeared to be smooth and spherical and some appeared to be bullet shaped which suggests that the uranium could have melted and undergone aerodynamic forces. X-ray spectra also suggest that the molten uranium had mixed with the dirt. All dirt particles examined were irregular (not smooth) in shape.

TABLE D-11

Summary of SEM-EDS Analysis of Full-Scale Test

SAMPLE	ELEMENTS DETECTED	PARTICLE MORPHOLOGY	FIGURE
GASP STA 1	Ca, Si, S, Al, Fe, Zn, Cu	Irregular 'dirt' particles from 1 to 100 μm	D-18
	U	~5 μm U particle	D-19, D-20
GASP STA 2	Ca, Si, Al, Fe	Irregular particles of 'dirt', No U detected	---
GASP STA 3	Ca, Si, S, K, Al, Fe, Zn, Ni, Ti, U	Irregular shaped particles of 'dirt'	---
		Smooth U particles ~10 μm	
GASP STA 4	Ca, Si, Al, Cu, Fe, U	~1 μm particles of 'dirt', agglomerates (10 to 15 μm) of U and 'dirt', Evidence of U melting	D-21, D-22, D-23, D-24
GASP STA 5	Ca, Si, Al, Fe, Pb	'dirt' particles identical to GASP Sta 2, No U detected	
GASP STA 6	Ca, Si, Al, Fe, Pb	Evidence of Pb melting, irregular particles of 'dirt', No U detected	D-25, D-26
PSA E03	Ca, Si, S, K, Al, P	Particles of 'dirt', Average particle size ~10 μm, No U detected	D-27
PSA N03	Ca, Si, Al, Fe, K	Particles of 'dirt', particle size ~5 μm No U detected	D-28
ESA V1	Ca, Si, Al, Fe, S	Particles of 'dirt', No U detected	---

TABLE D-11 (Continued)

Summary of SEM-EDS Analysis of Full Scale Test

SAMPLE	ELEMENTS DETECTED	PARTICLE MORPHOLOGY	FIGURE
ESA H2	Ca, Si, K, Fe, S	Particles of 'dirt', Particle size 15μm, No U detected	---
ESA H4	Ca, Si, K, S, Al, Fe, Mg, Cl	'dirt' particles, 1 to 100 μm particles, No U detected	D-29
ESA H6	Si, Al	'dirt' particles, 10 to 15 μm particles, No U detected	---
IIA2000	Ca, Si, Al, Cu, Fe K, Mg, organics	'dirt' particles, 20 μm, No U detected	---
IIIA5000	Ca, Si, K, Al, Cu, Fe, Zn	'dirt' particles 10 μm, No U detected	D-30
IIIE1000	Ca, Si, K, Al, Fe, Zn, Mg	'dirt particles, 10 to 50 μm, No U detected	---
IB2 BG1	Ca, Si, Al, Fe, Cu, Zn, Na, Cl	'dirt particles, No U detected	---
IIB2 BG1	Ca, Si, Cu, Zn, organics	Small particles of 'dirt' 50 μm, No U detected	---
IIE1 BG1	Ca, Si, Cu, Zn, organics	Small particles of 'dirt' 50 μm, No U detected	---
IID4 BG1	Ca, Si, Al, K, organics	Small particles of 'dirt', No U detected	---
IVB2 BG1	Ca, Si, K, Al, Cu, Fe, Mg, organics	Small particles of 'dirt', No U detected	---

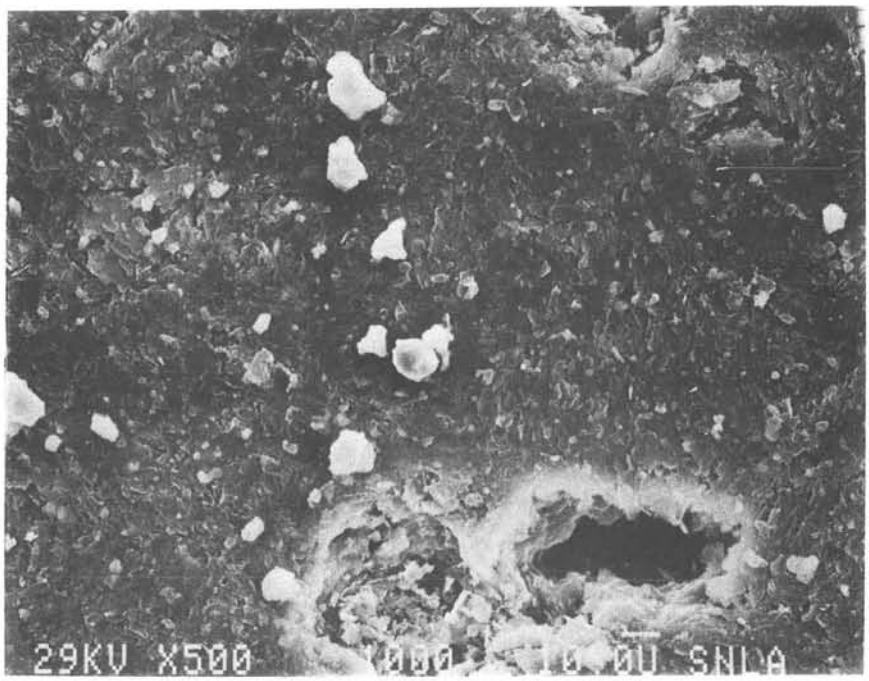

Figure D-18. SEM Micrograph of Carbon Planchet of GGASP Station 1 Showing Irregular Dirt Particles. Particles range from <1 μm to >100 μm.

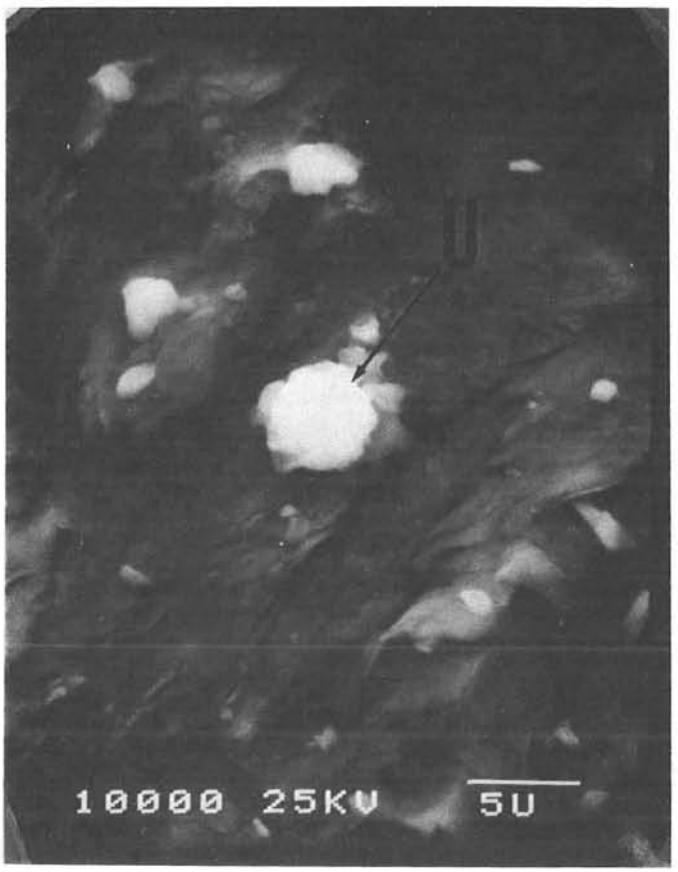

Figure D-19. SEM Micrograph of Carbon Planchet of GGASP Station 1 Showing Uranium Dirt Particle. Particle is a mixture of 'dirt' and uranium. Particle diameter (geometric) is 5 μm.

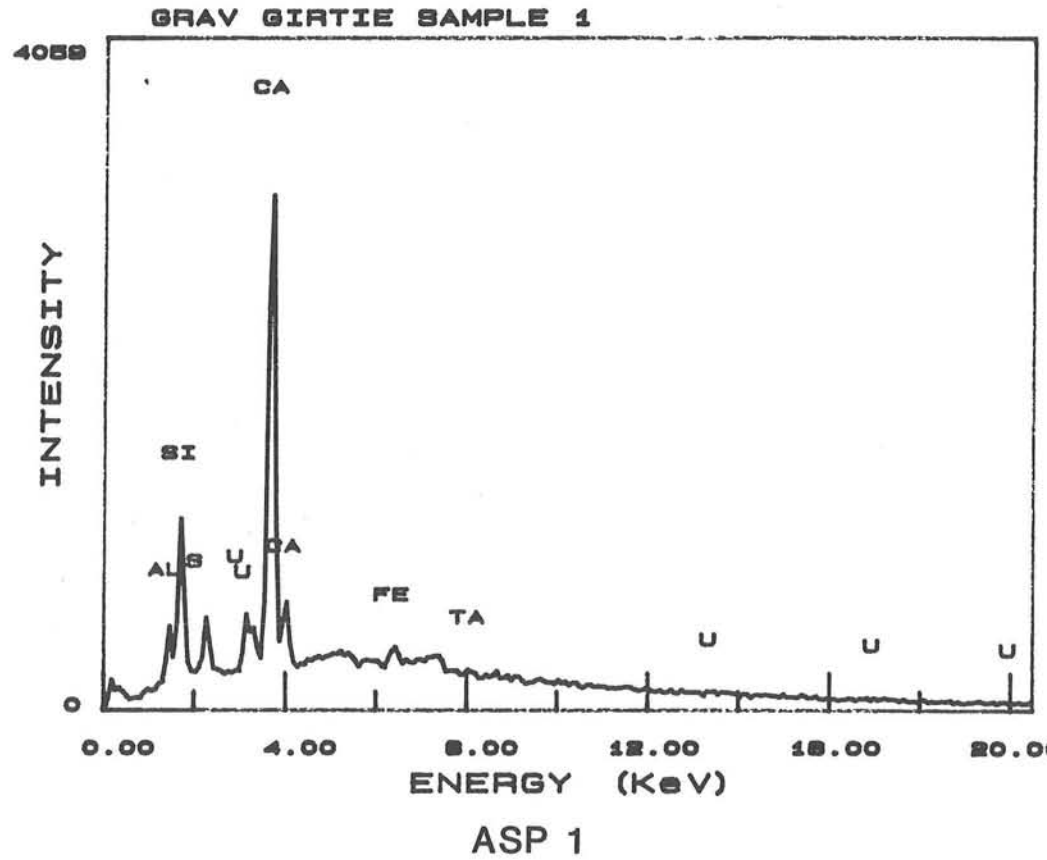

Figure D-20. X-ray Spectrum From Uranium Bearing Particle Shown in Figure D-19.

Figure D-21. SEM Micrograph of Planchet Taken From Sampling Chamber of GGASP Station 4. Uranium rich particle ($\sim$15 μm diameter) shows signs of uranium melting.

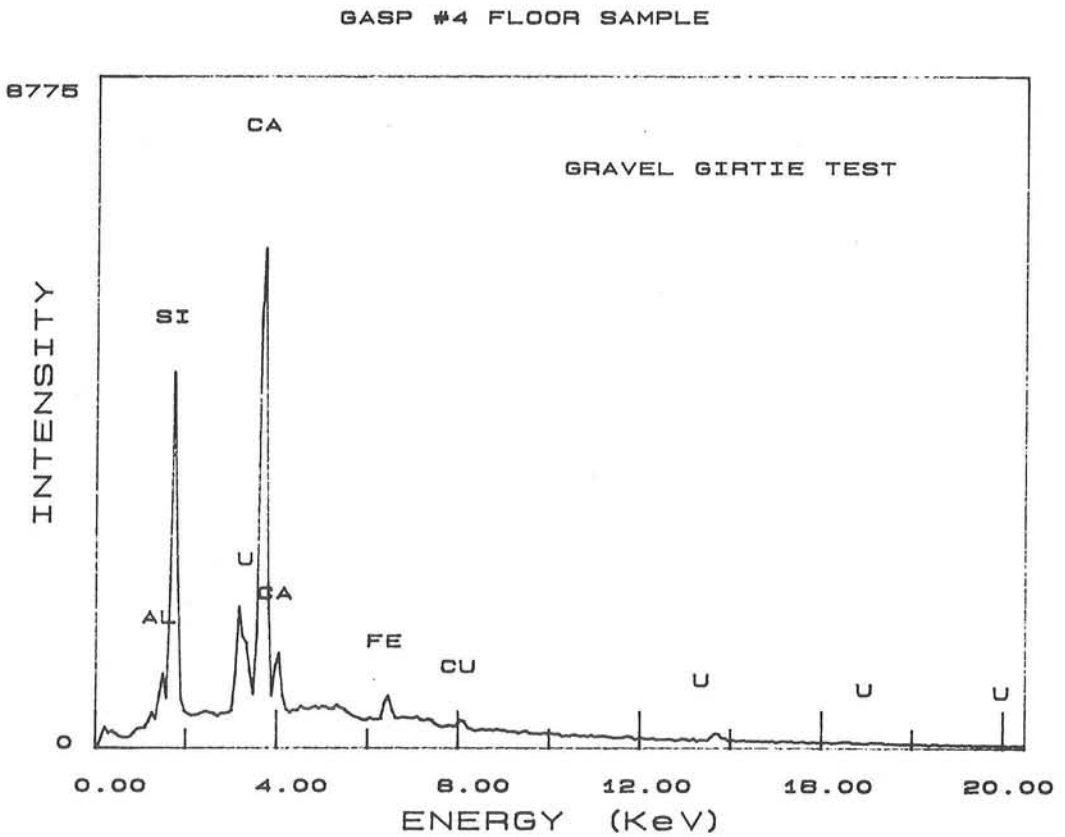

GASP 4 (floor)

Figure D-22. X-ray Spectrum of U-Rich Particle Shown in Figure D-21. Al, Si, Ca, and Fe indicate that the uranium particle was mixed with "dirt."

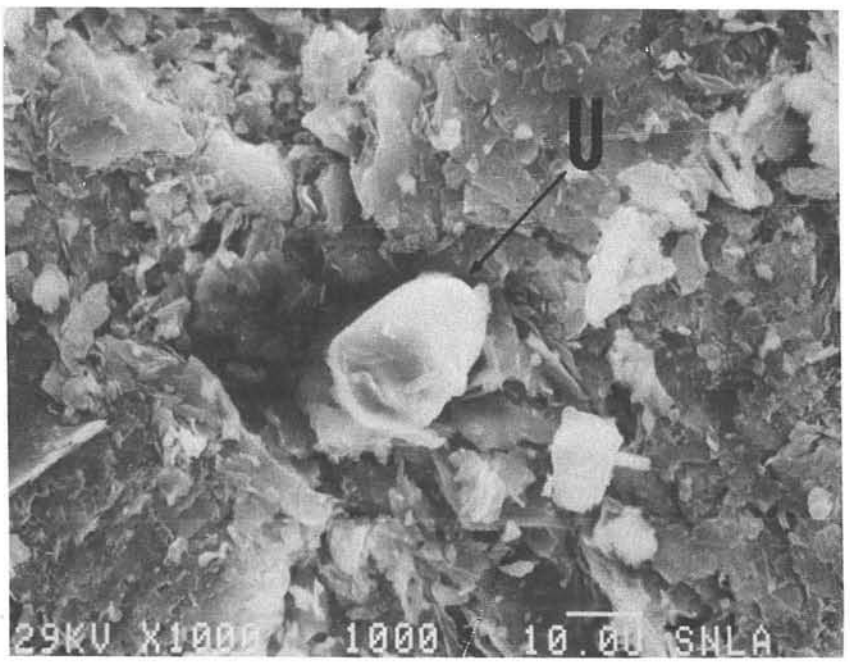

Figure D-23. SEM Micrograph of Carbon Planchet Taken From GGASP Station 4. Uranium-rich particle appears to be "bullet shaped" and is ~15 μm in diameter. Particle shape indicates a fully molten uranium droplet shaped by aerodynamic forces.

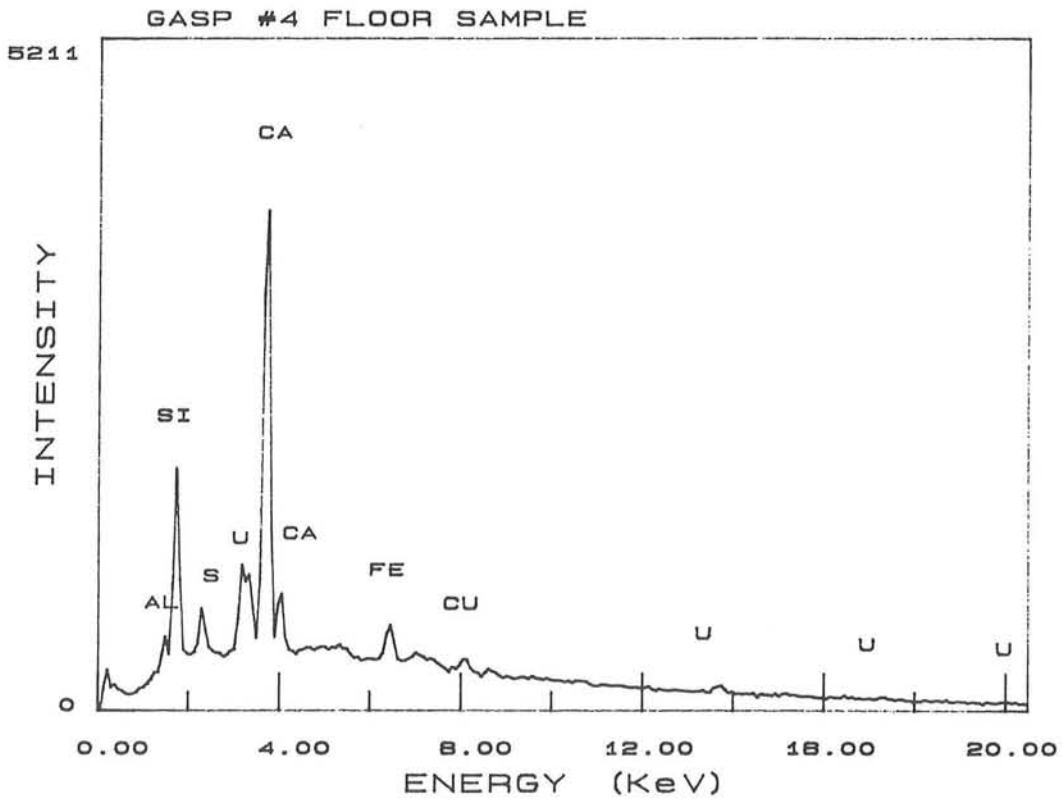

GASP 4 (floor)

Figure D-24. X-Ray Spectrum of U-Rich Particle Shown in Figure D-23. Presence of Al, Si, Ca, Fe, and U indicate a mixture of uranium and "dirt."

Figure D-25. SEM Micrograph of Debris on Planchet From GGASP Station 6. Typical "dirt" plus small deposits of Pb. Pb was once molten; may have been vaporized as indicated by wispiness of Pb deposits.

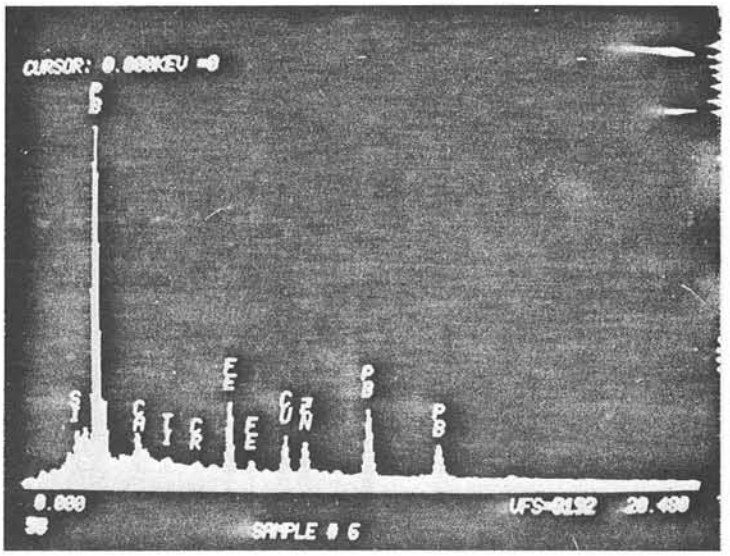

ASP 6

Figure D-26. X-Ray Spectrum of Pb-Rich Particle Shown in Figure D-26

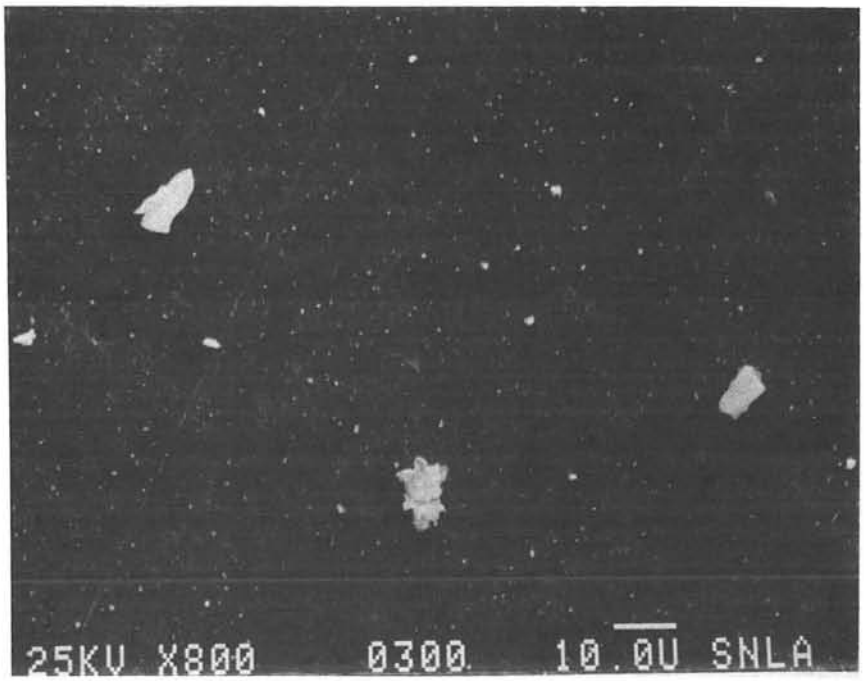

Figure D-27. SEM Micrograph of ESP Sample From PSA East 3. No uranium detected. Particles rich in Si, S, K, P, Cu, Al, and Ca. Average particle size is ~10 μm.

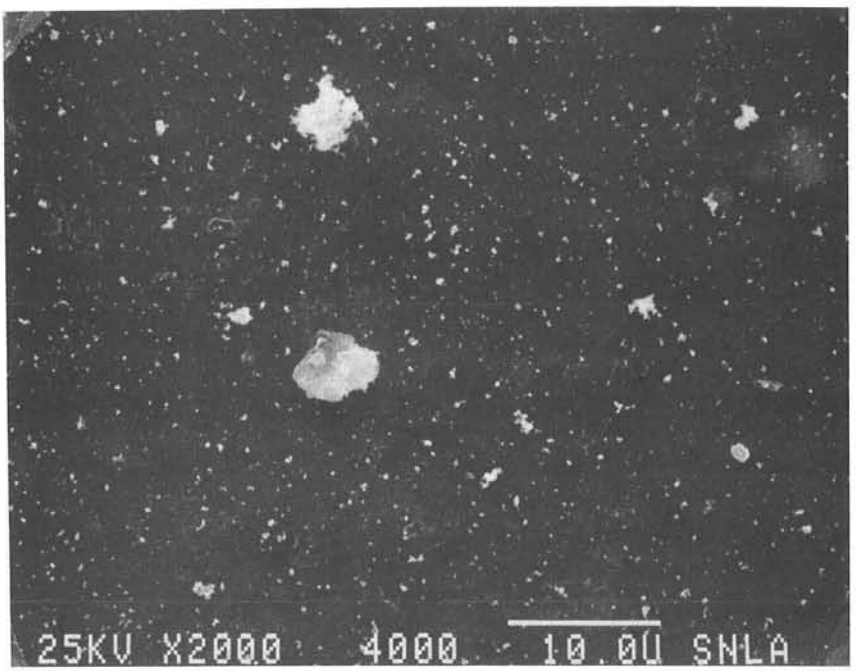

Figure D-28. SEM Micrograph of ESP Sample From PSA North 3. No uranium was detected. Sample contains particles of "dirt" (Al, Si, Ca, and Fe).

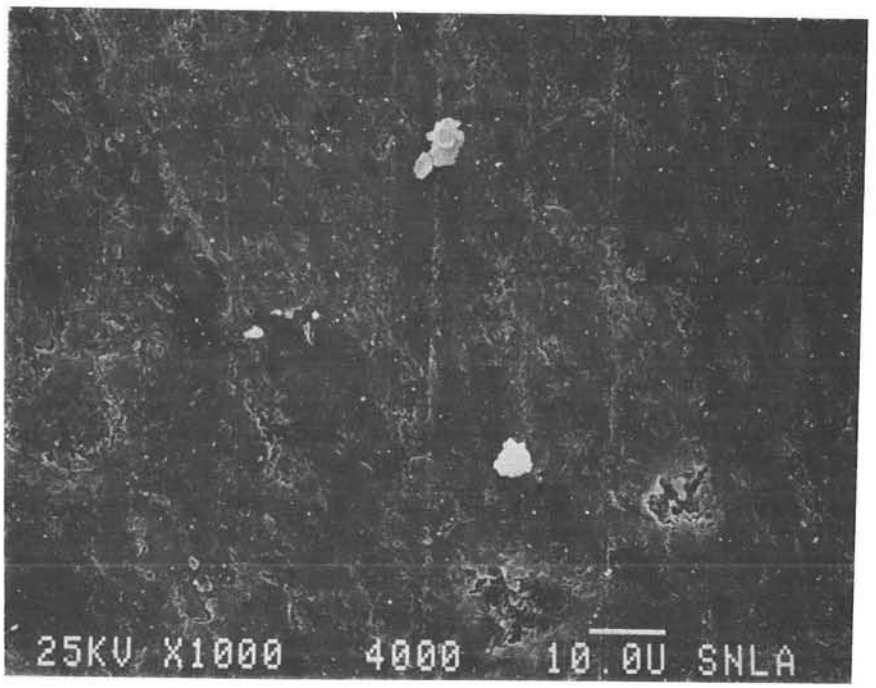

Figure D-29. SEM Micrograph of ESP Sample From ESA H4 Position. No uranium detected. Particles rich in Ca, Si, K, S, Al, Fe, Mg, and Cl ("dirt").

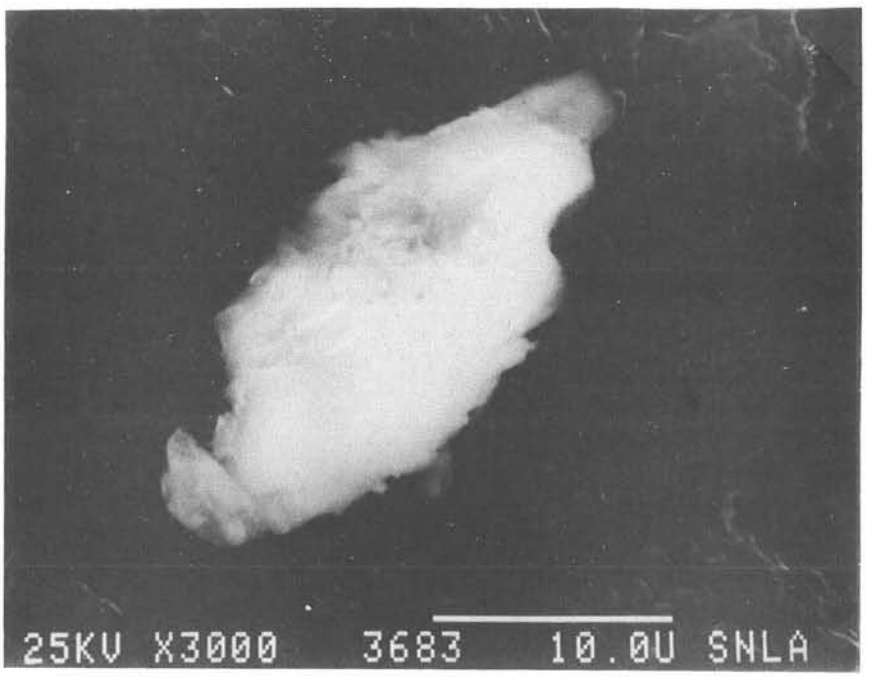

Figure D-30. SEM Micrograph of Planchet from CTA III-A 5-000 Showing Traces of Si, Al, Ca, K, Cu, Fe, and Zn. No uranium detected. Particle is approximately 10 μm wide and 20 μm long.

Appendix E
Full-Scale Test Pressure and Temperature Records

Ambient pressures were measured using fast response Kulite Gauges at each GGASP station, at the entrance door and at the LANL blast-valve experiment. In addition, temperature and pressure were measured within the sampling chambers of each GGASP using a Kulite pressure gage and thermocouples. Figure E-1 shows the location of each measurement station.

Figures E-2 to E-12 show the pressure and temperature data as obtained from the playback of the digital magnetic tape records. No attempt has been made to remove zero offsets or to smooth data in these records. It is clear, based on the pressure traces, that some zero offset may be present at long times when pressure should go to zero at the round room and staging area stations.

Figures E-13 through E-15 show three traces from SwRI pressure records in the round room and staging area for comparison with Figures E-2 and E-12. Of special note is the round room pressure record (Figure E-13) which is not confirmed by SNL records (Figure E-2). Private communication with Dr. W. E. Baker (SwRI) indicates that the SwRI record is likely in error as a result of temperature or impact damage. The entire sequence of SwRI measurements is documented in SW82.

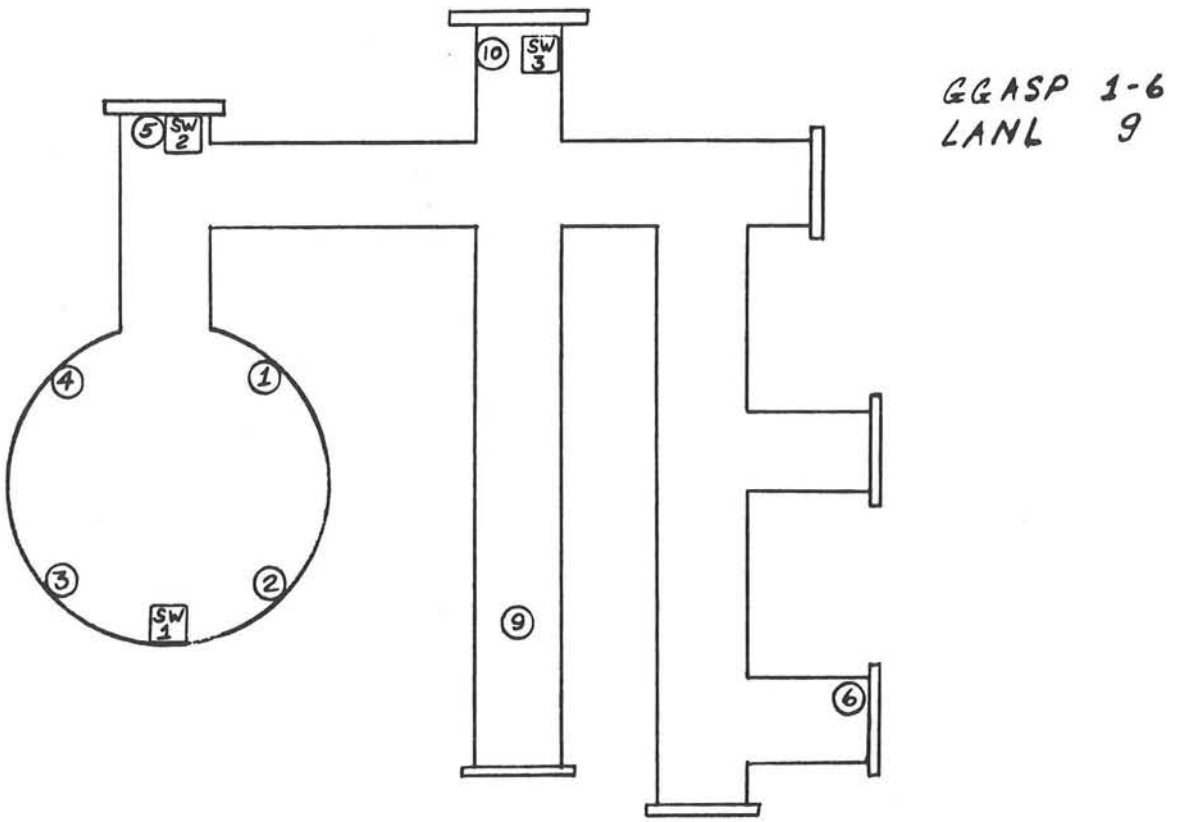

Figure E-1. Station Identification and Location

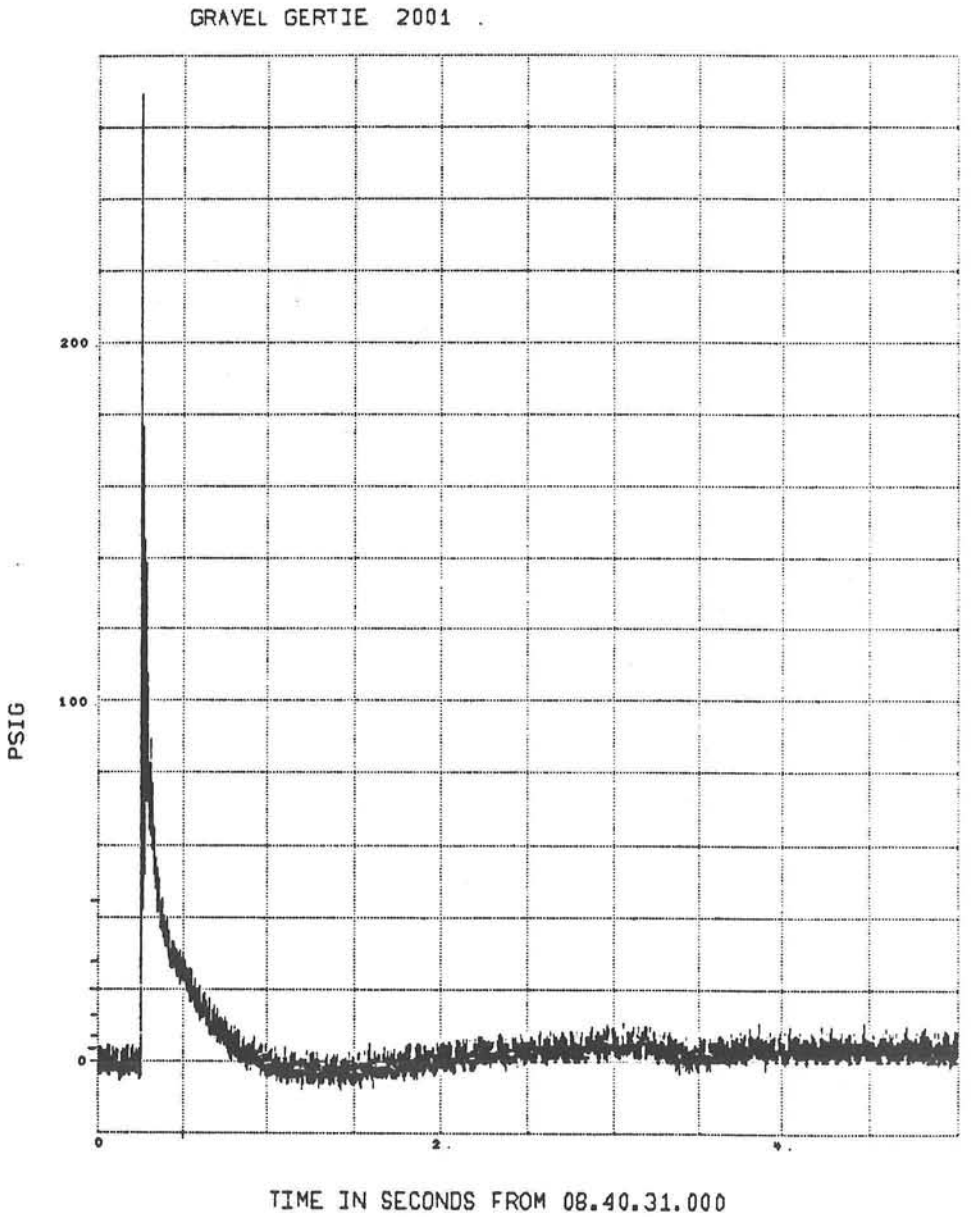

Figure E-2. Station 2 Round Room Pressure to 5 Seconds

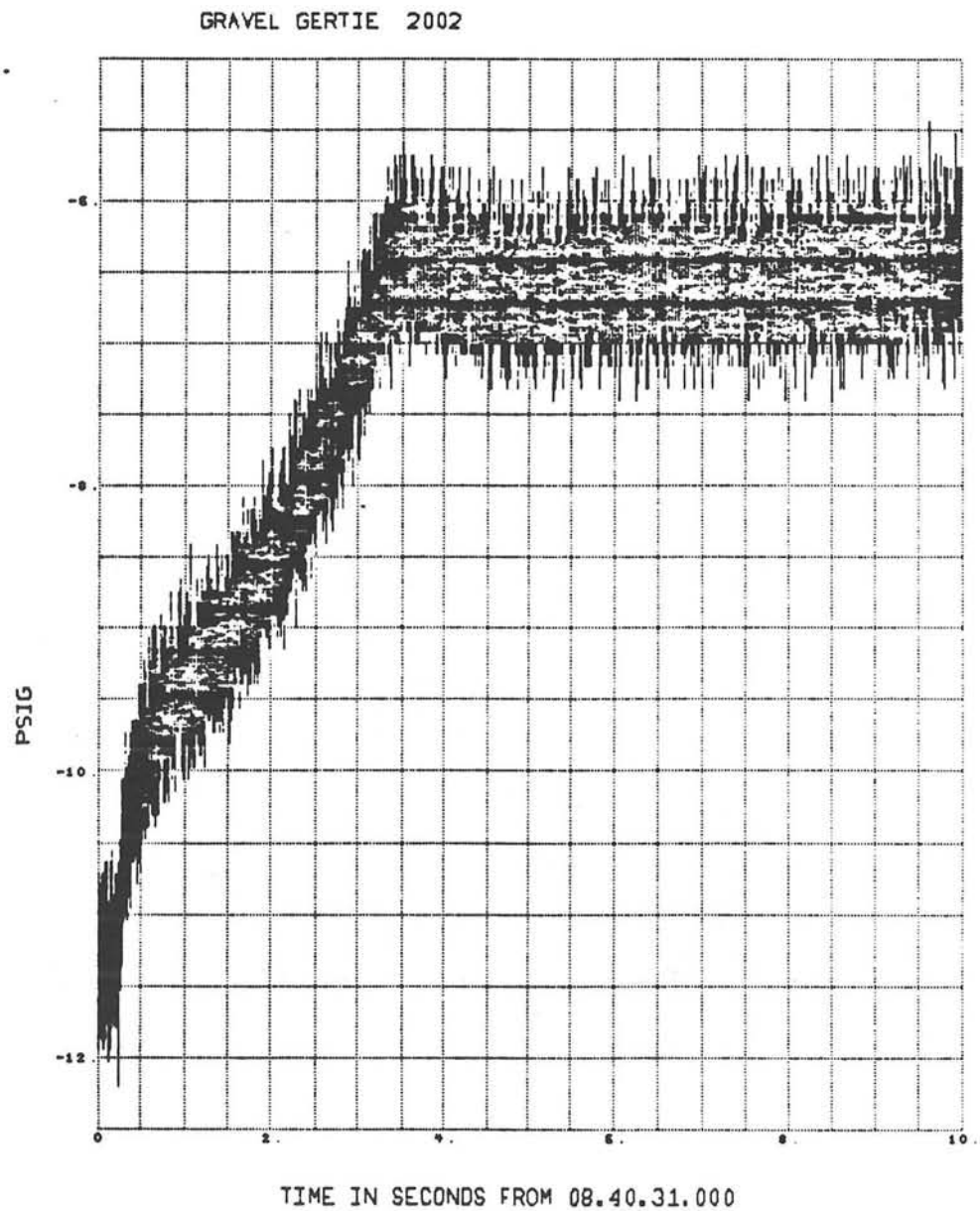

Figure E-3. Station 2 GGASP Internal Pressure to 10 Seconds

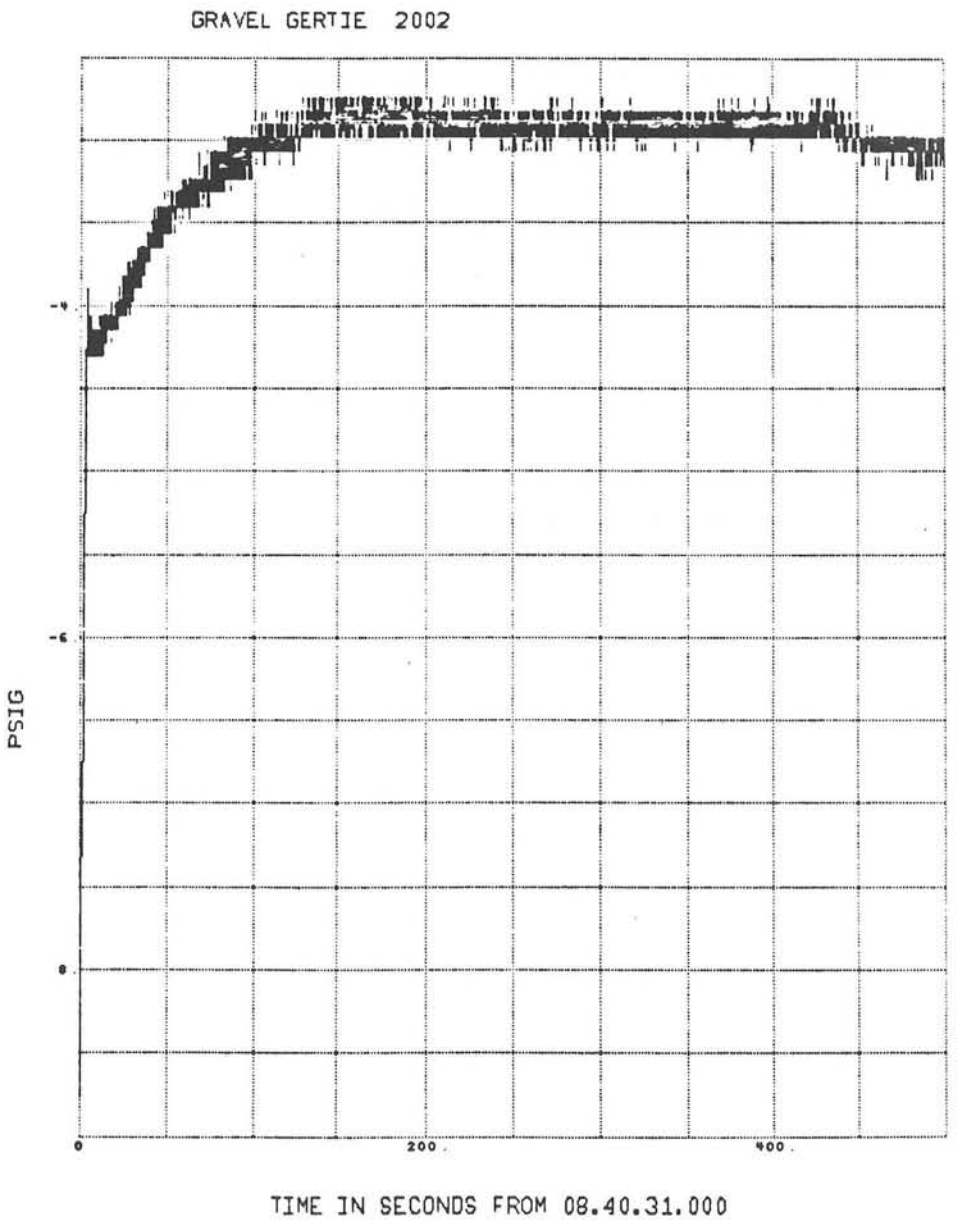

Figure E-4. Station 2 GGASP Internal Pressure to 500 Seconds

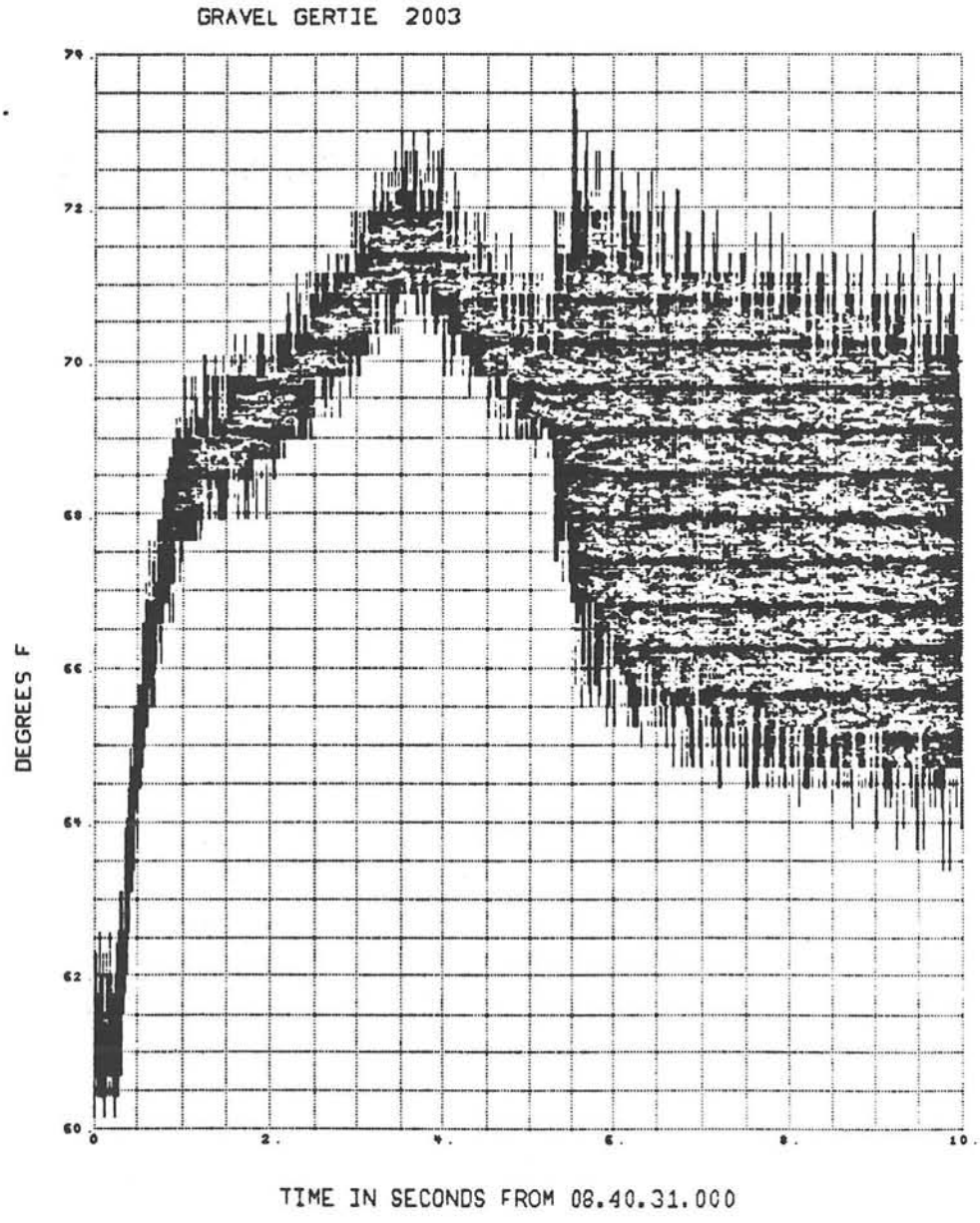

Figure E-5. Station 2 GGASP Internal Temperature to 10 Seconds

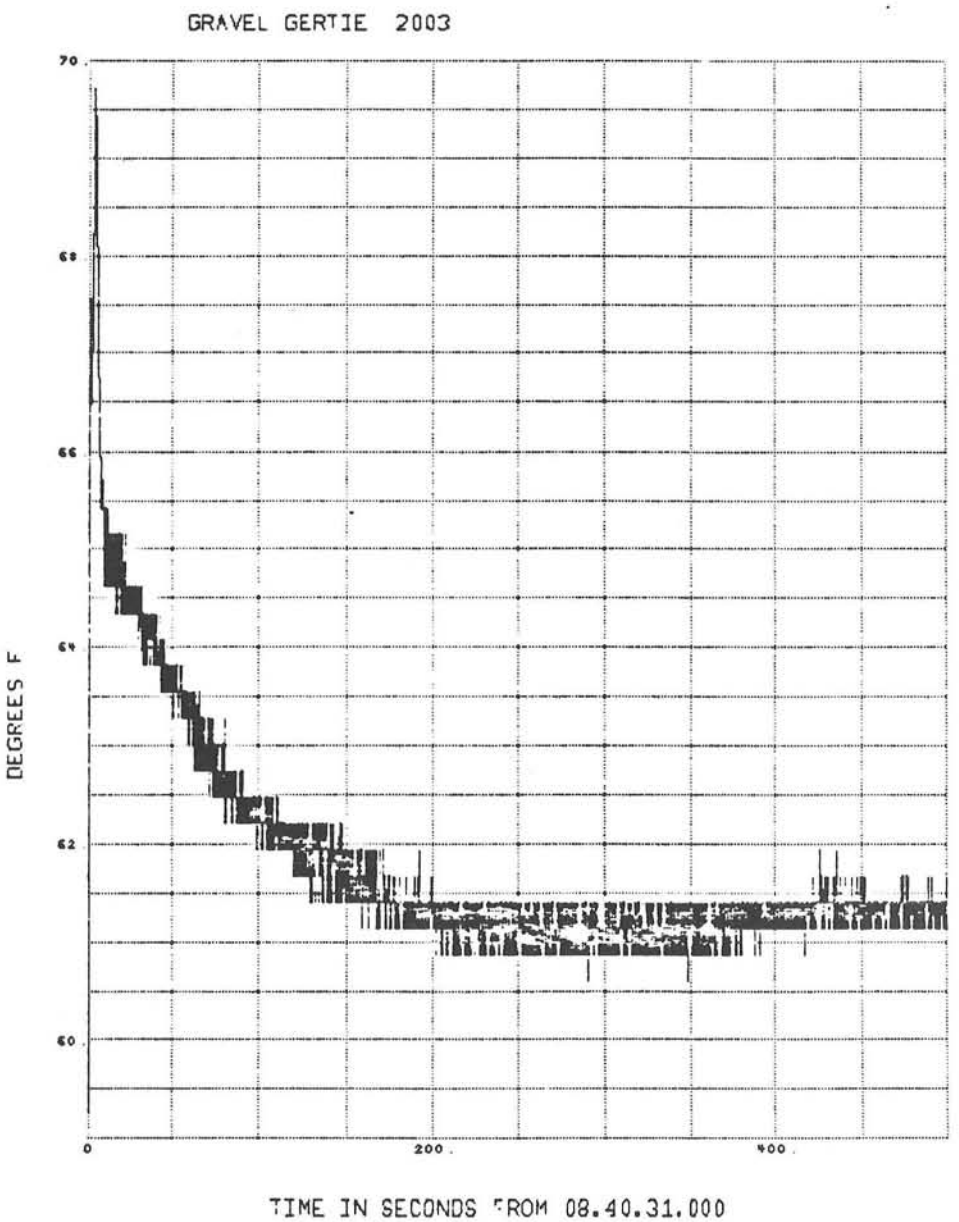

Figure E-6. Station 2 GGASP Internal Temperature to 500 Seconds

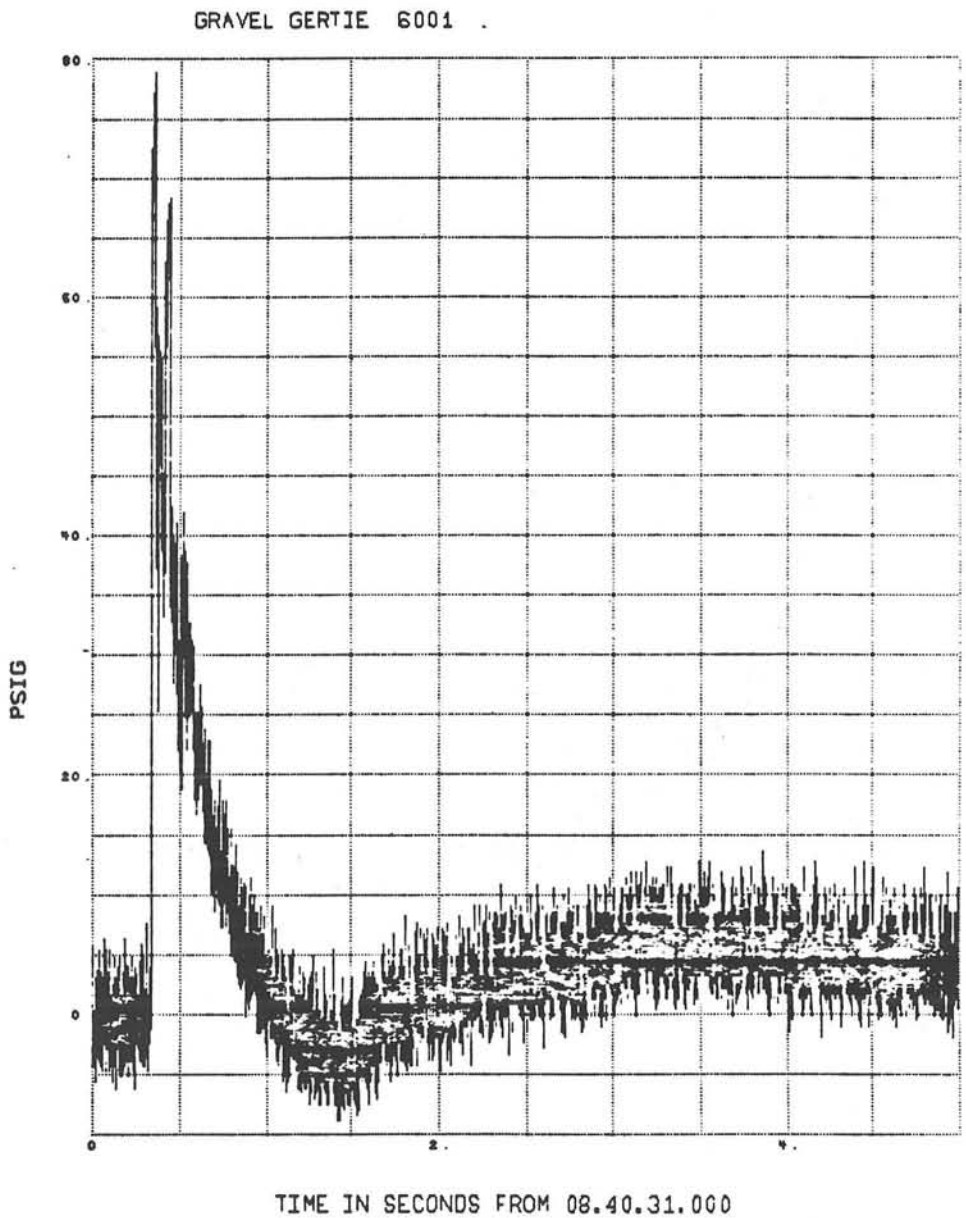

Figure E-7. Station 6 External Pressure to 5 Seconds

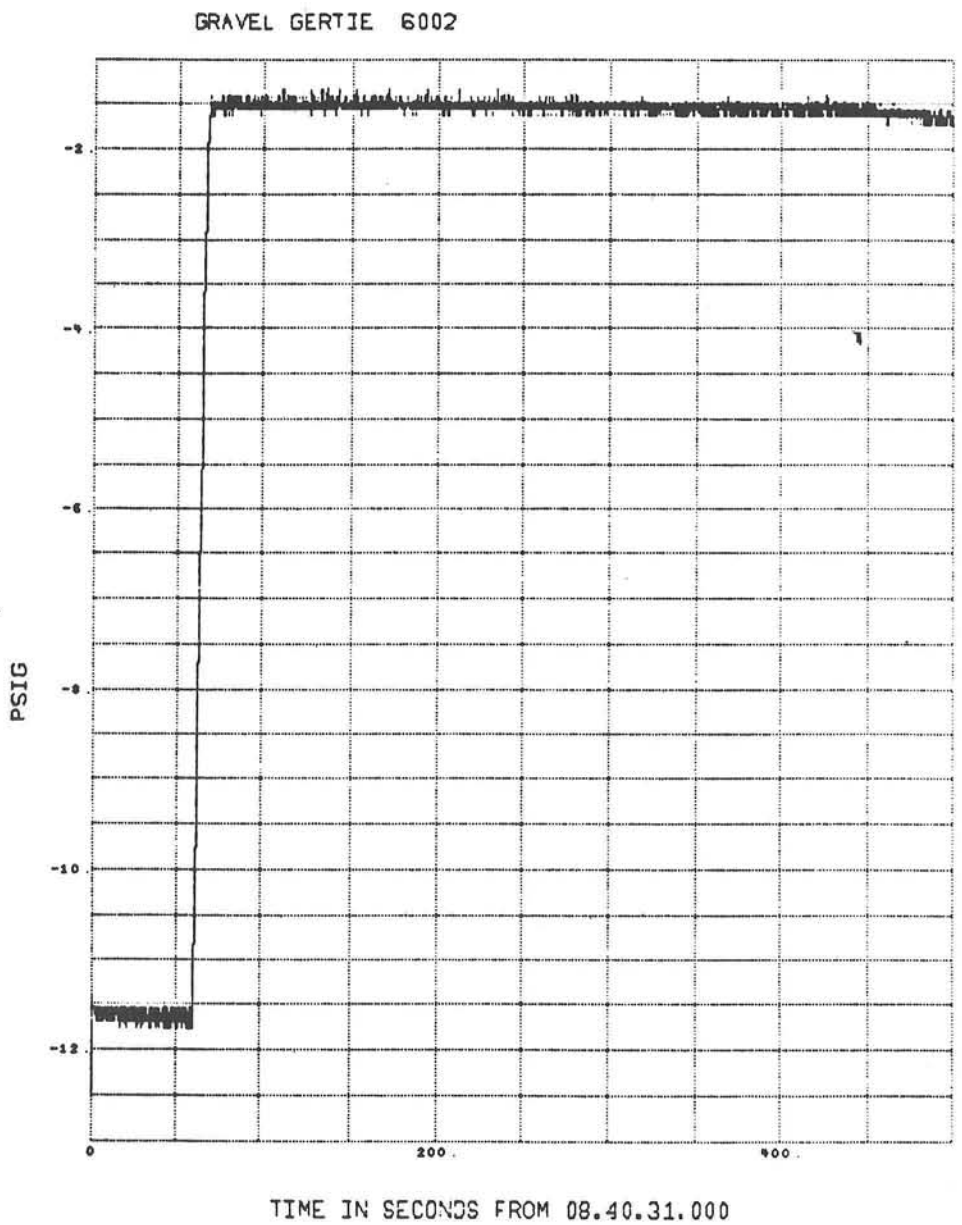

Figure E-8. Station 6 GGASP Internal Pressure to 500 Seconds

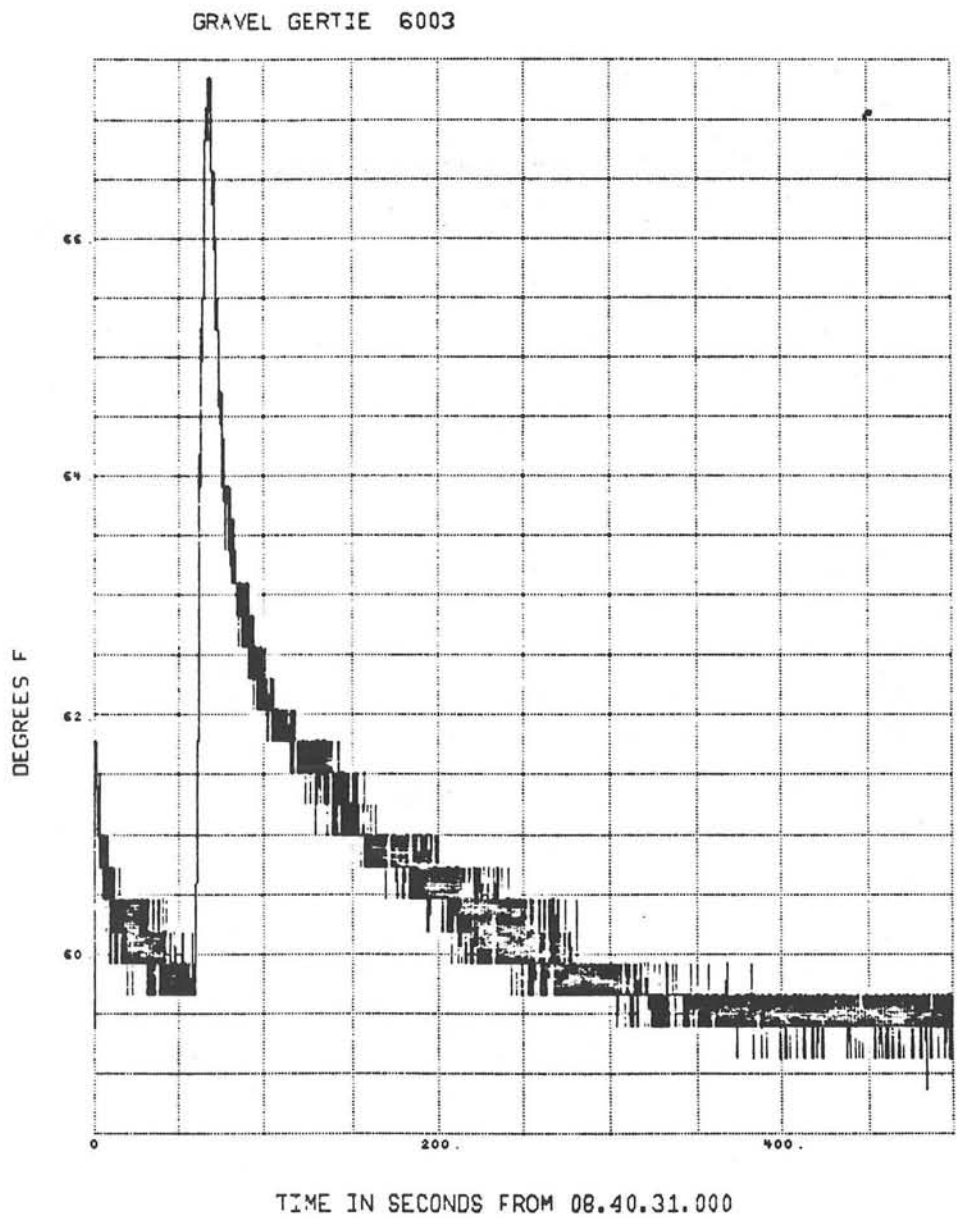

Figure E-9. Station 6 GGASP Internal Temperature to 500 Seconds

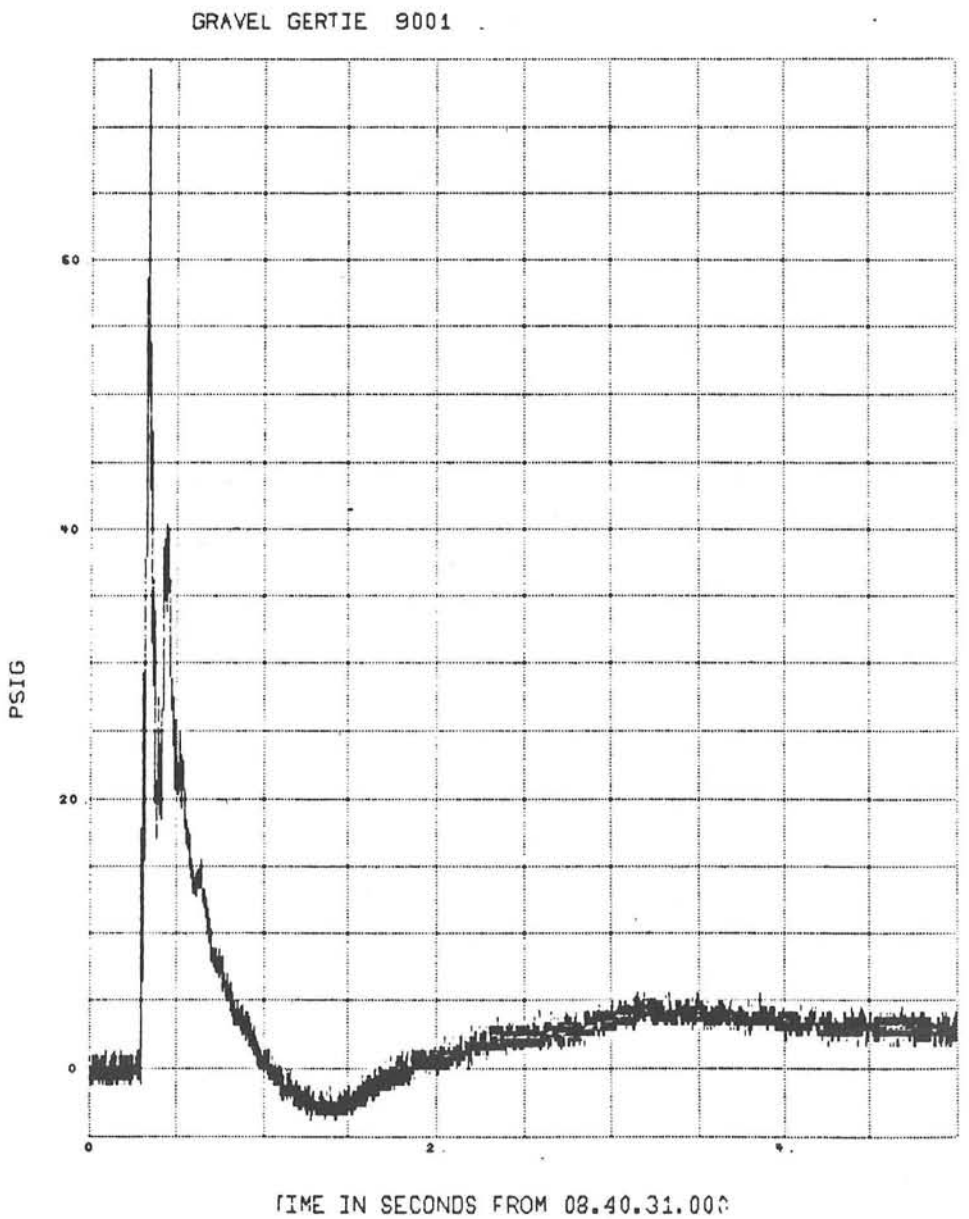

Figure E-10. Station 9 External Pressure to 5 Seconds for Gage Facing Wall

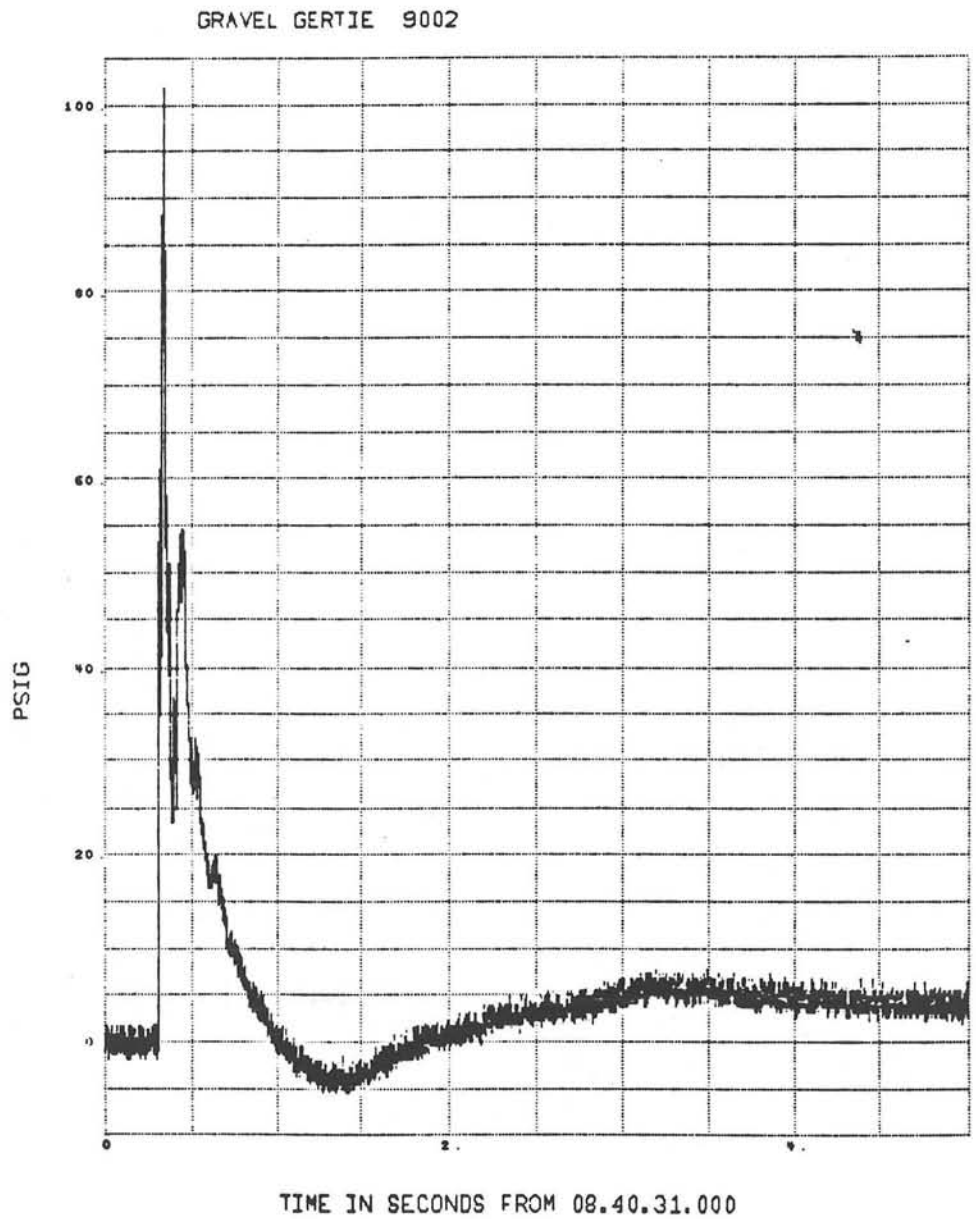

Figure E-11. Station 9 External Pressure to 5 Seconds for Gage Facing Station 10

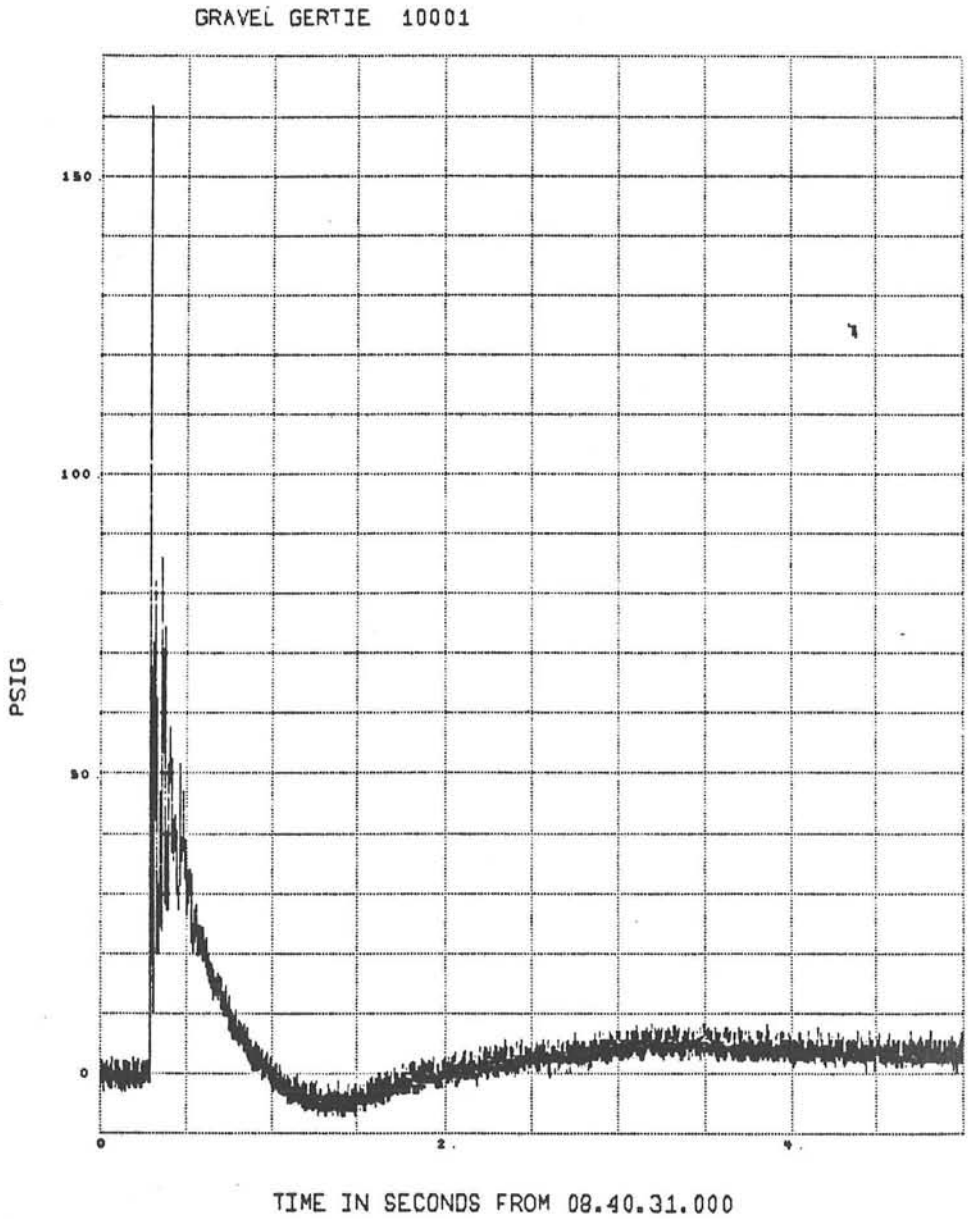

Figure E-12. Station 10 External Pressure to 5 Seconds

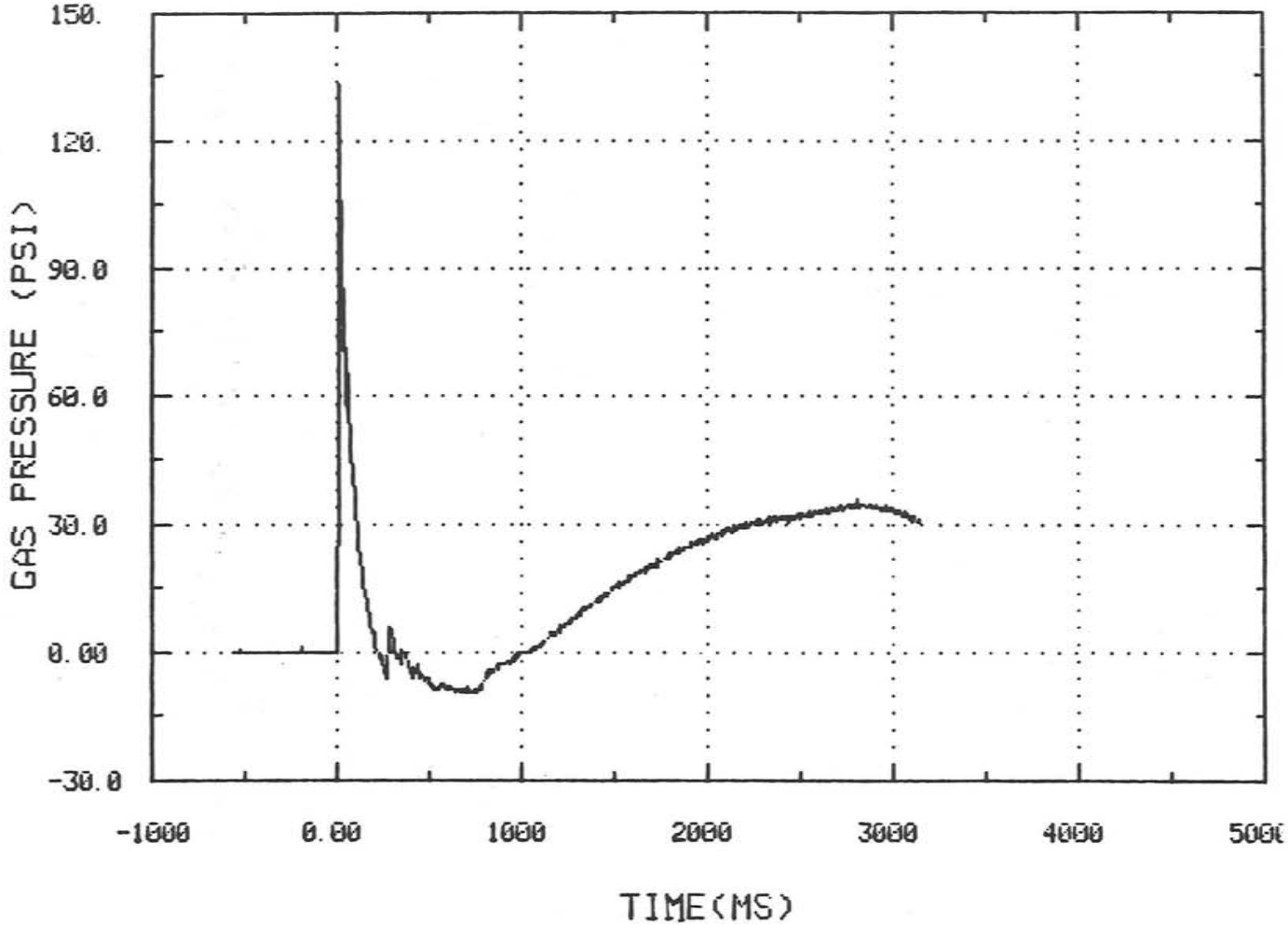

Figure E-13. Station SW1 External Pressure to 5 Seconds

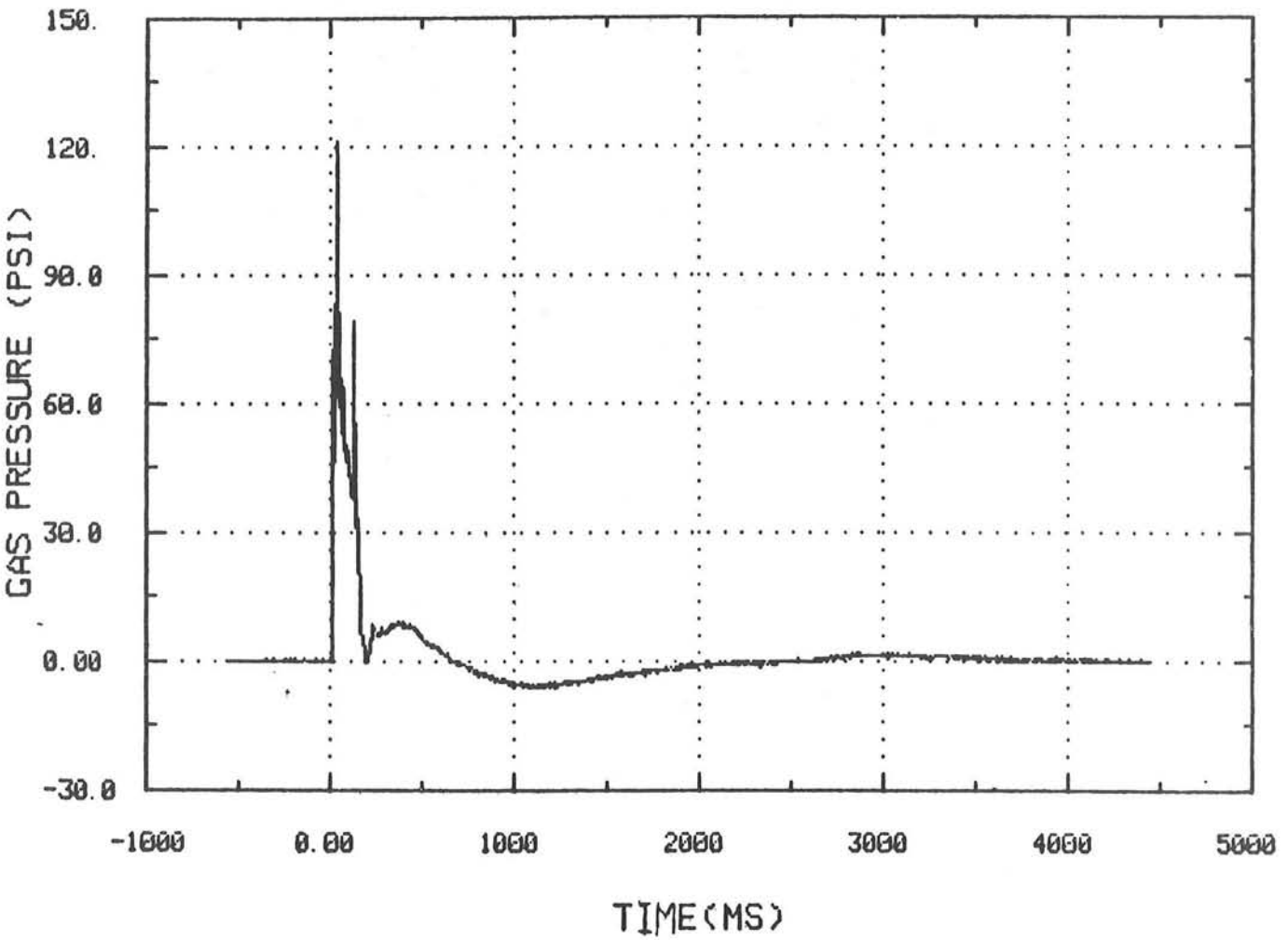

Figure E-14. Station SW2 External Pressure to 5 Seconds

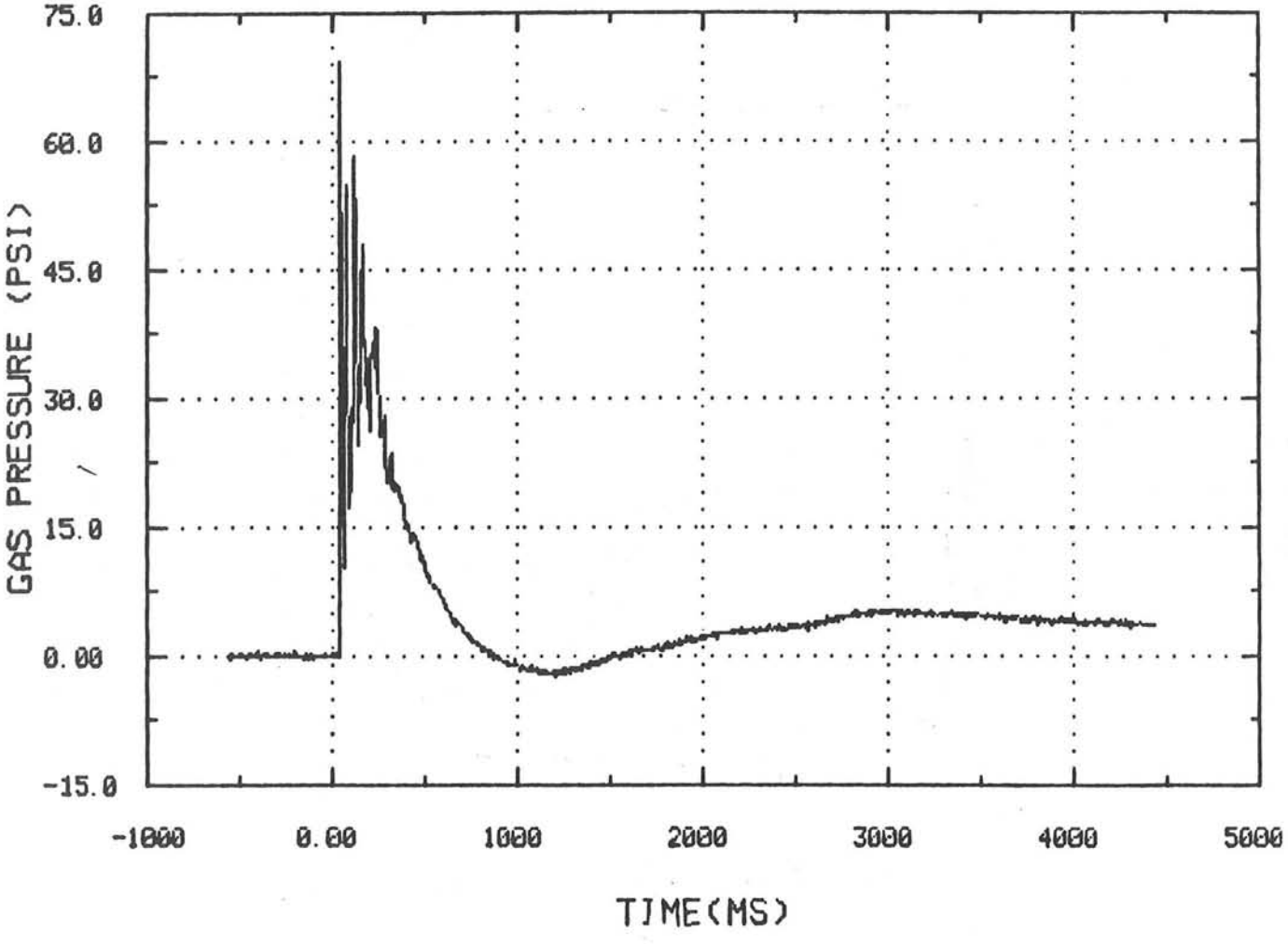

Figure E-15. Station SW3 External Pressure to 5 Seconds

Appendix F
Fragmentation Experiments Conducted During Full-Scale Test

The Gravel Gertie fragmentation measurement system consisted of three 6-foot panels constructed from 8-inch aluminum channel. Top and bottom cover plates, also aluminum, were welded on both ends of the channel. Witness plates made from annealed copper and softened aluminum were bolted to the inside of the channel and these completed arrays were bolted to the walls of the round room at a distance of approximately 5.18 m (17 ft) from the explosive charges. The installed panels are shown on Figure F-1 and a plan view of the installation is shown on Figure F-2. Figure F-3 shows the angular relationship between the charges and the panels and Figure F-4 shows the construction of the panels.

The panels were positioned in such a way that each had different "view" of the explosive assembly.

After the panels were removed from the excavated round room, they were packaged and sent to Albuquerque, where they were carefully inspected and disassembled and each individual witness plate was stamped with a unique identification number. The number scheme is shown on Figure F-5. Once the plates were labelled, they were ultrasonically cleaned in water and alcohol to remove residual dust particles.

The individual plates were analyzed optically to determine crater size distribution. Nine of the plates are either missing or sufficiently deformed to preclude determination of crater size distribution.

Approximately 26,000 individual craters were statistically analyzed. As shown on Figure F-6, there is essentially no variation in crater size distribution based on vertical or horizontal plate location or on the type of plate used. In addition, there is no apparent variation in the number of particles impacting a given area as a function of overall location. Within large horizontal and vertical zones there is some fluctuation in crater density but this appears to be a stochastic variation, not one which correlates directly to plate location.

Figure F-6 suggests a mean crater dimension (and, hence, an upper limit on particle diameter) of approximately 76 microns with a geometric standard of approximately 2.1. The distribution tails off in the smaller size regime due to the aerodynamic forces acting to stop smaller fragments before they reach the wall of the structure. Aerodynamic forces also act to break up the high-speed liquid droplets as they move toward the plates, causing the impacting droplets to be smaller than those formed during the detonation itself. A preshot code prediction indicated that these "prompt" droplets are distributed about a median diameter of approximately 125 microns, whereas the impact plates themselves suggest that the droplets have undergone some primary breakups (perhaps as much as a factor of 4 in diameter) in their 5 m flight.

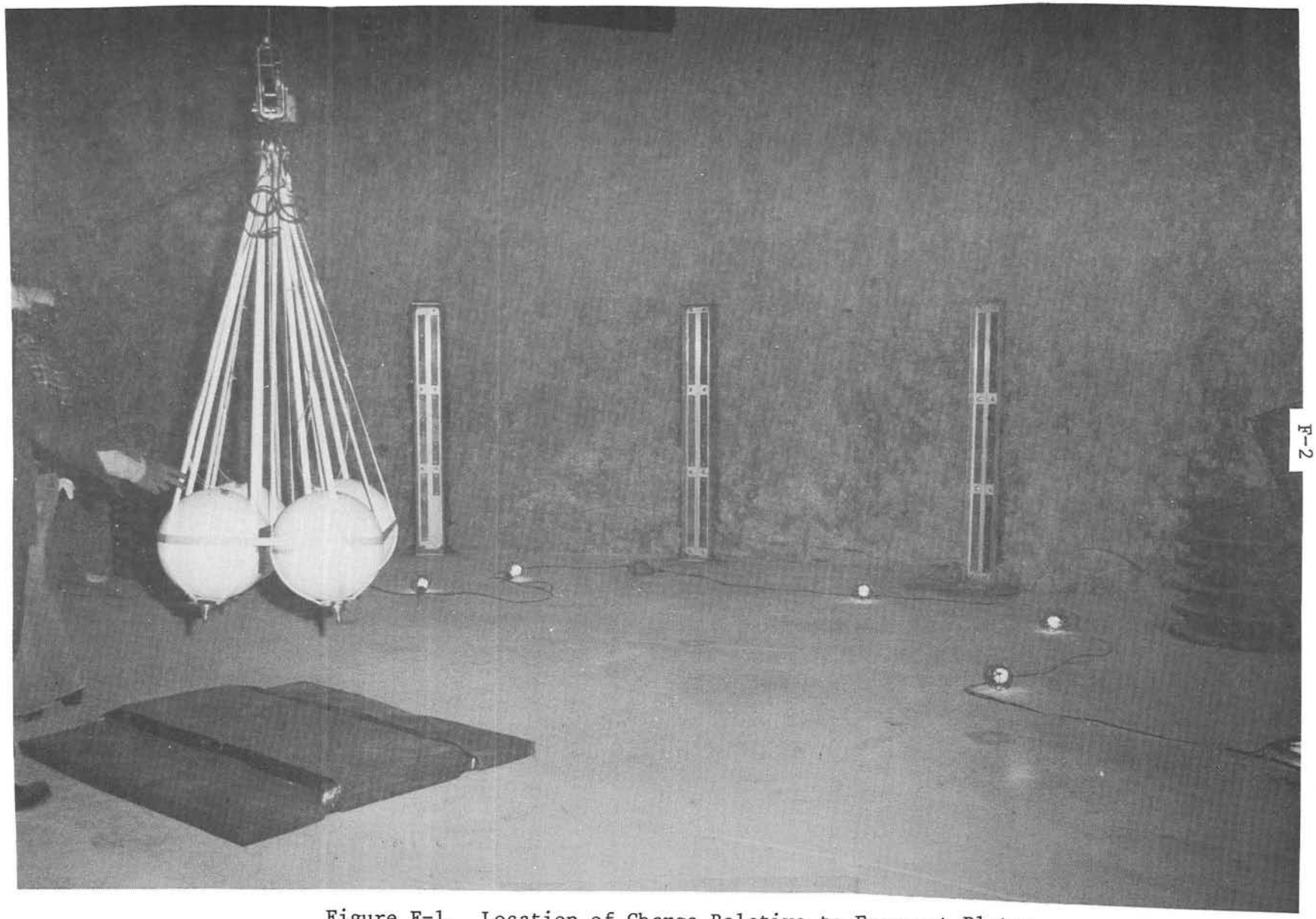

Figure F-1. Location of Charge Relative to Fragment Plates

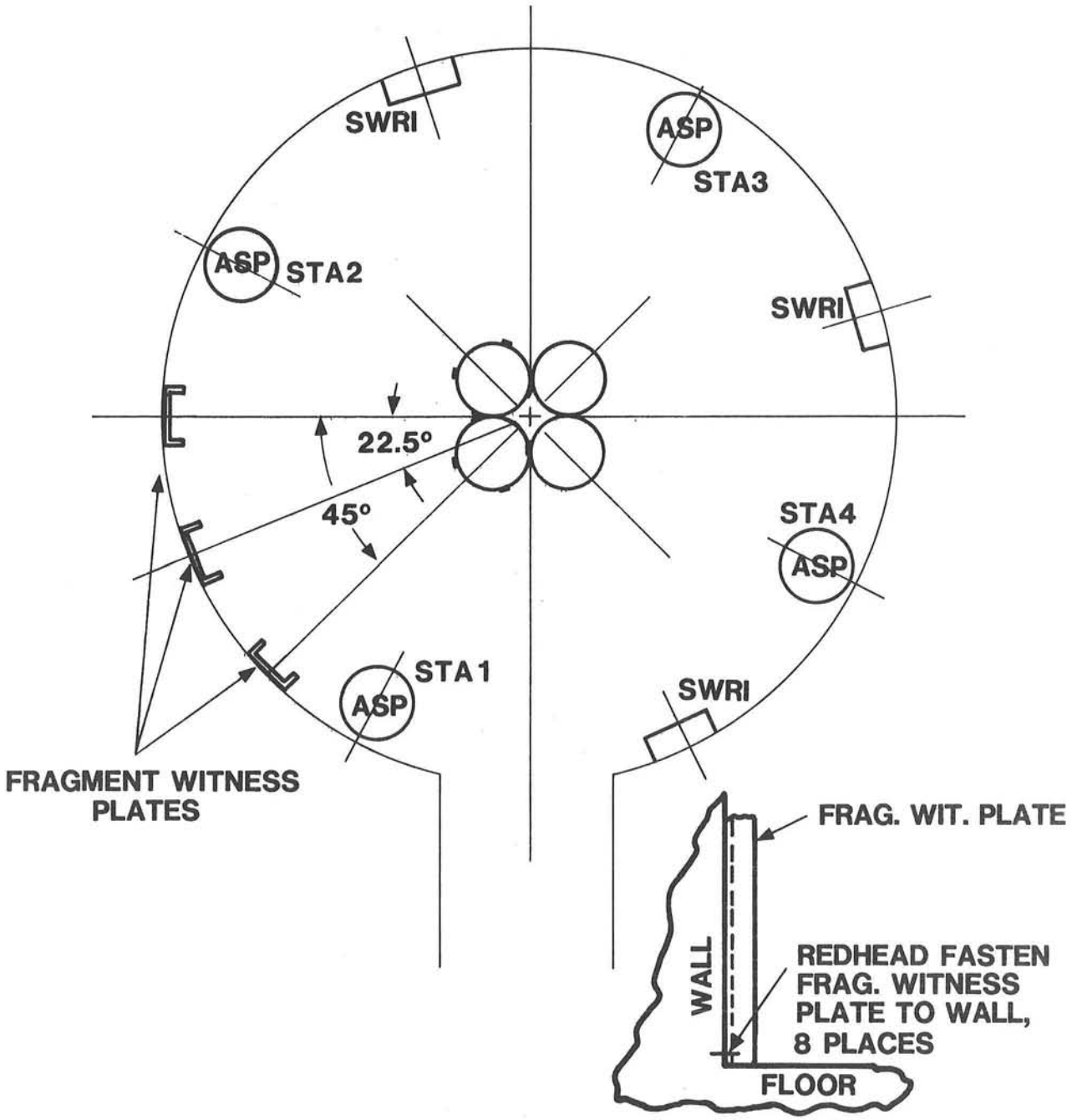

Figure F-2. Plan View of Fragment Detector Installation

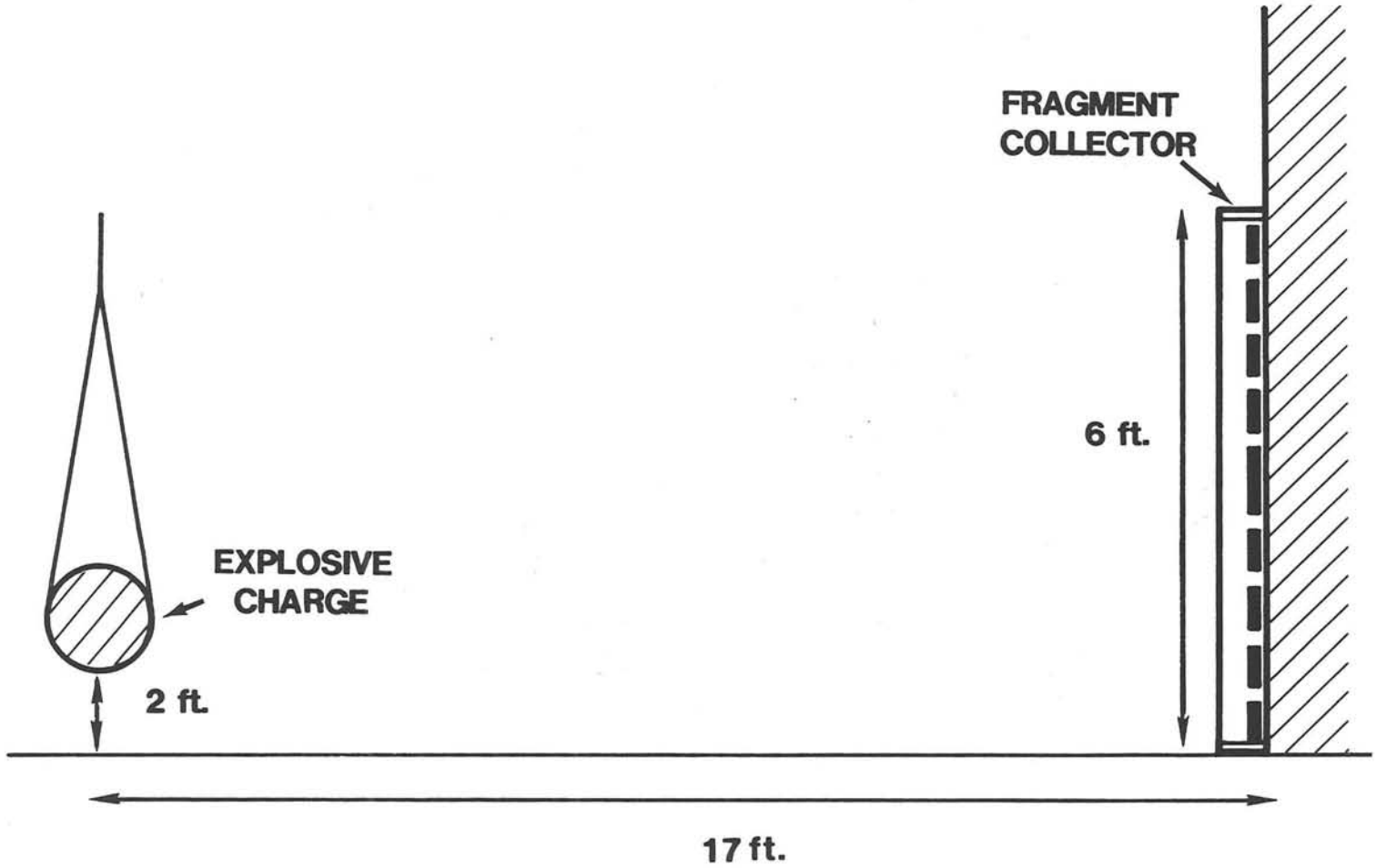

Figure F-3. Fragment Plate Location--Angular Layout

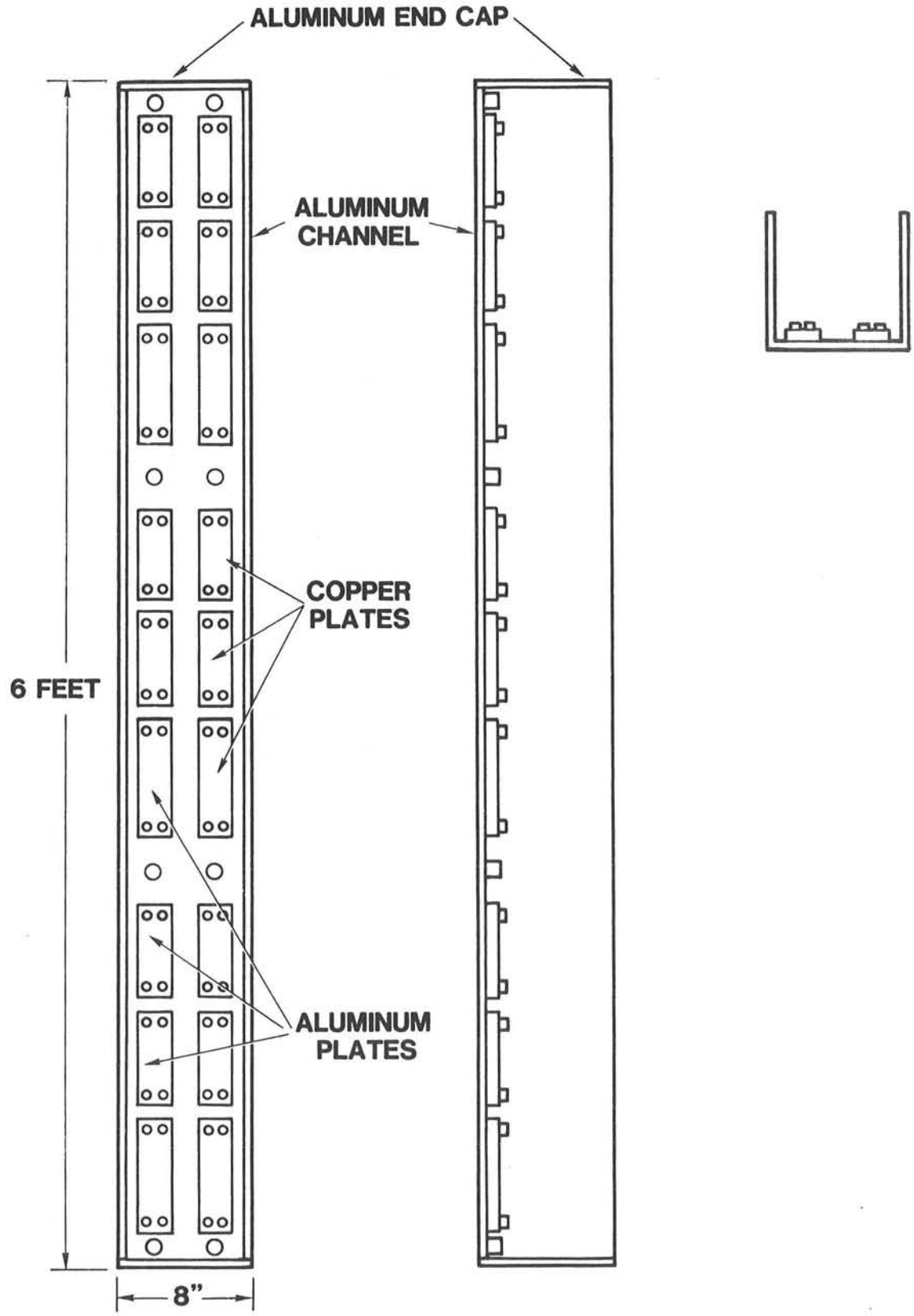

Figure F-4. Fragment Detector Construction

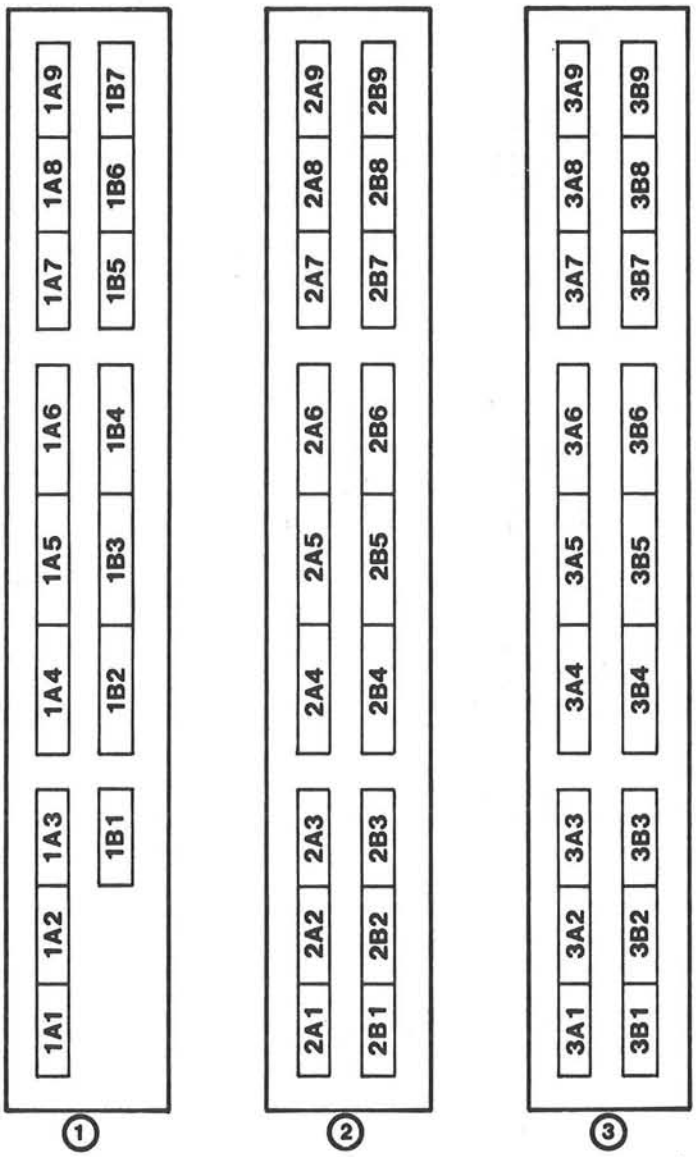

CLOCKWISE FROM PANEL NEAREST ENTRANCE

ALL "A" PLATES EXCEPT FOR 1A8 AND 1A9 ARE ALUMINUM
ALL "B" PLATES PLUS 1A8 AND 1A9 ARE COPPER

Figure F-5. Fragment Plate Numbering Schemes

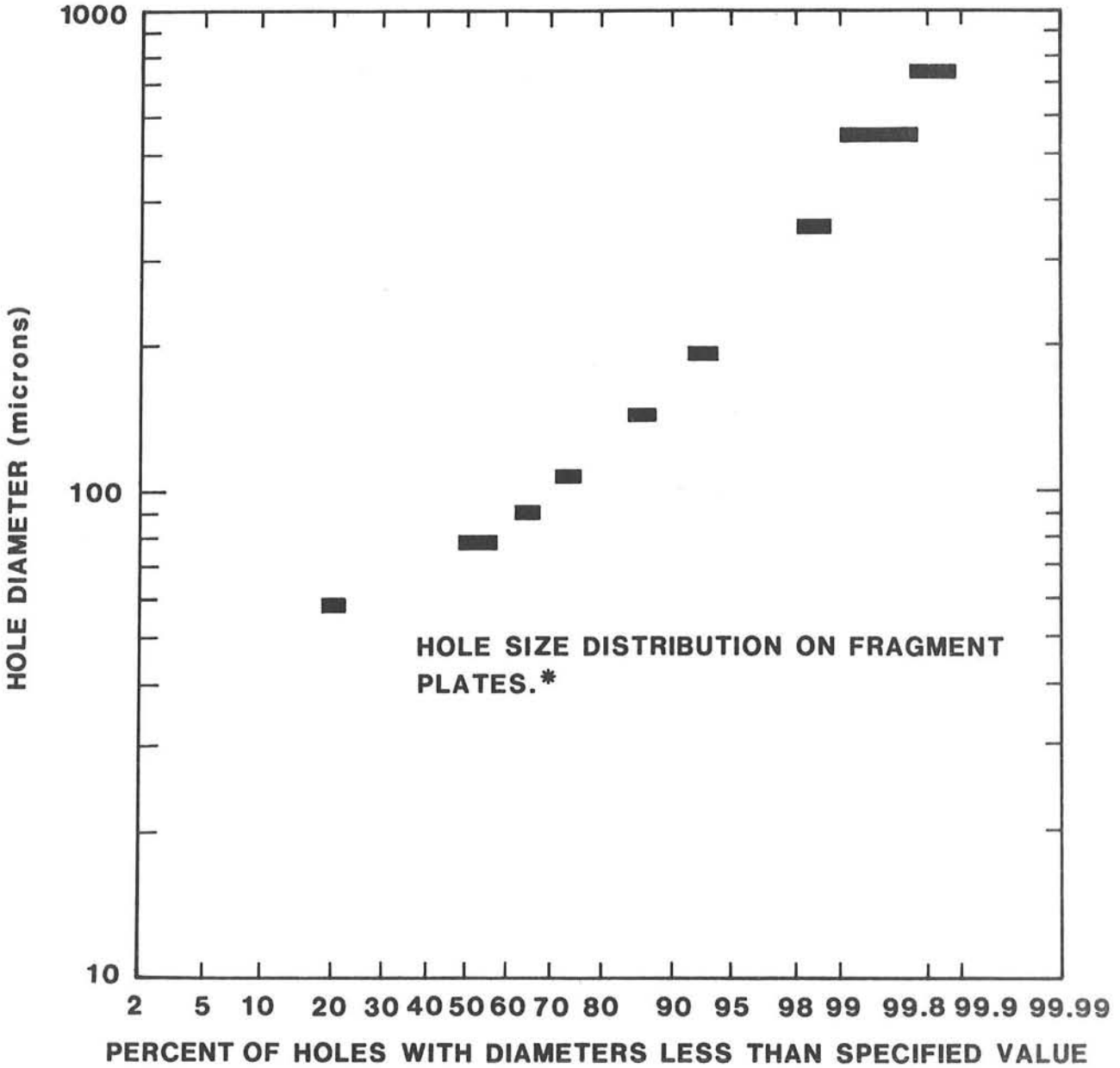

*EACH RECTANGLE REPRESENTS THE ENVELOPE OF POINTS WHEN SUBDIVIDED BY HORIZONTAL LOCATION, VERTICAL LOCATION, AND PLATE MATERIAL

Figure F-6. Crater Distribution on Fragment Plates

Appendix G
Full-Scale Test Blast Valve Experiment

Introduction

To verify the ability of commercially available, fast-acting ventilation closure systems to protect the external environment from aerosol releases following a blast within a facility, two of the most promising devices were chosen for full-scale testing. Both of the devices chosen are blast-actuated poppet-style ventilation valves as shown in Figure G-1.

The objectives of the test were to determine the amount of the blast wave that bypasses the valves during closure, and to determine if any radioactive material bypasses the valves by measuring:

- The side-on and face-on pressure-time histories of the blast wave upstream of the valves;
- The pressure-time history within the test fixture (simulating the downstream ductwork); and
- The closure time of the valves.

The interiors of the fixtures were also monitored for the presence of radioactive contamination following the test.

Physical Layout

Figure G-2 is a plan view of the test facility at NTS which shows the area chosen for the ventilation valve testing. This area is similar to the actual location of the ventilation openings into a Gravel Gertie assembly facility. In addition, the expected blast-wave characteristics at this point are similar to those expected in the Test Device Assembly Building (TDAB), an assembly facility currently being considered for construction at the Los Alamos National Laboratory.

Figure G-3 is a section view and plan view of the valve test area. Each of the two ventilation valves was mounted in the face of a separate gas-tight box that is mounted on the concrete floor. To provide protection, all instrument cables were run in conduit, most of which was embedded in the concrete floor. Figure G-4 shows the installation.

Definition of Equipment and Instrumentation

The two valves for testing were chosen on the basis of a competitive bid between US manufacturers of the blast-actuated poppet-style ventilation valves. The two valves are the following.

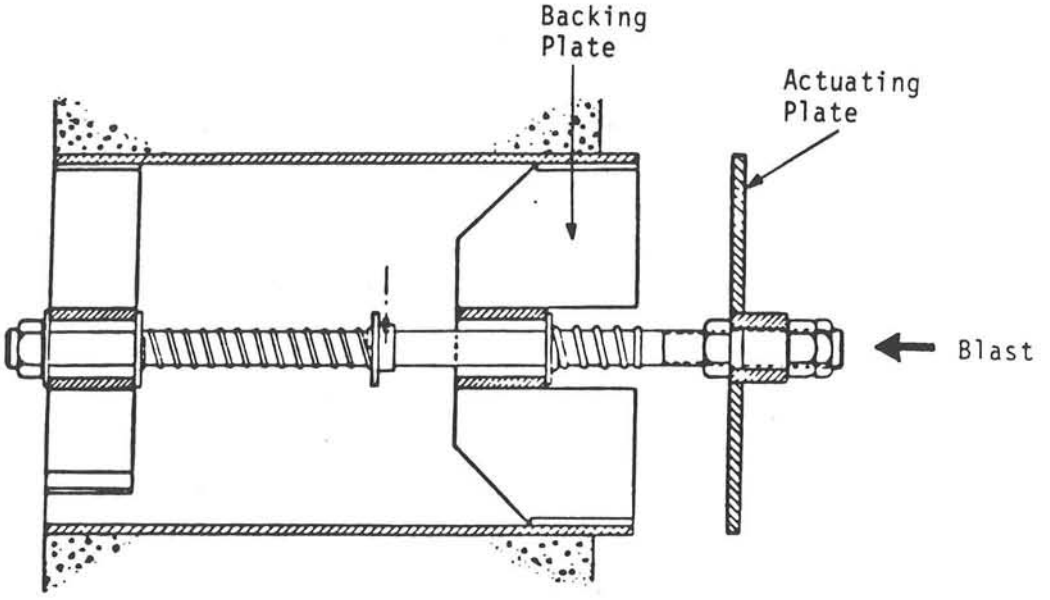

Figure G-1. Typical Blast-Actuated Poppet-Style Ventilation Valve

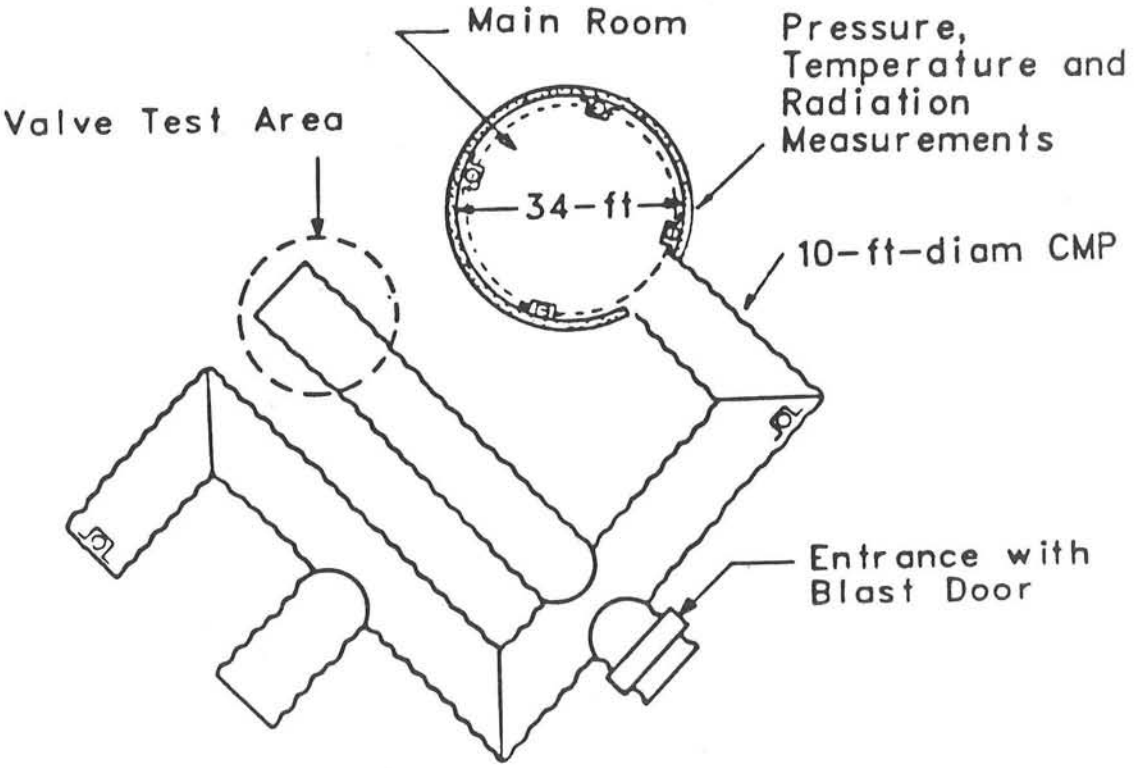

Figure G-2. Plan View of Gravel Gertie Test Facility

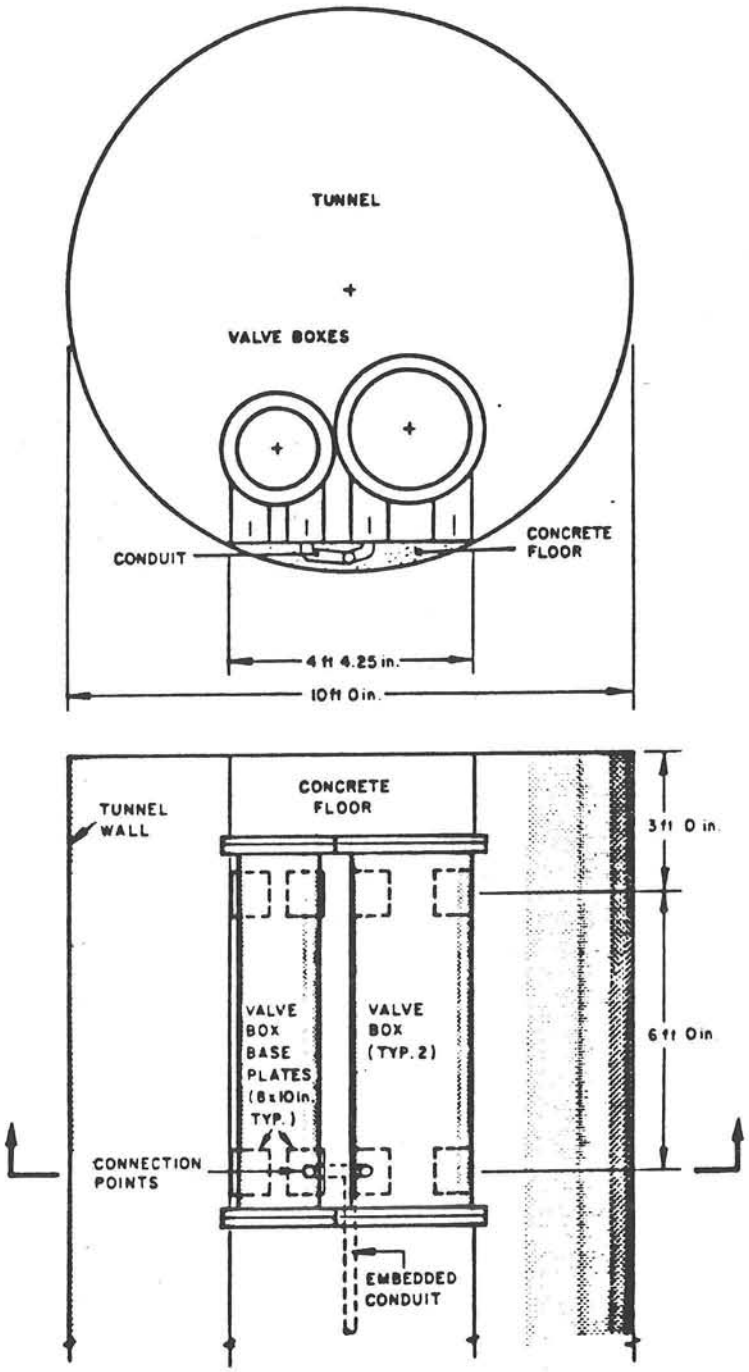

Figure G-3. Section and Plan View of Valve Test Area

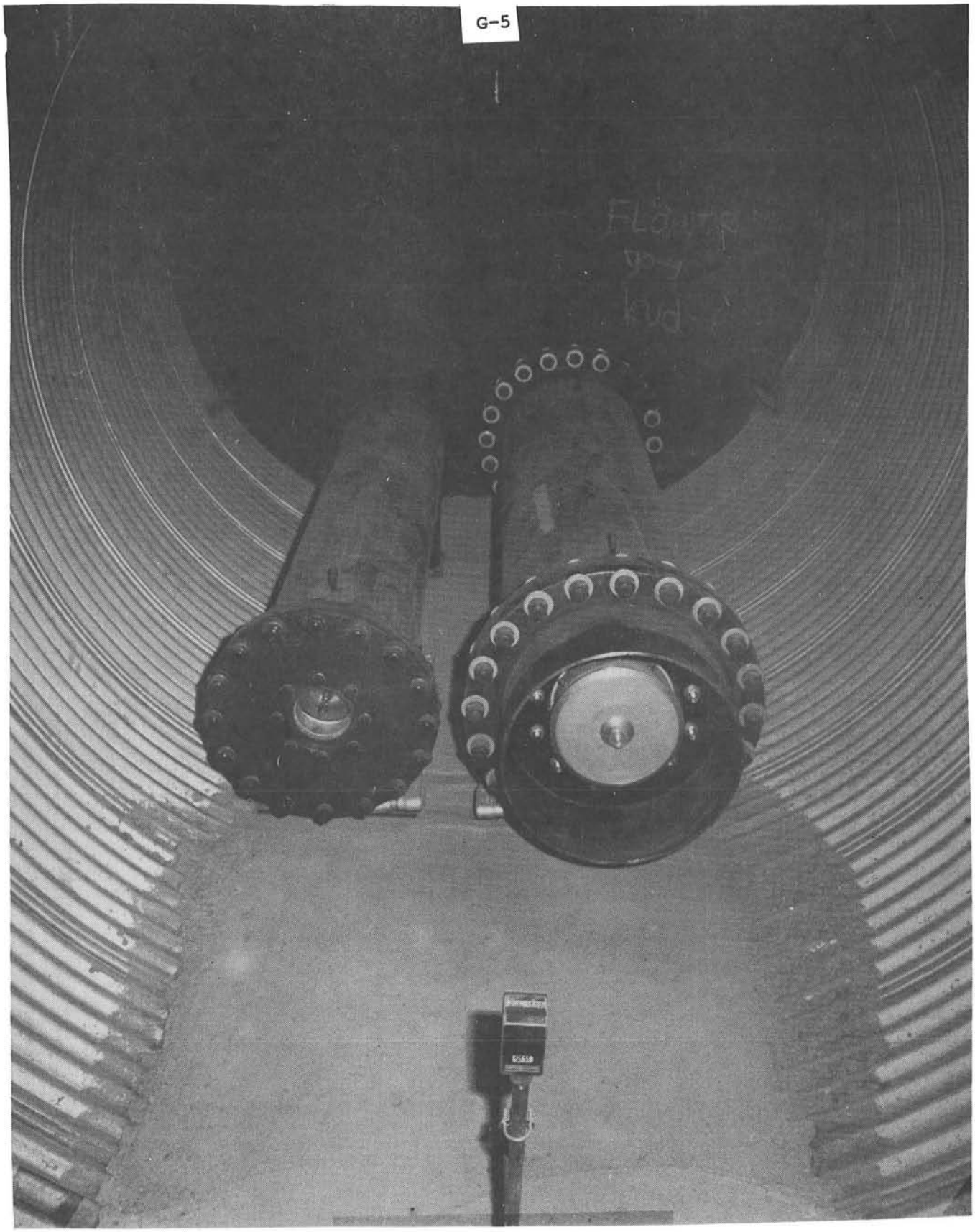

Figure G-4. LANL Valve Installation

- Temet USA model PV-6-150
- David Baclini, Inc., 12-in. ventilation valve

Temet, USA Model PV-6-150

The Temet, USA valve consists of a massive backing plate with a light-weight actuating plate. The valve is designed to rapidly close on positive pressures and then reopen on zero or negative pressures. This action provides protection to ventilation equipment; and, because of the very short closure time, it allows operation of the equipment without interruption. This feature will be useful in facilities that employ HEPA or other filter systems on the normal ventilation exhaust, because no action would be required by the operators to initiate cleanup following an accident. The HVAC equipment should be located outside of the blast-containment area.

David Baclini, Inc. 12-in. Valve

The David Baclini, Inc. valve employs a spider backing plate with a heavy actuating plate. The valve is designed to rapidly close and latch on a positive pressure pulse. The valve is sealed by an elastomer ring in the actuator plate. This type of valve would be used in a facility where complete closure of the ventilation system is desired for some period of time following the accident. This valve must be manually unlatched or bypassed to re-establish ventilation flow.

Pressure Sensors

Figure G-5 shows the location of the instrumentation in the valve test area. The four pressure sensors are Kulite Model XT 190-100A with the following ranges.

Side-on pressure: 0-500 psia
Face-on pressure: 0-500 psia
Fixture internal pressure (2 each): 0-25 psia

Valve Closure Switches

One Los Alamos stock microswitch was mounted in each valve to provide a step change in output voltage upon complete valve closure.

Data Acquisition

The valve test instrumentation was connected to the data acquisition equipment that Sandia National Laboratories provided to gather data for the full facility test.

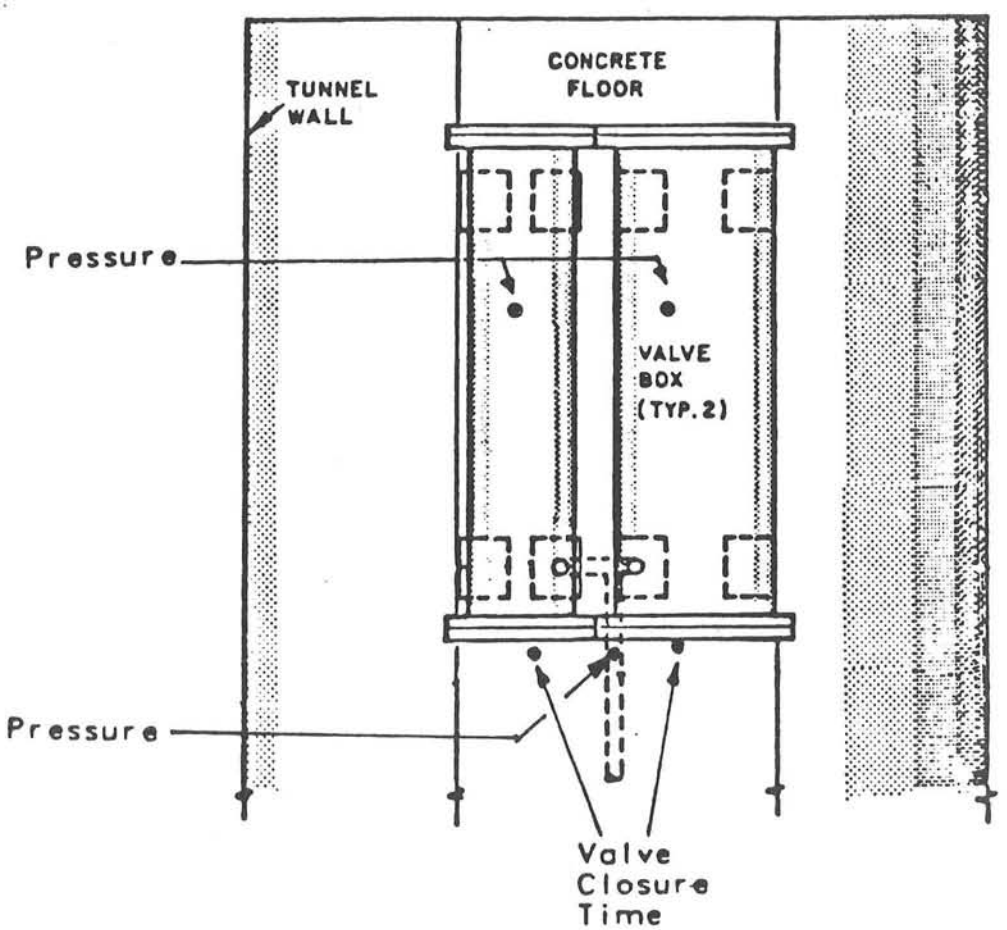

Figure G-5. Valve Test Area Instrumentation Locations

Test Results

Pressure-Time Histories

The blast wave that reached the valves had a measured peak over pressure of approximately 75 psig on one gage and 100 psig on the second. Peaks from both pressure sensors were reached 37 ms after the arrival of the blast wave. The time-history of pressure at the test location is shown on Figures G-6 and G-7.

The internal pressure of the valve fixture for the Temet, USA valve (nonlatching) reached a peak of 5.8 psig during the test. The internal pressure of the valve fixture with the David Baclini, Inc. valve (latching) reached a peak of 14.5 psig.

Closure-Time

The measured initial closure time of the Temet, USA valve was 5.5 $\pm$ 1.00 ms. With each successive surge in tunnel pressure (some as low as 5 psig), the valve reclosed and stayed closed until the tunnel pressure returned to zero or became negative.

The position switch on the David Baclini, Inc. valve was damaged during the test and no significant data could be obtained. However, based on the measured closure time and pressure rise in the Temet valve fixture and the rise time of the blast wave, an approximate ($\pm$50%) closure time can be calculated. The calculated closure time for this valve is 12 ms.

Visual Inspection

Both valves were inspected following the test and were found to be in excellent working condition with no evidence of any damage.

Results and Conclusions

The pressure rise within the fixtures was not sufficient to damage HVAC equipment or heavy walled ductwork. In addition, both valves closed well in advance of the arrival of the blast-wave pressure peak. The valve closure was, therefore, also well in advance of the arrival of the actual gas containing any particulate matter from the blast area.

The release expected into the HVAC equipment from the Temet, USA (nonlatching) valve would be on the order of 1×10^{-5} cm^3/s during periods of positive pressure within the facility. Continued operation of the HVAC equipment and filters during and after the accident would provide a means for rapid depressurization and cleanup of the facility atmosphere, which may significantly reduce the release from the facility through other openings.

The resulting release of contaminated gas into the HVAC ducting and equipment would be approximately 1×10^{-5} cm^3/s for the David Baclini, Inc. (latching) valve until the pressure decays to less than 10 psig. This number corresponds to the design leak rate of the valve in the closed position.

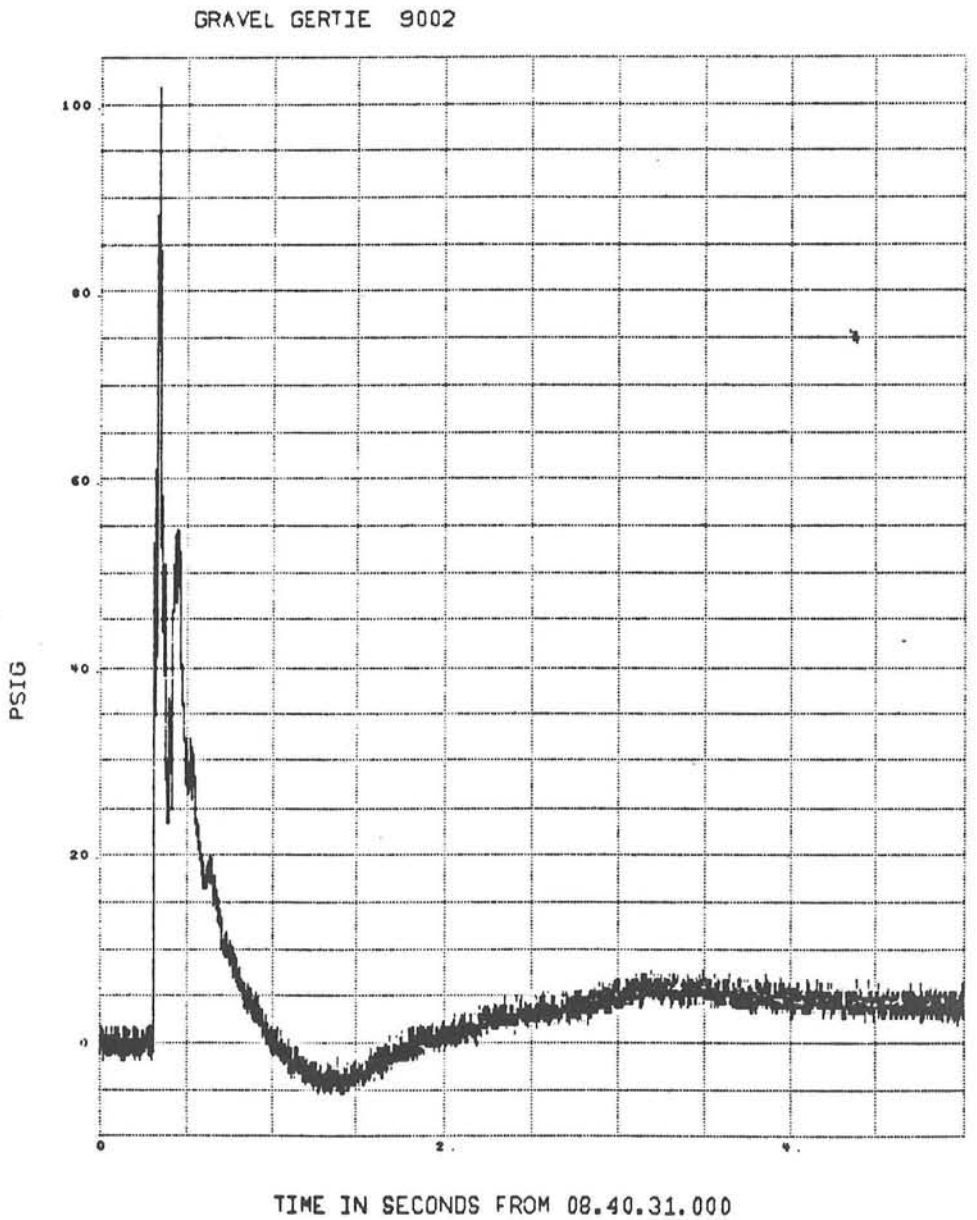

Figure G-6. Station 9 External Pressure to 5 Seconds for Gage Facing Station 10

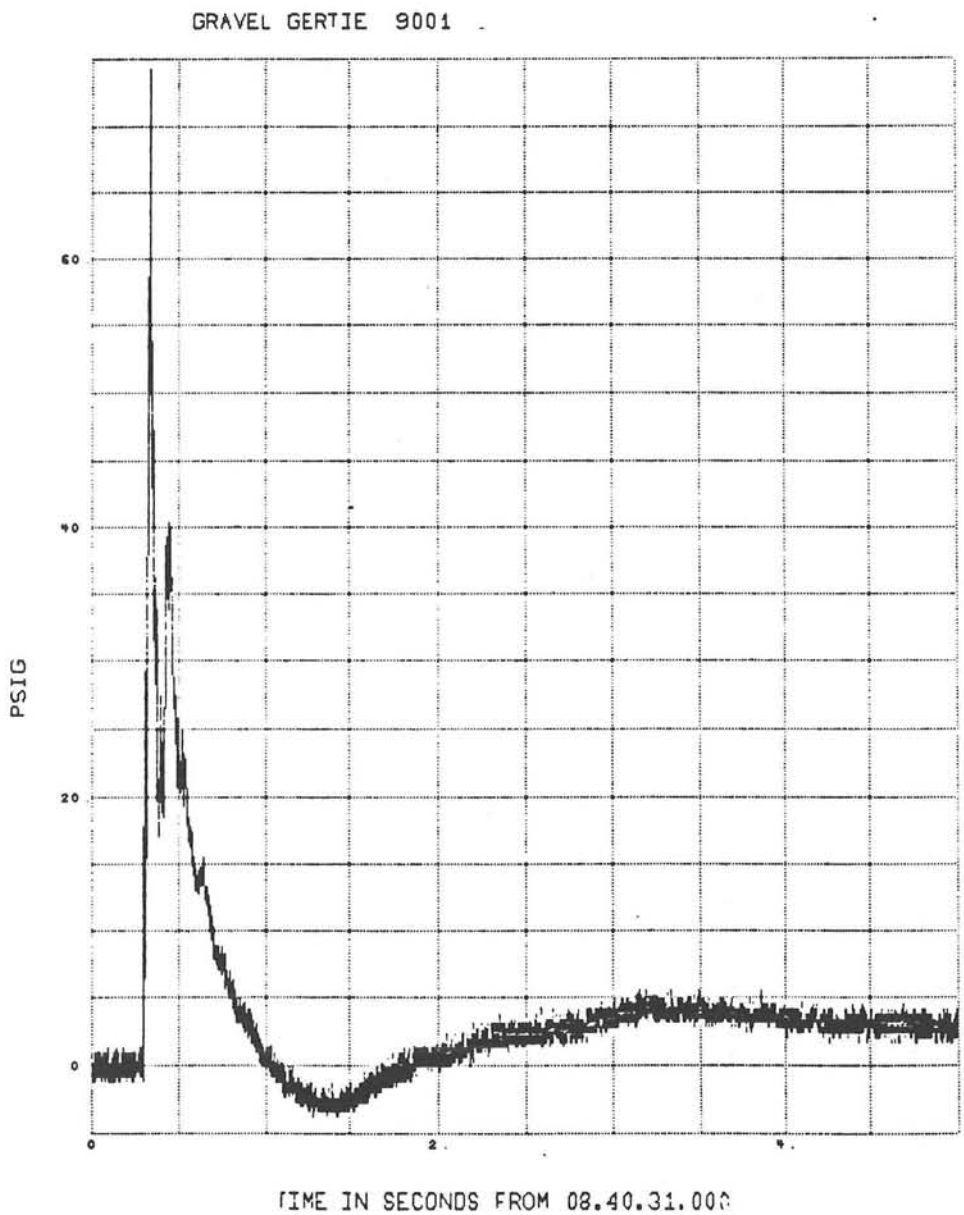

Figure G-7. Station 9 External Pressure to 5 Seconds For Gage Facing Wall

Appendix H
Full-Scale Test Meteorological Monitoring System Details and Data

Meteorological data before, during, and after t = 0 (0840 PST, 20 November 1982) was obtained from four on site sources: a fixed meteorological tower, a tethersonde, pilot balloon (PIBAL) flights, and portable equipment. Synoptic meteorology support was obtained through the National Weather Services support group at DOE/NVO for identification of weather trends in determining possible shot periods.

Fixed Meteorological Tower

A 30-m meteorological tower was installed approximately 100 m south of the center of the round room in July 1982. Continuous measurements of wind speed and wind direction were made at levels of 9 and 23 m and temperature measurements were made at levels of 3 and 28 m. All of these measurements were monitored in the control trailer as well as being telemetered to NTS CP-1 every 15 minutes. Between July and November, tower data was recorded and analyzed to characterize favorable shot conditions at the site.

Speed, direction, and temperature data obtained between 0700 PST and 1000 PST on November 20 are summarized in Table H-1.

Tethersonde

An AIR, Incorporated tethersonde was set up approximately 70 m southeast of the center of the round room near the control trailer. In the time 3 hours before test time and 2 hours after, soundings were taken as high as 1000 m (3300 ft) and were routinely taken between 0 and 200 m. The tethersonde was "parked" at a height of approximately 20 m at 0700 PST on November 20 and remained there until 0920 PST (40 minutes post shot) when another sounding was taken as high as 1000 m (3300 ft). The data obtained from the tethersonde system included wind speed, wind direction, temperature, and relative humidity. These data are summarized in Table H-2.

PIBAL System

Four pilot balloons (PIBAL) were released between 0400 and 0700 PST on November 20 from a location 100 m north northeast of the Gravel Gertie structure. Tracking these balloons visually using a theodolite provided a measure of wind speed and wind direction as a function of elevation above grade. The data obtained from the final PIBAL observation is contained in Table H-3.

TABLE H-1

Metorological Tower Data

Time (PST)[a]	Wind Data (speed(m/s)/direction[b](°)) h = 9m	h = 23 m
0700	≤1.0/080	2.5/090
0730	≤1.0/315	1.5/171
0800	0.0/015	0.5/000
0830	≤1.0/120	0.5/135
0835	≤1.0/110	≤1.0/085
0840	≤1.0/075	2.0/085
0845	≤1.0/090	2.5/095
0850	≤1.0/080	2.0/085
0855	≤1.0/085	3.0/085
0900	≤1.0/050	2.0/115
0905	≤1.0/070	2.5/050
0910	≤1.0/045	2.0/035
0915	2.0/050	2.0/060
0920	≤1.0/060	2.5/100
0925	≤1.0/090	2.5/090
0930	≤1.0/085	2.5/070
0945	≤1.0/110	1.5/100
1000	≤3.0/090	3.0/040

[a] November 20, 1983

[b] 0° is North, 90° is East

TABLE H-2

Tethersonde Data

Time[a] (PST)	Height Above Grade (m)	Wind Speed (m/s)	Wind Direction[b] (°)	Temperature (°C)	Relative Humidity (%)	
0636	0	0.4	140	2.5	80	
0638	45	0.8	333	3.7	67	
0640	142	1.0	263	5.1	58	Last
0641	205	0.6	013	5.4	61	Preshot
0645	134	0.7	291	5.6	61	Profile
0649	0	1.1	186	2.4	82	
0700	18	1.2	084	2.2	78	
0730	18	0.0	198	2.9	79	
0800	18	0.8	355	2.9	76	
0830	18	0.1	080	4.8	66	
0835	18	0.6	140	5.3	66	
0840	18	0.4	082	5.6	63	
0845	18	0.4	071	6.5	61	
0850	18	1.1	076	6.7	58	
0855	18	0.2	067	6.7	57	
0900	18	0.9	066	6.8	54	
0905	18	1.1	082	7.2	52	
0910	18	2.0	052	6.9	53	
0920	0	0.0	017	8.8	51	
0925	213	1.8	181	6.3	53	
0930	541	1.6	004	3.7	60	First
0935	829	1.4	015	2.2	60	Postshot
0938	971	2.1	009	1.3	60	Profile
0945	927	3.4	013	1.5	58	
0950	696	1.7	341	2.8	57	
0955	411	0.6	334	4.5	53	
1000	105	1.8	111	7.6	48	
1003	0	0.1	177	9.2	42	

[a] November 20, 1983

[b] 0° is North, 90° is East

TABLE H-3
PIBAL Data

Time[a] (PST)	Height Above Grade (ft)	Wind Speed (m/s)	Wind Direction[b] (°)
0400	3500	4	248
	4000	4	248
	4500	4	250
	5000	5	252
	5500	5	255
	6000	4	260
	6500	2	267
	7000	0	000
	7500	2	092
	8000	2	094
	8500	2	095
	9000	1	096
	9500	0	000
	10000	1	242
0500	3500	2	024
	4000	2	024
	4500	2	000
	5000	3	324
	5500	4	308
	6000	5	297
	6500	6	293
	7000	5	294
	7500	3	291
	8000	1	252
	8500	2	195
	9000	3	199
	9500	4	211
	10000	5	231
0600	3500	2	072
	4000	2	072
	4500	3	070
	5000	3	066
	5500	3	060
	6000	1	031
	6500	1	311
	7000	2	309
	7500	3	305
	8000	2	285
	8500	1	222

TABLE H-3
PIBAL Data
(continued)

Time[a] (PST)	Height Above Grade (ft)	Wind Speed (m/s)	Wind Direction[b] (°)
	9000	3	186
	9500	4	181
	10000	4	184
0700	3500	3	061
	4000	3	061
	4500	2	057
	5000	1	030
	5500	1	319
	6000	2	321
	6500	2	326
	7000	2	347
	7500	1	343
	8000	2	268
	8500	3	256
	9000	4	261
	9500	4	261
	10000	4	259

[a] November 20, 1983

[b] 0° is North, 90° is East

Portable Equipment

An aneroid barometer was installed in the test control trailer to provide barometric pressure data. The barometric pressure was observed to be 904.2 mbar at 0653, 905.5 mbar at 0753, and 906.2 mbar at 0920.

Appendix I
Photographic System

There are six sources of photographic information on the Gravel Gertie Test series: SNL still photos of the confinment and subscale tests, NTS still photos of the full-scale test, SNL movies of the subscale tests, SNL movies of the full-scale test, SNL video tape of the confinement and subscale tests, and SNL video tape of the full-scale test.

Still Photography

The available still photographs are listed by negative number and subject in Tables I-1 to I-3. Although many Polaroid photographs were also taken, they have not been logged.

Motion Picture Photographs: Full-Scale Test

High framing rate cameras (400 fps) with 25.4 mm lenses were placed at three orthogonal locations to determine the behavior of the gravel bed and earth fill and the early time aerosol cloud formation of the full-scale test (Figure I-1). The area immediately above the assembly cell was of primary importance, but the staging area and access door were also covered to document other potential vent pathways. These cameras were turned on 3 seconds before detonation by a sequencer in the A&F trailer, and turned themselves off as they ran out of film.

Standard framing rate cameras (24 fps) with 10 mm lenses were located at the same positions to backup the 400 fps cameras and to define the early aerosol cloud envelope. These cameras were turned on at T-35 sec by a sequencer in the A&F trailer, and turned themselves off when they ran out of film.

Slow framing rate cameras (6 fps) with 5.7 mm lenses were located at the same positions to backup the 24 fps cameras and to define the late aerosol cloud envelope. These cameras were turned on at T-35 sec by a sequencer in the A&F trailer, and turned themselves off when they ran out of film. All nine movie cameras were 16 mm format. T=0 was indicated by flash bulbs located at the interface between the gravel and the earth fill. Timing marks were also inserted at the edge of the film.

Table I-4 lists all available documentary films for the GGCVP.

Video Tape

Various aspects of the GGCVP were documented on video tape. A video camera was used to record the full-scale test construction details, the test, and the posttest activities. During the test, one video camera was located at about 206° and 136 m (447 ft) from the operating bay centerline. The other was located slightly east of south and at about 1.28 km (0.8 mile) from Gravel Gertie. All available video tapes are specified in Table I-5.

TABLE I-1

Confinment Chamber Test Documentary Photographs

Negative Number	Brief Description
SNLA C82 103252	Feedthrough protector plate
SNLA C82 103253	Feedthrough protector plate
SNLA C82 103264	8/27/83 - posttest
SNLA C82 103265	8/27/83 - pretest
SNLA C82 103266	Spinner installation
SNLA C82 103267	Protector plate - posttest
SNLA C82 103268	Spinner - posttest
SNLA C82 103269	Bottom port - posttest
SNLA C82 103270	Top port - posttest
SNLA C82 103271	Spinner plate prior to removal
SNLA C82 103287	8# - post-test
SNLA C82 103288	8# - post-test
A	External view of chamber
B	External view of chamber
C	8# - Spinner prior to removal
D	Charge configuration

TABLE I-2
Scale Model Test Documentary Photographs

Negative Number	Brief Description
SNLA C82 103236	SS-2 Structure pretest
SNLA C82 103237	SS-2 Structure posttest
SNLA C82 103238	SS-2 Structure pretest
SNLA C82 103239	SS-2 Wire fabric installation
SNLA C82 103240	SS-2 Structure posttest
SNLA C82 103246	SS-3 Wire fabric installation
SNLA C82 103247	SS-3 Overhead view - posttest
SNLA C82 103248	SS-3 Side view - posttest
SNLA C82 103249	SS-3 Fabric installation
SNLA C82 103250	SS-3 Top view - posttest
SNLA C82 103251	SS-3 Structure - pretest
SNLA C82 103254	SS-3 HE charge configuration
SNLA C82 103255	SS-3 Fabric installation
SNLA C82 103256	SS-5 Dropped ceiling fragments
SNLA C82 103257	SS-5 Membrane fragments
SNLA C82 103258	SS-5 Wire fabric - posttest
SNLA C82 103259	SS-5 Top view - posttest
SNLA C82 103260	SS-5 Wire fragments
SNLA C82 103261	SS-5 Wire fabric - posttest
SNLA C82 103262	SS-5 Membrane fragments
SNLA C82 103263	SS-5 Metal fragments
SNLA C82 103274	SS-4 HE installation
SNLA C82 103275	SS-4 Side view of structure - posttest
SNLA C82 103276	SS-4 Side view of structure - pretest
SNLA C82 103277	SS-4 Wire fabric installation
SNLA C82 103278	SS-4 GGASP installation
SNLA C82 103279	SS-4 Side view of structure - posttest
SNLA C82 103280	SS-4 Membrane installation
SNLA C82 103281	SS-4 Gravel bed - posttest
SNLA C82 103289	SS-5 Showing catenary
SNLA C82 103290	SS-5 Wire fabric being lowered
SNLA C82 103291	SS-5 Dropped ceiling
SNLA C82 103292	SS-5 Wire fabric showing cable cutters
SNLA C82 103293	SS-5 Dropped ceiling sample posttest

TABLE I-2 (Continued)
Scale Model Test Documentary Photographs

Negative Number	Brief Description
SNLA C82 103294	SS-5 Roof collapse
SNLA C82 103295	SS-5 Wire cabling posttest
SNLA C82 103296	SS-5 Charge pretest
SNLA C82 103297	SS-5 Wire cabling posttest
SNLA C82 103298	SS-5 Collapsed gravel
SNLA C82 103299	SS-5 Cable cutters posttest
SNLA C82 103300	SS-5 Bagged tracer hanging pretest
SNLA C82 103301	SS-5 Pretest
SNLA C82 103302	SS-5 Posttest
SNLA C82 103303	SS-4 Wire fabric installation
SNLA C82 103304	SS-4 Wire fabric installation
SNLA C82 103305	GGASP Posttest
SNLA C82 103306	Closeup of GGASP Top-Posttest
SNLA C82 103307	GGASP Posttest
SNLA C82 103308	GGASP Being raised out of SS facility
SNLA C82 103309	GGASP Posttest
SNLA C82 103310	GGASP Cover and charge being installed in SS facility
SNLA C82 103311	GGASP Being installed in SS facility
SNLA C82 103312	GGASP Being lowered into SS facility
SNLA C82 103313	GGASP Being raised out of SS facility

TABLE I-3
Full-Scale Test Documentary Photographs

Negative Number	Brief Description
NTS-A82-208	Gravel Gertie Site Pre-Excavation-1st visit
NTS-A82-286	Original structure prior to excavation from N
NTS-A82-287	Original structure prior to excavation from S
NTS-A82-288	Original structure prior to excavation from W
NTS-A82-289	Original structure prior to excavation from E
NTS-A82-290	Original crater fallback and misc. equipment
NTS-A82-291	Original crater fallback and misc. equipment
NTS-A82-292	Beginning of excavation
NTS-A82-293	PR
NTS-A82-294	PR
NTS-A82-295	During excavation
NTS-A82-296	PR
NTS-A82-297	During excavation
NTS-A82-298	During excavation
NTS-A82-299	Staging area during excavation
NTS-A82-300	Excavated round room from N
NTS-A82-301	Site from south-post-excavation
NTS-A82-302	Completely Excavated Structure from S
NTS-A82-303	Completely Excavated Structure from W
NTS-A82-304	Excavated spider ring assembly
NTS-A82-305	Excavated structure from E with large pipe
NTS-A82-431	View of original staging area construction
NTS-A82-432	View of original staging area showing shrapnel holes
NTS-A82-433	Crater in center of round room
NTS-A82-434	Exterior wall of round room showing cable connections
NTS-A82-435	Exterior wall of round room showing large horizontal crack
NTS-A82-436	Exterior wall of round room showing large vertical crack
NTS-A82-437	Interior view of entrance to round room

Table I-3 (continued)

Negative Number	Brief Description
NTS-A82-438	Exterior wall of round room showing vertical crack
NTS-A82-439	Interior wall of round room showing horizontal crack
NTS-A82-440	Interior wall of round room showing horizontal crack
NTS-A82-441	PR - J. Shinkle, B. G. Edwards, J. Burling inside round room
NTS-A82-442	Old entrance to round room showing culvert damage
NTS-A82-443	Crater in center of round room
NTS-A82-444	Totally excavated round room
NTS-A82-445	Cracks in external joint between culvert and round room
NTS-A82-446	External damage to entrance to round room
NTS-A82-447	Internal damage to entrance to round room
NTS-A82-448	Internal damage to entrance to round room
NTS-A82-449	Internal damage to entrance to round room
NTS-A82-450	Exterior of culvert leading out of round room
NTS-A82-451	Closeup of damage to exterior of round room door
NTS-A82-452	Damage to culvert near round room entrance
NTS-A82-453	PR - personnel on site inspection
NTS-A82-1257	Round room entrance showing rebar from S
NTS-A82-1258	Round room entrance showing rebar from SSW
NTS-A82-1259	Round room entrance showing rebar from SW
NTS-A82-1260	Round room entrance showing rebar from WSW
NTS-A82-1261	Round room from W
NTS-A82-1262	Round room from WNW
NTS-A82-1263	Round room from NW
NTS-A82-1264	Round room from NNW
NTS-A82-1265	Round room from N
NTS-A82-1266	Round room from NNE
NTS-A82-1267	Round room from NE

Table I-3 (continued)

Negative Number	Brief Description
NTS-A82-1268	Round room from NE
NTS-A82-1269	Round room from E
NTS-A82-1270	Round room from ESE
NTS-A82-1271	Round room from SW
NTS-A82-1272	Round room from SSE
NTS-A82-1273	Site and met tower from S
NTS-A82-1274	Site and met tower from SSW
NTS-A82-1275	Site and met tower from SW
NTS-A82-1276	Site and met tower from WSW
NTS-A82-1277	Site and met tower from W
NTS-A82-1278	Site and met tower from WNW
NTS-A82-1279	Site and met tower from NW
NTS-A82-1280	Site and met tower from NNW
NTS-A82-1281	Site and met tower from N
NTS-A82-1282	Site and met tower from NNE
NTS-A82-1283	Site and met tower from NE
NTS-A82-1284	Site and met tower from ENE
NTS-A82-1285	Site and met tower from E
NTS-A82-1286	Site and met tower from ESE
NTS-A82-1287	Site and met tower from SE
NTS-A82-1288	Site and met tower from SSE
NTS-A82-1289	Scaffolding inside round room
NTS-A82-1290	Cracks on round room floor
NTS-A82-1291	Scaffolding inside round room
NTS-A82-1292	Scaffolding inside round room
NTS-A82-1293	Scaffolding inside round room
NTS-A82-1294	Repair of crater in round room floor
NTS-A82-1295	Entrance to round room from inside showing repair zone
NTS-A82-1296	Entrance to round room from outside showing repair zone
NTS-A82-1297	Entrance to round room from outside (closeup)
NTS-A82-1298	Blast door in old culvert
NTS-A82-1299	Blast door
NTS-A82-1300	Meteorological tower
NTS-A82-1301	Cleanout of cable tubes
NTS-A82-1302	Cleanout of cable tubes
NTS-A82-1303	Culvert prior to installation
NTS-A82-1304	Rebar repair at round room entrance
NTS-A82-1305	Culvert prior to installation
NTS-A82-1306	Repaired rebar at entrance
NTS-A82-1307	Repaired rebar at entrance
NTS-A82-1308	Repaired rebar at entrance

Table I-3 (continued)

Negative Number	Brief Description
NTS-A82-1309	Round room and culvert from S
NTS-A82-1310	Round room from SW
NTS-A82-1553	Round room entrance from SW
NTS-A82-1554	New cable installed from outside
NTS-A82-1555	Round room from WSW
NTS-A82-1556	Old staging area being removed
NTS-A82-1557	Old staging area being removed
NTS-A82-1558	Installation of new round room entrance
NTS-A82-1559	Installation of new round room entrance
NTS-A82-1560	Main support cabling
NTS-A82-1561	Staging area joints
NTS-A82-1562	Round room entrance forms
NTS-A82-1563	Staging area joints
NTS-A82-1564	Round room entrance repair
NTS-A82-1565	Round room entrance repair
NTS-A82-1566	Round room entrance repair
NTS-A82-1567	Round room entrance repair
NTS-A82-1568	Round room entrance repair
NTS-A82-1569	Surface preparation for culvert
NTS-A82-1570	Surface preparation for culvert
NTS-A82-1571	Round room entrance repair
NTS-A82-1572	Round room entrance repair
NTS-A82-1573	Round room entrance repair
NTS-A82-1574	Surface preparation
NTS-A82-1575	Culvert installation
NTS-A82-1576	Culvert installation
NTS-A82-1577	Culvert joint preparation
NTS-A82-1578	Round room entrance repair
NTS-A82-1579	Round room entrance repair
NTS-A82-1580	Round room entrance repair
NTS-A82-1581	Round room entrance repair
NTS-A82-1582	Main support cables
NTS-A82-1583	Surface preparation & mounding
NTS-A82-1584	Culvert installation
NTS-A82-1585	Culvert installation
NTS-A82-1586	Culvert installation
NTS-A82-1587	Culvert installation
NTS-A82-1588	Culvert installation
NTS-A82-1589	Installation of N pole
NTS-A82-1590	Installation of N pole
NTS-A82-1591	Installation of N pole
NTS-A82-1592	Installation of end caps on culvert
NTS-A82-1593	Installation of N pole

Table I-3 (continued)

Negative Number	Brief Description
NTS-A82-1594	Installation of N pole
NTS-A82-1595	Installation of end caps on culvert
NTS-A82-1634	Inside of staging area drift
NTS-A82-1635	Inside of repaired round room entrance
NTS-A82-1636	Inside of staging area drift
NTS-A82-1637	Outside of culvert joint
NTS-A82-1638	Backfill around culvert
NTS-A82-1639	Backfill around perimeter
NTS-A82-1640	Backfill on slope
NTS-A82-1641	Backfill around culvert
NTS-A82-1642	Construction of sandbagged tunnel entrance
NTS-A82-1643	Construction of sandbagged tunnel entrance
NTS-A82-1644	Construction of sandbagged tunnel entrance
NTS-A82-1645	Construction of sandbagged tunnel entrance
NTS-A82-1646	Culvert joint
NTS-A82-1647	Culvert joint
NTS-A82-1648	Culvert before backfill
NTS-A82-1649	Installation of culvert end caps
NTS-A82-1650	Installation of west pole
NTS-A82-1651	Culvert joint
NTS-A82-1652	Installation of west pole
NTS-A82-1653	Tamping backfill
NTS-A82-1796	Spider ring from below
NTS-A82-1797	GGASP access port form
NTS-A82-1798	Conduit in round room
NTS-A82-1799	Conduit in round room
NTS-A82-1800	Conduit in round room
NTS-A82-1801	Conduit in round room
NTS-A82-1802	Conduit in round room
NTS-A82-1803	Conduit in round room
NTS-A82-1804	Conduit in round room
NTS-A82-1805	Conduit in staging area
NTS-A82-1806	Conduit in staging area
NTS-A82-1807	Conduit in staging area
NTS-A82-1808	Conduit in staging area
NTS-A82-1809	Backfill operations
NTS-A82-1810	Backfill operations
NTS-A82-1811	Backfill operations
NTS-A82-1812	Backfill operations
NTS-A82-1813	Backfill operations
NTS-A82-1814	Backfill operations

Table I-3 (continued)

Negative Number	Brief Description
NTS-A82-1915	Backfill operations
NTS-A82-1916	Backfill operations
NTS-A82-1917	Backfill operations
NTS-A82-1918	Backfill operations
NTS-A82-1919	Backfill operations
NTS-A82-1920	Backfill operations over tunnel entrance
NTS-A82-1921	Installation of 1st layer of wire mesh above cable
NTS-A82-1922	Installation of 1st layer of wire mesh above cable
NTS-A82-1923	Installation of 1st layer of wire mesh above cable
NTS-A82-1924	Installation of 1st layer of wire mesh above cable
NTS-A82-1925	Installation of 1st layer of wire mesh above cable
NTS-A82-1926	Installation of 1st layer of wire mesh above cable
NTS-A82-1927	Installation of 1st layer of wire mesh above cable
NTS-A82-1928	Installation of 1st layer of wire mesh above cable
NTS-A82-1929	Installation of 1st layer of wire mesh above cable
NTS-A82-1930	Installation of membrane above 1st mesh
NTS-A82-1931	Control trailers
NTS-A82-1932	Blast shields outside tunnel entrance
NTS-A82-1933	GGASP access port
NTS-A82-1934	Blast shield inside staging area
NTS-A82-1935	Staging area with poured floor
NTS-A82-1936	Staging area with poured floor
NTS-A82-1937	Blast shield in round room
NTS-A82-1938	Control trailers
NTS-A82-1939	Generators
NTS-A82-1940	External foundation form
NTS-A82-1941	Impermeable membrane installation
NTS-A82-1942	External foundation
NTS-A82-1943	Membrane prior to initial gravel fill
NTS-A82-1944	Protected cable runs to trailers

Table I-3 (continued)

Negative Number	Brief Description
NTS-A82-1945	Membrane 3/4 complete
NTS-A82-1946	Wire mesh being installed over first gravel layer
NTS-A82-1947	Overall structure during gravel installation
NTS-A82-1948	Protected cable runs from south
NTS-A82-2108	Preshot view of structure from ESE
NTS-A82-2109	Preshot view of structure from ESE
NTS-A82-2110	Preshot view of structure from ESE
NTS-A82-2111	Early time gravel bed expansion
NTS-A82-2112	During shot--cloud development
NTS-A82-2113	Preshot view of structure from ESE
NTS-A82-2114	Posttest view from NE camera site
NTS-A82-2115	Aerial view of structure from SE preshot
NTS-A82-2116	4 suspended charges pretest
NTS-A82-2117	4 suspended charges pretest
NTS-A82-2118	DSA 7 posttest
NTS-A82-2119	Crater backfall immediately posttest
NTS-A82-2120	Base of N pole posttest
NTS-A82-2121	Balloon support truck posttest
NTS-A82-2122	Closeup of DSA sampler posttest
NTS-A82-2123	ESA in place postshot
NTS-A82-2124	Internal staging area joint posttest
NTS-A82-2125	GGASP #5 pretest
NTS-A82-2126	GGASP #6 pretest
NTS-A82-2127	LANL experiment pretest
NTS-A82-2128	Fragment shields in place, with covers, pretest
NTS-A82-2129	Round room GGASP being installed
NTS-A82-2130	Fire set pretest
NTS-A82-2131	Joint of round room entrance posttest
NTS-A82-2132	Damage to gunnited joint posttest
NTS-A82-2133	Damage to gunnited joint posttest
NTS-A82-2134	GGASP #5 posttest
NTS-A82-2135	Rocks spilling through round room entrance posttest
NTS-A82-2136	A/C duct installation in staging area posttest
NTS-A82-2137	LANL experiment posttest

Table I-3 (continued)

Negative Number	Brief Description
NTS-A82-2151	Dismantling TSA samples posttest
NTS-A82-2152	Tunnel entrance posttest
NTS-A82-2153	Overhead view of control trailers posttest
NTS-A82-2154	View of structure from SE camera site posttest
NTS-A82-2155	View of structure from SW camera site posttest
NTS-A82-2156	PR--G.Gay at B48 with tethersonde gear
NTS-A82-2157	Aerial view of crater from SE posttest
NTS-A82-2158	Aerial view of crater from SE posttest
NTS-A82-2159	Edge of crater--posttest
NTS-A82-2160	Aerial view of structure from SE preshot
NTS-A82-2161	Northeast DSA posttest
NTS-A82-2162	Edge of crater looking to SE posttest
NTS-A82-2163	View of balloon tract to NW posttest
NTS-A82-2164	Detail of crater backfall
NTS-A82-2165	Close up of DSA to west posttest
NTS-A82-2166	Edge of crater and west pole posttest
NTS-A82-2167	Western slope of structure posttest
NTS-A82-2168	Northern slope of structure posttest
NTS-A82-2169	Western slope of structure posttest
NTS-A82-2170	AZ 290 marker posttest
NTS-A82-2171	AZ 320 marker posttest
NTS-A82-2172	AZ 330 marker posttest
NTS-A82-2173	AZ 340 marker posttest
NTS-A82-2174	AZ ? marker posttest
NTS-A82-2175	AZ 050 marker posttest
NTS-A82-2176	AZ 120 marker posttest
NTS-A82-2177	AZ 130 marker posttest
NTS-A82-2178	AZ 140 marker posttest
NTS-A82-2179	AZ 170 marker posttest
NTS-A82-2180	AZ 230 marker posttest
NTS-A82-2181	AZ 260 marker posttest
NTS-A82-2182	AZ 280 marker posttest
NTS-A82-2183	View of base of north pole posttest

Table I-3 (continued)

Negative Number	Brief Description
NTS-A82-2184	Northern edge of crater posttest
NTS-A82-2185	Outer edge of crater looking to NE posttest
NTS-A82-2186	Northeastern structure slope posttest
NTS-A82-2187	Northern structure slope posttest
NTS-A82-2188	Closeup of crater backfall
NTS-A82-2189	View of area to west posttest
NTS-A82-2190	Slope above tunnel entrance posttest
NTS-A82-2191	Western slope & balloon pickup posttest
NTS-A82-2192	Hanging charges
NTS-A82-2193	Hanging charges and entrance
NTS-A82-2194	Hanging charges
NTS-A82-2195	Hanging charges
NTS-A82-2196	Hanging charges and fragment collectors
NTS-A82-2197	Hanging charges
NTS-A82-2198	During shot view--cloud development
NTS-A82-2199	During shot view--cloud development
NTS-A82-2200	View of structure from east pretest
NTS-A82-2201	View of structure from east pretest
NTS-A82-2202	Slope of structure to south posttest
NTS-A82-2203	Bottom of crater with fines posttest
NTS-A82-2204	During shot view--cloud dispersion
NTS-A82-2205	View of structure from SE--posttest
NTS-A82-2206	SW toe of structure--posttest
NTS-A82-2207	SW toe of structure--posttest
NTS-A82-2208	PR-balloon crew posttest
NTS-A82-2209	GGASP unit pretest
NTS-A82-2210	Installation of GGASP in round room
NTS-A82-2211	Installation of fragment shield--GGASP #6
NTS-A82-2212	SWRI pressure transducer #3
NTS-A82-2213	SWRI pressure transducer and GGASP in round room pretest
NTS-A82-2214	Installation of round room GGASP #4
NTS-A82-2215	View of structure from SSE during gravel painting

Table I-3 (continued)

Negative Number	Brief Description
NTS-A82-2216	View of structure from NNE pretest
NTS-A82-2217	Balloon inflation pretest
NTS-A82-2218	Balloon inflation pretest
NTS-A82-2219	Balloon inflation pretest
NTS-A82-2220	View of structure from E during gravel painting
NTS-A82-2221	View of structure from E during gravel painting
NTS-A82-2222	ESA in place--pretest
NTS-A82-2223	View of structure from SE during gravel painting
NTS-A82-2224	SWRI round room pressure transducers pretest
NTS-A82-2225	Welded culvert joints--pretest
NTS-A82-2226	Uncovered fragment shields--pretest
NTS-A82-2227	GGASP #5--pretest
NTS-A82-2228	BSA control pickup--pretest
NTS-A82-2229	Fragment collectors in place and covered
NTS-A82-2230	Closeup of detonator installation
NTS-A82-2231	Plastic hose on reel--posttest
NTS-A82-2232	Tunnel entrance--posttest
NTS-A82-2233	BSA van posttest
NTS-A82-2234	ESA being lowered posttest
NTS-A82-2235	PR
NTS-A82-2236	ESA dismantling posttest
NTS-A82-2237	ESA sampler removal--posttest
NTS-A82-2238	ESA sampler removal--posttest
NTS-A82-2239	PR
NTS-A82-2240	PR
NTS-A82-2241	PR--Keller, Luna
NTS-A82-2242	PR
NTS-A82-2243	ESA sampler removal--posttest
NTS-A82-2244	Side view of north slope from W posttest
NTS-A82-2245	Side view of north slope from E posttest
NTS-A82-2246	Side view of south slope from E posttest
NTS-A82-2247	Side view of west slope from S posttest
NTS-A82-2248	Side view of west slope from SW posttest
NTS-A82-2249	AZ 240 marker--posttest
NTS-A82-2250	Side view of east slope from N posttest

Table I-3 (continued)

Negative Number	Brief Description
NTS-A82-2251	Closeup of gravel fallback through round room door
NTS-A82-2252	GGASP #5 posttest
NTS-A82-2253	Gunnite joint posttest
NTS-A82-2254	Vacuum pump--posttest
NTS-A82-2255	Circle through culvert--posttest
NTS-A82-2256	GGASP #6--posttest
NTS-A82-2257	Unbroken cables to NE--during posttest excavation
NTS-A82-2258	Unbroken cables to SE--during posttest excavation
NTS-A82-2259	Broken cables to SW--during posttest excavation
NTS-A82-2260	Cables to north--during posttest excavation
NTS-A82-2261	Unbroken cables to NE--during posttest excavation
NTS-A82-2262	Damage to poured staging area floor
NTS-A82-2263	Damage to poured staging area floor
NTS-A82-2264	Culvert joints--posttest
NTS-A82-2265	Staging area debris--posttest
NTS-A82-2266	Damage to round room door posttest excavation
NTS-A82-2267	Damage to cabling--posttest excavation
NTS-A82-2268	Damage to round room door posttest excavation
NTS-A82-2269	SWRI transducers and NE cabling posttest excavation
NTS-A82-2270	Damage to cabling--posttest excavation
NTS-A82-2271	Debris stored in staging area posttest excavation
NTS-A82-2272	View into staging area--posttest excavation
NTS-A82-2273	Cable damage--posttest excavation
NTS-A82-2274	PR-M. Martinez--posttest excavation
NTS-A82-2275	Overhead view of round room door posttest excavation
NTS-A82-2276	Culvert floor joints--posttest
NTS-A82-2277	Debris on culvert "shelves" posttest
NTS-A82-2278	PR-misc persons--posttest excavation

Table I-3 (continued)

Negative Number	Brief Description
NTS-A83-203	Postshot debris on floor of staging area
NTS-A83-204	Postshot debris on shelf in staging area
NTS-A83-205	Postshot debris on shelf in staging area
NTS-A83-206	Large piece of gypsum drywall in staging area
NTS-A83-207	Debris on shelf in staging area
NTS-A83-208	C Frederickson on postshot site visit
NTS-A83-209	Wire fabric on SE slope post-shot
NTS-A83-210	Close-up of heat damage to plastic vapor barrier
NTS-A83-211	Close-up of heat damage to plastic vapor barrier

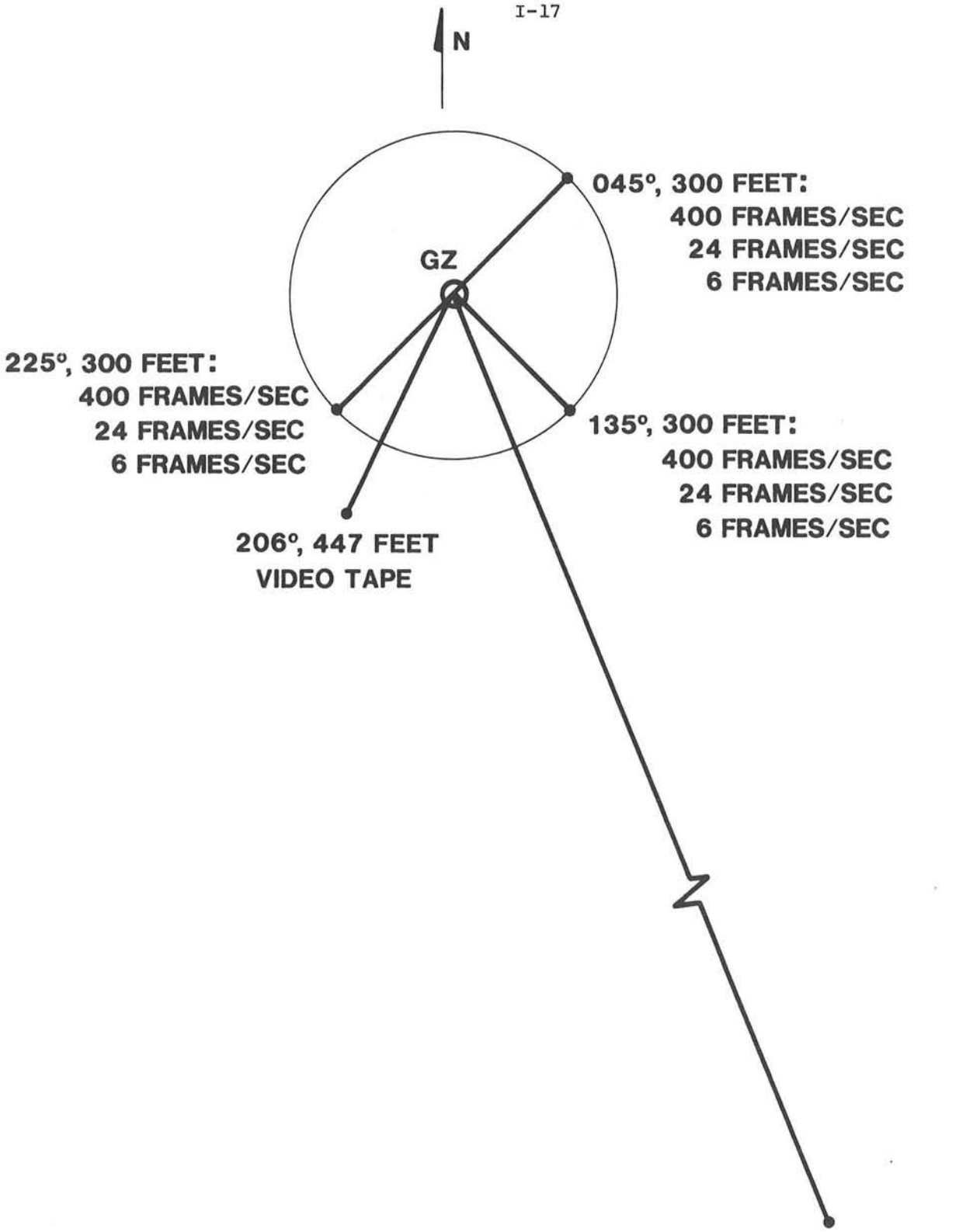

Figure I-1. Camera Locations

TABLE I-4

Available Documentary Films for GGCVP

Program Phase	Camera Location	Film Speed	Comments
Full-Scale Test	NE/91.5 m	400.0	Camera jammed at T + 1 sec
Full-Scale Test	NE/91.5 m	25.2	
Full-Scale Test	NE/91.5 m	10.0	
Full-Scale Test	SE/91.5 m	354.2	
Full-Scale Test	SE/91.5 m	22.7	
Full-Scale Test	SE/91.5 m	10.0	
Full-Scale Test	SW/91.5 m	284.0	
Full-Scale Test	SW/91.5 m	24.0	
Full-Scale Test	SW/91.5 m	9.9	

TABLE I-5
Available Documentary Video Tapes for GGCVP

Program Phase	Camera Location
Subscale Test 1 - 7/29/82	Various
Subscale Test 2 - 8/5/82	Various
Construction	Various
Full-Scale Test	206°/136.3 m
Full-Scale Test	160°/1281 m
Posttest	Various

Appendix J

Calculation of Internal Aerosol Mass Generated During Full-Scale Test

This appendix describes in detail the calculation of the respirable uranium airborne mass produced by the explosion in the Gravel Gertie round room. Round room and staging area aerosols were sampled using the GGASP instruments. Round room GGASPs filled during the time from t = 0 to t = 3.5 seconds and those in the staging area from 60 to 76 seconds. Key to the evaluation was the determination of the total volume of the sample compared to the total volume occupied by the aerosol. Two methods were used to quantify the uranium airborne mass sampled: (1) evaluation of the mass of gas collected using the critical flow function (assume choked flow through the sampling orifice) together with an estimate of the total gas mass in the round room and staging area, and (2) calculation of uranium concentration based upon fraction of filled GGASP volume compared with total aerosol volume. Both methods used measured quantities of uranium collected by each GGASP and the measured pressure histories internal and external to the GGASP collection chamber. Table J-1 lists the measured impactor and filter data for sampling stations 1 through 6. Also shown is the uranium mass determined by fluorometric analysis of debris washed from the collection chamber. A typical static overpressure history in the round room is shown in Figure J-1.

Internal pressures typical of the GGASP gas collection chamber are shown in the pressure trace of Figure J-2. The mass of airborne respirable uranium produced in the GG was determined as follows:

1. Computation By Critical Flow Function

A critical flow orifice was designed and fabricated to allow metering of the mass flow into the aerosol collection chamber of the GGASP. As long as the ratio between pressure inside the GGASP and pressure outside is smaller than 0.528, the mass flow rate is proportional to the upstream (round room) pressure and temperature and the orifice area. A smoothly converging nozzle design was used with a throat diameter of 0.413 $\pm$ 0.004 cm. The mass flow rate was determined according to the following equation:

$$\dot{m}(t) = \frac{3.2 \times 10^2 \times d^2 \times C \times P_o(t)}{(T_o)^{1/2}}, \qquad \text{(J-1)}$$

where P_o is the inlet stagnation pressure during the period of sampling (taken from Table J-2), T_o is the absolute stagnation temperature at the inlet, C is the discharge coefficient (a weak function of the back pressure ratio) and d is the orifice inlet diameter. Because the nozzles were well rounded, the value of C is taken to be 0.97 [AN61].

TABLE J-1

Gravel Gertie Aerosol Sampling Package Impactor/Filter Data

GGASP Station No.	Sampler No.	Substrate No.	Uranium Mass (ng)	a ECD_{aer} (μm)	t_{on} (sec)	t_{off} (sec)	Flow Rate (l/min)	MMAD (μm)	σ_g	Orifice Diameter (cm)
1	MI 1-15	4011	750	6.34	0	3.7	1.740	1.82	2.6	0.407
		4012	3981	4.19			1.740			0.407
		4013	3891	2.84			1.740			0.407
		4014	3741	1.92			1.740			0.407
		4015	2658	1.44			1.740			0.407
		4016	2794	0.97			1.740			0.407
		4017	3065	0.64			1.740			0.407
		4018	3997	----			1.740			0.407
	MI 1-18	4021	4312	6.17	0	3.7	1.835	2.3	3.0	0.407
		4022	5199	4.08						0.407
		4023	3576	2.77						0.407
		4024	3786	1.87						0.407
		4025	2599	1.41						0.407
		4026	2824	0.95						0.407
		4027	3004	0.63						0.407
		4028	3717	----						0.407
1	FL 1-7		53.4	----	0	3.7	----	----		0.407
1	FS 1-6		10,670	----	0	3.7	----	----		0.407
Bell Jar Wash			1.64×10^6							
Total			1.709×10^6							

[a] ECD_{ar} (μm) = $1.257 \times 10^3 \left[\frac{W^3}{F}\right]^{0.5}$, W in cm, F in cm^3/min

TABLE J-1

Gravel Gertie Aerosol Sampling Package Impactor/Filter Data (continued)

GGASP Station No.	Sampler No.	Substrate No.	Uranium Mass (ng)	ECD_{aer} (μm)	t_{on} (sec)	t_{off} (sec)	Flow Rate (l/min)	MMAD (μm)	σ_g	Orifice Diameter (cm)
2	MI 2-12	4041	1562	6.47	0	3.5	1.670	2.0	2.4	0.410
		4042	2554	4.38			1.670			0.410
		4043	3095	2.90			1.670			0.410
		4044	2238	1.96			1.670			0.410
		4045	1532	1.47			1.670			0.410
		4046	1622	0.99			1.670			0.410
		4047	1802	0.66			1.670			0.410
		4048	2539	----			1.670			0.410
2	MI 2-9	4031	86.4	6.78	0	3.5	1.520	1.5	2.5	0.410
		4032	1020	4.48			1.520			0.410
		4033	1231	3.04			1.520			0.410
		4034	1937	2.06			1.520			0.410
		4035	1381	1.55			1.520			0.410
		4036	1922	1.04			1.520			0.410
		4037	1441	0.69			1.520			0.410
		4038	2545	----			1.520			0.410
2	FL 2-3	2052	29.4					----	----	0.410
2	FS 2-3	3052	12,323					----	----	0.410
Bell Jar Wash			1.379×10^6							
Total			1.420×10^6							

TABLE J-1

Gravel Gertie Aerosol Sampling Package Impactor/Filter Data (continued)

GGASP Station No.	Sampler No.	Substrate No.	Uranium Mass (ng)	ECD_{aer} (μm)	t_{on} (sec)	t_{off} (sec)	Flow Rate (l/min)	MMAD (μm)	σ_g	Orifice Diameter (cm)
3	MI 3-4	4051	510	6.98	0	3.6	1.435	1.9	2.7	0.420
		4052	1411	4.61			1.435			0.420
		4053	1787	3.13			1.435			0.420
		4054	1652	2.12			1.435			0.420
		4055	1186	1.59			1.435			0.420
		4056	1216	1.07			1.435			0.420
		4057	1336	0.71			1.435			0.420
		4058	2373	----			1.435			0.420
3	MI 3-8	4061	1547	6.22	0	3.6	1.810	1.9	2.7	0.420
		4062	2794	4.11			1.810			0.420
		4063	1892	2.79			1.810			0.420
		4064	1336	1.89			1.810			0.420
		4065	1081	1.42			1.810			0.420
		4066	1201	0.95			1.810			0.420
		4067	1381	0.63			1.810			0.420
		4068	2749	----			1.810			0.420
3	FL 3-2	2053	32	----				----	----	
3	FS 3-2	3053	11,848	----				----	----	
Bell Jar Wash		1.27×10^6								
Total		1.164×10^6								

TABLE J-1

Gravel Gertie Aerosol Sampling Package Impactor/Filter Data (continued)

GGASP Station No.	Sampler No.	Substrate No.	Uranium Mass (ng)	ECD_{aer} (μm)	t_{on} (sec)	t_{off} (sec)	Flow Rate (l/min)	MMAD (μm)	σ_g	Orifice Diameter (cm)
4	MI 7-10	4071	960	7.76	0	3.5	1.16	1.8	2.6	0.413
		4072	1937	5.13			1.16			0.413
		4073	3080	3.48			1.16			0.413
		4074	3651	2.36			1.16			0.413
		4075	2343	1.77			1.16			0.413
		4076	2388	1.19			1.16			0.413
		4077	2974	0.79			1.16			0.413
		4078	4042	----			1.16			0.413
4	MI 7-10	4081	31	9.29	0	3.5	0.810	1.8	2.6	0.413
		4082	314	6.14			0.810			0.413
		4083	1321	4.17			0.810			0.413
		4084	2103	2.82			0.810			0.413
		4085	1592	2.12			0.810			0.413
		4086	1471	1.42			0.810			0.413
		4087	1727	0.94			0.810			0.413
		4088	3711	----			0.810			0.413
4	FL 7-5	2054	43	0.413				----	----	0.413
4	FS 7-4	3053	25,850	0.413				----	----	0.413
Bell Jar Wash		1.058×10^6								
Total		1.117×10^6								

TABLE J-1

Gravel Gertie Aerosol Sampling Package Impactor/Filter Data (continued)

GGASP Station No.	Sampler No.	Substrate No.	Uranium Mass (ng)	ECD_{aer} (μm)	t_{on} (sec)	t_{off} (sec)	Flow Rate (l/min)	MMAD (μm)	σ_g	Orifice Diameter (cm)
5	MI 4-11	4101	434	5.93	60	76	1.970	1.5	2.7	0.415
		4102	2088	3.93			1.970			0.415
		4103	2463	2.68			1.970			0.415
		4104	1787	1.81			1.970			0.415
		4105	1291	1.36			1.970			0.415
		4106	1742	0.91			1.970			0.415
		4107	2749	0.60			1.970			0.415
		4108	2884	----			1.970			0.415
5	MI 4-17	4091	1510	5.88	60	75	2.020			0.415
		4092	2268	3.89			2.020			0.415
		4093	2328	2.64			2.020			0.415
		4094	1877	1.79			2.020			0.415
		4095	1321	1.34			2.020			0.415
		4096	1802	0.90			2.020			0.415
		4097	2569	0.60			2.020			0.415
		4098	3140	----			2.020			0.415
5	FL 4-1	2055	20.4		60	75		----	----	0.415
5	FS 4-1	3055	21,041		60	75		----	----	0.415
Bell Jar Wash		2.216×10^5								
Total		2.739×10^5								

TABLE J-1

Gravel Gertie Aerosol Sampling Package Impactor/Filter Data (continued)

GGASP Station No.	Sampler No.	Substrate No.	Uranium Mass (ng)	ECD_{aer} (μm)	t_{on} (sec)	t_{off} (sec)	Flow Rate (l/min)	MMAD (μm)	σ_g	Orifice Diameter (cm)
6	MI 6-6	4111	1291	5.91	60	75	2.00	1.7	2.7	0.410
		4112	2629	3.91			2.00			0.410
		4113	1366	2.66			2.00			0.410
		4114	1411	1.79			2.00			0.410
		4115	1982	1.35			2.00			0.410
		4116	1952	0.91			2.00			0.410
		4117	2358	0.60			2.00			0.410
		4118	1998	----			2.00			0.410
6	MI 6-16	4121	2088	5.91	60	75	2.00	2.1	2.6	0.410
		4122	3606	3.91			2.00			0.410
		4123	2118	2.65			2.00			0.410
		4124	2088	1.79			2.00			0.410
		4125	1472	1.35			2.00			0.410
		4126	1757	0.91			2.00			0.410
		4127	2689	0.60			2.00			0.410
		4128	1577	----			2.00			0.410
6	FL 6-6	2156	22		60	75		----	----	0.410
6	FS 6-6	3056	39,664		60	75		----	----	0.410
Bell Jar Wash		3.672×10^5								
Total		4.39×10^5								

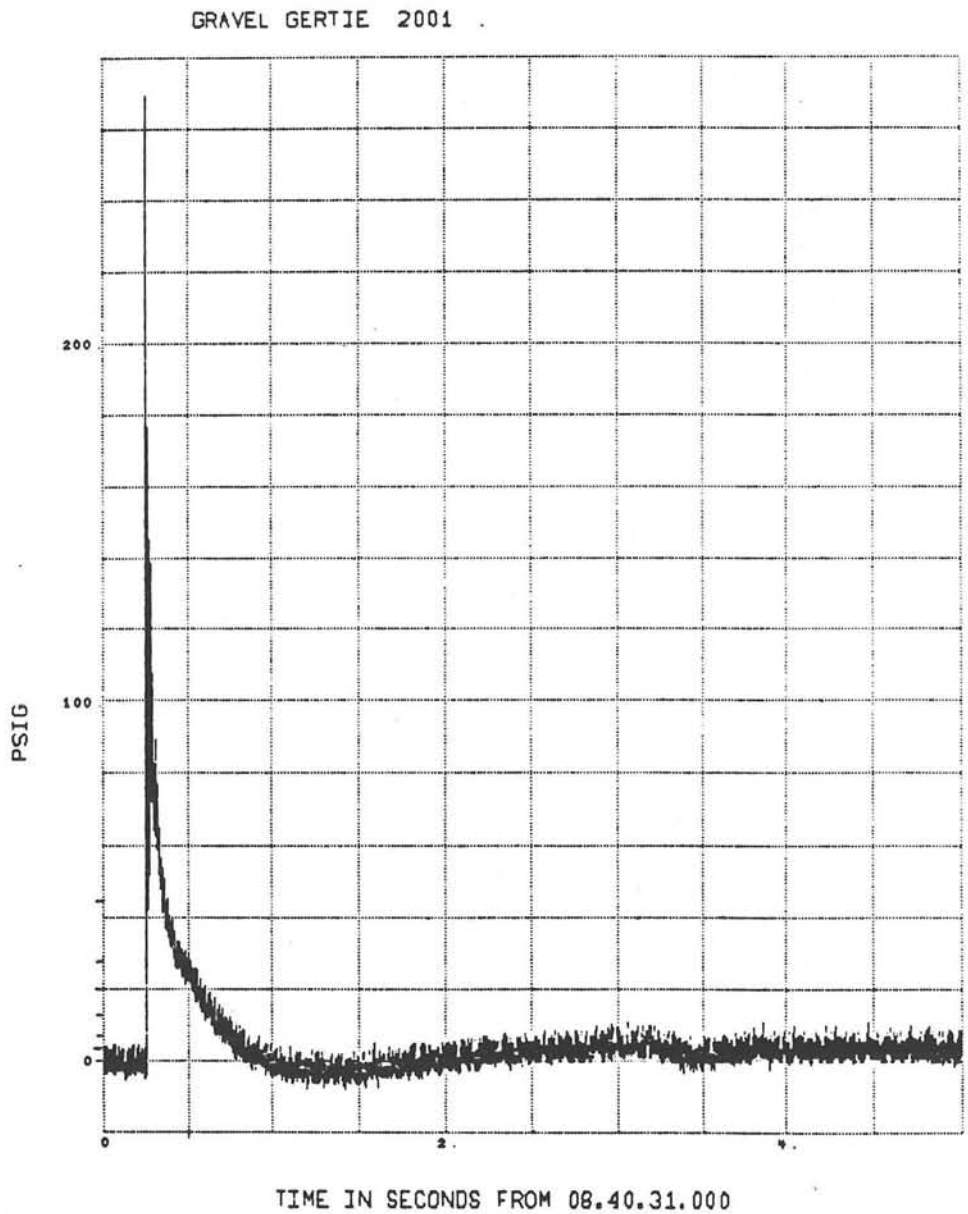

Figure J-1. Station 2 External Pressure to 5 Seconds

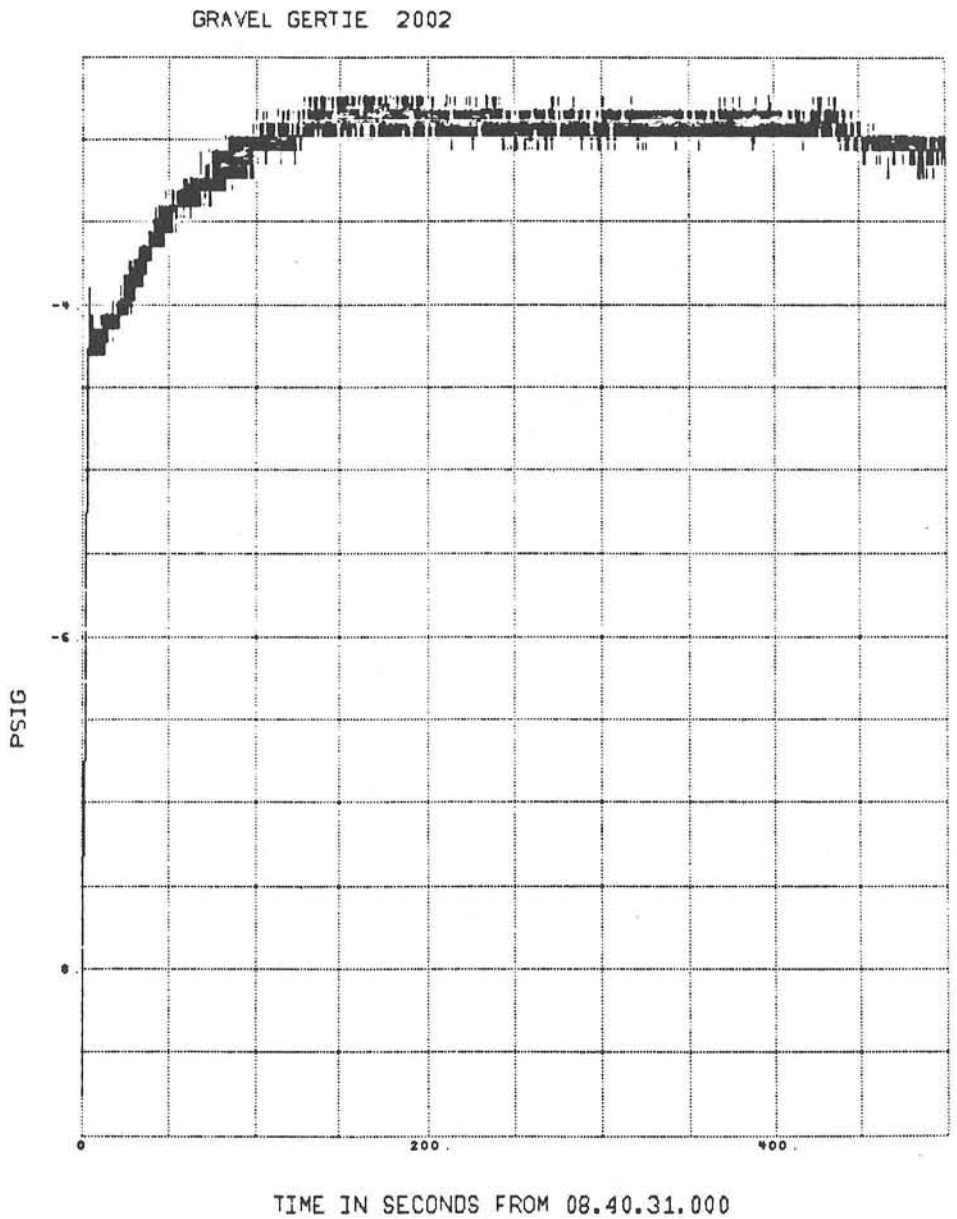

Figure J-2. Station 2 GGASP Internal Pressure to 500 Seconds

TABLE J-2

Input Parameters for Equation J-1

GGASP No.	M_U ($\times 10^{-3}$ g)	V_{SA} ($\times 10^5$ l)	V_{RR} ($\times 10^5$ l)	V_V ($\times 10^5$ l)	M_{CG} ($\times 10^5$ g)	To °K	d (cm)	C**	$P_o(t)dt$ (atmos-sec)	ρ_{air}* (g/l)
1	1.71	6.23	5.15	2.68	1.92	650	0.413	0.97	6.03	1.025
2	1.42	6.23	5.15	2.68	1.92	650	0.413	0.97	4.73	1.025
3	1.16	6.23	5.15	2.68	1.92	650	0.413	0.97	4.92	1.025
4	1.12	6.23	5.15	2.68	1.92	650	0.413	0.97	5.82	1.025
5	0.274	6.23	----	----	----	300K	0.413	0.97	15	1.025
6	0.439	6.23	----	----	----	300K	0.413	0.97	15	1.025

*at T = 30°C and P = 899 mbar
**no units
M_U = mass of uranium sampled
V_{SA} = volume of staging area
V_{RR} = volume of round room
V_V = rising gravel bed void volume
M_{CG} = mass of combustion gases
To = absolute stagnation temperature
d = orifice inlet diameter
C = discharge coefficient
ρ_{air} = density of air

The total mass of gas and aerosol sampled by each GGASP is determined by integrating Eq. (J-1) over the sampling period ($t_t - t_o$):

$$m_a = \int_{t_o}^{t_t} \dot{m}(t)dt \qquad \text{(J-2)}$$

The total mass of uranium produced in the structure (M_{tu}) is obtained by dividing the mass of uranium sampled (m_u) by the mass of gas sampled by each GGASP (m_a) and multiplying this ratio by the total mass of gas in the structure during the sampling period (M_g):

$$M_{tu} = \frac{m_u}{m_a} \cdot M_g \qquad \text{(J-3)}$$

During the 3.5 second sampling period in the round room, combustion product gases have been produced from the explosion and these gases have adiabatically expanded into a portion of the staging area. The volume of gas sampled by GGASPs 1-4 can be determined by assuming an adiabatic expansion of the gas in the round room V_{RR}.

If a gas at high pressure P_{RR}, confined in volume V_{RR}, is allowed to expand into a volume V_{SA} occupied by gas at ambient pressure P_{SA}, the expanded volume can be estimated by assuming that both gases expand/compress adiabatically. Assuming that, before expansion, the aerosol is confined to what was originally the round room volume, the fraction of the total volume occupied by this aerosol is:

$$f_{RR} = \frac{V_{RR}}{V_{RR} + V_{SA}} = \frac{1}{1 + \frac{V_{SA}}{V_{RR}}} \qquad \text{(J-4)}$$

The pressures and volumes are related through the adiabatic expansion relationship:

$$pV^{\gamma} = \text{constant.} \qquad \text{(J-5)}$$

If the final pressure in the round room and staging area at t = 100 msec is approximately 130 psig (143 psia) and initial pressure in the staging area is assumed to be 13 psia, then the value for f_{RR} is 0.90. If the initial pressure in the round room was 130 psig (essentially starting the expansion process earlier), then the value for f_{RR} is 0.82. In the calculation 0.90 has been used.

The volume of gas sampled by GGASPs 1-4 is then:

$$V_g = 0.90(V_{SA} + V_{RR} + V_{CG}) \qquad \text{(J-6)}$$

where V_{CG} is the volume of combustion gases produced in the round room.

In addition, after this initial expansion process, a fraction of this gas has expanded to fill the void produced by the rising gravel bed and this volume of gas V_V must be added to the volume available for sampling:

$$V_g = 0.90(V_{SA} + V_{RR} + V_{CG}) + V_V \qquad \text{(J-7)}$$

It is noted that, although a fraction of this void volume V_V contributes to the total volume sampled over the 3.5 second sampling period, the fractional contribution will be assumed to be 1.0 for the sake of simplicity.

The total mass of gases, M_g, available for sampling in Eq. (J-3) is then given by

$$M_g = 0.90(V_{SA} + V_{RR}) \cdot \rho_{air} + 0.9M_{CG} + V_V \rho_{air} \qquad \text{(J-8)}$$

The total mass of airborne uranium produced in the GG structure is then estimated using the data from GGASPs Nos. 1-4 and:

$$M_{TU} = \frac{M_U \; 0.90\left(V_{SA} + V_{RR}\right) \rho_{air} + V_V \rho_{air} + 0.9M_{CG}}{3.2 \times 10^2 d^2 C \int_{t=0}^{t=3.5} P_o(t)dt} T_o^{1/2} \qquad \text{(J-9)}$$

Equation (J-9) may be evaluated by using the data in Table J-2 which lists the pertinent input parameters. Table J-3 lists the calculated values of M_{TU} (Eq. (J-9)) for each GGASP. The average airborne aerosol mass as extrapolated to the GG structure from the GGASP samples obtained between t=0 and t=3.5 secs is 193 g. This corresponds to 2.4 percent of the initial uranium mass (8 kg).

2. Computation By Fraction of Filled Volume (Pressure Ratios)

Based upon pressure histories measured in the GGASP gas collection chambers, a change in pressure during the sampling period was determined for each GGASP. The total pressure change indicative of complete filling of the 21 liter collection volume was measured during calibration evaluation to be 13 psig. From these data, a ratio of pressure changes was determined and the fill fraction of each GGASP sampling volume was obtained. Uranium mass concentration for each GGASP was calculated by dividing the total mass of uranium collected by the fractional volume sampled for each GGASP. The total mass of airborne uranium in the GG structure was determined by using the volume of gas in the GG structure computed in Eq. (J-6) and the uranium mass concentration of each sampling station.

From the four sampling stations in the round room (GGASPs Nos. 1-4) an average mass of airborne uranium aerosol was determined. The computation is as follows:

TABLE J-3
Calculated Values for M_{TU} From Eq J-9

GGASP No.	M_{TU} (g)	AVM_{TU} (g)	% in Structure
1	217		
2	230	193	2.4
3	180		
4	147		
5	4		6.6×10^{-2}
6	6.5	5.3	(avg conc. = 8.5×10^{3} g/m^{3})

$$M_{iTU} = \frac{M_{iU} \cdot V_g}{\frac{P\Big|_{t_{on}}^{t_{off}}}{P_{cal}}} \cdot V_{GGASP} \qquad \text{(J-10)}$$

where

V_g = total volume of gas in GG structure
V_{GGASP} = volume of GGASP collection chamber
M_{iU} = mass of uranium collected per GGASP

$\frac{P\Big|_{t_{on}}^{t_{off}}}{P_{cal}}$ = ratio of pressure differentials

Table J-4 lists values of pertinent input parameters and calculated airborne uranium aerosol mass. Total released airborne uranium aerosol mass is shown in the last column and is based upon an average of extrapolated uranium masses from GGASPs Nos. 1-4.

Based on this computational method, approximately 2.5 percent of the initial uranium mass in the test assembly was produced as airborne material. This is in good agreement with the estimates from the first computational method, which suggested 2.4 percent production. The reduced pressure in some of the GGASP 20 litre chambers during sample processing by the measurement section had the effect of increasing the MMAD. However, because only the last stage of the Mercers (< 1 μm) were affected by the reduced pressure, the error is estimated to be less than +40% than the indicated value. An average value at 195 ± 40 g was estimated for the mass of uranium particles produced in the structure.

GGASPs 5 and 6 were located in the staging area and were not used in either method of determining the average airborne uranium mass because they did not sample until t = +60 seconds after detonation. The samples taken by GGASPs 5 and 6 characterize the residual aerosol left in the staging area after the major violence caused by the detonation, roof movement, gas escape, and roof fallback have been completed. During the period of sampling starting at t = 60 seconds, significant decreases in total suspended aerosol would have taken place as a result of agglomeration, gravitational fallout and diffusive and thermophoretic plateout.

Figures J-3 through J-8 show the particle sizes measured by the GGASP impactors. Uncertainties due to the flow rate, impactor jet parameters, pressures, etc., were propagated to estimate the cumulative MMAD uncertainty. The total uncertainty on the MMAD was calculated to be ±50%. The average MMAD of uranium particles collected by GGASPs in the round room was estimated to be 1.64 ± 0.82 μm. The average MMAD of uranium particles collected in the staging area by GGASPs 5 and 6 was estimated to be 2.08 ± 1.04 μm.

TABLE J-4

Summary of Calculation of Respirable Airborne Uranium Aerosol Produced in GG Structure

GGASP No.	M_{iU} ($\times 10^{-3}$ g)	$P_i(t_{on})$ (psig)	$P_i(t_{off})$ (psig)	P_{cal} (psig)	V_{GGASP} (l)	Concentration ($\times 10^{-4}$ g/l)	V_g ($\times 10^{6}$ l)	M_{TU} (g)	Average M_{TU} (g)	% in Structure
1	1.71	-11.5	-6.5	13	21	2.1	1.201	252		
2	1.42	-11.5	-6.5	13	21	1.8	1.201	216		
3	1.16	-12	-6.2	13	21	1.2	1.201	144	198	2.5
4	1.12	-12.25	-7.5	13	21	1.5	1.201	180		
5	0.274	-11.0	0	13	21	0.15	1.201	9	13	1.6×10^{-1}
6	0.439	-11.5	-1.5	13	21	0.27	1.201	17		
									(avg. conc = 2.1×10^{-2} g/m^3)	

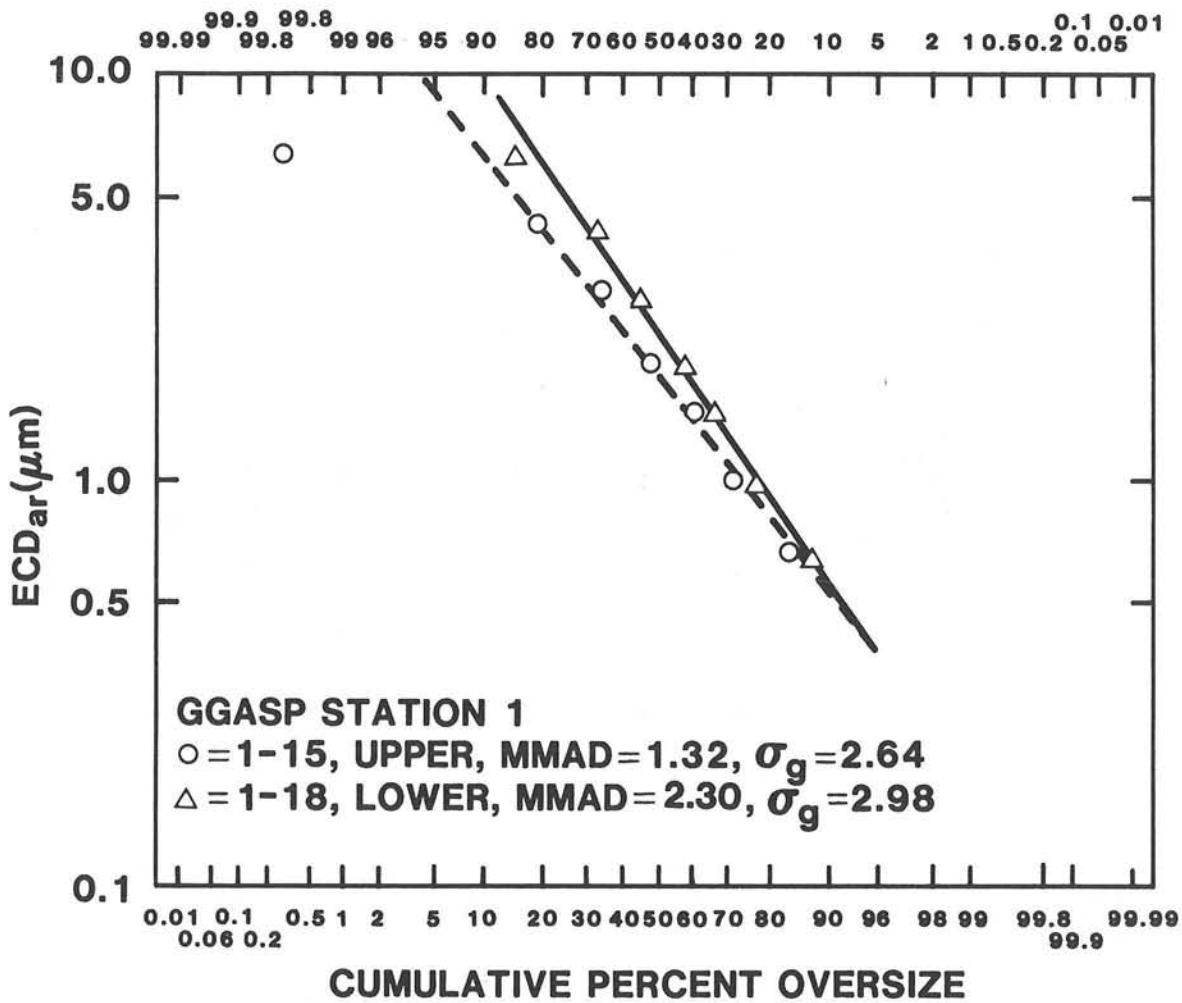

Figure J-3. A Log-Normal Fit to Mercer Impactor Data of GGASP No. 1, Station No. 1, Showing Effective Cutoff Diameter (μm) as a Function of Cumulative Percent of Mass Oversize.

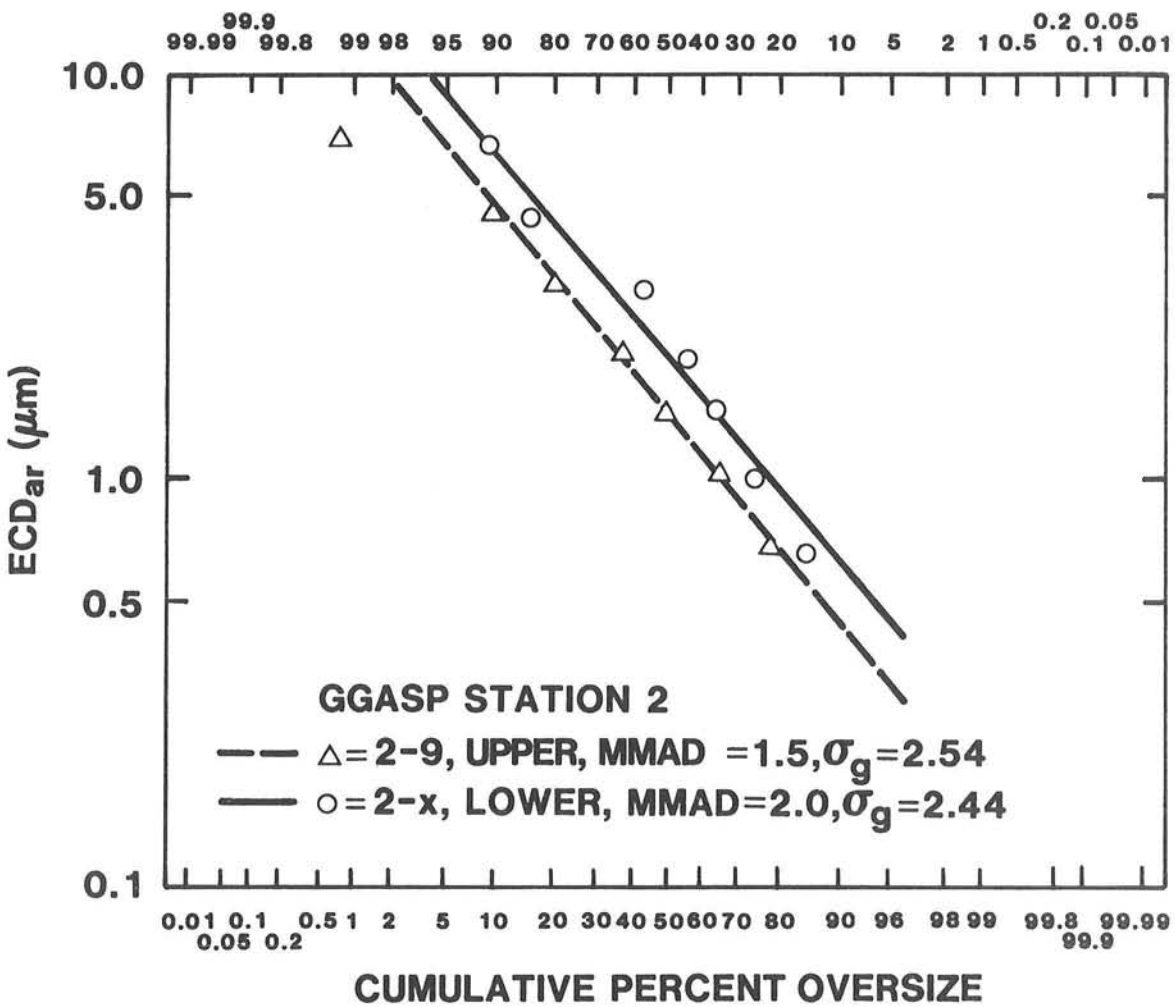

Figure J-4. A Log-Normal Fit to Mercer Impactor Data of GGASP No. 2, Station No. 2, Showing Estimated Cutoff Diameter (μm) as a Function of Cumulative Percent of Mass Oversize.

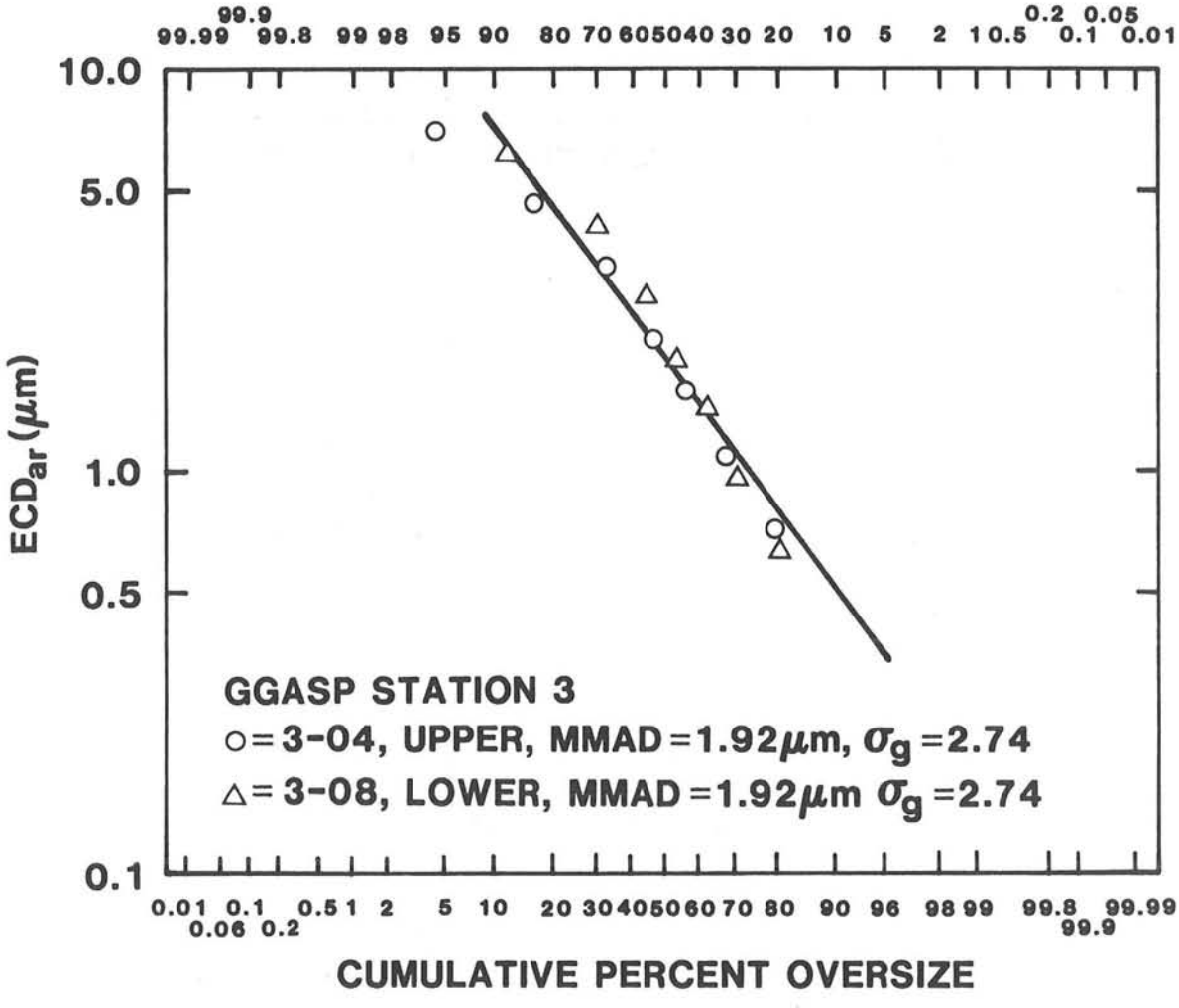

Figure J-5. A Log-Normal Fit to Mercer Impactor Data of GGASP No. 3, Station No. 3, Showing Effective Cutoff Diameter (μm) as a Function of Cumulative Percent of Mass Oversize.

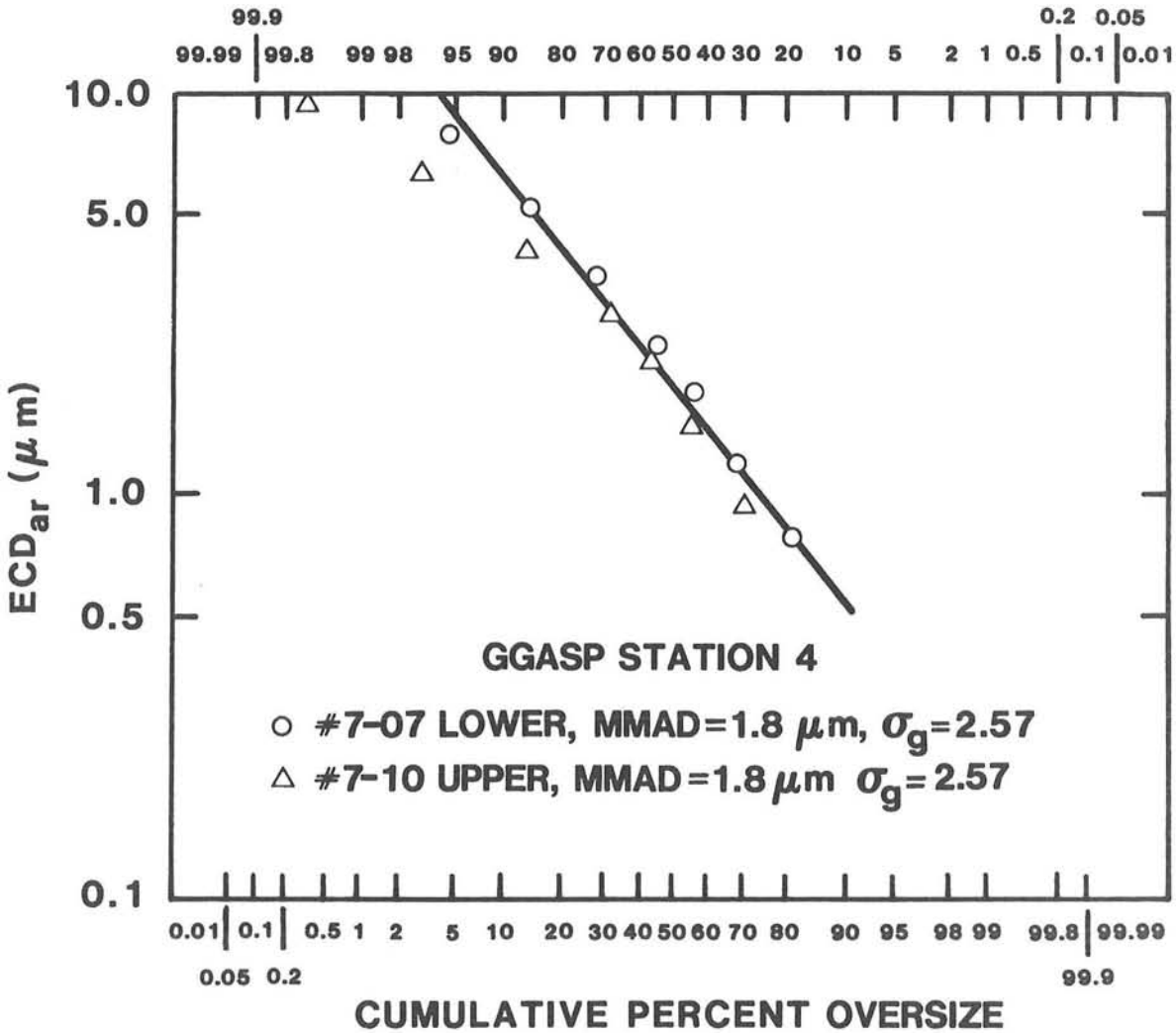

Figure J-6. A Log-Normal Fit to Mercer Impactor Data of GGASP No. 7, Station No. 4, Showing Effective Cutoff Diameter (μm) as a Function of Cumulative Percent of Mass Oversize.

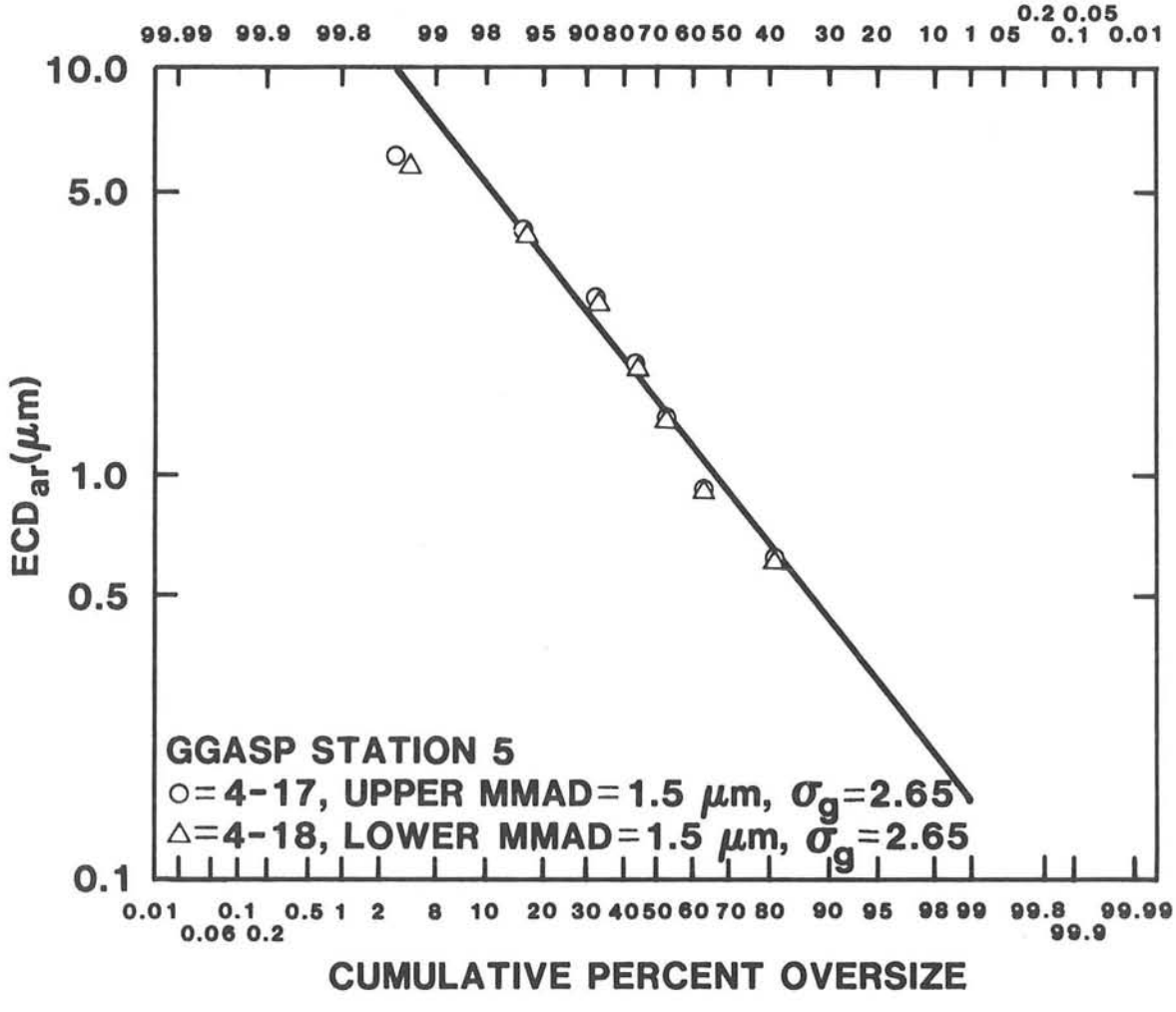

Figure J-7. A Log-Normal Fit to Mercer Impactor Data of GGASP No. 4, Station No. 5, Showing Effective Cutoff Diameter (μm) as a Function of Culmulative Percent of Mass Oversize.

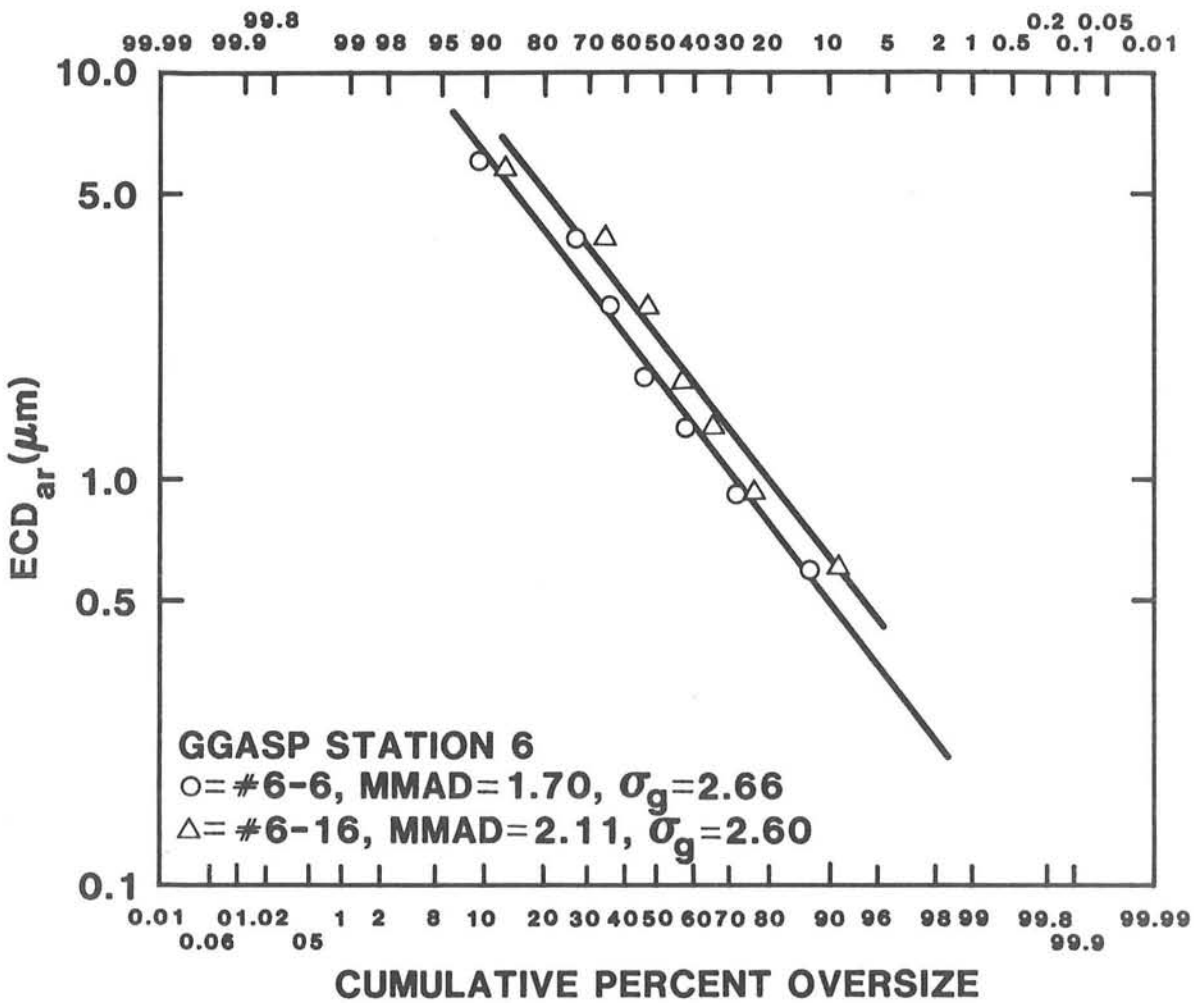

Figure J-8. A Log-Normal fit to Mercer Impactor Data of GGASP No. 6, Station No. 6, Showing Effective Cutoff Diameter (μm) as a Function of Cumulative Percent of Mass Oversize.

Appendix K
Analysis of Respirable Aerosol Release Fraction for Full-Scale Test

Uranium aerosol data obtained from cascade impactors was analyzed to infer mass versus size of the aerosol. Samplers deployed in the External Sampling Array, Pole Sampling Array, Balloon Sampling array, and Tunnel Sampling Array were used in this analysis.

External Sampling Array

Uranium mass (in nanograms) measured by flourometric analyses is shown in Table K-1 for each stage of cascade impactors used in the overhead External Sampling Array (ESA). Flow rate, effective stage cutoff diameter (ECD)*, and total mass collected per impactor stage are also shown in Table K-1. The last column shows the quantity of uranium after subtraction of assay error ($\pm$ 10 ng) and background uranium soil contribution (which was 3.4 ppm for gravel bed and overburden). The remaining quantity of uranium greater than or equal to two standard deviations of estimated error was considered to be a statistically significant quantity. From these data it is not possible to compute size distributions for airborne uranium since no impactor collected statistically significant quantities of uranium on more than two stages per impactor. In addition, no statistically significant amounts of uranium were detected on any filters deployed in the ESA. Of the five filters analyzed for Sb, no statistically significant amounts were detected.

Pole Sampling Array

Table K-2 shows the uranium and total mass analyses results for cascade impactors configured in the Pole Sampling Array (PSA). Flow rate, effective cutoff diameter (ECD_{aer}), and mass median aerodynamic diameter (MMAD) are also shown. The last column lists those impactor stages which collected statistically significant quantities of uranium. No more than two stages of any impactor used in the Pole Sampling Array collected significant quantities of uranium. A minimum of four stages are required to provide an acceptable "goodness of fit" test to an assumed log-normal function. From these data it was not possible to compute size distributions of pole-sampled airborne uranium particles. In addition, selected filters used in the Pole Sampling Array were analyzed for Sb using delayed neutron activation (DNA) analyses, and no statistically significant Sb quantities above soil background were detected.

Tunnel Sampling Array

Table K-3 shows uranium and total mass collected per stage for cascade impactors deployed in the Tunnel Sampler Array (TSA). The TSA-1 cascade impactor was located about 3 meters southwest of, and external to, the tunnel

*ECD: aerodynamic diameter at which 50 percent of particles are caught on the impactor stage. Smaller particles are caught with lower efficiency and larger particles with a greater efficiency.

TABLE K-1
External Sampling Array Cascade Impactor Data

Location	Sampler ID No.	Substrate No.	Flow Rate (l/min)	ECD_{aer} (μm)	Total Mass (mg)	Uranium (ng)	Significant Uranium (ng)
ESA-H1	LMJ-19	1031	14.7	12.6	1.40	0.0	0
ESA-H1	LMJ-19	1032	14.7	8.0	0.31	0.0	0
ESA-H1	LMJ-19	1033	14.7	5.2	0.08	0.0	0
ESA-H1	LMJ-19	1034	14.7	3.1	0.05	27.9	18
ESA-H1	LMJ-19	1035	14.7	2.0	0.0	0.0	0
ESA-H1	LMJ-19	1036	14.7	1.3	0.01	15.9	0
ESA-H1	LMJ-19	1037	14.7	0.8	0.04	0.0	0
ESA-H1	LMJ-19	1038	14.7	--	0.55	60.9	49
ESA-H2	LMJ-4	1061	17.3	11.6	1.00	296.1	283
ESA-H2	LMJ-4	1062	17.3	7.4	1.35	123.9	109
ESA-H2	LMJ-4	1063	17.3	4.8	0.76	5.9	0
ESA-H2	LMJ-4	1064	17.3	2.9	0.37	0.0	0
ESA-H2	LMJ-4	1065	17.3	1.8	0.41	0.0	0
ESA-H2	LMJ-4	1066	17.3	1.2	0.33	3.9	0
ESA-H2	LMJ-4	1067	17.3	0.7	0.16	0.0	0
ESA-H2	LMJ-4	1068	17.3	--	0.12	3.9	0
ESA-H3	LMJ-20	1071	14.3	12.8	0.39	0.0	0
ESA-H3	LMJ-20	1072	14.3	8.2	0.5	0.0	0
ESA-H3	LMJ-20	1073	14.3	5.3	0.20	0.0	0
ESA-H3	LMJ-20	1074	14.3	3.2	0.16	0.0	0
ESA-H3	LMJ-20	1075	14.3	2.0	0.06	0.0	0
ESA-H3	LMJ-20	1076	14.3	1.3	0.06	0.0	0
ESA-H3	LMJ-20	1077	14.3	0.8	0.28	0.0	0

TABLE K-1 (continued)
External Sampling Array Cascade Impactor Data

Location	Sampler ID No.	Substrate No.	Flow Rate (l/min)	ECD_{aer} (μm)	Total Mass (mg)	Uranium (ng)	Significant Uranium (ng)
ESA-H4	LMJ-10	1091	15.0	12.5	0.60	0.9	0
ESA-H4	LMJ-10	1092	15.0	8.0	0.14	0.0	0
ESA-H4	LMJ-10	1093	15.0	5.1	0.24	0.0	0
ESA-H4	LMJ-10	1094	15.0	3.1	0.09	0.0	0
ESA-H4	LMJ-10	1095	15.0	2.0	0.17	8.4	0
ESA-H4	LMJ-10	1096	15.0	1.2	0.0	8.4	0
ESA-H4	LMJ-10	1097	15.0	0.8	0.15	0.0	0
ESA-H4	LMJ-10	1098	15.0	--	0.26	0.0	0
ESA-H5	LMJ-5	1121	15.1	12.5	0.40	0.0	0
ESA-H5	LMJ-5	1122	15.1	7.9	0.0	0.0	0
ESA-H5	LMJ-5	1123	15.1	5.1	0.02	0.0	0
ESA-H5	LMJ-5	1124	15.1	3.1	0.0	0.0	0
ESA-H5	LMJ-5	1125	15.1	2.0	0.04	0.0	0
ESA-H5	LMJ-5	1126	15.1	1.2	0.0	0.0	0
ESA-H5	LMJ-5	1127	15.1	0.8	0.0	0.0	0
ESA-H5	LMJ-5	1128	15.1	--	0.33	0.0	0
ESA-H6	LMJ-9	1021	15.1	12.5	0.41	110.4	99
ESA-H6	LMJ-9	1022	15.1	7.9	0.26	0.0	0
ESA-H6	LMJ-9	1023	15.1	5.1	0.26	0.0	0
ESA-H6	LMJ-9	1024	15.1	3.1	0.14	0.0	0
ESA-H6	LMJ-9	1025	15.1	2.0	0.08	0.0	0
ESA-H6	LMJ-9	1026	15.1	1.2	0.04	6.9	0
ESA-H6	LMJ-9	1027	15.1	0.7	0.05	3.9	0
ESA-H6	LMJ-9	1028	15.1	--	0.57	5.4	0

TABLE K-1 (continued)
External Sampling Array Cascade Impactor Data

Location	Sampler ID No.	Substrate No.	Flow Rate (l/min)	ECD_{aer} (μm)	Total Mass (mg)	Uranium (ng)	Significant Uranium (ng)
ESA-H7	LMJ-7	1051	15.2	12.4	0.63	0.0	0
ESA-H7	LMJ-7	1052	15.2	7.9	0.25	0.0	0
ESA-H7	LMJ-7	1053	15.2	5.1	0.10	0.0	0
ESA-H7	LMJ-7	1054	15.2	3.1	0.16	0.0	0
ESA-H7	LMJ-7	1055	15.2	2.0	0.18	0.0	0
ESA-H7	LMJ-7	1056	15.2	1.2	0.19	0.0	0
ESA-H7	LMJ-7	1057	15.2	0.8	0.0	0.0	0
ESA-H7	LMJ-7	1058	15.2	--	0.41	0.0	0
ESA-H8	LMJ-8	1041	15.1	12.5	0.77	5.4	0
ESA-H8	LMJ-8	1042	15.1	7.9	0.15	5.4	0
ESA-H8	LMJ-8	1043	15.1	5.1	0.14	152.4	142
ESA-H8	LMJ-8	1044	15.1	3.1	0.0	0.0	0
ESA-H8	LMJ-8	1045	15.1	2.0	0.0	47.4	37
ESA-H8	LMJ-8	1046	15.1	1.2	0.02	0.0	0
ESA-H8	LMJ-8	1047	15.1	0.8	0.02	9.9	0
ESA-H8	LMJ-8	1048	15.1	--	0.29	0.0	0
ESA-H9	LMJ-6	1081	15.1	12.5	0.09	0.0	0
ESA-H9	LMJ-6	1082	15.1	7.9	0.04	0.0	0
ESA-H9	LMJ-6	1083	15.1	5.1	0.0	0.0	0
ESA-H9	LMJ-6	1084	15.1	3.1	0.0	96.9	87
ESA-H9	LMJ-6	1085	15.1	2.0	0.02	0.0	0
ESA-H9	LMJ-6	1086	15.1	1.2	0.03	0.0	0
ESA-H9	LMJ-6	1087	15.1	0.7	0.06	0.0	0
ESA-H9	LMJ-6	1088	15.1	--	0.30	0.0	0

TABLE K-1 (continued)
External Sampling Array Cascade Impactor Data

Location	Sampler ID No.	Substrate No.	Flow Rate (l/min)	ECD_{aer} (μm)	Total Mass (mg)	Uranium (ng)	Significant Uranium (ng)
ESA-V1	LMJ-2	1241	15.9	12.1	0.11	11.4	0
ESA-V1	LMJ-2	1242	15.9	7.7	0.0	11.4	0
ESA-V1	LMJ-2	1243	15.9	5.0	0.02	2.4	0
ESA-V1	LMJ-2	1244	15.9	3.0	0.0	0.0	0
ESA-V1	LMJ-2	1245	15.9	2.0	0.04	0.0	0
ESA-V1	LMJ-2	1246	15.9	1.2	0.0	15.9	0
ESA-V1	LMJ-2	1247	15.9	0.7	0.01	23.4	0
ESA-V1	LMJ-2	1248	15.9	--	0.37	20.4	0
ESA-V2	LMJ-1	1231	15.9	12.1	0.24	5.4	0
ESA-V2	LMJ-1	1232	15.9	8.1	0.02	0.0	0
ESA-V2	LMJ-1	1233	15.9	5.0	0.09	2.4	0
ESA-V2	LMJ-1	1234	15.9	3.0	0.01	0.0	0
ESA-V2	LMJ-1	1235	15.9	1.9	0.0	0.0	0
ESA-V2	LMJ-1	1236	15.9	1.2	0.0	0.0	0
ESA-V2	LMJ-1	1237	15.9	0.7	0.02	0.0	0
ESA-V2	LMJ-1	1238	15.9	--	0.23	3.9	0
ESA-V3	LMJ-3	1141	14.3	12.8	0.56	0.0	0
ESA-V3	LMJ-3	1142	14.3	8.2	0.21	0.0	0
ESA-V3	LMJ-3	1143	14.3	5.2	0.46	3.9	0
ESA-V3	LMJ-3	1144	14.3	3.2	0.33	0.0	0
ESA-V3	LMJ-3	1145	14.3	2.0	0.22	5.4	0
ESA-V3	LMJ-3	1146	14.3	1.3	0.25	2.4	0
ESA-V3	LMJ-3	1147	14.3	0.8	0.09	0.0	0
ESA-V3	LMJ-3	1148	14.3	--	0.35	0.0	0

TABLE K-1 (continued)

External Sampling Array Cascade Impactor Data

Location	Sampler ID No.	Substrate No.	Flow Rate (l/min)	ECD_{aer} (μm)	Total Mass (mg)	Uranium (ng)	Significant Uranium (ng)
ESA-V4	LMJ-25	1131	15.7	12.2	0.62	20.4	0
ESA-V4	LMJ-25	1132	15.7	7.8	0.35	3.9	0
ESA-V4	LMJ-25	1133	15.7	5.0	0.20	0.0	0
ESA-V4	LMJ-25	1134	15.7	3.0	0.13	9.9	0
ESA-V4	LMJ-25	1135	15.7	2.0	0.08	15.9	0
ESA-V4	LMJ-25	1136	15.7	1.2	0.07	0.0	0
ESA-V4	LMJ-25	1137	15.7	0.7	0.04	0.9	0
ESA-V4	LMJ-25	1138	15.7	--	0.28	0.9	0

TABLE K-2
Pole Sampling Array Cascade Impactor Data

Location	Sampler ID No.	Substrate No.	Flow Rate (l/min)	ECD_{aer} (μm)	Total Mass (mg)	Uranium (ng)	Significant Uranium (ng)
W-02	LMJ-14	1261	15.0	12.5	0.02	17.4	0
W-02	LMJ-14	1262	15.0	8.0	0.05	12.9	0
W-02	LMJ-14	1263	15.0	5.1	0.06	15.9	0
W-02	LMJ-14	1264	15.0	3.1	0.03	14.4	0
W-02	LMJ-14	1265	15.0	2.0	0.0	14.4	0
W-02	LMJ-14	1266	15.0	1.2	0.05	11.4	0
W-02	LMJ-14	1267	15.0	0.8	0.08	14.4	0
W-02	LMJ-14	1268	15.0	--	0.23	51.9	41
W-03	LMJ-12	1251	15.8	12.2	0.09	0.0	0
W-03	LMJ-12	1252	15.8	7.8	0.06	2.4	0
W-03	LMJ-12	1253	15.8	5.0	0.0	20.4	0
W-03	LMJ-12	1254	15.8	3.0	0.02	11.4	0
W-03	LMJ-12	1255	15.8	2.0	0.0	5.4	0
W-03	LMJ-12	1256	15.8	1.2	0.02	5.4	0
W-03	LMJ-12	1257	15.8	0.7	0.01	0.0	0
W-03	LMJ-12	1258	15.8	--	0.30	27.9	0
N-02	LMJ-016	1161	15.5	12.3	0.01	11.4	0
N-02	LMJ-016	1162	15.5	7.8	0.01	17.4	0
N-02	LMJ-016	1163	15.5	5.0	0.0	21.9	0
N-02	LMJ-016	1164	15.5	3.1	0.01	0.0	0
N-02	LMJ-016	1165	15.5	2.0	0.0	3.9	0
N-02	LMJ-016	1166	15.5	1.2	0.02	0.0	0
N-02	LMJ-016	1167	15.5	0.7	0.02	29.4	0
N-02	LMJ-016	1168	15.5	--	0.23	14.4	0

TABLE K-2 (continued)
Pole Sampling Array Cascade Impactor Data

Location	Sampler ID No.	Substrate No.	Flow Rate (l/min)	ECD_{aer} (μm)	Total Mass (mg)	Uranium (ng)	Significant Uranium (ng)
N-03	LMJ-26	1271	15.3	12.4	0.0	8.4	0
N-03	LMJ-26	1272	15.3	7.9	0.0	2.4	0
N-03	LMJ-26	1273	15.3	5.1	0.01	2.4	0
N-03	LMJ-26	1274	15.3	3.1	0.03	0.0	0
N-03	LMJ-26	1275	15.3	2.0	0.15	8.4	0
N-03	LMJ-26	1276	15.3	1.3	0.0	15.9	0
N-03	LMJ-26	1277	15.3	0.8	0.0	15.9	0
N-03	LMJ-26	1278	15.3	--	0.25	0.0	0
E-02	LMJ-23	1281	15.4	12.4	0.09	0.0	0
E-02	LMJ-23	1282	15.4	7.9	0.0	74.4	64
E-02	LMJ-23	1283	15.4	5.1	0.0	0.0	0
E-02	LMJ-23	1284	15.4	3.1	0.0	40.0	30
E-02	LMJ-23	1285	15.4	2.0	0.02	0.9	0
E-02	LMJ-23	1286	15.4	1.2	0.0	3.9	0
E-02	LMJ-23	1287	15.4	0.8	0.0	3.9	0
E-02	LMJ-23	1288	15.4	--	0.16	2.4	0
E-03	LMJ-27	1221	15.6	12.3	0.89	5.4	0
E-03	LMJ-27	1222	15.6	7.8	0.01	5.4	0
E-03	LMJ-27	1223	15.6	5.0	0.0	0.0	0
E-03	LMJ-27	1224	15.6	3.1	0.04	0.0	0
E-03	LMJ-27	1225	15.6	1.9	0.12	0.0	0
E-03	LMJ-27	1226	15.6	1.2	0.0	131.4	121
E-03	LMJ-27	1227	15.6	0.7	0.03	0.0	0
E-03	LMJ-27	1228	15.6	--	0.47	0.0	0

TABLE K-2 (continued)
Pole Sampling Array Cascade Impactor Data

Location	Sampler ID No.	Substrate No.	Flow Rate (l/min)	ECD_{aer} (μm)	Total Mass (mg)	Uranium (ng)	Significant Uranium (ng)
S-02	LMJ-11	1151	15.3	12.4	0.07	5.4	0
S-02	LMJ-11	1152	15.3	7.9	0.04	0	0
S-02	LMJ-11	1153	15.3	5.1	0	8.4	0
S-02	LMJ-11	1154	15.3	3.1	0.14	0	0
S-02	LMJ-11	1155	15.3	2.0	0.03	0	0
S-02	LMJ-11	1156	15.3	1.2	0.04	3.9	0
S-02	LMJ-11	1157	15.3	0.8	0	0	0
S-02	LMJ-11	1158	15.3	--	0.31	6.9	0
S-03	LMJ-17	1211	14.6	12.7	0.31	5.4	0
S-03	LMJ-17	1212	14.6	8.1	0.02	5.4	0
S-03	LMJ-17	1213	14.6	5.2	0	0	0
S-03	LMJ-17	1214	14.6	3.2	0.01	0	0
S-03	LMJ-17	1215	14.6	2.0	0	0	0
S-03	LMJ-17	1216	14.6	1.3	0.02	131.4	121
S-03	LMJ-17	1217	14.6	0.8	0	0	0
S-03	LMJ-17	1218	14.6	--	0.33	0	0

TABLE K-3
Tunnel Sampling Array Cascade Impactor Data

Location	Sampler ID No.	Substrate No.	Flow Rate (l/min)	ECD_{aer} (μm)	Total Mass (mg)	Uranium Mass (ng)	Significant U (ng)	MMAD U (μm)	σ_g
TSA-1+	LMJ-18	1111	15.1	12.4	4.88	1829	1802	3.3	33.0
TSA-1+	LMJ-18	1112	15.1	8.0	1.10	217	203	3.3	33.0
TSA-1+	LMJ-18	1113	15.1	5.1	0.53	272	260	3.3	33.0
TSA-1+	LMJ-18	1114	15.1	3.1	0.38	259	248	3.3	33.0
TSA-1+	LMJ-18	1115	15.1	2.0	0.26	233	222	3.3	33.0
TSA-1+	LMJ-18	1116	15.1	1.2	0.12	251	240	3.3	33.0
TSA-1+	LMJ-18	1117	15.1	0.8	0.03	164	154	3.3	33.0
TSA-1+	LMJ-18	1118	15.1	--	0.37	1829	1818	3.3	33.0
TSA-2#	LMJ-21	1101	15.3	12.4	9.70	27500	27456	6.5	15.5
TSA-2#	LMJ-21	1102	15.3	7.9	3.55	6549	6527	6.5	15.5
TSA-2#	LMJ-21	1103	15.3	5.1	3.15	5992	2971	6.5	15.5
TSA-2#	LMJ-21	1104	15.3	3.1	3.24	6083	6062	6.5	15.5
TSA-2#	LMJ-21	1105	15.3	2.0	2.57	5526	5507	6.5	15.5
TSA-2#	LMJ-21	1106	15.3	1.2	1.27	4655	4640	6.5	15.5
TSA-2#	LMJ-21	1107	15.3	0.8	0.54	6594	6582	6.5	15.5
TSA-2#	LMJ-21	1108	15.3	--	0.60	11418	11406	6.5	15.5

+TSA-1--Cascade Impactor was Outside Tunnel

#TSA-2--Cascade Impactor was Inside Tunnel

exit. The TSA-2 cascade impactor was located about 2 meters south of the door but inside the tunnel. Statistically significant quantities of uranium were detected using uranium fluorometric analyses on all eight stages of each impactor as shown in column 8. Column 9 shows the calculated mass median aerodynamic diameter (MMAD) in micrometers and column 10 shows the geometric standard deviation of the median diameter. The particle size distribution data of Table K-3 is plotted in Figure K-1, which shows the cumulative percent of uranium oversize as a function of aerodynamic diameter (AD) in micrometers. The size fractions were fitted by least squares to a log-normal size distribution. Note that both plots predict approximately 60 percent by mass of uranium is smaller than 10 μm aerodynamic diameter. The MMAD for TSA-1 (outside sampler) is 3.3 μm with a standard deviation of 33. The MMAD for TSA-1 (tunnel sampler) is 6.5 μm with a standard deviation of 15.5. Since it was observed during the disassembly and analysis of the impactor samples that the stages were heavily loaded with sampled material, these aerosol characterizations are not considered to be reliable. The large geometric standard deviations (33 and 15) imply a highly skewed distribution which is not reasonable in light of the typical soil size distributions and those of previous experiments with uranium tracers. It is, therefore, concluded that the size distribution data determined from the tunnel array impactors are impaired as a result of overloaded stages and are not representative of the true size distributions of released tracer material.

Balloon Sampling Array

Table K-4 shows cascade impactor data for Mercer impactors used in the Balloon Sampling Array (BSA). The uranium mass collected on each stage was determined by uranium fluorometry and by delayed neutron analysis for selected samples as shown in column 6. The MMAD and geometric standard deviations are shown in columns 8 and 9, respectively. Significant quantities of uranium were collected on four stages of impactors located at C-6 (76 ng), F-6 (80 ng), and C-3 (110 ng).

Figure K-2 shows the cumulative uranium mass distribution versus the effective cutoff diameter for impactors F-6, C-6, and C3 as well as a BSA composite. The calculated MMAD for F-6 was approximately 5 μm with a geometric standard deviation of 2.2. The MMAD for C-6 was calculated to be 2 μm with a standard deviation of 4. However, the fitted line for C-6 appears to be at odds with the significant stage collections. An approximate line suggests that a σ_g of 2.7 is more appropriate with a MMAD of 3.2 μm. For impactor C-3 no calculated fit was possible, but an estimated distribution is shown in Figure K-2. This suggests a MMAD of 7.2 m and a σ_g of 2. These distributions indicate respirable fractions from 62 to 88 percent. The goodness of-fit test performed on F-6 and C-6 impactor data was statistically significant at the 95 percent confidence level for C-6 and at the 99 percent confidence level for F-6. Approximately 70 percent of the uranium detected by the BSA impactors was smaller than 10 μm aerodynamic diameter. If it is assumed that all samplers saw the same aerosol and the stage collections are pooled, then a composite distribution shown in Figure K-2 with MMAD = 5 μm and σ_g = 3.6 is obtained.

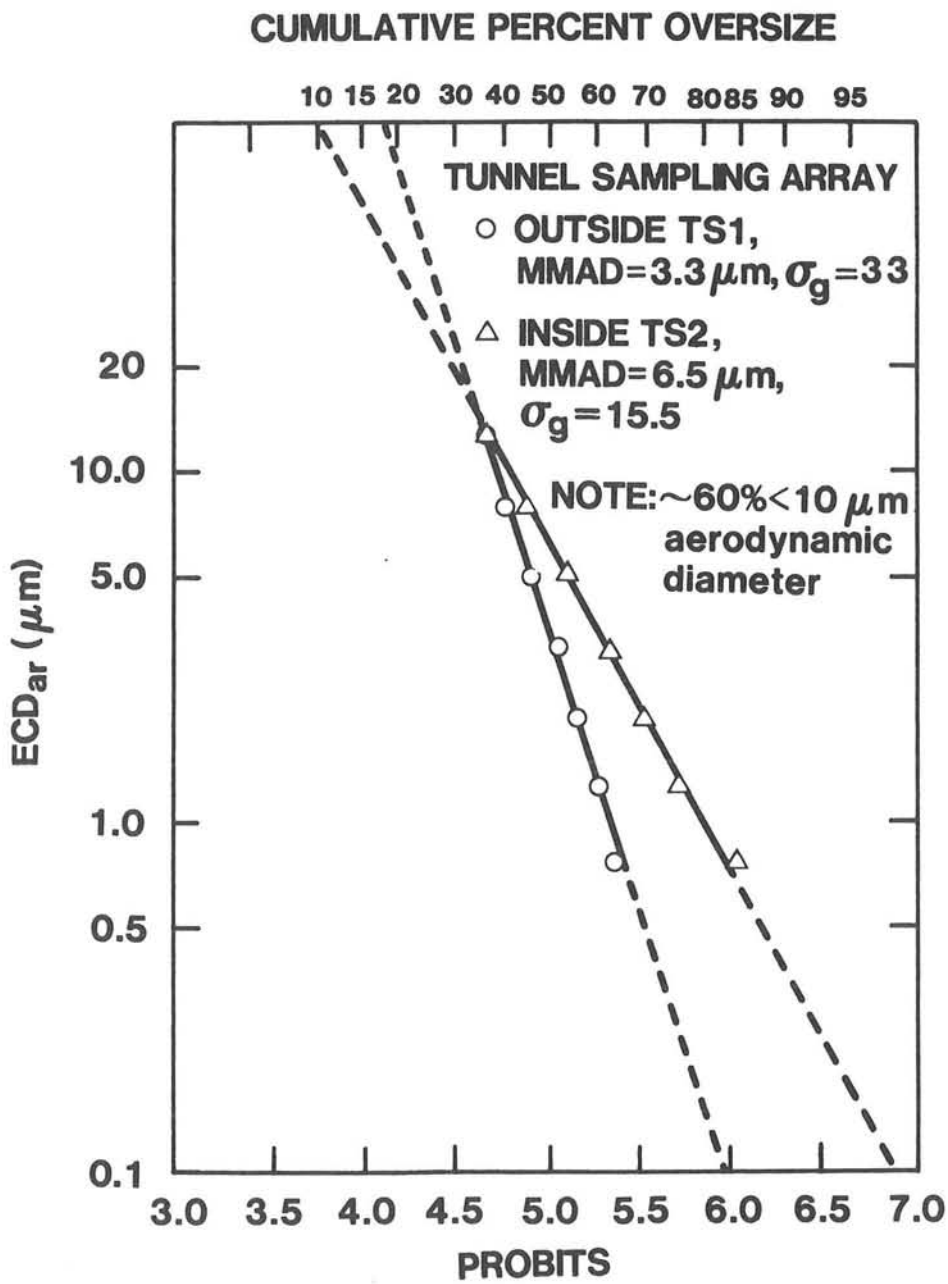

Figure K-1. Size Distribution for GGTSA Impactors

TABLE K-4
Balloon Sampling Array Cascade Impactor Data

Location	Sampler ID No.	Substrate No.	Flow Rate (l/min)	ECD_{aer} (μm)	Uranium Mass (ng)	Significant U (ng)	MMAD U (μm)	σ_g
C-6	EE-64	4161	0.600	6.1	21.9	22	2.0	4.03
C-6	EE-64	4162	0.600	3.8	3.9	4	2.0	4.03
C-6	EE-64	4163	0.600	2.7	0.9	0	2.0	4.03
C-6	EE-64	4164	0.600	2.1	0.0	0	2.0	4.03
C-6	EE-64	4165	0.600	1.4	0.0	0	2.0	4.03
C-6	EE-64	4166	0.600	1.0	38.4	38	2.0	4.03
C-6	EE-64	4167	0.600	0.4	8.4	8	2.0	4.03
C-6	EE-64	4168	0.600	--	0.0	0	2.0	4.03
D-6	EE-66	4211	0.635	6.0	0.0	0	-	-
D-6	EE-66	4212	0.635	3.7	0.9	0	-	-
D-6	EE-66	4213	0.635	2.8	0.0	0	-	-
D-6	EE-66	4214	0.635	2.0	0.0	0	-	-
D-6	EE-66	4215	0.635	1.4	0.0	0	-	-
D-6	EE-66	4216	0.635	1.1	0.9	0	-	-
D-6	EE-66	4217	0.635	0.4	0.0	0	-	-
D-6	EE-66	4218	0.635	-	-	-	-	-

TABLE K-4 (continued)
Balloon Sampling Array Cascade Impactor Data

Location	Sampler ID No.	Substrate No.	Flow Rate (l/min)	ECD_{aer} (μm)	Uranium Mass (ng)	Significant U (ng)	MMAD U (μm)	σ_g
E-6	CEOG69	4231	0.585	6.2	0.0	0	-	-
E-6	CEOG69	4232	0.585	3.8	0.0	0	-	-
E-6	CEOG69	4233	0.585	2.7	0.0	0	-	-
E-6	CEOG69	4234	0.585	2.1	0.0	0	-	-
E-6	CEOG69	4235	0.585	1.4	0.0	0	-	-
E-6	CEOG69	4236	0.585	0.9	0.9	0	-	-
E-6	CEOG69	4237	0.585	0.4	0.0	0	-	-
E-6	CEOG69	4238	0.585	--	0.9	0	-	-
F-6	AW-63	4151	0.600	6.2	35.4	35	5.1	2.2
F-6	AW-63	4152	0.600	3.8	17.4	17	5.1	2.2
F-6	AW-63	4153	0.600	2.7	0.9	0	5.1	2.2
F-6	AW-63	4154	0.600	2.1	18.9	19	5.1	2.2
F-6	AW-63	4155	0.600	1.4	0.9	0	5.1	2.2
F-6	AW-63	4156	0.600	0.9	5.4	5	5.1	2.2
F-6	AW-63	4157	0.600	0.4	0.9	0	5.1	2.2
F-6	AW-63	4158	0.600	-	0.0	0	5.1	2.2
C-3	AW-65	4171	0.600	6.2	65.4	65	7.8	3.0
C-3	AW-65	4172	0.600	3.8	14.4	14	7.8	3.0
C-3	AW-65	4173	0.600	2.7	12.9	13	7.8	3.0
C-3	AW-65	4174	0.600	2.1	17.4	17	7.8	3.0
C-3	AW-65	4175	0.600	1.4	0.0	0	7.8	3.0
C-3	AW-65	4176	0.600	0.9	0.0	0	7.8	3.0
C-3	AW-65	4177	0.600	0.4	0.0	0	7.8	3.0
C-3	AW-65	4178	0.600	-	0.0	0	7.8	3.0

TABLE K-4 (continued)
Balloon Sampling Array Cascade Impactor Data

Location	Sampler ID No.	Substrate No.	Flow Rate (l/min)	ECD_{aer} (μm)	Uranium Mass (ng)	Significant U (ng)	MMAD U (μm)	σ_g
D-3	AX-67	4221	0.600	6.1	0.0	0	-	-
D-3	AX-67	4222	0.600	3.8	0.9	0	-	-
D-3	AX-67	4223	0.600	2.7	0.0	0	-	-
D-3	AX-67	4224	0.600	2.1	0.0	0	-	-
D-3	AX-67	4225	0.600	1.4	0.0	0	-	-
D-3	AX-67	4226	0.600	0.95	0.0	0	-	-
D-3	AX-67	4227	0.600	0.4	0.0	0	-	-
D-3	AX-67	4228	0.600	--	0.0	0	-	-
E-3	CEDD-61	4181	0.625	6.2	0.0	0	-	-
E-3	CEDD-61	4182	0.625	3.8	2.5	2.5	-	-
E-3	CEDD-61	4183	0.625	2.7	0.0	0	-	-
E-3	CEDD-61	4184	0.625	2.1	0.0	0	-	-
E-3	CEDD-61	4185	0.625	1.4	0.0	0	-	-
E-3	CEDD-61	4186	0.625	0.9	0.0	0	-	-
E-3	CEDD-61	4187	0.625	0.4	0.0	0	-	-
E-3	CEDD-61	4188	0.625	-	4.0	4	-	-
F-3	CEDA-68	4191	0.600	6.1	0.0	0	-	-
F-3	CEDA-68	4192	0.600	3.7	0.9	0	-	-
F-3	CEDA-68	4193	0.600	2.8	0.0	0	-	-
F-3	CEDA-68	4194	0.600	2.0	0.0	0	-	-
F-3	CEDA-68	4195	0.600	1.4	0.0	0	-	-
F-3	CEDA-68	4196	0.600	0.9	0.0	0	-	-
F-3	CEDA-68	4197	0.600	0.4	0.0	0	-	-
F-3	CEDA-68	4198	0.600	-	0.0	0	-	-

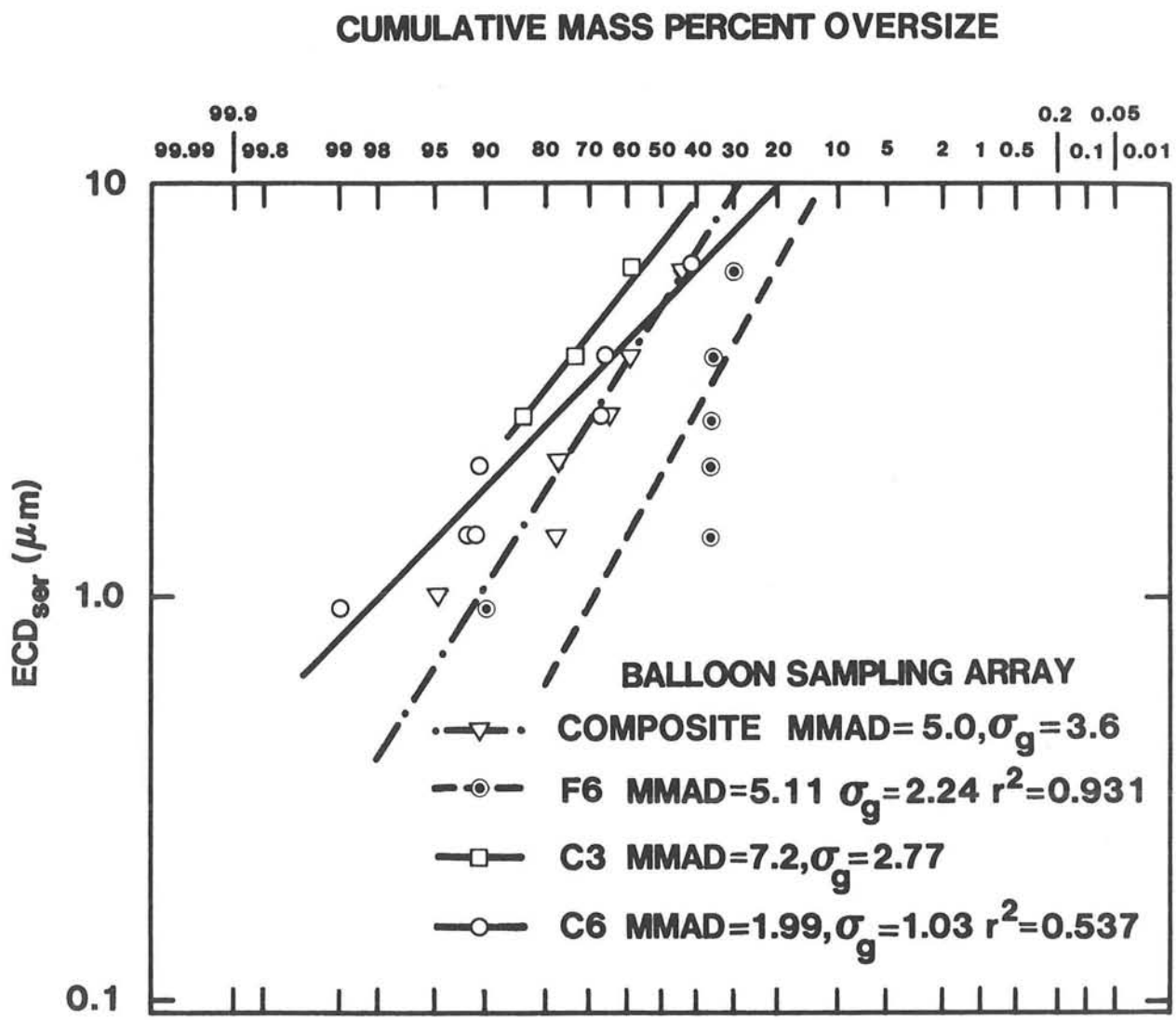

Figure K-2. Size Distribution for GGBSA Impactors With Significant Collections

Appendix L
Analysis of Cloud Growth, Release, and Particle Trajectories

Calculation of the maximum respirable airborne tracer material released from the Gravel Gertie confinement structure is presented in this Appendix. Two methods were used to compute the mass of released tracer aerosol: (1) calculation by cloud volume; and (2) calculation by cloud flux. Measurements of the displacement of the top of the gravel bed and its vertical velocity as a function of time are shown. Also provided are views of the cloud outline at various times and an analysis of the trajectories of the observed ballistic particles.

Gravel Bed Displacement

Figure L-1 shows the displacement of the gravel bed peak as a function of time. The 25 frame-per-second (fps) NE camera was used for this figure. Pictures were scanned digitally to detect the gravel interface and machine counts were converted to distance using ten readings taken before detonation to calibrate machine counter measurements. The frame containing the fiducial flash was frame 0. Figure L-2 shows the average vertical velocity using the data from Figure L-1.

Figures L-3, L-4, and L-5 illustrate cloud formation from three views (NE, SE, and SW) traced from the 10 fps films. First visible motion of gravel bed (apex) was chosen as t = 0. Each frame image was projected on graph paper with the five visible poles and instrument levels marked as distance/angle fiducials. The pretest outline of the gravel bed was traced for reference. The cloud was then traced at times of approximately t = 12 seconds and t = 36 seconds.

Figure L-6 illustrates the cloud formation using the SE 10 FPS camera at times t = 3, 4, and 8 seconds. Cloud information shown in Table L-1 was obtained from Figure L-6. The cloud appeared to stabilize (no significant further radial expansion) at times greater than or equal to 8 seconds. Less than 5 percent volumetric expansion was measured from t = 8 seconds to t = 12 seconds. The cloud transport velocity at a height of 11 meters was estimated to be 0.5 m/sec after t = 12 seconds. The direction of the transport velocity vector appeared to be approximately 75° east of north for times less than two minutes postdetonation. Cloud movement velocity at 3 meters above ground level was approximately 1 m/sec. Cloud arrival times at the DSA location (10.7 m) and BSA location (47.7 m) were 1.4 seconds and 8 seconds, respectively.

A stabilized cloud volume at t = 12 seconds was estimated from film measurements to be 4.64×10^4 m^3. At t = 6 seconds, the volume was approximately 3.3×10^4 m^3. The average cross-sectional area of the cloud transverse to the wind at t = 8 to 12 seconds was approximately 955 m^2. The following assumptions were made in calculating these volumes: (1) the

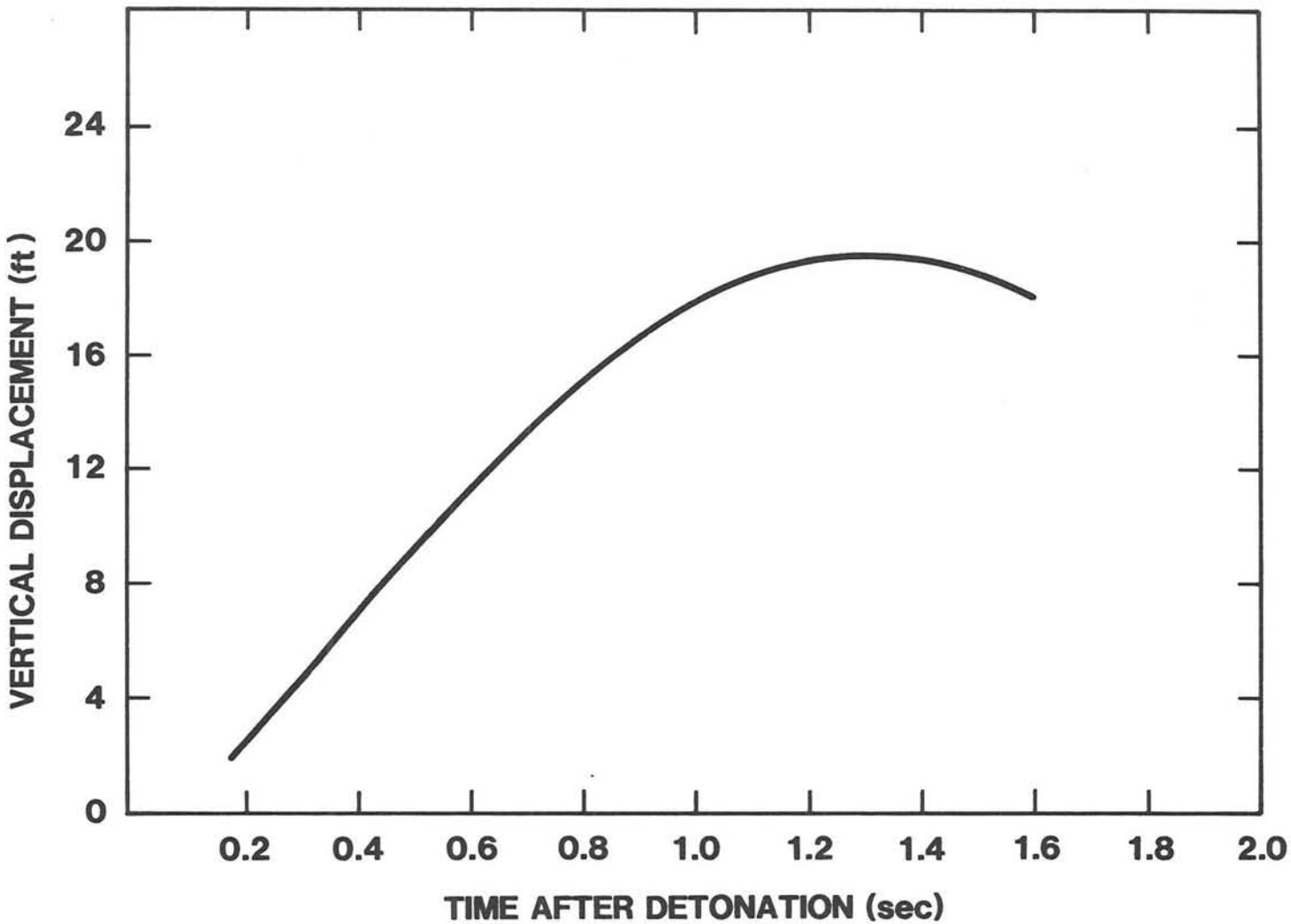

Figure L-1. Early Growth of Gravel Bed Dome

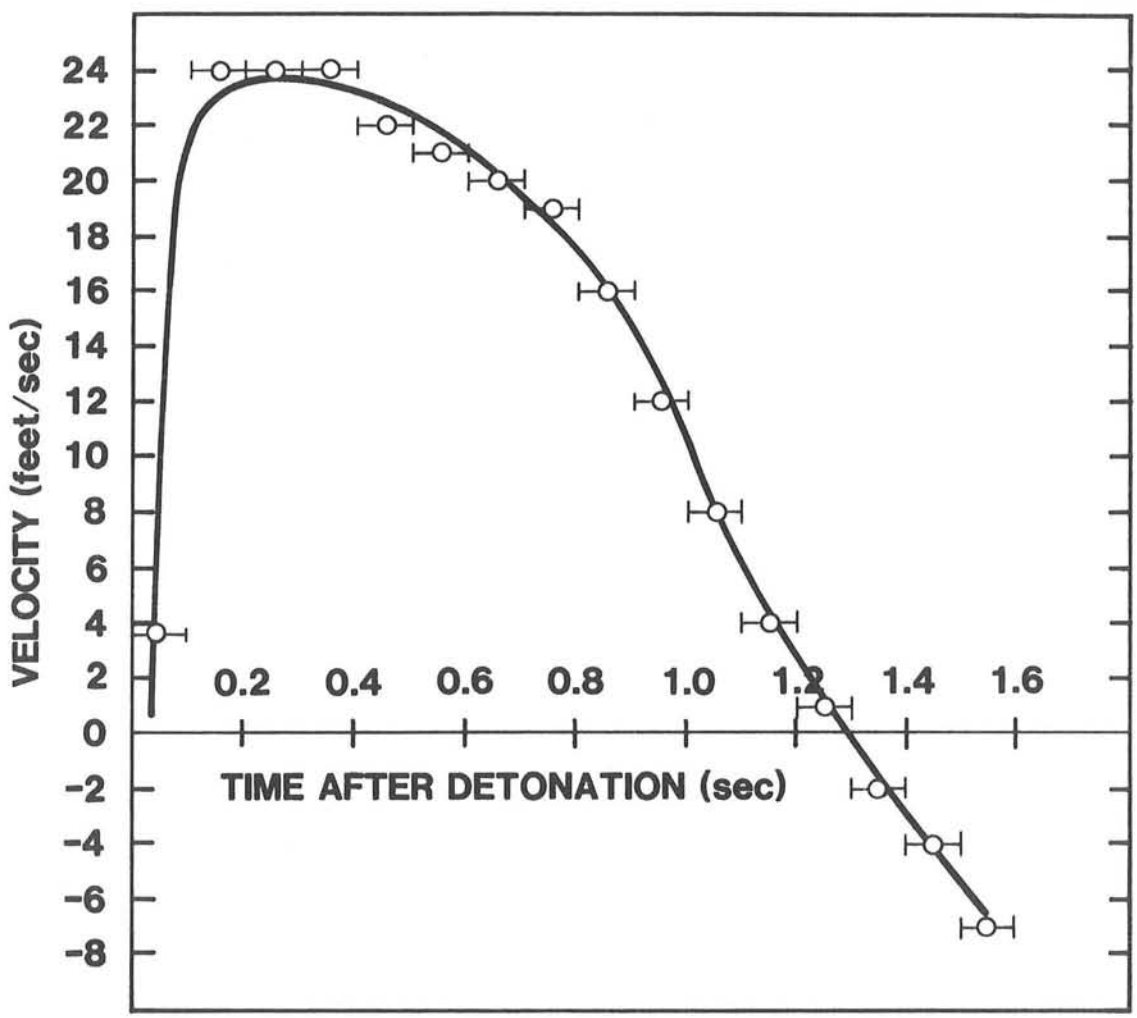

Figure L-2. Vertical Velocity of Gravel Bed

Figure L-3. Cloud Profiles From NE

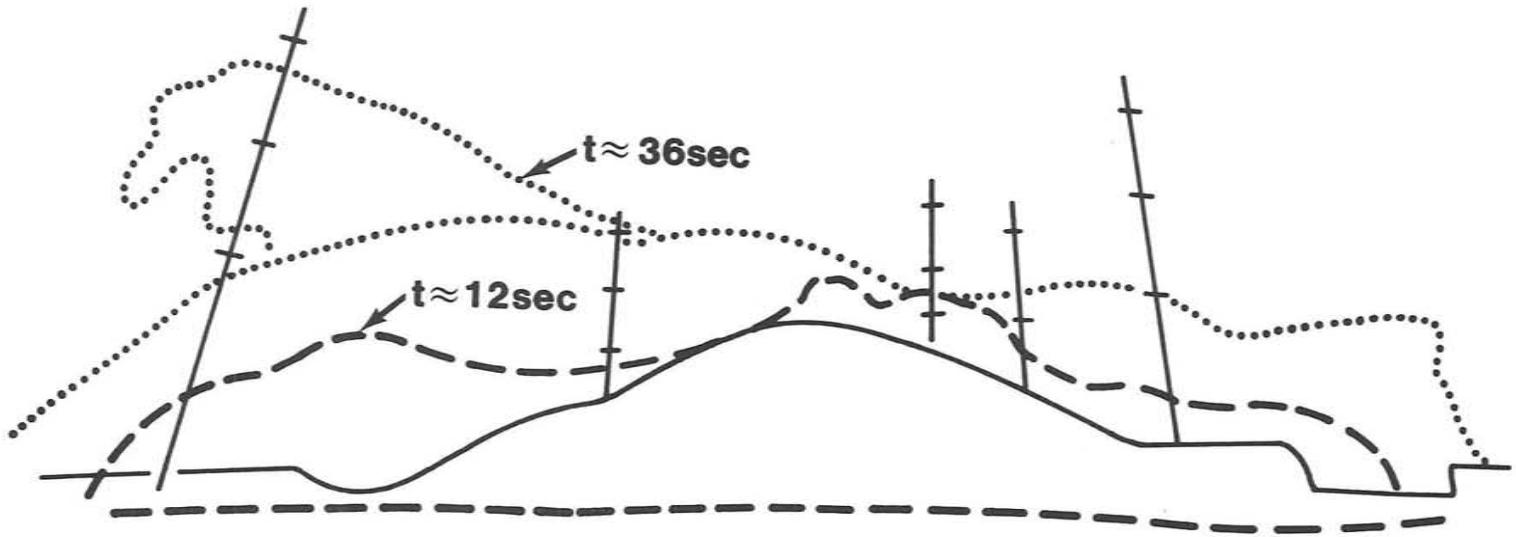

Figure L-4. Cloud Profiles From SE

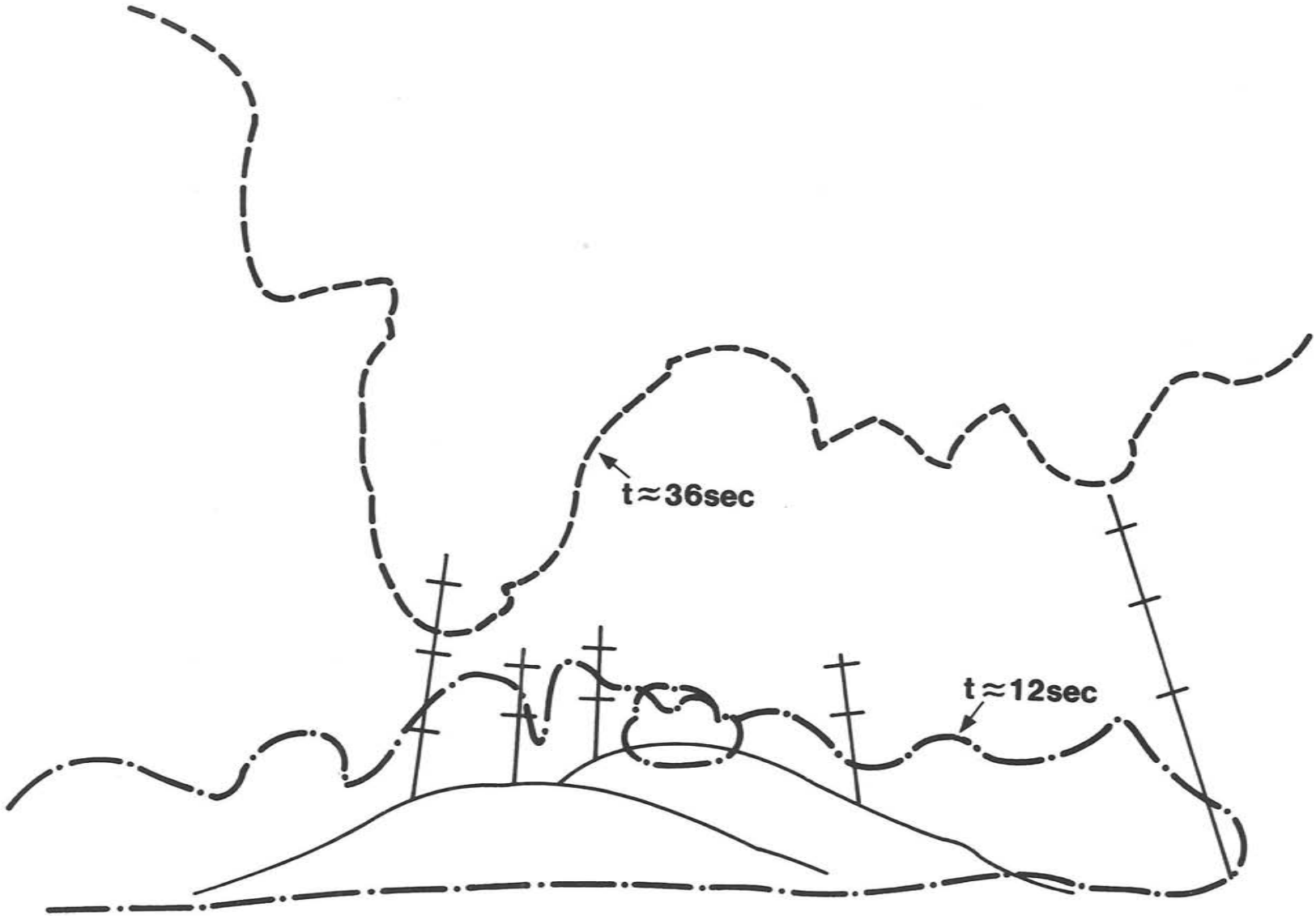

Figure L-5. Cloud Profiles from SW

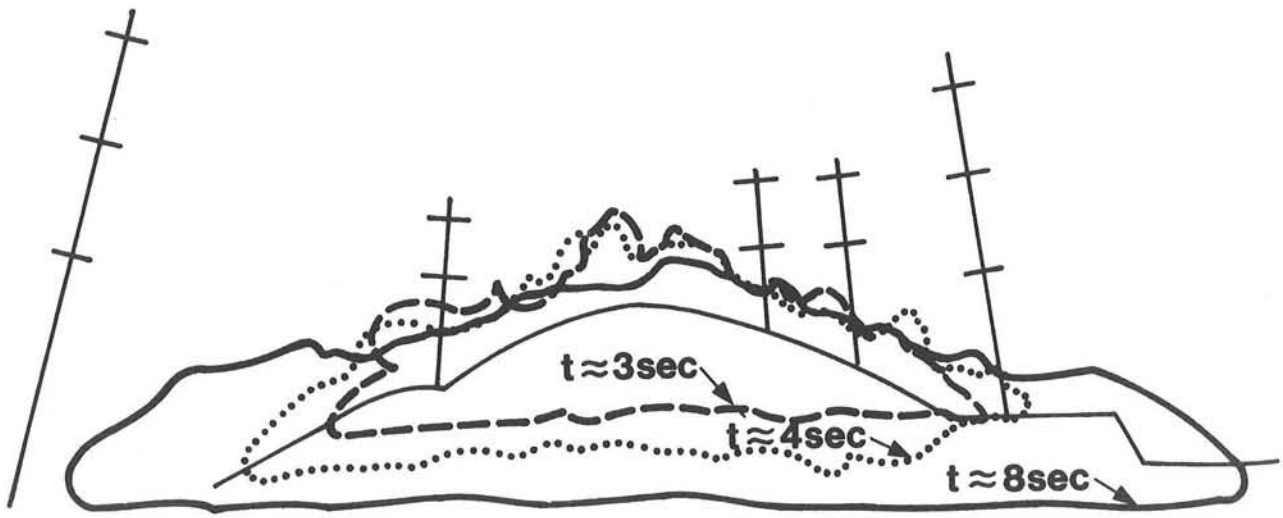

Figure L-6. Cloud Profiles at 3, 4, and 8 Seconds from SE

TABLE L-1
Summary of Measured Cloud Parameters

Sampling System	t_a	t_s	ν_t	Δs	V(4)	V(6)	V(12)	$A_c(8)$
	sec	sec	m/s	m	m^3	m^3	m^3	m^2
DSA	1.4	12	0.5	53	1.9×10^4	3.3×10^4	4.6×10^4	---
BSA	8	12	1.0	122	---	---		955

t_a = time of cloud arrival at sampling station

t_s = time of cloud stabilization (no further volumetric expansion)

ν_t = cloud transport velocity (by wind vector after cloud stabilization

Δs = distance over which cloud is transported past sampling station (after cloud stabilization)

V(4) = volume of cloud at t = 4 seconds postdetonation

V(6) = volume of cloud at t = 6 seconds

V(12) = volume of cloud at t = 12 seconds

$A_c(8)$ = cross-sectional area of cloud at t = 8 seconds postdetonation.

projected cloud images from the SE camera film were assumed to be semisymmetric (ie, the cloud was composed of a forward quarter sphere and an after quarter sphere, each with a different radius), and (2) the volume of gravel bed and overburden was estimated to be a spherical body having a radius of 45.3 m. The cloud volumes were then calculated using the equation:

$$V(t) = \frac{\pi \Delta h}{2} \sum_{i=1}^{n} r_i(t)^2 - 1/3\ \pi h^2 (3R-h) \qquad \text{(L-1)}$$

The parameters used in Eq. (L-1) are defined in Figure L-7. The assumption of a spherical gravel bed and overburden leads to an overestimate of cloud volume and, therefore, to an overprediction of the quantity of released tracer mass.

1. Calculation by Cloud Volume Using DSA Data

The maximum total respirable airborne uranium released from the GG structure may be calculated using uranium samples obtained from the DSA system as presented in Table L-2. The measured uranium airborne mass is a function of the flow rate (f), the sample time (Δt) and the time averaged aerosol density (assuming a uniform spatial concentration in the cloud) ($\overline{\rho}(\Delta t_1)$). Because there is a sample period during the radial expansion of the cloud ($\Delta t_1 = t_s - t_s$) and a sampling period corresponding to the transport period of the cloud past the sampling stations, an equation for the sampled airborne mass may be written as:

$$M_m = f(\Delta t_1 \cdot \overline{\rho}_1(\Delta t_1) + \Delta t_2 \cdot \overline{\rho}_2(\Delta t_2)) \qquad \text{(L-2)}$$

where

$\Delta t_1 = t_s - t_a$ (1st sample period)
$\Delta t_2 = \Delta s / \nu_t$ (2nd sample period)
Δs = distance cloud travels during sampling after cloud stabilization
ν_t = cloud transport velocity
t_s = time at which cloud stabilizes
t_a = time of arrival of cloud at sampling station

The total mass of airborne tracer in the cloud during sampling is given by:

$$M_T = \overline{\rho}_1\ (\Delta t_1) \cdot V\ (\Delta t_1) = \overline{\rho}_2\ \ (\Delta t_2) \cdot V\ (\Delta t_2) \qquad \text{(L-3)}$$

Therefore, the total mass of airborne tracer aerosol in the cloud during the sampling period is

$$M_T = \frac{M_m}{f \left[\frac{\Delta t_1}{V(\Delta t_1)} + \frac{\Delta t_2}{V(\Delta t_2)} \right]} \qquad \text{(L-4)}$$

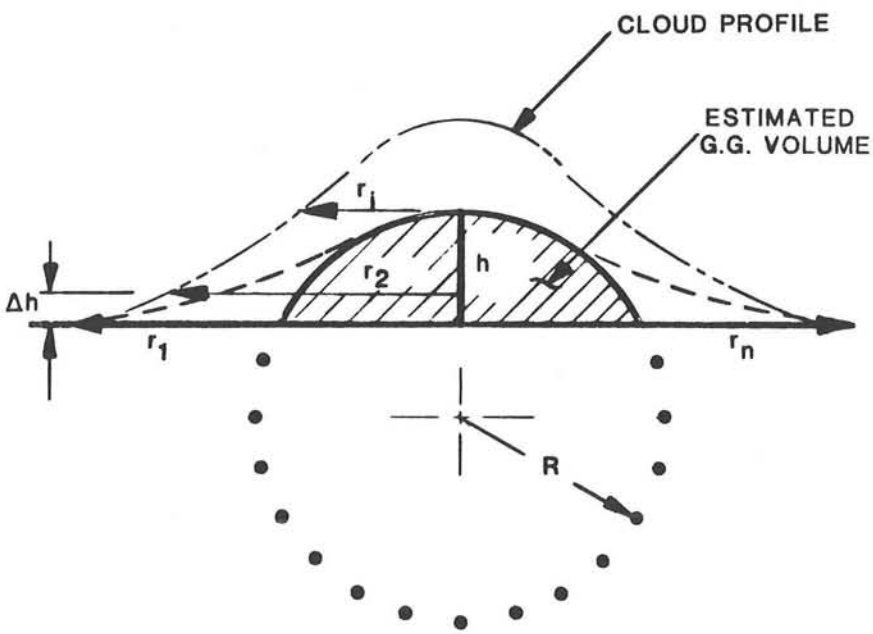

Figure L-7. Schematic Representation of Cloud Volume Calculation

TABLE L-2

Parameters Used to Evaluate Eq. (L-4) Based Upon DSA Data

Station Number	M_m	f	Δs	ν_t	t_s	t_a	V(6)	V(12)	M_T
	($\times 10^{-9}$ g)	(m^3/s)	(m)	(m/s)	(seconds)	(seconds)	(m^3)	(m^3)	(g)
DSA-1	11.0	3.6×10^{-5}	53	0.5	12	1.4	3.3×10^{4}	4.6×10^{4}	0.11
DSA-2	4.3	3.3×10^{-5}	53	0.5	12	1.4	3.3×10^{4}	4.6×10^{4}	0.05
DSA-3	10.8	3.2×10^{-5}	53	0.5	12	1.4	3.3×10^{4}	4.6×10^{4}	0.13
DSA-4	150.0	3.1×10^{-5}	53	0.5	12	1.4	3.3×10^{4}	4.6×10^{4}	1.9
DSA-5	120.0	3.4×10^{-5}	53	0.5	12	1.4	3.3×10^{4}	4.6×10^{4}	1.3
DSA-6	270.0	2.4×10^{-5}	53	0.5	12	1.4	3.3×10^{4}	4.6×10^{4}	4.2
DSA-7	18.5	3.7×10^{-5}	53	0.5	12	1.4	3.3×10^{4}	4.6×10^{4}	0.19
DSA-8	0.0	3.3×10^{-5}	53	0.5	12	1.4	3.3×10^{4}	4.6×10^{4}	0.0

$$\overline{M}_T = \frac{1}{8}\sum_{i=1}^{8} M_{T_i} = 0.98 \text{ g} \qquad \text{(L-5)}$$

where

$V(\Delta t_1)$ = average cloud volume over $(t_s - t_a)$ period
$V(\Delta t_2)$ = average cloud volume at $t > t_s$
$_1(\Delta t_1)$ = time-averaged aerosol density over sample period t_1
$_2(\Delta t_2)$ = time-averaged aerosol density over sample period t_2

Equation (L-4) was evaluated for each of the sampling stations in the GGDSA using Table L-2. The sampled uranium mass (M_m), corrected for background soil contribution and instrument error, is shown in column 1. Flow rates (F) are also shown. The distance which the cloud travels past each sampling station (Δs) is shown in column 3. A Δs of 53 meters corresponding to sampling station DSA6, which sampled the largest quantity of uranium, was selected for a conservative estimate of M_T. Cloud volumes averaged over the sampling period $(t_s - t_a)$ and $\Delta s/\nu_t$ were also calculated. The total mass (M_T) in the cloud as measured by each sampling station of the DSA is shown in the last column. The averaged total uranium mass in the cloud measured by the eight DSA stations is 0.98 $\pm$ 0.20 grams.

2. Calculation by Cloud Flux at BSA Station

The total respirable airborne uranium released from the GG structure may also be calculated by estimating the uranium aerosol flux impinging on the BSA curtain. The mass of uranium tracer aerosol intercepted by the balloon curtain may be calculated using the following:

$$M_{T,u} = \frac{\bar{M}_{s,u}}{f} \cdot \nu_t \cdot A_c \qquad \text{(L-6)}$$

where

$M_{s,u}$ = averaged uranium mass collected by BSA
ν_t = transport velocity of cloud
f = flow rate of samplers
A_c = cross-sectional area of cloud

Two techniques were used in estimating the cloud uranium mass from the BSA data. The first was an attempt to be conservative in these estimates. An upper limit value of the uranium aerosol sample mass was used in these calculations instead of an average value for $M_{s,u}$. Table L-3 lists the parameters used to evaluate Eq. (L-6). Using this conservative technique, a total uranium airborne aerosol mass of 2.8 g was estimated in the cloud at $t \approx 100$ seconds postdetonation based upon the uranium aerosol collected in the Balloon Sampling Array.

A more detailed calculation of the total aerosol mass from BSA data was attempted by utilizing each BSA data point and the area it represented. Aerosol mass in the area sampled by the lowest line of samplers was doubled to account for segments of the base surge cloud which were not intercepted by the

TABLE L-3

Parameters Used to Evaluate Eq. L-6 Based Upon BSA Data

$M_{s,u}$	ν_t	f	A_c	A_{BSA}	$M_{T,u}$
($x10^{-9}$g)	(m/s)	(m^3/s)	(m^2)	(m^2)	(g)
508	1.0	$1.7x10^{-4}$	955	2200	2.8

BSA array. Above the lowest level (F level), the cloud was almost fully intercepted by the BSA array. Details of this calculation, which yielded an estimated mass of 0.6 $\pm$ 0.3 grams, are shown in Table L-4.

The mass release value from the detailed calculation using the BSA data is in good agreement with the value calculated using the DSA Data, that is, about 0.98 g. It is emphasized that the total uranium aerosol releases calculated by these two methods are likely to be upper bounds because of the uniform distribution assumptions and generous estimate of cloud volume.

Analysis of Sb_2O_3 Tracer Release in the Full-Scale GG Test

One kg of Sb_2O_3 was suspended in four ashless filter paper bags from the Gravel Gertie round room ceiling as a backup tracer to uranium. Figure L-8 presents two preshot particle size distributions of the Sb_2O_3 powder. A particle size distribution based on particle weight was obtained from the supplier, Cerac, Inc. The other size distribution was determined at SNL by particle count using a scanning electron microscope (SEM). Although the curves are not log-normal, they both show that at least 90% of the Sb_2O_3 particles have a geometric diameter 10 μm in compliance with the manufacturer's specifications. The count median and count mean particle diameters are about 3.5 μm and 5.3 μm, respectively. The mass median diameter is about 1.2 μm. Count median and mean particle diameters determined by SEM are expected to be larger than actual particle size because of the effect of particle agglomeration.

Instrumental thermal neutron activation analysis of Sb deposits on Balloon Sampling Array (BSA) filter and cascade impactor samplers was performed at LANL. Table L-5 summarizes the results of the LANL analysis.

In this analysis the Y-Z plane of the BSA was divided into 48 sampling areas at the center of which a sampler was located. One-half the distance between adjacent samplers was assigned to sampler j and the other one-half to sampler j+1. For the outer perimeter samplers, the sides of the imaginary rectangle are extended an amount equal to one-half the distance between samplers. The bottom samplers (F1 through F8) were extended 4 feet to ground level. Sample areas are shown in Table L-5.

The total Sb tracer mass (Q) passing through the Balloon Sampler Array may be calculated from the following:

$$Q = \sum_{j=1}^{48} \frac{A_j D_j W_j}{S_j} \qquad \text{(L-8)}$$

TABLE L-4

BSA Cloud Intercept Flux Calculation

BSA STATION	$M_{s,u}/f$	ν_t	A*	S**	M_u
	$\mu g\text{-}s/m^3$	m/s	m^2		mg
F1	2239	0.5	28.8	2	64
F2	2735	0.5	28.8	2	79
F3	799	0.5	49.5	2	40
F4	1117	0.5	59.4	2	66
F5	536	0.5	60.4	2	32
F6	1335	0.5	51.4	2	69
F7	1113	0.5	30.0	2	33
F8	1920	0.5	30.0	2	58
E1	1240	0.4	31.5	1	16
E2	1038	0.4	31.5	1	13
E3	588	0.4	54.4	1	13
D1	477	0.5	28.7	1	7
C3	393	0.8	46.3	1	15
B3	593	1.0	86.9	1	52

*Areas were calculated using the Mid-Point distances between samplers.

**Factor used to account for that portion of cloud that missed samplers.

$$M_{T,u} = \sum_{i=1}^{14} M_{s,u_i}/f \cdot \left(\nu_t\right)_i \cdot A_i S_i \qquad \text{(L-7)}$$

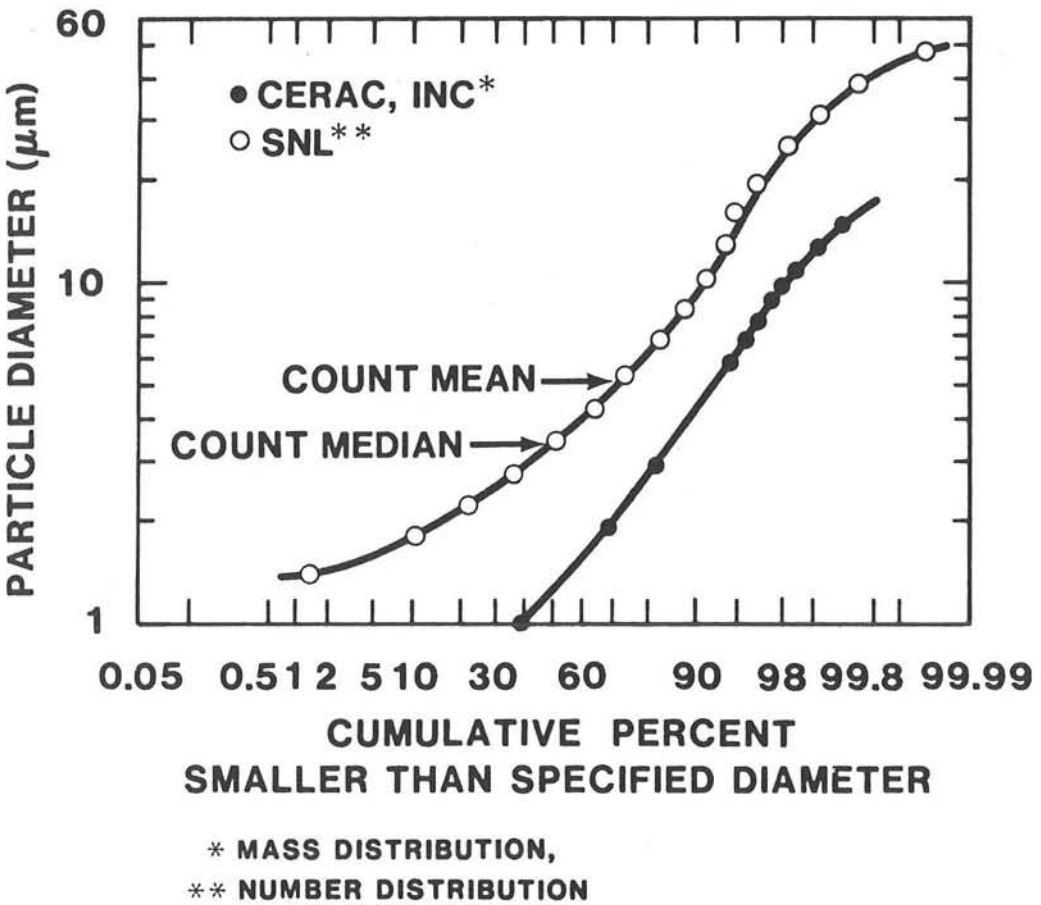

Figure L-8. Preshot Sb_2O_3 Particle Size Distribution

TABLE L-5

Data Used to Calculate Sb Release

BSA Sampler Location	Flow Rate (ℓ/min)	Sb Mass (ng)	Sb Concentration (ng-min/ℓ)	Wind Velocity (m/min)	Sample Area (m^2)
A1	10.0	.0	0.4	80	76.8
B1	10.0	--	--	61	52.5
C1	11.0	34.0	3.1	51	28.0
D1	11.0	5.0	0.4	39	28.0
E1	11.0	27.0	2.4	29	32.8
F1	11.0	75.0	6.8	30	30.0
A2	9.0	--	--	80	76.8
B2	10.0	--	--	61	52.5
C2	10.0	--	--	51	28.0
D2	10.0	10.0	1.0	39	28.0
E2	10.0	11.0	1.1	29	32.8
F2	11.0	53.0	4.8	30	30.0
A3	9.0	27.0	3.0	80	130.6
B3	10.0	--	--	61	89.0
C3	10.0	13.0	1.3	51	47.5
D3	10.0	--	--	39	47.5
E3	11.0	37.0	3.4	29	55.8
F3	10.0	21.0	2.1	30	51.0
A4	9.0	--	--	80	155.1
B4	9.0	2.0	0.2	61	105.7
C4	10.0	2.0	0.2	51	56.4
D4	10.0	6.0	0.6	39	56.4
E4	10.0	14.0	1.4	29	66.3
F4	10.0	2.0	0.2	30	60.6
A5	10.0	--	--	80	154.8
B5	9.0	--	--	61	105.6
C5	9.0	--	--	51	56.3

TABLE L-5

Data Used to Calculate Sb Release
(continued)

BSA Sampler Location	Flow Rate (ℓ/min)	Sb Mass (ng)	Sb Concentration (ng-min/ℓ)	Wind Velocity (m/min)	Sample Area (m^2)
D5	10.0	22.0	2.2	39	56.3
E5	10.0	--	--	29	66.2
F5	10.0	4.0	0.4	30	60.5
A6	10.0	2.0	0.2	80	130.2
B6	10.0	--	--	61	88.8
C6	10.0	5.0	0.5	51	47.4
D6	11.0	--	--	39	45.4
E6	11.0	1.0	0.09	29	55.6
F6	11.0	49.0	4.4	30	50.9
A7	9.0	--	--	80	76.7
B7	10.0	--	--	61	52.3
C7	11.0	--	--	51	27.9
D7	10.0	--	--	39	27.9
E7	10.0	9.0	0.0	29	32.8
F7	11.0	17.0	1.5	30	30.0
A8	9.0	--	--	80	76.7
B8	9.0	--	--	61	52.3
C8	10.0	--	--	51	27.9
D8	10.0	--	--	39	27.9
E8	10.0	--	--	29	32.8
F8	10.0	32.0	3.2	30	30.0

where A_j is the sampling area associated with sampler j, D_j is the tracer mass deposited on sampler j, W_j is the wind velocity at the position of sampler j, and S_j is the flow rate of sampler j.

Wind velocity as a function of height for the BSA was provided by the tethersonde system and the anemometers located on the Gravel Gertie meteorological tower. Table L-5 shows the wind velocities averaged over the two-minute sampling period (when the cloud was moving through the array) as a function of height for each sampler location. The uncertainty associated with these wind velocity estimates is approximately ±50%.

Table L-6 summarizes the results of calculations using Eq. (L-8) and Table L-5. A total of 92 mg of Sb was collected by the sampling array. This corresponds to 9.2×10^{-5} of the original Sb_2O_3 mass in the round room. These results do not take into account the total amount of Sb released in the base surge occurring around the circumference of the GG round room. Rather, only that portion of the base surge which radially subtends the balloon curtain is sampled and this portion <u>is</u> accounted for in the 92 mg. A rough estimate of 50% of the base surge cloud which is <u>not</u> accounted for in the 92 mg may be accounted for by doubling the mass collected in samplers F1 through F8. The total mass of Sb released from the GG structure including that contained in the base surge is approximately 118 mg. This corresponds to 1.2×10^{-4} of the original Sb_2O_3 mass placed in the GG round room. SEM particle size analysis of Sb deposits on ESA and PSA samplers indicated that 90% of the released mass (or 106 mg) was smaller than 10 m aerodynamic diameter. Because of substrate interference, no analysis for Sb deposits on GGASP samples in the round room were made.

The possible errors associated with wind velocity (±50%), ITNA analysis (25%) and estimation of sampling areas (±20%) may be propagated to determine the total error associated with the total released mass. The total error is estimated to be ± 60%. The total released respirable Sb is therefore estimated to be 106 ±64 mg. This corresponds to a release fraction of 1.1×10^{-4} $\pm 6.4 \times 10^{-5}$ of the initial Sb tracer mass. This is a factor of 27 smaller than the release fraction estimated for the uranium tracer (3×10^{-3}). The Sb was suspended from the ceiling in a powdered form about 4 m away from the uranium HEAGs, and it is reasonable to expect that the U and Sb materials responded differently to the high temperatures and shock environment. In light of these facts, it is plausible that the uranium metal and Sb_2O_3 powder would break-up and aerosolize differently and that roughly 4% of the initial one kg of Sb_2O_3 powder could have been aerosolized and dispersed into the round room during the gravel bed rise and collapse. This would correspond to less than 40 g of respirable Sb aerosol produced in the round room of which 106 mg was released into the environment. A respirable release fraction of 3×10^{-3} is therefore an acceptable upper bound estimate for both uranium and Sb_2O_3 tracers.

<u>Evaluation of Falling Particles</u>

High-speed film from the southwest camera station shows a number of particles moving in what appear to be ballistic trajectories down the southern face of the structure between times 2.7 s and 4.4 s. Examination of the

TABLE L-6
Sb Release Calculations Using Eq (L-8)

Location	Release Mass (mg)	Location	Release Mass (mg)
A1	2.46	A5	0
B1	0	B5	0
C1	4.43	C5	0
D1	0.44	D5	4.83
E1	2.28	D5	0
F1	6.12	F5	0.73
TOTAL	15.7	TOTAL	5.6
A2	0	A6	2.08
B2	0	B6	0
C2	0	C6	1.21
D2	1.09	D6	0
E2	1.05	E6	0.14
F2	4.32	F6	6.72
TOTAL	6.5		10.1
A3	31.3	A7	0
B3	0	B7	0
C3	3.15	C7	0
D3	0	D7	0
E3	5.50	E7	0.86
F3	3.21	F7	1.35
TOTAL	43.2	TOTAL	2.2

TABLE L-6 (continued)
Sb Release Calculations Using Eq (L-8)

Location	Release Mass (mg)	Location	Release Mass (mg)
A4	0	A8	0
B4	1.29	B8	0
C4	0.58	C8	0
D4	1.32	D8	0
E4	2.69	E8	0
F4	0.36	F8	2.9
TOTAL	6.2	TOTAL	2.9

high-speed film from the southeast camera station shows similar particles moving up out of the center of the structure, reaching an apex slightly left of center, between times 3.3 s and 4.9 s, and falling down towards the southern face.

Qualitatively, the particles appear as light colored, twinkling objects. They are readily visible when the high-speed film advanced rather rapidly but are less discernable on individuals frames. In addition, they are much more discernable when viewed against a dark background and are essentially invisible if viewed against the blue sky background.

Initial ballistic analysis was performed on the southeast film between frames 770 (t = 2.7 sec) and 1236 (t = 4.4 sec). Several particles were selected based on trajectories with significant vertical velocity components and durations of observable track on the film. The basic equations used for the ballistic analysis were:

$$V = at \qquad \text{(L-9)}$$

$$V = \sqrt{2\ as} \qquad \text{(L-10)}$$

where V = velocity
a = acceleration
t = time
s = distance traveled

In this instance, the only acceleration is assumed to be that due to gravity ($a = 9.8\ m/sec^2$).

Vertical components of velocities were computed by measuring the distance traveled in the vertical plane and noting the frame numbers during which the movement occurred. Once the velocity and height were determined, the apex of the trajectory was determined by solving Equation (L-10) for s and that distance was added to the height of the particle above the ground at the point where the velocity was initially determined. Similarly, the time at apex was computed by solving Equation (L-9) for t and subtracting the resulting time from the time at which the velocity was initially determined.

By assuming that all the fragments originated at the height of approximately 21 ft inside the gravel bed, an initial velocity and release time were also determined.

Figure L-9 shows the particle analysis done using the particles visible from the southwest camera station and Figure L-10 shows the particles passing through their apex, as viewed from the southeast camera. Table L-7 gives the trajectory details on the 12 particles selected from the southwest high-speed (400 fps) film.

With the exception of particle #2, the calculated release times and extrapolated point of origin of the particles on the southwest film were consistent with releases coincident with the jet visibly moving toward the south-

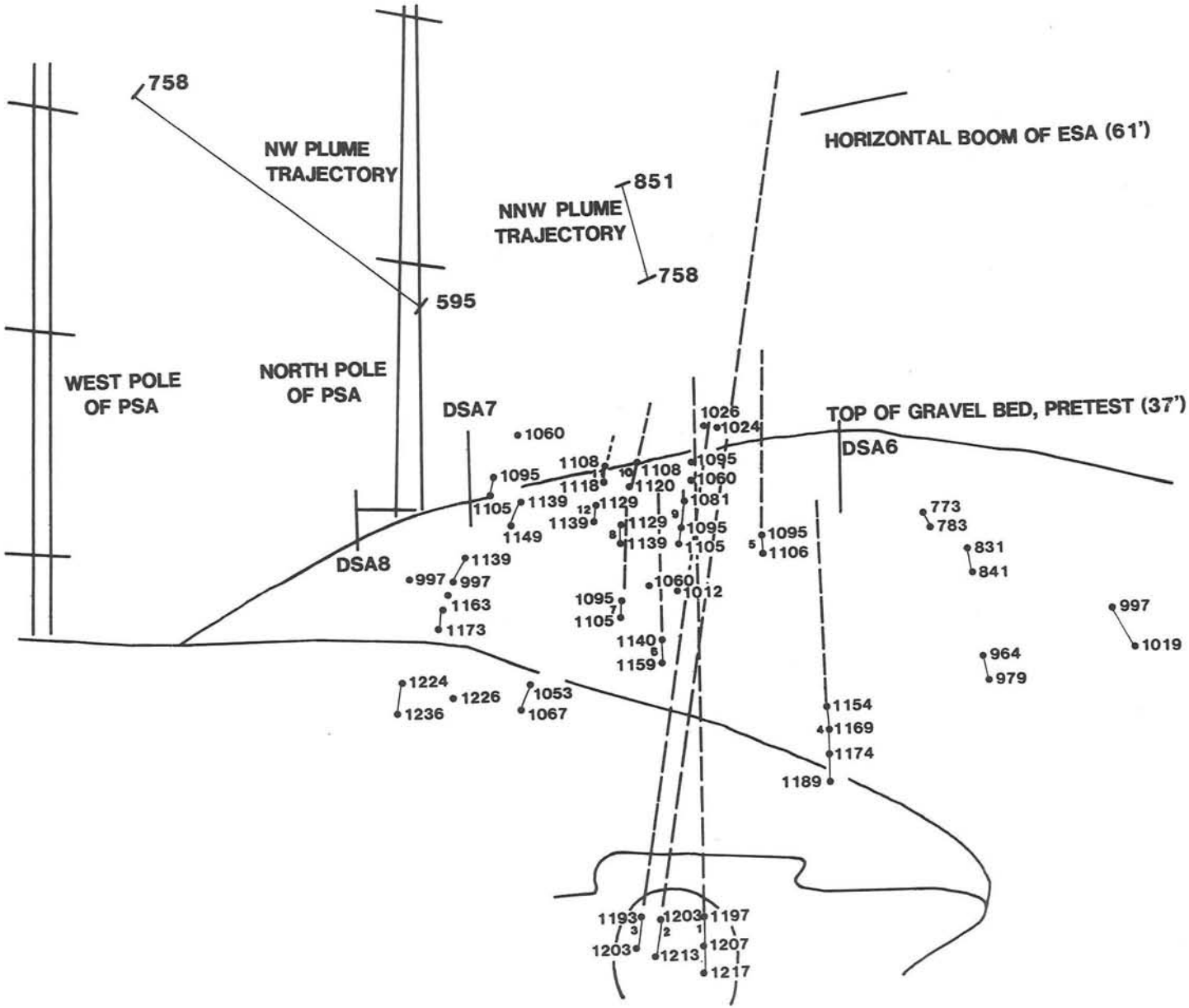

Figure L-9. Particle Trajectories Viewed from SW

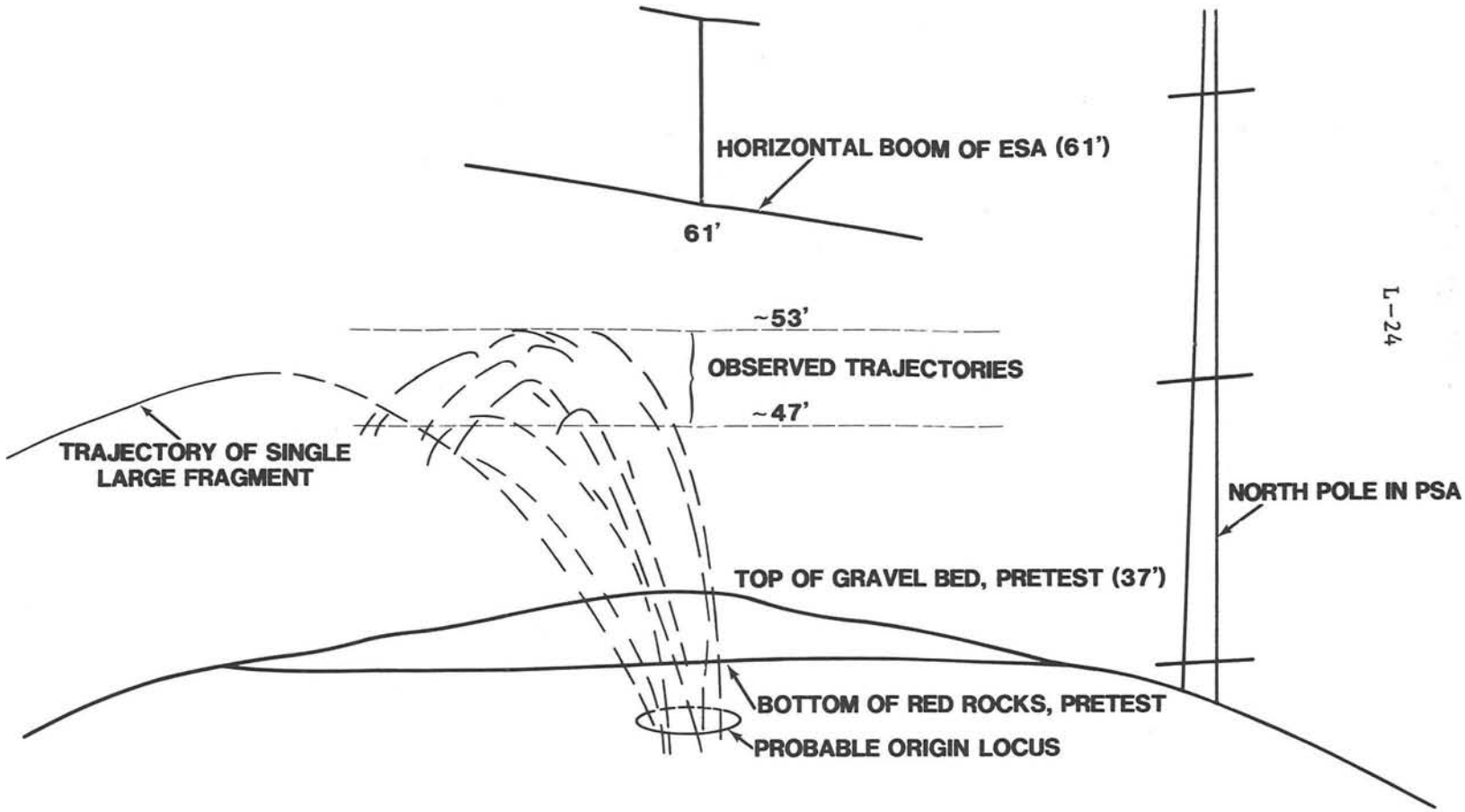

Figure L-10. Particle Trajectories Viewed from SE

TABLE L-7

Particle Trajectory Data

Summary of SW "400". Particle Data*

Particle #	V Measured V (ft/sec)	H_o Observed Ht (ft)	H_p Peak Ht (ft)	T_p Time at Peak Ht fr (sec)	V_{ij} Vel. at 21 ft (ft/sec)	Time at 21 ft fr	sec
1	51	1	41	767 (2.7)	36	450	1.6
2	63	1	63	657 (2.3)	52	198	0.7
3	48	2	38	780 (2.8)	33	488	1.7
4	32	13	29	907 (3.2)	23	706	2.5
5	36	23	43	788 (2.8)	38	456	1.6
6	32	17	33	877 (3.1)	28	632	2.2
7	24	20	29	893 (3.1)	23	693	2.4
8,10**	31	23	39	856 (3.0)	33	552	2.0
9	25	23	33	885 (3.1)	28	640	2.3
11,12**	29	24	37	883 (3.1)	32	600	2.1
			$\frac{V^2}{2g} + H_o$	$\frac{V}{g}$	$2g(H_p-21)$	$\frac{V_i}{g}$	

*actual frame rate 284 frames/sec

**Particles 8 and 10 as well as 11 and 12 are considered to be the same particle viewed at different times in their trajectory.

west at 1.8 seconds. The fragments visible on the southeast camera are coincident with the jet which appears at approximately 3.2 seconds moving to the south at an angle of approximately 30° from the vertical. It appears that the glittering objects visible from the southwest are pieces of the 1 to 2 inch gravel fill thrown upward from the bottom layers as the roof expanded. Those visible from the southeast appear to be pieces of gravel "launched" at about the time the main part of the roof collapsed onto the somewhat elastic cable structure and round room.

Appendix M
Analytical Prediction of Results Using Diffusion Modeling

Introduction

One technique which has been used to independently verify the Gravel Gertie performance is diffusion modeling. This technique basically consisted of the following steps:

1. Specifying each potential source of both respirable and depositable aerosol;

2. Modeling each source in terms of volume, location, particle size distribution, and activity distribution using unit quantity of released material;

3. Modeling the prevailing atmospheric conditions in terms of wind speed, wind direction, barometric pressure, temperature, and atmospheric stability;

4. Inserting each postulated cloud into a diffusion model and predicting the downwind concentration at locations where samples were located during the test;

5. Applying multiplicative factors to each source quantity to reproduce observed results; and

6. Using comparative results to draw conclusions concerning total release.

Each of these steps will be explored in turn.

Specification of Sources

Examination of films and samplers suggested that the total release could be subdivided into five sources:

1. A large, near-grade cylindrical source containing large particles;

2. A large, near-grade cylindrical source containing respirable-sized particles;

3. An elevated source containing respirable-sized particles;

4. A small, cylindrical source containing large particles; and

5. A small, cylindrical source containing respirable particles.

Large Deposit Source

The large deposit source modeled the contribution of background material in the gravel bed and overburden which is entrained in the base surge. The base surge was observed to expand to a diameter of approximately 100 m around GZ before moving downwind. The observed height of this cloud was approximately 5 m. Based on sieve results of gravel and overburden material (see Appendix N), the mean of the particle size distribution was 270 μm with a geometric standard deviation of 3.0. Uranium aerosol was assumed to be uniformly distributed in the cloud.

Large Respirable Source

The large respirable source modeled the contribution of respirable-sized material from inside the structure which may have "leaked" and become a part of the cloud generated by the base surge. This cloud was identical to the large-deposit cloud except that the particle size distribution was assumed to have a mean of 2.0 m and a geometric standard deviation of 2.5.

Elevated Source

A residual elevated source was observed above the structure after the base surge and ballistic phase of the detonation. This cloud is hypothesized to contain "leakage" which did not become entrained in the base surge. The cloud was considered to be a cylinder between heights of 10 and 25 m with a diameter of 5 m. The particle-size distribution was assumed to be identical to the one used in the large respirable source and the radioactivity was considered to be uniformly distributed throughout the cloud.

Small Deposit Source

Close examination of the films taken from the southwest and southeast camera stations coupled with preliminary data from samples located on the south side of the structure suggest a leakage source from the southwest portion of the round room. This source was modeled as a small cylindrical cloud, extending from the ground to 5 m with a diameter of 10 m. The particle-size distribution was identical to that used for the large deposit source. The material was assumed to be uniformly distributed.

Small Respirable Source

This source represented the respirable portion of the source described above. The only difference was the particle-size distribution, which was considered to be identical to that used for the respirable sources described earlier.

The source geometries are summarized in Table M-1 and Figures M-1 and M-2, and the particle-size distributions are shown in Figure M-3.

TABLE M-1

Source Summary

Source	Diameter (m)	Cloud Base (m)	Cloud Top (m)	Particle-Size Distribution	
				Mean (μm)	Standard Deviation
Large, Deposit	100	0	5	270.0	3.0
Large, Respirable	100	0	5	2.0	2.5
Elevated	20	5	30	2.0	2.5
Small, Deposit	10	0	5	270.0	3.0
Small, Respirable	10	0	5	2.0	2.5

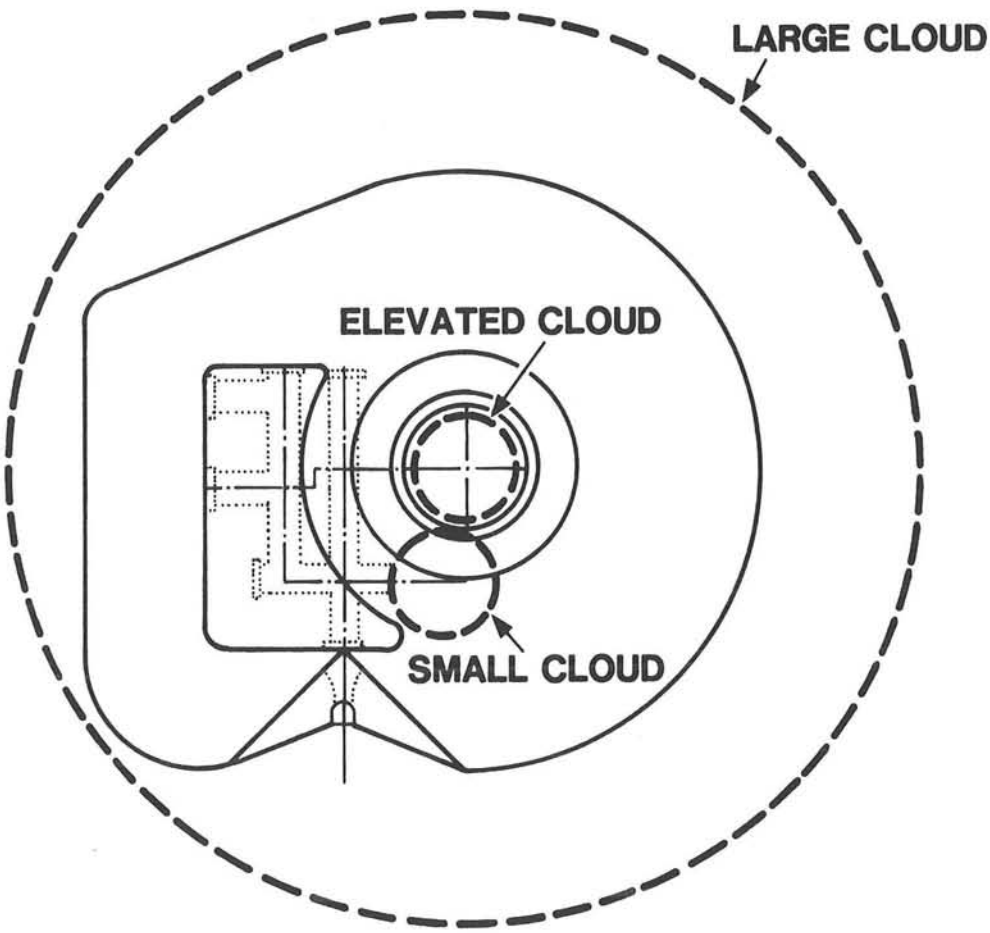

Figure M-1. Plan View of Clouds

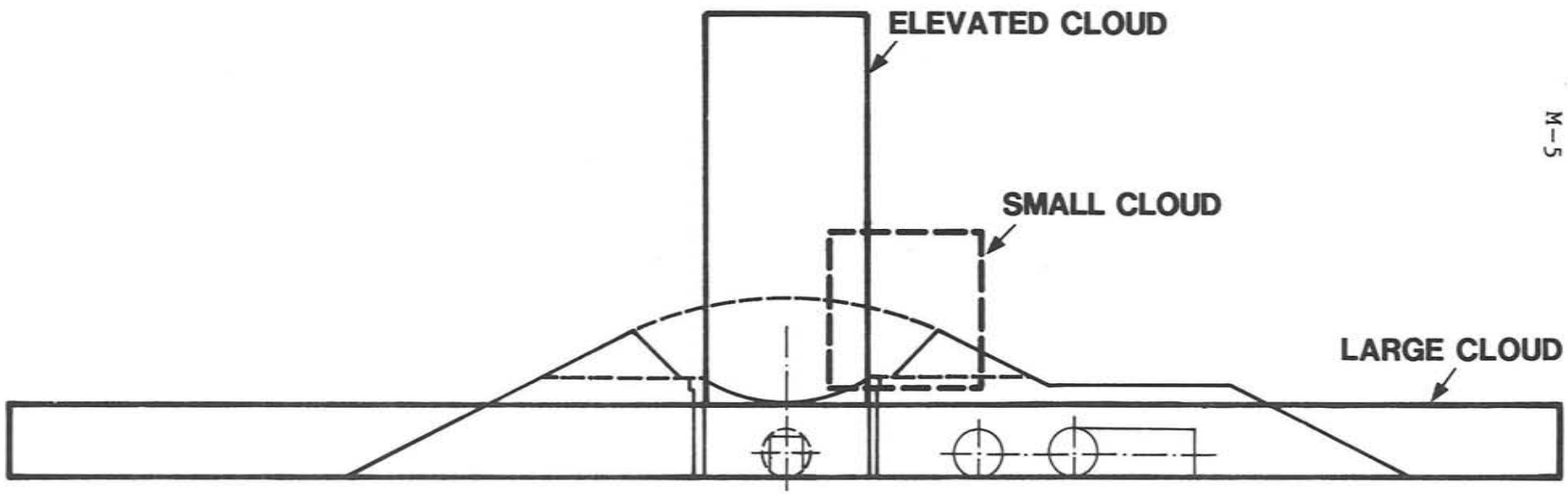

Figure M-2. Cloud Model--Elevation

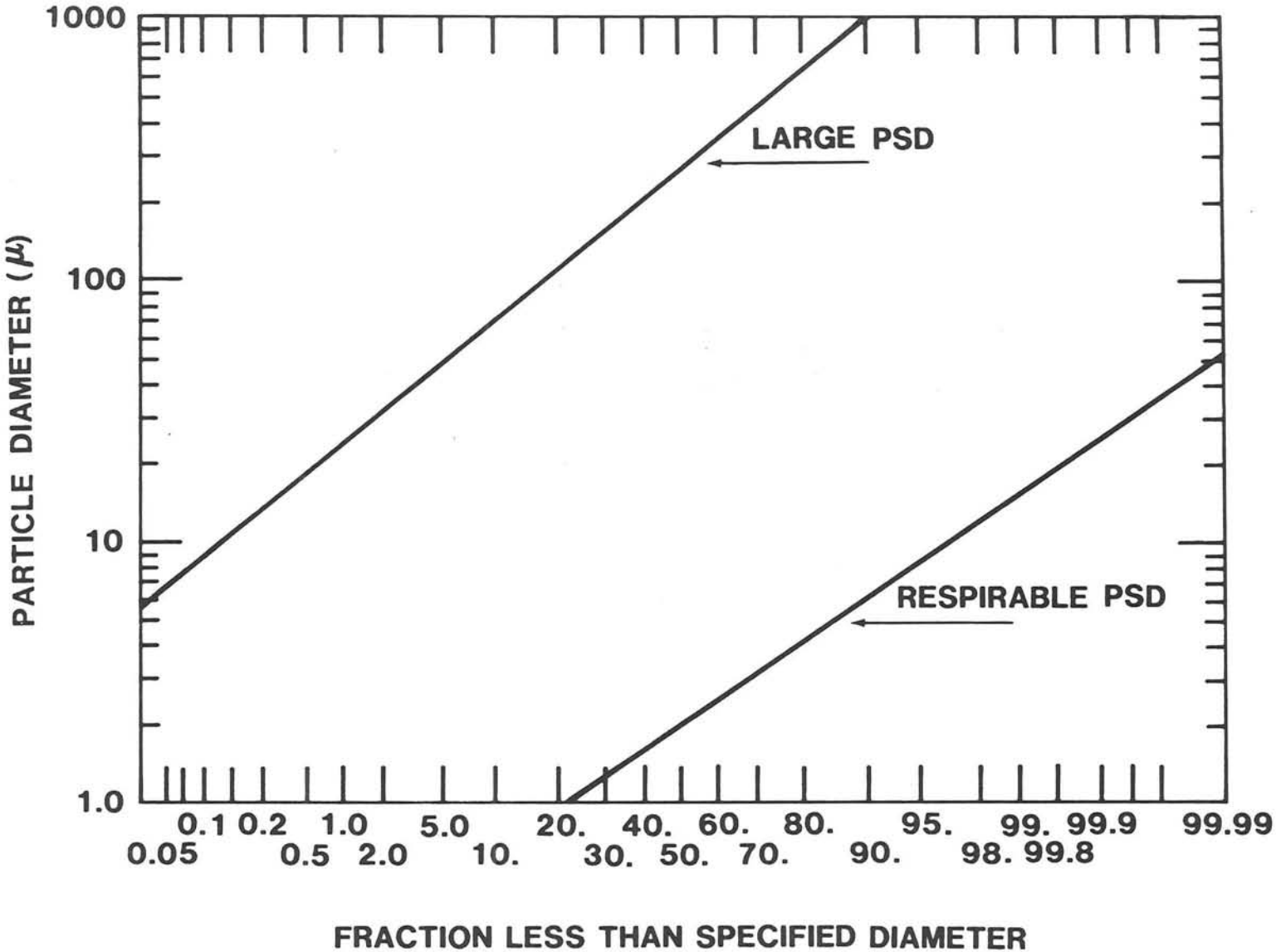

Figure M-3. Assumed Particle Size Distributions

Meteorological Assumptions

Examination of the meteorological records suggests that the wind speed and direction was approximately uniform in the first 50 m, blowing from 090° at approximately 0.5 m/s. Temperature, insolation, wind speed, and cloud observations suggest that Pasquill Category B best characterizes the underlying atmospheric stability.

Analytical Technique

Each of the five scenarios was used as input source data for the Gaussian diffusion code DIFOUT [LU69]. This three-dimensional, layered, Gaussian diffusion code combines the source data with the meteorological data and predicts the downwind concentrations of both respirable particles and deposited particles at various distances specified by the analyst. By setting these distances equal to distances at which particle samplers and deposit trays were located, analytical predictions of concentrations at these points were made.

Since each of the source scenarios is put into DIFOUT with a unit source of 1 g, applying scalar factors to the source quantity in each scenario to achieve a "best fit" to the observed values was attempted. By iterating source scaling and the order of trying to fit the data with the various sources, an "optimized" estimate was made for the total source of sampled respirable aerosol. Table M-2 shows the process. At the left, the data selected for fitting is shown. The data estimate at the location of each sampler is shown for a 1 gram source in the columns marked "orig." (original). The scaled value is marked "modif" (modified). The data less the modified prediction is shown in the column marked "net rem" (net remaining). Each model was applied successively to the "net rem" to simultaneously reduce all values to approximately zero. This procedure was approximate and somewhat subjective, but suggested a total aerosol source of approximately 0.9 g.

TABLE M-2

	Radius Meters	Azimuth Degrees	Weight Metres	Data ng, sln	Model 1 Orig.	Model 1 Modif.	Net Rem	Model 2 Orig.	Model 2 Modif.	Net 2 Rem	Model 5 Orig.	Model 5 Modif.	Net 5 Rem
BSAF1	45.7	249	2.4	2,274.0	4,150.0	1,038	1,236.5	2.2	198	1,038.5	4,000.0	1,000	38.5
F2	45.7	247	2.4	2,760.0	4,150.0	1,038	1,722.5	2.2	198	1,574.5	8,000.0	2,000	(475.5)
F3	45.7	256	2.4	834.0	4,270.0	1,068	(23.5)	2.3	207	(440.5)	-	-	(440.5)
F4	45.7	265	2.4	1,128.0	4,640.0	1,160	(32.0)	2.4	216	(248.0	-	-	(248.0)
F5	45.7	274	2.4	546.0	4,660.0	1,165	(619.0)	2.3	225	(844.0)	-	-	(844.0)
F6	45.7	286	2.4	1,350.0	4,300.0	1,075	273.0	2.3	207	68.0	-	-	68.0
F7	45.7	294	2.4	1,176.0	4,300.0	1,075	101.0	2.3	207	(106.0)	-	-	(106.0)
F8	45.7	302	2.4	1,920.0	4,300.0	1,075	845.0	2.2	198	647.0	100.0	200	447.0
E1	45.7	240	10.7	1,266.0	-	-	1,266.0	-	-	1,266.0	-	-	1,266.0
D1	45.7	240	16.8	400.0	-	-	480.0	-	-	480.0	-	-	480.0
E2	45.7	247	10.7	1,056.0	-	-	1,056.0	-	-	1,056.0	-	-	1,056.0
E3	45.7	236	10.7	636.0	-	-	636.0	-	-	636.0	-	-	636.0
D3	45.7	236	29.0	594.0	-	-	594.0	-	-	594.0	-	-	594.0
TOTAL	-	-	-	16,020.0	34,770.0	8,695	7,327.5	18.4	1,656	5,671.5	12,000.0	3,200	2,471.5
BSA4	10.4	135	1.0	5,140.0	20,000.0	7,000	(1,852.0)	16.3	1,467	(3,319.0)	-	-	(3,319.0)
BSA5	10.4	100	1.0	3,450.0	20,000.0	7,000	(3,550.0)	16.3	1,467	(5,017.0)	-	-	(5,017.0)
BSA6	10.4	225	1.0	10,914.0	20,000.0	7,000	3,914.0	16.3	1,467	2,447.0	54,000.0	13,500	(11,033.0)
BSA7	10.4	270	1.0	750.0	20,000.0	7,000	(6,250.0)	16.3	1,467	(7,717.0)	540.0	135	(7,852.0)
TOTAL	--	-	-	20,262.0	112,000.0	20,000	(7,730.0)	65.2	5,868	(13,606.0)	54,540.0	13,635	(27,241.0)
63 T	45.7	286	2.4	7,936.0	4,300.0	1,075	6,801.0	14.0	1,260	5,621.0	-	-	5,621.0
63 H	45.7	286	2.4	2,600.0	3,900.0	973	1,713.0	2.3	207	1,506.0	-	-	1,506.0
64 T	45.7	286	22.0	7,326.0	-	-	7,326.0	-	-	7,326.0	-	-	7,326.0
64 H	45.7	286	22.0	4,752.0	-	-	4,752.0	-	-	4,752.0	-	-	4,752.0
65 T	45.7	236	22.0	10,974.0	-	-	10,974.0	-	-	10,974.0	-	-	10,974.0
65 H	45.7	236	22.0	3,018.0	-	-	3,018.0	-	-	3,018.0	-	-	3,018.0
TOTAL	-	-	-	36,714.0	8,200.0	2,030	34,644.0	16.3	1,467	33,197.0	-	-	33,197.0
ESAM1	-	-	17.4	5,100.0	-	-	5,100.0	-	-	5,100.0	-	-	5,100.0
ESAM2	-	-	21.9	3,114.0	-	-	3,114.0	-	-	3,114.0	-	-	3,114.0
PSAV1	30.5	270	10.7	1,584.0	-	-	1,584.0	-	-	1,584.0	-	-	1,584.0
PSAM1	15.2	-	10.7	1,338.0	-	-	1,338.0	-	-	1,338.0	-	-	1,338.0
TSA1	36.6	225	2.1	20,100.0	11,000.0	2,730	17,350.0	32.0	2,000	14,470.0	90,000.0	20,000	(5,530.0)
TSA2	30.5	225	1.5	286,800.0	54,100.0	13,525	273,275.0	160.0	14,400	258,875.0	400,000.0	100,000	(58,875.0)
TSA1F	36.6	225	2.1	23,112.0	11,000.0	2,750	20,362.0	32.0	2,000	17,482.0	80,000.0	20,000	(2,518.0)
TSA2F	30.5	225	1.5	536,880.0	54,100.0	13,525	523,355.0	160.0	14,400	508,955.0	400,000.0	100,000	408,955.0
TOTAL	-	-	-	878,028.0	130,200.0	32,550	845,478.0	384.0	34,560	810,918.0	960,000.0	240,000	570,918.0
IIID1	61.0	270	-	386.0	40.0	10	376.0	4.2	378	(2.0)	24.0	6	(8.0)
IIIC1	121.9	270	-	210.0	19.0	5	205.3	1.0	92	113.5	8.2	2	111.4
IIIE1	243.0	270	-	2.9	6.0	2	1.4	0.2	21	(19.3)	1.0	0	(19.8)
IIIG1	365.0	270	-	2.6	2.7	1	1.9	0.1	8	(6.2)	0.7	0	(6.3)
IIII1	407.7	270	-	1.7	1.5	0	1.3	0.0	4	(2.8)	-	-	(2.8)
IIIK1	609.6	270	-	0.7	0.9	0	0.5	0.0	3	(2.2)	-	-	(2.2)
IIID2	86.3	223	-	9.2	20.0	5	4.2	1.5	135	(130.8)	45.0	11	(142.1)
IIIC2	136.2	244	-	1.3	4.0	1	0.3	0.2	18	(17.7)	50.0	13	(30.2)
IVD2	86.3	315	-	297.0	20.0	5	292.0	1.5	135	157.0	45.0	11	145.8
IVD3	136.2	333	-	2.9	4.0	1	1.9	0.2	18	116.21	50.0	13	(28.7)
IVC2	136.2	296	-	9.2	4.0	1	8.2	0.2	18	(9.8)	50.0	13	(22.3)
TOTAL	-	-	-	923.5	122.1	31	892.9	9.2	829	63.5	274.7	69	(5.2)
Proves Reason-able Overall	-	-	-	-	-	0.25 g			0.12 g			0.25 g	

TABLE M-2 (continued)

Model 4 Orig.	Model 4 Modif.	Net 4 Rem	Model 3 Orig.	Model 3 Modif.	Net 3 Rem	
-	-	38.5	-	-	38.5	BSAF1
-	-	(475.5)	-	-	(475.5)	F2
-	-	(440.5)	-	-	(440.5)	F3
-	-	(248.0)	-	-	(248.0)	F4
-	-	(844.0)	-	-	(844.0)	F5
-	-	68.0	-	-	68.0	F6
-	-	(106.0)	-	-	(106.0)	F7
-	-	447.0	-	-	447.0	F8
-	-	1,266.0	22,700.0	4,540	(3,274.0)	E1
-	-	480.0	22,700.0	4,540	(4,060.0)	D1
-	-	1,056.0	22,700.0	4,540	(3,484.0)	E2
-	-	636.0	27,700.0	4,540	(3,904.0)	E3
-	-	594.0	22,700.0	4,540	(3,966.0)	D3
-	-	2,471.5	113,500.0	22,700	(20,228.5)	TOTAL
12.0	300	(3,619.0)	-	-	(3,619.0)	BSA4
9.0	225	(5,242.0)	-	-	(5,242.0)	BSA5
30.0	750	(11,803.0)	-	-	(11,803.0)	BSA6
3.0	75	(7,927.0)	-	-	(7,927.0)	BSA7
54.0	1,350	(28,591.0)	-	-	(20,591.0)	TOTAL
-	-	5,621.0	-	-	5,621.0	63 T
-	-	1,506.0	-	-	1,506.0	63 R
-	-	7,326.0	22,700.0	4,540	2,786.0	64 T
-	-	4,752.0	22,700.0	4,540	212.0	64 R
-	-	10,974.0	22,700.0	4,540	6,434.0	65 T
-	-	3,018.8	22,700.0	4,540	(1,522.0)	65 R
-	-	33,197.0	90,800.0	18,160	15,037.0	TOTAL
-	-	5,100.0	22,700.0	4,540	560.0	ESAM1
-	-	3,114.0	22,700.0	4,540	(1,426.0)	ESAM4
-	-	1,584.0	22,700.0	4,540	(2,956.0)	PSAM1
-	-	1,338.0	22,700.0	4,540	(3,202.0)	PSAM1
400.0	10,000	(15,530.0)	-	-	(15,530.0)	TSA1
2,000.0	50,000	108,875.0	-	-	108,875.0	TSA2
400.00	10,000	(12,518.0)	-	-	(12,518.0)	TSA1F
2,000.0	50,000	358,955.0	-	-	358,955.0	TSA2F
4,800.0	120,000	450,918.0	90,800.0	18,160	432,758.0	TOTAL
25.0	625	(633.0)	-	-	(633.0)	IIIB1
4.5	113	(1.1)	-	-	(1.1)	IIIC1
0.7	18	(37.3)	-	-	(37.3)	IIIE1
0.2	6	(12.1)	-	-	(12.1)	IIIG1
0.1	3	(5.3)	-	-	(5.3)	III1I
0.1	1	(3.6)	-	-	(3.6)	IIIK1
-	-	(142.1)	-	-	(142.1)	IIIB2
4.0	100	(130.2)	-	-	(130.2)	IIIC2
-	-	145.0	-	-	145.0	IVD2
-	-	(28.7)	-	-	(28.7)	IVD3
-	-	(22.3)	-	-	(22.3)	IVC2
34.6	865	(869.8)	-	-	(869.8)	TOTAL

0.20 g 0.25 g TOTAL 0.90 g

Appendix N
Analysis of Control Samples, Background Soil, and Background Air Samples

Quality assurance for uranium determination by fluorometry and delayed neutron assay was provided by analyzing samples of known quantities of uranium prepared by SNL Organization 6324 and the alpha-chemistry group of the Lovelace Inhalation Toxicology Research Institute. Two solutions were used for these standards:

(1) A reference standard of 100.3 μg of uranium per ml of 0.2% HNO_3 solution, and

(2) A reference standard of 10 ml of Solution No. 1 in 100 ml of H_2O.

Quantities of 1.003×10^2 ng, 1.003×10^3 ng, 1.003×10^4 ng, and 1.003×10^5 ng of uranium were pipetted onto cellulose acetate filters, stainless steel, and glass substrates. Filter blanks, stainless steel, and glass substrate blanks were used as 0.0 ng uranium controls. Table N-1 summarizes the results of the DNA and uranium fluorometric analyses of these standards by the H-8 group at LANL and the alpha-chemistry group at ITRI, respectively. The quantity of uranium on each standard was not disclosed to either group before analysis.

Values for the known (spiked) quantities and measured uranium quantities are shown in Table N-1. Figure N-1 shows a log-log plot of the DNA measured quantities versus the known values of the uranium. For the DNA technique, good agreement was achieved between measured and standard values for quantities above 10 ng uranium. Figure N-2 shows a log-log plot of measured values obtained by uranium fluorometry versus the known control values. Good agreement between measured and standard values was achieved for values above 10 ng. It was concluded that the percentage error of the DNA technique applied to uranium quantities above 10 ng is less than 25%. The percentage error of the fluorometic technique for quantities above 10 ng is less than 20%.

Samples of soil from the surrounding NTS Gravel Gertie site, gravel bed, and dirt overburden were analyzed for uranium, antimony and scandium using uranium fluorometry (UF), neutron activation analysis (NAA), and delayed neutron assay (DNA). Mass spectroscopic analysis of these samples was also performed to determine the atomic mass ratio of U-235 to U-238. This analysis was necessary for the DNA technique. Table N-2 shows the results of these analyses. The gravel bed mix analyses indicated a natural uranium content (i.e., 0.7% U-235/U-238) of approximately 3.4 parts per million (PPM). The soil surrounding the Gravel Gertie structure contained 2 to 5 PPM of depleted uranium (i.e., 0.224% of U-235/U-238). The dirt overburden of the Gravel Gertie structure contained 1.5 PPM of natural occurring uranium (i.e., 0.7% U-235/U-238). In addition, paticle size distribuions for both the rock fill and the earth overburden were determined using an ultrasonic sifter. The results of this analysis are shown on Figure N-3.

TABLE N-1
Results of Control Sample Analysis

Substrate ID NO.	Spiked Quantity (ng)	Measured Quantity (ng)	Spiked By	Measured By (2,3)	Analytical Technique	Atomic % U-235
FL 210	1.00×10^2	1.01×10^2	SNL(1)	LANL H-8(2)	DNA	0.70
FS 211	1.00×10^4	9.40×10^3	SNL	LANL H-8	DNA	0.70
FS 212	1.00×10^3	1.03×10^3	SNL	LANL H-8	DNA	0.70
FS 213	1.00×10^1	3.70	SNL	LANL H-8	DNA	0.70
FL 214	1.0×10^3	NA	SNL	-	-	0.70
LMJ 1511	0	1.5	SNL	LANL H-8	DNA	0.70
LMJ 1512	1.00×10^2	8.70×10^1	SNL	LANL H-8	DNA	0.70
LMJ 1513	1.00×10^3	7.62×10^2	SNL	LANL H-8	DNA	0.70
LMJ 1514	1.00×10^4	6.89×10^3	SNL	LANL H-8	DNA	0.70
LMJ 1515	1.00×10^5	7.710×10^4	SNL	LANL H-8	DNA	0.70
FS 3030	0	9.0	SNL	LANL H-8	DNA	0.70
FL 3031	0	9.0	SNL	LANL H-8	DNA	0.70
FL 2041	0	9.0	SNL	LANL H-8	DNA	0.70
FL 2043	0	9.0	SNL	LANL H-8	DNA	0.70
FL 201	0	9.0	SNL	LANL H-8	DNA	0.70
FL 202	0	9.0	SNL	LANL H-8	DNA	0.70
FL 203	0	9.0	SNL	LANL H-8	DNA	0.70
FL 204	0	9.0	SNL	LANL H-8	DNA	0.70
FL 205	0	9.0	SNL	LANL H-8	DNA	0.70
FL 206	0	9.0	SNL	LANL H-8	DNA	0.70
FL 2040	0	0	SNL	LANL H-8	DNA	0.70
LMJ 1171	0	0	SNL	ITRI(3)	UF	NA
LMJ 1172	0	0	SNL	ITRI	UF	NA
LMJ 1173	0	5.4	SNL	ITRI	UF	NA
LMJ 1174	0	6.9	SNL	ITRI	UF	NA
LMJ 1175	0	5.9	SNL	ITRI	UF	NA
LMJ 1176	0	0	SNL	ITRI	UF	NA
LMJ 1177	0	2.4	SNL	ITRI	UF	NA
LMJ 1178	0	4.0×10^1	SNL	ITRI	UF	NA
LMJ 1181	0	0	SNL	ITRI	UF	NA
LMJ 1182	0	0	SNL	ITRI	UF	NA
LMJ 1183	0	0	SNL	ITRI	UF	NA
LMJ 1184	0	0	SNL	ITRI	UF	NA
LMJ 1185	0	0	SNL	ITRI	UF	NA
LMJ 1186	0	0	SNL	ITRI	UF	NA
LMJ 1187	0	0	SNL	ITRI	UF	NA
LMJ 1188	0	0	SNL	ITRI	UF	NA

TABLE N-1 (Continued)
Results of Control Sample Analysis

Substrate ID NO.	Spiked Quantity (ng)	Measured Quantity (ng)	Spiked By	Measured By (2,3)	Analytical Technique	Atomic % U-235
LMJ 1411	0	5.64×10^{1}	SNL	ITRI	UF	0.70
LMJ 1412	1.00×10^{2}	1.584×10^{2}	SNL	ITRI	UF	0.70
LMJ 1413	1.00×10^{3}	1.002×10^{3}	SNL	ITRI	UF	0.70
LMJ 1414	1.00×10^{4}	8.638×10^{3}	SNL	ITRI	UF	0.70
LMJ 1415	1.003×10^{5}	8.758×10^{4}	SNL	ITRI	UF	0.70
FL 2026	0	9.0×10^{-1}	SNL	ITRI	UF	NA
FL 2027	0	9.9	SNL	ITRI	UF	NA
FL 2028	0	2.4	SNL	ITRI	UF	NA
FL 2029	0	9.9	SNL	ITRI	UF	NA
FL 2030	0	1.89×10^{1}	SNL	ITRI	UF	NA
FL 2050	1.00×10^{3}	9.123×10^{2}	SNL	ITRI	UF	0.70
FL 2055	1.00×10^{2}	1.179×10^{2}	SNL	ITRI	UF	0.70
MSA 3019	0	1.74×10^{1}	SNL	ITRI	UF	0.70
MSA 3020	1.00×10^{4}	1.03×10^{3}	SNL	ITRI	UF	0.70
MSA 3021	1.00×10^{3}	7.932×10^{3}	SNL	ITRI	UF	0.70
MSA 3022	1.00×10^{2}	6.88×10^{1}	SNL	ITRI	UF	0.70
MI 8001	0	3.6	SNL	ITRI	UF	0.70
MI 8002	1.00×10^{2}	9.49×10^{1}	SNL	ITRI	UF	0.70
MI 8003	1.00×10^{3}	8.97×10^{2}	SNL	ITRI	UF	0.70
MI 8004	1.00×10^{4}	5.876×10^{3}	SNL	ITRI	UF	0.70
MI 8005	1.003×10^{5}	8.9613×10^{4}	SNL	ITRI	UF	0.70
LMJ 1311	0	0	ITRI	ITRI	UF	NA
LMJ 1312	1	3.90	ITRI	ITRI	UF	NA
LMJ 1313	0	2.49×10^{1}	ITRI	ITRI	UF	NA
LMJ 1314	0	8.64×10^{1}	ITRI	ITRI	UF	NA
LMJ 1315	0	1.59×10^{1}	ITRI	ITRI	UF	NA
LMJ 1316	0	0	ITRI	ITRI	UF	NA
LMJ 1317	1.0×10^{1}	1.14×10^{1}	ITRI	ITRI	UF	NA
LMJ 1318	1	5.40	ITRI	ITRI	UF	NA
LMJ 1301	0	0	ITRI	ITRI	UF	NA
LMJ 1302	0	0	ITRI	ITRI	UF	NA
LMJ 1303	0	0	ITRI	ITRI	UF	NA
LMJ 1304	0	0	ITRI	ITRI	UF	NA
LMJ 1305	0	0	ITRI	ITRI	UF	NA
LMJ 1306	0	0	ITRI	ITRI	UF	NA
LMJ 1307	0	9.30×10^{-1}	ITRI	ITRI	UF	NA
LMJ 1308	0	0	ITRI	ITRI	UF	NA

TABLE N-1 (Continued)
Results of Control Sample Analysis

Substrate ID NO.	Spiked Quantity (ng)	Measured Quantity (ng)	Spiked By	Measured By (2,3)	Analytical Technique	Atomic % U-235
FS 01	0	2.48	ITRI	ITRI	UF	NA
FS 02	0	0	ITRI	ITRI	UF	NA
FS 03	0	0	ITRI	ITRI	UF	NA
FL 01	0	0	ITRI	ITRI	UF	NA
FL 02	0	0	ITRI	ITRI	UF	NA
FL 01	0	2.48	ITRI	ITRI	UF	NA
FL 02	0	0	ITRI	ITRI	UF	NA
F37-01	0	0	ITRI	ITRI	UF	NA
F37-02	0	0	ITRI	ITRI	UF	NA
F47-03	0	0	ITRI	ITRI	UF	NA
MGLASS-1	0	0	ITRI	ITRI	UF	NA
MGLASS-2	0	0	ITRI	ITRI	UF	NA
MGLASS-3	0	0	ITRI	ITRI	UF	NA

(1) Sandia National Laboratories, Organization 6324.
(2) Los Alamos National Laboratories, Division H-8, Environmental Health.
(3) Lovelace Inhalation Toxicology Research Institute
DNA: Uranium Fluorometry
NA: Not Analyzed
LMJ: Lovelace Multijet Impactor
FL: Large (47 mm diameter) filter
FS: Small (25 mm diameter) filter

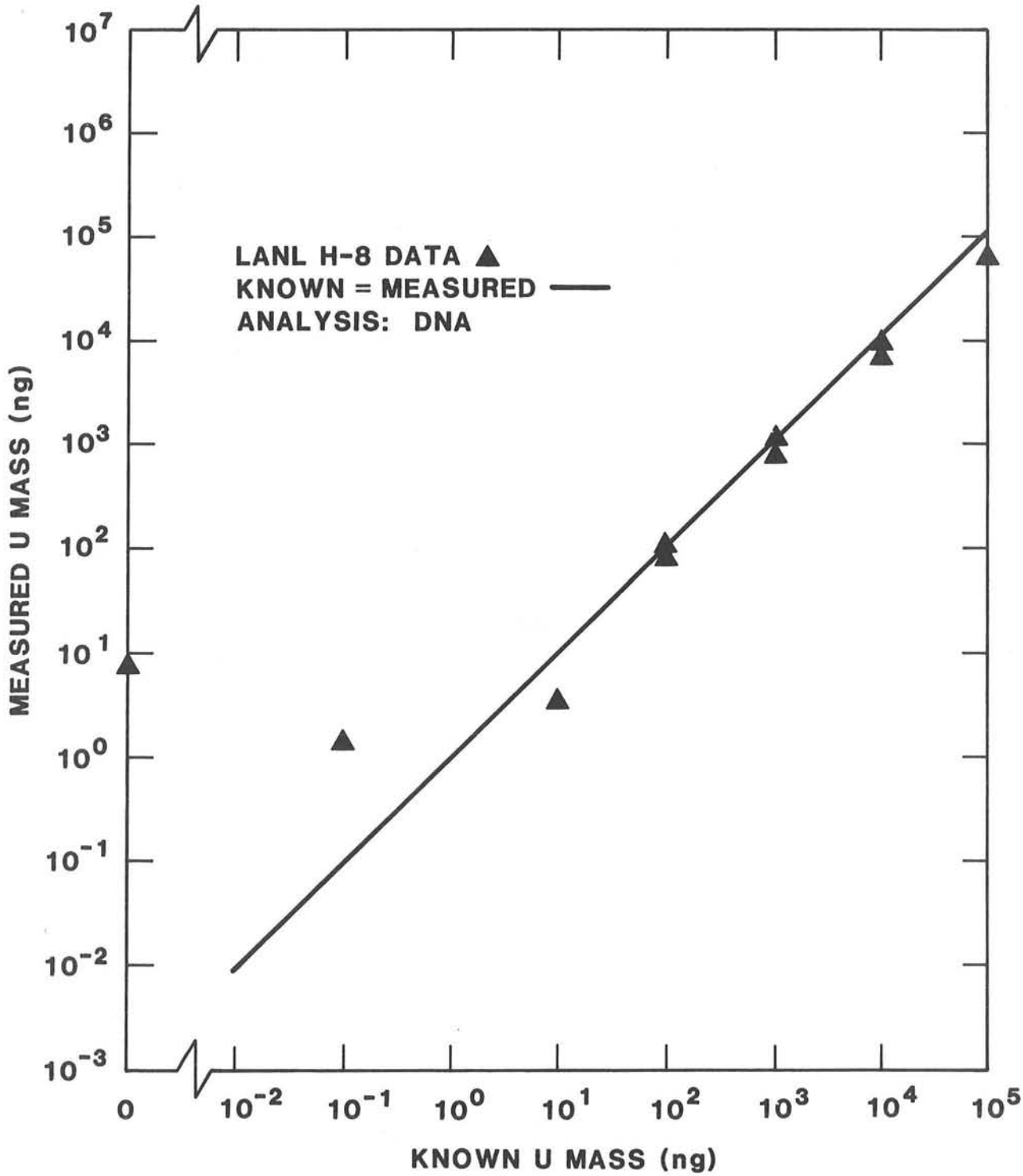

Figure N-1. DNA Measurements vs Known U Mass

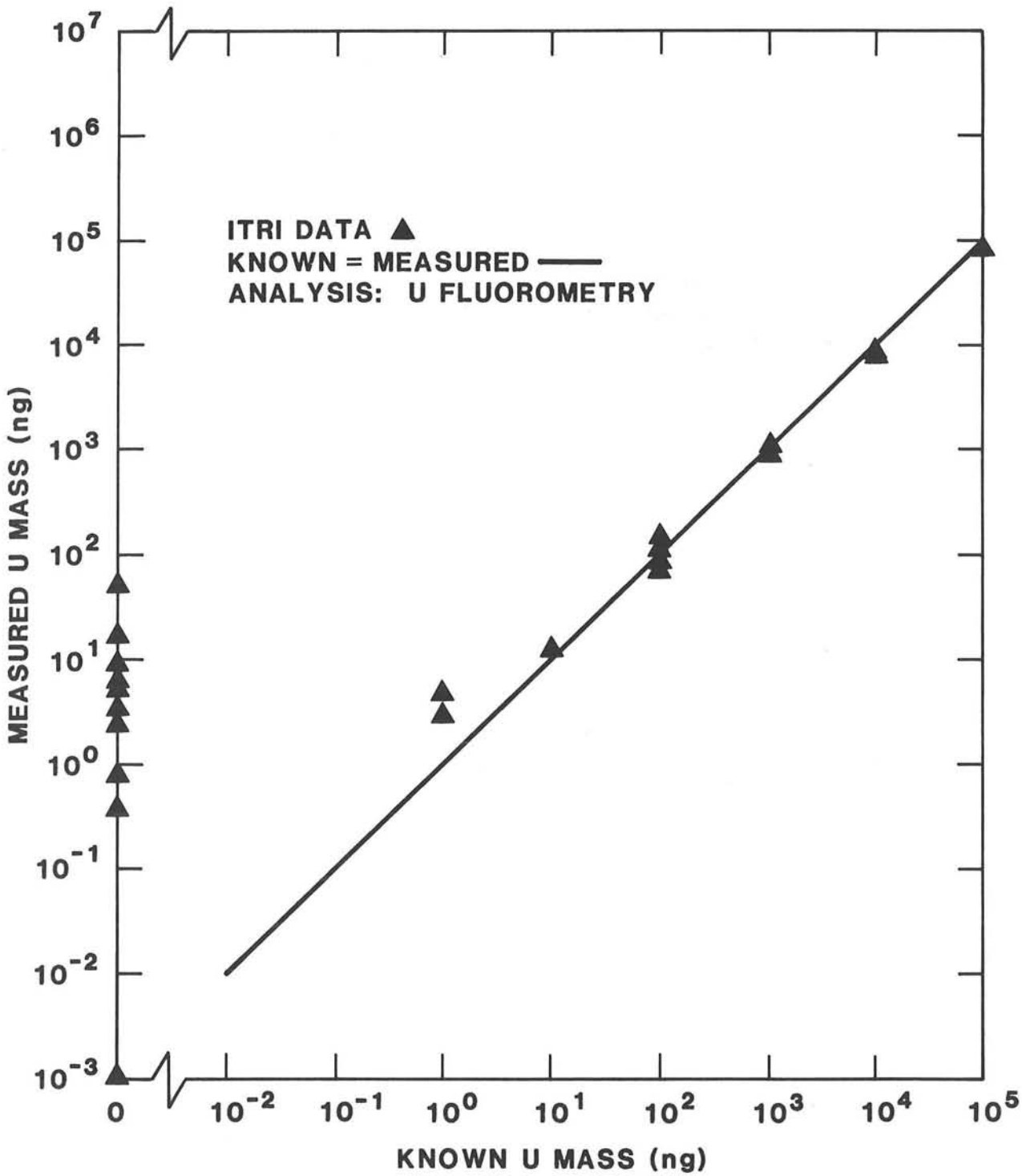

Figure N-2. U Fluorometry Measurements vs Known U Mass

TABLE N-2
Results of Soil Sample Analysis

Sample ID No.	Total Mass (g)	U (PPM)	Sb (PPM)	Sc (PPM)	Atomic % U-235	Analytical Technique	Analyzer
Gravel Pit Access Road	12.24	0.4*	-	-	-	UF	ITRI
100 yd N of GG	2.423	0.8*	-	-	-	UF	ITRI
100 yd S of GG	2.613	0.5*	-	-	-	UF	ITRI
E toe of GG	-	5.2 ± 1.8	0.82 ±0.09	NA	0.224	NAA	SNL Org 1821
100 yd W of GG	-	1.8 ± 0.2	0.79 0.05	NA	-	NAA	SNL Org 1821
200 yd N of GG	-	1.9 ± 0.2	0.85 ± 0.03	NA	-	NAA	SNL Org 1821
Gravel Bed Mix 1560	2.00	3.44 ± 0.24	1.7 0.2	6.5 ± 0.3	0.7	DNA	LANL H-8
Gravel Bed Mix 1561	2.00	3.44 ± 0.24	1.1 ± 0.2	7.4 ± 0.4	0.7	DNA	LANL H-8
GG Overburden E-T03 1562	5.00	1.58 ± 0.12	0.5 ± 0.1	2.3 ± 0.1	0.8	DNA	LANL H-8
GG Overburden 1563	8.00	1.41 ± 0.10	0.7 ± 0.1	2.2 + 0.1	0.7	DNA	LANL H-8

UF: Uranium Fluorometry
NAA: Neutron Activation Analyses
DNA: Delayed Neutron Assay
ITRI: Lovelace Inhalation Toxicology Institute
LANL: Los Alamos National Laboratories
SNL: Sandia National Laboratories, Albuquerque, NM
*These values are suspect because of operator error.

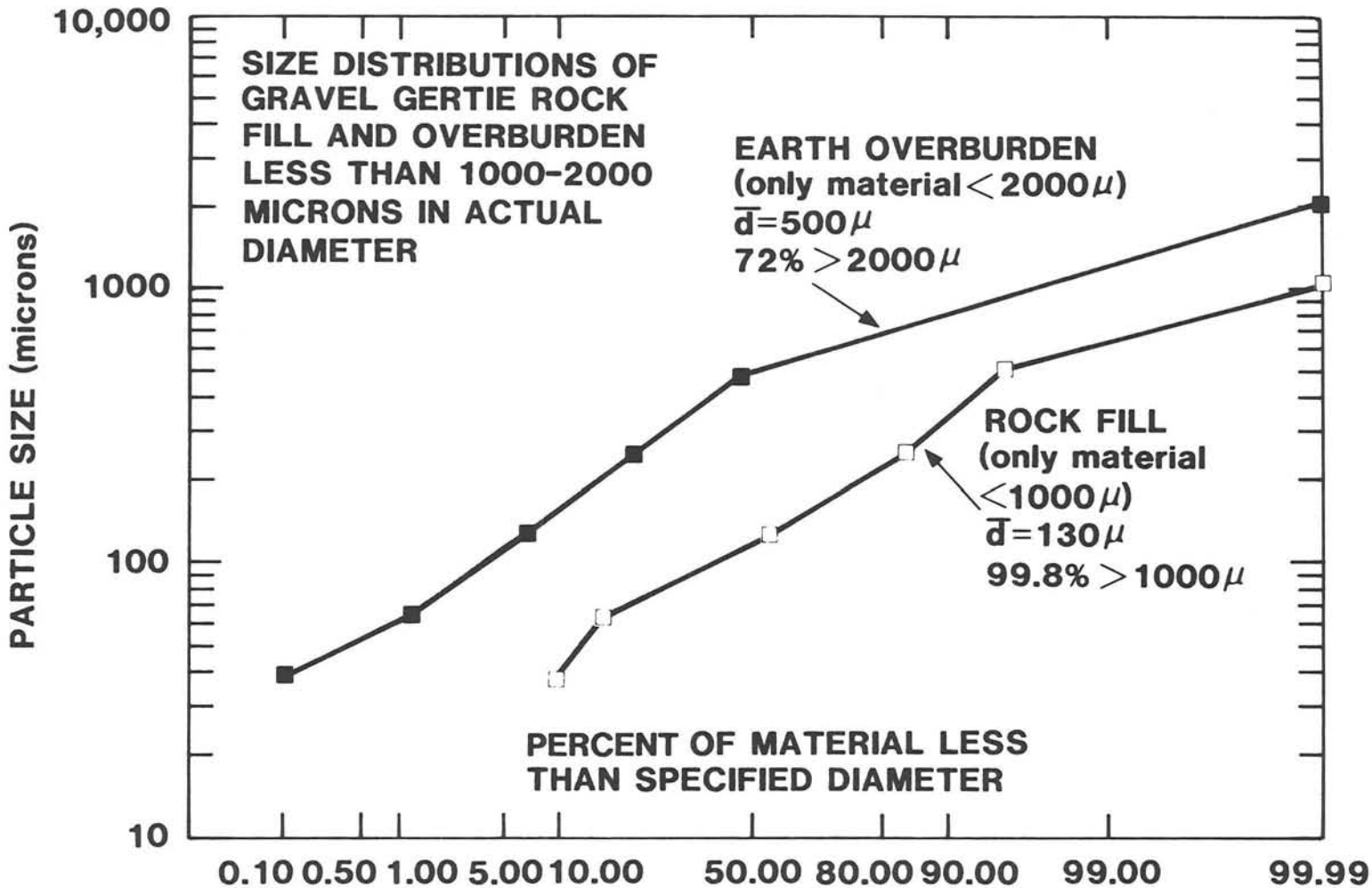

Figure N-3. Fraction of Material Less than Specified Diameter

Filter and cascade impactor samples of air surrounding the NTS Gravel Gertie site were also taken a day before the November 20 test for analysis by uranium fluorometry. Table N-3 shows the results of these analyses. An average uranium concentration of 2.5×10^{-6} PPM was determined for the ambient air. Analysis for the atomic ratio of U-235 to U-238 was not performed for these samples.

TABLE N-3

Results of Pretest Air Sample Analysis

Sample ID	Stage No.	Total Mass (mg)	Flow Rate (ℓ/min)	Sample Time (min)	Uranium Mass (ng)	ECD (μm)	U[a] (PPM)
FL 2001	-	0.32	8.82	206	8.4	-	3.8×10^{-6}
FL 2002	-	0.26	8.64	206	3.6	-	1.7×10^{-6}
LMJ 1011	1	0.31	~15	206	8.4	12.50	
LMJ 1011	2	0.01	~15	206	0.0	7.96	
LMJ 1011	3	0.05	~15	206	15.9	5.12	
LMJ 1011	4	0.01	~15	206	0.9	3.13	2.0×10^{-6}
LMJ 1011	5	0.00	~15	206	17.4	1.99	
LMJ 1011	6	0.01	~15	206	11.4	1.24	
LMJ 1011	7	0.05	~15	206	2.4	10.75	
LMJ 1011	8	0.43	~15	206	3.9	--	

[a] PPM = Mass Uranium/Mass Air

~ Estimated

Appendix O
Dynamic Analysis

Introduction

The phenomena that govern the behavior of the Gravel Gertie structure under accident conditions are numerous and highly interlinked. Formulation of a simple dynamic model was considered an important method for comparing this test with the 1957 tests and other scaled test data that are available. In particular, it was desired to be able to estimate the behavior of this test structure in comparison to what would have been observed had the construction produced an actual replica of a Pantex structure.

While numerous complex structural computer models are available, it was decided that a relatively simple semiempirical model might provide the necessary linking of the experiments without the time and cost of developing a full finite-difference model. To this end a set of assumptions were set down and developed into a modest computerized model. Although the assumptions were based largely on what was seen in the 1982 full-scale experiment, the model was validated by applying it to the 1957 tests and the 1982 scaled tests.

Model Development

The following general assumptions were made initially in conceptualizing the dynamic model:

1. The gas within the structure acts like a perfect gas with the properties of air.

2. The structure, except at very early time, consists of one large volume rather than a round room and staging area connected by a portal.

3. At very early times the pressure increases linearly to a pressure consistent with detonation of the nominal HE in a volume typical of the round room. The maximum pressure and the time at which maximum pressure is reached is estimated from the smallest dimension of the room by methods outlined in Reference BA82.

   Pressure decreases exponentially from the maximum to a value typical of the nominal HE in a volume equal to the total enclosed volume (round room plus staging area). The time at which this second pressure is reached is a function of the portal area between round room and staging area volume as outlined in Reference BA82.

4. From the time at which full volume equilibrum pressure is achieved, an effective air temperature is estimated from pressure, volume, and mass. This energy is subject to appropriate conservation laws thereafter. Effects included are radiation and conduction-convection to walls, p-v work and energy fluxes associated with the losses of mass.

5. Gravel fill is divided into two sections: a cylindrical volume defined by the upward extension of the round room walls (referred to as the plug) and the annular gravel fill outside the plug (called the wedge). The plug is assumed to translate only in the vertical direction and remains geometrically unchanged throughout the event. The wedge is assumed to take the form of a spherical segment linked to the top of the plug and sliding on the surface interface between gravel and earth fill (points A and B on Figure O-1). The speed of sliding on the gravel-fill interface is a function of the upward motion of the plug. The spherical segments making up the wedge are defined from points A, B, and a constraint that the sphere center is on the centerline of the round room. The wedge thickness, Δt is calculated to conserve the initial volume of gravel in the wedge.

6. Motion of the center of gravity of the gravel is calculated from the acceleration obtained from the net force acting on the full gravel mass. Pressure is assumed to act initially over the area out to point D and then, as motion begins, out to point C (see Figure O-1).

7. During a detonation event, gas escapes only through the gravel and at a rate proportional to the pressure difference, inside gravel surface area, thickness of gravel, and parameter relative to gravel porosity.

8. At the peak of plug rise, the wedge and plug are assumed to become disconnected and each falls subject to gravity and whatever pressure forces are appropriate.

9. Escape of aerosol from the structure was estimated from empirical relationships for aerosol capture in packed gravel bed filters exposed to steady flow conditions [MI74]. Aerosols were assumed to be uniformly mixed into the gas contained in the structure initially. Gas leakage through the gravel carried entrained aerosol which was either captured or released to the environment. That aerosol captured in the bed was assumed to be held for the duration of the experiment.

These and other sets of assumptions were translated into appropriate equations and relationships (see later sections of this Appendix) and used to calculate gravel rise and round room pressure in the 1982 GG Test. When results were clearly at variance with the observed behavior of the structure or data, assumptions were modified to relieve the problem. The assumptions listed above seemed to provide a reasonable fit to the 1982 test data (see Figures O-2 and O-3) and were adopted as a acceptable model.

Use of the Model

The model was used to examine three additional problems of interest. The first was the 1957 fully confined GG test, the second was the nominal 1982 test structure and the third was one of the scaled tests done in preparation for the 1982 full-scale tests. Results are shown in Figures O-4 for the 1957 test, O-5 for the 1982 nominal configuration, and O-6 for the scaled test. Table O-1 contains input data for all calculations.

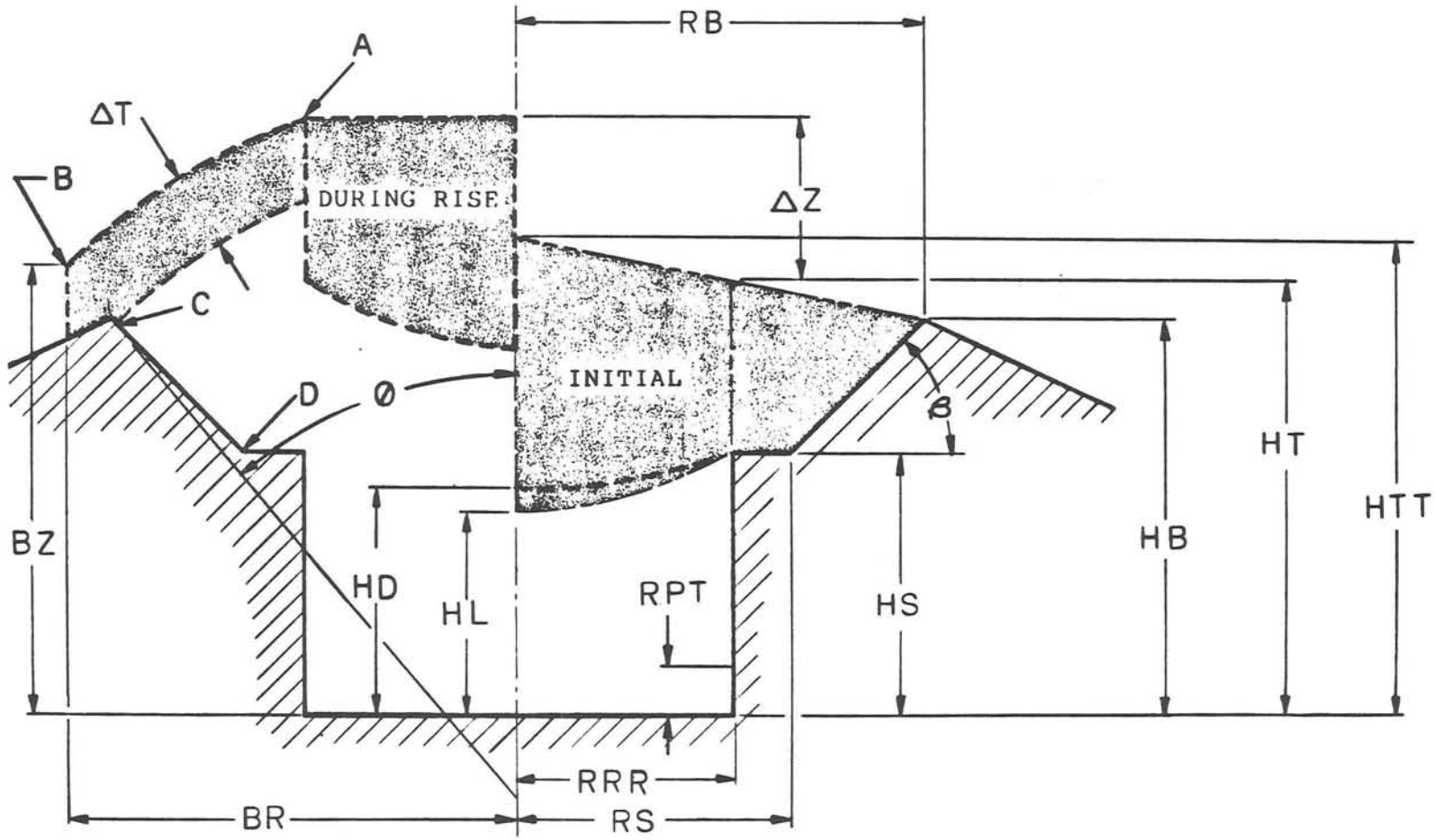

Figure O-1. Cross-section of full-scale gravel bed.

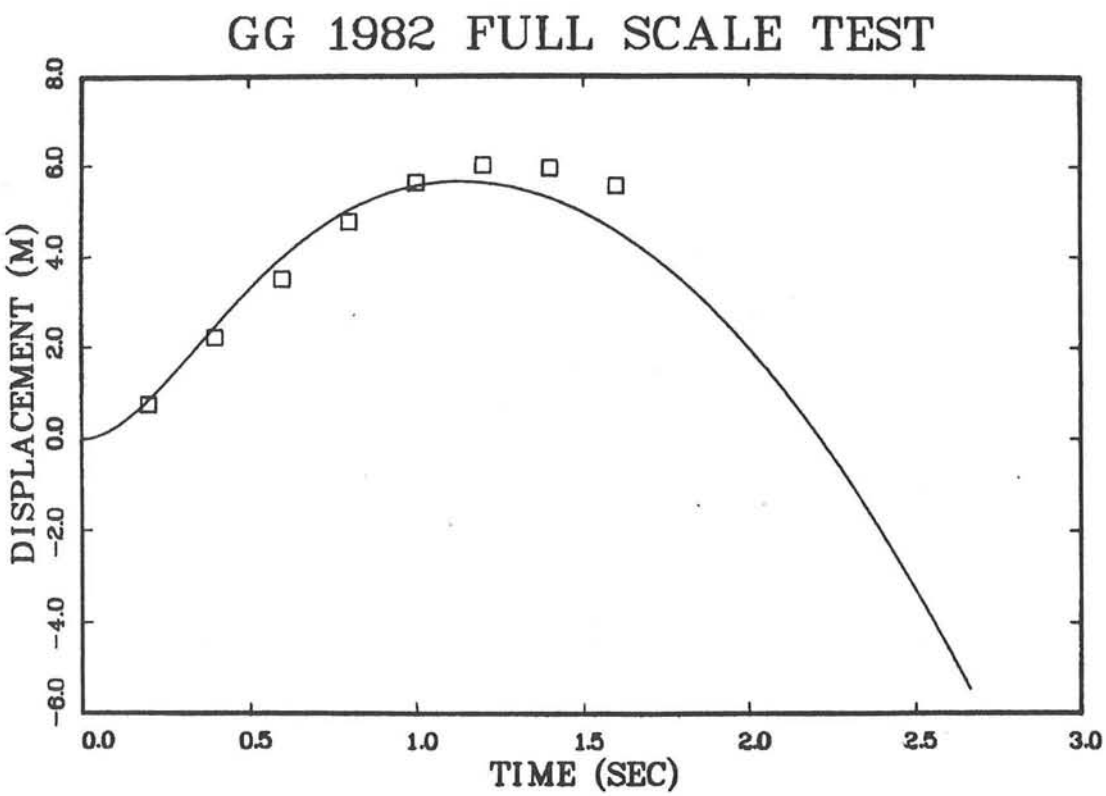

Figure O-2. Model Results and Motion Data for 82 Test

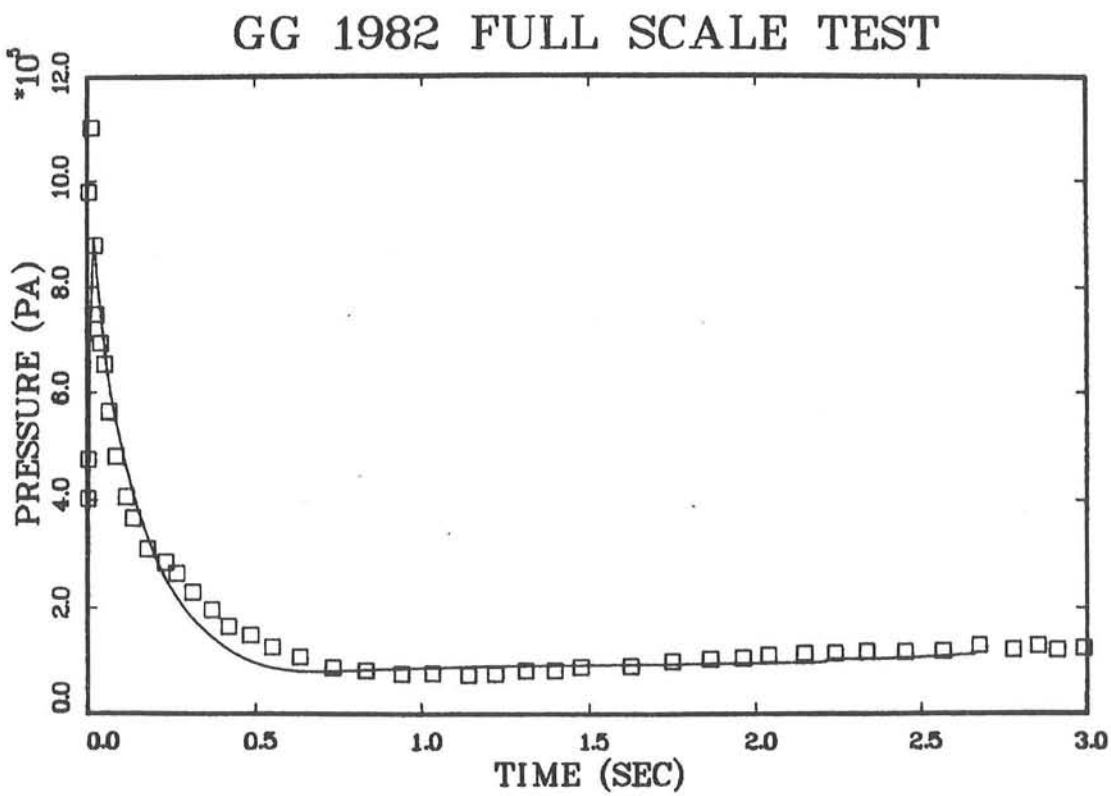

Figure O-3. Model Results and Pressure Data for 82 Test

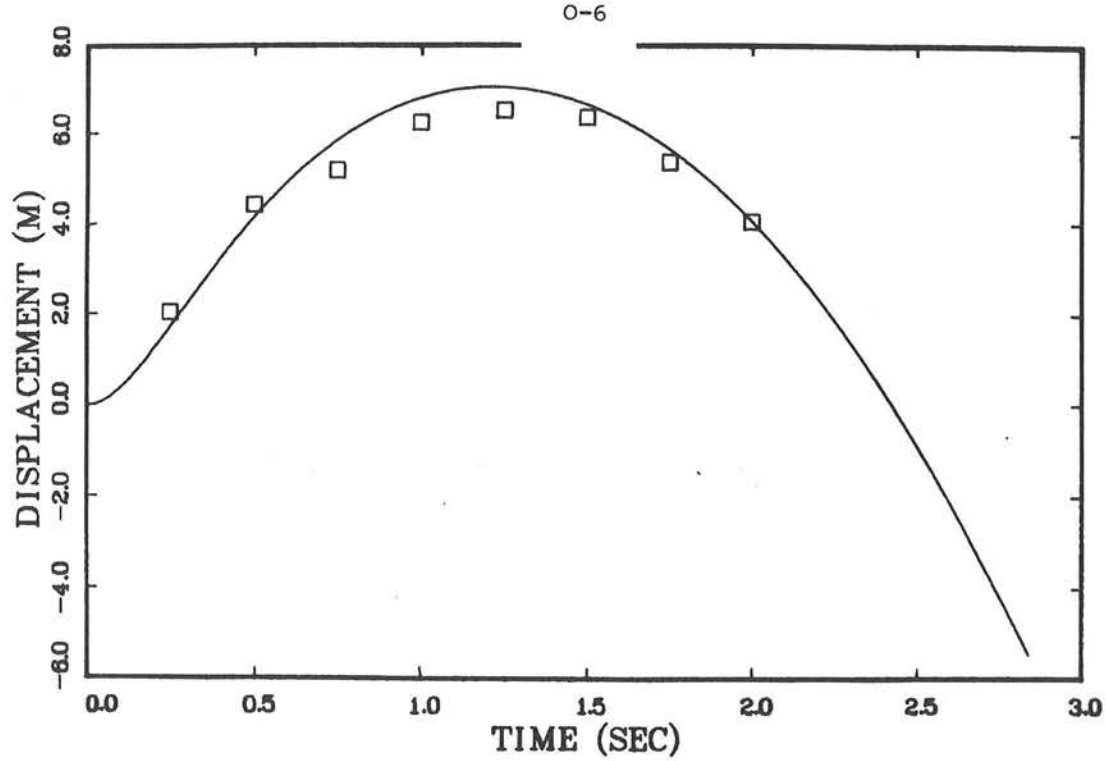

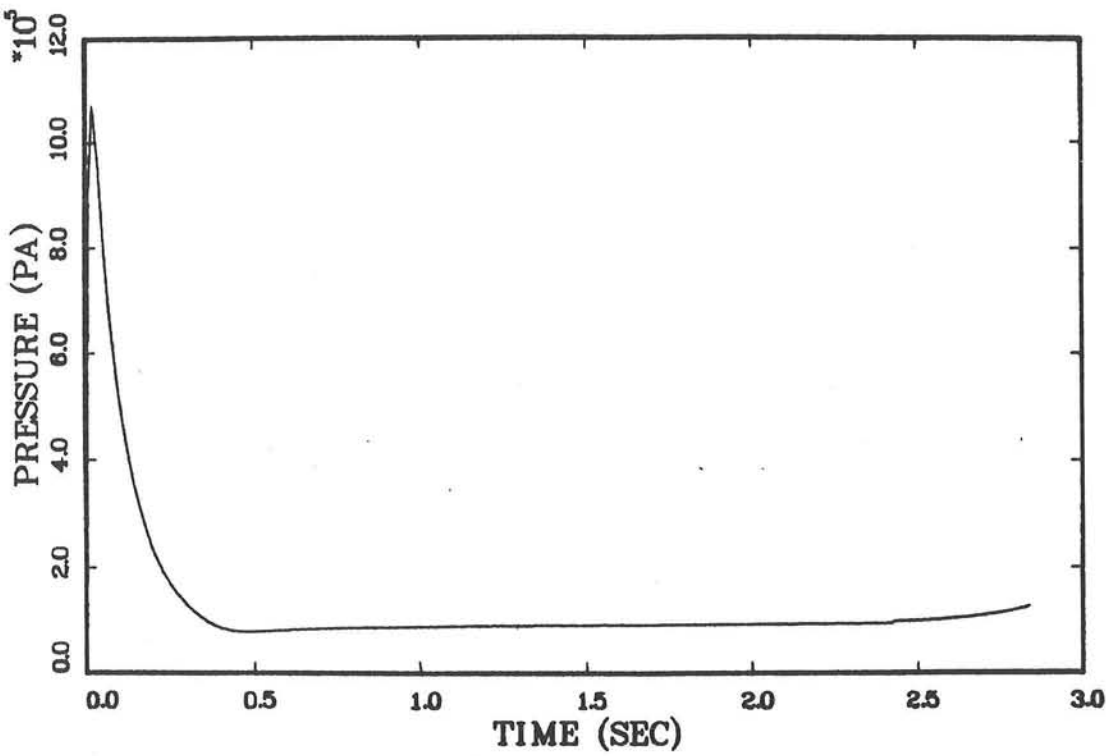

Figure O-4. Model Results for 1957 Full-Scale Test

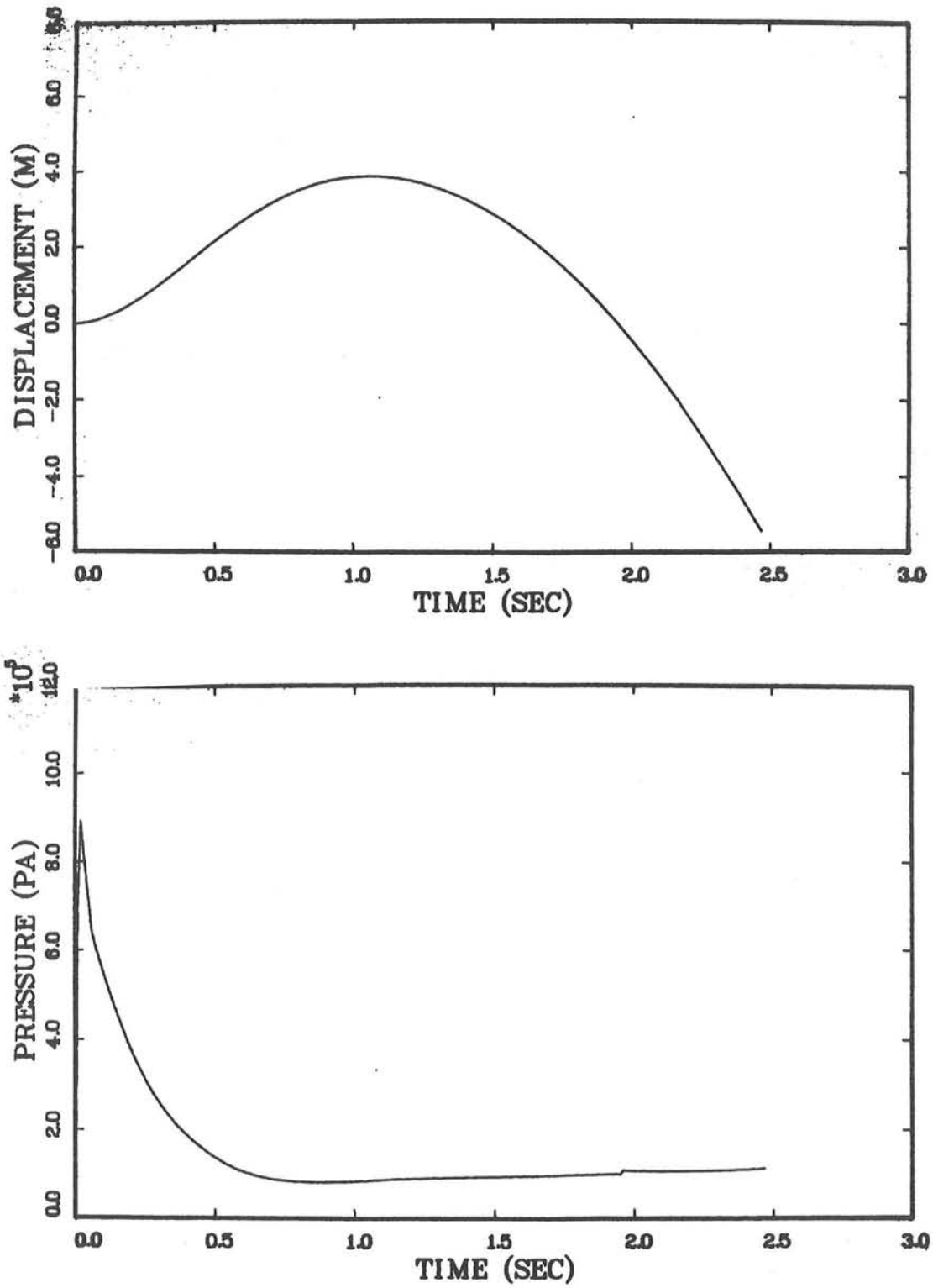

Figure O-5. Model Results for 1982 Nominal Configuration

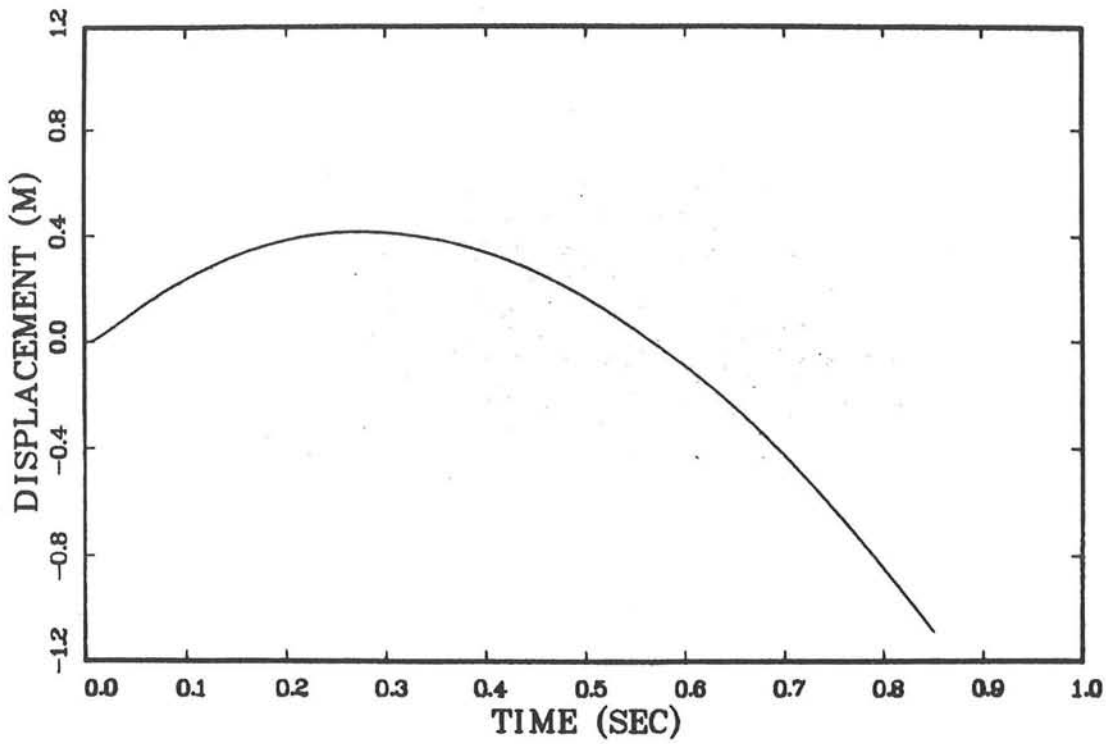

Figure O-6. Model Results for 1982 Scaled Test

TABLE O-1

Input Parameters for the 1982 Full Scale, Scaled and Nominal and 1957 Full Scale Simulations

Description* (units)	Variable Name	Full Scale 1957	Full Scale 1982	Scaled 1982	Nominal 1982
Radius of round room (m)	RRR	5.18	5.18	.915	5.18
Radius of Sill (m)	RS	6.71	6.71	1.185	6.71
Height of Sill (m)	HS	6.45	6.45	1.09	6.45
Radius of earth break (m)	RB	8.35	9.75	1.677	9.75
Height of earth break (m)	HB	8.23	9.6	1.549	9.6
Height of gravel @ center (m)	HTT	9.91	11.56	2.149	11.56
Height of gravel @ RRR (m)	HT	9.6	10.52	2.149	11.25
Height of cable (unloaded) (m)	HD	5.05	5.05	1.092	5.05
Height of cable (loaded) (m)	HL	4.95	4.95	.991	4.95
Radius of portal (m)	RPT	1.08	1.28	.432	1.28
Radius of staging area (m)	RCR	1.07	1.52	.305	1.52
Length of staging area (m)	LSA	40.0	71.63	6.0	71.63
Volume of plug (m^3)	VGP	346.0	450.0	2.79	497.0
Volume of wedge (m^3)	VGW	268.0	464.0	2.0	601.0
Volume of staging area (m^3)	VCR	141.7	522.6	3.554	522.6
High Explosive (kg)	HE	273.0	192.0	.264	192.0
Ambient Pressure (pa)	PA	8.97×10^4	8.97×10^4	8.61×10^4	8.97×10^4
Gravel Density (kg/m^3)	RHO	2.0×10^3	2.0×10^3	2.0×10^3	2.0×10^3

*See Figure O-1.

The model provides reasonable predictions for all of the cases attempted. Of particular interest is the 1957 test as compared to the 1982 test. The 1957 test had more HE, less gravel volume, and smaller total volume than the 1982 test and, therefore, might be expected to have produced much larger gravel rise. This was not observed. The proper behavior was predicted because the important effect of staging area volume in lengthening the pressure pulse and increasing impulse was modeled. Although decreased total volume does act to increase the initial pressure, the effect of that increase on overall roof behavior was contravened by a rapid pressure decrease caused by the increased ratio of expanded round room volume to total volume.

The predicted aerosol releases in the 1982 and 1957 tests and the 1982 nominal configurations are shown in Figure O-7 as a function of time after detonation. Total respirable release predicted for the 1982 test is not too different from that observed (considering the crude nature of the model). If the relative quantities of aerosol released are used as an index, it can be seen that the 1982 nominal might have been expected to release no more than the 1982 test structure did. This provides some comfort in using the 1982 test as a true indicator of the capability of the Pantex structure (like the 1982 nominal) to confine hazardous small aerosols.

Model Equations

A. Initial Pressures Versus Time (see Figure O-8):
(Reference BA82, p. 238)

$$t_1 = 5t_a + t_r$$

$$t_r = \frac{2i_r}{P_r}$$

where t_1 is the time at which the internal blast loading phase ends,
t_a is the shock arrival time at the roof,
i_r is the reflected specific impulse, and
P_r is the peak reflected overpressure.

$$P_1 = P_a + P_{qs}$$

$$P_2 = P_a + P'_{qs}$$

$$t_2 = t_1 + \Delta t$$

$$\Delta t = \frac{V_{rr}}{725\,\alpha\,A} \ln\left(\frac{P_1}{P_2}\right)$$

where P_a is atmospheric pressure

P_{qs} is the quasi-static pressure which is a function of the mass, W, of HE and the volume, V_{rr}, of the round room,

P'_{qs} is the quasi-static pressure which is a function of W and the combined volume, $V_{rr} + V_{sa}$, of round room and staging area,

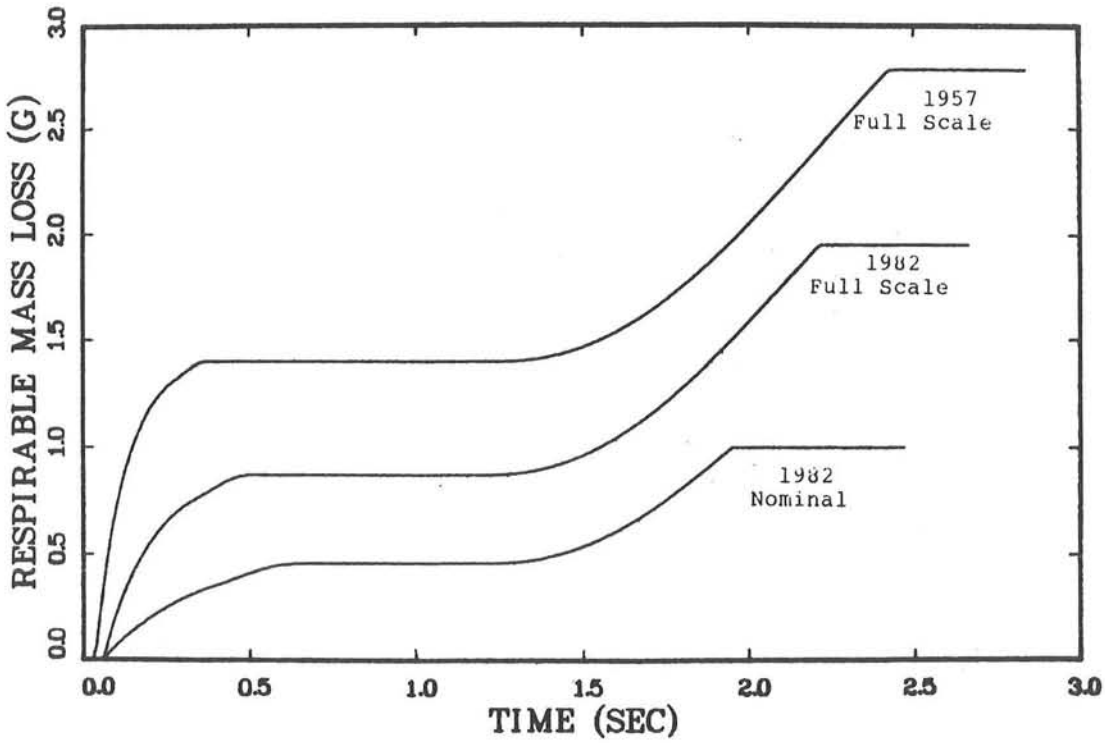

Figure O-7 Comparision of Estimated Respirable Mass Loss

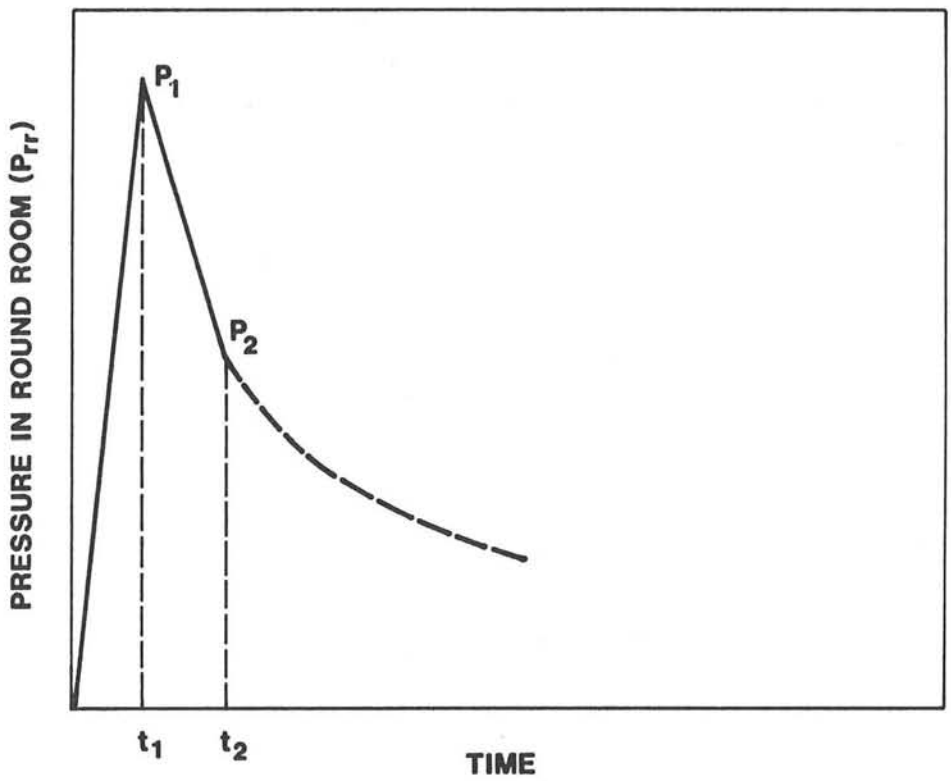

Figure O-8. Initial Pressure--Time Assumptions

α is a constant equal to 1.0, and

A is area of portal connecting round room to staging area.

B. Vertical Acceleration of Gravel

$$A_g = \frac{p \cdot \text{Area} + K\,(z_o - z) - \text{Weight}}{\text{gravel bed mass}}$$

where:

p is the pressure difference across the gravel and is equal to the difference between the dynamic pressure in round room and the atmospheric pressure P_a,

Area is the gravel bed cross sectional area over which the dynamic pressure acts,

$K(z_o-z)$ is the spring force resulting suspension cable elongation which goes to zero for z greater than or equal to z_o.

C. Conservation of Energy

$$M\,C_v\,(T_2-T_1) = \text{heat loss} - P_s\,\Delta V + \Delta M\,[C_v\,T_s + P_s\,V_s]$$

where:

M is the instantaneous mass of the gas in the structure,

C_v is specific heat at constant volume

T_2-T_1 is change in temperature over time step Δt

P_s is the average pressure of gas over time step Δt

ΔV is change in gas volume over time step Δt

ΔM is change in gas mass over time step Δt

T_s is the average temperature during time step Δt

V_s is average specific volume of gas (volume/mass) during time step Δt.

$$\text{heat loss} = A_w \left[\epsilon\sigma(T_1^4 - T_w^4) + h\,(T_1 - T_w)\,\Delta t\right]$$

where

σ is Stefann Boltzmann constant

h is heat transfer coefficient (56 $J/m^2/K/s$)

ϵ is effective gas emissivity (0.5)

T_w is wall temperature (300 K)

A_w is total surface area in contact with gas

Δt is time step of integration

D. Movement of Point B

$B_r(t) = B_r\,(t-\Delta t) + \Delta Z\,\sin\theta\,(t-\Delta t)\,\cos\beta$

$B_z(t) = B_z\,(t-\Delta t) + \Delta Z\,\sin\theta\,(t-\Delta t)\,\sin\beta$

$B_r(o) = RB$

$B_z(o) = HB$

ΔZ is change in center of gravity of plug over time Δt (see figure O-1 for θ, β, B_r, B_z, RB, HB, ΔZ)

Subscript r denotes the radial component and subscript z denotes the vertical component.

E. Gas Passed Through Gravel Bed

$$M = \frac{\rho \cdot \text{Area} \cdot \Delta p \cdot D_g^2}{\mu L} \left[\frac{\epsilon^3}{36\ K(1-\epsilon^2)} \right] \cdot \Delta t$$

where Area is surface area of bed exposed to gas.

μ	is viscosity of gas
ρ	is density of gas
Δp	is pressure drop on bed
L	is depth of bed
D_g	is gravel diameter
ϵ	is $\epsilon_o\ [1 - A_g/9.8]^{1.5}$ (Ref. HA65)
A_g	is acceleration of gravel
ϵ_o	is void fraction $[1 - \rho_g/\rho_r]$
ρ_g	is gravel density
ρ_r	is density of rock in gravel
K	is Kozeny constant (5)

F. Aerosol Capture Model (Ref. MI74)

Fraction released = $\exp - (2.74 \times 10^{-3} z)$

z	is $L/(D_g^{\ 1.43} \cdot U^{2/3})$
U	is $\Delta m/(\rho \cdot \text{Area} \cdot \Delta t)$

SPECIFIED EXTERNAL DISTRIBUTION ONLY:

M1163	Carl Forsberg (5) DP 221.1, GTN U.S. Department of Energy Washington, DC 20545
NE 0737	Los Alamos National Laboratories (1) Mail Station 5000 P.O. Box 5000 Los Alamos, NM Attn: Don Rose- WX-5 A. Stoker - WX-5 E. Gladney - WX-5
TB 0660	U.S. Department of Energy Amarillo Area Office P.O. Box 30030 Amarillo, TX 79120 Attn: Paul Wagner, Area Manager (6)
NE 0659	U.S. Department of Energy Albuquerque Operations Office P.O. Box 5400 Albuquerque, NM 87115 Attn: J. Schinkel, OSD (4) H. F. Mumma, FCMD (3)
300	R. L. Hagengruber (1) Attn: P. A. Stokes, 0311 Attn: J. M. Taylor, 0311
400	C. Winter
1220	M. Cowan
1533	P. Yarrington
1533	T. K. Bergstresser
1533	F. R. Norwood
1534	J. R. Asay
1534	D. E. Grady
2000	J. Mogford, U.K. Coordinator (2) Attn: Derek Vallis, AWRE, Aldermaston, England Attn: L. Huckstep, HRM Ord. Facility, Burghfield Common, England
3141	Technical Library (5)
3151	Technical Writing (3)
3311	D. R. Parker
5100	J. C. Crawford
5100	R. N. Brodie
5135	L. L. Keller
5256	M. R. Madsen
5256	W. R. Hartman
5256	G. W. Dykes
6000	E. H. Beckner
6300	R. W. Lynch

6320	R. M. Jefferson (1)
	Attn: R. E. Luna, 6321 (1)
	Attn: R. P. Sandoval, 6321 (1)
	Attn: N. R. Grandjean, 6321 (1)
	Attn: B. D. Zak, 6324 (1)
	H. W. Church, 6324
7130	J. D. Kennedy (1)
	Attn: B. G. Edwards
	Attn: V. E. Kerr
	Attn: A. Church
7230	W. L. Stevens
7233	F. H. Mathews (1)
	Attn: R. E. Bohannon
	Attn: M. G. Perdue
	Attn: J. P. Weber